

PRECAMBRIAN PALEONTOLOGY

EDITED BY: Juliana Leme, Shuhai Xiao and Dermeval Aparecido Do Carmo

PUBLISHED IN: *Frontiers in Earth Science* and *Frontiers in Ecology and Evolution*



frontiers

Frontiers eBook Copyright Statement

The copyright in the text of individual articles in this eBook is the property of their respective authors or their respective institutions or funders. The copyright in graphics and images within each article may be subject to copyright of other parties. In both cases this is subject to a license granted to Frontiers.

The compilation of articles constituting this eBook is the property of Frontiers.

Each article within this eBook, and the eBook itself, are published under the most recent version of the Creative Commons CC-BY licence.

The version current at the date of publication of this eBook is CC-BY 4.0. If the CC-BY licence is updated, the licence granted by Frontiers is automatically updated to the new version.

When exercising any right under the CC-BY licence, Frontiers must be attributed as the original publisher of the article or eBook, as applicable.

Authors have the responsibility of ensuring that any graphics or other materials which are the property of others may be included in the CC-BY licence, but this should be checked before relying on the CC-BY licence to reproduce those materials. Any copyright notices relating to those materials must be complied with.

Copyright and source acknowledgement notices may not be removed and must be displayed in any copy, derivative work or partial copy which includes the elements in question.

All copyright, and all rights therein, are protected by national and international copyright laws. The above represents a summary only. For further information please read Frontiers' Conditions for Website Use and Copyright Statement, and the applicable CC-BY licence.

ISSN 1664-8714

ISBN 978-2-83250-118-4

DOI 10.3389/978-2-83250-118-4

About Frontiers

Frontiers is more than just an open-access publisher of scholarly articles: it is a pioneering approach to the world of academia, radically improving the way scholarly research is managed. The grand vision of Frontiers is a world where all people have an equal opportunity to seek, share and generate knowledge. Frontiers provides immediate and permanent online open access to all its publications, but this alone is not enough to realize our grand goals.

Frontiers Journal Series

The Frontiers Journal Series is a multi-tier and interdisciplinary set of open-access, online journals, promising a paradigm shift from the current review, selection and dissemination processes in academic publishing. All Frontiers journals are driven by researchers for researchers; therefore, they constitute a service to the scholarly community. At the same time, the Frontiers Journal Series operates on a revolutionary invention, the tiered publishing system, initially addressing specific communities of scholars, and gradually climbing up to broader public understanding, thus serving the interests of the lay society, too.

Dedication to Quality

Each Frontiers article is a landmark of the highest quality, thanks to genuinely collaborative interactions between authors and review editors, who include some of the world's best academicians. Research must be certified by peers before entering a stream of knowledge that may eventually reach the public - and shape society; therefore, Frontiers only applies the most rigorous and unbiased reviews. Frontiers revolutionizes research publishing by freely delivering the most outstanding research, evaluated with no bias from both the academic and social point of view. By applying the most advanced information technologies, Frontiers is catapulting scholarly publishing into a new generation.

What are Frontiers Research Topics?

Frontiers Research Topics are very popular trademarks of the Frontiers Journals Series: they are collections of at least ten articles, all centered on a particular subject. With their unique mix of varied contributions from Original Research to Review Articles, Frontiers Research Topics unify the most influential researchers, the latest key findings and historical advances in a hot research area! Find out more on how to host your own Frontiers Research Topic or contribute to one as an author by contacting the Frontiers Editorial Office: frontiersin.org/about/contact

PRECAMBRIAN PALEONTOLOGY

Topic Editors:

Juliana Leme, University of São Paulo, Brazil

Shuhai Xiao, Virginia Tech, United States

Dermeval Aparecido Do Carmo, University of Brasilia, Brazil

Citation: Leme, J., Xiao, S., Do Carmo, D. A., eds. (2022). Precambrian Paleontology. Lausanne: Frontiers Media SA. doi: 10.3389/978-2-83250-118-4

Table of Contents

- 05 *Precambrian Paleobiology: Precedents, Progress, and Prospects***
J. William Schopf
- 26 *The Importance of Size and Location Within Gregarious Populations of *Ernietta plateauensis****
Brandt M. Gibson, Simon A.F. Darroch, Katie M. Maloney and Marc Laflamme
- 37 *New Species of Macroalgae from Tamengo Formation, Ediacaran, Brazil***
Cleber Q. C. Diniz, Juliana de Moraes Leme and Paulo C. Boggiani
- 48 *Orientations of Mistaken Point Fronds Indicate Morphology Impacted Ability to Survive Turbulence***
Philip B. Vixseboxse, Charlotte G. Kenchington, Frances S. Dunn and Emily G. Mitchell
- 63 *Evolution of Holdfast Diversity and Attachment Strategies of Ediacaran Benthic Macroalgae***
Xiaopeng Wang, Mengyin Wu, Bin Wan, Changtai Niu, Wentao Zheng, Chengguo Guan, Ke Pang, Zhe Chen and Xunlai Yuan
- 74 *Doushantuo-Pertatataka—Like Acritarchs From the Late Ediacaran Bocaina Formation (Corumbá Group, Brazil)***
L. Morais, T. R. Fairchild, B. T. Freitas, I. D. Rudnitzki, E. P. Silva, D. Lahr, A. C. Moreira, E. A. Abrahão Filho, J. M. Leme and R. I. F. Trindade
- 89 *Charniodiscus and Arborea Are Separate Genera Within the Arboreomorpha: Using the Holotype of *C. concentricus* to Resolve a Taphonomic/Taxonomic Tangle***
Daniel Pérez-Pinedo, Christopher McKean, Rod Taylor, Robert Nicholls and Duncan McIlroy
- 103 *What Happens Between Depositional Events, Stays Between Depositional Events: The Significance of Organic Mat Surfaces in the Capture of Ediacara Communities and the Sedimentary Rocks That Preserve Them***
Mary L. Droser, Scott D. Evans, Lidya G. Tarhan, Rachel L. Surprenant, Ian V. Hughes, Emmy B. Hughes and James G. Gehling
- 120 *Methodological Development of a Combined Preparation for Micropaleontological and Sedimentological Studies of Samples From the Proterozoic Record***
Matheus Denezine, Rodrigo Rodrigues Adorno, Dermeval Aparecido Do Carmo, Edi Mendes Guimarães, Detlef Hans Gert Walde, Carlos José Souza De Alvarenga, Gerard Germs, Lucas Silveira Antonietto, Christian Gianfranco Valdivia Rodríguez and Osvaldo De Oliveira Nunes Junior
- 134 *A New Conulariid (Cnidaria, Scyphozoa) From the Terminal Ediacaran of Brazil***
Juliana M. Leme, Heyo Van Iten and Marcello G. Simões

- 147** *New Facies Model and Carbon Isotope Stratigraphy for an Ediacaran Carbonate Platform From South America (Tamengo Formation—Corumbá Group, SW Brazil)*
Maria E. A. F. Ramos, Martino Giorgioni, Detlef H. G. Walde, Dermeval A. do Carmo, Gabriella Fazio, Lucieth C. Vieira, Matheus Denezine, Roberto V. Santos, Rodrigo R. Adôrno and Lucas Lage Guida
- 171** *New Material of Carbonaceous Compressions from the ~1.5 Ga Singhora Group, Chhattisgarh Supergroup, India, and their Interpretation as Benthic Algae*
Veeru Kant Singh and Mukund Sharma
- 196** *Evidence for Metabolic Diversity in Meso-Neoproterozoic Stromatolites (Vazante Group, Brazil)*
Flavia Callefo, Fresia Ricardi-Branco, Mírian Liza Alves Forancelli Pacheco, Alexandre Ribeiro Cardoso, Nora Noffke, Verônica de Carvalho Teixeira, Itamar Tomio Neckel, Lara Maldanis, Emma Bullock, Dina Bower, Adalene Moreira Silva, Dario Ferreira Sanchez, Fabio Rodrigues and Douglas Galante



Precambrian Paleobiology: Precedents, Progress, and Prospects

J. William Schopf*

Department of Earth, Planetary, and Space Sciences, University of California, Los Angeles, Los Angeles, CA, United States

OPEN ACCESS

Edited by:

Juliana Leme,
University of São Paulo, Brazil

Reviewed by:

Thomas Rich Fairchild,
University of São Paulo, Brazil
Guang-Hui Xu,
Institute of Vertebrate Paleontology
and Paleoanthropology, Chinese
Academy of Sciences, China

*Correspondence:

J. William Schopf
schopf@epss.ucla.edu

Specialty section:

This article was submitted to
Paleontology,
a section of the journal
Frontiers in Ecology and Evolution

Received: 08 May 2021

Accepted: 09 August 2021

Published: 27 August 2021

Citation:

Schopf JW (2021) Precambrian
Paleobiology: Precedents, Progress,
and Prospects.
Front. Ecol. Evol. 9:707072.
doi: 10.3389/fevo.2021.707072

In 1859, C. R. Darwin highlighted the “inexplicable” absence of evidence of life prior to the beginning of the Cambrian. Given this lack of evidence and the natural rather than theological unfolding of life’s development Darwin espoused, over the following 50 years his newly minted theory was disputed. At the turn of the 19th century, beginning with the discoveries of C. D. Walcott, glimmerings of the previously “unknown and unknowable” early fossil record came to light – but Walcott’s Precambrian finds were also discounted. It was not until the breakthrough advances of the 1950’s and the identification of modern stromatolites (1956), Precambrian phytoplankton in shales (1950’s), stromatolitic microbes in cherts (1953), and terminal-Precambrian soft-bodied animal fossils (1950’s) that the field was placed on firm footing. Over the following half-century, the development and application of new analytical techniques coupled with the groundbreaking contributions of the Precambrian Paleobiology Research Group spurred the field to its international and distinctly interdisciplinary status. Significant progress has been made worldwide. Among these advances, the known fossil record has been extended sevenfold (from ~0.5 to ~3.5 Ga); the fossil record has been shown consistent with rRNA phylogenies (adding credence to both); and the timing and evolutionary significance of an increase of environmental oxygen (~2.3 Ga), of eukaryotic organisms (~2.0 Ga), and of evolution-speeding and biota-diversifying eukaryotic sexual reproduction (~1.2 Ga) have been identified. Nevertheless, much remains to be learned. Such major unsolved problems include the absence of definitive evidence of the widely assumed life-generating “primordial soup”; the timing of the origin of oxygenic photosynthesis; the veracity of postulated changes in global photic-zone temperature from 3.5 Ga to the present; the bases of the advent of eukaryotic sexuality-requiring gametogenesis and syngamy; and the timing of origin and affinities of the small soft-bodied precursors of the Ediacaran Fauna.

Keywords: C. R. Darwin, great oxidation event (GOE), oldest fossils, Precambrian Paleobiology Research Group (PPRG), C. D. Walcott

EXPLANATORY COMMENT

Unlike the Editors and publishers of this volume, please note that I prefer to refer to this field of science as “Precambrian Paleobiology” – rather than “Precambrian Paleontology” – chiefly because the suffix “-biology” emphasizes its necessarily interdisciplinary character, a hallmark of the field that contrasts rather markedly from the long-established practices of Phanerozoic

paleontology. In addition, being the last surviving member of the so-called “vanguard” of workers in such Precambrian studies (Cloud, 1983) and having spent some 60 years investigating numerous aspects of the early history of life, please also note that this review article is written from my personal perspective.

BEGINNINGS OF THE SCIENCE

1859, Darwin’s Dilemma

In 1859, Charles Robert Darwin stated the problem: “*If the theory [of evolution] be true, it is indisputable that before the lowest Cambrian stratum was deposited... the world swarmed with living creatures. [Yet] why we do not find rich fossiliferous deposits belonging to these assumed earliest periods... I can give no satisfactory answer. The case at present must remain inexplicable; and may be truly urged as a valid argument against the views here entertained*” (Darwin, 1859, Chpt X).

Darwin’s evidence for his theory came not only from the multitude of specimens he collected as the naturalist on the 1831–1836 world-encircling voyage of the *H.M.S. Beagle* but even more-so from the then already reasonably well-outlined Phanerozoic fossil record. In Darwin’s time, however, the history of life prior the emergence of the oldest Cambrian-age invertebrate animal fossils was completely unknown, a deficiency that plagued Darwin and his theory. And though Darwin tried mightily to explain the problem away (perhaps primitive life was too small, too fragile to be preserved, or perhaps all truly ancient fossil-hosting rocks had eroded away), his notions about pre-trilobite pre-Cambrian life and the early rock record were mistaken. Nevertheless, for the following full century, from the 1860’s to the 1960’s, the Precambrian history of life was regarded as “*unknown and unknowable*,” claimed by some to be “*the greatest unsolved problem in all of natural science*.”

1860–1900, Distrust of Darwin’s Evolution

As with all newly minted paradigms, Darwin’s evolution addressed a previously unquestioned explanation of a major aspect of human understanding, namely the history and development of life on Earth. Throughout all of Europe for the previous nearly two millennia – dating from the Roman Empire that stretched across North Africa and from Italy to the British Isles – the prevailing view was that God, as documented in the Holy Christian Bible, had created all of life. Darwin’s theory of a naturally occurring rather than a Biblically ordained unfolding of life’s development flew in the face of accepted wisdom.

Darwin and his “Bible-disproving” ideas were soon lampooned in the British press, a pervasive criticism that spread the colonies. A prime example and strident critic was John William Dawson, appointed in 1855 to the influential position of Principal of McGill University, Canada, who was knighted by Queen Victoria in 1884. Of Scottish descent and a Calvinist staunch Creationist, in 1865 Dawson formally described *Eozoön canadense*, the “Dawn Animal of Canada” (Figure 1), a large multi-layered structure found in pre-trilobite, pre-Cambrian limestones near the Ottawa River west of Montreal, rocks



FIGURE 1 | J. W. Dawson’s “Dawn Animal of Canada,” *Eozoön canadense*, a specimen of non-biogenic serperpentinized limestone ~20 cm in largest dimension collected in early Neoproterozoic strata southwest of Quebec Canada, as depicted in *The Dawn of Life*, 1875, Plate III, p. 35.

now known to be ~1,100 Ma in age. Even though *Eozoön* was quite obviously far older than any fossils then known, Dawson regarded it to be assuredly biogenic, interpreting it to be the remains of a giant foraminiferal protozoan and – to him of utmost importance – direct evidence that disproved Darwin’s theory. As he wrote in his 1875 volume *The Dawn of Life*, “*There is no link whatever to connect Eozoön with younger fossils... all stand before us as distinct creations. Eozoön thus bears damaging negative testimony against evolution [a theory that] is incapable of proof and contrary to fact. Evolutionists are mere dreamers, having no scientific basis for their dogmas*” (Dawson, 1875, Chpt. VIII).

Eozoön was soon discounted. In 1866, a year after its announcement, Irish mineralogists William King and Thomas Rowley opined that the supposed fossil was “*purely mineralic, non-biologic*.” In 1879, based on studies of specimens sent to him by Dawson, the German zoologist and world expert on the Foraminifera Karl Möbius agreed with the King-Rowley assessment, writing that *Eozoön* was “*certainly not biologic*.” Finally, in 1894, two geologists at London’s British Museum, J. W. Gregory and H. J. Johnston-Lavis, collected specimens of *Eozoön* in volcanic blocks at Mt. Vesuvius in southern Italy and found them to be composed of coarsely crystalline calcite and serpentine, thus identifying Dawson’s “Dawn Animal” as a “*serpentinized limestone, entirely inorganic*.” In short – and though until his death in 1899, Dawson continued to maintain that he had “disproved evolution” – *Eozoön* has the unwelcome distinction of being the first Precambrian pseudofossil discovered and formally described.

1900–1950, Stage-Setting Events

In the late 1800’s, the American paleontologist Charles Doolittle Walcott entered the scene, a history masterfully recounted in the writings of Ellis Yochelson of the United States National Museum of Natural History (Yochelson, 1998). As a youth, Walcott attended Utica High School in upstate New York from which he

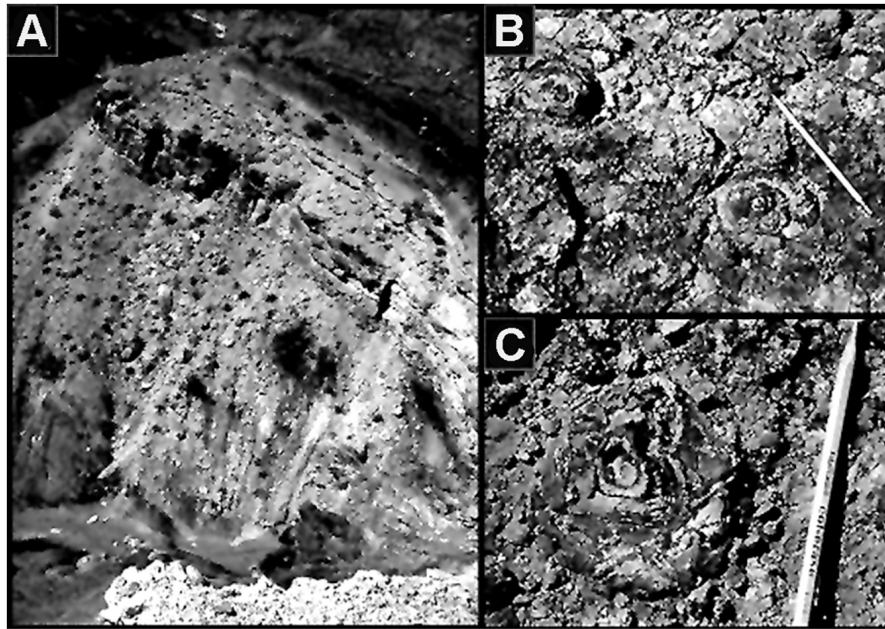


FIGURE 2 | (A) “Stromatolite Ridge” in the Neoproterozoic ~750 Ma Chuar Group Galeros Formation of the Grand Canyon of Arizona United States where C. D. Walcott discovered the *Cryptozoön*-like stromatolites shown in **(B,C)**, the first stromatolites to be reported from the Precambrian rock record.

departed at the age of 18 – two years before he was to graduate and after only 10 years of formal schooling. He then became a farmhand, toiling the fields and, in that process, augmenting the impressive collection of Cambrian trilobites he had begun to amass as a youth. Soon after being hired in 1876 by N.Y. State Geologist James Hall Jr., in 1879 Walcott was recruited to join the newly formed United States Geological Survey (USGS).

At about that time the recently appointed USGS Director, John Wesley Powell, set in place a series of expeditions down the Colorado River through the Grand Canyon of Arizona, each a harrowing passage down the rushing waters on large rowboats and unstable log rafts. Walcott eagerly signed-up. On one of the early ventures, in 1883, he discovered the first stromatolites known from the Precambrian rock record (**Figure 2**), layered microbe-produced mound-shaped structures much like the Cambrian “algal reefs” at Saratoga Springs NY that Hall had previously named *Cryptozoön* (meaning “hidden life”) and that Walcott had examined in 1878. This was an important “first,” stromatolites being now known to be both widespread and abundant in shallow-water marine strata throughout the Precambrian, the oldest dating from the beginning of the Paleoproterozoic.

On a later Grand Canyon trip, Walcott uncovered another major find, compressed specimens of the Precambrian spheroidal planktonic alga *Chuaria* (**Figure 3**) which he formally described and named in 1899 (Walcott, 1899). Although specimens much like *Chuaria* had previously been recorded from the ~800 Ma Neoproterozoic Visingsö Group of Sweden, they were unnamed and had not been illustrated (reviewed by Talyzina, 2000). Thus, Walcott deserves the credit for having formally described the first cellularly preserved Precambrian microfossils known to science.

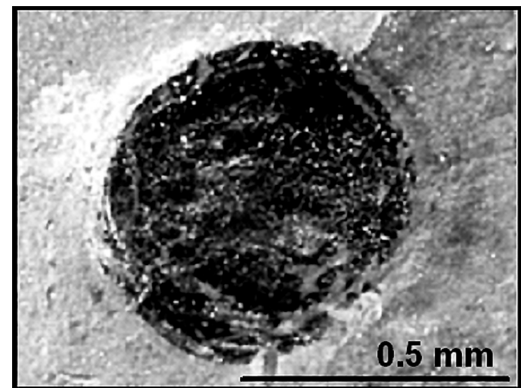


FIGURE 3 | A compressed flattened specimen of the megaplanktonic single-celled alga *Chuaria circularis* in the Neoproterozoic ~750 Ma Chuar Group of the Grand Canyon of Arizona United States, the first cellularly preserved microfossil formally described from Precambrian-age deposits.

In the following years, Walcott headed north along the spine of the Rocky Mountains and from 1902 to 1907 discovered numerous close-packed Precambrian stromatolites in the Lewis Range of northwestern Montana, important confirmation of his earlier discovery of their occurrence in the Chuar Group Grand Canyon strata. From there, he continued even farther north, up the Rocky Mountains into British Columbia where in 1909 he yet again had a huge success, discovery of the remarkably diverse and well-preserved animal fossils of the middle Cambrian (510 Ma) Burgess Shale, the all-important first prime evidence of the Cambrian Explosion of Life.

Walcott's career was spectacular. After joining the USGS in 1879, he rapidly rose through the ranks, in 1893 becoming Chief Paleontologist and then, in 1894 with the retirement of J. W. Powell, he was appointed the second Director of the United States Geological Survey. For Walcott, that was just the beginning. In 1902, he and a team of colleagues met with the exceedingly wealthy "Robber Barron" philanthropist Andrew Carnegie and established the Carnegie Institution of Washington to promote scientific discovery that from its inception has remained a highly distinguished research center. Walcott later went on to become Secretary (CEO) of Washington's Smithsonian Institution, President of the National Academy of Sciences, and President of the American Association for the Advancement of Science. Additionally, as a close advisor to United States President Theodore Roosevelt, he was instrumental to the establishment of the United States National Park system.

Despite these accomplishments, not all of Walcott's finds were warmly received, most notably his claims of Precambrian life (stromatolites and cellular fossils). Walcott had ascended to scientific stardom so it would take another luminary to take him down. Albert Charles Seward, Vice-Chancellor (CEO) of Cambridge University United Kingdom and the world's leading paleobotanist, filled the bill. Delivering his verdict from his position of unquestioned authority – Walcott's Precambrian finds being evidence of ancient algae and microbes and, thus, under the purview of paleobotany – Seward lowered the boom in his 1931 textbook, his discussion being brief but to the point. According to Seward, "[Walcott's interpretation of] *Cryptozoön* [the Precambrian stromatolites] is, I venture to think, not justified by the facts. It is clearly impossible to maintain that such bodies are attributable to algal activity. . . we can hardly expect to find in Pre-Cambrian rocks any actual proof of the existence of bacteria." Seward's assessment of Walcott's discoveries then concluded with a bit of artful doggerel about Walcott's Precambrian finds: "Creatures borrowed and again conveyed, from book to book – the shadows of a shade" (Seward, 1931, pp. 86, 87). Walcott could not offer a rejoinder – he had died 4 years before Seward's views were published.

Walcott's problem was that the Precambrian fossils he reported were not only previously unknown but were far too old to fit the widely accepted dogma. Nevertheless, numerous paleontologists were intrigued by Walcott's reports (perhaps the best known being Harvard's Percy E. Raymond) and investigated his finds, primarily in the Rocky Mountains of Montana. Walcott's reports of Precambrian stromatolites were easily confirmed, but the biological origin of these enigmatic structures remained in dispute as it had been since the early 1800's (their lithified modern analogs remaining undiscovered until 1956). And Walcott's claim of Precambrian cellular fossils fell to the wayside, his well-intentioned followers repeatedly misinterpreting encrusting mud flakes and similar mineralic objects as bits and pieces of bona fide fossils, chiefly trilobite carapaces. From then on, not surprisingly, the scientific community regarded any claim of the discovery of evidence of Precambrian life with unbridled skepticism.

In retrospect, we can now see that C. D. Walcott had brought the study of Precambrian fossils to the brink of

success, only to have his prescient findings dismantled by the errors of his fellow paleontologists and demolished by Seward's authoritative assertions.

1950–1965, Breakthrough Advances

In the 1950's and 1960's the tide began to turn, four initially seemingly unrelated field-charting breakthroughs dating from this seminal period.

Modern Stromatolites

The possible biogenicity of stromatolites, a subject of controversy since the early 1800's, was finally laid to rest in 1956 by Australian geologist Philip Playford who discovered living examples at Hamelin Pool, Shark Bay Western Australia. The modern forms, laminated mound-shaped structures lithified by precipitated calcium carbonate in the intertidal regions of this hypersaline lagoon (Figure 4), were in numerous respects similar to Hall's Cambrian-age *Cryptozoön* "algal reefs." Playford gave specimens from the site to Brian W. Logan, a graduate student at the University of Western Australia who by identifying their mat-building cyanobacterial components established their biogenicity (Logan, 1961). Though this was a major step forward for studies of Precambrian life – at present, stromatolites being known from shallow marine environments throughout the Precambrian rock record – it would not have been a surprise to the microbiological community, the unlithified equivalents of stromatolites having been referred to by microbiologists since the early 1900's as "microbial mat communities."

Microfossils in Shales

A second breakthrough advance came from the studies of Boris Vasil'evich Timofeev and his assistant Tamara Nikolaevna Hermann of the USSR Institute of Precambrian Geochronology in Leningrad (now St. Petersburg, Russia). In the late-1950's they initiated studies of microfossils in Precambrian shales, using the acid-maceration technique well known to palynologists and other micropaleontologists. Of their many seminal studies,

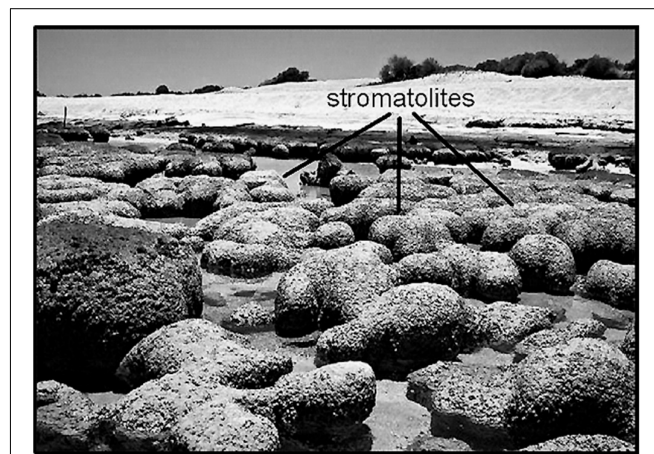


FIGURE 4 | Modern carbonate-lithified stromatolites discovered by P. Playford in the intertidal zone of Hamelin Pool, Shark Bay, Western Australia, shown here at low tide.

perhaps the best known is their 1979 discovery of the ~1,020 Ma Lakhanda Microflora of southeastern Siberia, among the oldest highly diverse phytoplankton-dominated biotas yet discovered (Timofeev and Hermann, 1979). Due to international politics and the then on-going East-West Cold War, the Timofeev-Hermann findings were for many years little known and rarely credited among the non-Soviet scientific community. Nevertheless, their groundbreaking studies have proven to be a prime factor in stimulating paleobiologic investigations of Precambrian carbonaceous shales worldwide.

Microfossils in Cherts

Here the major credit for the science-changing discovery belongs to Stanley A. Tyler, an economic geologist at the University of Wisconsin who in 1953 discovered microscopic fossils in stromatolitic carbonaceous cherts of the ~1,900 Ma Gunflint Formation of Ontario Canada, an iron-rich unit he was studying because of its economic importance to the Lake Superior-encircling taconite industry. Unschooled in paleontology, Tyler sought the advice of paleontologist Robert Shrock of the Massachusetts Institute of Technology who introduced him to Harvard's paleobotanist, Elso S. Barghoorn. In 1954, they published a paper announcing their discovery of cellularly preserved Paleoproterozoic fossil microbes (Tyler and Barghoorn, 1954).

During the following several months, Tyler prepared a manuscript illustrating the fossils and reporting the geologic details of the find to which Barghoorn was to add formal taxonomic descriptions of the newly discovered microbes. Unfortunately, however, due to a series of unforeseen difficulties the manuscript remained unattended until a decade later, finally published in 1965 (Barghoorn and Tyler, 1965) and less than a year after Tyler's unexpected death. Although the paper illustrated numerous obviously cellularly preserved ancient microbes (Figure 5), given the long-established dogma that Precambrian life was "unknown and unknowable" it is perhaps not surprising that this paper met with widespread skepticism, the critics opining publicly and privately that *"the fossils are far too old... simply not believable... there must be some mistake!"* Some 6 months later a second report of chert-preserved Precambrian fossils appeared (Barghoorn and Schopf, 1965), this time from the ~850 Ma Bitter Springs Formation of central Australia. In the development of the science, this second 1965 paper proved to be the "deal-sealer" – different rocks, different continent, different age, and chock-full of abundant, varied, remarkably well preserved microscopic fossils, many easily relatable to microbes living today (Figure 6). Taken together, these two seminal papers laid a firm foundation for the now thriving field of Precambrian paleobiology, especially after they were updated by the addition of new telling data, for the Gunflint assemblage by Awramik and Barghoorn (1977) and for the Bitter Springs Microbiota by Schopf (1968) and Schopf and Blacic (1971).

Precambrian Animal Fossils

The fourth in this series of breakthrough discoveries dates to 1946 and the work of Reginald Claude Sprigg, an Australian

geologist who discovered imprints of fossil jellyfish in strata of the Pound Quartzite in the Ediacara Hills north of Adelaide, South Australia. Sprigg named the fossils *Mawsonites* in honor of the Australian geologist and Antarctic explorer Douglas Mawson, but being uncertain of the fossils' age, Sprigg assumed they were most likely Cambrian.

Beginning in 1950, with the arrival at the University of Adelaide of paleontologist Martin Fritz Glaessner, the situation markedly changed. Indeed, by the end the 1950's, aided by his assistant Mary Julia Wade, Glaessner uncovered firm evidence showing that not only were the fossils pre-trilobite and pre-Cambrian (if barely so) but that the fauna was richly diverse, including many soft-bodied animals previously unknown to science (Figure 7). Like the reticence toward Walcott's earlier breakthrough finding of Precambrian stromatolites and fossil phytoplankton, Glaessner's discoveries were a poke in the eye to traditionalists who were convinced that it was impossible for pre-Cambrian animals to exist... *"after all,"* the naysayers exclaimed, *"that is the way the beginning of the Cambrian Period of geological history is defined!"*

A prime leader of this traditionalist school was Preston Eccelle Cloud, Jr. Over time, the Glaessnerian and Cloudian views of the definition of the base of the Phanerozoic Eon came to loggerheads. Glaessner argued that a new geological period should be established to include pre-trilobite soft-bodied animals. Cloud argued the opposite, that the base of the Cambrian should simply be extended downward, that no new geological period was needed. Clearly, Cloud's idea would not work – each new sequentially older finding would require that the Phanerozoic-Precambrian boundary be moved to a lower stratigraphic level making it impossible to be certain when the Phanerozoic truly began. But Glaessner's idea was at odds with long-established practice. The controversy was ultimately resolved by the International Commission on Stratigraphy and ratified in 2004 by the International Union of Geological Sciences (IUGS), establishing the first new geological period declared in 120 years – the 635–541 Ma Ediacaran Period, assigned to the uppermost Precambrian, not the overlying Phanerozoic.

NEW TECHNIQUES

Breakthrough discoveries are fundamentally defined by that which has not been known before, a lack of knowledge that in turn is not uncommonly a function of the techniques and instrumentation available to carry out the evidence-providing investigations. Thus, realization that the Precambrian fossil record was dominated by carbonaceous microscopic organisms rather than the skeletonized remains of Phanerozoic megascopic animals familiar to paleontologists presented a major challenge to the community, one difficult to meet by use solely of long-established research techniques. Not surprisingly, therefore – in part concurrent with but largely subsequent to the seminal discoveries noted above – a series of new techniques emerged, many now used routinely worldwide. Although the following synopsis focuses on the innovative techniques applied to

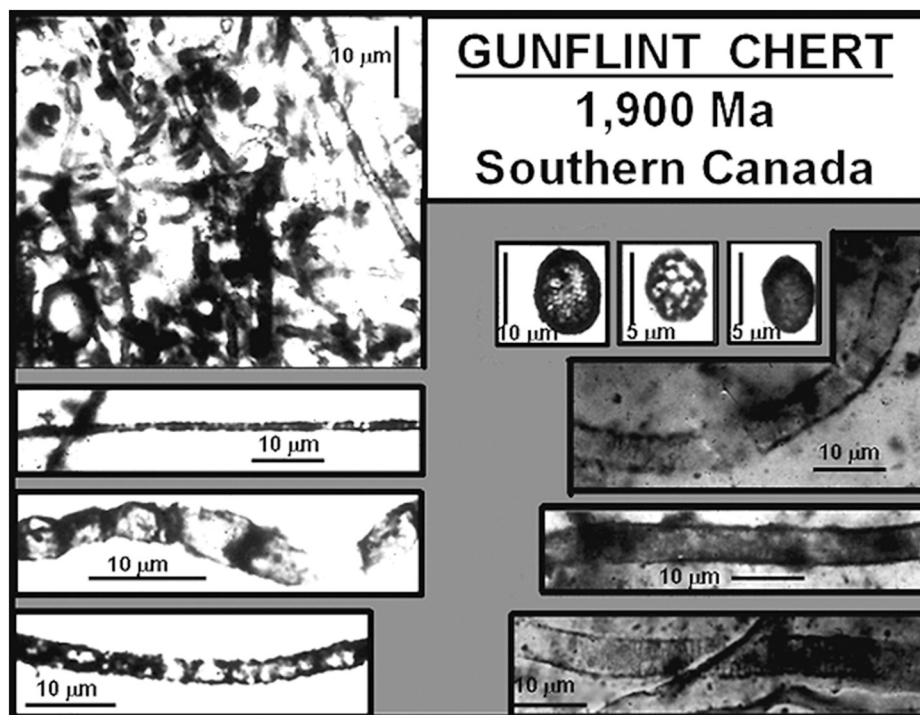


FIGURE 5 | Representative filamentous and ellipsoidal fossil microorganisms preserved by permineralization in large, meter-diameter mound-shaped carbonaceous stromatolites of the Paleoproterozoic ~1,900 Ma Gunflint chert of southern Ontario Canada.

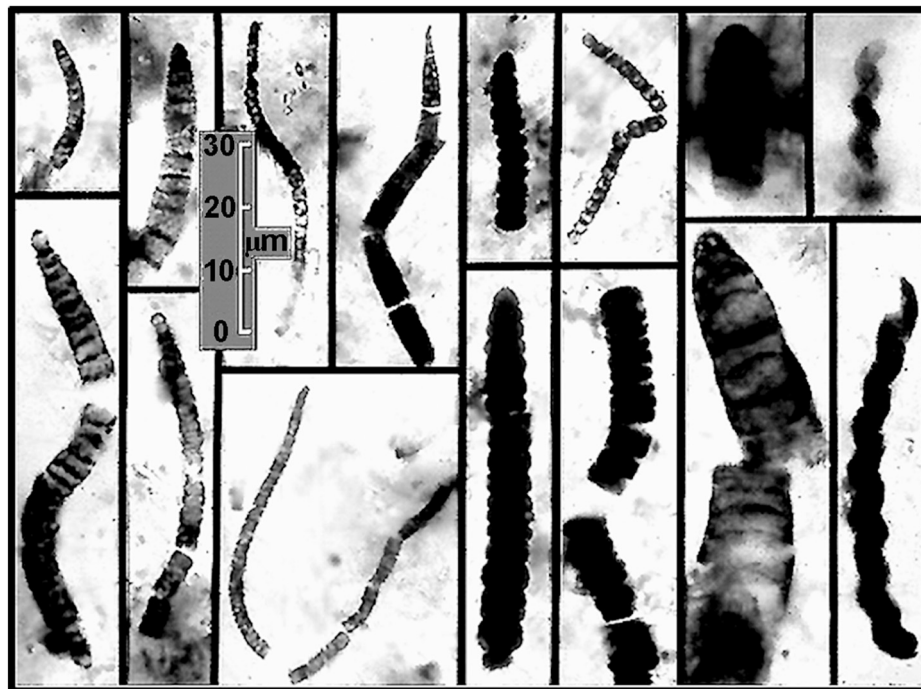


FIGURE 6 | Representative fossil Oscillatoriacean and Nostocacean cyanobacteria preserved by permineralization in flat-lying carbonaceous black chert stromatolites of the Neoproterozoic ~850 Ma Bitter Springs Formation of central Australia deposited in a quiescent, probably lagoonal setting. In both organismal and cellular morphology, the specimens shown are essentially indistinguishable from modern species of such cyanobacteria as *Oscillatoria*, *Rivularia*, *Spirulina*, and *Nostoc*.

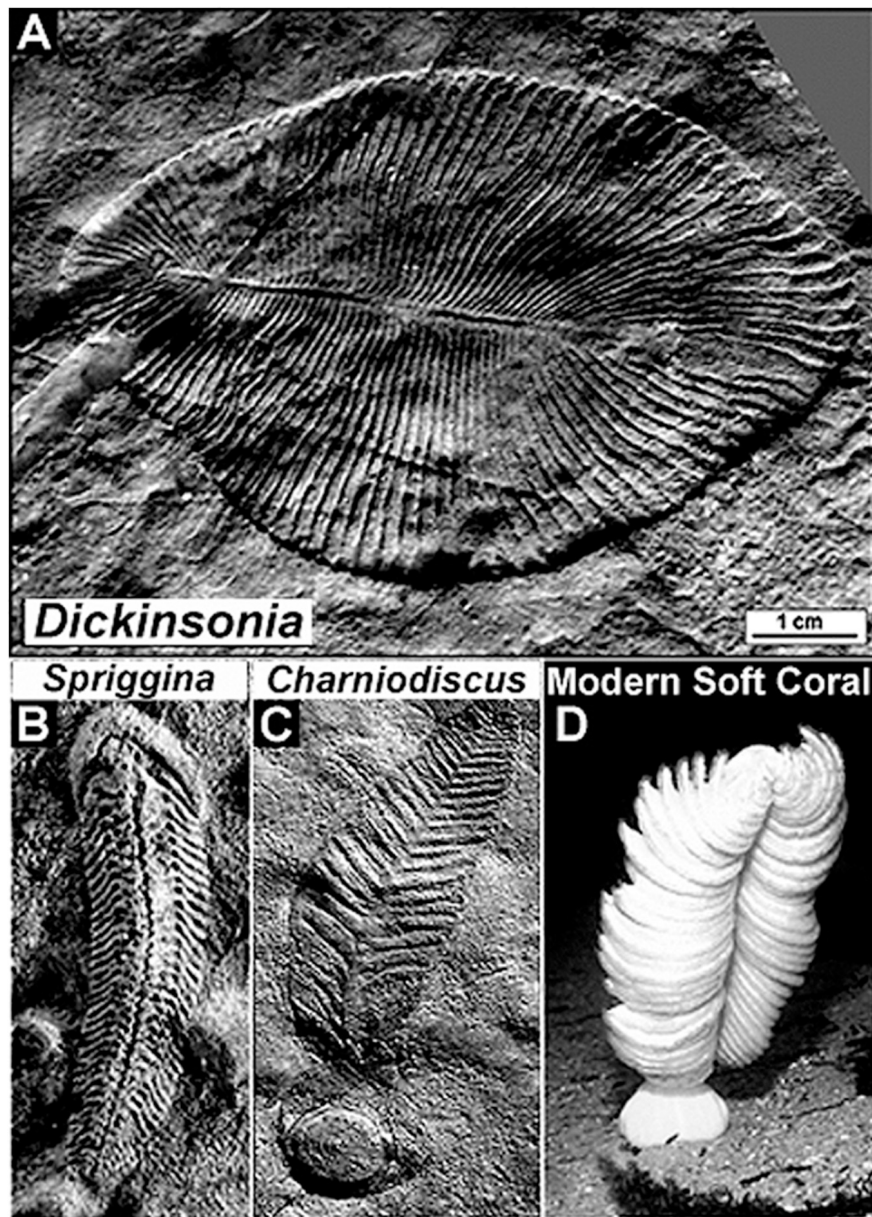


FIGURE 7 | Representative soft-bodied animal fossils of the latest Neoproterozoic Ediacaran Fauna of the Pound Quartzite of South Australia. **(A)** *Dickinsonia*, a disk-shaped worm-like animal. **(B)** *Spriggina*, a polychaete worm-like animal and the oldest known fossil to exhibit an identifiable head, thickened to protect its contained sensory apparatus. **(C)** *Charniodiscus*, a stationary animal that lived anchored to the sandy seabed held in place by a basal holdfast, an Ediacaran fossil similar to **(D)** a modern soft coral.

studies of microscopic Precambrian fossils, several have also been used quite effectively in investigations of early-evolved metazoans.

The breakthrough Timofeev-Hermann studies of shale microfloras and Tyler-Barghoorn-Schopf chert microbiotas discussed above highlight the differences in preservation between these two matrices. Fossils preserved in shale are compressed, flattened and commonly distorted, best studied freed from their matrix in acid macerations. In contrast, microfossils permineralized in chert are three-dimensional and

cellularly intact, the permineralizing microcrystalline silica having infilled and replaced watery spaces within the cells and cell walls to produce unflattened “life-like” geochemically altered carbonaceous fossils that are studied most effectively *in situ*, embedded within petrographic thin sections. Of the two types of preservation, three-dimensional permineralization (whether in silica, calcite or gypsum) is clearly the paleontologically preferable, providing far more little altered morphological information by which to assess the biological affinities of the fossils studied.

Photomontage

Despite the obvious advantages of permineralized fossils, their study presents problems, primarily and ironically because of their “life-like” three-dimensional form. The great majority of Precambrian fossils are microscopic, their detailed study requiring high-resolution 100 \times oil-immersion optical microscopy. Moreover, most are minute sinuous cellular filaments that bend in and out of a single thin optical plane whereas others comprise larger three-dimensional colonies that cannot be depicted in a single thin in-focus high magnification photomicrograph. To address these problems, in 1968 the technique of photomontage was introduced (Schopf, 1968), a matter of literally pasting together a series of photomicrographs taken at sequential optical depths to thereby reconstruct the three-dimensional form of a fossil studied (**Figure 8**). This simple technique, an innovation necessary for the publication of research findings and immediately adopted by workers worldwide, is now accomplished far easier by use of the Photoshop computer program.

Electron Microscopy

In the 1960's and 1970's, transmission electron microscopy (TEM) and scanning electron microscopy (SEM), both techniques having exceptionally high spatial resolution and both borrowed from the biological sciences, were first applied to Precambrian microbes. TEM was used to identify bacterium-like fossils in the \sim 1,900 Ma Gunflint chert (Schopf et al., 1965) and, a few years later, to document the preservation of nuclei in permineralized unicellular phytoplankton of the \sim 850 Ma Bitter springs Formation (Schopf and Oehler, 1976). Similarly, SEM proved useful to analyze diverse

Precambrian microbes isolated from their encompassing matrices by acid maceration (Schopf, 1970; Schopf and Blacic, 1971). Such studies have continued to the present, most recently illustrated by the use of SEM to document filamentous fungi and associated siphonole green algae in Ediacaran stromatolites of the southern Siberian Platform (Kolosov, 2016).

Secondary Ion Mass Spectrometry

The introduction of secondary ion mass spectrometry (SIMS) in the field of geochemistry, where it was primarily applied to analyzing the carbon isotopic composition of isolated Archean zircon grains, represented a promising opportunity to Precambrian paleobiology by which to document the metabolism-indicating carbon isotopic signatures of individual microscopic fossils. SIMS was first applied to Precambrian microfossils in 2000, an analysis of the carbon isotopic composition of microfossils permineralized in the \sim 850 Ma Bitter Springs Formation of central Australia selected for this initial study because it would permit the SIMS data to be compared with a body of previously obtained bulk carbon isotopic measurements of co-occurring detrital carbonaceous matter. The veracity of the SIMS data was thus confirmed (House et al., 2000) and, like the use of photomontage, this technique, where available, has been applied in numerous studies worldwide.

Nevertheless, and although the application of secondary ion mass spectrometry to analyses of ancient microscopic fossils was a major step forward in Precambrian paleobiological studies, its use has drawbacks. The required equipment is expensive and not widely available, and though SIMS establishes the metabolism-evidencing carbon isotopic composition of the fossils analyzed, its application is exceedingly time-consuming and limited to single fossils exposed at the upper surface of a petrographic thin section.

Raman Spectroscopy

What was needed was a faster more widely applicable technique, one that could not only establish the carbonaceous composition of the fossils analyzed but that could also document their morphology and molecular chemical signature at depth below the thin section surface. This need was soon met by the introduction to such studies of Raman spectroscopy. As first illustrated by analyses of microfossils of the \sim 3,465 Ma Apex chert of Western Australia (Kudryavtsev et al., 2001; Schopf et al., 2002), Raman spectra establish the molecular-structural carbonaceous composition of minute Precambrian permineralized fossil microbes whether surface-exposed or rock-encased and plunging below the surface of a translucent thin section (Schopf and Kudryavtsev, 2005). Moreover, and at the same submicron spatial resolution, such spectra can be used to document the mineralogy of the fossil-hosting matrix, the three-dimensional cellular morphology and molecular chemistry of the fossils studied, and establish as well, by use of the Raman Index of Preservation (RIP), the fidelity of preservation of their macromolecular carbonaceous components (Schopf et al., 2005).

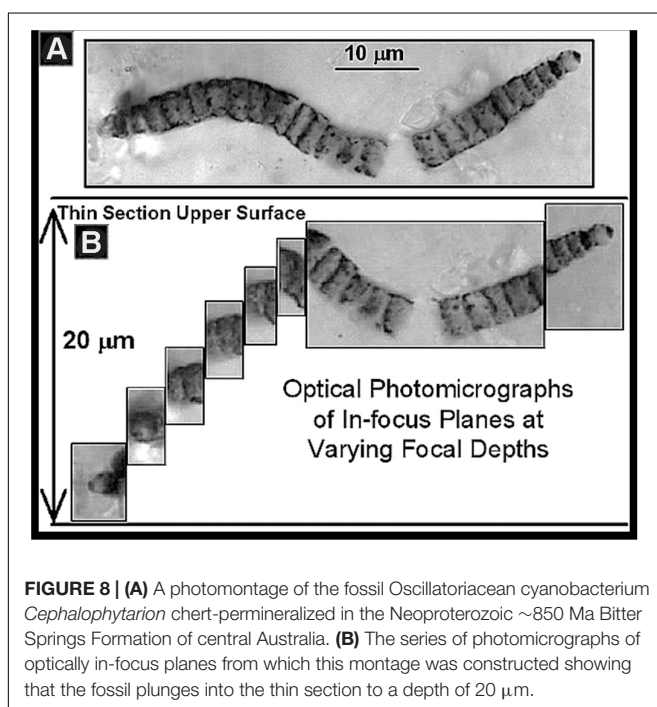


FIGURE 8 | (A) A photomontage of the fossil Oscillatoriacean cyanobacterium *Cephalophytarion* chert-permineralized in the Neoproterozoic \sim 850 Ma Bitter Springs Formation of central Australia. **(B)** The series of photomicrographs of optically in-focus planes from which this montage was constructed showing that the fossil plunges into the thin section to a depth of 20 μ m.

X-Ray Tomography

In 2003, yet another new analytical technique was introduced, X-ray microtomography (XTM). Unlike the previously discussed techniques, XTM was initially used for analyses of Neogene hominids (Chaimanee et al., 2003) and, soon thereafter, Phanerozoic fossil plants and amber-entombed insects (Feist et al., 2005; Tafforeau et al., 2006; Friis et al., 2007). Like TEM, SEM and SIMS, XTM is a high-resolution technique primarily useful for analyses of surface-exposed specimens and, thus, has been used principally to investigate the morphological characteristics of specimens separated from their rock matrices by acid maceration. Notably, however, and unlike these other techniques, XTM permits 3-D examination of such specimens from multiple vantage points and visualization of their internal structures. In studies of Precambrian fossils, XTM has been used for analyses of 600–800 μm diameter metazoan embryos and their contents phosphatized in the Weng'an biota of the Ediacaran Doushantuo Formation of southwest China (Chen et al., 2006, 2009; Donoghue et al., 2006; Tafforeau et al., 2006), studies recently amplified and expanded by Yin et al. (2020). Given this success, increased application of XTM can easily be predicted.

Confocal Laser Scanning Microscopy

With these advances – photomontage, electron microscopy, SIMS, 2-D and 3-D Raman spectroscopy, and X-ray tomography – most of the obvious instrumental needs of the field had been addressed. But one glaring deficiency remained, namely, what additional information about the taxonomically crucial morphology of such minute objects could be gleaned by imagining them *in situ*, embedded in their rock matrix, at high resolution and not only from their top, as required by most of these techniques, but by visualizing them from their sides and bottoms as well? This final problem was answered in 2006 by the introduction to paleobiological studies of 3-D confocal laser scanning microscopy (CLSM), a high-resolution technique borrowed and modified (Schopf et al., 2006) from its use in detailed morphological studies of the fine-scale internal architecture of modern cells. Although not yet widely adopted by the international Precambrian paleobiological community – primarily because few scientific journals provide means for the incorporation of the rotating three-dimensional video images provided by CLSM – the instrument used for such studies is readily available in many university biology departments. CLSM is a highly effective research tool and the only technique now available for complete morphological investigation of minute fossils rock-embedded at depth, permitting their images to be rotated parallel to the thin section surface and thus viewed from multiple perspectives.

Applied in tandem, these techniques provide unprecedented opportunity to document the intracellular structure of kerogenous microscopic fossils (Figure 9), their indigenosity to and syngenicity with the fossil-hosting mineral matrix, their biogenicity-indicating molecular and isotopic kerogenous composition and three-dimensional form, and their degree of geochemical maturity, all at submicron spatial resolution.

Applications to Megascopic Body Fossils

Many of these techniques initially designed for studies of minute Precambrian fossil microbes have been applied as well to early-evolved multicellular organisms. A good example is their use in investigations of *Eocyathispongia*, the earliest fossil sponge now known, reported in 2015 from the Ediacaran Doushantuo Formation of Guizhou Province in southwestern China (Yin et al., 2015). This richly fossiliferous unit, well known to the paleontological community, is actively mined for its economically important phosphate. However, and although much of the diverse Doushantuo biota is thus permineralized in phosphatic fluorapatite, this earliest known fossil sponge is embedded in non-phosphatic limestone. To fully analyze the fossil, the investigating scientists therefore used hydrochloric acid to dissolve the enclosing carbonate matrix and liberate the organic-walled fossil – an example of the application of the acid maceration technique pioneered for Precambrian studies by Timofeev and Hermann – and analyzed its inner wall submicron sponge-distinctive morphology by scanning electron microscopy.

Other of the techniques initially devised for the analysis of Precambrian microfossils have similarly been applied to ancient megafossils. A prime example is the late-stage embryo of a ctenophore coelenterate (“comb jelly”) from the basal Cambrian Meishucun fossil assemblage of Shaanxi Province China reputed to contain the oldest complex skeletonized organisms known in the geological record. In this case, the fine structure of the specimen was documented by confocal laser scanning microscopy and shown by Raman spectroscopy to be composed of carbonaceous kerogen permineralized in apatite (Chen et al., 2007). Additional examples could be cited, but these two, the oldest known fossil sponge and oldest known comb jelly, are sufficient to prove the point. Clearly, the techniques devised for the study of microscopic Precambrian life have applicability to megafossils as well.

INTERNATIONAL INTERDISCIPLINARITY

One additional aspect of the study of Precambrian life remains to be addressed, namely its distinctive international interdisciplinary character, a hallmark of the science introduced early in its modern development that has led to its marked success over the past half-century.

In the 1960's as seminal findings laid the groundwork for the field, international interdisciplinary science was far from the norm. Internationalism had been repeatedly thwarted by geopolitical strife and interdisciplinary science was generally discounted, the assumption being that adherents of this approach were likely to be “jacks of all trades but masters of none.” Quite clearly, that does not apply to practitioners of Precambrian paleobiology today. It is thus germane to inquire how the current mindset originated, what are its roots? The following discussion will help to answer this question and elucidate how interdisciplinary studies of Precambrian life have risen to their current global status.

In 1978, using prize money provided the United States National Science Board's 1977 Alan T. Waterman Award I

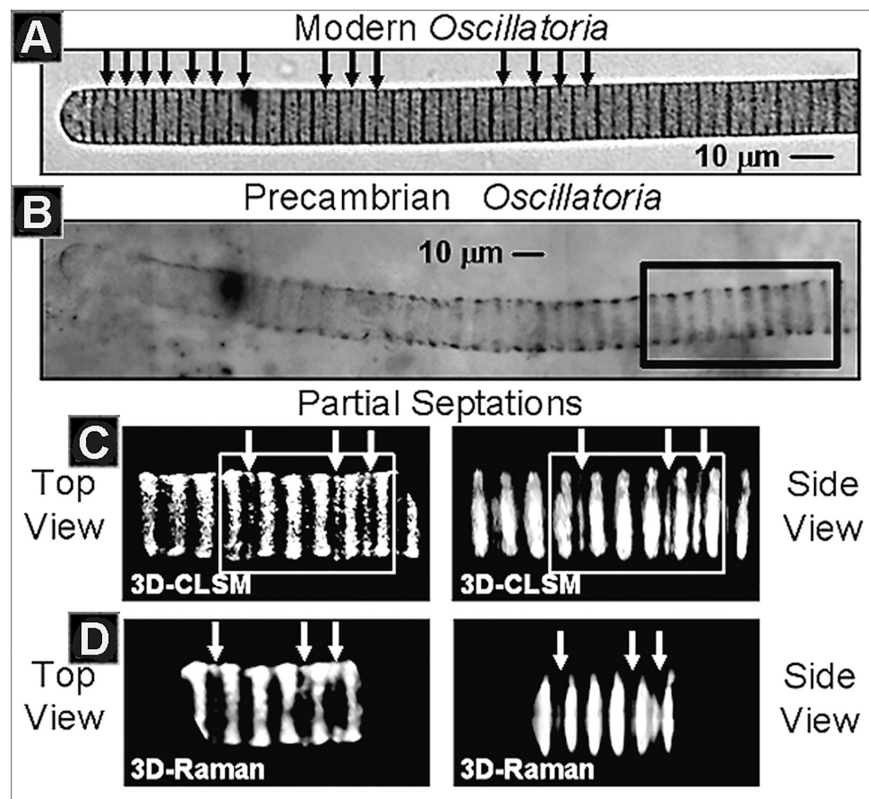


FIGURE 9 | (A) The modern cyanobacterium *Oscillatoria*, denoting (black arrows) its intracellular partial septations, the precursors of subsequent cells walls and cellular binary division. **(B)** Optical photomicrograph of fossil *Oscillatoria* persevered in carbonaceous stromatolitic chert of the Neoproterozoic ~750 Ma Chichkan Formation of South Kazakhstan, denoting the region (black rectangle) depicted in the CSM and Raman images immediately below. **(C)** Three-dimensional CLSM images of the Chulaktau fossil in top and side views, denoting its partial septations (white arrows). **(D)** Three-dimensional Raman images of the same region of the fossil in top and side views, denoting the same partial septations (white arrows).

elected to establish the Precambrian Paleobiology Research Group (PPRG), an effort to promote the advancement of the science and lay a framework for its further development. Unfortunately, however, the monies available were insufficient to fund the planned 14-month stay of the envisioned international interdisciplinary team of “Young Turks” and their families at UCLA. Matching funds were therefore sought from NASA’s Exobiology Program, a proposal that was reviewed and immediately rejected by the two leading experienced specialists in the field, Elso Barghoorn (because “science is done by individuals, not by groups”) and Preston Cloud (because “the group lacks senior leadership”). Despite the negative assessments of these luminaries, the proposal was funded.

This first version of the PPRG included 19 members from four countries, Australia, Canada, Germany and the United States. Included in its ranks were established and up-and-coming workers focused on Earth’s formative Hadean development, prebiotic organic syntheses, Archean geology, organic and isotopic geochemistry, microbiology, Archean microfossils and stromatolites, and Archean atmospheric and environmental evolution. The group pooled its rock collections, carried out laboratory research together as a team, and each Wednesday evening became educated about the specialty of one of the other

members. The product of this venture, *Earth’s Earliest Biosphere, its Origin and Evolution* (Schopf(ed.), 1983), was published. In 1983, an extensive 543-page tome presenting new research results and summarizing the interrelated biologic-environmental evolution of the earliest two billion years of Earth history.

Given the success of this Hadean-Archean-focused project, in 1984 I set in place its sequel, this time adding participants from Denmark, South Africa, Sweden and the USSR and increasing the roster to include a total of 42 members incorporating workers having expertise in the 2.5–0.5 Ga Proterozoic segment of Precambrian biotic and environmental Earth history. Again carrying out international field expeditions (generously funded by the National Geographic Society) and working together at UCLA for a 14-month period, in 1992 the product of this second PPRG study was published, *The Proterozoic Biosphere, A Multidisciplinary Study* (Schopf and Klein, 1992), a mammoth 1,348-page volume.

This second study, like its predecessor, had considerable impact on the development of the field. Each of the volumes produced received the Association of American Publishers’ Professional and Scholarly Publishing Award in its year of publication and virtually all of the participants in the two PPRG ventures continued on to become acknowledged leaders in the

science, some two-thirds of the members having been elected to their country's national academy of science. Moreover, and of considerable interest to the broader scientific community, the influence of the international interdisciplinarity of the PPRG continued unabated even after the conclusion of its two-part, almost two-decade-long effort. Indeed, this successful experiment provided the model on which NASA Deputy Director Jerry Soffen based the NASA Astrobiology Institute, in his words designed to be a "virtual PPRG," that has had enormous impact in promoting and advancing the science of astrobiology and establishing the foundation for NASA's current search for evidence of past life on Mars.

PROGRESS

The developments summarized above – from the breakthrough advances of 1950 to 1965, to the subsequent decades-long introduction of new analytical techniques, to the international interdisciplinary field-establishing PPRG – set the stage for the science today. What progress has been made?

Oldest Records of Life

Over the past half-century, the science has prospered, mightily. Spurred by early publications elucidating the mode of formation and abundance of fossil stromatolites (Walter, 1973; Walter, 1977), a great majority of this progress has focused on the Proterozoic (2.5–0.541 Ga) segment of the Precambrian from which many hundreds of stromatolitic and/or microfossiliferous units have been reported. Taken as a whole, life's Proterozoic fossil record is now known to include prokaryotes, acritarchs, testate protists, microscopic problematica, megascopic algae, soft-bodied metazoans and diverse trace fossils (for comprehensive early summaries of such taxa see Mendelson et al., 1992; Sepkoski and Schopf, 1992; and Towe et al., 1992; and for an up-to-date review of such finds from the 2.5 to 1.6 Ga Paleoproterozoic, see Javaux and Lepot, 2018).

Unsurprisingly, far fewer fossiliferous units are known from the underlying older Archean (4.0–2.5 Ga) segment of the Precambrian, a result of the paucity of such ancient sedimentary rocks that have survived to the present. Estimated to include only about 5% of the surviving rock record (Garrels and Mackenzie, 1971, pp. 255–276), not only have virtually all originally deposited Archean sediments been geologically recycled but those that have survived, particularly those older than 3.2 Ga, have experienced varying degrees of fossil-altering or -destroying metamorphism. Indeed, only three major regions are known to contain appreciable sequences of such Paleoproterozoic strata, the relatively less metamorphosed Pilbara Craton of northwestern Western Australia, the moderately altered Barberton Mountain Land of South Africa, and the typically rather severely metamorphosed Isua Supracrustal Group and associated units of southwestern Greenland (for a tabulation of fossils reported from these and other Archean units see Tomescu et al., 2016, **Table 3.2**). Interestingly, given the current and ongoing episode of global warming and the easily predictable continued melting of the Greenland ice sheet, an ever-increasing array of even more

ancient potentially fossiliferous strata is likely to become exposed, a promising future source of new evidence of life's earliest history.

Nevertheless, despite the obvious impediments imposed by the metamorphically altered, areally limited Paleoproterozoic rock record available for study, early records of life are well established – again, not surprisingly, from the least metamorphosed of the three major Paleoproterozoic terrains. At present, the oldest widely accepted fossils known are stromatolites of ~3.48 Ga Dresser Formation of the northwestern Australian Pilbara Craton (Van Kranendonk et al., 2021). Although devoid of preserved stromatolite-forming microorganisms, the abundance, distinctive laminar fabric, hot springs setting, and comparability of these stromatolites both to modern examples and to fossil specimens occurring in similarly Paleoproterozoic units leave little doubt as to their biogenicity.

Moreover, the Dresser stromatolites are only slightly older than the oldest diverse fossil microbiota now known, that of the ~3.465 Ga Apex chert, also of the Pilbara Craton. First reported nearly 30 years ago (Schopf, 1993), the 11 taxa described from the partially degraded primarily filamentous microbial assemblage on the bases of measurements of nearly 1,900 cells ranging from 0.5 to 19.5 μm in diameter preserved in 173 specimens, have stood the test of time (**Figure 10**). Over the ensuing years, the indigenosity, syngenesis and biogenicity of the Apex fossils – including their organismal morphology, cellularity and carbonaceous composition and kerogenous molecular structure – have been repeatedly established at submicron spatial resolution by optical microscopy, photomontage, TEM, Raman spectrometry and CLSM, making this the most thoroughly investigated fossil microbiota known from the geological record. In addition, and perhaps of even greater significance, the biologic affinities of five of the 11 taxa have recently been documented by SIMS (Schopf et al., 2018) showing the assemblage to include anoxygenic photosynthetic bacteria and both anaerobic methane-producing and anaerobic methane-consuming archaea. All three of these lineages are situated near the base of the rRNA phylogenetic Tree of Life, their documentation in this oldest known diverse biota thus reinforcing the credibility of Precambrian microfossil studies, of molecular biologic phylogenetic analyses of the extant counterparts of ancient microbes, and of geochemistry-based inferences of the low oxygen content of the Paleoproterozoic environment.

In sum, as Precambrian paleobiology has matured over the past half-century, workers worldwide have amassed a voluminous body of telling evidence, even from the relatively sparse Archean rock record. Included among the particularly ancient examples are well more than a score of reports of stromatolites and cellular microbial fossils dating from earlier than 3.2 Ga (those from the Barberton Mountain Land recently reviewed by Homann, 2019) and SIMS analyses of the carbon isotopic composition of possibly biogenic graphite in pre-3.5 Ga zircons (Bell et al., 2014, 2015; Tang et al., 2019). Among all these, the diverse microbial assemblage of the Apex chert stands out as a definitive benchmark, the most thoroughly scrutinized, evaluated and repeatedly affirmed finding in the history of the science. Taken as a whole, such evidence not only resolves Darwin's dilemma, extending the known fossil record by a remarkable sevenfold

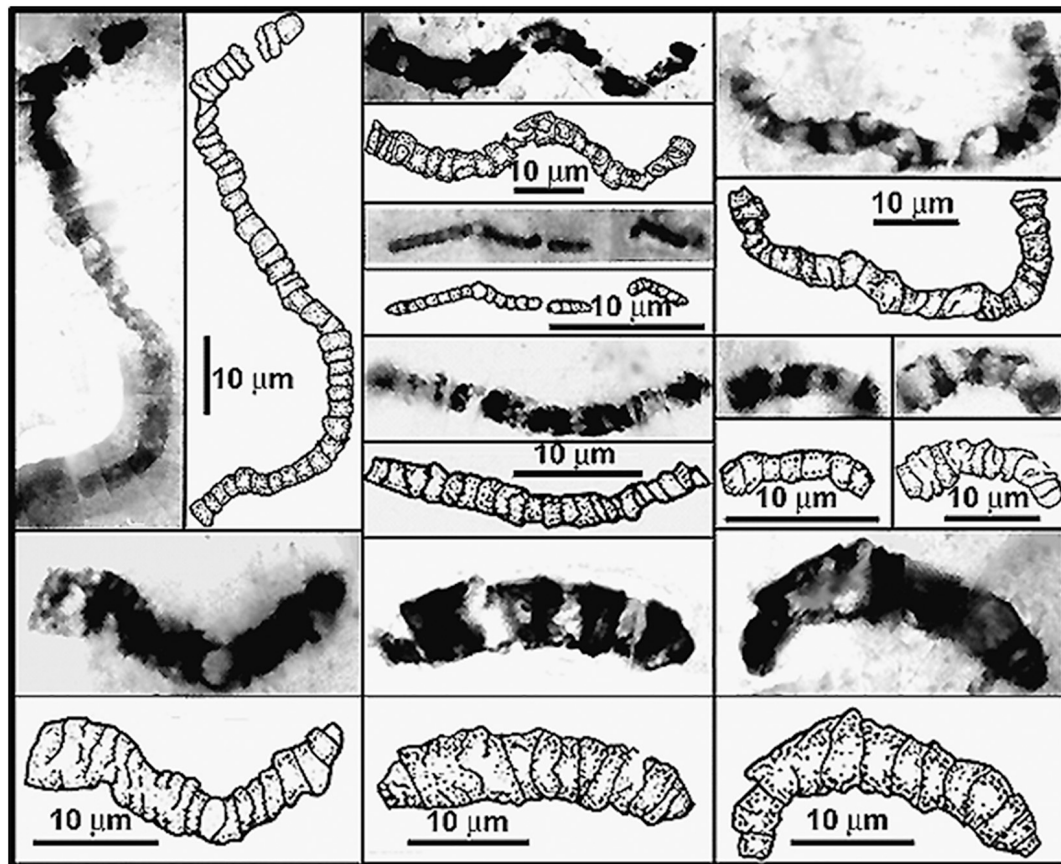


FIGURE 10 | Representative filamentous microfossils from the Paleoproterozoic ~2.3 Ga Apex chert of northwestern Western Australia.

from that known when *The Origin* first appeared, but it establishes as well that primordial life evolved early, far and fast – a largely unexpected, and thus rather remarkable insight into life’s earliest development.

Mid-Precambrian Origin of Eukaryotes

Recognition of the occurrence of a mid-Precambrian significant increase of global environmental oxygen – the great oxidation event, “GOE,” biotically important as providing the abundance of oxygen necessary to fuel biologic obligate aerobic respiration – dates from the geological-paleoenvironmental studies of H. D. Holland (2006). His postulate was based on analyses of the temporal distribution of banded iron formations, globally widespread deposits typified by cyclically repeating alternating bands of fine-grained hematite (Fe_2O_3) and iron-deficient layers of fine-grained chert that provide the foundation of the world’s steel industry (Figure 11). Holland found that many such deposits were situated in the shallow portions of inland seas and that they spanned the time from about 3.0 to 2.0 Ga ago, rising slowly in abundance to a peak at about 2.5 Ga and then gradually petering out. Reasoning that their banded character reflected seasonal changes, he postulated that their cyclicity reflected the yearly upwelling of ferrous iron from deep-sea volcanic fumaroles and that the environmental oxygen required for deposition

of their distinctive oxidized hematitic bands was a result of cyanobacterial oxygenic photosynthesis.

Resulting from the studies of M. H. Thiemens, who was first to investigate the mass-independent fractionation (MIF) of oxygen (Thiemens and Heidenreich, 1983) and subsequent studies of the MIF of sulfur by Thiemens’ student J. Farquhar, the date of the GOE was more precisely set at ~2.3 Ga (Farquhar et al., 2000). The data are convincing. Mass-independent fractionation of sulfur isotopes in Archean sediments is a strong indicator of an anoxic Archean atmosphere, substantiated by numerous independent lines of evidence, and the MIF of sulfur isotopes is known in numerous sediments of the Archean and early Proterozoic but not in rocks younger than ~2.3 Ga. This is not to imply, however, that Earth’s atmosphere became “fully oxygenated” at 2.3 Ga. Indeed, current estimates indicate that permanent oxygenation was not attained until ~2.2 Ga, 100 Ma later (Poulton et al., 2021), and even then remained at low concentrations, far below current atmospheric levels, for the following billion years or more (Olson et al., 2018).

Independent of these important breakthroughs, Precambrian paleobiologists had previously noted the presence in Paleoproterozoic deposits ~2.1 Ga and younger of large-celled spheroidal phytoplankton, far too large to be comparable to extant prokaryotes. There was thus no doubt that these

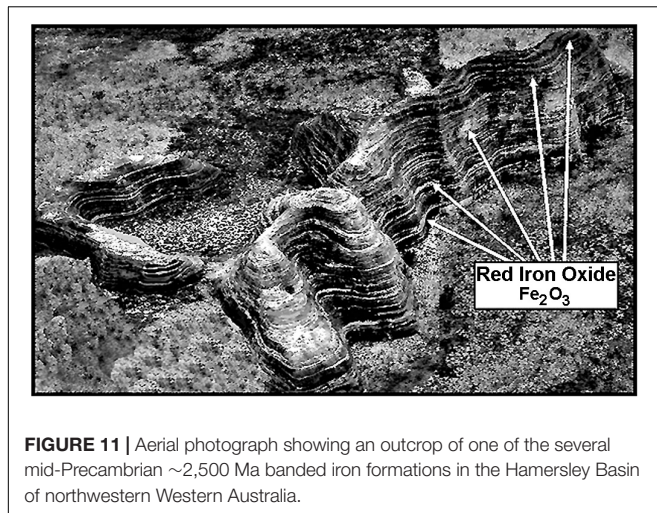


FIGURE 11 | Aerial photograph showing an outcrop of one of the several mid-Precambrian ~2,500 Ma banded iron formations in the Hamersley Basin of northwestern Western Australia.

megaspheeromorphs were unicellular algal eukaryotes, not prokaryotes, but because their precise affinities to modern algal groups were uncertain they were collectively grouped together in the taxonomically non-committal “Acritarcha” (Evitt, 1963), taxa of which are known today from many Proterozoic and Phanerozoic deposits (Knoll, 1992; Colbath and Grenfell, 1995; Tomescu et al., 2016, **Table 3.3**).

Because all eukaryotes are oxygen-dependent, the geochemical-paleoecological MIF data and the post-GOE fossil evidence mesh together, the advent of eukaryotes being enabled by the increase of environmental oxygen. This sequential co-occurrence seems well established. The MIF-indicated ~2.3 Ga date of the onset of the GOE is holding firm. Acritarchs are well documented in the Paleoproterozoic (**Figure 12**), including the ~1631 Ma (Ray et al., 2002). Deonar Formation of Madhya Pradesh, India (Prasad et al., 2005), the ~1,650 Ma Changzhougou Formation of North China (Miao et al., 2019) and the ~1650 Ma Mallapunyah Formation of northern Australia (Javaux et al., 2004). Similarly, >300 μm -diameter specimens of the sphaeromorph acritarch *Leiosphaeridia* occur in the ~1.9 Ga Kondopoga Formation of Karelia, Russia (Javaux and Lepot, 2018) and even older sphaeromorphs – including *Leiosphaeridia*, *Dictyosphaera*, *Dongyesphaera*, and *Satka* – have been recorded from the ~2,090 Ma (Wilde et al., 2004) Hutuo Group of Shanxi Province in northern China (Yin et al., 2020).

With regard to larger putatively eukaryotic algal fossils, two particularly ancient examples can be noted. Thin, wedge- and tongue-shaped compressions up to 18 cm long and 4 cm broad, some longitudinally striated or having possible basal holdfasts, have been reported from the 1,560 Ma Mesoproterozoic Goayuzhuang Formation of northern China (Zhu et al., 2016). Although assuredly thallus-like and thus presumably remnants of multicellular eukaryotic algae, the available evidence is insufficient to firmly establish their biological relationships. The second example is of even more uncertain affinities. One to two millimeter-broad specimens of the coiled strand-like macrofossil *Grypania* have been recorded from the ~1,890 Ma (Pietrzak-Renaud and Davis, 2014) Paleoproterozoic Negaunee

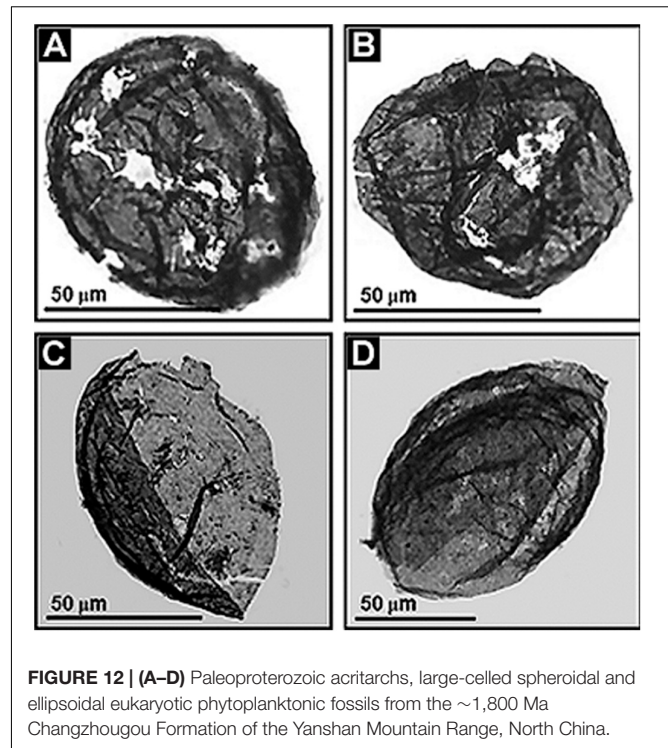


FIGURE 12 | (A–D) Paleoproterozoic acritarchs, large-celled spheroidal and ellipsoidal eukaryotic phytoplanktonic fossils from the ~1,800 Ma Changzhougou Formation of the Yanshan Mountain Range, North China.

Iron Formation of northern Michigan, United States (Han and Runnegar, 1992). Although previously regarded by Runnegar (1994) to be a chlorophycean green alga, other workers have backed away from this assessment, regarding *Grypania* to be a eukaryote of undetermined affinities (Knoll et al., 2006) or, more recently, as representing either a eukaryote or possibly a large-size prokaryote, a fossil thus classed as *Incertae Sedis* (Sharma and Shukla, 2009a,b).

Thus, taken as a whole – the established record of Paleoproterozoic acritarch microfossils and the reports of plausible, if as yet unsubstantiated mid- to possibly early-Proterozoic algal macrofossils – affirm the mid-Precambrian origin of eukaryotic life. This second major feature of life’s Precambrian history, the timing and GOE-related paleoenvironmental impetus for the origin of eukaryotic cells, seems well established.

Late Precambrian Advent of Eukaryotic Sexuality

Progress has also been made in defining the time of origin of a third great advance in life’s Precambrian evolutionary development, the advent of eukaryotic sexuality.

Beginning with the origin of single-celled eukaryotic acritarchs about 2.1 Ga, biotic evolution appears to have stalled, virtually shutting down for the following billion or so years, in retrospect a striking anomaly given the subsequent Neoproterozoic rapid rise in eukaryotic diversity and abundance. And not only did biotic advance seemingly grind to a halt, but major global geological and climatic change seem also to have markedly quieted, prompting this ensuing period of stasis to

have been described as “the dullest time in Earth’s history” (Buick et al., 1995), the “boring billion” (Brasier, 2012).

In retrospect, it is notable that this long-term stasis of biological evolution, at least among ancient prokaryotic microorganisms, was not unexpected. As early as the detailed descriptions of the stromatolitic ~850 Ma Bitter Springs microflora (Schopf, 1968; Schopf and Blacic, 1971) it had been recognized that many types of Precambrian prokaryotic cyanobacteria are essentially indistinguishable from modern counterpart genera and even species. This marked morphological comparability, in concert with evidence of virtually identical fossil-modern developmental life cycles, was soon established by a great many workers worldwide for fossil cyanobacteria in innumerable Proterozoic stromatolitic assemblages. Such similarity is well illustrated by the common practice of naming newly discovered fossil taxa by adding the prefixes “archaeo-” (ancient), “paleo-” (old) or “eo-” (early), or the suffix “-opsis” (resembling) to the genus name of a modern cyanobacterial generic name to highlight the apparent identity of the fossil and modern analogs. Indeed, a recent compilation of such taxa from a mere seven Proterozoic deposits lists some 21 such fossil-modern namesake taxa (Schirrmeister et al., 2016).

Ultimately, after 25 years and the repeated confirmation of this remarkably slow rate of prokaryotic evolutionary change, it was codified as “hypobradely” (Schopf, 1994), literally, the “slowest of the slow” referring to a taxon longevity of $\pm 1,000$ Ma. This seemingly arcane term was coined to parallel Simpson’s (1944) fossil-record established rate-distributions of Phanerozoic taxa: “tachytelic” (fast evolving short-lived species having a longevity of ± 1 Ma), “horotelic” (typical species having lifetimes of ± 10 Ma) and “bradytelic” (long-lived species, having a longevity of ± 100 Ma). It is important to note, however, that prokaryotic hypobradely does not imply that such microbes did not evolve. They certainly did, not morphologically but biochemically as they slowly adapted to gradual, virtually imperceptible changes in oxygen availability, day-length, UV-flux, salinity and other aspects of their environment.

In contrast with such hypobradelytic prokaryotic evolutionary stasis, about 1 billion years ago eukaryotic acritarchs began to markedly increase in abundance, diversity, size, complexity of shape, and especially the size and number of their surficial spines, a development first documented by Timofeev and Hermann (1979; **Figure 13**). These evolutionary advances were soon paralleled by the appearance of testate protozoans (Schopf et al., 1973a; Bloeser et al., 1977), diverse multicellular algae (Xiao et al., 2004) and filamentous fungi (Butterfield, 2005; Kolosov, 2016), a series of accelerating advances well summarized by Knoll (1994); Knoll et al. (2006), and Butterfield (2014). What is this basis of this late Precambrian dramatic surge in biotic diversity and evolutionary rate?

A plausible explanation was first suggested in 1973 in a paper noting that prokaryotes – whether unicellular, colonial, or multicellular and filamentous – are uniformly asexual, reproducing by binary division, a “cloning” of their cells, their genetic components being passed to subsequent generations unchanged except for random mutations. The paper went on to point out that that this prokaryotic mode of reproduction

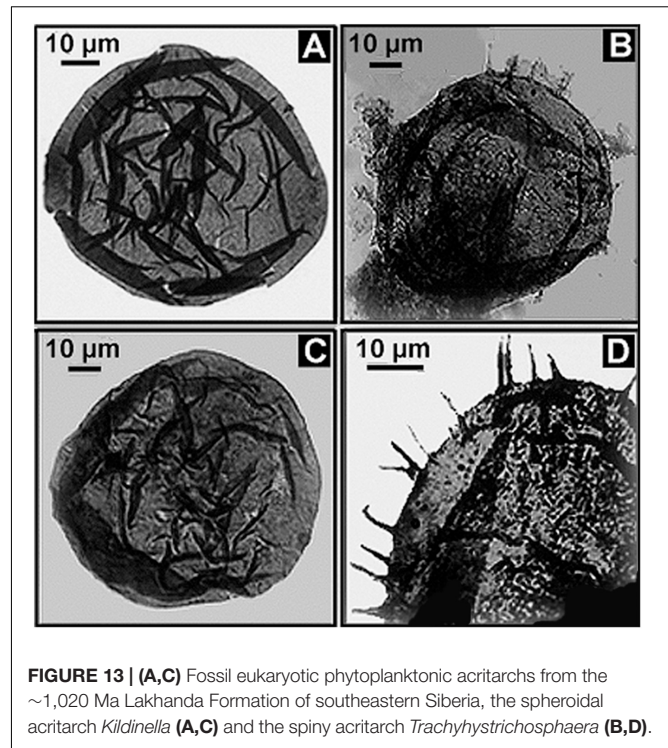


FIGURE 13 | (A,C) Fossil eukaryotic phytoplanktonic acritarchs from the ~1,020 Ma Lakhanda Formation of southeastern Siberia, the spheroidal acritarch *Kildinella* (**A,C**) and the spiny acritarch *Trachyhystrichosphaera* (**B,D**).

differs markedly from the sexual reproduction characteristic of eukaryotes, a process that combines the genetic information from two differing parental stocks to produce offspring that (except for identical siblings) differ one from another. Reasoning that increased genetic diversity would result in increases in adaptation to diverse environments and, thus, of biotic diversity, biotic interactions and evolutionary rates, the paper proposed that the origin of eukaryotic sexuality presented a plausible explanation for the rise of late Precambrian eukaryotic life (Schopf et al., 1973b).

Based on the foregoing, the origin of eukaryotic sexuality at ~1 Ga was pegged as the cause of the now firmly established rise in the rate of change and biotic diversity of Neoproterozoic life, another “old idea” that seems to have withstood the test of time.

Note, however, that somewhat older evidently sexually reproducing eukaryotes are now known, in particular the ~1,198 Ma red alga *Bangiomorpha pubescens* of the Hunting Formation of Arctic Canada (Butterfield, 2000) – the red algal affinities of which are not unexpected given that this clade is generally regarded to be the phylogenetically most closely allied of all algal groups to their asexual photosynthesizing cyanobacterial precursors. Moreover, if the origin of eukaryotic sexuality is the correct explanation for the change in rate and marked increase of biotic diversity of Neoproterozoic life, it implies that earlier evolving acritarchs and the few other particularly ancient possible eukaryotes now known were asexual and that the development of sexual reproduction did not occur until a billion years after the eukaryotic lineage originated. Though this is not implausible, such modern eukaryotic green algae as *Chlorococcus*, *Chlorella*, and *Chlorococcum* being entirely

asexual, the mode of reproduction of pre-1.2 Ga eukaryotes has yet to be documented.

Thus, the question posed by the Neoproterozoic surge of biotic diversification and evolutionary rate seems answered, at least for the present, with much remaining to be learned from the fossil record about the transition from asexual to sexual reproduction and the biotic impact of the rise in atmospheric oxygen content that would surely have accompanied the sex-derived proliferation and diversification of O₂-producing phototrophs. Evidently, the preceding so-called “boring billion” was paleobiologically not so boring after all.

PROSPECTS

Numerous major questions about life’s early history remain unanswered. Some are obvious, some less so, unknowns quite effectively posed by Javaux (2019). The following is a synopsis of five such topics, temporally ranging from the Paleoarchean to the Neoproterozoic, quandaries for which viable solutions would greatly advance the field.

Missing Evidence of the Life-Generating “Primordial Soup”

In the 1920’s, A. I. Oparin (1924) and J. B. S. Haldane (1929) independently hypothesized that life originated from a “primordial soup” produced abiotically in Earth’s early anoxic environment. A quarter-century later, in the 1950’s, this concept was shown to be plausible by the laboratory syntheses of abiotic organics under pre-biotic conditions by Miller (1953) and his mentor, H. C. Urey (Miller and Urey, 1959). Nevertheless, and although widely accepted by the scientific community, the Oparin-Haldane hypothesis has yet to be confirmed by direct evidence from the geological record establishing the existence of the postulated life-generating abiotic broth.

At first glance, this absence of evidence seems surprising. After all, Miller-Urey-type syntheses have been studied for many decades and found to generate an enormous array of biologically important organic compounds (amino acids, sugars, monomers of nucleic acids and many others). Moreover, such syntheses are primarily inhibited only by the presence of molecular oxygen, shown by paleoenvironmental studies to have been absent or present in only trace concentrations until ~2.3 Ga ago. Given this, it might well be imagined that evidence of residual remnants of the primordial abiotic soup should exist in the sedimentary rock record throughout the Archean and into the earliest Paleoproterozoic.

Placed in context, however, the lack of evidence of such abiotic organics in the rock record can be easily explained. Sedimentary carbonaceous matter, “kerogen” – for example that of coal, black shales and fossiliferous black cherts – is derived from buried partially decayed remnants of previously living systems. Once life had originated and proliferated, the biota became a far more voluminous producer of organics than relatively inefficient abiotic syntheses. Thus, even if abiotic organic matter is present in the sedimentary rock record up to early Proterozoic, it would be virtually undetectable, “swamped

out” at a ratio of hundreds of thousands to one by the organics produced by life.

Thus, in the absence of the pre-4.0 Ga Hadean sedimentary rock record which would have harbored evidence of a pre-life stage in Earth’s development, the search for remnants of the primordial soup resolves into a proverbial “needle in a haystack hunt.” But success is not out of the question. Stemming from the seminal studies of Abelson and Hoering (1961), the preservation in sedimentary kerogens of the stable isotopes of carbon, ¹²C and ¹³C, has been long established, their relative abundance being a function of enzyme-mediated biological mass-dependent kinetic isotopic fractionation. Documented in thousands of kerogenous Phanerozoic and Precambrian sediments, data from the Phanerozoic generated largely by the petroleum industry in their search for productive oil reservoirs, carbon isotopic ratios have been used to trace the record of biologic photosynthesis, whether O₂-producing or anoxygenic, to ~3.5 Ga (Schidlowski et al., 1983), an assessment later up-dated to ~3.8 Ga (Schidlowski, 1991).

Kerogens, however, are geochemically altered remnants of originally deposited organics which, as they mature toward their lasting endpoint, graphite, become increasingly modified into increasingly larger aggregates of geochemically stable plate-like polycyclic aromatic hydrocarbons (PAHs). As a result, much of their original enzyme-determined detailed molecular structure is destroyed. Nevertheless, in relatively less mature kerogens, unaltered molecular bridges link such PAHs together and it is here that residuums of the abiotic soup might be detected.

As demonstrated by the pioneering studies of J. M. Hayes (reviewed in Hayes, 2001), the intramolecular distribution of the stable isotopes of carbon and hydrogen in biosynthesized organic matter is, like the isotopic properties of bulk samples of carbonaceous kerogen, a result of enzymatic synthesis with such products having a regular distribution of ¹²C and ¹³C, and ¹H and ²H atoms. In contrast, the products of Miller-Urey and all other types of abiotic syntheses are composed of randomly distributed carbon and hydrogen atoms. Thus, the intramolecular carbon and hydrogen isotopic distribution in the linkage groups of kerogenous PAHs seems a promising source of data by which to distinguish biotic and abiotic carbonaceous sedimentary organic matter. Though the abiotic signal can be expected to be small, it might well be discernable and, thus, provide telling evidence of the hypothesized non-biological production of organic matter early in Earth history.

Timing of the Origin of Oxygenic Photosynthesis

As noted above, stromatolite-, microfossil-, and carbon isotopic-evidence of biological photosynthesis extend to at least ~3.5 Ga. But a cardinal question remains unanswered, namely, when did oxygen-producing cyanobacteria evolve from their anoxygenic bacterial ancestors, an important precursor to subsequent biotic evolution including the early Proterozoic development of oxygen-dependent eukaryotes.

Although the uppermost surface of modern stromatolites – both of lithified and unlithified mat-forming microbial

communities – is occupied by O₂-producing cyanobacteria, the ~3.5 Ga presence of stromatolites (Van Kranendonk et al., 2021) does not solve the problem. Formed by communities of mobile phototrophs as they spread across surfaces to absorb light, modern microbial mats include a thin anoxic zone directly beneath the cyanobacterial layer that is inhabited by anoxygenic photosynthetic bacteria, primarily green sulfur bacteria such as *Chlorobium* and purple sulfur bacteria such as *Thiospirillum* (Figure 14). These and other co-occurring non-O₂-producing photosynthesizers are able to “see through” the overlying layer and power their photosynthesis by absorbing parts of the solar spectrum not absorbed by cyanobacterial chlorophyll (Figure 15). Thus, prior to the advent of oxygenic cyanobacteria, anoxygenic photosynthetic bacteria would be expected to have formed stromatolites morphologically similar to those dominated by cyanobacteria, with such microbial non-oxygen producers known to have been existed at least as early as ~3.5 Ga (Schopf et al., 2018).

Given the foregoing, the quandary posed regarding the time of origin of O₂-producing photosynthesis resolves to the problem of distinguishing between the preserved cellular remnants of early-evolved anoxic and oxygenic microbial phototrophs, the search centered in the Paleoproterozoic when the rock record, though scant and metamorphically altered, still exists. Unfortunately, however, this problem is compounded by the morphological similarity between members of the two groups, bacteriochlorophyll-containing anoxygenic photosynthetic bacteria being evolutionary precursors of biochemically modified chlorophyll-containing oxygen-producing cyanobacteria. Indeed, members of the two groups are primarily distinguished not by their morphology but by the terminal reductant used in their differing types of photosynthesis, hydrogen sulfide for the anoxygenic bacterial photosynthesizers – rather than water, as for the cyanobacteria – and, hence, by the byproducts produced, elemental sulfur for the non-oxygen producers instead of the molecular oxygen of cyanobacteria.

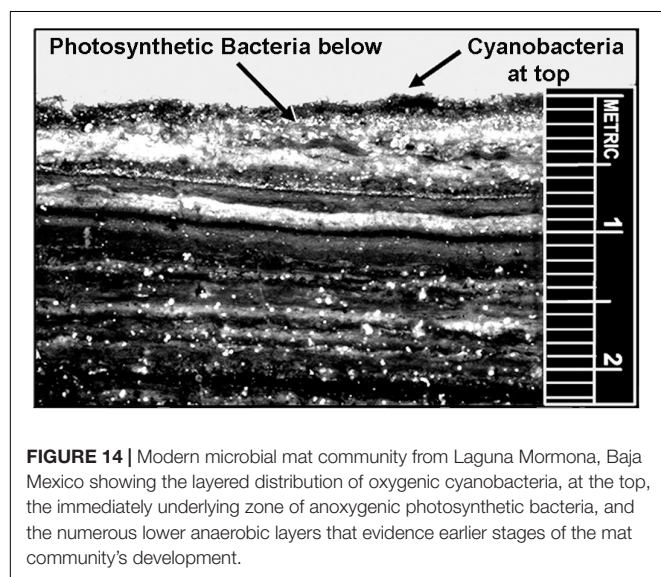


FIGURE 14 | Modern microbial mat community from Laguna Mormona, Baja Mexico showing the layered distribution of oxygenic cyanobacteria, at the top, the immediately underlying zone of anoxygenic photosynthetic bacteria, and the numerous lower anaerobic layers that evidence earlier stages of the mat community's development.

This difference in the byproducts of the two processes presents a potential means to address this conundrum. Elemental sulfur is geologically short-lived and in the anoxic Paleoproterozoic environment would have been especially so, reacting with ferrous iron to form pyrite as is well established for a ~3.4 Ga sulfur-cycling microbial sulfuretum recently reported from the ~3.4 Ga Strelley Pool Formation of the Pilbara Craton (Schopf et al., 2017). As this study shows, the characteristic seemingly random “cobweb-like” fabric such sulfur-cycling consortia is easily distinguishable from the well-laminated phototroph-formed fabric of stromatolites. Nevertheless, because the metabolic cycle of such sulfuretums involves the production of elemental sulfur, like that generated by anoxygenic photosynthesis, this fossilized assemblage contains copious amounts of microgranular pyrite. From this it would follow that stromatolites produced by solely anoxygenic photosynthetic bacteria might contain appreciable concentrations of fine-grained (<1 μm-sized) pyrite, as a cursory perusal of relevant specimens and the literature seems to suggest, the presence and then relative absence of such grains centering at about 3.0 Ga. Clearly, detailed in-depth investigation of this supposition or some more telling solution will be needed to properly pin down the time of origin of oxygen-producing photosynthesis.

Long-Term Secular Environmental Change

Stemming from their pioneering studies of the paleotemperature-indicating ratios of the stable ¹⁶O to ¹⁸O isotopes in the SiO₂ of Precambrian cherts, Knauth and Lowe (1978, 2003) and Knauth (2005) postulated that Earth's surface temperature decreased over geological time to its present ~15°C from a high of 70°±15°C during the Paleoproterozoic. Soon thereafter, this inference was reinforced by analyses of the stable ²⁹Si to ³⁰Si isotopes of silicon in cherts (Robert and Chaussidon, 2006). These interpretations, however, have been much contested due to uncertainties associated with possible changes in oceanic isotopic compositions (Perry, 1967; Kasting et al., 2006; Hren et al., 2009) and age-related diagenetic and/or metamorphic resetting of the reported isotopic signatures (Degens and Epstein, 1962; Weis and Wasserburg, 1987; Chakrabarti et al., 2012).

What was needed to resolve these ambiguities was a different line of evidence, one wholly independent of the isotopic ratios of cherts. A possible solution emerged, stimulated by the groundbreaking studies of Akihiko Yamagishi and his colleagues at the Tokyo University of Pharmacy and Life Science who pioneered the reconstruction of ancient enzymes to unravel the potentially telling data encoded in their original compositions. The success of this approach was demonstrated in 1998 when Yamagishi and his team used the reconstructed enzymes of the phylogenetically inferred last universal common ancestor of life, “LUCA,” to suggest it to have been a thermophile (Yamagishi et al., 1998). To follow this lead, UCLA graduate student Amanda Garcia spent two extensive stays in Yamagishi's Tokyo lab investigating temperature-indicative reconstructed enzymes of photic-zone inhabiting modern photoautotrophs having fossil-record established times of phylogenetic divergence.

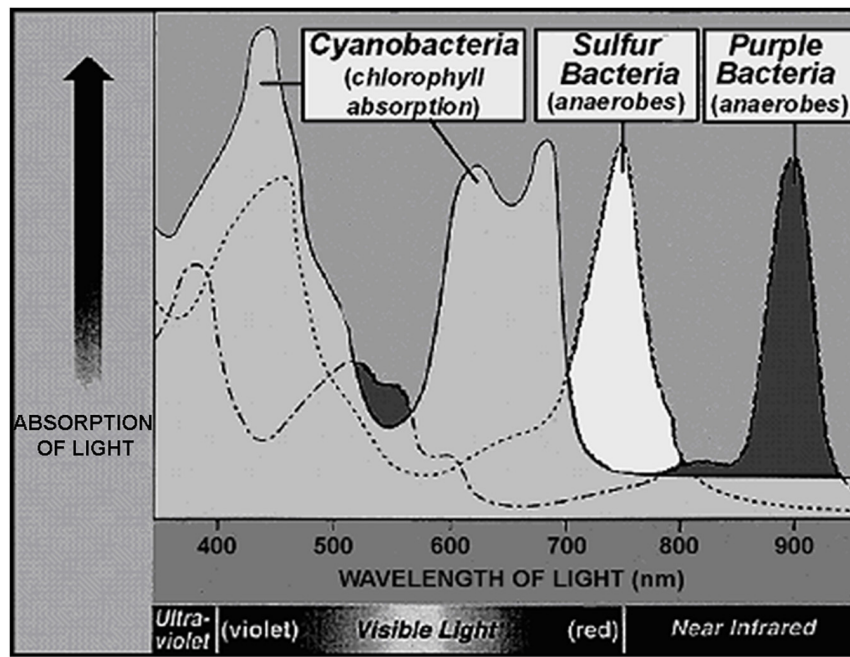


FIGURE 15 | Absorption spectrum comparing the wavelengths of light absorbed by the chlorophyll of cyanobacteria, the surface-inhabitants of modern microbial mat communities, and those of the bacteriochlorophylls of the immediately underlying green and purple sulfur bacteria.

The biomolecule selected to be reconstructed for the resulting study (Garcia et al., 2017) was nucleoside diphosphate kinase, “NDK,” an enzyme virtually ubiquitous among extant organisms for which the thermostability had been shown to correlate strongly with organismal growth temperature (Akanuma et al., 2013, 2015). Measurements were made of the thermostabilities of reconstructed ancestral NDK from photic-zone-limited early- and later-evolving cyanobacteria, green algae, and land plants, groups and subgroups of which have temporally widely spaced fossil-record-indicated divergence ages. Notably, the results obtained, consonant with the previous chert isotope-based studies, indicated a cooling of Earth’s surface temperature from ~75°C in the Archean (~3.0 Ga) to ~35°C in the Devonian (~420 Ma) and a finding consistent as well with other such studies of reconstructed biomolecules (Gaucher et al., 2008; Risso et al., 2013).

The success of such “proof of concept” studies showing the use of reconstructed biomolecules to resolve uncertainties about long-term environmental change suggests its further application to additional paleobiological questions. For example, changes in day-length over geological time, first elucidated for the Phanerozoic by John Wells’ seminal studies of Devonian fossil corals (Wells, 1963) and shown also to apply to fossil and modern brachiopods, have yet to be extended into the Precambrian. Such data would be important to document some 90% of the history of the temporally evolving Earth-Moon system and, thereby, possible perturbations of this system by early events in the evolution of the Solar System. A solution to this problem might be provided by stripping away evolution-imposed modifications of the circadian rhythm-defining modules

of extant phototrophs to reveal their original day-length-determined parameters. Similarly, such analyses in extant organisms of the intracellular DNA-repair mechanisms of the damage induced by UV-radiation, particularly in cyanobacterial and anoxygenic phototrophic bacterial lineages that pre-date the mid-Precambrian GOE and the resulting increase in the UV-absorbing ozone layer, might well document the early evolution of the Sun when it became gradually more luminous and its UV-flux decreased by ~30%. In short, many such major questions have yet to be addressed, the use of reconstructed ancient enzymes appearing to provide a promising pathway toward their solution, perhaps augmented by better understanding of the impetus presumably provided by mid-Precambrian increases in environmental oxygen.

Bases of Eukaryotic Sexuality

As discussed above, the advent of eukaryotic sexuality near the beginning of the Neoproterozoic was evidently one of the foremost advances in the history of life. Nevertheless, given its postulated overriding significance, it is surprising that we know so little about the origins of this game-changing process.

Quite obviously, meiosis, the “reduction division” required for the genesis of sperm and egg, the gametes of sexual reproduction, is an evolutionary derivative of earlier established eukaryotic mitotic body cell division, shown by the shared essentially identical first cell-division stages of the two processes. And it is both plausible and presumably likely that the earliest unicellular phytoplanktonic acritarchs were mitotically reproducing asexual algae like such modern unicellular eukaryotic Chlorococcaleans as *Chlorococcus*, *Chlorella*, and *Chlorococcum*.

Nevertheless, there is no direct evidence from the fossil record of the timing or even the presence of the process of sexual reproduction, its existence inferred solely from its presumed evolutionary products rather than from the evidence of the process itself. Given that meiotic cell division has been established in permineralized (calcified) Carboniferous seed ferns (Millay and Eggert, 1974) as has the presence of preserved nuclei in similarly fossilized (silicified) Triassic cycads (Gould, 1971) and chert-embedded Neoproterozoic algal unicells (Schopf and Oehler, 1976), it is possible and perhaps likely that meiotically produced gametes could also be preserved, evidence that has yet to be uncovered by paleobiologic studies of Precambrian eukaryotes. Such studies of early evolved life cycles might well be aided by understanding of the biochemical bases of the evolutionary roots of eukaryotic sexuality – specifically, of the gametogenesis and syngamy on which it is based – a question as yet little investigated even in modern eukaryotes. The answer obtained might well shed light on the impetus, whether biological or environmental, for the advent of the history of life-altering process of eukaryotic sexual reproduction.

Soft-Bodied Precursors of the Ediacaran Fauna

The precursors of the large many-celled animals of the Ediacaran Fauna were no doubt soft-bodied and much smaller, so small that their fossil record is yet unknown. Plausible candidates for such pre-Ediacaran animals include nematodes of which the best-known living example is the roundworm *Caenorhabditis elegans*, a taxon more commonly known simply as *C. elegans*. Used by biologists since the early 1960's as a "model organism," its genetics are thoroughly defined showing that it shares many genes and gene-defined molecular biochemical pathways with humans and, therefore, has proved to be a useful model for studying human diseases. The bodies of such nematodes are not divided into orderly regular segments – as, for example, are those of the common annelid earthworm *Lumbricus* – so *C. elegans* is appreciably more primitive.

Roundworms such as *C. elegans* are small, about one millimeter in length and live in the soil where they survive by feeding on bacteria and similar microscopic fodder. But because they are so tiny they cannot nudge aside stony particles and leave identifiable burrows or trails in their wake as do larger annelid worms. Moreover, their body wall is thin and soft, too fragile to be readily preservable in clastic-dominated sediments. Thus, like all other multicelled precursors of the Ediacaran Fauna, they have no known fossil record. A possible solution to this lack of evidence is, as suggested above for the uncertainties enshrouding the origin of eukaryotic sexuality, intensive paleobiologic investigation of chemical deposited, rather than clastic strata. Such permineralized evidence might well exist, whether of pre-Ediacaran roundworms or of some other such lineage, but this probability has yet to be fully investigated.

DÉNOUEMENT

There are, of course, a myriad of other unanswered outstanding questions about life's early history, not least of which is whether or not Earth's early biotic record will prove relevant to the search for evidence of past life on other planets, an assumption exemplified by the hunt for potentially microfossiliferous stromatolites by NASA's current Mars 2020 Mission. Nevertheless, as this review of the roots of Precambrian paleobiologic studies and their progress and prospects illustrates, the field has made great strides over the past half century. The future is bright as the field surges forward to discover more and more about the interrelated evolution of life and its environment over the stupendously long span of Precambrian time, new findings being amassed at an ever-quicken pace as is well exemplified by the following papers in this volume.

AUTHOR CONTRIBUTIONS

The author confirms being the sole contributor of this work and has approved it for publication.

REFERENCES

- Abelson, P. H., and Hoering, T. C. (1961). Carbon isotope fractionation in formation of amino acids by photosynthetic organisms. *Proc. Natl. Acad. Sci. U.S.A.* 47, 623–632. doi: 10.1073/pnas.47.5.623
- Akanuma, S., Nakajima, Y., Yokobori, S.-I., Kimura, M., Nemoto, N., Mase, T., et al. (2013). Experimental evidence for the thermophilicity of ancestral life. *Proc. Natl. Acad. Sci. U.S.A.* 110, 11067–11072. doi: 10.1073/pnas.1308215110
- Akanuma, S., Yokobori, S., Nakajima, Y., Bessho, M., and Yamagishi, A. (2015). Robustness of predictions of extremely thermally stable proteins in ancient organisms. *Evolution* 69, 2954–2962. doi: 10.1111/evo.12779
- Awramik, S. M., and Barghoorn, E. S. (1977). The gunflint microbiota. *Precamb. Res.* 5, 121–142. doi: 10.1016/0301-9268(77)90025-0
- Barghoorn, E. S., and Schopf, J. W. (1965). Microorganisms from the late precambrian of Central Australia. *Science* 150, 337–339. doi: 10.1126/science.150.3694.337
- Barghoorn, E. S., and Tyler, S. A. (1965). Microorganisms from the gunflint chert. *Science* 147, 563–577. doi: 10.1126/science.147.3658.563
- Bell, E. A., Boehnke, P., Harrison, T. M., and Mao, W. L. (2015). Potentially biogenic carbon preserved in a 4.1 billion-year-old zircon. *Proc. Natl. Acad. Sci. U.S.A.* 112, 14518–14521. doi: 10.1073/pnas.1517557112
- Bell, E. A., Harrison, T. M., Kohl, I. E., and Young, E. D. (2014). Eoarchean crustal evolution of the Jack Hills zircon source and loss of Hadean crust. *Geochim. Cosmochim. Acta* 146, 27–42. doi: 10.1016/j.gca.2014.09.028
- Bloeser, B., Schopf, J. W., Horodyski, R. J., and Breed, W. J. (1977). Chitinozoans from the late precambrian chuar group of the Grand Canyon, Arizona. *Science* 195, 676–679. doi: 10.1126/science.195.4279.676
- Brasier, M. (2012). *Secret Chambers: The Inside Story of Cells and Complex Life*. Oxford: Oxford University Press.
- Buick, R., Des Marais, D. J., and Knoll, A. H. (1995). Stable isotopic compositions of carbonates from the mesoproterozoic bangemall group, northwestern Australia. *Chem. Geol.* 123, 153–171. doi: 10.1016/0009-2541(95)00049-r
- Butterfield, N. J. (2000). *Bangiomorpha pubescens* n. gen., n. sp.: implications for the evolution of sex, multicellularity, and the mesoproterozoic/neoproterozoic radiation of eukaryotes. *Paleobiology* 26, 386–404. doi: 10.1666/0094-8373(2000)026<0386:bpngns>2.0.co;2

- Butterfield, N. J. (2005). Probable proterozoic fungi. *Paleobiology* 31, 165–182. doi: 10.1666/0094-8373(2005)031<0165:ppf>2.0.co;2
- Butterfield, N. J. (2014). Early evolution of the eukaryota. *Palaeontology* 58, 5–17. doi: 10.1111/pala.12139
- Chaimanee, Y., Jolly, D., Benammi, M., Tafforeau, P., Duzer, D., Moussa, I., et al. (2003). A middle miocene hominoid from Thailand and orangutan origins. *Nature* 422, 61–65. doi: 10.1038/nature01449
- Chakrabarti, R., Knoll, A. H., Jacobsen, S. B., and Fischer, W. W. (2012). Si isotope variability in proterozoic cherts. *Geochim. Cosmochim. Acta* 91, 187–201. doi: 10.1016/j.gca.2012.05.025
- Chen, J.-Y., Bottjer, D. J., Davidson, E. H., Dornbos, S. Q., Gao, X., Yang, Y.-H., et al. (2006). Phosphatized polar lobe-forming embryos from the precambrian of southwest China. *Science* 312, 1644–1646. doi: 10.1126/science.1125964
- Chen, J.-Y., Bottjer, D. J., Davidson, E. H., Li, G., Gao, F., Cameron, R. A., et al. (2009). Phase contrast synchrotron X-ray microtomography of Ediacaran (Doushantuo) metazoan microfossils: phylogenetic diversity and evolutionary implications. *Precamb. Res.* 173, 191–200. doi: 10.1016/j.precamres.2009.04.004
- Chen, J.-Y., Schopf, J. W., Bottjer, D. J., Zhang, C.-Y., Kudryavtsev, A. B., Tripathi, A. B., et al. (2007). Raman spectra of a lower cambrian ctenophore embryo from southwestern Shaanxi, China. *Proc. Natl. Acad. Sci. U.S.A.* 104, 6289–6292. doi: 10.1073/pnas.0701246104
- Cloud, P. E. (1983). “Early biogeologic history: the emergence of a paradigm,” in *Earth's Earliest Biosphere, Its Origin and Evolution*, ed. J. W. Schopf (Princeton, NJ: Princeton University Press), 14–31.
- Colbath, G. K., and Grenfell, H. R. (1995). Review of biological affinities of paleozoic acid-resistant, organic-walled eukaryotic algal microfossils (including “acritarchs”). *Rev. Palaeobot. Palynol.* 86, 287–314. doi: 10.1016/0034-6667(94)00148-d
- Darwin, C. R. (1859). *On the Origin of Species*. London: John Murray.
- Dawson, J. W. (1875). *The Dawn of Life*. London: Hodder and Stoughton.
- Degens, E. T., and Epstein, S. (1962). Relationship between O^{18}/O^{16} ratios in coexisting carbonates, cherts, and diatomites. *Am. Assoc. Pet. Geol. Bull.* 46, 534–542.
- Donoghue, P. C. J., Bengtson, S., Dong, X.-P., Gostling, N., Hultgren, T., Cuninghame, J. A., et al. (2006). Synchrotron X-ray tomographic microscopy of fossil embryos. *Nature* 442, 680–683. doi: 10.1038/nature04890
- Evitt, W. R. (1963). A discussion and proposals concerning fossil dinoflagellates, hystrichospheres and acritarchs. *Proc. Natl. Acad. Sci. U.S.A.* 49, 158–164. doi: 10.1073/pnas.49.2.158
- Farquhar, J., Bao, H., and Thieme, M. H. (2000). Atmospheric influence of Earth's earliest sulfur cycle. *Science* 289, 756–758. doi: 10.1126/science.289.5480.756
- Feist, M., Liu, J., and Tafforeau, P. (2005). New insights into paleozoic charophytes morphology and phylogeny. *Am. J. Bot.* 92, 1152–1160. doi: 10.3732/ajb.92.7.1152
- Friis, E. M., Crane, P. R., Pedersen, K. R., Bengtson, S., Donoghue, P. C. J., Grimm, G. W., et al. (2007). Phase-contrast X-ray microtomography links Cretaceous seeds with gnetales and bennettitales. *Nature* 450, 549–553. doi: 10.1038/nature06278
- Garcia, A. K., Schopf, J. W., Yokobori, S.-I., Akanuma, S., and Yamagishi, A. (2017). Reconstructed ancestral enzymes suggest long-term cooling of Earth's photic zone since the Archean. *Proc. Natl. Acad. Sci. U.S.A.* 91, 4619–4624. doi: 10.1073/pnas.1702729114
- Garrels, R. M., and Mackenzie, F. T. (1971). *Evolution of Sedimentary Rocks*. New York: Norton.
- Gaucher, E. A., Govindarajan, S., and Ganesh, O. K. (2008). Palaeotemperature trend for precambrian life inferred from resurrected proteins. *Nature* 451, 704–707. doi: 10.1038/nature06510
- Gould, R. E. (1971). *Lysoxylon grigsbyi*, a cycad trunk from the Upper Triassic of Arizona and New Mexico. *Am. J. Bot.* 58, 239–248. doi: 10.1002/j.1537-2197.1971.tb09968.x
- Haldane, J. B. S. (1929). Origin of life. *Ration. Ann.* 148, 3–10.
- Han, T.-M., and Runnegar, B. (1992). Megascopic eukaryotic algae from the 2.1 billion-year-old neogee iron formation, Michigan. *Science* 257, 232–235. doi: 10.1126/science.1631544
- Hayes, J. M. (2001). Fractionation of carbon and hydrogen isotopes in biosynthetic processes. *Rev. Miner. Geochem.* 43, 225–277. doi: 10.1515/9781501508745-006
- Holland, H. D. (2006). The oxygenation of the atmosphere and oceans. *Philos. Trans. R. Soc. Biol. Sci.* 361, 903–915. doi: 10.1098/rstb.2006.1838
- Homann, M. (2019). Earliest life on earth: evidence from the barberton greenstone belt, South Africa. *Earth Sci. Rev.* 196:102888. doi: 10.1016/j.earscirev.2019.102888
- House, C. H., Schopf, J. W., McKeegan, K. D., Coath, C. D., Harrison, T. M., and Stetter, K. O. (2000). Carbon isotopic composition of individual Precambrian microfossils. *Geology* 28, 707–710. doi: 10.1130/0091-7613(2000)028<0707:cicoip>2.3.co;2
- Hren, M. T., Tice, M. M., and Chamberlain, C. P. (2009). Oxygen and hydrogen isotope evidence for a temperate climate 3.42 billion years ago. *Nature* 462, 205–208. doi: 10.1038/nature08518
- Javaux, E. J. (2019). Challenges in evidencing the earliest traces of life. *Nature* 572, 451–460. doi: 10.1038/s41586-019-1436-4
- Javaux, E. J., and Lepot, K. (2018). The paleoproterozoic fossil record: implications for the evolution of the biosphere during Earth's middle-age. *Earth Sci. Rev.* 176, 68–86. doi: 10.1016/j.earscirev.2017.10.001
- Javaux, E. J., Knoll, A. H., and Walter, M. R. (2004). TEM evidence for eukaryotic diversity in mid-proterozoic oceans. *Geobiology* 2, 121–132. doi: 10.1111/j.1472-4677.2004.00027.x
- Kasting, J. F., Howard, M. T., Wallmann, K., Veizer, J., Shields, G., and Jaffés, J. (2006). Paleoclimates, ocean depth, and the oxygen isotopic composition of seawater. *Earth Planet. Sci. Lett.* 252, 82–93. doi: 10.1016/j.epsl.2006.09.029
- Knauth, L. P. (2005). Temperature and salinity history of the precambrian ocean: implications for the course of microbial evolution. *Palaeogeogr. Palaeoclimatol. Palaeoecol.* 219, 53–69. doi: 10.1016/b978-0-444-52019-7.50007-3
- Knauth, L. P., and Lowe, D. R. (1978). Oxygen isotope geochemistry of cherts from the Onverwacht group (3.4 billion years), Transvaal, South Africa, with implications for secular variations in the isotopic composition of cherts. *Earth Planet. Sci. Lett.* 41, 209–222. doi: 10.1016/0012-821x(78)90011-0
- Knauth, L. P., and Lowe, D. R. (2003). High Archean climatic temperature inferred from oxygen isotope geochemistry of cherts in the 3.5 Ga Swaziland supergroup, South Africa. *Geol. Soc. Am. Bull.* 115, 566–580. doi: 10.1130/0016-7606(2003)115<0566:hactif>2.0.co;2
- Knoll, A. H. (1992). The early evolution of eukaryotes: a geological perspective. *Science* 256, 622–627. doi: 10.1126/science.1585174
- Knoll, A. H. (1994). Proterozoic and early cambrian protists – evidence for accelerating evolutionary tempo. *Proc. Natl. Acad. Sci. U.S.A.* 91, 6743–6750. doi: 10.1073/pnas.91.15.6743
- Knoll, A. H., Javaux, E. J., Hewitt, D., and Cohen, P. A. (2006). Eukaryotic organisms in proterozoic oceans. *Philos. Trans. R. Soc. Biol. Sci.* 361, 1023–1038. doi: 10.1098/rstb.2006.1843
- Kolosov, P. N. (2016). New microorganisms from the Vendian (Ediacaran) of the Berezovsky trough, southern Siberian platform. *Paleontol. J.* 50, 549–556. doi: 10.1134/s0031030116060071
- Kudryavtsev, A. B., Schopf, J. W., Agresti, D. G., and Wdowiak, T. J. (2001). In situ laser-Raman imagery of precambrian microscopic fossils. *Proc. Natl. Acad. Sci. U.S.A.* 98, 823–826. doi: 10.1073/pnas.98.3.823
- Logan, B. W. (1961). Cryptozoon and associate stromatolites from the recent, Shark Bay, Western Australia. *J. Geol.* 69, 517–533. doi: 10.1086/626769
- Mendelson, C. V., Bauld, J., Horodyski, R. J., Lipps, J. H., Moore, T. B., and Schopf, J. W. (1992). “Proterozoic and selected early cambrian microfossils: prokaryotes and protists,” in *The Proterozoic Biosphere, A Multidisciplinary Study*, eds J. W. Schopf and C. Klein (Cambridge: Cambridge University Press), 175–244. doi: 10.1017/cbo9780511601064.007
- Miao, L., Moczyłowska, M., Zhu, S., and Zhua, M. (2019). New record of organic-walled, morphologically distinct microfossils from the late paleoproterozoic changcheng group in the Yanshan range, North China. *Precamb. Res.* 321, 172–198. doi: 10.1016/j.precamres.2018.11.019
- Millay, M. A., and Eggert, D. A. (1974). Microgametophyte development in the paleozoic seed fern family callistophytaceae. *Am. J. Bot.* 61, 1067–1075. doi: 10.1002/j.1537-2197.1974.tb12324.x
- Miller, S. L. (1953). Production of amino acids under possible primitive earth conditions. *Science* 117, 528–529. doi: 10.1126/science.117.3046.528
- Miller, S. L., and Urey, H. C. (1959). Organic compound synthesis on the primitive earth. *Science* 130, 245–251.

- Olson, S. L., Schwieterman, E. W., Reinhard, C. T., and Lyons, T. W. (2018). "Earth: atmospheric evolution of a habitable planet," in *Handbook of Exoplanets*, eds H. Deeg and J. Belmonte (Cham: Springer). doi: 10.1007/978-3-319-30648-3_189-1
- Oparin, A. I. (1924). *Proiskhozhdenie Zhizni [The Origin of Life]*. Moscow: Izd. Moskhovhii Rabochii. (in Russian).
- Perry, E. C. (1967). The oxygen isotope chemistry of ancient cherts. *Earth Planet. Sci. Lett.* 3, 62–66. doi: 10.1016/0012-821x(67)90012-x
- Pietrzak-Renaud, N., and Davis, D. (2014). U–Pb geochronology of baddeleyite from the belleview metadiabase: age and geotectonic implications for the negaunee iron formation, Michigan. *Precamb. Res.* 250, 1–5. doi: 10.1016/j.precamres.2014.05.018
- Poulton, S. W., Bekker, A., Cumming, V. M., Zerkle, A. L., Canfield, D. E., and Johnston, D. T. (2021). A 200-million-year delay in permanent atmospheric oxygenation. *Nature* 592, 232–236. doi: 10.1038/s41586-021-03393-7
- Prasad, B., Uniyal, S. N., and Asher, R. (2005). Organic-walled microfossils from the proterozoic vindhyan supergroup of Son Valley, Madhya Pradesh, India. *Palaeobotanist* 54, 13–60.
- Ray, J. S., Martin, M. W., Veizer, J., and Bowring, S. A. (2002). U–Pb zircon dating and Sr isotope systematics of the Vindhyan supergroup, India. *Geology* 30, 131–134.
- Risso, V. A., Gavira, J. A., and Mejia-Carmona, D. F. (2013). Hyperstability and substrate promiscuity in laboratory resurrections of precambrian β -lactamases. *J. Am. Chem. Soc.* 135, 2899–2902. doi: 10.1021/ja311630a
- Robert, F., and Chaussidon, M. (2006). A palaeotemperature curve for the precambrian oceans based on $\delta^{18}\text{O}$ silicon isotopes in cherts. *Nature* 443, 969–972. doi: 10.1038/nature05239
- Runnegar, B. (1994). "Proterozoic eukaryotes: evidence from biology and geology," in *Early Life on Earth*, Nobel Symposium No. 84, ed. S. Bengtson (New York, NY: Columbia University Press), 287–297.
- Schidlowski, M. (1991). Organic carbon isotope record: index line of autotrophic carbon fixation over 3.8 Gyr of earth history. *J. Southeast Asian Earth Sci.* 5, 333–337. doi: 10.1016/0743-9547(91)90045-Y
- Schidlowski, M., Hayes, J. M., and Kaplan, I. R. (1983). "Isotopic inferences of ancient biochemistries: carbon, sulfur, hydrogen, and nitrogen," in *Earth's Earliest Biosphere, Its Origin and Evolution*, ed. J. W. Schopf (Princeton, NJ: Princeton University Press), 149–186.
- Schirmermeister, B. E., Sanchez-Baracaldo, P., and Wacey, D. (2016). Cyanobacterial evolution during the precambrian. *Int. J. Astrobiol.* 15, 187–204. doi: 10.1017/S1473550415000579
- Schopf, J. W. (1968). Microflora of the bitter springs formation, late precambrian, Central Australia. *J. Paleontol.* 42, 651–688.
- Schopf, J. W. (1970). Electron microscopy of organically preserved precambrian microorganisms. *J. Paleontol.* 44, 1–6.
- Schopf, J. W. (1993). Microfossils of the early Archaean apex chert: new evidence of the antiquity of life. *Science* 260, 640–646. doi: 10.1126/science.260.5108.640
- Schopf, J. W. (1994). Disparate rates, differing fates: the rules of evolution changed from the precambrian to the phanerozoic. *Proc. Natl. Acad. Sci. U.S.A.* 91, 6735–6742. doi: 10.1073/pnas.91.15.6735
- Schopf, J. W. (ed.) (1983). *Earth's Earliest Biosphere, Its Origin and Evolution*. Princeton, NJ: Princeton University Press.
- Schopf, J. W., and Blacic, J. M. (1971). New microorganisms from the bitter springs formation (late precambrian) of the north-central Amadeus Basin, Australia. *J. Paleontol.* 45, 925–960.
- Schopf, J. W., and Klein, C. (eds) (1992). *The Proterozoic Biosphere, A Multidisciplinary Study*. Cambridge: Cambridge University Press. doi: 10.1017/CBO9780511601064
- Schopf, J. W., and Kudryavtsev, A. B. (2005). Three-dimensional Raman imagery of precambrian microscopic organisms. *Geobiology* 3, 1–12. doi: 10.1111/j.1472-4669.2005.00044.x
- Schopf, J. W., and Oehler, D. Z. (1976). How old are the eukaryotes? *Science* 193, 47–49.
- Schopf, J. W., Barghoorn, E. S., Maser, M. D., and Gordon, R. O. (1965). Electron microscopy of fossil bacteria two billion years old. *Science* 149, 1365–1367. doi: 10.1126/science.149.3690.1365
- Schopf, J. W., Ford, T. D., and Breed, W. J. (1973a). Microorganisms from the late precambrian of the Grand Canyon, Arizona. *Science* 179, 1319–1321.
- Schopf, J. W., Haugh, B. N., Molnar, R. E., and Satterthwait, D. F. (1973b). On the development of metaphytes and metazoans. *J. Paleontol.* 47, 1–9.
- Schopf, J. W., Kitajima, K., Spicuzza, M. J., Kudryavtsev, A. B., and Valley, J. W. (2018). SIMS analyses of the oldest known assemblage of microfossils document their taxon-correlated carbon isotope compositions. *Proc. Natl. Acad. Sci. U.S.A.* 115, 53–58. doi: 10.1073/pnas.1718063115
- Schopf, J. W., Kudryavtsev, A. B., Agresti, D. G., Czaja, A. D., and Wdowiak, T. J. (2005). Raman imagery: a new approach to assess the geochemical maturity and biogenicity of permineralized precambrian fossils. *Astrobiology* 5, 333–371. doi: 10.1089/ast.2005.5.333
- Schopf, J. W., Kudryavtsev, A. B., Agresti, D. G., Wdowiak, T. J., and Czaja, A. D. (2002). Laser-Raman imagery of Earth's earliest fossils. *Nature* 416, 73–76. doi: 10.1038/416073a
- Schopf, J. W., Kudryavtsev, A. B., Osterhout, J. T., Williford, K. H., Kitajima, K., Valley, J. W., et al. (2017). An anaerobic ~3400 Ma shallow-water microbial consortium: presumptive evidence of Earth's paleoarchean anoxic atmosphere. *Precamb. Res.* 299, 309–318. doi: 10.1016/j.precamres.2017.07.021
- Schopf, J. W., Tripathi, A. B., and Kudryavtsev, A. B. (2006). Three-dimensional confocal optical microscopy of precambrian microscopic organisms. *Astrobiology* 6, 1–16. doi: 10.1089/ast.2006.6.1
- Sepkoski, J. J., and Schopf, J. W. (1992). "Biotic diversity and rates of evolution during proterozoic and earliest phanerozoic time," in *The Proterozoic Biosphere, A Multidisciplinary Study*, eds J. W. Schopf and C. Klein (Cambridge: Cambridge University Press), 521–566.
- Seward, A. C. (1931). *Plant Life Through the Ages*. Cambridge: Cambridge University Press.
- Sharma, M., and Shukla, Y. (2009a). Mesoproterozoic coiled megascopic fossil *Grypania spiralis* from the rohtas formation, semri group, Bihar, India. *Curr. Sci.* 96, 1636–1640.
- Sharma, M., and Shukla, Y. (2009b). Taxonomy and affinity of early mesoproterozoic megascopic helically coiled and related fossils from the rohtas formation, the Vindhyan supergroup, India. *Precamb. Res.* 173, 105–122.
- Simpson, G. G. (1944). *Tempo and Mode in Evolution*. New York, NY: Columbia University Press.
- Tafforeau, P., Boistel, R., Boller, E., Bravin, A., Brunet, M., Chaimanee, Y., et al. (2006). Applications of X-ray synchrotron microtomography for non-destructive 3D studies of paleontological specimens. *Appl. Phys. A Mater. Sci. Process.* 83, 195–202. doi: 10.1007/s00339-006-3507-2
- Talyzina, N. M. (2000). Ultrastructure and morphology of *Chuarina circularis* (Walcott, 1899) Vidal and Ford (1985) from the neoproterozoic visingsö group, Sweden. *Precamb. Res.* 102, 123–134. doi: 10.1016/S0301-9268(00)00062-0
- Tang, H., Trail, D., Bell, E. A., and Harrison, T. M. (2019). Zircon halogen geochemistry: insights into Hadean-Archean fluids. *Geochem. Perspect. Lett.* 9, 49–53. doi: 10.7185/geochemlet.1905
- Thiemens, M. H., and Heidenreich, J. E. (1983). The mass-independent fractionation of oxygen: a novel effect and its possible cosmochemical implications. *Science* 219, 1073–1075. doi: 10.1126/science.219.4588.1073
- Timofeev, B. F., and Hermann, T. N. (1979). "Dokembriiskaya microbiota Lachandinskoi svity [Precambrian microbiota of the Lakhanda formation]," in *Paleontologiya Dokembriya I Rannego Kembriya [Paleontology of the Precambrian and Early Cambrian]*, ed. B. S. Sokolov (Leningrad: Nauka), 137–147. (in Russian).
- Tomescu, A. M. F., Klymiuk, A. A., Matsunaga, K. K. S., Bippus, A. C., and Shelton, G. W. K. (2016). "Microbes and the fossil record: selected topics in paleomicrobiology," in *Their World: A Diversity of Microbial Environments*, Advances in Environmental Microbiology 1, ed. C. J. Hurst (Cham: Springer), 69–169.
- Towe, K. M., Bengtson, S., Fedonkin, M. A., Hofmann, H. J., Mankiewicz, C., and Runnegar, B. N. (1992). "Proterozoic and earliest cambrian carbonaceous remains: trace and body fossils," in *The Proterozoic Biosphere, A Multidisciplinary Study*, eds J. W. Schopf and C. Klein (Cambridge: Cambridge University Press), 343–402.
- Tyler, S. A., and Barghoorn, E. S. (1954). Occurrence of structurally preserved plants in pre-cambrian rocks of the Canadian shield. *Science* 119, 606–608. doi: 10.1126/science.119.3096.606
- Van Kranendonk, M. J., Baumgartner, R., Djokic, T., Ota, T., Steller, L., Garbe, U., et al. (2021). Elements for the origin of life on land: a deep-time perspective

- from the Pilbara Craton of Western Australia. *Astrobiology* 21, 39–59. doi: 10.1089/ast.2019.2107
- Walcott, C. D. (1899). Precambrian fossiliferous formations. *Geol. Soc. Am. Bull.* 10, 199–244. doi: 10.1130/GSAB-10-199
- Walter, M. R. (1977). Interpreting stromatolites. *Am. Sci.* 65, 563–571.
- Walter, M. R. (ed.) (1973). *Stromatolites: Advances in Sedimentology*, Vol. 20. Amsterdam: Elsevier.
- Weis, D., and Wasserburg, G. J. (1987). Rb-Sr and Sm-Nd isotope geochemistry and chronology of cherts from the Onverwacht group (3.5 AE), South Africa. *Geochim. Cosmochim. Acta* 51, 973–984. doi: 10.1016/0016-7037(87)90109-8
- Wells, J. W. (1963). Coral growth and geochronometry. *Nature* 197, 948–950. doi: 10.1038/197948a0
- Wilde, S. A., Zhao, G., Wang, K., and Sun, M. (2004). First SHRIMP zircon U-Pb ages for hutuo group in Wutaishan: further evidence for palaeoproterozoic amalgamation of North China Craton. *Chin. Sci. Bull.* 49, 83–90. doi: 10.1007/BF02901747
- Xiao, S., Knoll, A. H., Yuan, X., and Poeschel, C. M. (2004). Phosphatized multicellular algae in the neoproterozoic doushantuo formation, China, and the early evolution of florideophyte red algae. *Am. J. Bot.* 91, 214–227. doi: 10.3732/ajb.91.2.214
- Yamagishi, A., Kon, T., Takahashi, G., and Oshima, T. (1998). “From the common ancestor of all living organisms to protoeukaryotic cell,” in *Thermophiles: The Key To Molecular Evolution And The Origin of Life?* eds J. Wiegand and M. Adams (London: Taylor and Francis), 287–295.
- Yin, L., Meng, F., Kong, F., and Niu, C. (2020). Microfossils from the paleoproterozoic hutuo group, Shanxi, North China: early evidence for eukaryotic metabolism. *Precamb. Res.* 342:105650. doi: 10.1016/j.precamres.2020.105650
- Yin, Z., Zhu, M., Davidson, E. H., Bottjer, D. J., Zhao, F., and Tafforeau, P. (2015). Sponge grade body fossil with cellular resolution dating 60 Myr before the cambrian. *Proc. Natl. Acad. Sci. U.S.A.* 112, E1453–E1460. doi: 10.1073/pnas.1414577112
- Yochelson, E. (1998). *Charles Doolittle Walcott, Paleontologist*. Kent, OH: Kent State University Press.
- Zhu, S., Zhu, M., Knoll, A. H., Yin, Z., Zhao, F., Sun, S., et al. (2016). Decimetre-scale multicellular eukaryotes from the 1.56-billion-year-old gaoyuzhuang formation in North China. *Nat. Commun.* 7:11500. doi: 10.1038/ncomms11500

Conflict of Interest: The author declares that the research was conducted in the absence of any commercial or financial relationships that could be construed as a potential conflict of interest.

Publisher's Note: All claims expressed in this article are solely those of the authors and do not necessarily represent those of their affiliated organizations, or those of the publisher, the editors and the reviewers. Any product that may be evaluated in this article, or claim that may be made by its manufacturer, is not guaranteed or endorsed by the publisher.

Copyright © 2021 Schopf. This is an open-access article distributed under the terms of the Creative Commons Attribution License (CC BY). The use, distribution or reproduction in other forums is permitted, provided the original author(s) and the copyright owner(s) are credited and that the original publication in this journal is cited, in accordance with accepted academic practice. No use, distribution or reproduction is permitted which does not comply with these terms.



The Importance of Size and Location Within Gregarious Populations of *Ernietta plateauensis*

Brandt M. Gibson^{1,2*}, Simon A.F. Darroch^{2,3*}, Katie M. Maloney¹ and Marc Laflamme¹

¹Department of Chemical and Physical Sciences, University of Toronto Mississauga, Mississauga, ON, Canada, ²Department of Earth & Environmental Sciences, Vanderbilt University, Nashville, TN, United States, ³Senckenberg Museum of Natural History, Frankfurt, Germany

OPEN ACCESS

Edited by:

Shuhai Xiao,
Virginia Tech, United States

Reviewed by:

Alex Liu,
University of Cambridge,
United Kingdom
Linda Satour,
University of Oran 2, Algeria

*Correspondence:

Brandt M. Gibson
brandt.m.gibson@vanderbilt.edu
Simon A.F. Darroch
simon.a.darroch@vanderbilt.edu

Specialty section:

This article was submitted to
Paleontology,
a section of the journal
Frontiers in Earth Science

Received: 29 July 2021

Accepted: 04 October 2021

Published: 18 October 2021

Citation:

Gibson BM, Darroch SAF,
Maloney KM and Laflamme M (2021)
The Importance of Size and Location
Within Gregarious Populations of
Ernietta plateauensis.
Front. Earth Sci. 9:749150.
doi: 10.3389/feart.2021.749150

Ernietta plateauensis is a semi-infaunal macroscopic eukaryote of unknown affinities common in latest Ediacaran (~548–539 Ma) shallow marine settings in Namibia. The discovery of *in-situ* assemblages of *Ernietta* has demonstrated that these organisms lived in aggregated populations, while studies employing computational fluid dynamics (CFD) modeling have supported the hypothesis that these organisms were likely behaving as gregarious suspension feeders, analogous to many extant invertebrate phyla in present-day marine environments. Careful census and measurement of individuals within these *in-situ* populations offers an opportunity to examine how their size and location within a larger population affect nutrient delivery dynamics. In this study, we build on previous work by simulating fluid flow over aggregations of *Ernietta* comprising individuals of disparate sizes, and additionally reconstruct a population of *Ernietta* preserved *in-situ* from Farm Hansburg, Namibia. We use a combination of stationary and time-dependent CFD to reconstruct nutrient carrying flow paths, and compare the efficiency with which nutrients are partitioned between individuals of different shapes and sizes. Our results demonstrate that smaller *Ernietta* experience limited recirculation within their cavities compared to larger individuals. Furthermore, in spatially-accurate distributions, reduced recirculation is limited to isolated individuals of any size, while smaller individuals found downstream of larger ones receive enhanced cavity mixing. These reconstructed flow patterns illustrate that the disadvantage associated with small size is apparently mediated by location within the overall aggregation, suggesting a complex interplay of controls on feeding efficiency. This in turn suggests that aggregations of adult *Ernietta* would likely have performed a ‘nursery’ function, creating localized conditions ideal for the settlement and growth of younger individuals.

Keywords: Ediacara biota, computational fluid dynamics (CFD), large eddy simulation (LES), Spalart-Allmaras, Nama assemblage

INTRODUCTION

Ediacaran fossil assemblages preserve the earliest evidence of macroscopic communities in the fossil record (Narbonne, 2005; Knoll et al., 2006). These fossils have historically been divided into three distinct assemblages referred to as the “Avalon”, “White Sea”, and “Nama” (Waggoner, 2003; Boag et al., 2016), which reflect a combination of distinct preservational (Gehling, 1999; Narbonne, 2005;

Droser et al., 2017), paleoenvironmental (Grazhdankin, 2004; Grazhdankin, 2014; Gehling and Droser, 2013; Liu et al., 2015), and evolutionary (Grazhdankin, 2014; Droser et al., 2017) stages. The older Avalon assemblages (e.g., see Liu et al., 2015) are characterized primarily by arboreomorphs, rangeomorphs, and triradialomorphs that persist into the younger White Sea and Nama assemblages (Laflamme et al., 2013). The middle White Sea Assemblage has the greatest morphological and species diversity (Shen et al., 2008), while the youngest Nama Assemblage preserves communities dominated by erniettomorphs, and which are characterized by relatively low species richness and community structures suggestive of limited levels of competition and/or ecological stress (Muscente et al., 2019; Darroch et al., 2015; 2018a,b; although see Vaziri et al., 2021). Previous analyses that have investigated the role of size in *in-situ* Ediacaran populations have typically focused on Avalon-aged (~571–558 Ma) rangeomorph communities from Mistaken Point, Newfoundland (Clapham and Narbonne, 2002; Clapham et al., 2003; Darroch et al., 2013; Mitchell et al., 2015; Mitchell and Kenchington, 2018; Boddy et al., 2021). Building off these, more recent numerical studies have focused on how the spatial arrangement of individual organisms within communities may reflect paleoecological and -biological aspects of individual taxa, including potential reproductive modes, dispersal distances, and interspecific interactions (Hall et al., 2015; Mitchell et al., 2015, 2018; Mitchell and Butterfield, 2018; Mitchell and Kenchington, 2018). However, to date no studies have applied these approaches to the latest Ediacaran Nama-aged (~548–539 Ma) assemblages, which in southern Namibia can be found preserved as large monospecific accumulations in life position (Gibson et al., 2019). In this study, we investigate the size and spatial distributions of individuals within *in-situ* populations of *Ernietta plateauensis* from Farm Hansburg, Namibia. We test hypotheses surrounding how these dense populations reflect aspects of life history, and/or adaptations to feeding. Given that communities of erniettomorph Ediacara biota thrived immediately prior to the Cambrian boundary (e.g., Elliott et al., 2016; Meyer et al., 2014; Darroch et al., 2018a; Darroch et al., 2021), understanding the structure and function of their communities will shed valuable light on ecological dynamics during the Ediacaran-Cambrian transition (Darroch et al., 2018a).

Ernietta plateauensis is an iconic Ediacaran taxon that is found in a range of paleoenvironments up until the Ediacaran–Cambrian boundary (Bouougri et al., 2011; Laflamme et al., 2013; Darroch et al., 2015; Smith et al., 2017; Maloney et al., 2020). It is a sack-like organism constructed from modular, tubular elements in a double-walled palisade structure that are alternately stitched along a basal medial seam (Jenkins et al., 1981; Elliott et al., 2016; Ivantsov et al., 2016). Individuals lived semi-infaunally with the basal portion buried within the seafloor, and with an upper portion extended above the sediment-water interface (Seilacher, 1992; Seilacher et al., 2003; Bouougri et al., 2011; Seilacher and Gishlick, 2014; Elliott et al., 2016; Ivantsov et al., 2016). Based on their presence in ripple-laminated fine-grained sandstones preserving evidence of microbial mats, *Ernietta* is interpreted to have lived in protected, high-to

medium-energy shallow marine settings with periodic clastic sediment supply (Bouougri et al., 2011; Ivantsov et al., 2016; Maloney et al., 2020). These inner-to outer-ramp environments are characterized by unstable marine redox conditions indicating that *Ernietta* was likely capable of living in environments characterized by low or fluctuating oxygen levels (Hall et al., 2013; Wood et al., 2015; Bowyer et al., 2017; 2020). Similar to trends observed in other macroscopic eukaryotes (*Pteridinium*, *Windermeria*) observed in the Blueflower Formation of Northwestern Canada (Sperling et al., 2016), *Ernietta* may also have been able to opportunistically colonize environments that experienced transient pulses of oxygenation (Hall et al., 2013; Bowyer et al., 2020). Furthermore, *Ernietta* fossils are often found in large accumulations and have been interpreted to be in life position based on their vertical orientation (Bouougri et al., 2011; Maloney et al., 2020), lacking apparent biostratinomic compaction (Elliott et al., 2016; Ivantsov et al., 2016), and detailed sedimentological analyses suggesting continued vertical growth (Jenkins et al., 1981; Jenkins, 1992). Previous work employing computational fluid dynamics (CFD) modeling has suggested both that *Ernietta* likely functioned as a sessile suspension feeder based on the consistent presence of recirculation within its cavity, and that living in aggregated patches led to increased mixing above populations, replenishing nutrients and helping to diffuse any potential waste (i.e., “commensalism” though technically ecological facilitation—see Gibson et al., 2019).

Previous studies (Ivantsov et al., 2016; Gibson et al., 2019) noted that populations of *Ernietta* in southern Namibia tend to comprise individuals with a wide range of sizes, and non-random spatial organizations. While Gibson et al. (2019) demonstrated certain advantages of gregarious living using simplified, idealized spatial arrangements of uniformly sized *Ernietta*, these are not entirely representative of the original system, and potentially mask subtle interactions that result from these more complex community structures. By analogue with modern marine benthic organisms that live gregariously, this raises the question: how might individual size and position within aggregations affect the success of individuals within the broader population? Individual success in modern marine organisms is influenced by a combination of external (environmental) and intrinsic (conspecific) controls. External controls are typically density-independent and may include: local water temperature (Pepin, 1991); local sedimentation rates, volumes, and type (Gilmour, 1999); and the area of available substrate suitable for settlement/recruitment (Harrington et al., 2004). In contrast, intrinsic controls, such as population growth rates, are more likely to be density-dependent (Caley et al., 1996). Interactions between these external and intrinsic controls can regulate the magnitude and direction of density-dependent effects (Hixon et al., 2002; White, 2007; Vermeij and Sandin, 2008; Doropoulos et al., 2017). Examples include prey mortality severity (Raymundo and Maypa, 2004; White, 2007), larval settlement and survivability (Gaines and Roughgarden, 1985; Raimondi, 1990; Doropoulos et al., 2017), and food delivery (Bertness and Grosholz, 1985; Bertness et al., 1991; Leonard et al., 1998). Furthermore, individual survivability at low settlement densities can be

density-independent, but there is increasing evidence to suggest that gregarious settlement has the potential to increase survivability depending on environment (Bertness and Grosholz, 1985; Raymundo and Maypa, 2004; Linden and Rinkevich, 2017). This is particularly important in the absence of predation [such as during the Ediacaran (Xiao and Laflamme, 2009)]—as predation is the most frequent cause of post-settlement, density-dependent mortality (Gaines and Roughgarden, 1985). As an example, population assessments of the extant ribbed mussel (*Geukensia*) residing along the seaward margins of salt marshes have shown that during colder seasons with high tide, low density aggregations have higher mortality rates when compared to denser aggregations (Bertness and Grosholz, 1985).

While these patterns are possible to observe in modern ecosystems, detecting similar interactions within Ediacaran communities is more challenging and requires strategies for indirect assessment. In this study, we explore individual size- and location-specific controls on individual success (measured as inferred feeding efficiency) within *Ernieetta* populations, using the strength of recirculation within the cavities of individuals as a proxy for feeding efficiency. Previous work on *Ernieetta* feeding has suggested that cavity recirculation is linked to suspension feeding implying a positive correlation between recirculation and nutrient acquisition, such that individuals within a population that experience greater cavity recirculation are interpreted to have greater feeding success (Gibson et al., 2019; 2021). To test the effect of size and location on feeding efficiency within populations, we compare patterns of recirculation within idealized arrays of *Ernieetta*, alongside those within a reconstructed population recorded during fieldwork. The results of these analyses reveal whether there are advantages associated with specific locations within populations, and thus whether monospecific communities of *Ernieetta* may have been characterized by competition for space.

MATERIALS AND METHODS

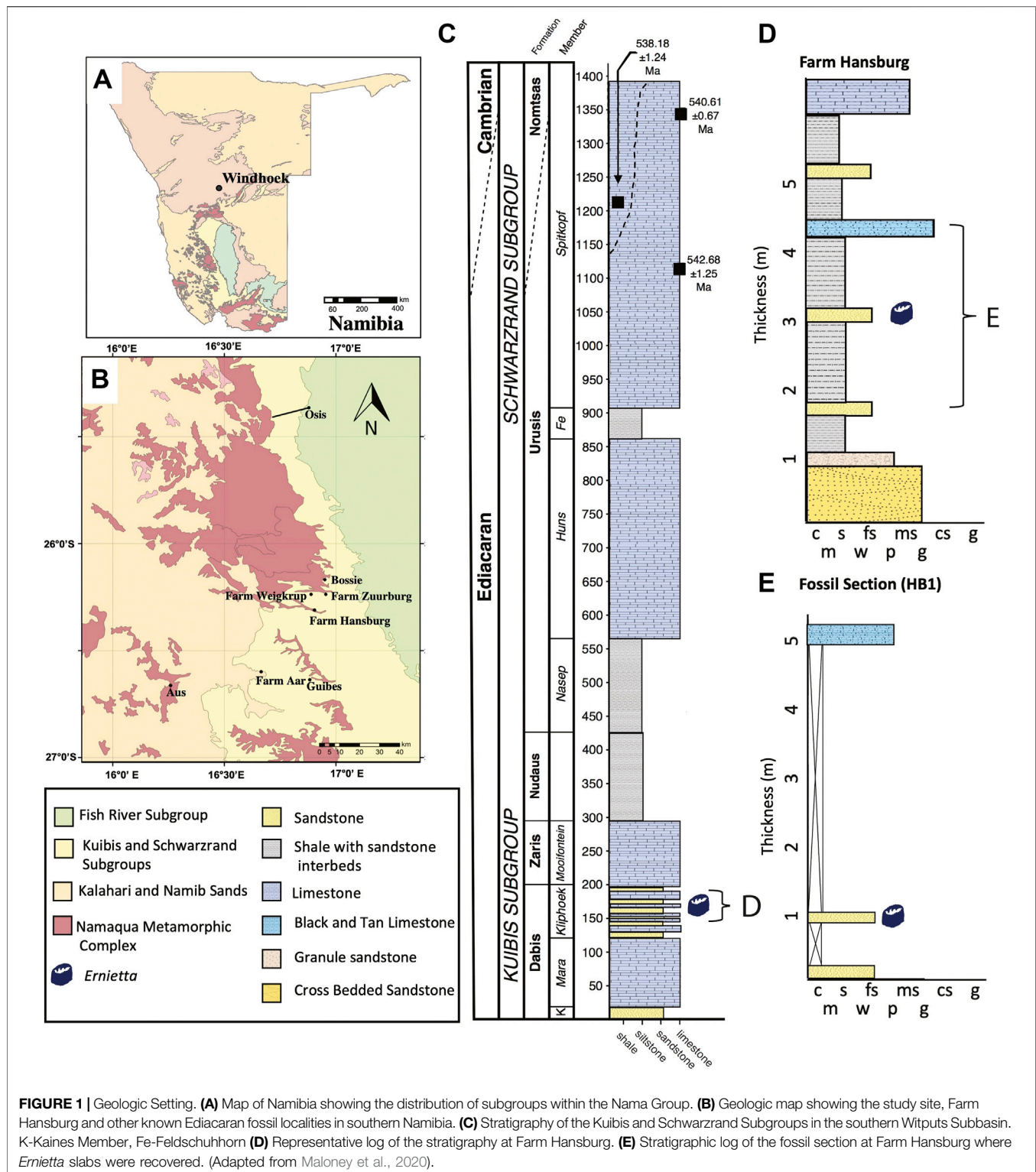
All simulation parameters and models from this study were based on latest Ediacaran material from Namibia that have been published elsewhere. For a detailed description of the geologic background, see Maloney et al. (2020) and Bouougri et al. (2011). For all simulations, we used a previously published 3D *Ernieetta* model (Gibson et al., 2019) scaled to dimensions reported by Ivantsov et al. (2016). We conducted three groups of simulations: 1) single individual simulations, where a “large” individual was scaled identical to Gibson et al. (2019) simulations, and the “small” individual was isotropically half that size. 2) Idealized populations where we created square arrays comprised of four individuals. And, 3) a spatially-accurate reconstructed population of *Ernieetta*. Within the idealized population arrays, we varied the size of individuals iteratively, producing arrays with smaller individuals upstream (translated by 0.025 m) and downstream (translated by 0.15 m). Again, smaller individuals were isotropically scaled to half of the larger individuals, which fell

well within the range reported by previous studies (Ivantsov et al., 2016; Elliott et al., 2016; Gibson et al., 2019). In order to recreate real *in-situ* populations, we used as a reference a slab from the Kliphoeck Member of the Dabis Formation from Farm Hansburg, Namibia, that preserves an *in-situ* *Ernieetta* population (**Figure 1; Supplementary Figure S1**; Bouougri et al., 2011; Gibson et al., 2019; Maloney et al., 2020). This slab was collected from the ripple laminated, fine grained sandstone Facies 3 of Maloney et al. (2020), and was solely examined and photographed in the field due to its large size. We digitally reconstructed the Hansburg slab by placing and anisotropically scaling individuals to visually match the exposed surface. Individual dimensions were taken by measuring the long axis length and the length of the axis normal to the long axis. While such techniques did not perfectly replicate the population due to differential burial depths (thus affecting size reconstructions), they did allow us to more accurately replicate Ediacaran populations for CFD analyses than what had been presented elsewhere (Ghisalberti et al., 2014; Gibson et al., 2019). In both sets of analyses, all sizes fell within the published ranges of *Ernieetta* sizes (Gibson et al., 2019).

Because CFD is a computationally intensive technique, we optimized our simulation setups and methods employed based on the question of interest. For all idealized population simulations, we used stationary (time-averaged) Reynolds-Averaged Navier-Stokes (RANS) simulations with the Spalart-Allmaras one-equation eddy viscosity turbulence model (Bardina et al., 1997; Blazek, 2001) as described in *Idealized Populations CFD Protocol (Reynolds-Averaged Navier-Stokes)*. For our Hansburg population analysis, we employed both Spalart-Allmaras RANS and Large Eddy Simulation (LES) turbulence closures using the methods described in *Hansburg Population CFD Protocol (Reynolds-Averaged Navier-Stokes and Large Eddy Simulation)*. Because LES is more accurate and time-dependent, it allowed for more precisely resolved fluid flow patterns in the more complex population setup; however, the time required to solve LES simulations limited its use in idealized populations. For a more in-depth discussion the benefits of LES over RANS, see Gibson et al. (2021). For a more in-depth discussion of turbulence models in general, see Blazek (2001). All CFD simulations were performed in COMSOL Multiphysics 5.6 (COMSOL Multiphysics, RRID:SCR_014,767).

Idealized Populations CFD Protocol (Reynolds-Averaged Navier-Stokes)

CFD simulations using our idealized arrays were set up using a hexahedron flow domain (1.75 m × 0.71 m × 0.25 m; W × D × H) that was sufficiently large to reconstruct flow patterns without influence from boundaries. Following previous setups (e.g., Rahman, 2017), our seafloor and *Ernieetta* individuals were assigned no-slip conditions (e.g., fixing the velocity at 0 m/s), the upper face and flow-parallel faces were assigned slip conditions, and the inlet and outlet conditions were assigned on the upstream and downstream faces, respectively. For the inlet boundary condition, a fully-developed, depth-averaged velocity was prescribed (Gibson et al., 2021), and a zero-pressure condition was assigned to the outlet. We chose $U = 0.1, 0.2, 0.5$ m/s following previous *Ernieetta*



CFD analyses (Gibson et al., 2019). Liquid water material properties [density $\rho = 1000 \text{ kg/m}^3$, dynamic viscosity $\mu = 0.001 \text{ kg/(s}\cdot\text{m)}$] were assigned to the flow domain. The domain was meshed using free tetrahedral elements with two layers of additional hexahedral elements proximal to the no-slip conditions to better resolve the

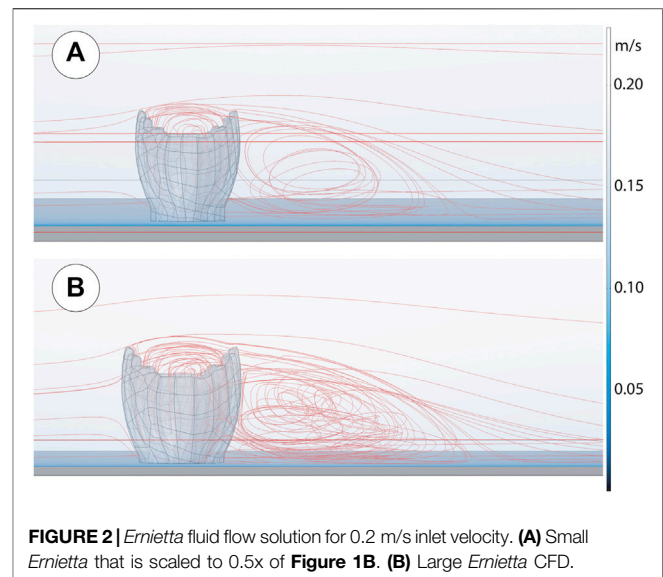
viscous sublayer. Because our system Reynolds number was $Re = 74,826$ (Supplementary 1), turbulent flow was solved using the Spalart-Allmaras one-equation eddy viscosity RANS turbulence model. This turbulence model was chosen to more accurately resolve flow separation from adverse pressure gradients (Bardina et al., 1997;

Blazek, 2001), such as between the smaller and larger individuals in our populations.

Hansburg Population CFD Protocol (Reynolds-Averaged Navier-Stokes and Large Eddy Simulation)

Recent analyses have demonstrated that LES can produce fluid flow results that are more accurate than the widely-employed RANS approach (Gibson et al., 2021). This improvement stems from solving the Navier-Stokes equations without implementing a Reynolds stress tensor (Blazek, 2001). For this reason, we used COMSOL's LES residual-based variational multiscale (RBVM) turbulence closure on the Hansburg population CFD simulation. For computational ease, we initiated our LES simulations with a previously computed stationary RANS solution following the protocol presented in *Idealized Populations CFD Protocol (Reynolds-Averaged Navier-Stokes)*. We used a hexahedron flow domain ($150\text{ cm} \times 80\text{ cm} \times 15\text{ cm}$; $W \times D \times H$) that was sufficiently large to reconstruct flow patterns with minimal influence on the population from boundaries in the initial stationary simulation. Following *Idealized Populations CFD Protocol (Reynolds-Averaged Navier-Stokes)*, we applied the same boundary conditions, fluid material properties, and performed a mesh sensitivity analysis (**Supplementary 2**). Following the idealized population methods, we used the simpler Spalart-Allmaras turbulence closure to solve the flow fields that were used to speed the convergence of the LES simulation. Using the mesh-independent solution ("Normal"; **Supplementary Figure S2**), we integrated pressure (p) on the upstream and downstream faces to calculate the pressure differential (Δp) that was required to drive flow at the desired $U = 0.5\text{ m/s}$ depth-averaged velocity. As there were no paleocurrent markers preserved within the slab, we chose the direction of flow based off of our hypothesis framework. While flow could feasibly have come from other directions, this orientation was chosen to better reconstruct the flow dynamics of smaller individuals behind larger individuals while simultaneously reconstructing flow over isolated individuals both at the leading edge of the population and downstream (see **Supplementary Figure S3**). Because LES is so computationally intensive, only the 0.5 m/s depth-averaged velocity was solved for in this study.

Using the same flow domain and mesh procedures described in *Idealized Populations CFD Protocol (Reynolds-Averaged Navier-Stokes)*, we modified our design for the LES analysis by changing the flow-parallel hexahedron slip faces that are orthogonal to the no slip seafloor to be periodic boundaries with a pressure differential $\Delta p = 0\text{ Pa}$. In a physical sense, this allowed fluid that intersected these boundaries to exit the domain on a face and be reintroduced on the opposing face while preserving momentum and continuity. We then changed the inlet and outlet faces to also be periodic boundaries, but additionally prescribed a pressure differential of $\Delta p = 2\text{ Pa}$ to approximate flow at the desired depth-averaged velocity 0.5 m/s . A pressure point constraint was placed on the no slip seafloor away from *Ernietta* individuals (see Gibson et al., 2021), which provided a known pressure point for calculating variations within the pressure field. We used the solution derived from the Spalart-Allmaras



preliminary simulation as the first time step (e.g., initial conditions, $t = 0$) for the flow field, and ran the simulation for 30 s using COMSOL's dynamic time stepping to ensure adequate time resolution was solved between time steps (but only output flow fields every 0.01 s). Additionally, due to non-linearities from the fully-coupled flow field turbulent solver, we used an Automatic Fully Non-linear Newton solver instead of the default Constant Newton Iterations solver settings. Finally, we verified our flow fields were in agreement with theoretical constraints by computing the time-averaged velocity profile throughout multiple points in the flow domain. As described in theory (Prandtl, 1905; Gibson et al., 2021), these profiles follow the logarithmic law of the wall.

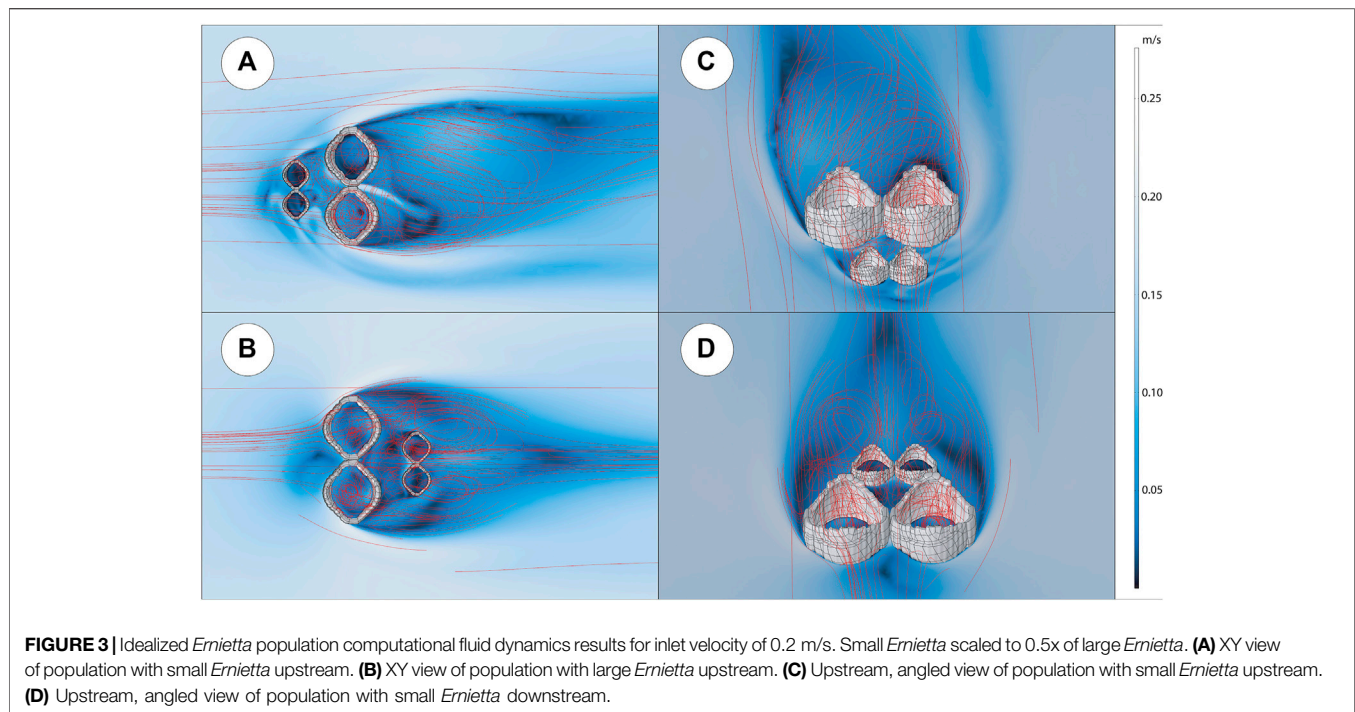
RESULTS

Individual Results

As shown in **Figure 2**, both the small and large *Ernietta* individual flow patterns show patterns consistent with CFD descriptions elsewhere (Gibson et al., 2019; 2021). In the small individual simulations, flow enters the cavity from above, is directed to the downstream interior face, and is then forced upstream toward the interior and upstream face, where it is finally directed out of the cavity by mixing with the current above the cavity. A wake of slower, more turbulent water is formed directly downstream of the individual. These patterns are stronger or weaker with faster and slower far field velocities, respectively. The larger individual developed the same patterns of recirculation within the cavity and downstream with a similar relationship between recirculation speed and far field velocity, but the velocities and mixing were greater than those experienced by the smaller individual.

Idealized Populations Results

Figure 3 show the results for each of the idealized population CFD studies. In all simulations, there is recirculation in both large and small individuals in the population simulation, though



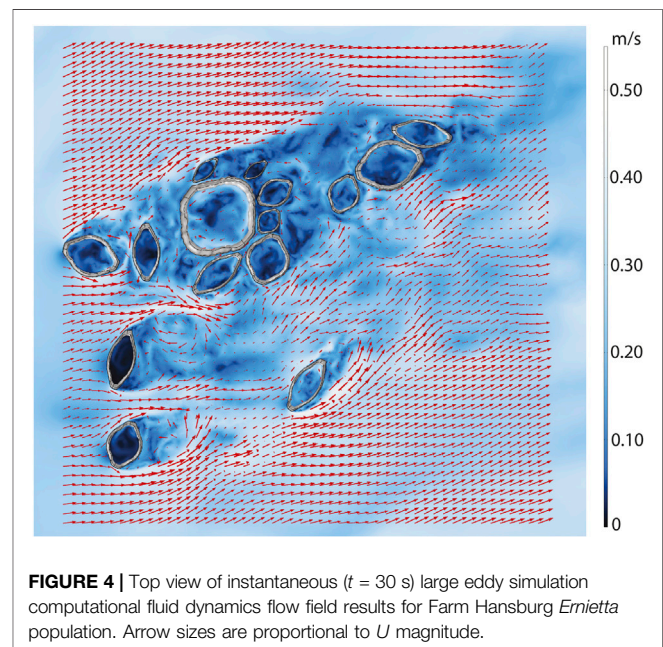
absolute velocities vary depending on size, location, and proximity to neighbouring individuals. Cavity velocities are always slower than the far field velocities, and there is a higher-pressure region upstream of the population where fluid is directed around and over the aggregate. A wake is also formed downstream of the population in all simulations.

Smaller Upstream

Slower velocities are observed in cavities of the smaller individuals found upstream (**Figures 3A,C**), while faster velocities are observed in the larger, downstream ones. At the slowest far field velocity (0.1 m/s), small cavities are mostly stagnant upstream. This stagnation decreases when the prescribed flow is increased (0.2 m/s and further at 0.5 m/s). In the larger downstream individuals, flow velocities are faster with minimal stagnation in the lower region of the cavity, regardless of far field velocity. In between the upstream and downstream individuals, there are areas of recirculation that increase in velocity as the far field velocity increases. Vortex shedding occurs on the downstream exterior surfaces, where eddies form and travel downstream in an alternating von Kármán vortex street fashion. As these are stationary solutions, this asymmetry likely results from individual placement as well as asymmetry within the individual *Ernietta* model.

Smaller Downstream

When smaller *Ernietta* are placed downstream of larger individuals (**Figures 3B,D**), consistent cavity recirculation is still present in both upstream and downstream individuals. On average, the larger, upstream individuals experience faster cavity velocities than downstream smaller individuals with a low



velocity core within the larger individuals' cavities. Downstream individuals experience this same pattern at reduced velocities. The viscous sublayer and turbulent boundary layer are disrupted by the large, upstream individuals, where flow is directed between and around these individuals. Vortices are shed off of the downstream face of the larger upstream individuals, where flow then reattaches to the no-slip seafloor downstream of the smaller individuals. This

leads to a recirculation of water upstream towards the smaller individuals as evidenced by the streamlines. Lastly, there is less asymmetry in the downstream wake compared to the simulations where the smaller *Ernietta* are translated upstream of the larger individuals.

In-Situ Hansburg Population Results

Figure 4 and **Supplementary Figure S4** show that flow patterns within the reconstructed Hansburg slab broadly follow those described for idealized arrays, with some key distinctions. All individuals receive recirculation within their cavities, and these cavity velocities are reduced compared to the far field velocity. While there is consistent mixing within cavities, most fluid is preferentially directed around and above individuals. Slower velocities are observed in upstream individuals, while faster velocities are observed within the aggregations and within the downstream individuals' cavities. Smaller *Ernietta* within the aggregate that are located directly downstream of the largest individual consistently receive fast recirculation—faster than even larger individuals located closer to the upstream face of the largest individual (**Figure 4**; **Supplementary Figure S4**). Narrow individuals have slower cavity velocities. Eddies are shed off of all individuals, but orientation to flow, individual shape, and individual location dictate how far downstream eddies persist. Narrow individuals that are oriented broad-side into flow typically exhibit rapid mixing, including upstream recirculation directly behind the individual, while the wakes of those individuals that form part of aggregates are typically disrupted by wakes of neighbouring individuals, leading to additional turbulence. Isolated individuals typically develop small vortex streets that are disrupted by individuals further downstream.

DISCUSSION

The effect of individual size on flow patterns varied with the quantity and arrangement of individuals. In single *Ernietta* simulations, smaller sized individuals developed lower amounts of recirculation. This observation is mirrored in idealized populations, suggesting a potential size control on intra-specific competition, whereby larger individuals should consistently receive greater volumes of fluid required for feeding. However, on the reconstructed Hansburg slab (**Figure 4**, **Supplementary Figure S4**) reconstructed flow patterns illustrate that the disadvantage associated with small size is apparently mediated by location within the overall aggregation, suggesting a complex interplay of controls on feeding efficiency, and thus individual success. Below we discuss how the flow pattern results presented here compare with previous CFD studies, both for individuals and idealized populations. We then compare the results of the idealized populations with those of the Hansburg slab to detail ecological signals that emerge from both. Finally, we use these results to address previously suggested hypotheses regarding *Ernietta* paleobiological reconstructions.

Individuals and Idealized Populations vs Previous Work

Previous CFD analyses on *Ernietta* individuals and idealized populations investigated how burial depth and individual spacing may have controlled feeding efficiency (Gibson et al., 2019). This work demonstrated that turbulence increased above downstream individuals in addition to generating faster recirculation within the cavities of the same individuals (see Gibson et al., 2019 **Figure 3**), suggesting that the facultatory lifestyle exhibited by *Ernietta* may have imparted a selective advantage for feeding and waste dispersion. While the new CFD results targeting individuals of mixed sizes presented here broadly support the previous results regarding cavity recirculation and suspension feeding, these new data provide additional insights that were not available in the previous analyses. Recirculation is faster within the cavity of larger individuals than in smaller ones, regardless of far field velocity. This indicates that a greater volume of fluid should cycle through larger individuals, potentially delivering larger quantities of food. Also, these new idealized population simulation results partially agree with previous work suggesting that mixing is increased above and within the cavities of downstream individuals. This agreement is strongest for simulations where the larger individuals are downstream of the smaller ones. When smaller individuals were upstream of larger individuals, they received slower velocities than those that were placed downstream (**Figure 3**). Interestingly, our results demonstrate that the locations of smaller individuals in idealized populations of *Ernietta* directly affect flow patterns, and thus impact our interpretation of their feeding efficiency. In idealized populations constructed with smaller individuals downstream of larger individuals (**Figure 3**), smaller individuals experience slower cavity recirculation than the larger individuals (*contra* Gibson et al., 2019). Based on these comparisons, this would signal that, while vertical mixing is enhanced above aggregations of similarly sized *Ernietta*, those individuals that are smaller and downstream of larger ones might be flow starved compared to the larger individuals. These idealized populations would then suggest that it might be optimal for *Ernietta* to form populations of similarly-sized individuals, (i.e., as single cohorts that result from reproduction with spat-fall, however, see below).

Idealized Populations Compared to Hansburg Population

Previous studies have noted that individual *Ernietta* fossils can vary in shape, with authors attributing these shape variations to a combination of individual growth response to the local environment and/or taphonomy (Elliott et al., 2016; Ivantsov et al., 2016; Smith et al., 2017). In our idealized population models, individuals were identical in shape but were binarily scaled. While cavity velocity magnitudes differed depending on location, the overall recirculation patterns were still comparable between simulations. In contrast, our Hansburg individuals were asymmetrically scaled to better approximate the spatial

reconstruction of the Farm Hansburg *in-situ* population (**Supplementary Figure S1**). Those results demonstrate cavity and downstream flow patterns are strongly affected by overall individual shape (e.g., slender vs round). Slender individuals receive slower and more asymmetric recirculation compared to rotund individuals. These patterns were present within aggregated and isolated individuals, indicating that overall shape exerts a strong control over internal cavity flow. There may, therefore, have been strong selective pressure for individuals to grow with a more uniform cavity diameter, as evident in many *Ernietta* deposits (see figures and descriptions from Jenkins et al., 1981; Ivantsov et al., 2016; Elliott et al., 2016; Smith et al., 2017), while cavity filling by deposited sediment would serve to retain the overall oval to circular shape of the cavity.

Our results also show that an individual's location (or proximity) to neighbors is an equally important control on the generation of flow patterns thought to be important for feeding. Isolated individuals within our Hansburg population experience slower cavity recirculation even when having a more uniform cavity diameter (**Figure 4; Supplementary Figure S4**), while aggregated individuals experience comparatively faster cavity recirculation. Flow patterns around our individual *Ernietta* and idealized arrays (*Individuals and Idealized Populations vs Previous Work*) suggest that smaller individuals experience slower cavity velocities when downstream of larger individuals. However, our Hansburg population results demonstrate that even when smaller individuals were placed immediately downstream of larger individuals, the smaller individuals were constantly exposed to faster velocity flow when compared to isolated forms. At first impression this appears contradictory, but it may highlight the importance of modeling natural systems as opposed to overly simplified (i.e., idealized) ones. Furthermore, our reconstructed population simulations agree with previous results that demonstrated increased mixing above and within downstream cavities (Gibson et al., 2019). This suggests that smaller individuals within aggregates are not hampered when behind a larger individual, but in fact are likely to receive more and better-mixed fluid flow. Thus, while it is less advantageous for an individual to be near the edge of the aggregation, smaller individuals would likely gain access to additional resources that they might not otherwise receive should they be on the edge of the population, or entirely isolated. While little is known about the ontogenetic history of *Ernietta*, it is reasonable to assume that younger individuals would be smaller; our results suggest that there would thus have been an advantage to settling, or living near, larger individuals within the greater population. In this fashion, aggregations of adult *Ernietta* would likely have performed a “nursery” function, creating localized conditions favoring the settlement and growth of younger individuals.

This complex interplay of controls on individual feeding success has some parallels in extant benthic marine ecosystems. Studies focused on intraspecific competition arising from spatial density within populations of sessile suspension feeders demonstrate that, in multi-sized aggregations, intraspecific competition can affect both individual size and spatial distribution (Werner and Gilliam, 1984). When different sizes preferentially exploit disparate

resources, the competition between adults and juveniles is reduced (Werner and Gilliam, 1984). However, in such cases where exploited resources overlap as is plausible with *Ernietta*—and size does determine the outcome of competition, younger individuals are often less successful due to metabolic constraints (Peters, 1983). Importantly, the magnitude of this general relationship is greatly influenced by resource availability. While a paucity of resources does typically lead to increased competition, when resources are abundant this can decrease levels of exploitative competition (Hazlett et al., 1975; Werner and Gilliam, 1984). This distinction is important when applying these models to Ediacaran-aged communities in Namibia; recent geochemical work on the Nama Group suggests large scale unstable redox conditions accompanied by decreasing nutrient delivery to inner ramp habitats where *Ernietta* are typically found (Bowyer et al., 2017; 2020). In combination with the evidence presented here for relatively low-levels of intraspecific competition, this would indicate that populations of *Ernietta* on Farm Hansburg either: 1) locally received short-lived, adequate nutrient levels to offset multi-sized intraspecific competition; or, 2) *Ernietta* was an ecological generalist not endemic to oxygenated, nutrient-saturated environments (Darroch et al., 2018b).

Broader Speculation on the Paleobiology of *Ernietta*

While our simulations were designed as an extension of recent work (Gibson et al., 2019, 2021) with the goal of moving towards reconstructing fluid flow over spatially-accurate 3D populations of Ediacaran taxa, they do allow us to evaluate other hypotheses regarding the paleobiology and life habit of *Ernietta*. For example, Bouougri et al. (2011) suggested that living *Ernietta* may have been covered in a slime or mucus layer, based on the orientation of sediment detrital mica flakes associated with fossil molds. While our results cannot support or refute this suggestion, our simulations do at least show that recirculation in the wakes of individual *Ernietta* would provide one possible mechanism for fine-grained sediment (presumably together with suspended food particles) delivery to downstream surfaces. Given that many modern suspension feeding organisms make use of mucus nets and other structures as a means for capturing food particles (see discussion of aerosol capture mechanisms in Rubenstein and Koehl, 1977; and LaBarbera, 1984), we suggest that an external slime- or mucus-covered surface could have been used to capture suspended particulate material, and which could then have been sorted and/or transported to other feeding organs (see, for example, LaBarbera, 1978). However, without additional evidence for mucus membranes, or indeed any other evidence revealing how food particles are ingested and processed, this model remains highly speculative.

In a similar vein, Ivantsov et al. (2016) suggested that the “apical fan” of *Ernietta* (i.e., the portion of the organism raised into the water column) may have been used for respiration. While no previous CFD studies have interpreted this anatomy in the context of respiration, many of the flow patterns modelled around

Ernietta could have been useful for bringing oxygen-rich water closer to respiratory organs. The increased turbulence modelled in these areas could plausibly have served to replenish dissolved gases, as well as diffuse any exhalants. Although we cannot directly address hypotheses surrounding respiration without substantially adjusting the methods employed here, future coupling of fluid dynamics simulations with oxygen diffusion/uptake models (see, for example, Ghisalberti et al., 2014) may offer an elegant means to test this idea. Future work using this combination of methods could plausibly be used to test the hypothesis that *Ernietta* was opportunistic, and able to colonize shallow marine environments that were only transiently oxygenated (see Hall et al., 2013; Bowyer et al., 2020).

Summary

Previous paleoecological work focused on the latest Ediacaran Nama interval has suggested that communities of soft-bodied Ediacara biota were relatively depauperate, possessing lower species richness than older Ediacaran communities, as well as having relatively “simple” structures consistent with either competition for a limited number of ecological resources and/or ecological stress (Darroch et al., 2015; 2018a,b). This study adds nuance to this picture, illustrating that, while species poor and relatively simple, the structure of Nama-aged erniettomorph communities was likely influenced by a wide-range of intraspecific ecological factors, including size, location, and (potentially) developmental stage. In this study, we show that individual size and location within a population can have large effects on flow within and around the body cavities, affecting their access to nutrients and well-mixed water. Given the lack of any evidence for asexual reproductive modes such as budding in *Ernietta*, it is reasonable to hypothesize that these factors might have been crucial during the recruitment and settlement of new individuals. In addition, while not directly assessed here, our flow patterns showing increased fluid delivery downstream of larger individuals also suggests a potential ‘nursery’ effect, with competition for space adjacent to larger *Ernietta*. Many of these density-dependent factors continue to influence the structure of communities in today’s oceans (Caley et al., 1996; Gilmour, 1999; Harrington et al., 2004), and so reinforce the point that, while we still have little idea where taxa like *Ernietta* fit (if at all) in the metazoan tree of life, in many respects they experienced similar ecological pressures—and may have utilized similar ecological strategies—as modern benthic marine organisms.

REFERENCES

- Bardina, J. E., Huang, P. G., and Coakley, T. J. (1997). Turbulence Modeling Validation, Testing, and Development. *NASA Tech. Memorandum* 110446, 1–88. doi:10.2514/6.1997-2121
- Bertness, M. D., Gaines, S., Bermudez, D., and Sanford, E. (1991). Extreme Spatial Variation in the Growth and Reproductive Output of the Acorn Barnacle *Semibalanus balanoides*. *Mar. Ecol. Prog. Ser.* 75, 91–100. doi:10.3354/meps075091
- Bertness, M. D., and Grosholz, E. (1985). Population Dynamics of the Ribbed Mussel, *Geukensia demissa*: the Costs and Benefits of an Aggregated Distribution. *Oecologia* 67, 192–204. doi:10.1007/bf00384283

DATA AVAILABILITY STATEMENT

The raw data supporting the conclusion of this article will be made available by the authors, without undue reservation.

AUTHOR CONTRIBUTIONS

All authors collected field measurements and contributed in writing to this work. BMG and ML generated the digital reconstruction, and BMG conducted the fluid simulations.

FUNDING

BG received funding from the University of Toronto Mississauga Postdoctoral Fellowship Award and Vanderbilt University’s Alberstadt, Reeseman, and Sterns grant. SD acknowledges NSF-NERC EAR 2007928, National Geographic 9968–16, and a Paleontological Society Arthur J. Boucot Award. SD also acknowledges generous support from the Alexander von Humboldt Foundation, which is sponsored by the Federal Ministry for Education and Research in Germany. KM was supported by the Natural Sciences and Engineering Research Council of Canada (NSERC) postgraduate scholarship and the Chemical and Physical Sciences Research Visit Program (University of Toronto Mississauga). ML was funded by the NSERC Discovery Grant (RGPIN 435402) and National Geographic 9241–14.

ACKNOWLEDGMENTS

We thank B. Viljoen and L. Viljoen for their hospitality and access to field sites; D. Furbish, M. Schmeeckle, and I. Rahman for fluid mechanics discussions; G. Gualda for access to computational workstations.

SUPPLEMENTARY MATERIAL

The Supplementary Material for this article can be found online at: <https://www.frontiersin.org/articles/10.3389/feart.2021.749150/full#supplementary-material>

- Blazek, J. (2001). *Computational Fluid Dynamics: Principles and Applications*. Amsterdam: Elsevier.
- Boag, T. H., Darroch, S. A. F., and Laflamme, M. (2016). Ediacaran Distributions in Space and Time: Testing Assemblage Concepts of Earliest Macroscopic Body Fossils. *Paleobiology* 42, 574–594. doi:10.1017/pab.2016.20
- Boddy, C. E., Mitchell, E. G., Merdith, A., and Liu, A. G. (2021). Palaeolatitudinal Distribution of the Ediacaran Macrobiota. *J. Geol. Soc.*, jgs2021-030. doi:10.1144/jgs2021-030
- Bouougri, E. H., Porada, H., Weber, K., and Reitner, J. (2011). “Sedimentology and Palaeoecology of *Ernietta*-Bearing Ediacaran Deposits in Southern Namibia: Implications for Infaunal Vendobiont Communities,” in *Advances in Stromatolite Geobiology*. Editors J. Reitner, N.V. Quéric, and A. Gernot (Berlin, Heidelberg): Springer, 473–506. doi:10.1007/978-3-642-10415-2_29

- Bowyer, F. T., Shore, A. J., Wood, R. A., Alcott, L. J., Thomas, A. L., Butler, I. B., et al. (2020). Regional Nutrient Decrease Drove Redox Stabilisation and Metazoan Diversification in the Late Ediacaran Nama Group, Namibia. *Sci. Rep.* 10, 1–11. doi:10.1038/s41598-020-59335-2
- Bowyer, F., Wood, R. A., and Poulton, S. W. (2017). Controls on the Evolution of Ediacaran Metazoan Ecosystems: A Redox Perspective. *Geobiology* 15, 516–551. doi:10.1111/gbi.12232
- Caley, M. J., Carr, M. H., Hixon, M. A., Hughes, T. P., Jones, G. P., and Menge, B. A. (1996). Recruitment and the Local Dynamics of Open marine Populations. *Annu. Rev. Ecol. Syst.* 27, 477–500. doi:10.1146/annurev.ecolsys.27.1.477
- Clapham, M. E., and Narbonne, G. M. (2002). Ediacaran Epifaunal Tiering. *Geol.* 30, 627–630. doi:10.1130/0091-7613(2002)030<0627:et>2.0.co;2
- Clapham, M. E., Narbonne, G. M., and Gehling, J. G. (2003). Paleoeology of the Oldest Known Animal Communities: Ediacaran Assemblages at Mistaken Point, Newfoundland. *Paleobiology* 29, 527–544. doi:10.1666/0094-8373(2003)029<0527:potoka>2.0.co;2
- Darroch, S. A. F., Cribb, A. T., Buatois, L. A., Germs, G. J. B., Kenchington, C. G., Smith, E. F., et al. (2021). The Trace Fossil Record of the Nama Group, Namibia: Exploring the Terminal Ediacaran Roots of the Cambrian Explosion. *Earth-Science Rev.* 212, 103435. doi:10.1016/j.earscirev.2020.103435
- Darroch, S. A. F., Laflamme, M., and Clapham, M. E. (2013). Population Structure of the Oldest Known Macroscopic Communities from Mistaken Point, Newfoundland. *Paleobiology* 39, 591–608. doi:10.1666/12051
- Darroch, S. A. F., Laflamme, M., and Wagner, P. J. (2018a). High Ecological Complexity in Benthic Ediacaran Communities. *Nat. Ecol. Evol.* 2, 1541–1547. doi:10.1038/s41559-018-0663-7
- Darroch, S. A. F., Smith, E. F., Laflamme, M., and Erwin, D. H. (2018b). Ediacaran Extinction and Cambrian Explosion. *Trends Ecol. Evol.* 33, 653–663. doi:10.1016/j.tree.2018.06.003
- Darroch, S. A. F., Sperling, E. A., Boag, T. H., Racicot, R. A., Mason, S. J., Morgan, A. S., et al. (2015). Biotic Replacement and Mass Extinction of the Ediacara Biota. *Proc. R. Soc. B.* 282, 20151003. doi:10.1098/rspb.2015.1003
- Doropoulos, C., Evensen, N. R., Gómez-Lemos, L. A., and Babcock, R. C. (2017). Density-dependent Coral Recruitment Displays Divergent Responses during Distinct Early Life-History Stages. *R. Soc. Open Sci.* 4, 170082. doi:10.1098/rsos.170082
- Droser, M. L., Tarhan, L. G., and Gehling, J. G. (2017). The Rise of Animals in a Changing Environment: Global Ecological Innovation in the Late Ediacaran. *Annu. Rev. Earth Planet. Sci.* 45, 593–617. doi:10.1146/annurev-earth-063016-015645
- Elliott, D. A., Trusler, P. W., Narbonne, G. M., Vickers-Rich, P., Morton, N., Hall, M., et al. (2016). Ernieeta from the Late Ediacaran Nama Group, Namibia. *J. Paleontol.* 90, 1017–1026. doi:10.1017/jpa.2016.94
- Gaines, S., and Roughgarden, J. (1985). Larval Settlement Rate: a Leading Determinant of Structure in an Ecological Community of the marine Intertidal Zone. *Proc. Natl. Acad. Sci.* 82, 3707–3711. doi:10.1073/pnas.82.11.3707
- Gehling, J. G., and Droser, M. L. (2013). How Well Do Fossil Assemblages of the Ediacara Biota Tell Time? *Geology* 41, 447–450. doi:10.1130/g33881.1
- Gehling, J. G. (1999). Microbial Mats in Terminal Proterozoic Siliciclastics: Ediacaran Death Masks. *Palaio* 14, 40–57. doi:10.2307/3515360
- Ghisalberti, M., Gold, D. A., Laflamme, M., Clapham, M. E., Narbonne, G. M., Summons, R. E., et al. (2014). Canopy Flow Analysis Reveals the Advantage of Size in the Oldest Communities of Multicellular Eukaryotes. *Curr. Biol.* 24, 305–309. doi:10.1016/j.cub.2013.12.017
- Gibson, B. M., Furbish, D. J., Rahman, I. A., Schmeeckle, M. W., Laflamme, M., and Darroch, S. A. F. (2021). Ancient Life and Moving Fluids. *Biol. Rev.* 96, 129–152. doi:10.1111/brv.12649
- Gibson, B. M., Rahman, I. A., Maloney, K. M., Racicot, R. A., Mocke, H., Laflamme, M., et al. (2019). Gregarious Suspension Feeding in a Modular Ediacaran Organism. *Sci. Adv.* 5, eaaw0260. doi:10.1126/sciadv.aaw0260
- Gilmour, J. (1999). Experimental Investigation into the Effects of Suspended Sediment on Fertilisation, Larval Survival and Settlement in a Scleractinian Coral. *Mar. Biol.* 135, 451–462. doi:10.1007/s002270050645
- Grazhdankin, D. (2014). Patterns of Evolution of the Ediacaran Soft-Bodied Biota. *J. Paleontol.* 88, 269–283. doi:10.1666/13-072
- Grazhdankin, D. (2004). Patterns of Distribution in the Ediacaran Biotas: Facies versus Biogeography and Evolution. *Paleobiology* 30, 203–221. doi:10.1666/0094-8373(2004)030<0203:podite>2.0.co;2
- Hall, C. M. S., Droser, M. L., Gehling, J. G., and Dzaugis, M. E. (2015). Paleoeology of the Enigmatic *Tribrachidium*: New Data from the Ediacaran of South Australia. *Precambrian Res.* 269, 183–194. doi:10.1016/j.precamres.2015.08.009
- Hall, M., Kaufman, A. J., Vickers-Rich, P., Ivantsov, A., Trusler, P., Linnemann, U., et al. (2013). Stratigraphy, Palaeontology and Geochemistry of the Late Neoproterozoic Aar Member, Southwest Namibia: Reflecting Environmental Controls on Ediacara Fossil Preservation during the Terminal Proterozoic in African Gondwana. *Precambrian Res.* 238, 214–232. doi:10.1016/j.precamres.2013.09.009
- Harrington, L., Fabricius, K., De'ath, G., and Negri, A. (2004). Recognition and Selection of Settlement Substrata Determine post-settlement Survival in Corals. *Ecology* 85, 3428–3437. doi:10.1890/04-0298
- Hazlett, B. A., Rubenstein, D., and Rittschof, D. (1975). Starvation, Energy Reserves, and Aggression in the Crayfish *Orconectes Virilis* (Hagen, 1870) (Decapoda, Cambaridae). *Crustaceana* 28, 11–16.
- Hixon, M. A., Pacala, S. W., and Sandin, S. A. (2002). Population Regulation: Historical Context and Contemporary Challenges of Open vs. Closed Systems. *Ecology* 83, 1490–1508. doi:10.2307/3071969
- Ivantsov, A. Y., Narbonne, G. M., Trusler, P. W., Greentree, C., and Vickers-Rich, P. (2016). Elucidating Ernieeta: New Insights from Exceptional Specimens in the Ediacaran of Namibia. *Lethaia* 49, 540–554. doi:10.1111/let.12164
- Jenkins, R. J. F. (1992). “Functional and Ecological Aspects of Ediacaran Assemblages,” in *Origin and Early Evolution of the Metazoa*. Editors J.H. Lipps and P.W. Signor (New York: Plenum Press), 131–176. doi:10.1007/978-1-4899-2427-8_5
- Jenkins, R. J. F., Plummer, P. S., and Moriarty, K. C. (1981). Late Precambrian Pseudofossils from the Flinders Ranges, South Australia. *Trans. R. Soc. South Aust.* 105, 67–83.
- Knoll, A., Walter, M., Narbonne, G., and Christie-Blick, N. (2006). The Ediacaran Period: a New Addition to the Geologic Time Scale. *Lethaia* 39, 13–30. doi:10.1080/00241160500409223
- LaBarbera, M. (1984). Feeding Currents and Particle Capture Mechanisms in Suspension Feeding Animals. *Am. Zool.* 24, 71–84. doi:10.1093/icb/24.1.71
- LaBarbera, M. (1978). Particle Capture by a Pacific Brittle star: Experimental Test of the Aerosol Suspension Feeding Model. *Science* 201, 1147–1149. doi:10.1126/science.201.4361.1147
- Laflamme, M., Darroch, S. A. F., Tweedt, S. M., Peterson, K. J., and Erwin, D. H. (2013). The End of the Ediacara Biota: Extinction, Biotic Replacement, or Cheshire Cat? *Gondwana Res.* 23, 558–573. doi:10.1016/j.gr.2012.11.004
- Leonard, G. H., Levine, J. M., Schmidt, P. R., and Bertness, M. D. (1998). Flow-driven Variation in Intertidal Community Structure in a Maine Estuary. *Ecology* 79, 1395–1411. doi:10.1890/0012-9658(1998)079[1395:fdvii]2.0.co;2
- Linden, B., and Rinkevich, B. (2017). Elaborating an Eco-Engineering Approach for Stock Enhanced Sexually Derived Coral Colonies. *J. Exp. Mar. Biol. Ecol.* 486, 314–321. doi:10.1016/j.jembe.2016.10.014
- Liu, A. G., Kenchington, C. G., and Mitchell, E. G. (2015). Remarkable Insights into the Paleoeology of the Avalonian Ediacaran Macrobiota. *Gondwana Res.* 27, 1355–1380. doi:10.1016/j.gr.2014.11.002
- Maloney, K. M., Boag, T. H., Faccioli, A. J., Gibson, B. M., Cribb, A., Koester, B. E., et al. (2020). Paleoenvironmental Analysis of Ernieeta-Bearing Ediacaran Deposits in Southern Namibia. *Palaeogeogr. Palaeoclimatol. Palaeoecol.* 556, 109884. doi:10.1016/j.palaeo.2020.109884
- Meyer, M., Elliott, D., Schiffbauer, J. D., Hall, M., Hoffman, K. H., Schneider, G., et al. (2014). Taphonomy of the Ediacaran Fossil *Pteridinium Simplex* Preserved Three-Dimensionally in Mass Flow Deposits, Nama Group, Namibia. *J. Paleontol.* 88, 240–252. doi:10.1666/13-047
- Mitchell, E. G., and Butterfield, N. J. (2018). Spatial Analyses of Ediacaran Communities at Mistaken Point. *Paleobiology* 44, 40–57. doi:10.1017/pab.2017.35
- Mitchell, E. G., Kenchington, C. G., Harris, S., and Wilby, P. R. (2018). Revealing Rangeomorph Species Characters Using Spatial Analyses. *Can. J. Earth Sci.* 55, 1262–1270. doi:10.1139/cjes-2018-0034

- Mitchell, E. G., Kenchington, C. G., Liu, A. G., Matthews, J. J., and Butterfield, N. J. (2015). Reconstructing the Reproductive Mode of an Ediacaran Macro-Organism. *Nature* 524, 343–346. doi:10.1038/nature14646
- Mitchell, E. G., and Kenchington, C. G. (2018). The Utility of Height for the Ediacaran Organisms of Mistaken Point. *Nat. Ecol. Evol.* 2, 1218–1222. doi:10.1038/s41559-018-0591-6
- Muscente, A. D., Bykova, N., Boag, T. H., Buatois, L. A., Mángano, M. G., Eleish, A., et al. (2019). Ediacaran Biozones Identified with Network Analysis Provide Evidence for Pulsed Extinctions of Early Complex Life. *Nat. Commun.* 10, 911. doi:10.1038/s41467-019-08837-3
- Narbonne, G. M. (2005). The Ediacara Biota: Neoproterozoic Origin of Animals and Their Ecosystems. *Annu. Rev. Earth Planet. Sci.* 33, 421–442. doi:10.1146/annurev.earth.33.092203.122519
- Pepin, P. (1991). Effect of Temperature and Size on Development, Mortality, and Survival Rates of the Pelagic Early Life History Stages of marine Fish. *Can. J. Fish. Aquat. Sci.* 48, 503–518. doi:10.1139/f91-065
- Peters, R. H. (1983). *The Ecological Implications of Body Size*. Cambridge: Cambridge University Press.
- Prandtl, L. (1905). “über Flüssigkeitsbewegung bei sehr kleiner Reibung,” in *Verhandlungen des III Internationalen Mathematiker Kongresses* (Heidelberg/Leipzig, 1904, 484–491).
- Rahman, I. A. (2017). Computational Fluid Dynamics as a Tool for Testing Functional and Ecological Hypotheses in Fossil Taxa. *Palaeontology* 60, 451–459. doi:10.1111/pala.12295
- Raimondi, P. T. (1990). Patterns, Mechanisms, Consequences of Variability in Settlement and Recruitment of an Intertidal Barnacle. *Ecol. Monogr.* 60, 283–309. doi:10.2307/1943059
- Raymundo, L. J., and Maypa, A. P. (2004). Getting Bigger Faster: Mediation of Size-specific Mortality via Fusion in Juvenile Coral Transplants. *Ecol. Appl.* 14, 281–295. doi:10.1890/02-5373
- Rubenstein, D. I., and Koehl, M. A. R. (1977). The Mechanisms of Filter Feeding: Some Theoretical Considerations. *The Am. Naturalist* 111, 981–994. doi:10.1086/283227
- Seilacher, A., and Gishlick, A. D. (2014). “Vendobionts: Lost Life Forms of Ediacaran Times,” in *Morphodynamics*. Editors A. Seilacher and A.D. Gishlick (Boca Raton: CRC Press, Taylor & Francis Group), 133–148. doi:10.1201/b17557-16
- Seilacher, A., Grazhdankin, D., and Legouta, A. (2003). Ediacaran Biota: The Dawn of Animal Life in the Shadow of Giant Protists. *Paleontological Res.* 7, 43–54. doi:10.2517/prpsj.7.43
- Seilacher, A. (1992). Vendobionta and Psammocorallia: Lost Constructions of Precambrian Evolution. *J. Geol. Soc.* 149, 607–613. doi:10.1144/gsjgs.149.4.0607
- Shen, B., Dong, L., Xiao, S., and Kowalewski, M. (2008). The Avalon Explosion: Evolution of Ediacara Morphospace. *Science* 319, 81–84. doi:10.1126/science.1150279
- Smith, E. F., Nelson, L. L., Tweedt, S. M., Zeng, H., and Workman, J. B. (2017). A Cosmopolitan Late Ediacaran Biotic Assemblage: New Fossils from Nevada and Namibia Support a Global Biostratigraphic Link. *Proc. R. Soc. B.* 284, 20170934. doi:10.1098/rspb.2017.0934
- Sperling, E. A., Carbone, C., Strauss, J. V., Johnston, D. T., Narbonne, G. M., and Macdonald, F. A. (2016). Oxygen, Facies, and Secular Controls on the Appearance of Cryogenian and Ediacaran Body and Trace Fossils in the Mackenzie Mountains of Northwestern Canada. *Geol. Soc. America Bull.* 128, 558–575. doi:10.1130/b31329.1
- Vaziri, S. H., Majidifard, M. R., Darroch, S. A. F., and Laflamme, M. (2021). Ediacaran Diversity and Paleocology from central Iran. *J. Paleontol.* 95, 236–251. doi:10.1017/jpa.2020.88
- Vermeij, M. J. A., and Sandin, S. A. (2008). Density-dependent Settlement and Mortality Structure the Earliest Life Phases of a Coral Population. *Ecology* 89, 1994–2004. doi:10.1890/07-1296.1
- Waggoner, B. (2003). The Ediacaran Biotas in Space and Time. *Integr. Comp. Biol.* 43, 104–113. doi:10.1093/icb/43.1.104
- Werner, E. E., and Gilliam, J. F. (1984). The Ontogenetic Niche and Species Interactions in Size-Structured Populations. *Annu. Rev. Ecol. Syst.* 15, 393–425. doi:10.1146/annurev.es.15.110184.002141
- White, J. W. (2007). Spatially Correlated Recruitment of a marine Predator and its Prey Shapes the Large-Scale Pattern of Density-dependent Prey Mortality. *Ecol. Lett.* 10, 1054–1065. doi:10.1111/j.1461-0248.2007.01098.x
- Wood, R. A., Poulton, S. W., Prave, A. R., Hoffmann, K.-H., Clarkson, M. O., Guilbaud, R., Lyne, J. W., Tostevin, R., Bowyer, F., Penny, A. M., and Curtis, A., and (2015). Dynamic Redox Conditions Control Late Ediacaran Metazoan Ecosystems in the Nama Group, Namibia. *Precambrian Res.* 261, 252–271. doi:10.1016/j.precamres.2015.02.004
- Xiao, S., and Laflamme, M. (2009). On the Eve of Animal Radiation: Phylogeny, Ecology and Evolution of the Ediacara Biota. *Trends Ecol. Evol.* 24, 31–40. doi:10.1016/j.tree.2008.07.015

Conflict of Interest: The authors declare that the research was conducted in the absence of any commercial or financial relationships that could be construed as a potential conflict of interest.

The handling Editor declared a past co-authorship with the authors KM, ML.

Publisher's Note: All claims expressed in this article are solely those of the authors and do not necessarily represent those of their affiliated organizations, or those of the publisher, the editors, and the reviewers. Any product that may be evaluated in this article, or claim that may be made by its manufacturer, is not guaranteed or endorsed by the publisher.

Copyright © 2021 Gibson, Darroch, Maloney and Laflamme. This is an open-access article distributed under the terms of the Creative Commons Attribution License (CC BY). The use, distribution or reproduction in other forums is permitted, provided the original author(s) and the copyright owner(s) are credited and that the original publication in this journal is cited, in accordance with accepted academic practice. No use, distribution or reproduction is permitted which does not comply with these terms.



New Species of Macroalgae from Tamengo Formation, Ediacaran, Brazil

Cleber Q. C. Diniz^{1*}, Juliana de Moraes Leme² and Paulo C. Boggiani²

¹Institute of Geosciences, University of São Paulo, São Paulo, Brazil, ²Department of Sedimentary and Environmental Geology, Institute of Geosciences, University of São Paulo, São Paulo, Brazil

OPEN ACCESS

Edited by:

Haijun Song,
China University of Geosciences,
China

Reviewed by:

Katie Maloney,
University of Toronto Mississauga,
Canada
Qin Ye,
China University of Geosciences,
China

*Correspondence:

Cleber Q. C. Diniz
cleber.diniz@hotmail.com.br

Specialty section:

This article was submitted to
Paleontology,
a section of the journal
Frontiers in Earth Science

Received: 28 July 2021

Accepted: 14 September 2021

Published: 29 October 2021

Citation:

Diniz CQC, Leme JM and Boggiani PC
(2021) New Species of Macroalgae
from Tamengo Formation,
Ediacaran, Brazil.
Front. Earth Sci. 9:748876.
doi: 10.3389/feart.2021.748876

The Tamengo Formation (Corumbá Group) is an important Ediacaran stratigraphic unit in South America due to the presence of metazoan fossils and geochemistry data of carbonate rocks, with excellent geochronological delimitation (between 555–541 Ma) obtained by U–Pb dating on volcanic zircons. The present work shows three new species of macroalgae found as carbonaceous compressions and studied for their morphology and taxonomy. All new taxa are characterized as centric macroalgae; *Tamengophyton espinosa* sp. nov. is a fan-shaped alga with striated thalli, dichotomous branches, trichomes with perpendicular growth, and a connecting membrane. *Ladariella hidria* sp. nov. is formed by a set of striated and branched thalli in a cylindrical form with almond-shaped structures in the top. *Ladariophyton veinosa* sp. nov. is characterized by the main growth thallus and an enlarged longitudinal structure at the center. These new occurrences of macroalgae add to the largest life assemblages in the Neoproterozoic of South America, which contributes to documentation of the evolutionary history of macroalgae and the paleoecological settings of the Late Ediacaran.

Keywords: Macroalgae, taxonomy, Ediacaran, Tamengo, Brazil

INTRODUCTION

The evolution of eukaryotic organisms changed the dynamic of the Earth. Even though the timing of their appearance is debated, through the paleontological data and molecular clock analysis, we have an estimative age for the last eukaryotic ancestor appearance between 1.8 and 2.3 Ga in the Paleoproterozoic Era (Hedges et al., 2004; Knoll et al., 2006; Parfrey et al., 2011). These evolutions brought new cellular behaviors, which were capable of sensing and reacting to environmental change (Cohen and McDonald, 2015; Wan and Jekély, 2021). Reaching a higher level of multicellular organization, they could expand and differentiate the cells to adapt to new opportunities.

During the Ediacaran, such new life forms were mainly represented by macroalgae (Bykova et al., 2020). They still are defined as eukaryotic multicellular organisms capable of doing photosynthesis, megascopic with a size larger than 1 mm, and possible to see with the naked eye, whose oldest fossil record dates to the Neoproterozoic (Xiao and Dong, 2006; Tang et al., 2020). Their complexity and diversity have records in China (Xiao et al., 1998), India (Srivastava, 2012), the United States (Rowland and Rodriguez, 2014), Russia (Nagovitsin et al., 2015), Mongolia (Dornbos et al., 2016), and Canada (Maloney et al., 2021). Interacting with other organisms of their time, the macroalgae form biotas, which serve as protection sites or creating oxygen niches (Xiao et al., 2002; Zhao et al., 2004). Here, we present three new species of macroalgae from Mato Grosso do Sul Brazil and discuss their significance to the Ediacaran assemblage from Tamengo Formation and the influence of the depositional process from the Corumbá Group in their preservation.

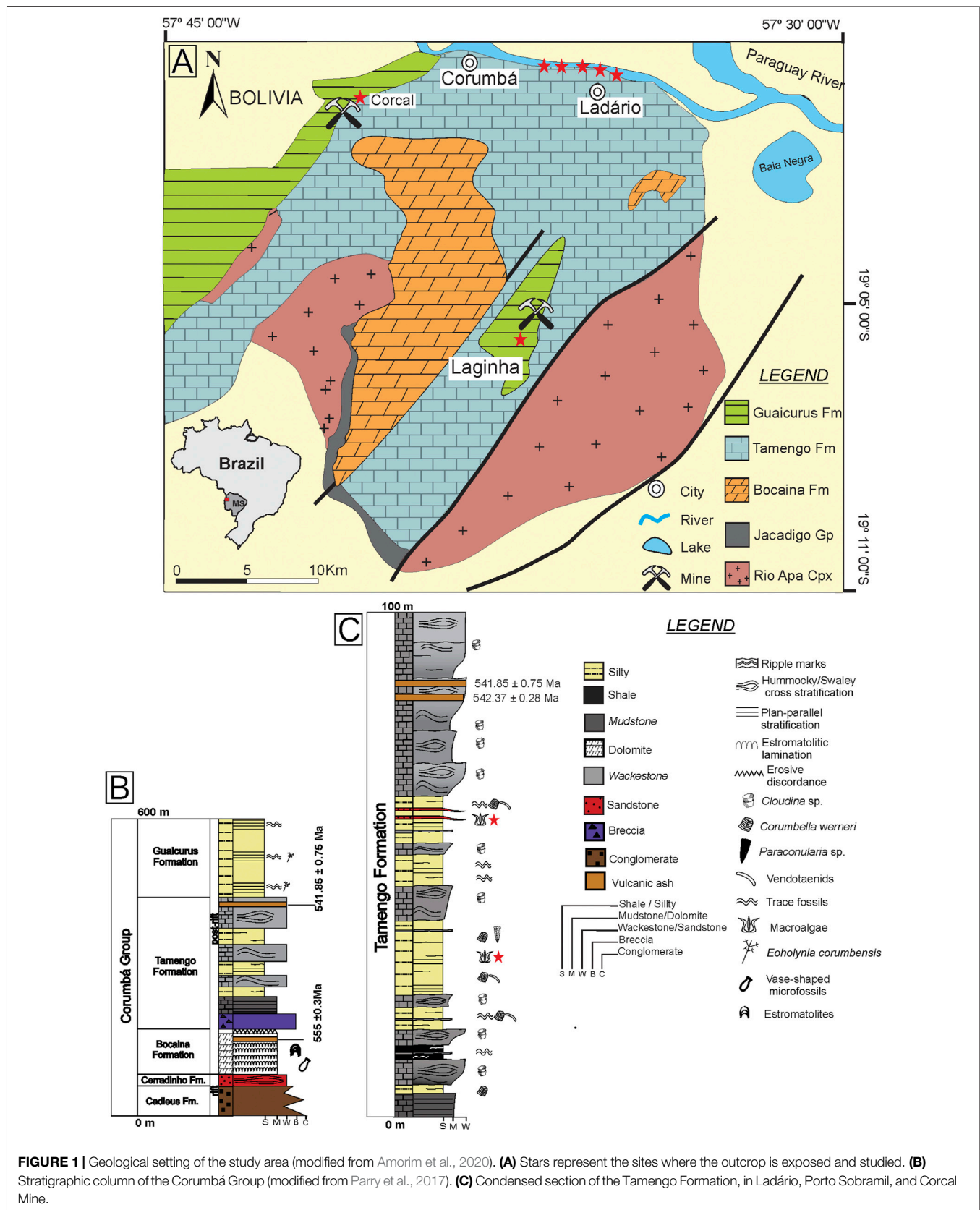


FIGURE 1 | Geological setting of the study area (modified from Amorim et al., 2020). **(A)** Stars represent the sites where the outcrop is exposed and studied. **(B)** Stratigraphic column of the Corumbá Group (modified from Parry et al., 2017). **(C)** Condensed section of the Tamengo Formation, in Ladário, Porto Sobramil, and Corcal Mine.

GEOLOGICAL CONTEXT

The Corumbá Group exposes in Serra da Bodoquena and Corumbá region (**Figure 1A**) (Mato Grosso do Sul State, SW Brazil), close at Urucum Massif. The fossiliferous sites are located in the cities of Corumbá, Ladário, in mines and at the margin of the Paraguay River, in the Pantanal plain. The lowest units in the Corumbá Group (**Figure 1B**) are the Cadieus and Cerradinho formations representing a terrigenous sedimentation. Follow-up by the Bocaina Formation containing stromatolitic dolomites and a volcanic ash at the top dating 555.18 ± 0.30 Ma. The Tamengo Formation is the best-known unit from the Corumbá Group, around 200 m thick, characterized by black limestones, grainstones, organic siltstones, where the macroalgae occur, and shales. Follow-up by the the Guaicurus Formation containing laminated siltstones and macroalgae named *Eoholynia corumbensis*-up (Boggiani, 1998; Boggiani et al., 2010; Parry et al., 2017).

The Tamengo Formation (**Figure 1C**) is marked at the base by carbonatic breccia, overlain by carbonate facies of grainstones and mudstones with sedimentary structures, such as hummocky cross-stratification and wave marks with a volcanic ash at the top, in which zircons are dated at 541.85 ± 0.75 Ma. Packages of shales, siltstones, and fine sandstones with parallel plane lamination are interspersed with the carbonate facies (Boggiani et al., 2010; Parry et al., 2017; Amorim et al., 2020).

The Ediacaran Tamengo Formation exhibits paleontological remains with metazoan fossils such as *Corumbella werneri* (Pacheco et al., 2015; Walde et al., 2019), *Cloudina* sp. (Adorno et al., 2017; Becker-Kerber et al., 2017), *Paraconularia* sp. (Van Iten et al., 2014), and trace fossils such as *Multina minima* (Parry et al., 2017). Based on geological and paleontological evidence, the Tamengo Formation represents a carbonatic ramp in a marine environment, between the fair-weather wave base level and storm wave base level during a transgression phase. The facies characterized by siliciclastic rocks, metazoans, trace fossils, and plane parallel structures suggest an environment of low energy, associated with the offshore zone. The facies with limestone, hummocky cross-stratification, wave ripples, and *Cloudina* sp., is associated with the shoreface zone (Boggiani et al., 2010; Oliveira et al., 2019; Amorim et al., 2020).

MATERIALS AND METHODS

The fossils described here were collected in the siltstones of Tamengo Formation near Ladário city from Mato Grosso do Sul state. Each species has one specimen deposited in the Geoscience Institution, University of São Paulo. The samples were analyzed and photographed under a Zeiss stereomicroscope, and the fossil measurement data from each specimen were made with digital images using software Zen™ (ZEISS), where we catalog and measure the entire dimension containing their morphological features.

The samples were subjected to analysis in a scanning electron microscopy (SEM) to observe main morphological features in

high resolution and energy dispersive spectroscopy (EDS) to make elemental mapping, allowing for the characterization of the chemical composition of the macroalgae.

SYSTEMATIC PALEONTOLOGY

Usually, the morphological features of the fossils are fundamental to the taxonomy, since other characteristics such as biochemistry or the cellular structure is more difficult and rarely. The use of morphological characters to propose a new taxon needs to be approached with caution because the convergent evolution process does not make it a conclusive tool to identify phylogenetic affinity (Xiao and Dong, 2006). Also, the morphological features can be altered or lost through taphonomic processes, which strongly affects fossil algae. Their soft bodies are often recorded as broken, flattened, or distorted, and their most fragile structures can be dissolved and lost. But despite taphonomic processes, information can also be interpreted based on the fossil record.

The systematics of the fossils presented here is based only on their morphology, taking into account the taphonomic bias. The characteristics and description of the structures are based on Xiao et al. (2002) and Ye et al. (2019) who proposed the distinction of each genus considering the general morphology, branching pattern, the width of the thallus, the change in width along the length, the internode length flexibility, and the presence of microstructures. The phylogenetic affinities of the macroalgae are still uncertain because it needs a cellular information that the fossil record cannot provide. The systematic description is based on the genus and species levels. The descriptions of the new taxa follow the international code for plant, fungi, and algae nomenclature (IAPT global).

Genus *Tamengophyton* C.Q.C. Diniz & J.M. Leme sp. nov.

Type species: Tamengophyton espinosa C.Q.C. Diniz & J.M. Leme sp. nov.

Material: One specimen preserved.

Diagnosis: As for type species, by monotype.

Etymology: Tamengo Formation, where it was found.

Type locality: Ladário city located in the west of Mato Grosso do Sul state, Brazil.

Type horizon and stratigraphy: Ediacaran, Tamengo Formation, Brazil.

Tamengophyton espinosa C.Q.C. Diniz & J.M. Leme sp. nov.

Holotype: GP/1E - 10,990 (**Figure 2**), from the Tamengo Formation, Ediacaran, Corumbá Group, Ladário, Brazil (Repository: IGc-USP).

Diagnosis: A centimeter-scale fan-shaped macroalgal fossil. Possess thalli with heterogeneous thickness (**Figure 2B**), striated, and with dichotomous ramifications (**Figures 2C,D**). Along the thalli, microstructures projects in the edges (**Figure 2E**). In the apical part, a membrane is preserved that connects the stems (**Figure 2F**).

Description: The sample preserved in two-dimensional carbonaceous compression, with a size of 2.9 cm and a minimum width of 0.5 cm at base and a maximum width of 3.5 cm, formed by a set of approximately 27 striated thalli that branch per segment,

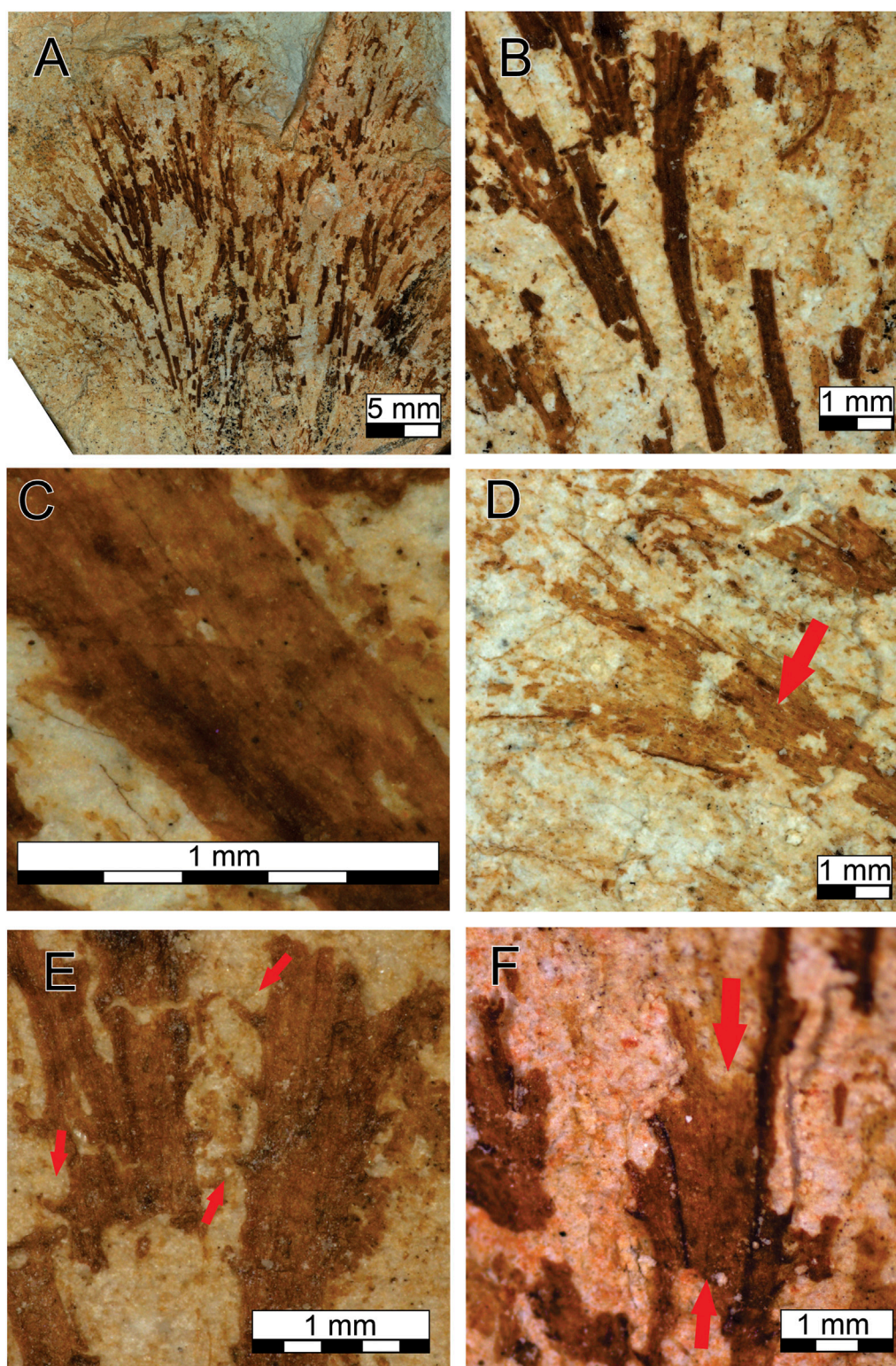


FIGURE 2 | *Tamengophyton espinosa*. **(A)** Complete fossil. **(B)** Widening in width through the length of thalli. **(C)** Details of the striation. **(D)** branching (arrow). **(E)** Details of the trichomes (arrows). **(F)** Details of the membrane (between the arrows).

widening at the top. The thalli do not overlap each other and are arranged in a straight pattern. The thickness of each thallus varies from 0.2 mm to 0.8 mm along the fossil species, with the base thinner than the top; this heterogeneity is repeated along the entire fossil. Parts preceding the branches tend to be thicker, appearing from the base through the top but can be observed only once per thallus. The preserved striation pattern follows the same longitudinal direction of the thalli. Microstructures are projecting throughout the thalli; there is no pattern for their positioning, and some are quadrilateral grouped, while others are arranged horizontally or vertically. They are preserved in different sizes, their length varies from 0.1 to 0.25 mm, and their width varies from 0.06 to 0.09 mm. The membrane is present in the distal part of the fossil, where a connection between the thalli is visible, and has the same composition as the thallus but is not striated.

Etymology: The fossil species name is determined by the presence of the microstructures that resemble thorns.

Remarks: *Tamengophyton* gen. nov. is characterized by the overall fan shape caused by the spreading of the stalks due the branching at the top; the straight thallus indicates little flexibility, the micro-triangle-shaped structures that grow perpendicularly throughout the thalli here is known as trichomes. No cellular structure has been preserved, but the presence of longitudinal striations implies a more complex internal structure resembling a pseudoparenchyma.

T. spinosa is similar to other species of macroalgae from Ediacaran around the world. The phylogeny of higher grades is uncertain, but the specimen fits into the family of Eoholyneacea (Hoffman 1994) and could be attributed to macroalgae of the Neoproterozoic due to the presence of branching. In addition, similar morphological features such as compressed cylindrical bifurcated thalli and a width < than 2 mm can also be observed with the morphogroup denominated delicately dichotomously branched, as proposed by LoDuca et al. (2017) for specimens of early Paleozoic seaweeds.

T. spinosa can be compared with genera of *Doushantuophyton* (Steiner, 1994), *Konglingiphyton* (Chen and Xiao, 1992) emend. Xiao et al. (2002) and *Maxiphyton* Ye et al. (2019) because it presents similar characteristics such as straight and rigid branches, regular dichotomy, and the capacity to widen the thallus toward the distal part. But their size does not combine; *Doushantuophyton* is 0.04–0.2 mm wide per thallus and *Konglingiphyton* can reach 1.4 mm, while the size of *T. spinosa* stays between the two genera. However, the principal diagnosis for distinguishing them is that the other taxa have smooth branches, while *T. spinosa* possesses the trichome projections and the connecting membrane to assign a new genus and new species.

Genus *Ladariella* C.Q.C. Diniz & J.M. Leme gen. nov.

Type species: *Ladariella hidria* C.Q.C. Diniz & J.M. Leme sp. nov.

Material: One specimen preserved.

Diagnosis: As for type species, by monotype.

Etymology: After the city of Ladário, located close to the type section where the fossil genus was found.

Type locality: Ladário city located in the west of Mato Grosso do Sul state, Brazil.

Type horizon and stratigraphy: Ediacaran, Tamengo Formation.

Ladariella hidria C.Q.C. Diniz & J.M. Leme sp. nov.

Holotype: GP/1E - 10,989 (Figure 3), from the Tamengo Formation, Ediacaran, Corumbá Group, Ladário, Brazil (Repository: IGc-USP).

Diagnosis: Centimeter-sized fossil preserved as a set of irregular curved thalli (Figures 3A,B). Presents rhizoidal holdfasts (Figure 3C) with a central axis and secondary elements at the base of the specimens. Possesses dichotomous striated branches (Figures 3D,E) and almond-shaped structures formed at the top (Figures 3F,G).

Description: The sample consists of a two-dimensional carbonaceous compression. With an elongate rhizoidal holdfast structure that grows perpendicular from the base of the thallus with 0.13 to 0.20 mm in width. It has a set of 20 thalli, with 1.5 cm maximum length. Each thallus is arranged obliquely and overlap each other from varied angles and difficult to measure their length, but the overall size varies from 5 to 15 mm. The width also varies between 0.15 and 0.9 mm, getting thinner in the top. The branching occurs once per thallus, and the striation follows the same longitudinal direction. The almond-shaped structures at the end ranges in size from 0.08 to 0.2 mm and are positioned obliquely with no apparent direction.

Etymology: Reference to the Greek mythological creature named hydra based on the similarity of the structure of the thalli arranged as one set and the multiple heads of the hydra in mythology.

Remarks: In the basal part, one structure at each side grows a central axis perpendicular to the thallus, most likely attributed to rhizoidal holdfasts. The branching of the thallus only occurs in the basal part of the fossil so the thickness in that area can be caused due to the enlargement of the branching process. The curvature state of the thalli indicates a flexibility that could help in a better response to hydrodynamics, and the almond-shaped structures has more accumulation of organic matter.

The phylogeny of higher grades remains uncertain, and the specimen fits into the Eoholyneacea family proposed by Hoffman (1994) because of the presence of branching and also shares the same features of *T. spinosa*, such as compressed cylindrical bifurcated thalli and a width < 2 mm that fits in the morphogroup proposed by LoDuca et al. (2017) based on delicately dichotomously branches.

L. hidria and *Miaohephyton* (Xiao et al. 1998) share a characteristic of a possible apical meristem. Nevertheless, considering the entire morphology, branching pattern, the heterogeneity, and especially the flexibility of the thallus as well as the almond structures, a new genus needs to be established.

Genus *Ladariophyton* C.Q.C. Diniz & J.M. Leme gen. nov.

Type species: *Ladariophyton veinosa* C.Q.C. Diniz & J.M. Leme sp. nov.

Material: One specimen preserved.

Diagnosis: As for type species, by monotype.

Etymology: Named after the city of Ladário, in where it was found.

Type locality: Ladário city located in the west of Mato Grosso do Sul state, Brazil.

Type horizon and stratigraphy: Ediacaran, Tamengo Formation, Brazil.

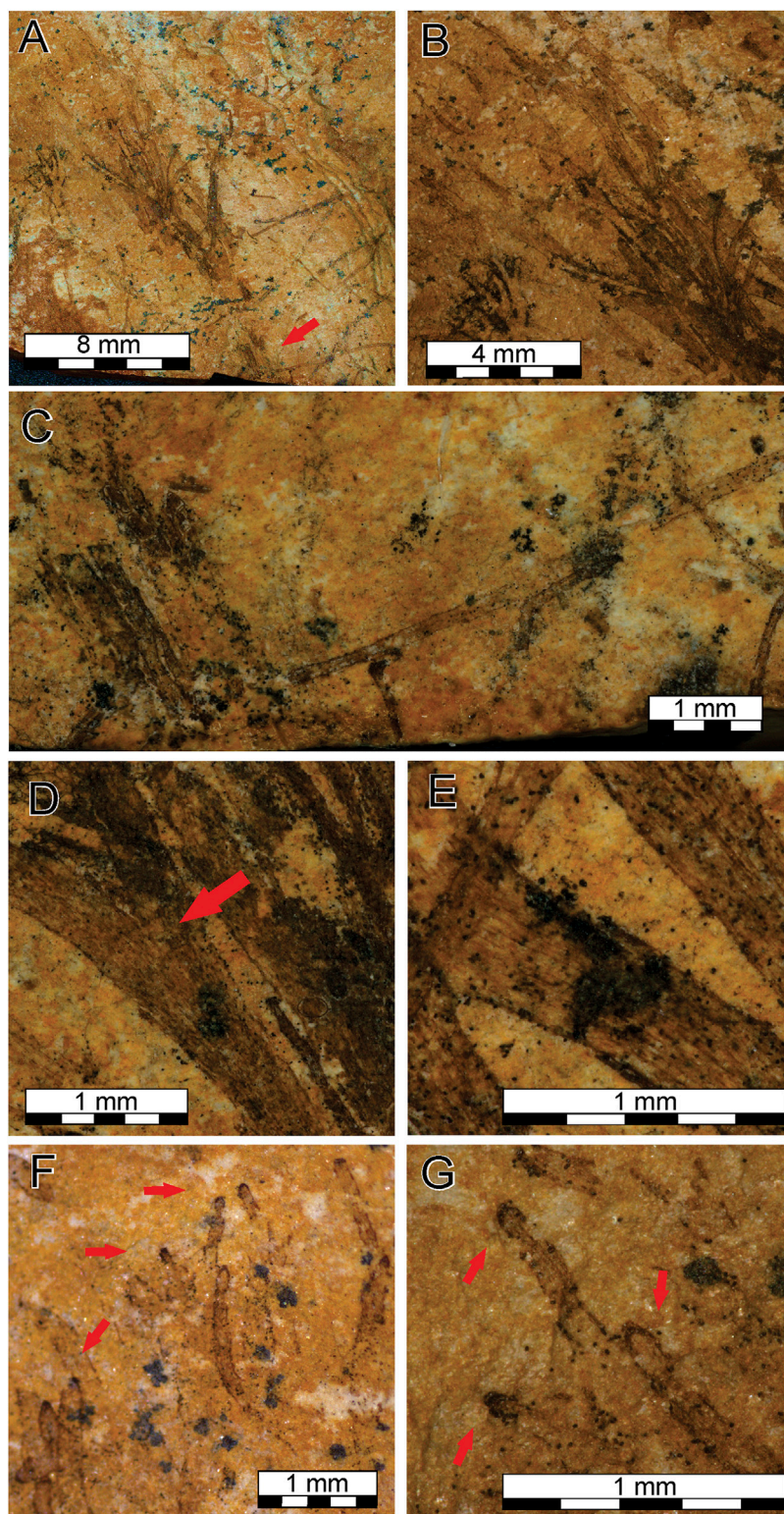


FIGURE 3 | *Ladariella hidria*. (A,B) Complete fossil with the arrow pointed out to the rhizoidal holdfasts in (A). (C) Details of the rhizoidal holdfasts. (D) Branching (arrow). (E) Details of the striation in the thalli. (F,G) Details of the almond structure (arrows).

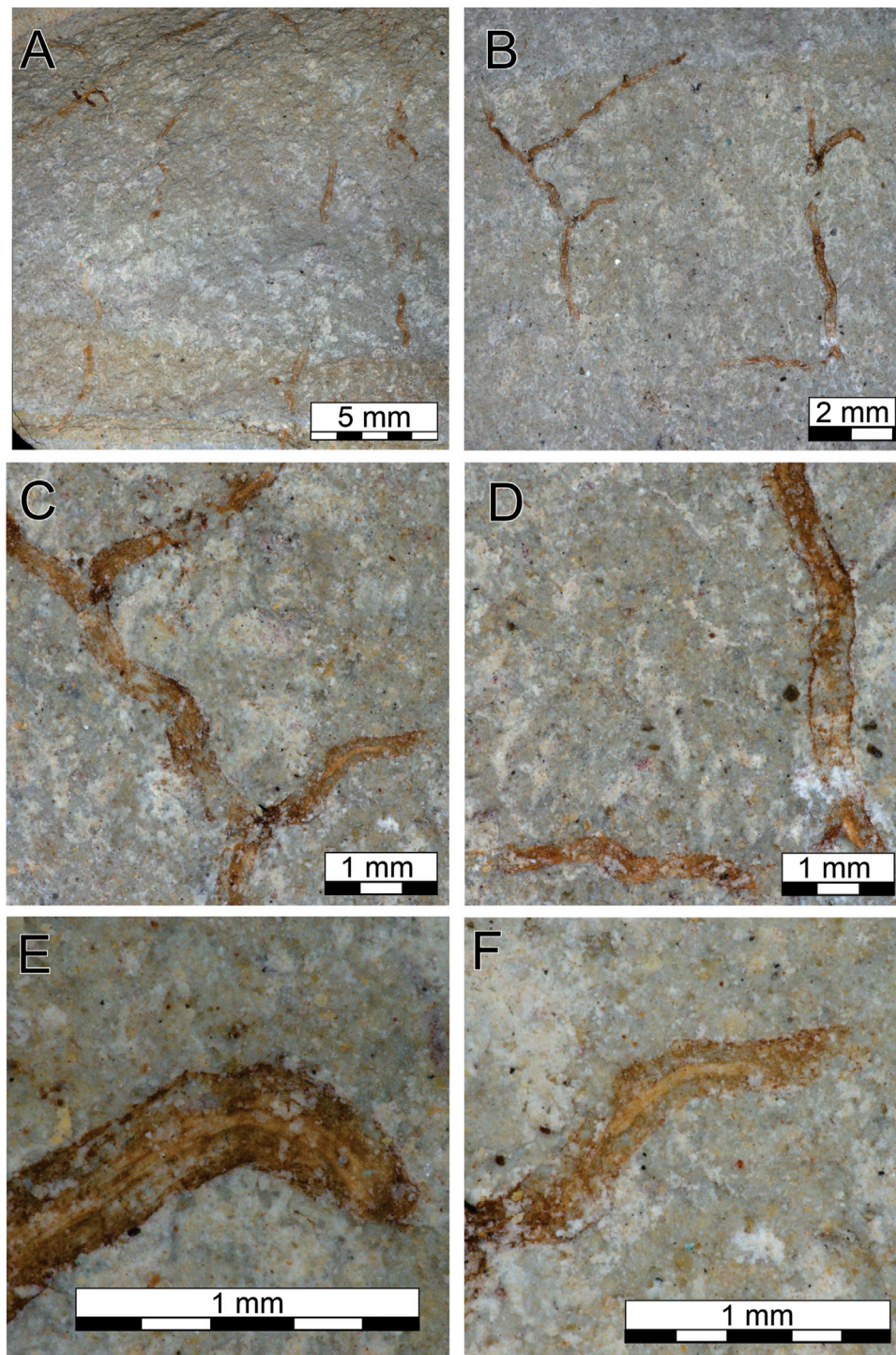


FIGURE 4 | *Ladariophyton veinosa*. **(A,B)** The complete fossil. **(C)** Details of the branching. **(D)** Details of the edge. **(E,F)** Details of the thickness of the longitudinal structure.

Ladariophyton veinosa C.Q.C. Diniz & J.M. Leme sp. nov.

Holotype: GP/1E - 11,187 (**Figure 4**), from the Tamengo Formation, Ediacaran, Corumbá Group, Ladário, Brazil (Repository: IGc-USP).

Diagnosis: Fossil organism of centimeter-scale with pseudomonopodial irregular branches (**Figure 4B**). It presents a defined border and has an enlarged

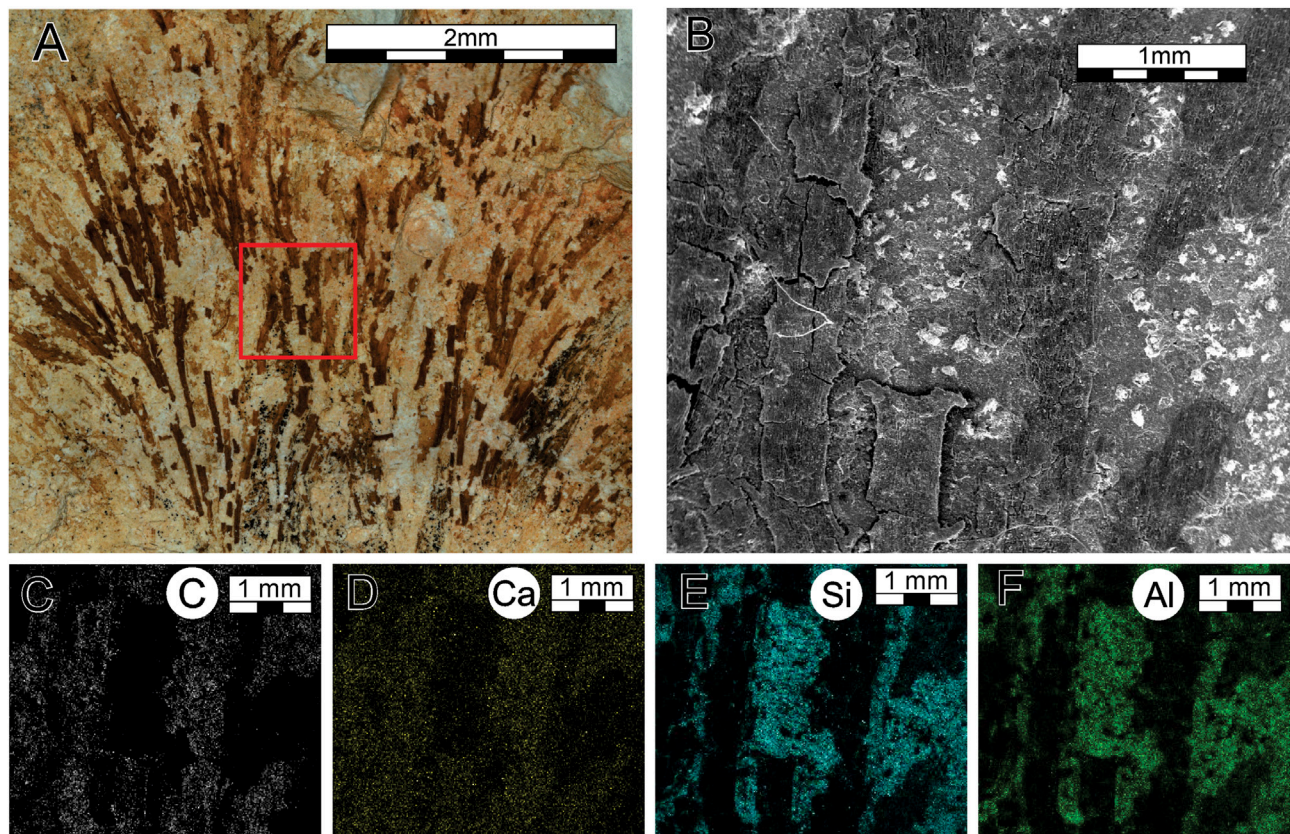


FIGURE 5 | Analysis of SEM and EDS of *T. espinosa*. **(A)** The complete fossil, where the red square highlights the zoom made in image **(B)**. **(B)** Analysis of SEM. **(C)** Concentration of carbon. **(D)** Concentration of calcium. **(E)** Concentration of silica. **(F)** Concentration of aluminum.

longitudinal structure on the center of each thallus (Figure 4D–F).

Description: The sample has a set of thalli, which are arranged in a specific direction without overlapping each other. They vary in length, with the longer thallus being 1.1 cm. This does not represent the full length of the organism because none of the thallus is complete without a basal and an apical part. The thalli are homogeneous in width, measuring between 0.2 and 0.35 mm. Branching can be observed more than once, but one thallus represents the principal growth of the alga where the branching always occurs. The fossil has well-demarcated edges with a corrugated shape. The characteristic, which differentiates and defines this fossil, is a thickening in the longitudinal structure present at the center of the thalli of approximately 0.1 mm.

Etymology: Reference for veins, based on the central structure along the thalli.

Remarks: This specimen fits into the Eoholyniaceae family proposed by Hoffman (1994) for macroalgae of the Neoproterozoic because of the presence of branches and the presence of characteristics of the morphogroup of delicately dichotomous branches as proposed by LoDuca et al. (2017) for specimens of early Paleozoic seaweeds.

L. veinosa sp. nov. is a very simple macroalga difficult to attribute a major group, can be compared to *Chinggiskhaania bifurcata* (Dornbos et al. 2016) due to its a thin filament with an average width of 0.45 mm, does not densely assemble and without distal tapering in width, but lacks a longitudinal striation. Macroalgae from Dolores Creeks Formation, Canada (Maloney et al., 2021), presents a longitudinal division but have septa along the fossil, structure that our specimen does not have; the aspects differentiating *L. veinosa* are the corrugated edges and the thick longitudinal structure in the center of the thallus.

DISCUSSION

The different records of Ediacaran fossils have various modes of exceptional preservation, such as phosphatization (e.g., Xiao et al., 2004), permineralization (e.g., Zhang et al., 1998), pyritization (e.g., Cai et al., 2010), and silicification (e.g., Liu, 2016). Analysis using energy-dispersive X-ray spectroscopy (EDS) of two samples was performed (Figures 5, 6), which indicated a high carbon and a low aluminum and silica content in the fossil in relation to the matrix.

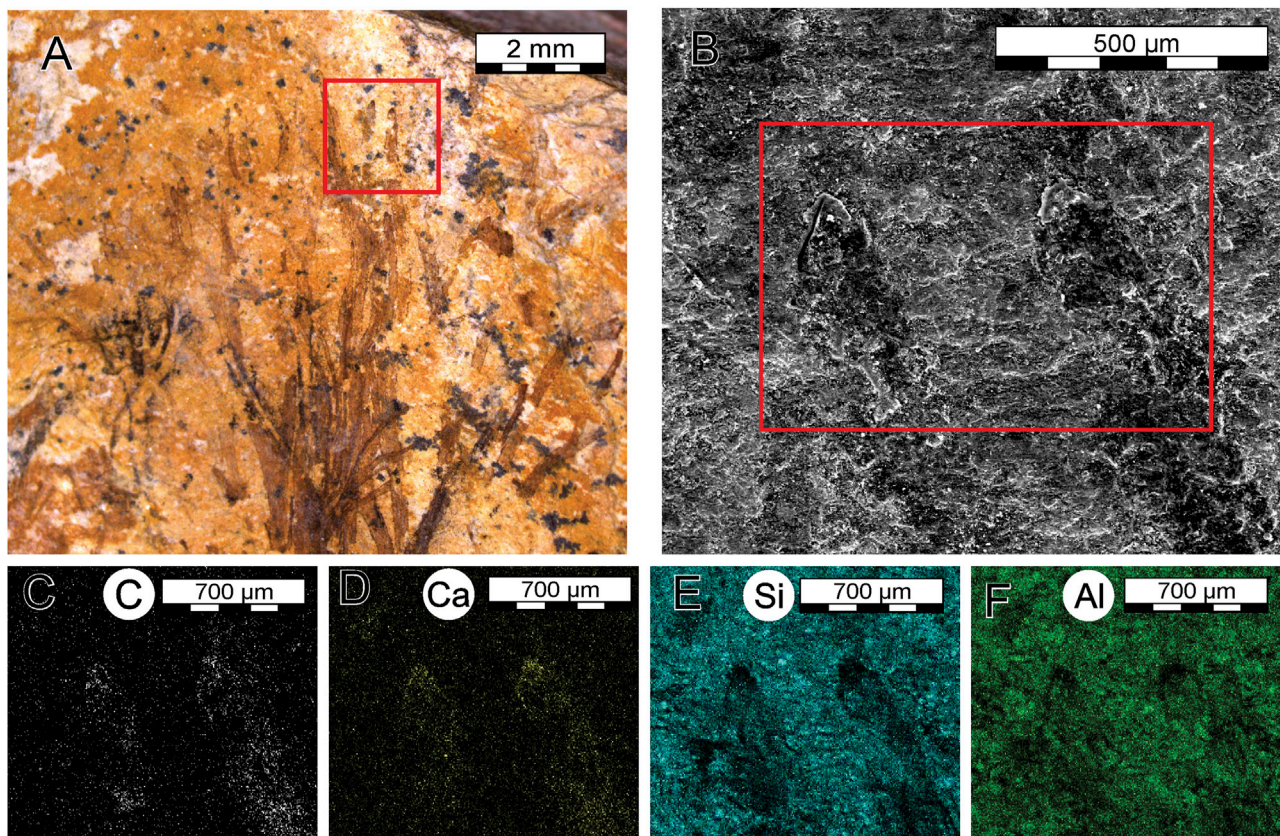


FIGURE 6 | Analysis of SEM and EDS of *L. hidria*. **(A)** The complete fossil, where the red square highlights the zoom made in image **(B)**. **(B)** Analysis of SEM, where the red rectangle highlights the zoom made in the other images. **(C)** Concentration of carbon. **(D)** Concentration of calcium. **(E)** Concentration of silica. **(F)** Concentration of aluminum.

The macroalgal fossils are preserved as carbonaceous compressions in pelite, from the information provided by SEM and EDS, which can be compared to Cambrian Burgess Shale-type preservation (Butterfield, 1995; Xiao et al., 2002; Butterfield, 2005). In addition, the preservation occurred because of a transformation of the non-mineralized soft tissues (organic matter) to a stable kerogen is a process named kerogenization (Cai et al., 2012).

Amorim et al. (2020) propose a facies association in the deposits from the Tamengo Fm. where the macroalgae were found. The silty shale facies have a parallel lamination with wide paleodiversity, such as fossils of *Corumbella weneri*, *Paraconularia* sp., and vendotaenids. It is intercalated with carbonated facies such as massive to poorly laminated calcimudstone, laminated wackestone, and hummocky/swaley cross-stratified packstone. The alternation between fossiliferous pelites with tempestites (carbonates) suggested the preservation of the fragile macroalgae during the interval of the storms, during the suspension fallout of fine sediments (Labaj and Pratt, 2016; Amorim et al., 2020).

The absence of hard structures in the macroalgae makes these fossils difficult to be preserved, especially their delicate characteristics as presented in the two samples (*T. espinosa* and *L. hidria*). The fossil *T. espinosa* have a basal part

incomplete, where the distal part is more preserved, which has been difficult to measure the full length of individual thallus. The absence of structures such as trichomes and membranes at the base of the fossil could be explained by an influence of taphonomic processes shaping the preserved morphology of the algae. The flattening of the fossil is visible, creating a two-dimensional form, affecting the trichomes forming small circles, and causing rupture in the thalli.

In *Ladariella hidria*, taphonomic processes influenced the preservation and shape of the fossil organism, including flattening throughout the structure. Better preservation occurs in the almond structures, where a thicker and darker layer was reported due to a larger accumulation of organic matter. This might indicate an apical meristem, where greater cell division for algae growth is expected.

In the case of *Ladariophyton veinosa*, a connection between the thalli is missing, together to an indication of a basal and top parts. Therefore, it is hard to acknowledge the total length of the fossil. The corrugated shape of the edges could also have been formed by a taphonomic influence; when body parts start to lose humidity, they tend to wrinkle.

Even though the macroalgae are not preserved in life position, a fossil of higher fragility could not be transported over long

distances or remain in the active high-energy zone for a long period of time without significant destruction. So, the presence of the macroalgae could indicate a depth when they would receive enough sunlight to enable photosynthesis and with energy sufficient to partially destroy their body.

Other fossils of metazoan are preserved in the same stratigraphic level such as *Corumbella weneri*; they also miss the basal part but present an overall well-preserved level in their carapace (Amorim et al., 2020). *Corumbella weneri* possess a thin organic and delicate wall (Pacheco et al., 2015; Walde et al., 2019), so the well-preserved fossil associated with the silty shale facies can indicate a minimal transportation or rework at a low-energy environment (Warren et al., 2012; Amorim et al., 2020).

The preservation of macroalgae together with carapaces of metazoan in the siltstone bed in the Tamengo Formation can be explained by environmental variations in higher sedimentation rates, probably a sedimentary deposit under offshore condition in a depth below storm wave base, with a low-energy environment representing an outer to distal mid-ramp.

CONCLUSION

Three specimens of macroalgae are described for the Brazilian Ediacaran, Tamengo Formation in Mato Grosso do Sul, representing new taxonomic species and genera. The new descriptions contribute to the local paleobiodiversity along with metazoans, ichnofossils, and microfossils previously documented in this formation. This further reinforces the contribution of Brazil to the knowledge of the Ediacaran fossils. These three genera and species add new evidence to evolutionary issues of macroalgae during the Ediacaran, especially *T. espinosa* with its more complex features such as differentiated trichome and an interconnecting membrane. This also emphasizes more complex organisms already existed before

the Cambrian but remain extremely rare in the fossil record due to their fragile structures.

DATA AVAILABILITY STATEMENT

The original contributions presented in the study are included in the article/supplementary materials; further inquiries can be directed to the corresponding author.

AUTHOR CONTRIBUTIONS

CD, JL, and PB collected the fossils. CD performed laboratory work and morphological taxon identifications. JL assisted with the interpretation. PB collaborated with hypothesis in the discussion. All authors contributed to the article and approved the submitted version.

FUNDING

This study was supported by the Coordenação de Aperfeiçoamento de Pessoal de Nível Superior – CAPES (167787/2017-9) and Fundação de Amparo à Pesquisa – FAPESP (Proc. 13/17835-8; 16/06114-6; 17/25433-8; 17/25433-8).

ACKNOWLEDGMENTS

We thank you the engineer Isaac Jamil Sayeg for providing SEM and EDS data. We are grateful to Andrea K. Kern from the Department of Sedimentary and Environmental Geology (GSA) of the University of São Paulo for their language help. Our gratitude goes to the editor and reviewers for their work and suggestions.

REFERENCES

- Adorno, R. R., do Carmo, D. A., Germs, G., Walde, D. H. G., Denezine, M., Boggiani, P. C., et al. (2017). Cloudina Lucianoi (Beurlen & Sommer, 1957), Tamengo Formation, Ediacaran, Brazil: Taxonomy, Analysis of Stratigraphic Distribution and Biostratigraphy. *Precambrian Res.* 301, 19–35. doi:10.1016/j.precamres.2017.08.023
- Amorim, K. B., Afonso, J. W. L., Leme, J. M., Diniz, C. Q. C., Rivera, L. C. M., Gómez-Gutiérrez, J. C., et al. (2020). Sedimentary Facies, Fossil Distribution and Depositional Setting of the Late Ediacaran Tamengo Formation (Brazil). *Sedimentology* 67, 3422–3450. doi:10.1111/sed.12749
- Becker-Kerber, B., Pacheco, M. L. A. F., Rudnitzki, I. D., Galante, D., Rodrigues, F., and Leme, J. M. (2017). Ecological Interactions in Cloudina From the Ediacaran Of Brazil: Implications for the Rise of Animal Biomineralization. *Sci. Rep.* 7, 5482–5487. doi:10.1038/s41598-017-05753-8
- Boggiani, P. C. (1998). Análise estratigráfica da Bacia Corumbá (Neoproterozoico) - Mato Grosso do Sul. Ph.D. Thesis, Brasil: Universidade de São Paulo, 181.
- Boggiani, P. C., Gaucher, C., Sial, A. N., Babinski, M., Simon, C. M., Riccomini, C., et al. (2010). Chemostratigraphy of the Tamengo Formation (Corumbá Group, Brazil): A Contribution to the Calibration of the Ediacaran Carbon-Isotope Curve. *Precambrian Res.* 182, 382–401. doi:10.1016/j.precamres.2010.06.003
- Butterfield, N. J. (1995). Secular Distribution of Burgess-shale-type Preservation. *Lethaia* 28, 1–13. doi:10.1111/j.1502-3931.1995.tb01587.x
- Butterfield, N. (2005). Reconstructing a Complex Early Neoproterozoic Eukaryote, Wynnatt Formation, Arctic Canada. *Lethaia* 38, 155–169. doi:10.1080/00241160510013231
- Bykova, N., LoDuca, S. T., Ye, Q., Marusin, V., Grazhdankin, D., and Xiao, S. (2020). Seaweeds Through Time: Morphological And Ecological Analysis of Proterozoic And Early Paleozoic Benthic Macroalgae. *Precambrian Res.* 350, 105875. doi:10.1016/j.precamres.2020.105875
- Cai, Y., Hua, H., Xiao, S., Schiffbauer, J. D., and Li, P. (2010). Biostratigraphy of the Late Ediacaran Pyritized Gaojiashan Lagerstätte from Southern Shaanxi, South China: Importance of Event Deposits. *Palaio* 25, 487–506. doi:10.2110/palo.2009.p09-133r
- Cai, Y., Schiffbauer, J. D., Hua, H., and Xiao, S. (2012). Preservation Modes in the Ediacaran Gaojiashan Lagerstätte: Pyritization, Aluminosilicification, and Carbonaceous Compression. *Palaogeogr. Palaeoclimatol. Palaeoecol.* 326–328, 109–117. doi:10.1016/j.palaeo.2012.02.009
- Chen, M., and Xiao, S. (1992). Macrofossil Biota from Upper Doushantuo Formation In Eastern Yangtze Gorges, China. *Acta Palaeontologica Sinica* 31, 513–529.
- Cohen, P. A., and Macdonald, F. A. (2015). The Proterozoic Record Of Eukaryotes. *Paleobiology* 41, 610–632. doi:10.1017/pab.2015.25

- Dornbos, S. Q., Oji, T., Kanayama, A., and Gonchigdorj, S. (2016). A New Burgess Shale-type deposit from the Ediacaran Of Western Mongolia. *Sci. Rep.* 6, 23438. doi:10.1038/srep23438
- Hedges, S., Blair, J. E., Venturi, M. L., and Shoe, J. L. (2004). A Molecular Timescale of Eukaryote Evolution and the Rise of Complex Multicellular Life. *BMC Evol. Biol.* 4, 2. doi:10.1186/1471-2148-4-2
- Hofmann, H. J. (1994). "Proterozoic Carbonaceous Compressions ('metaphytes' and 'worms')," in *Early Life on Earth*. Editor S. Bengtson (New York: Columbia University Press), 342–357.
- Knoll, A. H., Javaux, E. J., Hewitt, D., and Cohen, P. (2006). Eukaryotic Organisms in Proterozoic Oceans. *Phil. Trans. R. Soc. B* 361, 1023–1038. doi:10.1098/rstb.2006.1843
- Labaj, M. A., and Pratt, B. R. (2016). Depositional Dynamics in a Mixed Carbonate-Siliciclastic System: Middle-Upper Cambrian Abrigo Formation, southeastern Arizona. *U.S.A. J. Sed. Res.* 86, 11–37.
- Liu, A. G. (2016). Framboidal Pyrite Shroud Confirms the 'Death Mask' Model for Moldic Preservation of Ediacaran Soft-Bodied Organisms. *Palaios* 31, 259–274. doi:10.2110/palo.2015.095
- LoDuca, S. T., Bykova, N., Wu, M., Xiao, S., and Zhao, Y. (2017). Seaweed Morphology and Ecology during the Great Animal Diversification Events of the Early Paleozoic: a Tale of Two Floras. *Geobiology* 15, 588–616. doi:10.1111/gbi.12244
- Maloney, K. M., Halverson, G. P., Schiffbauer, J. D., Xiao, S., Gibson, T. M., Gibson, T. M., Lechte, M. A., et al. (2021). New Multicellular marine Macroalgae from the Early Tonian Of Northwestern Canada. *Geology* 49, 6. doi:10.1130/G48508.1
- Nagovitsin, K. E., Rogov, V. I., Marusin, V. V., Karlova, G. A., Kolesnikov, A. V., Bykova, N. V., et al. (2015). Revised Neoproterozoic And Terreneuvian Stratigraphy of the Lena-Anabar Basin and north-western Slope of the Olenek Uplift, Siberian Platform. *Precambrian Res.* 270, 226–245. doi:10.1016/j.precamres.2015.09.012
- Oliveira, R. S. d., Nogueira, A. C. R., Romero, G. R., Truckenbrodt, W., and da Silva Bandeira, J. C. (2019). Ediacaran Ramp Depositional Model of the Tamengo Formation, Brazil. *J. South Am. Earth Sci.* 96, 102348. doi:10.1016/j.jsames.2019.102348
- Pacheco, M. L., Galante, D., Rodrigues, F., Leme, J. M., Bidola, P., Hagadorn, W., et al. (2015). Insights Into the Skeletonization, Lifestyle, and Affinity of the Unusual Ediacaran Fossil Corumbella. *PLoS ONE* 10, e0114219–19. doi:10.1371/journal.pone.0114219
- Parfrey, L. W., Lahr, D. J. G., Knoll, A. H., and Katz, L. A. (2011). Estimating The Timing of Early Eukaryotic Diversification with Multigene Molecular Clocks. *Proc. Natl. Acad. Sci.* 108, 13624–13629. doi:10.1073/pnas.1110633108
- Parry, L. A., Boggiani, P. C., Condon, D. J., Garwood, R. J., Leme, J. M., McIlroy, D., et al. (2017). Ichnological Evidence for Meiofaunal Bilaterians from the Terminal Ediacaran And Earliest Cambrian Of Brazil. *Nat. Ecol. Evol.* 1, 1455–1464. doi:10.1038/s41559-017-0301-9
- Steiner, R. (1994). Einführung. *Berliner geowissenschaftliche Abhandlungen* 15, 1–4. doi:10.1007/978-3-322-84265-7_1
- Rowland, S. M., and Rodriguez, M. G. (2014). A Multicellular Alga with Exceptional Preservation from the Ediacaran Of Nevada. *J. Paleontol.* 88, 263–268. doi:10.1666/13-075
- Srivastava, P. (2012). "Morphodiversity, Complexity and Macroevolution: Revealed by the Megascopic Life of the Palaeo-Neoproterozoic Vindhyan Supergroup, India, 365," In *Palaeoproterozoic Of India*, eds. R. Mazumder and D. Saha London, Geological Society, Special Publications, 247–262. doi:10.1144/sp365.13
- Tang, Q., Pang, K., Yuan, X., and Xiao, S. (2017). Electron Microscopy Reveals Evidence for Simple Multicellularity in the Proterozoic fossil Chuaria. *Geology* 45, 75–78. doi:10.1130/G38680.1
- Van Iten, H., Marques, A. C., Leme, J. M., Pacheco, M. L. A. F., and Simões, M. G. (2014). Origin and Early Diversification of the Phylum Cnidaria Verrill: Major Developments in the Analysis of the Taxon's Proterozoic-Cambrian History. *Palaeontology* 57, 677–690. doi:10.1111/pala.12116
- Walde, D. H.-G., Weber, B., Erdtmann, B. D., and Steiner, M. (2019). Taphonomy of Corumbella Wernerifrom the Ediacaran of Brazil: Sinotubulitid Tube or Conulariid Test. *Alcheringa: Australas. J. Palaeontology* 43, 335–350. doi:10.1080/03115518.2019.1615551
- Wan, K. Y., and Jékely, G. (2021). Origins Of Eukaryotic Excitability. *Phil. Trans. R. Soc. B* 376, 20190758. doi:10.1098/rstb.2019.0758
- Warren, L. V., Pacheco, M. L. A. F., Fairchild, T. R., Simões, M. G., Riccomini, C., and Boggiani, P. C. (2012). The Dawn of Animal Skeletogenesis: Ultrastructural Analysis of the Ediacaran Metazoan Corumbella Werner. *Geology* 40, 691–694.
- Xiao, S., and Dong, L. (2006). "On The Morphological and Ecological History of Proterozoic Macroalgae," in *Neoproterozoic Geobiology And Paleobiology*, eds. S. Xiao and A. J. Kaufman (Dordrecht, Springer), 57–90.
- Xiao, S., Knoll, A. H., and Yuan, X. (1998). Morphological Reconstruction of Miaohephyton Bifurcatum, a Possible Brown Alga from the Neoproterozoic Doushantuo Formation, South China. *J. Paleontol.* 72, 1072–1086. doi:10.1017/s0022336000027414
- Xiao, S., Knoll, A. H., Yuan, X., and Poeschel, C. M. (2004). Phosphatized Multicellular Algae in the Neoproterozoic Doushantuo Formation, China, and the Early Evolution of Florideophyte Red Algae. *Am. J. Bot.* 91, 214–227. doi:10.3732/ajb.91.2.214
- Xiao, S., Yuan, X., Steiner, M., and Knoll, A. H. (2002). Macroscopic Carbonaceous Compressions in a Terminal Proterozoic Shale: a Systematic Reassessment of the Miaohhe Biota, South China. *J. Paleontol.* 76, 347–376. doi:10.1017/s0022336000041743
- Ye, Q., Tong, J., An, Z., Hu, J., Tian, L., Guan, K., et al. (2019). A Systematic Description of New Macrofossil Material from the Upper Ediacaran Miaohhe Member In South China. *J. Syst. Palaeontology* 17, 183–238. doi:10.1080/14772019.2017.1404499
- Zhang, Y., Yin, L., Xiao, S., and Knoll, A. H. (1998). Permineralized Fossils from the Terminal Proterozoic Doushantuo Formation, South China, *Memoir Paleontological Society*, 72, 1–52. doi:10.1017/s0022336000059977
- Zhao, Y., Chen, M. e., Peng, J., Yu, M., He, M., Wang, Y., et al. (2004). Discovery Of a Miaohhe-type Biota from the Neoproterozoic Doushantuo Formation in Jiangkou County, Guizhou Province, China. *Chin. Sci. Bull.* 49, 2224–2226. doi:10.1007/bf03185792

Conflict of Interest: The authors declare that the research was conducted in the absence of any commercial or financial relationships that could be construed as a potential conflict of interest.

Publisher's Note: All claims expressed in this article are solely those of the authors and do not necessarily represent those of their affiliated organizations, or those of the publisher, the editors and the reviewers. Any product that may be evaluated in this article, or claim that may be made by its manufacturer, is not guaranteed or endorsed by the publisher.

Copyright © 2021 Diniz, Leme and Boggiani. This is an open-access article distributed under the terms of the Creative Commons Attribution License (CC BY). The use, distribution or reproduction in other forums is permitted, provided the original author(s) and the copyright owner(s) are credited and that the original publication in this journal is cited, in accordance with accepted academic practice. No use, distribution or reproduction is permitted which does not comply with these terms.



Orientations of Mistaken Point Fronds Indicate Morphology Impacted Ability to Survive Turbulence

Philip B. Vixseboxse^{1,2*}, Charlotte G. Kenchington², Frances S. Dunn³ and Emily G. Mitchell⁴

¹School of Earth Sciences, University of Bristol, Bristol, United Kingdom, ²Department of Earth Sciences, University of Cambridge, Cambridge, United Kingdom, ³Oxford University Museum of Natural History, University of Oxford, Oxford, United Kingdom, ⁴Department of Zoology, University of Cambridge, Cambridge, United Kingdom

OPEN ACCESS

Edited by:

Shuhai Xiao,
Virginia Tech, United States

Reviewed by:

Simon Darroch,
Vanderbilt University, United States
Marc Laflamme,
University of Toronto Mississauga,
Canada

*Correspondence:

Philip B. Vixseboxse
pbv22@cam.ac.uk

Specialty section:

This article was submitted to
Paleontology,
a section of the journal
Frontiers in Earth Science

Received: 22 August 2021

Accepted: 01 November 2021

Published: 07 December 2021

Citation:

Vixseboxse PB, Kenchington CG,
Dunn FS and Mitchell EG (2021)
Orientations of Mistaken Point Fronds
Indicate Morphology Impacted Ability
to Survive Turbulence.
Front. Earth Sci. 9:762824.
doi: 10.3389/feart.2021.762824

The Ediacaran fossils of the Mistaken Point E surface have provided crucial insight into early animal communities, including how they reproduced, the importance of Ediacaran height and what the most important factors were to their community dynamics. Here, we use this iconic community to investigate how morphological variation between eight taxa affected their ability to withstand different flow conditions. For each of *Beothukis*, *Bradgatia*, *Charniodiscus procerus*, *Charniodiscus spinosus*, *Plumeropriscum*, *Primocandelabrum*, *Thectardis* and *Fractofusus* we measured the orientation and length of their stems (if present) and their fronds. We statistically tested each taxon's stem and frond orientation distributions to see whether they displayed a uniform or multimodal distribution. Where multimodal distributions were identified, the stem/frond length of each cohort was tested to identify if there were differences in size between different orientation groups. We find that *Bradgatia* and *Thectardis* show a bimodal felling direction, and infer that they were felled by the turbulent head of the felling flow. In contrast, the frondose rangeomorphs including *Beothukis*, *Plumeropriscum*, *Primocandelabrum*, and the arboreomorphs were felled in a single direction, indicating that they were upright in the water column, and were likely felled by the laminar tail of the felling flow. These differences in directionality suggests that an elongate habit, and particularly possession of a stem, lent greater resilience to frondose taxa against turbulent flows, suggesting that such taxa would have had improved survivability in conditions with higher background turbulence than taxa like *Bradgatia* and *Thectardis*, that lacked a stem and had a higher centre of mass, which may have fared better in quieter water conditions.

Keywords: Ediacaran, Mistaken Point, orientations, turbidite, rangeomorphs, arboreomorphs

INTRODUCTION

The Ediacaran macrobiota is a polyphyletic assemblage of organisms (Darroch et al., 2018) which appear in the fossil record ~575 million years ago and contain some of the oldest animals in the fossil record (Xiao and Laflamme 2009; Budd and Jensen 2017; Bobrovskiy et al., 2018; Dunn et al., 2018, 2021; Hoyal Cuthill and Han 2018; Wood et al., 2019). The morphologies of Ediacaran organisms from Newfoundland and the United Kingdom have few clear points of homology with living animal lineages or Phanerozoic fossil groups, which has historically limited our understanding of their phylogenetic affinities and hampers our understanding of the functional ecology of these organisms (Laflamme et al., 2013; Liu et al., 2015).

The Ediacaran communities of Eastern Newfoundland are dominated by the perhaps most distinct members of the Ediacaran macrobiota—the sessile, frondose rangeomorphs (Narbonne and Gehling 2003; Narbonne 2005). Rangeomorphs are characterised by a “fractal” branching architecture (Narbonne 2004; Hoyal Cuthill and Conway Morris 2014), and which increasing data supports as a clade of stem-group eumetazoans (Hoyal Cuthill and Han 2018; Dunn et al., 2021). Rangeomorphs numerically dominate these late-Ediacaran sea floors, but they lived alongside a number of different groups, the most abundant of which are the arboreomorphs (Clapham et al., 2003; Xiao and Laflamme 2009). These are similarly frondose, but unlike the rangeomorphs which can possess many orders of hierarchical branching, Newfoundland arboreomorphs possess only two orders (Laflamme et al., 2004; Laflamme and Narbonne 2008; Laflamme et al., 2018). Non-frondose fossils are also present, though rare in these fossil deposits—the most well-known is *Thectardis*, a conical to triangular organism which has been interpreted as a sponge (Clapham et al., 2004; Sperling et al., 2011).

Of these groups, rangeomorphs are not only the most diverse but display the greatest anatomical variation (Shen et al., 2008; Xiao and Laflamme 2009). Some rangeomorphs are preserved as single fronds (e.g., *Charnia*), but others were bushy (e.g., *Bradgatia*), spindle-shaped (e.g., *Fractofusus*) or arborescent (e.g., *Primocandelabrum*) (Gehling and Narbonne 2007; Bamforth et al., 2008; Flude and Narbonne 2008; Bamforth and Narbonne 2009; Dunn et al., 2019). Rangeomorph branches differentiated directly from one another or from a central stalk (Dunn et al., 2019) and some rangeomorphs additionally exhibited a naked stem that elevated the frond into the water column (Laflamme et al., 2012). Most rangeomorphs possessed a spheroidal-discoidal holdfast that anchored them within the sediment (Laflamme et al., 2004; Burzynski and Narbonne 2015), attaching the organism to the substrate and from which the stem or frond derived. Previous functional studies have demonstrated that the high surface area of the repeatedly branched frond maximised nutrient or gas exchange (Laflamme et al., 2009; Sperling et al., 2011; Liu et al., 2015). The phylogenetic relationship between frondose rangeomorphs and the coeval arboreomorphs is currently unclear (Decechi et al., 2017; Hoyal Cuthill and Han 2018); some have argued that arboreomorphs are members of the Rangeomorpha (Brasier and Antcliffe 2009), but clear anatomical differences between at least some arboreomorphs and rangeomorphs mean that this view is not universally held, with others suggesting that overtly similar gross morphologies may have arisen through convergence (Laflamme et al., 2018). Indeed, in the modern, a sessile, frondose bodyplan is found in myriad different groups, such as ferns, cnidarians and bryozoans and has been acquired through different developmental processes, demonstrating that such a bodyplan can be the product of similar ecologies or function and is not necessarily indicative of close phylogenetic relationship.

Stems were originally thought to facilitate height-driven tiering in Avalonian communities, allowing taller fronds to

reach higher-velocity conditions (Clapham and Narbonne, 2002; Ghisalberti et al., 2014), but more recent work has suggested that not all communities were tiered and that increased height may have additionally functioned in offspring dispersal (Mitchell and Kenchington 2018). Thickening of the stem close to the holdfast—optimisation of the stem as a cantilever beam—is observed in cnidarians (Koehl 1977a, b), and crinoids (Baumiller and Ausich 1996), where it permits orientation of the crown with the aboral surface facing the flow, initiating aboral inflow and recirculation (Dynowski et al., 2016). Rangeomorphs have been documented as showing a basal thickening of the stem and so may have functioned in the same way (Kenchington and Wilby 2017). By examining the different functional ecology of stemmed and non-stemmed organisms, we can investigate what the advantages of stems were in Ediacaran organisms.

These fossils are found preserved within turbiditic sequences, under thin layers of ash which blanketed large swathes of sea floor and smothered thousands of macro-organisms in a single event bed (Wood et al., 2003). Communities are exceptionally preserved and provide a near-census record of the benthos (Wood et al., 2003). This *in-situ* preservation, combined with the sessile habit of the organisms, means that detailed spatial ecological analyses can be used to investigate reproductive strategies (Mitchell et al., 2015), taxonomy (Mitchell et al., 2018), community interactions (Mitchell and Butterfield 2018) and evolutionary drivers (Mitchell et al., 2019, 2020), and in this study supplement functional ecology analyses of the organisms.

Here, we use statistical analyses of the orientations of 8 taxa from the E surface, Mistaken Point, Newfoundland: *Beothukis*, *Bradgatia*, *Charniodiscus procerus*, *Charniodiscus spinosus*, *Plumeroprisicum*, *Primocandelabrum*, *Thectardis*, and *Fractofusus*. We determine the extent to which orientation distributions of populations of complete specimens, stems and fronds are randomly, normally and/or uniformly distributed, and how many sub-groups within each population exist. Where taxa exhibit multi-modal orientation distributions, we use random labelling spatial analyses to determine whether there are any spatial patterns to taxa orientations. These analyses enable us to investigate how morphological features, such as stems and number of folia influenced the stability of these organisms in the ancient oceans and their ability to withstand burial events of differing magnitudes.

Geological Setting

The Avalon Assemblage records the evolution of deep marine metazoan communities from the ~574 Ma Drook Formation (Matthews et al., 2021), to the late Ediacaran Bradgate Formation [556.6 ± 6.4 Ma, (Noble et al., 2015)]. One of the three assemblages originally proposed by Waggoner 2003, it traces the marine margin of the Avalonian Terrane through the British Isles and Newfoundland. In both regions, sedimentation was dominated by turbidite deposition (Wood et al., 2003; Noble et al., 2015). Throughout the Newfoundland succession, there is a transition in tectonic setting and depositional character (**Figure 1**), from the basin plain setting of the lower Conception Group to the shallowing-upwards slope

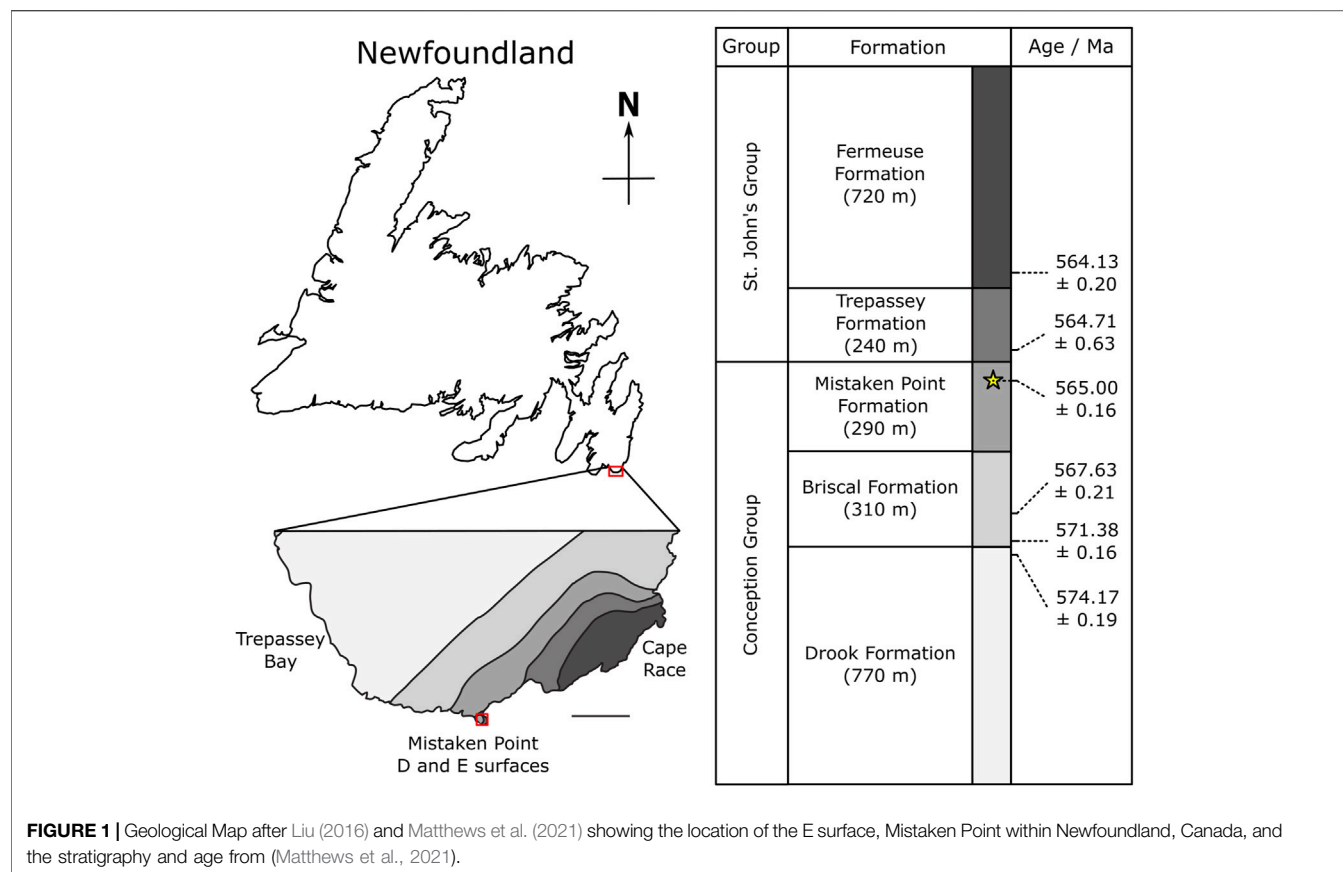


FIGURE 1 | Geological Map after Liu (2016) and Matthews et al. (2021) showing the location of the E surface, Mistaken Point within Newfoundland, Canada, and the stratigraphy and age from (Matthews et al., 2021).

setting of the upper Conception and St John's groups, with a concomitant increase in depositional energy and rate of deposition and a basinwards progradation of the locus of sedimentation (Wood et al., 2003; Matthews et al., 2021).

The Mistaken Point Formation is dominated by thick-bedded, mud-rich and ashy turbidites, punctuated by tuffaceous horizons (Wood et al., 2003; Ichaso et al., 2007; Matthews et al., 2021). The bed over the E surface has a thin, coarse crystal tuff, a lower graded portion and an upper portion that consists of alternating dark-light bands (above the chlorite-carbonate band; **Supplementary Figure S4**; Matthews et al., 2021). The exact mode of emplacement of the tuffaceous horizons was long thought to be primarily from water-lain ashfall events (where ashy material enters the basin, and gradually settles out through the water column). However, recent work suggests that at least some of these horizons were instead the product of ashy turbidites, and that they contain variable proportions of volcanoclastic (eruptive and/or unlithified reworked) and epiclastic (lithified and reworked) material (Noble et al., 2015; Kenchington et al., 2018; Matthews et al., 2021).

The mode of emplacement has direct implications for understanding the process that felled the fronds within the palaeocommunities, and therefore their preserved orientations. If the tuffs were water-lain, they are not necessarily associated with a gravity-driven flow, and accordingly the fronds were interpreted as having been felled by basin contour-parallel currents (Wood et al., 2003). However, if the smothering ashes

are a product of turbidity flows, then it is likely that the fronds were felled by these same flows (Matthews et al., 2021). In the specific case of the E surface, however, there is no contention that there is a gravity-driven flow origin for the alignment of fronds on the E Surface (F12 of Wood et al., 2003; Matthews et al., 2021)—though this may be atypical for the Mistaken Point Formation (Wood et al., 2003).

Gravity Flows and Their Expression in the Rock Record

Turbidites are the lithological record of deposition via sediment-laden turbidity currents, and exist on a continuum with other gravity-driven flows and their deposits (Haughton et al., 2009; Talling et al., 2012). The lack of evidence of fluvial input, together with the slump horizons that occur throughout the Mistaken Point Formation (Wood et al., 2003), suggests that the source of the flows in the Mistaken Point Formation are more likely to be those dominantly sourced from slope failure (slumping), rather than rivers. Therefore, here we focus only on the former. Gravity flow behaviour, and thus classification, is principally driven by two factors: the fraction of cohesive components within the sediment, and the overall concentration of sediments within the flow (e.g., Haughton et al., 2009). Higher sediment concentrations, and higher fractions of cohesive components (clay minerals and reworked muds), act to dampen turbulence at the sediment-water interfaces (Cantero et al., 2012; Talling

et al., 2012), and within dilute turbidity currents (Baas and Best 2002; Baas et al., 2009).

The coarse tuff immediately above the E surface could be indicative of particle sorting and winnowing within the more turbulent head of the turbidity current (Sparks and Wilson 1983), while the structure within the rest of the bed is consistent with the hybrid flow model of Haughton et al., 2009 (Matthews et al., 2021). On a broad scale, this mixed/hybrid flow interpretation may be reflected in the increased turbidite thickness within the Mistaken Point Formation [previously interpreted as turbidite ponding, (Ichaso et al., 2007)]. Surface weathering, synsedimentary and early diagenetic alteration of the volcanoclastic source for the Mistaken Point turbidites would have produced a clay-rich source sediment (cf. Kiipli et al., 2007), enhanced by addition of deposition from nepheloid plumes or as hemipelagic fallout (cf. Kenchington et al., 2018). This high clay content and high sediment load would have increased the cohesion within the flow and so dampened its turbulence (see Shringarpure et al., 2012), potentially generating conditions conducive to internal laminar flow (Fisher 1983), while dilution of the head of the turbidity flow likely brought concentrations below the threshold for a laminar-dominated regime (similar to the high-density turbidity or lower density mixed flows of Haughton et al., 2009), with turbulent conditions within the head of the turbidity flow.

As a flow moves down a slope, it can change character and concentration, reflected in different depositional products (Houghton et al., 2009). For example, after slumping, entrainment of water rapidly dilutes the head of the turbidity flow, inhibiting sediment-induced turbulence dampening (Hallworth et al., 1993; Cartigny et al., 2013). In contrast, entrainment of clay-rich material would have the opposite effect. Differential dilution-driven turbulence often manifests as Kelvin-Helmholtz instabilities (Liu and Jiang 2014), wherein turbulent eddies rotate about a horizontal axis orthogonal to the direction of turbidity current propagation (see “roll waves” of Cartigny et al., 2013)—important when we are thinking about the processes controlling frond orientation.

MATERIALS AND METHODS

Data Processing

In this study we used mapped data from the E surface taken from Mitchell et al., 2019. Mitchell et al. LiDAR scanned the E surface using a Faro Focus 330X to ensure spatial accuracy was maintained over large areas. The LiDAR scans resulted in a 3D surface mesh of 1 mm resolution. In order to get sufficient resolution to resolve taxonomic identity, Mitchell et al. also laser scanned the E surface using a Faro Scan Arm v6LLP, resulting in surface meshes of ~0.050 mm resolution. The high-resolution scanning was done in grids of ~1 m × 1 m. Due to large file sizes, these high-resolution scans could not all be viewed simultaneously, so control points were marked in each high-resolution scan, and in the LiDAR scan, enabling accurate combination of the high-resolution scans with the LiDAR surface data (performed using Geomagic 2015). A photomap

was created by photographing the specimens along a horizontal and vertical grid, then using Agisoft Photoscan software v1.3.5 to create a photogrammetric render of the surface. The LiDAR scan was then imported into Photoscan, and the photographs aligned on the LiDAR scan to ensure large-scale accuracy. An orthomosaic of the surface was produced within Agisoft PhotoScan, from which the data was collected. The combination of LiDAR, LLP and photogrammetry enabled accurate retention of angle data between photographs, with minimal perspective projection distortion (Mitchell et al., 2019). Specimens were binned into 8 morphogroups: *Beothukis*—a unifoliate, spatulate-fronded rangeomorph, with a short—or absent—stem and holdfast (Brasier and Antcliffe 2009; Hawco et al., 2020; **Figure 2A, C**); *Bradgatia*—a multifoliate rangeomorph consisting of up to eight folia from a central branching point on an inferred holdfast (Boynton and Ford 1995; Flude and Narbonne 2008; **Figure 2B**); *Charniodiscus procerus*—a unifoliate arboreomorph possessing a circular holdfast, elongate stem, and a lanceolate frond (often laterally displaced) without fractal, rangeomorph-style branching (Laflamme et al., 2004; **Figure 2A**); *Charniodiscus spinosus*—a unifoliate arboreomorph with a large ovate frond, lacking rangeomorph-style branching, tipped with an elongate spine, connected to a large holdfast via a short cylindrical stem (Laflamme et al., 2004; **Figure 2D**); *Fractofusus*—a spindle-shaped rangeomorph with bundled frondlets offset along a central axis (Gehling and Narbonne 2007; Mitchell et al., 2015; **Figure 2F**); *Plumeropriscum*—a multifoliate rangeomorph composed of at least nine first order branches furcating from an elongate cylindrical stem, attached to the substrate by a discoidal holdfast (Mason and Narbonne 2016; **Figure 2F**); *Primocandelabrum*—a multifoliate rangeomorph consisting of a large holdfast, elongate stem, and substantial crown composed of three first order branches (Hofmann et al., 2008; Kenchington and Wilby 2017; **Figure 2G** and *Thectardis*—an erect conical taxon lacking evidence of a holdfast (Clapham et al., 2004; **Figure 2E**). We used the size and orientation data from Mitchell et al. (2019) for *Fractofusus*. We identified 18 *Beothukis*, 52 *Bradgatia*, 61 *C. procerus*, 31 *C. spinosus*, 20 *Plumeropriscum*, 47 *Primocandelabrum* and 27 *Thectardis* and 1,593 *Fractofusus* across 85.42 m² of the E surface bedding plane.

Retrodeformation

The E surface has undergone tectonic deformation so prior to any analyses, retrodeformation needs to be performed to re-engineer the organisms back to their in-death dimensions (Wood et al., 2003; Gehling and Narbonne 2007; **Figure 3**). To perform the retrodeformation, we collected the dimensions and orientations of 24 representative, large, discs across the E Surface (**Supplementary Figure S1**). Utilising a constant area retrodeformation method, the principal axis lengths for each disc were extracted. Following the methodology of Mitchell et al. (2015), a regression was fitted to determine the retrodeformation ratio (1.75, within the confidence interval (1.71 ± 0.08) of Mitchell et al. (2015), which was applied across the entire E surface. To apply this retrodeformation, the annotated photosquares were aligned and stitched together in

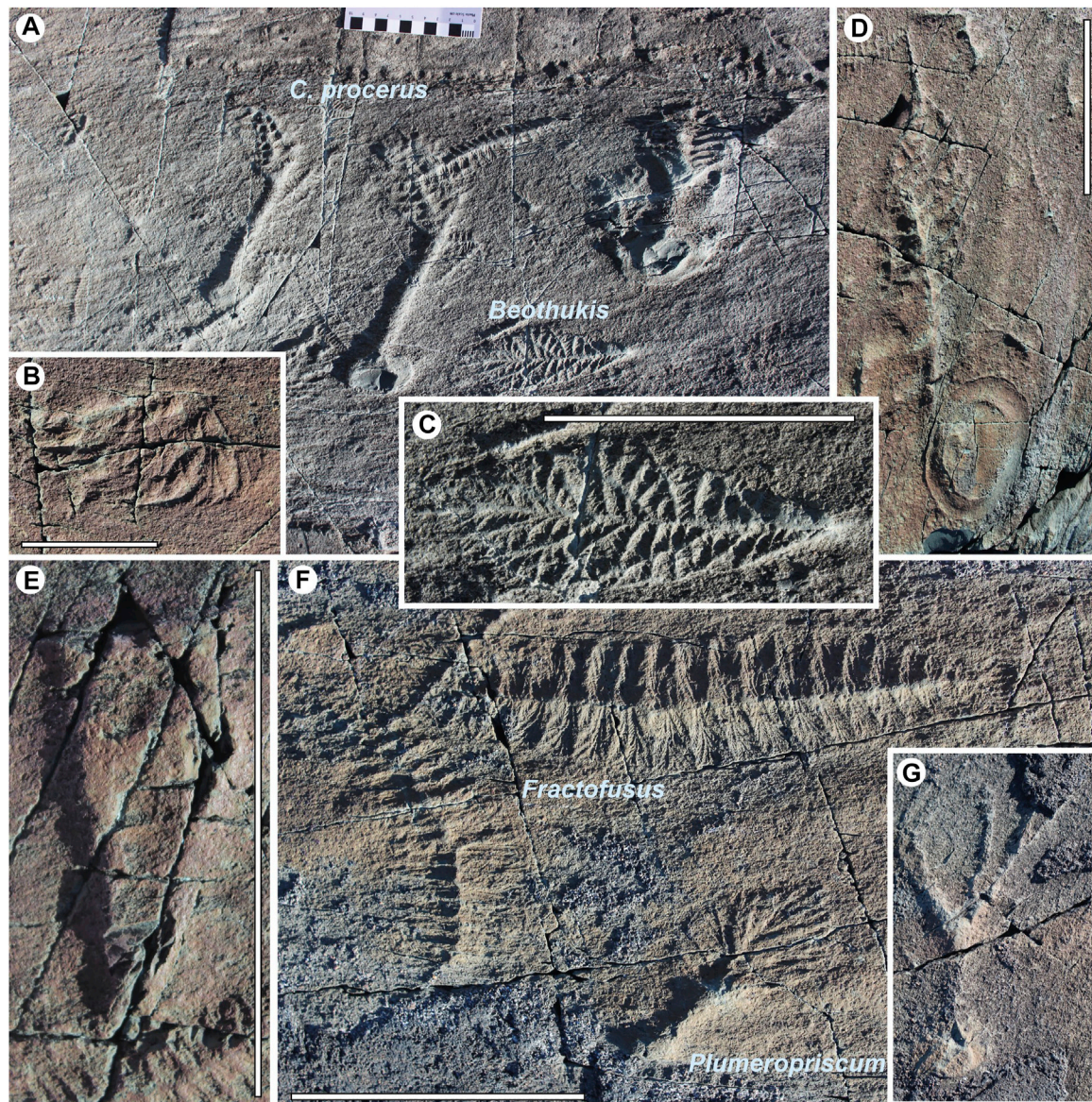


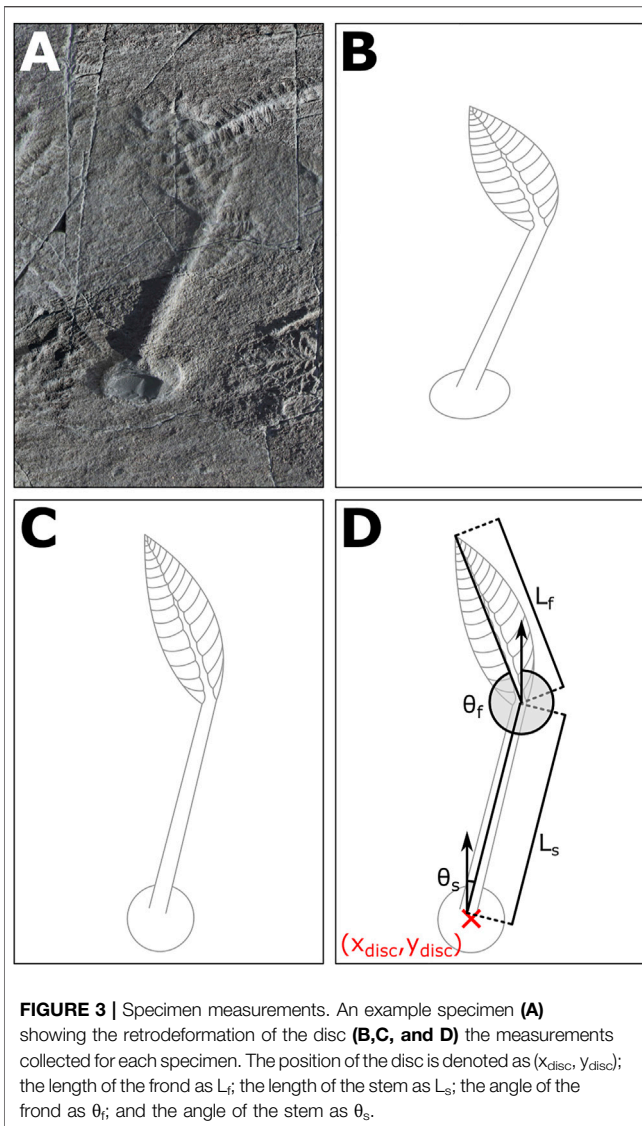
FIGURE 2 | E surface taxa included in this study. (A) *Charniodiscus procerus* and *Beothukis* and (B) Close up of *Bradgatia* (C) *Beothukis* (D) *Charniodiscus spinosus* (E) *Thectardis*, (F) *Fractofusus* and *Plumeropriscum* and (G) *Primocandelabrum*. Scale bar is 5 cm.

Inkscape v0.92.4, and rotated to align the principal axes of the mean disc with the vertical and horizontal axes of the document—thus aligning the eigenvectors of retrodeformation with the axes of the document. From here, constant area retrodeformation can be characterised as a deformation, which can be achieved with shortening and elongation of the vertical and horizontal axes. The retrodeformed surface was then rotated to the original orientation. Overall, the photosquares were shortened by 26.7% along the eigenvector oriented 78.5°, and elongated 36.8% along the orthogonal eigenvector of 168.5° (Supplementary Figure S1). We note that, whilst retrodeformation techniques have the potential to introduce error (Liu et al., 2011), the strong correlation of the regression

($R^2 = 0.86$) (Supplementary Figure S1) suggests that our retrodeformation technique is suitable for the spatial scale of the mapped E Surface. The orientation measurements are different for *Fractofusus* because unlike the frondose organisms there is no differentiation between the top and bottom half of the organism, such as a disc. As such, the angles are limited to a 180° range of 0° to 180° with the angle of e.g., 200° being equivalent to 20°.

Statistical Analyses

For each taxon population we performed four tests in R v4.0.4. To test for non-uniform distributions of orientation data we used the Rao's Spacing Test of Uniformity using the package CircStats



v0.2-6 (Agostinelli and Agostinelli 2018), with a p -value < 0.05 indicating a non-uniform distribution (Rao 1976). For our data, a significant p -value indicates non-random felling of organisms, with some orientations exhibiting a greater frequency than would otherwise be expected from random felling. In order to test for multimodal distributions within angular data we used the Hermans-Rasson test (HR test of Landler et al., 2019) using the package CircMLE v3.0.0 (Fitak and Johnsen 2017). Where multi-modal distributions were found, the mean values for each peak were identified utilising the Gaussian finite mixture model-based clustering algorithms of mclust v5.4.7 (Fraley and Raftery 2017). To account for the circular nature of angular data, the density distribution was inspected and split at a minimum to ensure any peaks coincident with 0° were not bisected. This split produced a continuous 360° density distribution with no assumed peak bisection. When more than one distribution was present (i.e. bidirectional distributions), the data were partitioned into two peaks, whilst unimodal distributions (including those found to be

composed of multiple coincident distributions) were left unpartitioned. The circular equivalent to a normal distribution is the von Mises distribution, tested using a Watson's goodness of fit (Agostinelli and Agostinelli 2018). A statistically significant p -value output corroborates a von Mises distribution—where a significant von Mises distribution was found, the models of Schnute and Groot (1992) were employed to test for a variety of modelled orientation scenarios. For bimodally-distributed taxa, the constituent distributions were partitioned and frond lengths cross-compared utilising a Mann-Whitney test. Statistical significance would suggest non-uniform sampling from the same parent population; in essence, the orientation-partitioned data would exhibit different frond length distributions.

In order to investigate the spatial distribution of populations which exhibited significant multi-modal orientations, random labelling analyses (RLA) were used. RLA are a type of spatial point process analysis whereby the position of each point (here fossil specimen) is kept constant, but the label (here the orientation group) is randomly permuted about the points (Illian et al., 2008). As such, RLAs do not directly measure the aggregation or segregation between labels (here orientation patterns), so do not test the processes that resulted in labels, but instead measure the differences in spatial distributions of the labels independently of the positions of the fossil specimens (cf. Mitchell et al., 2018). Spatial distributions are commonly described using pair correlation functions (PCFs) which describe how the density of points (i.e. fossil specimens) changes as a function of distance from the average specimen (e.g., Illian et al., 2008). RLAs assess the differences between two characters (orientation group 1 or group 2) of the populations by calculating variations between PCFs by considering the Difference test and the Quotient test (Wiegand and Moloney 2013). The Difference test is the calculation of the difference the distribution of each group in turn (PCF₁₁ is the distribution of group 1 and PCF₂₂ the distribution of group 2) i.e. PCF₁₁—PCF₂₂. These differences test the relative aggregation (or segregation) of the spatial distributions of the orientations compared to each other. If PCF₁₁—PCF₂₂ = 1 then the orientation groups are randomly distributed about the surface. The Quotient test calculates how the relative group (Diggle et al., 2005) changed with respect to the total density (i.e. the joined distribution of both group 1 and group 2). The distribution of group 1 relative to the joined groups PCF_{1,1+2}, and group 2 relative to the joined groups PCF_{2,2+1} with the Quotient test as the calculation: PCF_{1,1+2}—PCF₂₁/PCF_{2,2+1}. If PCF₁₂/PCF_{1,1+2}—PCF₂₁/PCF_{2,2+1} > 0 then group 2 is mainly located in areas with high density of the joint pattern, and group 1 is in low density areas (i.e., group 2 has more neighbours than group 1. If this Quotient is significantly non-zero, then the process underlying the characters is density-dependent. In order to test whether any observed patterns were significantly different from a random distribution we follow Mitchell and Harris 2020 and use two different methods, which are commonly used to establish acceptance or rejection of the null hypotheses for ecological data (e.g., Illian et al., 2008 and references therein): 1) Monte Carlo simulations, and 2) Diggle's goodness-of-fit test p_d , which represents the total squared deviation between the observed pattern and the simulated pattern across the studied

TABLE 1 | Results of uniformity tests, with 5% significance levels used to indicate rejection of the null models i.e., non-random orientations for the Rao's spacing and Hermans-Rasson tests and von Mises distribution (normally distributed orientation data) for the Watson's test.

Taxa	Measurement	Rao's Test <i>p</i> -value	Hermans-Rasson test <i>p</i> -value	Watson's Test <i>p</i> -value
<i>Beothukis</i>	Fronds	<0.001	0.0001	>0.10
<i>Bradgatia</i>	Fronds	<0.001	0.0001	>0.10
				<0.05
<i>C. procerus</i>	Stems	<0.001	0.0001	>0.10
	Fronds	<0.001	0.0001	>0.10
<i>C. spinosus</i>	Stems	<0.001	0.0001	>0.10
	Fronds	<0.001	0.0001	>0.10
<i>Fractofusus</i>	Length	<0.001	0.0010	<0.01
<i>Plumeropriscum</i>	Stems	<0.001	0.0001	>0.10
	Fronds	<0.001	0.0001	>0.10
<i>Primocandelabrum</i>	Stems	<0.001	0.0001	<0.01
	Fronds	<0.001	0.0001	<0.05
<i>Thectardis</i>	Cones	<0.010	0.0001	>0.10
				>0.10

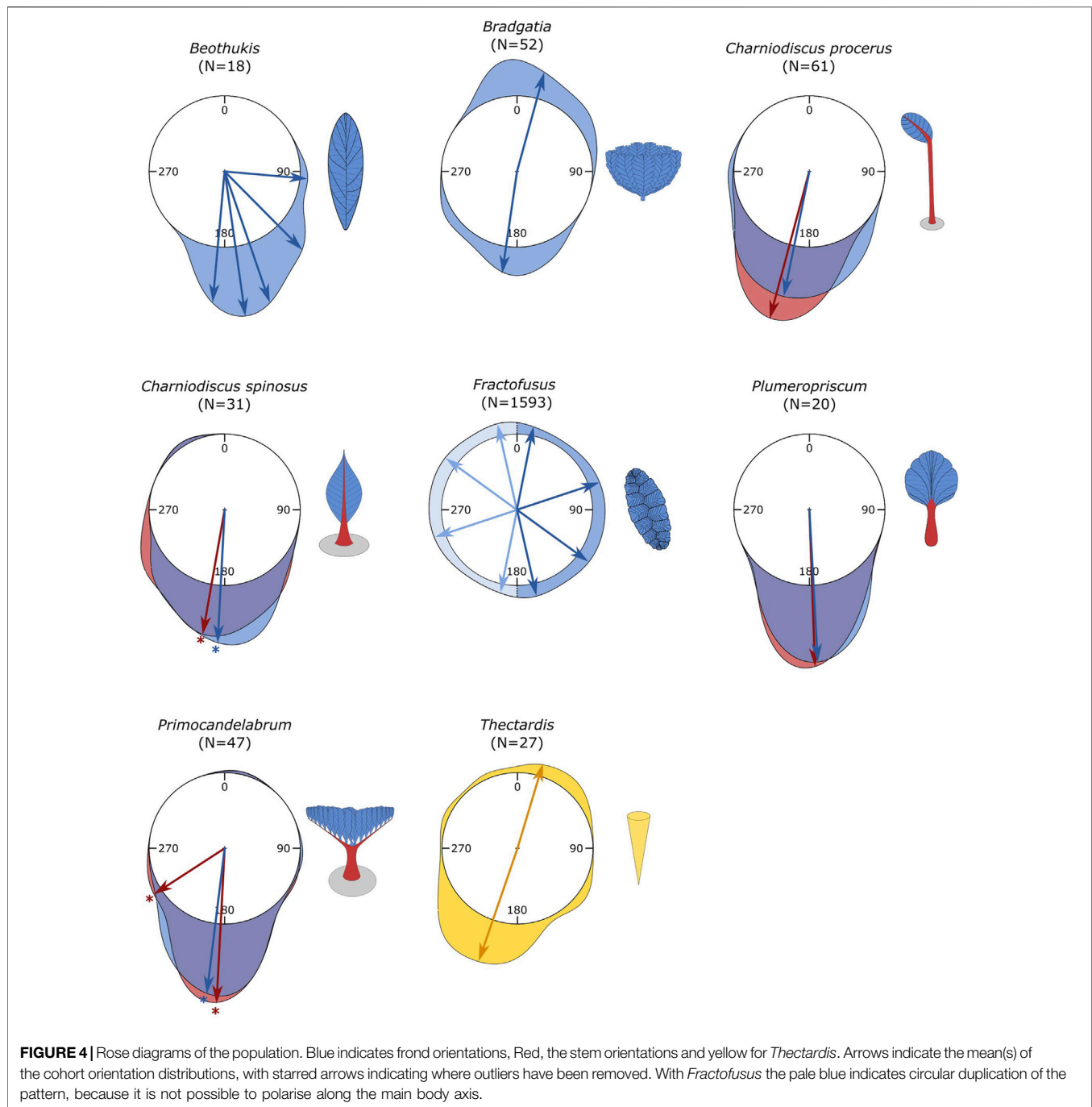
Where more than one cohort is found (such as for *Bradgatia*) there will be a Watson's Test for each cohort.

TABLE 2 | Cohort analyses for each morphogroup orientation distribution. σ indicates the standard deviation of each cohort with respect to the provided mean orientation. Where all cohorts within a population have equal standard deviation (such as *Beothukis*) a single σ is given, and where each σ varies according to the cohort (unequal variance) then a value is given for each cohort. Note that the *Fractofusus* data represents the simplest of two statistically-indistinguishable BIC models (**Supplementary Figure S2**). Note for *C. spinosus* and *Primocandelabrum* the cohorts of one represents outliers, which were not well resolved by cohort-analyses (**Supplementary Figure S3**).

Taxa	Measured	N	Mean Orientation (°)	σ	Proportion (%)
<i>Beothukis</i>	Fronds	1	95	2.45	5.56
		4	135		22.22
		5	161		27.78
		3	172		16.67
		5	185		27.78
<i>Bradgatia</i>	Fronds	30	15	26.79	57.69
		22	188		42.31
<i>C. procerus</i>	Stems	61	195	18.89	100.00
	Fronds	61	192	30.23	100.00
<i>C. spinosus</i>	Stems	30	190	30.87	96.77
		1	326	NA	3.23
	Fronds	30	183	24.83	96.77
		1	328	NA	3.23
<i>Fractofusus</i>	Fronds	206	11 (191)	10.47	12.93
		602	72 (252)	24.83	37.79
		517	126 (306)	18.96	32.45
		268	167 (347)	7.28	16.82
<i>Plumeropriscum</i>	Stems	20	178	16.73	100.00
	Fronds	20	177	17.26	100.00
<i>Primocandelabrum</i>	Stems	42	183	13.74	89.36
		3	237	13.74	6.38
		1	11	NA	2.13
		1	119	NA	2.13
	Fronds	45	187	19.05	95.74
		1	14	NA	2.13
		1	98	NA	2.13
<i>Thectardis</i>	Cones	7	17	33.00	25.93
		20	199		74.07

distances (Diggle et al., 2005). For each RLA test performed, 999 Monte Carlo simulations were used to generate simulation envelopes around the random PCF difference (e.g.,

$PCF_{11} - PCF_{22} = 0$) and the p_d values were calculated using Diggle's goodness-of-fit test. If the observed test (either Difference or Quotient) fell outside the RLA generated Monte



Carlo envelopes and also had $p_d < 0.1$, then the distributions were found to be significantly different. RLAs were performed in Programita (Wiegand and Moloney 2013).

RESULTS

For all taxa we found statistically significant non-random distributions using the Rao's Spacing Test of Uniformity and the improved Hermans-Rasson—all $p < 0.01$, **Table 1**. The

majority of taxa exhibited a non-von Mises (i.e., non-normal) distributions as per the Watson's test (**Table 1**). One *Bradgatia* cohort ($p < 0.05$), and the *Primocandelabrum* stems ($p < 0.01$), and fronds ($p < 0.05$) exhibited von Mises distributions (**Table 1**). The von Mises distributions for *Primocandelabrum* enabled model fitting to the orientation distributions of *Primocandelabrum*, which were found to exhibit bi-modal distributions (**Supplementary Figure S2**).

Analyses of the number of cohorts within each morphogroup orientation distribution varied between 1 and 5 (**Table 2**;

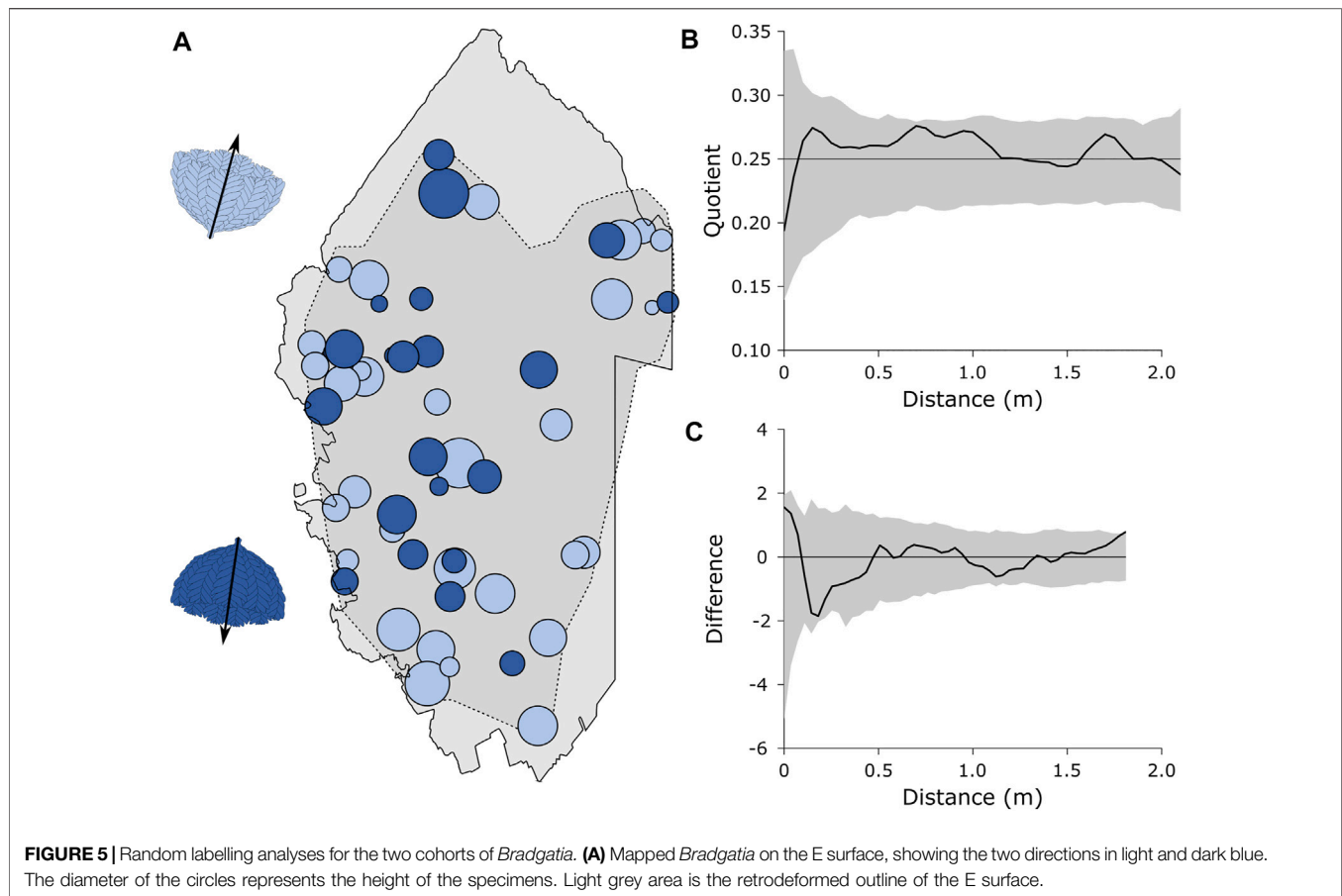


Figure 4). For *C. procerus* and *Plumeropriscum*, the stems and fronds exhibited uni-modal distributions, with similar mean orientations of 195° and 192° for *C. procerus* stems and fronds and 178° and 177° for *Plumeropriscum* (Table 2; Figure 4). The majority (96.77%) of *C. spinosus* stems and fronds exhibited a unimodal distribution (190° and 183° respectively), with a single outlier orientated at 326° for stem and 328° for frond (Table 2; Figure 4, Supplementary Figure S3). Similarly, *Primocandelabrum* specimens exhibit a unimodal distribution for their fronds (95.74%, 187°) and with a minor bimodal component for the stems (89.36%, 183°; 6.38%, 237°), with two singleton outliers, and frond at 14° and the second with its stem at 119° and frond at 98° (Table 2; Figure 4, Supplementary Figure S3). *Thectardis* and *Bradgatia* exhibited bi-modal distributions, with different distributions indicated by the mean orientations being notably different between the two groups, in contrast to *Primocandelabrum* and *C. spinosus* (Table 2; Figure 4). The majority of *Bradgatia* specimens (57.69%) formed a cohort with the mean orientation of 15°, with the remainder (42.31%) within the cohort at 188° (Table 2; Figure 4). The majority of *Thectardis* specimens (74.07%) formed a cohort with the mean orientation of 199°, with the remainder (25.93%) within the cohort at 17° (Table 2; Figure 4). The distribution of sampled *Beothukis* specimens formed 5 distinct cohorts

(Table 2), with one specimen notably different at 95° to the other four cohorts, which had similar mean orientations with the unimodal taxa orientations. The small number of specimens within the *Beothukis* distributions indicates that the relatively high number of cohorts could be an artefact of small sample sizes. *Fractofusus* exhibited a multi-modal distribution, with four cohorts at 11°, 72°, 126° and 167° within a 180° distribution (Table 2; Figure 4).

Inspection of the distributions in Figure 4 shows that while the number of statistically significant cohorts within each taxon varies, the stemmed taxa (*C. spinosus*, *C. procerus*, *Plumeropriscum* and *Primocandelabrum*) and *Beothukis* were all orientated in similar directions, while *Bradgatia* and *Thectardis* had a significant proportion of specimens with an antipodal orientation (Table 2; Figure 4). While the mean orientations of the multiple *Beothukis* cohorts were all tightly clustered, showing clear directionality in a single direction, the *Fractofusus* mean orientations were evenly distributed across the range, with no such directionality (Figure 4).

Analyses of the bimodally distributed taxa found no significant differences mean frond length for *Bradgatia* ($p = 0.1850$), or cone length for *Thectardis* ($p = 0.4547$) between cohorts. *Bradgatia* was the only taxon that exhibited significant bidirectionality in numbers sufficient for RLA (Figure 5A). The Quotient test RLA, which describes the relative density dependence of different factors within a spatial population found that there was no

density dependence between the two *Bradgatia* orientation groups ($p_d = 0.8040$, **Figure 5B**). The Difference test RLA, which tests for the difference between the spatial distributions of the two orientation groups, were not significantly different ($p_d = 0.4104$, **Figure 3C**), although the observed difference was close to the outside the simulation envelope which could indicate a larger spatial scale pattern not captured within our data.

DISCUSSION

The orientation distributions of fossil specimens are well established as a mechanism to indicate palaeocurrent directions (Toots 1965; Jones and Dennison 1970; Ichaso et al., 2007). The orientation distribution of a given taxon depends on its mode of life, with erect benthic organisms exhibiting strong directionality, in contrast to non-erect organisms which have limited directionality (Toots 1965; Jones and Dennison 1970; Smith 1980; Demko 1995). These explanations of orientation distributions have been used to understand the mode-of-life of Ediacaran taxa, with qualitative examination of *Fractofusus* specimens showing even orientation distribution suggestive of a reclining mode of life (Gehling and Narbonne 2007). In contrast, Ediacaran fronds such as *Charniodiscus* and *Charnia* have been interpreted as erect organisms, due to the morphological similarities to extant benthos such as sea pens (Seilacher 1992; Laflamme and Narbonne 2008; Laflamme et al., 2012) and—crucially—the orientation of these fronds are noted to have a strongly preferred orientation, suggested to be aligned to the contour-parallel current which felled them (Wood et al., 2003; Narbonne 2005; Ichaso et al., 2007; Laflamme et al., 2012). Strongly orientated organisms have been interpreted as erect because an organism attached to the seafloor at a single point will have the majority of its body pulled by the current, orientating it with its long axis parallel to this current (Hofmann et al., 2008). In contrast, if an organism is reclining on the substrate, it will not be subject to such currents, so will not display strong orientations (Gehling and Narbonne 2007; Bamforth and Narbonne 2009; Mitchell et al., 2015).

The relationship between fossil orientation and mode-of-life is pertinent because there has recently been revived debate surrounding the nature of the life habit of the Ediacaran rangeomorphs (e.g., McIlroy et al., 2020). Where fronds have historically been interpreted as displaying a mixture of upright and recumbent lifestyles (Ford 1958; Laflamme and Narbonne 2004; Laflamme and Narbonne 2008; Wilby et al., 2011), recent work has posited that recumbent lifestyles are more likely for some rangeomorph fronds. Orientation analyses allows us to test between these two different life habits in a statistically robust way. This study reflects the most statistically rigorous attempt to quantitatively test the orientation distributions of multiple E surface taxa, and quantify differences in orientations between the stems and fronds of these taxa. We find significant differences in felling behaviour between the stemless *Bradgatia* (*sensu* Flude and Narbonne 2008) and *Thectardis* (in broad agreement with Clapham et al., 2004), *Fractofusus* (Gehling and

Narbonne 2007), and all other taxa (*Beothukis*, the arboreomorphs, *Primocandelabrum*, and *Plumeropriscum*), which show unidirectional felling all oriented towards the south. *Fractofusus* shows no notable directionality in any direction, whereas orientation distributions of *Bradgatia* and *Thectardis* both exhibit evidence of bidirectional felling. We found no significant height/sized-based correlations with orientation or outliers. Our results confirm the qualitative results of previous authors (Wood et al., 2003; Narbonne et al., 2005; Gehling and Narbonne 2007; Laflamme et al., 2012) whereby frondose taxa such as *Beothukis*, *Charniodiscus* and *Primocandelabrum* were erect in the water-column, anchored to the sea-floor, while *Fractofusus* lived close to the substrate in a reclined habit. Our results do not support recent suggestions that the fronds like *Beothukis* reclined on the sediment in life (McIlroy et al., 2020). The orientation distributions we find for *Bradgatia* and *Thectardis* are also consistent with an upright mode of life (Clapham et al., 2004; Flude and Narbonne 2008) and felling in a (bidirectional) current. All of our results and interpretations are based on the behaviour of the majority of specimens within a taxon, and confirm the utility of populations of specimens rather than outliers to infer the ecology for the entire population of a given taxon (e.g., Benhadi-Marin 2018). Describing population distributions enables intra-specific variability to be captured, and thus enables comparison between populations. Indeed, it is not possible to compare the orientations of two specimens in a statistically rigorous and robust way without accounting for intra-specific variability, i.e., without quantifying the population behaviour. There are, notably, multiple cohorts within the orientation distributions of *Beothukis*. However, while *C. procerus*, for example, exhibits different mean orientation directionality to *Beothukis*, the 95% confidence interval (as given by two sigma) places all but one specimen of *Beothukis* (the holotype, oriented at 95°) within the *C. procerus* confidence interval—and indeed, within the 95% confidence intervals of all other southerly-oriented taxa. Thus, the *Beothukis* and *C. procerus* populations do not have significantly different orientations. It is possible of course that the *Beothukis* holotype belongs to a different species than the remainder of the population assigned by us to that taxon based on branching characters (McIlroy et al., 2020). However, recent work on the taxonomy of *Beothukis*, which demonstrates that the holotype is well within all other specimens with comparable morphology, and which were assigned by those authors to that taxon (Hawco et al., 2020) renders this unlikely. Indeed, an outlier of *Primocandelabrum*—whose morphology, and the orientations of the rest of the population, are entirely at odds with a reclined mode of life—is also oriented at 95°. Our orientation analyses of the *Beothukis* population demonstrates how the holotype orientation is an outlier and not representative of the population. Our results thus confirm an erect lifestyle for *Beothukis* (Wood et al., 2003; Laflamme and Narbonne 2008; Laflamme et al., 2012), contra McIlroy et al., 2020.

Charniodiscus procerus specimens—the taxon with the proportionally longest stem of any studied here (Laflamme et al., 2004)—are all oriented south, in a single cohort, with 1

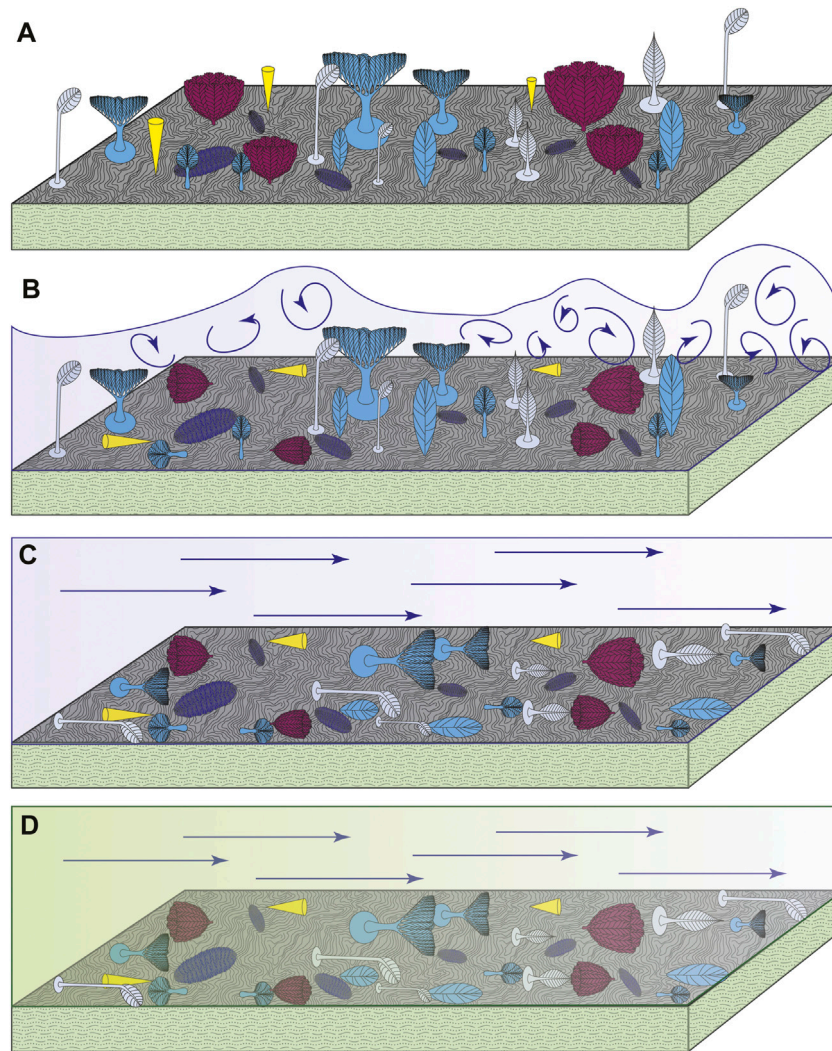


FIGURE 6 | Schematic illustrating the sequence of events that yield the preserved orientation distributions. **(A)** E surface community in life, with all fronds bar *Fractofusus* having an upright mode of life. **(B)** The dilute, turbid head of the gravity flow fells organisms with a high centre of gravity, including *Thectardis* and *Bradgatia*, producing a bimodal orientation distribution pattern. Note the orientation of the turbulent eddies (indicated by curled dark blue lines) relative to the direction of overall flow. **(C)** The laminar tail of the gravity flow fells all other upright fronds on the surface. Increased sediment concentrations within the tail of the gravity flow dampen turbulence, so the remaining fronds are felled in a solely laminar flow regime (indicated by straight dark blue lines). **(D)** Ash settles out of the flow, and smothers the community with the preserved distribution of orientations. Yellow = *Thectardis*; pink = *Bradgatia*; dark blue = *Fractofusus*; grey = *Chamiodiscus procerus* and *Chamiodiscus spinosus*; blue = upright fronds felled with a unimodal orientation (*Beothukis*, *Plumeropriscum* and *Primocandelabrum*).

outlier individual oriented antipodally (**Supplementary Figure S3**). All bar one specimen of *Beothukis* is oriented south, although notably with greater variance than the stemmed arboreomorphs (**Figure 4**). All *Plumeropriscum* specimens are oriented south, along with the majority of *Primocandelabrum* (**Figure 4**). Two *Primocandelabrum* specimens are oriented in a different orientation, away from the main direction (**Figure 4**, **Supplementary Figure S3**). In contrast, *Bradgatia* specimens are divided almost equally between north and south felling directions (**Figure 4**). These data would suggest that there is a correlation between proportional stem length and felling direction, and for the multifoliate taxa, there seems to be a strong correlation between presence of a stem and felling

direction. *Thectardis*—with its narrow base and wide top—like *Bradgatia*, also shows a significant portion felled in the northern direction (**Figure 4**).

Together, our data suggest that those taxa with bases that are proportionally narrow compared to the widths of their tops (*Thectardis* and *Bradgatia*) show significantly different felling behaviours to those taxa that are more elongate and equal in shape, and that those taxa with the longest and thickest stems show the most consistent felling direction. *Beothukis*, for example, appears to show a sympodial central axis (Brasier et al., 2012; Hawco et al., 2020), and has the widest spread of any of the unifoliate and dominantly south-felled taxa. Equally, although *Primocandelabrum* has a sturdy stem, it has a

proportionally wide top, and two specimens that are felled at a different angle from the main population. *Charniodiscus spinosus* has a much shorter stem than *C. procerus*, and also has a few specimens that are felled antipodally. The top-heavy morphology of *Primocandelabrum*, *Bradgatia* and *Thectardis* would presumably induce greater drag compared to the more streamlined unifoliate fronds, making them more susceptible to felling—and also potentially to adhesion to the matground—though the sturdy stems of *Primocandelabrum* helping to redress this susceptibility in all but a few individual cases.

Random labelling analyses suggest that these differences are not an artifact of different flow regimes in different areas, indicating that differences in orientations between stemmed and stemless organisms may reflect genuine differences in the effect of flow on stemmed and stemless taxa. Fronds and stems behave differently in flow: at a flow velocity of 0 ms^{-1} , both the frond and the stem will be fully upright, with no deflection, but as the flow velocity increases the tubular cross-section of the stem maximises the second moment of area, thus reducing the extent of bending under stress, and so this tubular morphology would serve to reduce the probability of failure via buckling (Wegst and Ashby 2007). Indeed, the high and positive epirelief of *Charniodiscus procerus* stems (Figure 2A) may indicate further biomechanical adaptation to flow conditions via wall thickening or changes in tissue rheology. Perhaps, because of this morphology the stem impeded felling of stemmed taxa within the enhanced velocities of the turbulent head of a turbidity flow, according with studies concerning the mechanical properties of stems, for example crinoids and aquatic plants (Baumiller and Ausich 1996; Ming-Chao and Chang-Feng 1996; Luhar and Nepf 2011).

Our interpretations are further supported by differential resolution of preservation between taxa. We observe the finest resolution of rangeomorph element preservation within *Bradgatia* (Figure 2B) and *Beothukis* (Figure 2A,C), whereas the primary branching units of *Primocandelabrum* and *Plumeropriscum* are rarely well-defined (Figure 2F,G). Though this may reflect a taphonomic signature, common membership within Rangeomorpha suggests similar modes of element construction, and instead we favour an interpretation comparable to that of Laflamme et al. (2004), wherein increasing volumes of sediment between the mat and the organism reduce preservation. This corroborates our model of comparatively rapid felling of the stemless *Bradgatia* and *Beothukis* (*Thectardis* does not possess rangeomorph branching, and thus cannot be considered here), whereas the stemmed *Primocandelabrum* and *Plumeropriscum* remained upright while small quantities of sediment were deposited out of the flow and onto the mat, precluding fine-scale preservation of the frondlets. Indeed, most *Charniodiscus procerus* specimens exhibit poorly-preserved fronds, consistent with our model—though note that arboreomorph tissue properties may differ from those of rangeomorphs, and thus may limit intercomparability.

These data support a two-phase model of felling (Figure 6), corresponding to the different flow regimes within a gravity flow. We infer that during the turbulent head of the flow, most fronds

were buffeted by Kelvin-Helmholtz vortices. However, some easily-felled taxa (*Bradgatia* and *Thectardis*) were felled by this turbulence, producing a bimodal distribution of felling orientations (Figures 4, 6). The transition to laminar flow within the body of the turbidity flow led to the felling of most remaining fronds, in a unimodal distribution (Figures 4, 6). In Charnwood Forest, we know that at least some fronds were capable of surviving small-scale disturbance events (Wilby et al., 2015). Wilby et al. focussed on the bimodal population structures of the unifoliate rangeomorph *Charnia*, but documented other, stemmed taxa that were also preserved with a bimodal population structure (*Primocandelabrum*, *Hylaeacullulus* and *Charniodiscus*). Together with our data, this suggests that stemmed and elongate taxa showed greater survivability in high velocity flow. Height in the water column has previously been demonstrated to increase propagule dispersal, and doesn't appear to provide refuge from resource competition (Mitchell and Kenchington 2018). Our work suggests that stems may have had an additional function—lending greater resilience to felling in turbulent and high velocity flow regimes. These insights hint at potential environmental influences on the morphological composition of Ediacaran organisms.

CONCLUSIONS

We provide robust quantitative analyses of the orientation of populations of specimens from the Mistaken Point E surface. Our data support traditional palaeobiological models for the life habits of different organisms which lived in this community, with the majority of frondose organisms living upright in the water column while the spindle-shaped *Fractofusus* lived flat on the seafloor. Previous authors have suggested that current type and flow rate may impact community composition, but we demonstrate for the first time how the presence or absence of anatomical features impact survivability in different flow regimes. Specifically, we find that the presence of a stem (and potentially its proportional length) lends greater resilience to turbulent currents. Future work may find that such traits affect the presence and abundance of different morphologies under different environmental conditions, and potentially even the structuring of communities as they experience changing flow conditions.

DATA AVAILABILITY STATEMENT

The original contributions presented in the study are included in the article/Supplementary Material, further inquiries can be directed to the corresponding author.

AUTHOR CONTRIBUTIONS

PV conceived and designed the project. Analyses were performed PV and EM. PV, EM and CK contributed to data collection from

photosquares and all authors (PV, CK, FD and EM) contributed to the writing up of the final manuscript.

FUNDING

This work has been supported by the Natural Environment Research Council Independent Research Fellowship NE/S014756/1 to EGM and a Natural Environment Research Council grant NE/V010859/1 to FSD. FSD acknowledges support from the Royal Commission for the Exhibition of 1851 and Merton College, Oxford. CGK was supported by Leverhulme Trust (ECF-2018-542) and by the Isaac Newton Trust 18.08(H).

REFERENCES

- Agostinelli, C., and Agostinelli, M. C. (2018). "CircStats Package," in *Topics in Circular Statistics*.
- Baas, J. H., Best, J. L., Peakall, J., and Wang, M. (2009). A Phase Diagram for Turbulent, Transitional, and Laminar Clay Suspension Flows. *J. Sediment. Res.* 79, 162–183. doi:10.2110/jsr.2009.025
- Baas, J. H., and Best, J. L. (2002). Turbulence Modulation in Clay-Rich Sediment-Laden Flows and Some Implications for Sediment Deposition. *J. Sediment. Res.* 72, 336–340. doi:10.1306/120601720336
- Bamforth, E. L., Narbonne, G. M., and Anderson, M. M. (2008). Growth and Ecology of a Multi-Branched Ediacaran Rangeomorph from the Mistaken Point Assemblage, Newfoundland. *J. Paleontol.* 82, 763–777. doi:10.1666/07-112.1
- Bamforth, E. L., and Narbonne, G. M. (2009). New Ediacaran Rangeomorphs from Mistaken Point, Newfoundland, Canada. *J. Paleontol.* 83, 897–913. doi:10.1666/09-047.1
- Baumiller, T. K., and Ausich, W. I. (1996). Crinoid Stalk Flexibility: Theoretical Predictions and Fossil Stalk Postures. *Lethaia* 29, 47–59. doi:10.1111/j.1502-3931.1996.tb01836.x
- Benhadi-Marin, J. (2018). A Conceptual Framework to deal with Outliers in Ecology. *Biodivers. Conserv.* 27, 3295–3300. doi:10.1007/s10531-018-1602-2
- Bobrovskiy, I., Hope, J. M., Ivantsov, A., Nettersheim, B. J., Hallmann, C., and Brocks, J. J. (2018). Ancient Steroids Establish the Ediacaran Fossil *Dickinsonia* as One of the Earliest Animals. *Science* 361, 1246–1249. doi:10.1126/science.aat7228
- Boynton, H., and Ford, T. D. (1995). Ediacaran Fossils from the Precambrian (Charnian Supergroup) of Charnwood Forest, Leicestershire, England. *Mercian Geologist* 13, 165–182. Available at: http://www.emgs.org.uk/files/mercian_voll3on/Mercian%20Geologist%20volume%2013%201992-1995/MG13_4_1995_165_Boynton&Ford_Ediacaran%20fossils%20from%20Charnian%20of%20Charnwood%20Forest.pdf
- Brasier, M. D., and Antcliffe, J. B. (2009). Evolutionary Relationships within the Avalonian Ediacara Biota: New Insights from Laser Analysis. *J. Geol. Soc.* 166, 363–384. doi:10.1144/0016-76492008-011
- Brasier, M. D., Antcliffe, J. B., and Liu, A. G. (2012). The Architecture of Ediacaran Fronds. *Palaeontology* 55, 1105–1124. doi:10.1111/j.1475-4983.2012.01164.x
- Budd, G. E., and Jensen, S. (2017). The Origin of the Animals and a 'Savannah' Hypothesis for Early Bilateral Evolution. *Biol. Rev.* 92, 446–473. doi:10.1111/brv.12239
- Burzynski, G., and Narbonne, G. M. (2015). The Discs of Avalon: Relating Discoid Fossils to Frondose Organisms in the Ediacaran of Newfoundland, Canada. *Palaeogeogr. Palaeoclimatol. Palaeoecol.* 434, 34–45. doi:10.1016/j.palaeo.2015.01.014
- Cantero, M. I., Cantelli, A., Pirmez, C., Balachandar, S., Mohrig, D., Hickson, T. A., et al. (2012). Emplacement of Massive Turbidites Linked to Extinction of Turbulence in Turbidity Currents. *Nat. Geosci.* 5, 42–45. doi:10.1038/ngeo1320
- Cartigny, M. J. B., Eggenhuisen, J. T., Hansen, E. W. M., and Postma, G. (2013). Concentration-Dependent Flow Stratification in Experimental High-Density Turbidity Currents and Their Relevance to Turbidite Facies Models. *J. Sediment. Res.* 83, 1047–1065. doi:10.2110/jsr.2013.71
- Clapham, M. E., and Narbonne, G. M. (2002). Ediacaran Epifaunal Tiering. *Geology* 30 (7), 627–630. doi:10.1130/0091-7613(2002)030<0627:EET%3E2.0.CO;2
- Clapham, M. E., Narbonne, G. M., Gehling, J. G., Greentree, C., and Anderson, M. M. (2004). *Thectardis Avalonensis*: A New Ediacaran Fossil from the Mistaken Point Biota, Newfoundland. *J. Paleontol.* 78, 1031–1036. doi:10.1017/s0022336000043857
- Clapham, M. E., Narbonne, G. M., and Gehling, J. G. (2003). Paleoeecology of the Oldest Known Animal Communities: Ediacaran Assemblages at Mistaken Point, Newfoundland. *Paleobiology* 29, 527–544. doi:10.1666/0094-8373(2003)029<0527:potoka>2.0.co;2
- Darroch, S. A. F., Smith, E. F., Laflamme, M., and Erwin, D. H. (2018). Ediacaran Extinction and Cambrian Explosion. *Trends Ecol. Evol.* 33, 653–663. doi:10.1016/j.tree.2018.06.003
- Dececchi, T. A., Narbonne, G. M., Greentree, C., and Laflamme, M. (2017). Relating Ediacaran Fronds. *Paleobiology* 43, 171–180. doi:10.1017/pab.2016.54
- Demko, T. (1995). in *Proceedings of the Third Annual Fossils of Arizona Symposium, November 18, 1995*. Editor M. S. Museum (American Traveler Press), 111.
- Diggle, P., Zheng, P., and Durr, P. (2005). Nonparametric Estimation of Spatial Segregation in a Multivariate point Process: Bovine Tuberculosis in Cornwall, UK. *J. R. Stat. Soc. C* 54, 645–658. doi:10.1111/j.1467-9876.2005.05373.x
- Dunn, F. S., Liu, A. G., Grazhdankin, D. V., Vixseboxse, P., Flannery-Sutherland, J., Green, E., et al. (2021). The Developmental Biology of *Charnia* and the Eumetazoan Affinity of the Ediacaran Rangeomorphs. *Sci. Adv.* 7, eabe0291. doi:10.1126/sciadv.abe0291
- Dunn, F. S., Liu, A. G., and Donoghue, P. C. J. (2018). Ediacaran Developmental Biology. *Biol. Rev.* 93, 914–932. doi:10.1111/brv.12379
- Dunn, F. S., Wilby, P. R., Kenchington, C. G., Grazhdankin, D. V., Donoghue, P. C. J., and Liu, A. G. (2019). Anatomy of the Ediacaran rangeomorph *Charnia Masoni*. *Pap. Palaeontol.* 5, 157–176. doi:10.1002/spp2.1234
- Dynowski, J. F., Nebelsick, J. H., Klein, A., and Roth-Nebelsick, A. (2016). Computational Fluid Dynamics Analysis of the Fossil Crinoid *Encrinurus liliiformis* (Echinodermata: Crinoidea). *PLOS ONE* 11, e0156408. doi:10.1371/journal.pone.0156408
- Fisher, R. V. (1983). Flow Transformations in Sediment Gravity Flows. *Geol.* 11, 273–274. doi:10.1130/0091-7613(1983)11<273:ftisgf>2.0.co;2
- Fitak, R. R., and Johnsen, S. (2017). Bringing the Analysis of Animal Orientation Data Full circle: Model-Based Approaches with Maximum Likelihood. *J. Exp. Biol.* 220, 3878–3882. doi:10.1242/jeb.167056
- Flude, L. I., and Narbonne, G. M. (2008). Taphonomy and Ontogeny of a Multibranched Ediacaran Fossil: *Bradgatia* from the Avalon Peninsula of Newfoundland. *Can. J. Earth Sci.* 45, 1095–1109. doi:10.1139/e08-057
- Ford, T. D. (1958). Pre-Cambrian Fossils from Charnwood Forest. *Proc. Yorks. Geol. Soc.* 31, 211–217. doi:10.1144/pygs.31.3.211

ACKNOWLEDGMENTS

The Parks and Natural Areas Division (PNAD), Department of Environment and Conservation, Government of Newfoundland and Labrador, provided permits to conduct research within the Mistaken Point Ecological Reserve (MPER) in 2010, 2016 and 2017. Readers are advised that access to MPER is by scientific research permit only.

SUPPLEMENTARY MATERIAL

The Supplementary Material for this article can be found online at: <https://www.frontiersin.org/articles/10.3389/feart.2021.762824/full#supplementary-material>

- Fraley, C., and Raftery, A. E. (2017). *MCLUST Version 3 for R: Normal Mixture Modeling and Model-Based Clustering*. Washington: MCLUST, 57.
- Gehling, J. G., and Narbonne, G. M. (2007). Spindle-shaped Ediacara Fossils from the Mistaken Point Assemblage, Avalon Zone, Newfoundland. *Can. J. Earth Sci.* 44, 367–387. doi:10.1139/e07-003
- Ghisalberti, M., Gold, D. A., Laflamme, M., Clapham, M. E., Narbonne, G. M., Summons, R. E., et al. (2014). Canopy Flow Analysis Reveals the Advantage of Size in the Oldest Communities of Multicellular Eukaryotes. *Curr. Biol.* 24, 305–309. doi:10.1016/j.cub.2013.12.017
- Hallworth, M. A., Phillips, J. C., Huppert, H. E., and Sparks, R. S. J. (1993). Entrainment in Turbulent Gravity Currents. *Nature* 362, 829–831. doi:10.1038/362829a0
- Houghton, P., Davis, C., McCaffrey, W., and Barker, S. (2009). Hybrid Sediment Gravity Flow Deposits - Classification, Origin and Significance. *Mar. Pet. Geology* 26, 1900–1918. doi:10.1016/j.marpetgeo.2009.02.012
- Hawco, J. B., Kenchington, C. G., Taylor, R. S., and McIlroy, D. (2020). A Multivariate Statistical Analysis of the Ediacaran Rangeomorph Taxa *Beothukis* and *Culmofrons*. *PALAIOS* 35, 495–511. doi:10.2110/palo.2020.049
- Hofmann, H. J., O'Brien, S. J., and King, A. F. (2008). Ediacaran Biota on Bonavista Peninsula, Newfoundland, Canada. *J. Paleontol.* 82, 1–36. doi:10.1666/06-087.1
- Hoyal Cuthill, J. F., and Conway Morris, S. (2014). Fractal Branching Organizations of Ediacaran Rangeomorph Fronds Reveal a Lost Proterozoic Body Plan. *Proc. Natl. Acad. Sci.* 111, 13122–13126. doi:10.1073/pnas.1408542111
- Hoyal Cuthill, J. F., and Han, J. (2018). Cambrian Petalonamid *Stromatoveris* Phylogenetically Links Ediacaran Biota to Later Animals. *Palaeontology* 61, 813–823. doi:10.1111/pala.12393
- Ichaso, A. A., Dalrymple, R. W., and Narbonne, G. M. (2007). Paleoenvironmental and basin Analysis of the Late Neoproterozoic (Ediacaran) Upper Conception and St. John's Groups, West Conception Bay, Newfoundland. *Can. J. Earth Sci.* 44, 25–41. doi:10.1139/e06-098
- Illian, J., Penttinen, P. A., Stoyan, D. H., and Stoyan, D. D. (2008). *Statistical Analysis and Modelling of Spatial Point Patterns*. Wiley, 560.
- Jones, M. L., and Dennison, J. M. (1970). Oriented Fossils as Paleocurrent Indicators in Paleozoic Lutites of Southern Appalachians. *J. Sediment. Res.* 40, 642–649. doi:10.1306/74d71ff5-2b21-11d7-8648000102c1865d
- Kenchington, C. G., Harris, S. J., Vixseboxse, P. B., Pickup, C., and Wilby, P. R. (2018). The Ediacaran Fossils of Charnwood Forest: Shining New Light on a Major Biological Revolution. *Proc. Geologists' Assoc.* 129, 264–277. doi:10.1016/j.pgeola.2018.02.006
- Kenchington, C. G., and Wilby, P. R. (2017). Rangeomorph Classification Schemes and Intra-specific Variation: Are All Characters Created Equal? *Geol. Soc. Lond. Spec. Publications* 448, 221–250. doi:10.1144/sp448.19
- Kiipli, T., Kiipli, E., Kallaste, T., Hints, R., Somelar, P., and Kirsimäe, K. (2007). Altered Volcanic Ash as an Indicator of marine Environment, Reflecting Ph and Sedimentation Rate - Example from the Ordovician Kinnekulle Bed of Baltoscandia. *Clays Clay Miner.* 55, 177–188. doi:10.1346/ccmn.2007.0550207
- Koehl, M. A. R. (1977a). Effects of Sea Anemones on the Flow Forces They Encounter. *J. Exp. Biol.* 69, 87–105. doi:10.1242/jeb.69.1.87
- Koehl, M. A. R. (1977b). Mechanical Organization of Cantileverlike Sessile Organisms: Sea Anemones. *J. Exp. Biol.* 69, 127–142. doi:10.1242/jeb.69.1.127
- Laflamme, M., Darroch, S. A. F., Tweedt, S. M., Peterson, K. J., and Erwin, D. H. (2013). The End of the Ediacara Biota: Extinction, Biotic Replacement, or Cheshire Cat? *Gondwana Res.* 23, 558–573. doi:10.1016/j.gr.2012.11.004
- Laflamme, M., Flude, L. I., and Narbonne, G. M. (2012). Ecological Tiering and the Evolution of a Stem: the Oldest Stemmed Frond from the Ediacaran of Newfoundland, Canada. *J. Paleontol.* 86, 193–200. doi:10.1666/11-044.1
- Laflamme, M., Gehling, J. G., and Droser, M. L. (2018). Deconstructing an Ediacaran Frond: Three-Dimensional Preservation of *Arborea* from Ediacara, South Australia. *J. Paleontol.* 92, 323–335. doi:10.1017/jpa.2017.128
- Laflamme, M., Narbonne, G. M., and Anderson, M. M. (2004). Morphometric Analysis of the Ediacaran Frond *Charniodiscus* from the Mistaken Point Formation, Newfoundland. *J. Paleontol.* 78, 827–837. doi:10.1666/0022-3360(2004)078<0827:maotef>2.0.co;2
- Laflamme, M., and Narbonne, G. M. (2008). Ediacaran Fronds. *Palaeogeogr. Palaeoclimatol. Palaeoecol.* 258, 162–179. doi:10.1016/j.palaeo.2007.05.020
- Laflamme, M., Xiao, S., and Kowalewski, M. (2009). Osmotrophy in Modular Ediacara Organisms. *Proc. Natl. Acad. Sci.* 106, 14438–14443. doi:10.1073/pnas.0904836106
- Landler, L., Ruxton, G. D., and Malkemper, E. P. (2019). The Hermans-Rasson Test as a Powerful Alternative to the Rayleigh Test for Circular Statistics in Biology. *BMC Ecol.* 19, 30. doi:10.1186/s12898-019-0246-8
- Liu, A. G. (2016). Framboidal Pyrite Shroud Confirms the 'Death Mask' Model for Mouldic Preservation of Ediacaran Soft-Bodied Organisms. *PALAIOS* 31 (5), 259–274. doi:10.2110/palo.2015.095
- Liu, A. G., Kenchington, C. G., and Mitchell, E. G. (2015). Remarkable Insights into the Paleoeology of the Avalonian Ediacaran Macrobiota. *Gondwana Res.* 27, 1355–1380. doi:10.1016/j.gr.2014.11.002
- Liu, A. G., McIlroy, D., Antcliffe, J. B., and Brasier, M. D. (2011). Effaced Preservation in the Ediacara Biota and its Implications for the Early Macrofossil Record. *Palaeontology* 54, 607–630. doi:10.1111/j.1475-4983.2010.01024.x
- Liu, X., and Jiang, Y. (2014). Direct Numerical Simulations of Boundary Condition Effects on the Propagation of Density Current in wall-bounded and Open Channels. *Environ. Fluid Mech.* 14, 387–407. doi:10.1007/s10652-013-9283-6
- Luhar, M., and Nepf, H. M. (2011). Flow-induced Reconfiguration of Buoyant and Flexible Aquatic Vegetation. *Limnol. Oceanogr.* 56, 2003–2017. doi:10.4319/lo.2011.56.6.2003
- Mason, S. J., and Narbonne, G. M. (2016). Two New Ediacaran Small Fronds from Mistaken Point, Newfoundland. *J. Paleontol.* 90, 183–194. doi:10.1017/jpa.2016.14
- Matthews, J. J., Liu, A. G., Yang, C., McIlroy, D., Levell, B., and Condon, D. J. (2021). A Chronostratigraphic Framework for the Rise of the Ediacaran Macrobiota: New Constraints from Mistaken Point Ecological Reserve, Newfoundland. *GSA Bull.* 133:612–624. doi:10.1130/b35646.1
- McIlroy, D., Hawco, J., McKean, C., Nicholls, R., Pasinetti, G., and Taylor, R. (2020). Palaeobiology of the Reclining Rangeomorph *Beothukis* from the Ediacaran Mistaken Point Formation of southeastern Newfoundland. *Geol. Mag.*, 1–15. doi:10.1017/s0016756820000941
- Ming-Chao, L., and Chang-Feng, D. (1996). Drag, Morphology and Mechanical Properties of Three Species of Octocorals. *J. Exp. Mar. Biol. Ecol.* 1 (2), 13–22.
- Mitchell, E. G., Bobkov, N., Bykova, N., Dhungana, A., Kolesnikov, A. V., Hogarth, I. R. P., et al. (2020). The Influence of Environmental Setting on the Community Ecology of Ediacaran Organisms. *Interf. Focus* 10, 20190109. doi:10.1098/rsfs.2019.0109
- Mitchell, E. G., and Butterfield, N. J. (2018). Spatial Analyses of Ediacaran Communities at Mistaken Point. *Paleobiology* 44, 40–57. doi:10.1017/pab.2017.35
- Mitchell, E. G., Harris, S., Kenchington, C. G., Vixseboxse, P., Roberts, L., Clark, C., et al. (2019). The Importance of Neutral over Niche Processes in Structuring Ediacaran Early Animal Communities. *Ecol. Lett.* 22, 2028–2038. doi:10.1111/ele.13383
- Mitchell, E. G., and Harris, S. (2020). Mortality, Population and Community Dynamics of the Glass Sponge Dominated Community "The Forest of the Weird" from the Ridge Seamount, Johnston Atoll, Pacific Ocean. *Front. Mar. Sci.* 7. doi:10.3389/fmars.2020.565171
- Mitchell, E. G., Kenchington, C. G., Harris, S., and Wilby, P. R. (2018). Revealing Rangeomorph Species Characters Using Spatial Analyses. *Can. J. Earth Sci.* 55, 1262–1270. doi:10.1139/cjes-2018-0034
- Mitchell, E. G., Kenchington, C. G., Liu, A. G., Matthews, J. J., and Butterfield, N. J. (2015). Reconstructing the Reproductive Mode of an Ediacaran Macro-Organism. *Nature* 524, 343–346. doi:10.1038/nature14646
- Mitchell, E. G., and Kenchington, C. G. (2018). The Utility of Height for the Ediacaran Organisms of Mistaken Point. *Nat. Ecol. Evol.* 2, 1218–1222. doi:10.1038/s41559-018-0591-6
- Narbonne, G. M., and Gehling, J. G. (2003). Life after Snowball: The Oldest Complex Ediacaran Fossils. *Geol* 31, 27–30. doi:10.1130/0091-7613(2003)031<0027:lastoc>2.0.co;2
- Narbonne, G. M. (2004). Modular Construction of Early Ediacaran Complex Life Forms. *Science* 305, 1141–1144. doi:10.1126/science.1099727
- Narbonne, G. M. (2005). The Ediacara Biota: Neoproterozoic Origin of Animals and Their Ecosystems. *Annu. Rev. Earth Planet. Sci.* 33, 421–442. doi:10.1146/annurev.earth.33.092203.122519
- Noble, S. R., Condon, D. J., Carney, J. N., Wilby, P. R., Pharaoh, T. C., and Ford, T. D. (2015). U-pb Geochronology and Global Context of the Charnian

- Supergroup, UK: Constraints on the Age of Key Ediacaran Fossil Assemblages. *Geol. Soc. America Bull.* 127, 250–265. doi:10.1130/b31013.1
- Rao, J. S. (1976). Some Tests Based on Arc-Lengths for the Circle. *Sankhyā: Indian J. Stat.* 38, 329–338.
- Schnute, J. T., and Groot, K. (1992). Statistical Analysis of Animal Orientation Data. *Anim. Behav.* 43, 15–33. doi:10.1016/s0003-3472(05)80068-5
- Seilacher, A. (1992). Vendobionta and Psammocorallia: Lost Constructions of Precambrian Evolution. *J. Geol. Soc.* 149, 607–613. doi:10.1144/gsjgs.149.4.0607
- Shen, B., Dong, L., Xiao, S., and Kowalewski, M. (2008). The Avalon Explosion: Evolution of Ediacara Morphospace. *Science* 319, 81–84. doi:10.1126/science.1150279
- Shringarpure, M., Cantero, M. I., and Balachandar, S. (2012). Dynamics of Complete Turbulence Suppression in Turbidity Currents Driven by Monodisperse Suspensions of Sediment. *J. Fluid Mech.* 712, 384–417. doi:10.1017/jfm.2012.427
- Smith, P. L. (1980). Determining the *In Situ* Orientation of Fossil Bilateral Symmetry Planes during Paleocurrent Analysis. *J. Paleontol.* 54, 1121–1123. Available at: <https://www.jstor.org/stable/1304378>
- Sparks, R. S. J., and Wilson, C. J. N. (1983). Flow-head Deposits in Ash Turbidites. *Geol.* 11, 348–351. doi:10.1130/0091-7613(1983)11<348:fdiat>2.0.co;2
- Sperling, E. A., Peterson, K. J., and Laflamme, M. (2011). Rangeomorphs, *Thectardis* (Porifera?) and Dissolved Organic Carbon in the Ediacaran Oceans. *Geobiology* 9, 24–33. doi:10.1111/j.1472-4669.2010.00259.x
- Talling, P. J., Masson, D. G., Sumner, E. J., and Malgesini, G. (2012). Subaqueous Sediment Density Flows: Depositional Processes and deposit Types. *Sedimentology* 59, 1937–2003. doi:10.1111/j.1365-3091.2012.01353.x
- Toots, H. (1965). *Orientation and Distribution of Fossils as Environmental Indicators*. Springs: Sedimentation of Late Cretaceous and Tertiary Outcrops, 219–229.
- Waggoner, B. (2003). The Ediacaran Biotas in Space and Time. *Integr. Comp. Biol.* 43, 104–113. doi:10.1093/icb/43.1.104
- Wegst, U. G. K., and Ashby, M. F. (2007). The Structural Efficiency of Orthotropic Stalks, Stems and Tubes. *J. Mater. Sci.* 42, 9005–9014. doi:10.1007/s10853-007-1936-8
- Wiegand, T., and Moloney, K. A. (2013). *Handbook of Spatial Point-Pattern Analysis in Ecology*. Boca Raton, FL: CRC Press.
- Wilby, P. R., Carney, J. N., and Howe, M. P. A. (2011). A Rich Ediacaran Assemblage from Eastern Avalonia: Evidence of Early Widespread Diversity in the Deep Ocean. *Geology* 39, 655–658. doi:10.1130/g31890.1
- Wilby, P. R., Kenchington, C. G., and Wilby, R. L. (2015). Role of Low Intensity Environmental Disturbance in Structuring the Earliest (Ediacaran) Macrobenthic Tiered Communities. *Palaeogeogr. Palaeoclimatol. Palaeoecol.* 434, 14–27. doi:10.1016/j.palaeo.2015.03.033
- Wood, D. A., Dalrymple, R. W., Narbonne, G. M., Gehling, J. G., and Clapham, M. E. (2003). Paleoenvironmental Analysis of the Late Neoproterozoic Mistaken Point and Trepassy Formations, southeastern Newfoundland. *Can. J. Earth Sci.* 40, 1375–1391. doi:10.1139/e03-048
- Wood, R., Liu, A. G., Bowyer, F., Wilby, P. R., Dunn, F. S., Kenchington, C. G., et al. (2019). Integrated Records of Environmental Change and Evolution challenge the Cambrian Explosion. *Nat. Ecol. Evol.* 3, 528–538. doi:10.1038/s41559-019-0821-6
- Xiao, S., and Laflamme, M. (2009). On the Eve of Animal Radiation: Phylogeny, Ecology and Evolution of the Ediacara Biota. *Trends Ecol. Evol.* 24, 31–40. doi:10.1016/j.tree.2008.07.015

Conflict of Interest: The authors declare that the research was conducted in the absence of any commercial or financial relationships that could be construed as a potential conflict of interest.

The handling Editor declared a past co-authorship with one of the authors (EM).

Publisher's Note: All claims expressed in this article are solely those of the authors and do not necessarily represent those of their affiliated organizations, or those of the publisher, the editors and the reviewers. Any product that may be evaluated in this article, or claim that may be made by its manufacturer, is not guaranteed or endorsed by the publisher.

Copyright © 2021 Vixseboxse, Kenchington, Dunn and Mitchell. This is an open-access article distributed under the terms of the Creative Commons Attribution License (CC BY). The use, distribution or reproduction in other forums is permitted, provided the original author(s) and the copyright owner(s) are credited and that the original publication in this journal is cited, in accordance with accepted academic practice. No use, distribution or reproduction is permitted which does not comply with these terms.



Evolution of Holdfast Diversity and Attachment Strategies of Ediacaran Benthic Macroalgae

Xiaopeng Wang^{1,2}, Mengyin Wu³, Bin Wan^{1,2*}, Changtai Niu^{1,4}, Wentao Zheng^{1,2}, Chengguo Guan¹, Ke Pang^{1,2}, Zhe Chen^{1,2} and Xunlai Yuan^{1,2}

¹State Key Laboratory of Palaeobiology and Stratigraphy, Nanjing Institute of Geology and Palaeontology and Center for Excellence in Life and Palaeoenvironment, Chinese Academy of Sciences, Nanjing, China, ²College of Earth and Planetary Sciences, University of Chinese Academy of Sciences, Beijing, China, ³School of Economics and Management, Guiyang University, Guiyang, China, ⁴School of Earth and Space Sciences, University of Science and Technology of China, Hefei, China

OPEN ACCESS

Edited by:

Juliana Leme,
University of São Paulo, Brazil

Reviewed by:

Manuel F. G. Weinkauff,
Charles University, Czechia
Natalia Bykova,
Institute of Petroleum Geology and
Geophysics (RAS), Russia
Katie Maloney,
University of Toronto Mississauga,
Canada

*Correspondence:

Bin Wan
binwan@nigpas.ac.cn

Specialty section:

This article was submitted to
Paleontology,
a section of the journal
Frontiers in Earth Science

Received: 26 September 2021

Accepted: 22 November 2021

Published: 08 December 2021

Citation:

Wang X, Wu M, Wan B, Niu C,
Zheng W, Guan C, Pang K, Chen Z and
Yuan X (2021) Evolution of Holdfast
Diversity and Attachment Strategies of
Ediacaran Benthic Macroalgae.
Front. Earth Sci. 9:783427.
doi: 10.3389/feart.2021.783427

Holdfast morphologies and attachment strategies of benthic macroalgae are somewhat flexible and controlled by both the substrate condition and species. Six forms (tapered base, globose holdfast, composite globose holdfast, discoidal holdfast, rhizoids and horizontal rhizomes) of attachment structures of Ediacaran benthic macroalgae are recognized from the early Ediacaran Lantian biota and late Ediacaran Miaohu biota in South China based on functional morphology. Each form is considered either adapted to firm substrates that dominate the Precambrian seafloor, or soft substrates that are more common in the Phanerozoic. The results show a diversification in both holdfast morphology and attachment strategies of macroalgae during the Ediacaran Period. In the early Ediacaran Lantian biota, none of the benthic macroalgae is adapted to soft substrates, while in the late Ediacaran Miaohu biota, a considerable number (41%) of species are adapted to relatively soft substrates. This shift might be an adaptive response to the diversification of macroalgae and a changing substrate condition during the Ediacaran Period: the decline of microbial mats and increase of water content in the sediments in the Ediacaran.

Keywords: Ediacaran, macroalgae, holdfast, South China, substrate condition

INTRODUCTION

Benthic macroalgae are important components of modern and past ecosystems. They are more efficient primary producers than phytoplankton (Bunt, 1975) and provide food and habitats for many other organisms (e.g., Steneck et al., 2002).

The evolution of benthic macroalgae experienced a prolonged stasis since its first appearance (Du et al., 1986; Dong et al., 2008; Xiao, 2013) in the Mesoproterozoic to early Neoproterozoic, and a sudden expansion in morphospace in the Ediacaran (Xiao and Dong, 2006; Bykova et al., 2020). The cause of the increase in morphological disparity might be the drop of pCO_2 in the atmosphere and seawater after the Cryogenian Snowball Earth glaciations (Xiao and Dong, 2006).

The morphology of the holdfast of benthic macroalgae also diversified with the expansion in morphospace. Holdfasts attach macroalgae to substrates, and their morphologies are greatly influenced by the property of substrates and reflect the attachment strategy adopted by the macroalgae. As a result, the morphology of holdfasts may serve as a proxy, to some extent, for

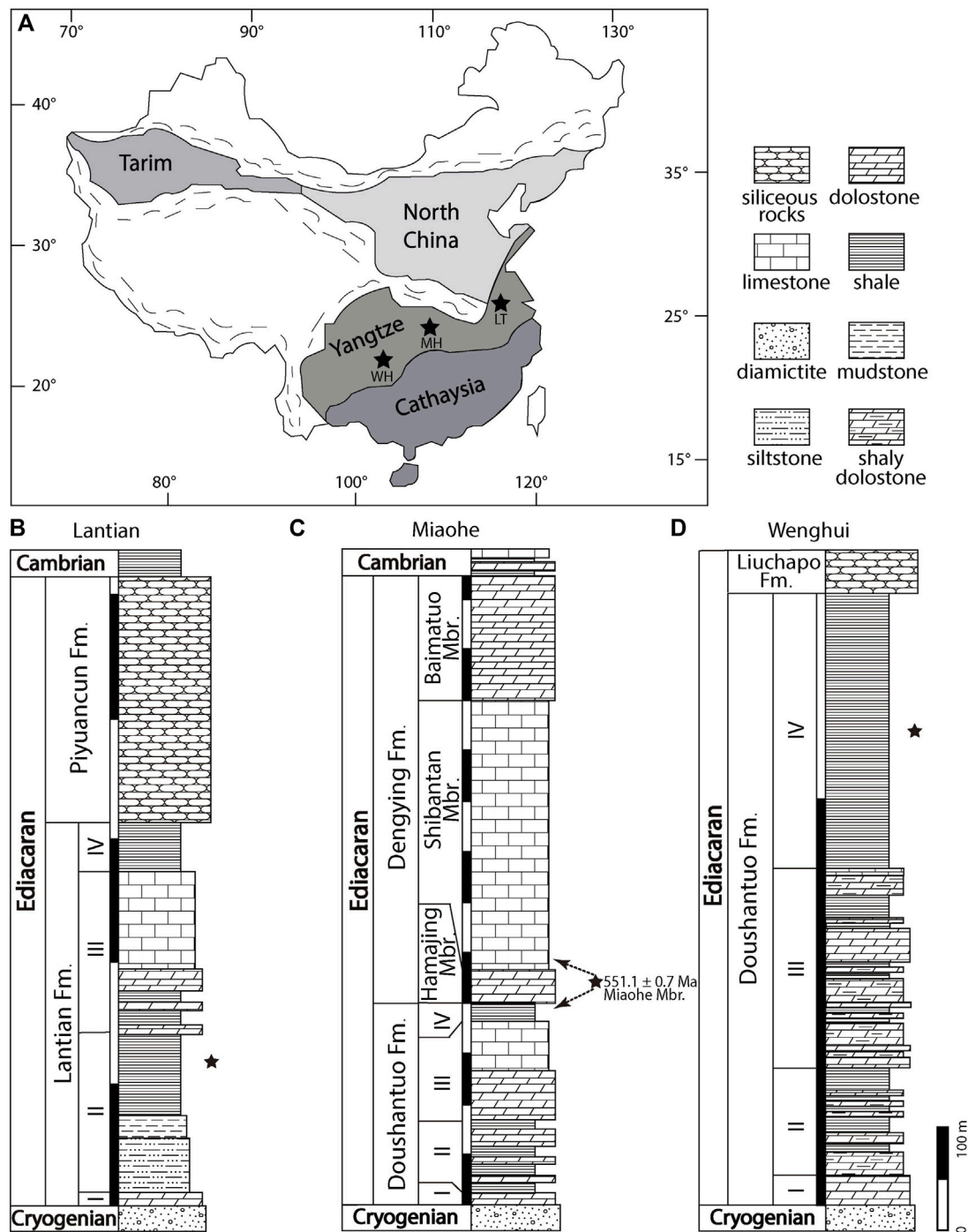


FIGURE 1 | Map and stratigraphic columns of the study areas. Modified from Wan et al. (2020) and Wang Y. et al. (2020). **(A)** Map showing fossil localities: Lantian (LT), Miaohé (MH), and Wenghui (WH). **(B-D)** Stratigraphic columns of Lantian, Miaohé, and Wenghui, respectively. Stars mark the fossil horizons in **(B-D)**. Dashed arrows mark alternative correlations of the Miaohé Member. Fm. = Formation; Mbr. = Member.

the substrate conditions. For instance, Dornbos et al. (2005) and Lei et al. (2014) have investigated the evolution of attachment strategies of benthic metazoans as a response to the changing substrate conditions in the Cambrian.

The agronomic revolution (AR) or the Cambrian substrate revolution (CSR) is one of the greatest shifts in substrate conditions, transforming from Proterozoic-style substrates to Phanerozoic mixed layers. Typical Proterozoic-style substrates

were firm and well-layered, with low water content and ubiquitous microbial mats; in contrast, typical Phanerozoic-style soft substrates were soupy, water-rich mixed layers (Bottjer et al., 2000). The AR was driven by increasing bioturbation that incorporated water into the sediment (Kloss et al., 2015), but its exact timing and extent have not been yet clearly defined. In the early Cambrian, the AR has already had an effect (Dornbos et al., 2005), and had almost been finished in the late Cambrian (Bottjer et al., 2000). Considering the relatively diverse and abundant trace fossils in the late Neoproterozoic (e.g., Chen et al., 2018; Chen et al., 2019; Xiao et al., 2019), the AR is supposed to have a root back in the Precambrian, but the scarcity of Precambrian biotas restrained the insight to the evolution of substrate conditions during this period. Recently, a large number of specimens of fossil macroalgae with holdfasts preserved intact yielded from the Lantian biota (Yuan and Cao, 1999; Yuan et al., 2011; Bin et al., 2013) and the Miaohu biota (Xiao et al., 2002; Ye et al., 2019a) offered a chance to examine the evolution of substrate conditions in the Ediacaran.

This study focuses on the evolution of macroalgal holdfasts, attachment strategies and substrate conditions during the Ediacaran Period by examining Lagerstätten in South China: the early Ediacaran Lantian biota and the late Ediacaran Miaohu biota. Both biotas are preserved in black shales, and they also share comparable geological settings and depositional environments. We described holdfast morphologies of benthic macroalgae and analyzed their attachment strategies to understand the dynamic of substrate conditions in the early and late Ediacaran.

GEOLOGICAL SETTING

The Lantian biota is preserved in the Member II black shale of the Ediacaran Lantian Formation in the Anhui province (**Figures 1A,B**). Underlain by the Cryogenian Leigongwu diamictite and topped by the latest Ediacaran Piyuancun Formation, the Lantian Formation holds the fossil record of life between the end of the Snowball Earth to the eve of the Cambrian Explosion. It consists of four lithological members at the Lantian section (**Figure 1B**), i.e., in ascending order, Members I–IV. The lowest Member I is the cap carbonate (4 m thick); the Member II consists of siltstone (23 m thick), mudstone (8.6 m thick) and fossiliferous black shale (34 m thick); the Member III consists of dolomite interbedded with black shale (26 m thick) and limestone (40 m thick); the uppermost Member IV consists of black mudstone, 20 m in thickness (Guan et al., 2014; Wan et al., 2014; Wan et al., 2016). The Lantian Formation is the lithostratigraphic equivalent to the Doushantuo Formation in the Hubei Province (Yuan et al., 2011), which has been constrained to be between 635 Ma to 551 Ma (Condon et al., 2005), and therefore the age of the Lantian biota is considered between 635 and 590 Ma (Yuan et al., 2011; Wan et al., 2016).

The sedimentary environment of the Lantian Formation was a restricted shelf basin (Zhu et al., 2007) at low to middle paleolatitudes (Li et al., 2008; Zhang et al., 2015). The *in situ* preserved benthic macroalgae and fine parallel laminations

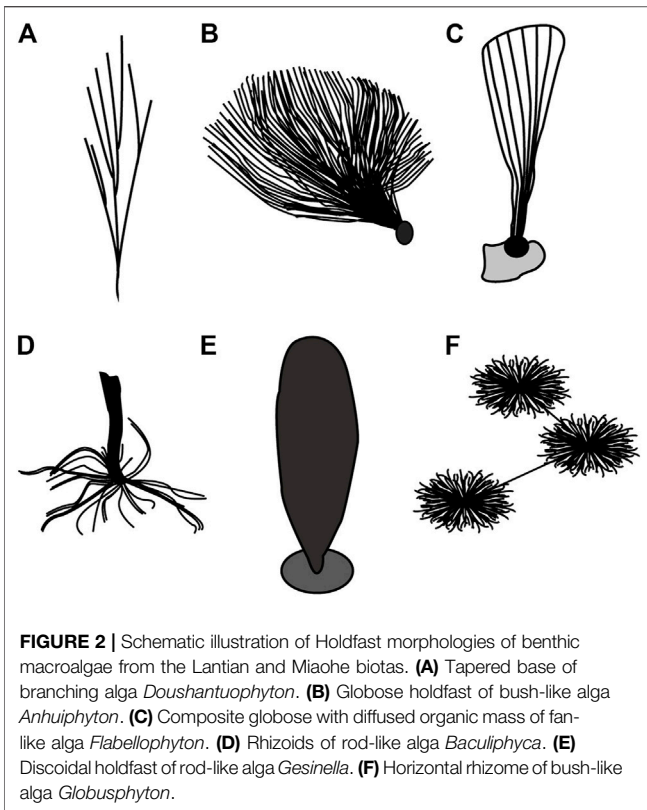
suggest that the deposition probably took place in a quiet environment below the storm wave base but within the photic zone (Yuan et al., 2011). Nevertheless, occasionally alignments of fossils in parallel and/or perpendicular directions indicate relatively weak current or wave movements.

The Miaohu biota refers to the fossil assemblage preserved in a siliceous black shale unit known as the Miaohu Member of the Ediacaran Doushantuo Formation (**Figures 1C,D**) which crops out in the Hubei and Guizhou provinces. Traditionally, the Miaohu Member is considered the equivalent of the uppermost black shale member of the Ediacaran Doushantuo Formation (Jiang et al., 2011; Xiao et al., 2017; Zhou et al., 2017). The Doushantuo Formation, as mentioned above, is a lithostratigraphic equivalent of the Lantian Formation. In the Miaohu area of the Hubei province and Wenghui area of the Guizhou province, the Doushantuo Formation overlain the Cryogenian Nantuo Formation and is overlaid by the latest Ediacaran Dengying and Liuchapo formations respectively. The Doushantuo Formation is 255 m thick at Miaohu and 79 m thick at Wenghui. Within the Doushantuo Formation, four members are discerned, in ascending order: a cap carbonate unit at the bottom (Member I, 5 m thick at Miaohu and 7 m thick at Wenghui), black shale interbedded with dolomite (Member II, 150 m thick at Miaohu and 10 m thick at Wenghui), laminated dolomite (Member III, 80 m thick at Miaohu and 17 m thick at Wenghui), and black shale and organic-rich mudstone at the top (Member IV, 20 m thick at Miaohu and 45 m thick at Wenghui). Nevertheless, An et al. (2015) proposed an alternative correlation that regards the Miaohu Member as an equivalent of the lower Shibantan Member of the Dengying Formation. The Miaohu Member yields diverse macroscopic fossils in the Miaohu area and several other localities in Hubei (Xiao et al., 2002; An et al., 2015; Ye et al., 2019a), and also in the Wenghui area in Guizhou (Zhao et al., 2004; Wang et al., 2014; Wang et al., 2016). Its age is constrained to 551 Ma (TIMS U–Pb dating, Condon et al., 2005). This black shale member is interpreted as transgressive sediments deposited during sea-level rise (Jiang et al., 2007; Jiang et al., 2011), which may represent a restricted intra-shelf basin setting in the Yangtze Gorges area (Zhu et al., 2013) at low paleolatitudes (Li et al., 2008), and probably represent a continental slope environment in the Wenghui area (Jiang et al., 2011). The surface sediment of the Wenghui area was considered to be soupy (Wang and Wang, 2008).

MATERIAL AND METHODS

Specimens from the Lantian and Miaohu biotas are deposited in the Nanjing Institute of Geology and Palaeontology, except for the *Gesinella* and *Globusphyton* specimens which are deposited in Guizhou University.

In order to determine attachment strategies of benthic macroalgae in the Lantian and Miaohu biotas, a detailed examination of macroalgal holdfasts was conducted. Observations and measurements were carried out directly on fossil specimens or pictures of fossils from these biotas. Based on



functional morphology, the holdfasts were classified into forms that were either adapted to firm and coherent substrates which dominated the Precambrian seafloor, or soft and soupy substrates that are more common in the Phanerozoic.

As a part of interpreting the adaptive morphology of globular holdfasts, a bivariate Spearman rank-order correlation (Spearman, 1904) was performed to determine if there is a correlation between the size of the thallus and the holdfast of *Flabellophyton*, which is the most representative and abundant taxon in the Lantian biota. A relatively small holdfast compared to the thallus may reflect minimal or no bioturbation (Loduca et al., 2017), hence the correlation (or lack thereof) would indicate if substrate conditions were relevant to the survival of benthic macroalgae or not. We focused on holdfasts instead of the amorphous organic mass here, because the organic mass may represent adhesive polypeptides (e.g., Levi and Friedlander, 2004) exuded from the holdfast rather than an anatomical structure. Two variables used here are the thallus area and the cross-section area of the globular holdfast. The thallus of *Flabellophyton* was an inverted hollow cone originally, and its fan-like fossil represents a projection of a cone on a two-dimensional surface (Wan et al., 2020). The projection is also equal to the frontal area facing into the flow direction, making it an important parameter for benthic macroalgae to withstand moving water. The cross-section area of the globular holdfast is calculated from the diameter which could be directly measured.

Fossil specimens were photographed under a Nikon DSLR D850, a Zeiss stereo microscope Axio Zoom V16. Measurements were made from photos of specimens using ImageJ, version 1.52a

(Rasband, 2018). Statistical analysis was carried out by using SPSS, version 23 (IBM Corp, 2015).

RESULTS AND DISCUSSION

Functional Morphology of Holdfasts in the Early Ediacaran Lantian Biota

Tapered Base

The base of the macroalgae tapers downwards to a point (Figure 2A; Figures 3A,B), with no differentiated holdfast. This could be an adaption for shallow insertion into sediments, similar to the strategy adopted by benthic invertebrates referred to shallow sediment stickers (Seilacher, 1999). The tapered base is an uncommon style of attachment for Lantian algae, which only have been found in simple dichotomously branching macroalgae, such as *Doushantuophyton* and *Enteromorpha*. Fragile structures such as rhizoidal holdfasts can be lost in some fossil specimens (Ye et al., 2019a). However, we have not found any other structures attach to the taper base in all specimens.

The tapered base can be generally regarded as an analogue to the bare rhizome holdfast (Wang Y. et al., 2020) from the Miaohu biota in the Wenghui area, but the latter may be associated with filamentous rhizoids which have never been found in the tapered base. The possible alga *Protoconites* from the Miaohu biota also bears a tapered base. *Protoconites* is fan-like compression with a tapered basal end, lacking obvious means of attachment. The interpretation of the affinity of *Protoconites* varies from scyphozoan to eukaryotic alga (Xiao et al., 2002). Comparable functional morphology has also been found in Cambrian suspension feeders, such as shallow sediment sticking demosponge *Takakkawia* (Dornbos et al., 2005) and helicoplacoid echinoderms (Dornbos and Bottjer, 2000).

A tapered morphology shows that their entire body mass was centered over a single point, which suggests that the substrates were not a water-rich mixed layer as we expect to find in typical Phanerozoic-style substrates, because these organisms might easily sink into the soupy sediment and die. Hence, shallow sediment stickers and algae that possess tapered bases are considered adapted to Proterozoic-style substrates, which were firm and well-layered and had low water content and ubiquitous microbial mats.

Globose Holdfast

A globose holdfast is globular to subglobular and buried shallow in the sediment (Figure 2B; Figures 3C,D). Globose holdfasts are found in bush-like algae, including *Anhuiphyton*, *Huangshanphyton*, and *Marpolia* from the Lantian biota. Occasionally, at the bottom of the globose holdfast, a tiny cone protrudes downwards. Comparable forms have also been found in the Miaohu biota in the Wenghui area and categorized into canopy rhizome holdfast (Wang Y. et al., 2020).

The globose holdfast in Ediacaran macroalgae would not be an effective anchoring structure on Phanerozoic mixed layers, because a sphere is not the optimal shape to resist upward

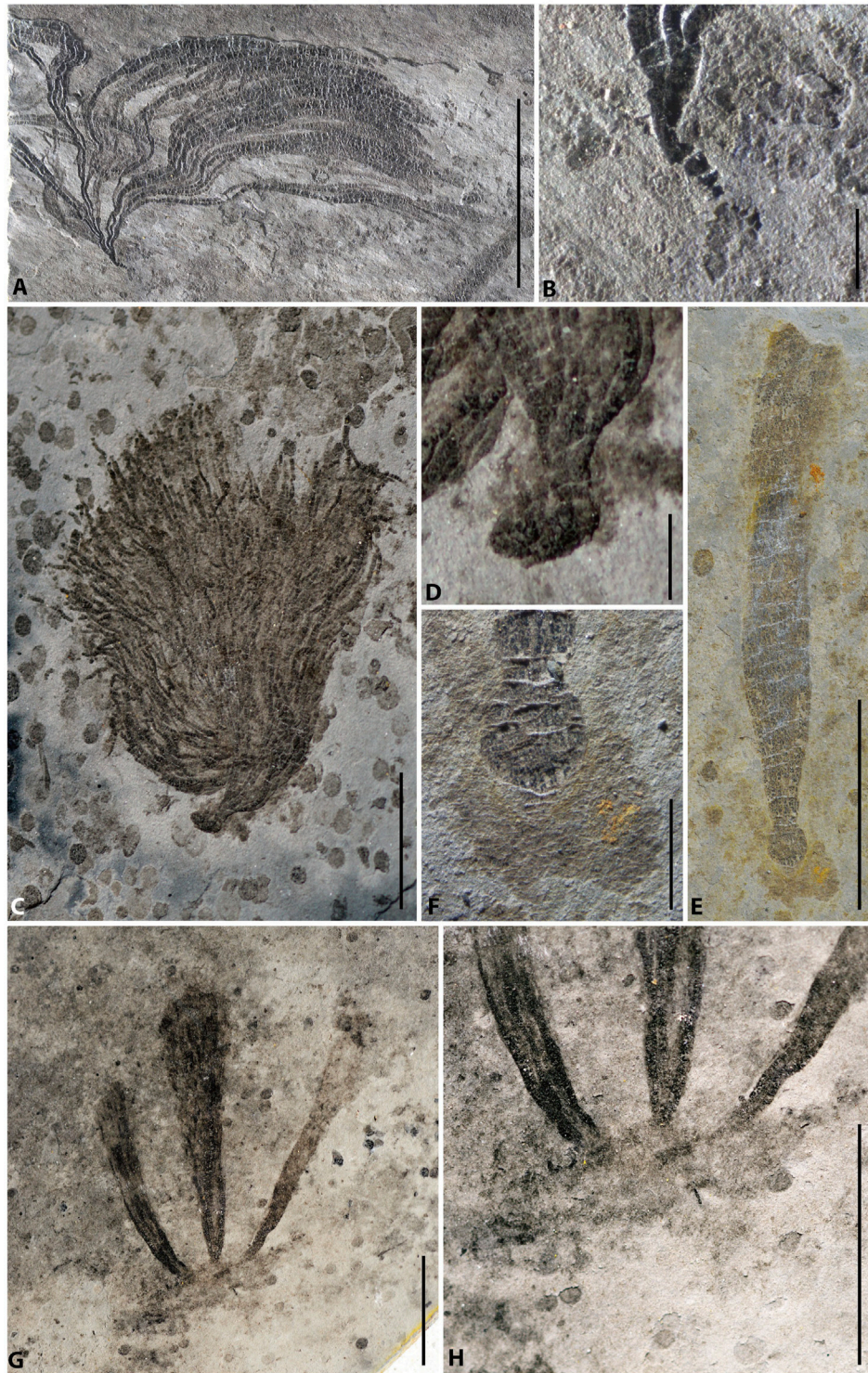
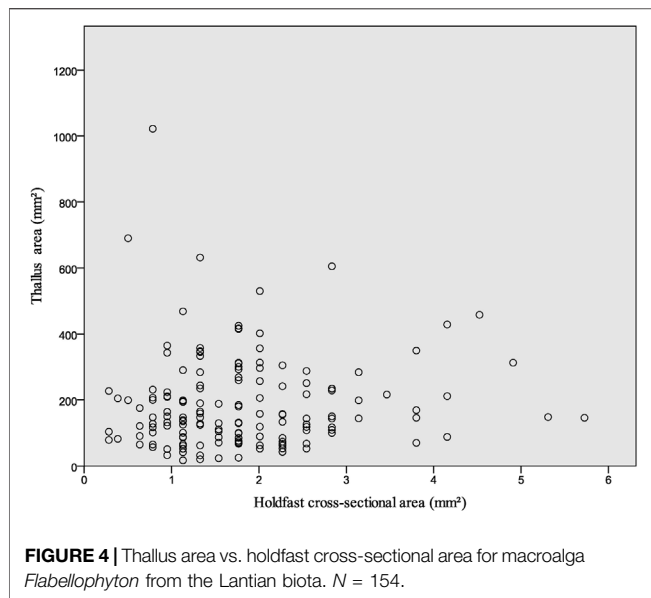


FIGURE 3 | Macroalgae and their holdfasts from the Lantian biota. **(A)** *Doushantuophyton cometa*, PB23767. **(B)** Enlargement of the holdfast in **(A)** showing a simple tapered morphology. **(C)** *Anhuiphyton lineatum*, PB23769. **(D)** Enlargement of the globular holdfast in **(C)**. **(E)** *Flabelliphyton lantianense*, PB23768. **(F)** Enlargement of the globular holdfast in **(E)**, with amorphous organic mass. **(G)** Three *Flabelliphyton* thalli rise from a common organic mass, PB23770. **(H)** Enlargement of the holdfast in **(G)**. Scale bars represent 10 mm **(A,C,E,G)** and 1 mm **(B,D,F,H)**.



movements. As an uprooting experiment showed (Mickovski and Ennos, 2003), among the common shapes of holdfasts, it was the second easiest to uproot. The force required to uproot the globose holdfast model was very close to the shape of an inverted conical model, which was the easiest shape to uproot. Interestingly, inverted conical is also the shape of attachment structures of the benthic organisms referred to as shallow sediment stickers discussed above.

From the perspective of the holdfast, all the factors that affect attachment [i.e., shape, depth of embedment, the size of the holdfast (Mickovski and Ennos, 2003)] are hardly favorable for effective attachment of a globose holdfast. As a result, the property of the substrate seems to be decisive for the success of globose holdfasts. The substrates had to be relatively firm to provide enough support for the globose holdfast to resist uprooting or sinking, but not completely sealed by microbial mats and had to have ample water content to allow the globose to penetrate the top several millimeters of the substrates. Hence, we consider globular holdfasts are adaptive to less typical Proterozoic-style substrates, potentially represents the transition to soupy substrates.

Composite Globose Holdfast

In some conical algae, especially in well preserved *Flabellophyton* specimens, an amorphous organic mass may be found surrounding the globose holdfast (Figure 2C). We categorized it into composite globose holdfast, as a variation of the simple globose holdfast discussed above. The mass is usually thinner and has a fainter appearance than the holdfast itself (Figures 3E,F); it probably represents adhesive polypeptides (e.g., Levi and Friedlander, 2004) exuded from the holdfast for agglutinating sediment particles. In other cases, the globose holdfast may attach to a platy carbonaceous structure at its bottom. Moreover, multiple thalli may arise from a common organic mass (Figures 3G,H) reminiscent of some individual *Longfengshania* specimens which can be merged into a

common, irregular carbonaceous mass as well (Hofmann, 1985). Both the amorphous mass and platy structure potentially provide additional anchorage strength for the alga.

Most of the *Flabellophyton* specimens were uprooted from the substrates before being buried, due to the relatively weak current or wave movements. As a result, their holdfasts are preserved as spheres without surrounding amorphous mass. The size of the holdfast is not correlated with the size of the conical thallus, as depicted in Figure 4. Small globose holdfasts are found in both large and small specimens. The correlation analysis also shows there is no statistically significant correlation between the cross-section area of the holdfast and the area of the thallus for *Flabellophyton*, $r_s(154) = 0.091$, $p = 0.262$. In contrast, there is a positive correlation between the wet weight/surface area of the above-sediment part and holdfast volume in modern algae (Anderson et al., 2006; Bedinger et al., 2013), possibly due to larger size, which experiences more dragging and have greater attachment strength (e.g., Denny et al., 1985; Wernberg and Thomsen, 2005).

Functional Morphology of Holdfasts in the Late Ediacaran Miaohu Biota

Rhizoid

Rhizoid holdfasts are the most common type in the Miaohu biota, exhibiting root-like filaments diverging from the base of thallus (Figure 2D). Rhizoid holdfasts are well-developed in algae such as *Longifuniculum* (Figure 5A), *Baculiphyca* (Figures 5C,D), *Konglingiphyton* (Figure 5F), and *Gesinella* (Figure 5E).

Rhizoids are sophisticated structures that increase the surface area of the anchoring device and are common in modern algae living on soft substrate. A larger surface area provides more frictional force between sediment grains and rhizoids (e.g., Yang et al., 2021) to stabilize the alga in soft sediments. Rhizoids also have the ability to bind grains to form clusters. The weight of grains adhered by rhizoids contributes to the anchorage of the alga as well, however, we did not observe any grains coarser than ambient sediments in studied specimens. Similar to rhizoids in morphology, a root-like holdfast is suggested to be an adaptation of benthic metazoans that developed to live on soft mud, and are common in fossil crinoids (Sprinkle and Guensburg, 1995). Root-like holdfasts are considered to be one of the indicators for typical Phanerozoic-style life mode for benthic metazoans (Dornbos et al., 2005) that lived on soupy mixed layers. As this conclusion is based on merely functional morphology, the interaction between the substrate property and holdfast morphology, it is also applicable to organisms with comparable morphology besides benthic metazoans, such as algae.

Discoidal Holdfast

Discoidal holdfasts are common in the Miaohu biota, displaying a disc-like structure, attached to the base of the thallus (Figure 2E, Figure 5B). Globose structures may be compressed to become discs that resemble discoidal holdfasts. However, discoidal holdfasts are more flattened and often have an elliptical appearance with a stem attached to the center. Discoidal holdfasts also do not exhibit thickened edges as flattened spheres do. Simple basal discs found in the early

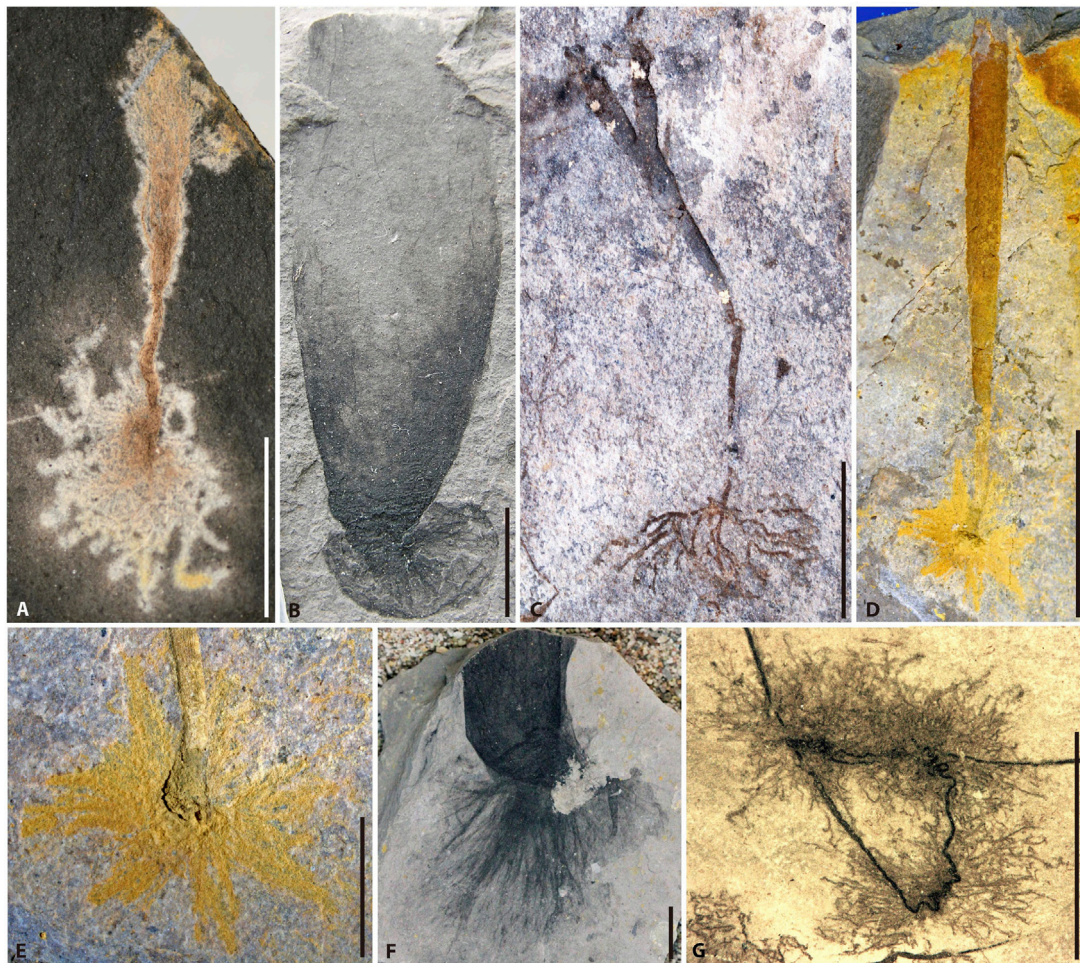


FIGURE 5 | Macroalgae and their holdfasts from the Miaohu biota. **(A)** *Longifuniculum dissolutum* with a rhizoidal holdfast, PB23771. **(B)** *Gesinella hunanensis* with a discoidal holdfast, MH-40-245B. **(C)** *Konglingiphyton erecta*, PB23773. **(D)** *Baculiphyca taeniata*, PB23772. **(E)** Enlargement of the rhizoidal holdfast in **(D)**. **(F)** *Gesinella hunanensis* with rhizoids, MH-57-1058B. **(G)** *Globusphyton lineare* with horizontal rhizomes, MH-40-0248. Scale bars represent 10 mm.

Neoproterozoic macroalgae *Longfengshania* and *Protoarenicola* may represent some of the earliest holdfasts (Du et al., 1986; Dong et al., 2008). In typical Ediacara-type fossil Lagerstätten, disc-like holdfasts are prevalent, for instance, in Ediacaran fronds *Arborea* (Hofmann et al., 2008; Wang X. et al., 2020) and *Primocandelabrum* (Kenckington and Wilby, 2017). Seilacher (1999) suggested that these Ediacara-type organisms were attached on the surface of the seafloor, which was relatively firm due to the presence of microbial mats. Any immobile benthic metazoans that simply lived by attaching to unconsolidated substrates, were well adapted to Proterozoic-style substrates (Dornbos et al., 2005). Considering the resemblance of discoidal holdfasts between macroalgae and other Ediacaran benthic organisms, they probably served as basal attachments in the same manner. As a result, the discoidal holdfast was the adaptation for both macroalgae and Ediacara-type organisms to Proterozoic-style firm substrates.

Horizontal Rhizome

The horizontal rhizome (Figure 2F) is another anchorage structure found in the Miaohu biota. Several pompom-like individuals of *Globusphyton* are interconnected by horizontal rhizomes which may creep on the seafloor or were shallowly buried within the sediment (Figure 5G). In terms of anchorage capacity, horizontal rhizomes join numerous individuals together, forming a network that provides more effective attachment than a solitary individual could achieve.

Wang Y. et al. (2020) proposed a classification of macroalgal holdfasts in the late Ediacaran Miaohu biota in the Wenghui area. Among the four major types recognized by them, bare and canopy rhizomes resemble tapered and globular holdfasts in the early Ediacaran Lantian biota, whereas pithy and differentiated rhizomes can be roughly correlated to the aforementioned filamentous rhizoids and horizontal rhizomes, respectively.

The Evolution of Holdfast Diversity

Holdfasts of macroalgae that predate the Ediacaran Period were simple and small, the prevalent holdfast type at that period was disc-like. In the Mesoproterozoic, discoidal structures attached to rod-like macroalgae *Tawuia* may represent the first unequivocal holdfast (Kumar, 2001; Xiao and Dong, 2006). Such type of holdfast was also ubiquitous in the Tonian (Dong, et al., 2008; Li et al., 2020) and persisted to the Ediacaran. The simple and invariable holdfast morphology at that time reflects the low diversity of macroalgae and the microbial mat ecosystem was dominant before the Ediacaran. The small discoidal holdfast provided sufficient anchorage to attach on the microbial mat.

During the Ediacaran, holdfasts of macroalgae remarkably diversified, at least six functional morphotypes were recognized. This morphological diversification of macroalgal holdfasts was probably triggered by ocean oxygenation and macroalgae radiation in the Ediacaran Period. The deep sea became intermittently oxic at the beginning of the Ediacaran (Sahoo et al., 2012; Wang et al., 2017; Xiao and Narbonne, 2020). The microbial mat ecosystem declined, and a new ecosystem dominated by erect benthic macroalgae and animals started to establish (Liu et al., 2015; Wan et al., 2020). For example, the benthic macroalga *Flabelllophyton* is a common member of the Lantian, Shibantan, and typical Ediacara biotas distributed in both China and Australia (Wan et al., 2020; Xiao et al., 2020). Through the Ediacaran, the holdfast of *Flabelllophyton typicum* found in both China and Australia (Xiao et al., 2020; Wan et al., 2020) maintained a composite globose shape and was invariable to the significant change of size of the thallus. The morphological stability suggests that the holdfast morphology was at least partially species-specific. As a result, the drastic increase of macroalgae diversity (Ye, 2019b; Bykova et al., 2020) may have also contributed to the diversification of holdfasts during this period.

Attachment Strategy Innovations for Changing Substrate Condition

One of the major factors that determine the attachment strategy of benthic macroscopic algae is the substrate condition (Verbruggen, 2008). The representative case is the comparison between *Flabelllophyton lantianense* (Figures 3E,F) from the Lantian biota and *Baculiphyca taeniata* (Figures 5D,E) from the Miaohu biota, both of them possess thalli that are very similar in shape and size. The only conspicuous difference between these two species is the morphology of the holdfast: *B. taeniata* possesses rhizoids whereas *F. lantianense* does not. The almost identical above-sediment part and comparable paleoenvironments indicate that the occurrence of rhizoids is a response to changed substrate conditions. Benthic macroalgae have already occurred in the Mesoproterozoic, however, the rhizoids have not been found in any fossil macroalgae that predates late Ediacaran (Ye, 2019b). The absence of rhizoids in such a vast time interval probably indicates the predominance of Proterozoic-style firm substrates in this period. Therefore, the lack of rhizoids in the Lantian macroalgae indicates that they were not necessary for effective attachment at that time because the

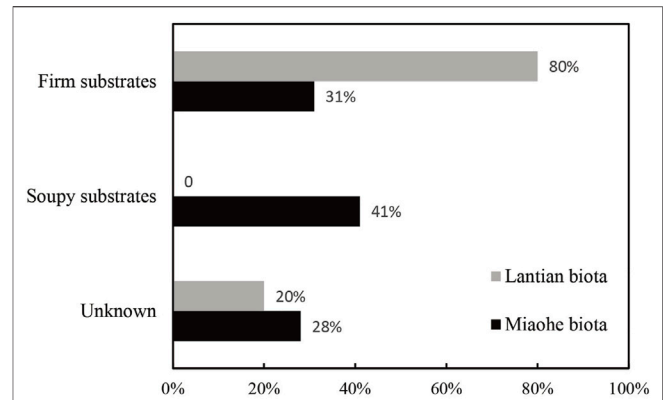


FIGURE 6 | The percentage of benthic macroalgae species more adapted to relatively firm and soupy substrates in the Lantian (10 species) and Miaohu biotas (29 species). Species not suitable for attachment strategy analyses classified as Unknown.

substrates were firm. The ubiquitous rhizoids in the younger late Ediacaran Miaohu biota may represent an adaptation to the changing substrate condition: from Proterozoic-style towards Phanerozoic-style substrates.

In order to determine whether the benthic macroalgae from the early Ediacaran Lantian biota to late Ediacaran Miaohu biota were adapted to the firm or soupy substrates, the morphology of their holdfasts was scrutinized in terms of functional adaptation. These holdfasts were categorized into six general forms which have implications for substrate conditions. As discussed above, tapered base, globose, composite globose, and discoidal forms were interpreted as adaptations to relatively firm substrates which were dominant most of the time of the Precambrian; filamentous rhizoids and horizontal rhizomes are considered to be adaptations to substrates with higher water content comparing to typical Proterozoic-style substrates.

The results show that, in the early Ediacaran Lantian biota, 80% of the benthic macroalga species (10 species in total) are adapted to firm substrates (Figure 6; Supplementary Material S1). The remaining 20% were incompletely preserved and their attachment strategies could not be determined, and were hence classified as unknown. The great majority of firm substrate dwellers suggests that the Lantian biota lived on firm Proterozoic-style substrates. In the late Ediacaran Miaohu biota, 31% of the benthic macroalga species (29 species in total) are adapted to firm substrates (Figure 6; Supplementary Material S1), 41% are adapted to soupy substrates, and 28% are unrecognizable, suggesting the substrates that the Miaohu biota lived on were soupy. Considering the similar depositional environments, the rise of soupy substrate adaptors in the Miaohu biota may indicate the onset of the transformation from firm substrates to soupy substrates had taken place between the age of the Lantian and Miaohu biotas.

During the great transition from the microbial mat to benthic macroscopic ecosystems in the Ediacaran-Cambrian periods (Butterfield, 2007; Wan et al., 2020; Xiao and Narbonne, 2020), the substrate condition also dramatically

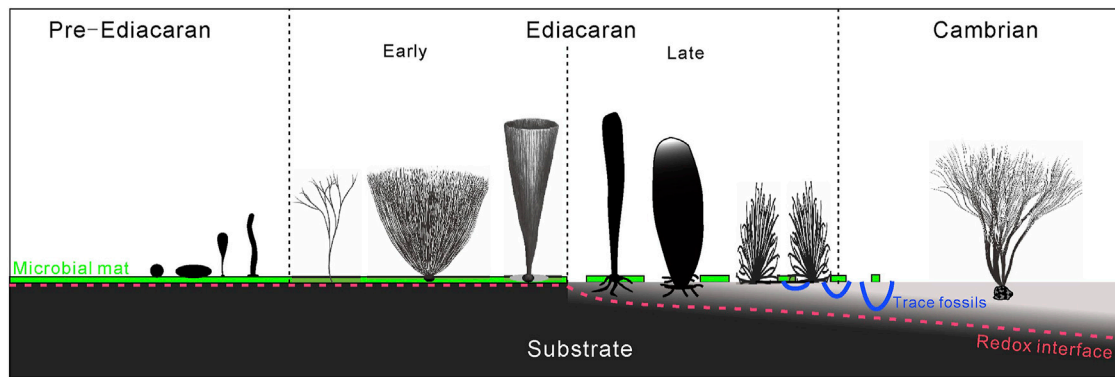


FIGURE 7 | Schematic illustration of macroalgal holdfast morphology and attachment strategy responding to a changing substrate condition.

transformed from the firm, microbial sealed sediments to the soft, water-rich sediments. Moreover, the redox interface migrated downwards to a deeper depth (Figure 7). Although benthic macroalgae (represented by the *Chuaria-Tawuia* assemblage) are not rare in pre-Ediacaran strata, the fossil record of erect benthic macroalgae, such as *Longfengshania* and *Protoarenicola/Pararenicola* (Tang et al., 2021) remains scarce. Macroalgae in the early Ediacaran, despite various shapes of the thalli, e.g., simple dichotomously branching, bush-like, or conical, were adapted to sticking on the surface of microbial mats while mats were still somewhat developed on the seafloor. Attachment innovations in macroalgae in the late Ediacaran, such as developed rhizoids and horizontal rhizomes, are typical adaptations for survival on unstable substrates with a higher water content compared to the early Ediacaran. It may represent adaptive responses to a changing substrate condition in the late Ediacaran, i.e., the decline of microbial mats and the increase of water content in the sediments. Holdfasts of macroalgae became more sophisticated in trapping grains to anchor on mixed substrates in the Cambrian. For example, *Thamnophyton* from the Cambrian Kaili biota show grains coarser than ambient sediments bound in its rhizoids (Yang et al., 2004; Zhao et al., 2011). In summary, the attachment strategy of benthic macroscopic algae became increasingly complex from Pre-Ediacaran to Cambrian, and exhibited some great innovations in the late Ediacaran, adapting to substrate condition and an ecosystem in transformation.

CONCLUSION

Adaptive morphological analysis indicates there are 6 holdfast forms (tapered base, globose holdfast, composite globose holdfast, discoidal holdfast, filamentous rhizoid, and horizontal rhizome) for benthic macroalgae from the early Ediacaran Lantian biota and late Ediacaran Miaohu biota in South China. The morphological variations between holdfasts

may reflect various attachment strategies and further imply general conditions of substrates. In the Lantian biota, all the benthic macroalgae with attachment structures are adapted to firm substrates, while in the Miaohu biota, a significant number (41%) of species are adapted to relatively soft substrates. The great diversification in holdfast morphology and attachment strategies which was marked by the appearance of complex rhizoidal holdfasts was a response to the diversification of macroalgae and changing substrate conditions during this period, i.e., the decline of microbial mat ecosystem and the founding of a benthic algae-dominated ecosystem. The results also provide evidence that the onset of the agronomic revolution (the Cambrian substrate revolution) likely predates the Cambrian and had a protracted effect on paleoecology and evolution onwards.

DATA AVAILABILITY STATEMENT

The original contributions presented in the study are included in the article/Supplementary Materials, further inquiries can be directed to the corresponding author.

AUTHOR CONTRIBUTIONS

BW and XW designed the research. XW, MW, WZ, BW, CN, KP, ZC, and XY collected fossils. All authors contributed feedback on drafts, revised and approved the manuscript.

FUNDING

This research was supported by National Natural Science Foundation of China (41972005 and 41921002), Chinese Academy of Sciences (XDB26000000), National Key Research and Development Program of China (2017YFC0603101), State Key Laboratory of Palaeobiology and Stratigraphy (2102108 and 20201102), and the Youth Innovation Promotion Association of the CAS (grant 2021307).

ACKNOWLEDGMENTS

We thank Chengxi Wu and Yarong Liu for assistance in fieldworks, and journal reviewers for their constructive feedback.

REFERENCES

- An, Z., Jiang, G., Tong, J., Tian, L., Ye, Q., Song, H., et al. (2015). Stratigraphic Position of the Ediacaran Miaohu Biota and its Constraints on the Age of the Upper Doushantuo $\delta^{13}\text{C}$ Anomaly in the Yangtze Gorges Area, South China. *Precambrian Res.* 271, 243–253. doi:10.1016/j.precamres.2015.10.007
- Anderson, K., Close, L., Dewreede, R. E., Lynch, B. J., Ormond, C., and Walker, M. (2006). Biomechanical properties and holdfast morphology of coenocytic algae (Halimedales, Chlorophyta) in Bocas del Toro, Panama. *J. Exp. Mar. Biol. Ecol.* 328, 155–167. doi:10.1016/j.jembe.2005.07.005
- Bedinger, L. A., Bell, S. S., and Dawes, C. J. (2013). Rhizophytic Algal Communities of Shallow, Coastal Habitats in Florida: Components above and below the Sediment Surface. *BMS* 89, 437–460. doi:10.5343/bms.2011.1151
- Bin, W., Xunlai, Y., Zhe, C., Chengguo, G., Ke, P., Qing, T., et al. (2013). Quantitative Analysis of *Flabellophyton* from the Ediacaran Lantian Biota, South China: Application of Geometric Morphometrics in Precambrian Fossil Research. *Acta Geol. Sin.* 87, 905–915. doi:10.1111/1755-6724.12099
- Bottjer, D. J., Hagadorn, J. W., and Dornbos, S. Q. (2000). The Cambrian Substrate Revolution. *GSA Today* 10, 1–7.
- Bunt, J. S. (1975). "Primary Productivity of marine Ecosystems," in *Primary Productivity of the Biosphere* (New York: Springer), 169–183. doi:10.1007/978-3-642-80913-2_8
- Butterfield, N. J. (2007). Macroevolution and Macroecology through Deep Time. *Palaeontology* 50, 41–55. doi:10.1111/j.1475-4983.2006.00613.x
- Bykova, N., Loduca, S. T., Ye, Q., Marusin, V., Grazhdankin, D., and Xiao, S. (2020). Seaweeds through Time: Morphological and Ecological Analysis of Proterozoic and Early Paleozoic Benthic Macroalgae. *Precambrian Res.* 350, 105875. doi:10.1016/j.precamres.2020.105875
- Chen, Z., Chen, X., Zhou, C., Yuan, X., and Xiao, S. (2018). Late Ediacaran Trackways Produced by Bilaterian Animals with Paired Appendages. *Sci. Adv.* 4, eaao6691. doi:10.1126/sciadv.aao6691
- Chen, Z., Zhou, C., Yuan, X., and Xiao, S. (2019). Death March of a Segmented and Trilobate Bilaterian Elucidates Early Animal Evolution. *Nature* 573, 412–415. doi:10.1038/s41586-019-1522-7
- Condon, D., Zhu, M., Bowring, S., Wang, W., Yang, A., and Jin, Y. (2005). U–pb Ages from the Neoproterozoic Doushantuo Formation, China. *Science* 308, 95–98. doi:10.1126/science.1107765
- Denny, M. W., Daniel, T. L., and Koehl, M. A. R. (1985). Mechanical Limits to Size in Wave-Swept Organisms. *Ecol. Monogr.* 55, 69–102. doi:10.2307/1942526
- Dong, L., Xiao, S., Shen, B., Yuan, X., Yan, X., and Peng, Y. (2008). Restudy of the Worm-like Carbonaceous Compression Fossils *Protoarenicola*, *Pararenicola*, and *Sinosabellidites* from Early Neoproterozoic Successions in North China. *Palaeogeogr. Palaeoclimatol. Palaeoecol.* 258, 138–161. doi:10.1016/j.palaeo.2007.05.019
- Dornbos, S. Q., and Bottjer, D. J. (2000). Evolutionary Paleocology of the Earliest Echinoderms: Helicoplacoids and the Cambrian Substrate Revolution. *Geology* 28, 839–842. doi:10.1130/0091-7613(2000)028<0839:epotee>2.3.co;2
- Dornbos, S. Q., Bottjer, D. J., and Chen, J.-Y. (2005). Paleocology of Benthic Metazoans in the Early Cambrian Maotianshan Shale Biota and the Middle Cambrian Burgess Shale Biota: Evidence for the Cambrian Substrate Revolution. *Palaeogeogr. Palaeoclimatol. Palaeoecol.* 220, 47–67. doi:10.1016/j.palaeo.2003.11.016
- Du, R., Tian, L., and Li, H. (1986). Discovery of Megafossils in the Gaoyuzhuang Formation of the Changchengian System, Jixian. *Acta Geol. Sin.* 60, 115–120.
- Guan, C., Zhou, C., Wang, W., Wan, B., Yuan, X., and Chen, Z. (2014). Fluctuation of Shelf basin Redox Conditions in the Early Ediacaran: Evidence from Lantian Formation Black Shales in South China. *Precambrian Res.* 245, 1–12. doi:10.1016/j.precamres.2014.01.003
- Hofmann, H. J., O'Brien, S. J., and King, A. F. (2008). Ediacaran Biota on Bonavista Peninsula, Newfoundland, Canada. *J. Paleontol.* 82, 1–36. doi:10.1666/06-087.1
- Hofmann, H. J., and Altken, J. D. (1979). Precambrian Biota from the Little Dal Group, Mackenzie Mountains, Northwestern Canada. *Can. J. Earth Sci.* 16, 150–166. doi:10.1139/e79-014
- IBM Corp (2015). *IBM SPSS Statistics for Windows*. Version 23.0. Armonk, NY: IBM Corp.
- Jiang, G., Kaufman, A. J., Christie-Blick, N., Zhang, S., and Wu, H. (2007). Carbon Isotope Variability across the Ediacaran Yangtze Platform in South China: Implications for a Large Surface-To-Deep Ocean $\delta^{13}\text{C}$ Gradient. *Earth Planet. Sci. Lett.* 261, 303–320. doi:10.1016/j.epsl.2007.07.009
- Jiang, G., Shi, X., Zhang, S., Wang, Y., and Xiao, S. (2011). Stratigraphy and Paleogeography of the Ediacaran Doushantuo Formation (Ca. 635–551Ma) in South China. *Gondwana Res.* 19, 831–849. doi:10.1016/j.jgr.2011.01.006
- Kenchington, C. G., and Wilby, P. R. (2017). Rangeomorph Classification Schemes and Intra-specific Variation: Are All Characters Created Equal? *Geol. Soc. Lond. Spec. Publ.* 448, 221–250. doi:10.1144/sp448.19
- Kloss, T. J., Dornbos, S. Q., and Chen, J. (2015). Substrate Adaptations of Sessile Benthic Metazoans during the Cambrian Radiation. *Paleobiology* 41, 342–352. doi:10.1017/pab.2014.22
- Kumar, S. (2001). Mesoproterozoic Megafossil *Chuarina-Tawuia* Association May Represent Parts of a Multicellular Plant, Vindhyan Supergroup, Central India. *Precambrian Res.* 106, 187–211. doi:10.1016/s0301-9268(00)00093-0
- Lei, Q.-P., Han, J., Ou, Q., and Wan, X.-Q. (2014). Sedentary Habits of Anthozoa-like Animals in the Chengjiang Lagerstätte: Adaptive Strategies for Phanerozoic-Style Soft Substrates. *Gondwana Res.* 25, 966–974. doi:10.1016/j.jgr.2013.01.007
- Levi, B., and Friedlander, M. (2004). Identification of Two Putative Adhesive Polypeptides in *Caulerpa Prolifera* Rhizoids Using an Adhesion Model System. *J. Appl. Phycol.* 16, 1–9. doi:10.1023/B:JAPH.0000019034.12015.87
- Li, Z. X., Bogdanova, S. V., Collins, A. S., Davidson, A., De Waele, B., Ernst, R. E., et al. (2008). Assembly, Configuration, and Break-Up History of Rodinia: A Synthesis. *Precambrian Res.* 160, 179–210. doi:10.1016/j.precamres.2007.04.021
- Li, G., Chen, L., Pang, K., Zhou, G., Han, C., Yang, L., et al. (2020). An Assemblage of Macroscopic and Diversified Carbonaceous Compression Fossils from the Tonian Shiwangzhuang Formation in Western Shandong, North China. *Precambrian Res.* 346, 105801. doi:10.1016/j.precamres.2020.105801
- Liu, A. G., Kenchington, C. G., and Mitchell, E. G. (2015). Remarkable Insights into the Paleocology of the Avalonian Ediacaran Macrobiota. *Gondwana Res.* 27, 1355–1380. doi:10.1016/j.jgr.2014.11.002
- Loduca, S. T., Bykova, N., Wu, M., Xiao, S., and Zhao, Y. (2017). Seaweed Morphology and Ecology during the Great Animal Diversification Events of the Early Paleozoic: A Tale of Two Floras. *Geobiology* 15, 588–616. doi:10.1111/gbi.12244
- Mickovski, S. B., and Ennos, A. R. (2003). Model and Whole-Plant Studies on the anchorage Capabilities of Bulbs. *Plant Soil* 255, 641–652. doi:10.1023/A:1026007229517
- Rasband, W. S. (2018). *ImageJ*. Bethesda, Maryland, USA: U. S. National Institutes of Health. Available at: <https://imagej.nih.gov/ij/>.
- Sahoo, S. K., Planavsky, N. J., Kendall, B., Wang, X., Shi, X., Scott, C., et al. (2012). Ocean Oxygenation in the Wake of the Marinoan Glaciation. *Nature* 489, 546–549. doi:10.1038/nature11445

SUPPLEMENTARY MATERIAL

The Supplementary Material for this article can be found online at: <https://www.frontiersin.org/articles/10.3389/feart.2021.783427/full#supplementary-material>

- Seilacher, A. (1999). Biomat-related Lifestyles in the Precambrian. *Palaio* 14, 86–93. doi:10.2307/3515363
- Spearman, C. (1904). The Proof and Measurement of Association between Two Things. *Am. J. Psychol.* 15, 72–101. doi:10.2307/1412159
- Sprinkle, J., and Guensburg, T. E. (1995). Origin of Echinoderms in the Paleozoic Evolutionary Fauna: The Role of Substrates. *Palaio* 10, 437–453. doi:10.2307/3515046
- Steneck, R. S., Graham, M. H., Bourque, B. J., Corbett, D., Erlandson, J. M., Estes, J. A., et al. (2002). Kelp forest Ecosystems: Biodiversity, Stability, Resilience and Future. *Envir. Conserv.* 29, 436–459. doi:10.1017/S0376892902000322
- Tang, Q., Pang, K., Li, G., Chen, L., Yuan, X., and Xiao, S. (2021). One-billion-year-old Epibionts Highlight Symbiotic Ecological Interactions in Early Eukaryote Evolution. *Gondwana Res.* 97, 22–33. doi:10.1016/j.gr.2021.05.008
- Verbruggen, H. (2008). Resegmenting Halimeda. Molecular and Morphometric Studies of Species Boundaries within a green Algal Genus. Doctoral Dissertation. Ghent: Ghent University.
- Wan, B., Xiao, S., Yuan, X., Chen, Z., Pang, K., Tang, Q., et al. (2014). Orbisiana Linearis from the Early Ediacaran Lantian Formation of South China and its Taphonomic and Ecological Implications. *Precambrian Res.* 255, 266–275. doi:10.1016/j.precamres.2014.09.028
- Wan, B., Yuan, X., Chen, Z., Guan, C., Pang, K., Tang, Q., et al. (2016). Systematic Description of Putative Animal Fossils from the Early E Diacaran L Antian F Formation of S Outh C Hina. *Palaeontology* 59, 515–532. doi:10.1111/pala.12242
- Wan, B., Chen, Z., Yuan, X., Pang, K., Tang, Q., Guan, C., et al. (2020). A Tale of Three Taphonomic Modes: The Ediacaran Fossil *Flabellophyton* Preserved in limestone, Black Shale, and sandstone. *Gondwana Res.* 84, 296–314. doi:10.1016/j.gr.2020.04.003
- Wang, Y., and Wang, X. (2008). Macroalgal Holdfasts and Their Interaction with Environments from the Neoproterozoic Doushantuo Formation in Guizhou, South China. *Front. Biol. China* 3, 113–122. doi:10.1007/s11515-008-0009-y
- Wang, Y., Wang, Y., Du, W., and Wang, X. (2014). The Correlation between Macroscopic Algae and Metazoans in the Ediacaran: a Case Study on the Wenghui Biota in Northeastern Guizhou, South China. *Aust. J. Earth Sci.* 61, 967–977. doi:10.1080/08120099.2014.956231
- Wang, Y., Wang, Y., Du, W., and Wang, X. (2016). New Data of Macrofossils in the Ediacaran Wenghui Biota from Guizhou, South China. *Acta Geol. Sin.* 90, 1611–1628. doi:10.1111/1755-6724.12805
- Wang, W., Guan, C., Zhou, C., Peng, Y., Pratt, L. M., Chen, X., et al. (2017). Integrated Carbon, Sulfur, and Nitrogen Isotope Chemostratigraphy of the Ediacaran Lantian Formation in South China: Spatial Gradient, Ocean Redox Oscillation, and Fossil Distribution. *Geobiology* 15, 552–571. doi:10.1111/gbi.12226
- Wang, X., Pang, K., Chen, Z., Wan, B., Xiao, S., Zhou, C., et al. (2020a). The Ediacaran Frondose Fossil Arborea from the Shibantan limestone of South China. *J. Paleontol.* 94, 1034–1050. doi:10.1017/jpa.2020.43
- Wang, Y., Wang, Y., Tang, F., and Zhao, M. (2020b). Ediacaran Macroalgal Holdfasts and Their Evolution: a Case Study from China. *Palaeontology* 63, 821–840. doi:10.1111/pala.12485
- Wernberg, T., and Thomsen, M. S. (2005). The Effect of Wave Exposure on the Morphology of *Ecklonia Radiata*. *Aquat. Bot.* 83, 61–70. doi:10.1016/j.aquabot.2005.05.007
- Xiao, S., and Dong, L. (2006). “On the Morphological and Ecological History of Proterozoic Macroalgae,” in *Neoproterozoic Geobiology and Paleobiology*. Editors S. Xiao and A. J. Kaufman (Netherlands: Springer), 57–90.
- Xiao, S., Gehling, J. G., Evans, S. D., Hughes, I. V., and Droser, M. L. (2020). Probable Benthic Macroalgae from the Ediacara Member, South Australia. *Precambrian Res.* 350, 105903. doi:10.1016/j.precamres.2020.105903
- Xiao, S. H., and Narbonne, G. M. (2020). “The Ediacaran Period,” in *Geologic Time Scale 2020* (Amsterdam, Netherland: Elsevier), 521–561. doi:10.1016/b978-0-12-824360-2.00018-8
- Xiao, S., Yuan, X., Steiner, M., and Knoll, A. H. (2002). Macroscopic Carbonaceous Compressions in a Terminal Proterozoic Shale: A Systematic Reassessment of the Miaohu Biota, south China. *J. Paleontol.* 76, 3472–4376. doi:10.1017/s0022336000041743
- Xiao, S., Bykova, N., Kovalick, A., and Gill, B. C. (2017). Stable Carbon Isotopes of Sedimentary Kerogens and Carbonaceous Macrofossils from the Ediacaran Miaohu Member in South China: Implications for Stratigraphic Correlation and Sources of Sedimentary Organic Carbon. *Precambrian Res.* 302, 171–179. doi:10.1016/j.precamres.2017.10.006
- Xiao, S., Chen, Z., Zhou, C., and Yuan, X. (2019). Surfing in and on Microbial Mats: Oxygen-Related Behavior of a Terminal Ediacaran Bilaterian Animal. *Geology* 47, 1054–1058. doi:10.1130/g46474.1
- Xiao, S. (2013). “Written in Stone: the Fossil Record of Early Eukaryotes,” in *Evolution from the Galapagos: Two Centuries after Darwin*. Editors G. Trueba and C. Montúfar (New York: Springer), 107–124. doi:10.1007/978-1-4614-6732-8_8
- Xunlai, Y., Jun, L., and Ruiji, C. (1999). A Diverse Metaphyte Assemblage from the Neoproterozoic Black Shales of South China. *Lethaia* 32, 143–155. doi:10.1111/j.1502-3931.1999.tb00533.x
- Yang, R., Mao, J., Zhang, W., Jiang, L., and Gao, H. (2004). Bryophyte-like Fossil (*Parafunaria Sinensis*) from Early-Middle Cambrian Kaili Formation in Guizhou Province, China. *Acta Bot. Sin.* 46, 180–185. doi:10.3321/j.issn:1672-9072.2004.02.009
- Yang, Q., Zhang, C., Liu, P., and Jiang, J. (2021). The Role of Root Morphology and Pulling Direction in Pullout Resistance of Alfalfa Roots. *Front. Plant Sci.* 12, 580825. doi:10.3389/fpls.2021.580825
- Ye, Q., Tong, J., An, Z., Hu, J., Tian, L., Guan, K., et al. (2019a). A Systematic Description of New Macrofossil Material from the Upper Ediacaran Miaohu Member in South China. *J. Syst. Palaeontol.* 17, 183–238. doi:10.1080/14772019.2017.1404499
- Ye, Q. (2019b). Study on the Macroalgae in the Late Neoproterozoic of the Shennongjia and Huangling Area, South China. Doctoral Dissertation. Wuhan: China University of Geosciences.
- Yuan, X., Chen, Z., Xiao, S., Zhou, C., and Hua, H. (2011). An Early Ediacaran Assemblage of Macroscopic and Morphologically Differentiated Eukaryotes. *Nature* 470, 390–393. doi:10.1038/nature09810
- Zhang, S., Li, H., Jiang, G., Evans, D. A. D., Dong, J., Wu, H., et al. (2015). New Paleomagnetic Results from the Ediacaran Doushantuo Formation in South China and Their Paleogeographic Implications. *Precambrian Res.* 259, 130–142. doi:10.1016/j.precamres.2014.09.018
- Zhao, Y., Chen, M. e., Peng, J., Yu, M., He, M., Wang, Y., et al. (2004). Discovery of a Miaohu-type Biota from the Neoproterozoic Doushantuo Formation in Jiangkou County, Guizhou Province, China. *Chin.Sci.Bull.* 49, 2224–2226. doi:10.1007/BF03185792
- Zhao, Y., Zhu, M., Babcock, L., and Peng, J. (2011). *The Kaili Biota: Marine Organisms from 508 Million Years Ago*. Guiyang: Guizhou Science and Technology Press.
- Zhou, C., Xiao, S., Wang, W., Guan, C., Ouyang, Q., and Chen, Z. (2017). The Stratigraphic Complexity of the Middle Ediacaran Carbon Isotopic Record in the Yangtze Gorges Area, South China, and its Implications for the Age and Chemostratigraphic Significance of the Shuram Excursion. *Precambrian Res.* 288, 23–38. doi:10.1016/j.precamres.2016.11.007
- Zhu, M., Zhang, J., and Yang, A. (2007). Integrated Ediacaran (Sinian) Chronostratigraphy of South China. *Palaeogeogr. Palaeoclimatol. Palaeoecol.* 254, 7–61. doi:10.1016/j.palaeo.2007.03.025
- Zhu, M., Lu, M., Zhang, J., Zhao, F., Li, G., Aihua, Y., et al. (2013). Carbon Isotope Chemostratigraphy and Sedimentary Facies Evolution of the Ediacaran Doushantuo Formation in Western Hubei, South China. *Precambrian Res.* 225, 7–28. doi:10.1016/j.precamres.2011.07.019

Conflict of Interest: The authors declare that the research was conducted in the absence of any commercial or financial relationships that could be construed as a potential conflict of interest.

Publisher's Note: All claims expressed in this article are solely those of the authors and do not necessarily represent those of their affiliated organizations, or those of the publisher, the editors and the reviewers. Any product that may be evaluated in this article, or claim that may be made by its manufacturer, is not guaranteed or endorsed by the publisher.

Copyright © 2021 Wang, Wu, Wan, Niu, Zheng, Guan, Pang, Chen and Yuan. This is an open-access article distributed under the terms of the Creative Commons Attribution License (CC BY). The use, distribution or reproduction in other forums is permitted, provided the original author(s) and the copyright owner(s) are credited and that the original publication in this journal is cited, in accordance with accepted academic practice. No use, distribution or reproduction is permitted which does not comply with these terms.



Doushantuo-Pertatataka—Like Acritarchs From the Late Ediacaran Bocaina Formation (Corumbá Group, Brazil)

L. Morais^{1,2*}, T. R. Fairchild², B. T. Freitas³, I. D. Rudnitzki⁴, E. P. Silva⁵, D. Lahr⁶, A. C. Moreira⁷, E. A. Abrahão Filho⁸, J. M. Leme² and R. I. F. Trindade⁹

¹Department of Geophysics, Institute of Astronomy, Geophysics and Atmospheric Sciences, University of São Paulo, São Paulo, Brazil, ²Department of Sedimentary and Environmental Geology, Institute of Geosciences, University of São Paulo, São Paulo, Brazil, ³Geology Lab, School of Technology, University of Campinas, Limeira, Brazil, ⁴Departament of Geology, Federal University of Ouro Preto – DEGEO/UFOP, Ouro Preto, Brazil, ⁵Department of Astronomy, Institute of Astronomy, Geophysics and Atmospheric Sciences, University of São Paulo, São Paulo, Brazil, ⁶Department of Zoology, Institute of Biosciences, University of São Paulo, São Paulo, Brazil, ⁷Laboratory of Porous Media and Thermophysical Properties, University Federal of Santa Catarina, Florianópolis, Brazil, ⁸EDEM, Empresa De Desenvolvimento em Mineração e Participações Ltda., Goiânia, Brazil, ⁹Department of Geophysics, Institute of Astronomy, Geophysics and Atmospheric Sciences, University of São Paulo, São Paulo, Brazil

OPEN ACCESS

Edited by:

Haijun Song,
China University of Geosciences
Wuhan, China

Reviewed by:

Qing Ouyang,
Nanjing Institute of Geology and
Palaeontology (CAS), China
Sebastian Willman,
Department of Earth Sciences,
Uppsala University, Sweden

*Correspondence:

L. Morais
Moraisluanamoraiss@usp.br

Specialty section:

This article was submitted to
Paleontology,
a section of the journal
Frontiers in Earth Science

Received: 30 September 2021

Accepted: 23 November 2021

Published: 09 December 2021

Citation:

Morais L, Fairchild TR, Freitas BT, Rudnitzki ID, Silva EP, Lahr D, Moreira AC, Abrahão Filho EA, Leme JM and Trindade RIF (2021) Doushantuo-Pertatataka—Like Acritarchs From the Late Ediacaran Bocaina Formation (Corumbá Group, Brazil). *Front. Earth Sci.* 9:787011. doi: 10.3389/feart.2021.787011

Acritarchs, a polyphyletic group of acid-resistant organic-walled microfossils, dominate the eukaryotic microfossil record in the Proterozoic (2500–541 Ma) yet exhibit significant reduction in diversity and size at the transition to the Phanerozoic (541–520 Ma). Despite the difficulty of tracing phylogenetic relationships among acritarchs, changes in their complexity and diversity through time have allowed their use in paleoecological and biostratigraphic schemes. The Doushantuo-Pertatataka Ediacaran acritarch assemblage, for example, is usually considered as restricted to the early Ediacaran between 635 and 580 Ma. But similar, diverse acritarchs have been recovered from younger rocks in Mongolia and Arctic Siberia and are now reported here from phosphatized horizons of the upper Bocaina Formation (ca. 555 Ma), Corumbá Group, SW Brazil. In the overlying black limestones and shales of the latest Ediacaran Tamengo Formation (542 Ma) acritarch diversity is low, but the skeletal metazoans *Cloudina* and *Corumbella* are abundant. The Bocaina acritarch assemblage shares forms referable to the genera *Leiosphaeridia*, *Tanarium*, *Asseserium* and *Megasphaera* with the Doushantuo-Pertatataka assemblage, but also includes specimens similar to the Phanerozoic genus *Archaeodiscina* in addition to two new complex acritarchs. The first is covered by rounded low conical bumps, similar to *Eotylotopalla* but differs in having a distinct opening suggestive of greater (multicellular?) complexity. The second, identified here as Morphotype 1, is a double-walled acanthomorph acritarch with scattered cylindrical processes between the walls. The contrast in acritarch diversity and abundance between the Bocaina and Tamengo formations is likely due in part to paleoenvironmental and taphonomic differences (absence of the phosphatization window in the latter), as well as to the appearance of both suspension-feeding skeletal metazoans (*Cloudina* and *Corumbella*). The occurrence of Doushantuo-Pertatataka acritarchs in SW Brazil,

northern Mongolia, and Arctic Siberia extend the biostratigraphic range of this assemblage up to the terminal Ediacaran *Cloudina* biozone.

Keywords: acanthomorph acritarchs, phosphatized microfossils, Neoproterozoic, Paraguay belt, Ediacaran

INTRODUCTION

Acritarchs represent a polyphyletic group of resistant organic-walled eukaryotic unicellular organisms (Evitt, 1963), fundamental to our understanding of early eukaryotic evolution and biostratigraphy (Knoll, 2003; Grey, 2005). They dominate the Proterozoic fossil record of plankton from 2500 to 541 Ma, having successfully endured the “Boring Billion” and survived Neoproterozoic icehouse intervals and bolide impacts (Grey et al., 2003; Huntley et al., 2006; Moczyłowska, 2008). Yet, they waned at the end of the Ediacaran and beginning of the Cambrian, between 541 and 520 Ma, as invertebrates began to flourish (Downie et al., 1963; Huntley et al., 2006).

From the Paleoproterozoic to the Early Neoproterozoic, the acritarch record is dominated by simple spheroids (Huntley et al., 2006) of limited biostratigraphic utility. During the rest of the Neoproterozoic, palynomorphs are often large, complex, process-bearing acritarchs having more restricted ranges and thus greater biostratigraphic usefulness, especially in the Ediacaran (Grey et al., 2003).

Ediacaran acritarch biozones were first established in Australia (Grey, 2005; Grey and Calver, 2007), where an older one dominated by simple spheroidal acritarchs is referred to as the Ediacaran Leiosphere Palynoflora (ELP) zone, and a younger one, characterized by ornamented, spheroidal microfossils, is called the Ediacaran Complex Acritarch-dominated Palynoflora (ECAP) zone (Grey, 2005; Grey and Calver, 2007; Gaucher and Sprechmann, 2009). Within the ECAP zone, larger ornamented acanthomorphs ranging in size from 100 to 700 μm are collectively known as the Doushantuo-Pertatataka-assemblage (Zang and Walter 1992; Grey, 2005), originally recognized in the <580 Ma Pertatataka Formation, Australia (Grey et al., 2003; Grey, 2005; McKirdy et al., 2006; Grey and Calver, 2007) and the 635 ± 0.6 to 551.1 ± 0.7 Ma Doushantuo Formation, China (Chen and Liu, 1986; Condon et al., 2005). Attempts to extend these zones to other regions have met with limited success, but, in general, complex large acanthomorphs are largely limited to strata older than the Gaskiers glaciation at about 580 Ma (see discussion in Xiao and Narbonne, 2020).

Even without definitive geochronological constraints, the ELP zone has been considered earliest Ediacaran and the ECAP zone younger, but probably not younger than 560 Ma (Grey 2005; Grey and Calver, 2007; Gaucher and Sprechmann, 2009; Golubkova et al., 2015; Rud'ko et al., 2017; Anderson et al., 2017), making it the last explosive acritarch radiation of the Proterozoic (Moczyłowska, 1991; Vidal and Moczyłowska-Vidal, 1997; Gaucher and Sprechmann, 2009). The decline of the ECAP has usually been attributed to the rise of metazoans within the Nama Assemblage (550–541 Ma) (Fedonkin and Waggoner, 1997; Huntley et al., 2006; Gaucher and Sprechmann, 2009; Xiao and Narbonne, 2020).

Recently, diverse Doushantuo-Pertatataka-like acritarchs have been reported from in the latest Ediacaran of northern Mongolia (Anderson et al., 2017, 2019) and latest Ediacaran to early Cambrian of Arctic Siberia (Grazhdankin et al., 2020). Here, we describe a similar assemblage from shale-hosted phosphatic nodules and phosphatic microbialites of the upper Ediacaran Bocaina Formation (555.18 ± 0.30 Ma; Parry et al., 2017), Corumbá Group, SW Brazil. Overlying this unit is the *Cloudina*- and *Corumbella*-bearing, leiosphaerid-dominated (Gaucher et al., 2003) Tamengo Formation (542 ± 0.75 Ma; Parry et al., 2017), also within the Corumbá Group.

The acritarchs in the Bocaina Formation consist of single- and double-walled vesicles, with or without processes, representing sphaeromorphs, acanthomorphs, netromorphs and pteromorphs (Downie et al., 1963). The great variation in shape and dimensions of the acanthomorph vesicles observed in the Bocaina Formation is a feature shared with Doushantuo-Pertatataka-like Mongolian and Siberian acanthomorphs of similar age (Chen and Liu, 1986; Zang and Walter, 1992; Grey, 2005; Anderson et al., 2017; Grazhdankin et al., 2020).

Our results provide paleogeographic, stratigraphic and chronologic constraints for the first occurrence of Doushantuo-Pertatataka-like acritarchs described from South America and further corroborate the extension of the ECAP into Ediacaran rocks just below the terminal Ediacaran *Cloudina* biozone.

GEOLOGICAL SETTING

The Corumbá Group is part of the southern Paraguay Belt, cropping out in the Urucum District and the Serra da Bodoquena, Mato Grosso do Sul, Brazil, central South America (Figure 1) (Almeida, 1946; 1965). In the Urucum District, the Corumbá Group comprises a carbonate-dominated succession deposited upon Paleoproterozoic granite and gneiss-dominated basement of the Rio Apa Block, as well as upon Cryogenian successions of the Jacadigo Group (Freitas et al., 2011; 2021) and the Puga Formation (Maciel, 1959; Freitas et al., 2011). There are two main carbonate sequences in the Corumbá Group: the lower, dominated by light grey dolostone enriched in phosphate near its top - the Bocaina Formation; and the upper, dominated by dark grey limestone with organic-rich shale intercalations and the metazoan fossils *Cloudina* and *Corumbella*—the Tamengo Formation (Figure 1A; Gaucher et al., 2003). Zircon crystals from ash beds near the top of both units have provided U-Pb ID-TIMS (CA-ID-TIMS) minimum ages of $555.18 \pm 0.30/0.34/0.70$ Ma for the Bocaina Formation and 541.2 to 548 Ma for the Tamengo Formation (Figure 1A; Parry et al., 2017). Conformably overlying the Tamengo Formation and finalizing the Corumbá Group are fine-grained siliciclastic deposits of the <541 Ma Guaicurus Formation (Figure 1A; Parry et al.,

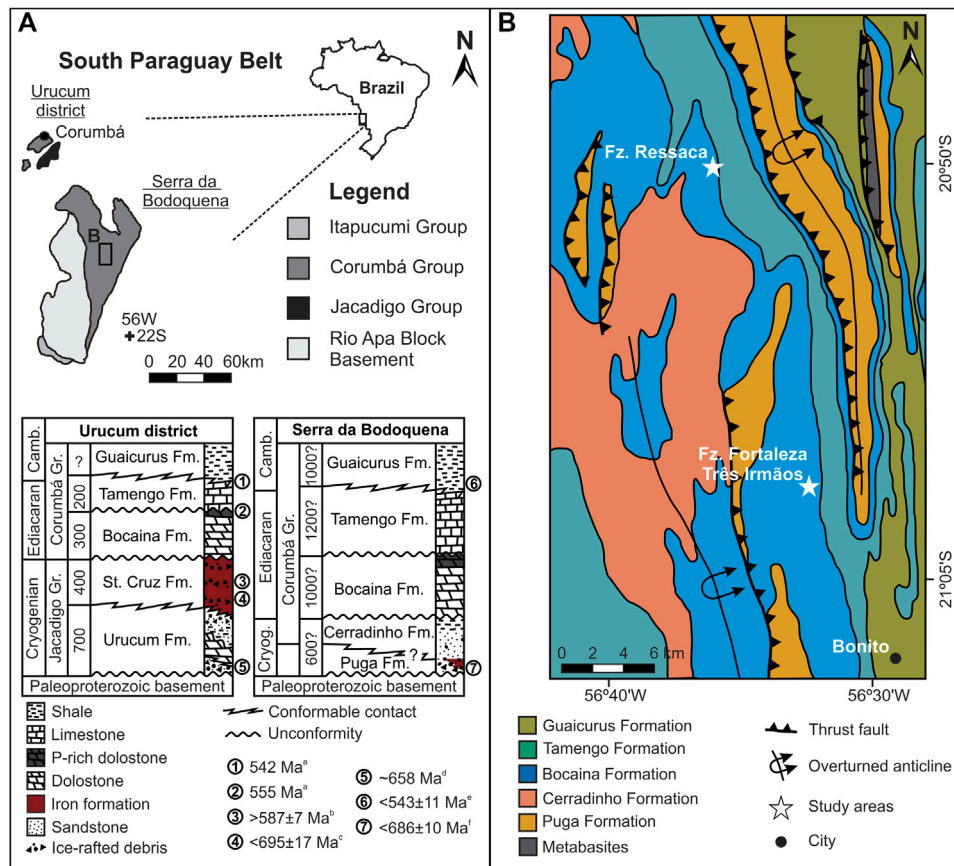


FIGURE 1 | Geological setting. **(A)** Neoproterozoic units, main outcropping areas and simplified stratigraphic charts of the South Paraguay Belt, western Mato Grosso do Sul, Brazil. Numbers in the stratigraphic charts are maximum estimated stratigraphic thickness in meters, for each formation, mostly based on composite sections. For the Urucum district area, maximum thickness estimates are from Gaucher et al. (2003), Boggiani et al. (2010) and Freitas et al. (2021). For Serra da Bodoquena, maximum stratigraphic thicknesses are estimates presented in the pioneer work of Almeida (1965). Time constraints: ^aAsh bed zircon, U-Pb, ID-TIMS (CA-ID-TIMS) (Parry et al., 2017); ^bCryptomelane, Ar-Ar (Piacentini et al., 2013); ^cDetrital zircon, U-Pb, LA-ICP-MS (Frei et al., 2017); ^dSequence and chemostratigraphic correlation with Neoproterozoic cryochrons (Freitas et al., 2021); ^eDetrital zircon, U-Pb, SHRIMP (McGee et al., 2018); ^fDetrital zircon, U-Pb, LA-ICP-MS (McGee et al., 2018). **(B)** Geological sketch map of study area, after Campanha et al. (2011).

2017). This same succession and bounding stratigraphic sequences of the Corumbá Group are also recognized in the Serra da Bodoquena, overlying the siliciclastic-dominated succession of the Puga, and Cerradinho formations (Figures 1A,B; Almeida, 1965; Campanha et al., 2011). Geochronology of detrital zircon from phyllite of the Guaicurus Formation in the Serra da Bodoquena provides a maximum depositional age of 543 Ma ± 11 (McGee et al., 2018), consistent with results obtained by Parry et al. (2017) in the Urucum District (Figure 1A).

The Bocaina Formation records shallow marine conditions as indicated by abundant ooid grainstone and stromatolitic dolostone, as well as by phosphate-rich horizons, observed in both the Urucum District and the Serra da Bodoquena (Almeida 1945; Gaucher et al., 2003; Freitas et al., 2011). The unit is truncated at the top by a regional erosional unconformity (Figure 1B), overlain by polymictic breccia having clasts of crystalline basement, dolostone and phosphorite at the base of the Tamengo Formation (Gaucher et al., 2003; Campanha et al., 2011; Amorim et al., 2020). The overlying Tamengo Formation

was deposited in a shallow to relatively deep storm-influenced carbonate ramp, as interpreted from cross-bedded fine grainstones, mudstones and shales associated with metazoan fossils and meiofaunal trace fossils (Zaine and Fairchild, 1987; Gaucher et al., 2003; Van Iten et al., 2014; Pacheco et al., 2015; Adorno et al., 2017; Parry et al., 2017; Amorim et al., 2020).

The microfossils reported here were recovered from the upper Bocaina Formation at Serra da Bodoquena (Figure 1B) in samples from a drill core (ALW-DD004) and three trenches cutting phosphate-rich horizons mined by EDEM (Empresa de Desenvolvimento em Mineração e Participações Ltda) at Fazenda Ressaca and Fazenda Fortaleza Três Irmãos, between Bonito and Bodoquena, Mato Grosso do Sul (Figures 1, 2).

MATERIALS AND METHODS

Stratigraphic sections are shown in Figure 2 for drill core DD004, trenches TR2 and TR3 at Fazenda Ressaca and TR6 at Fortaleza Três

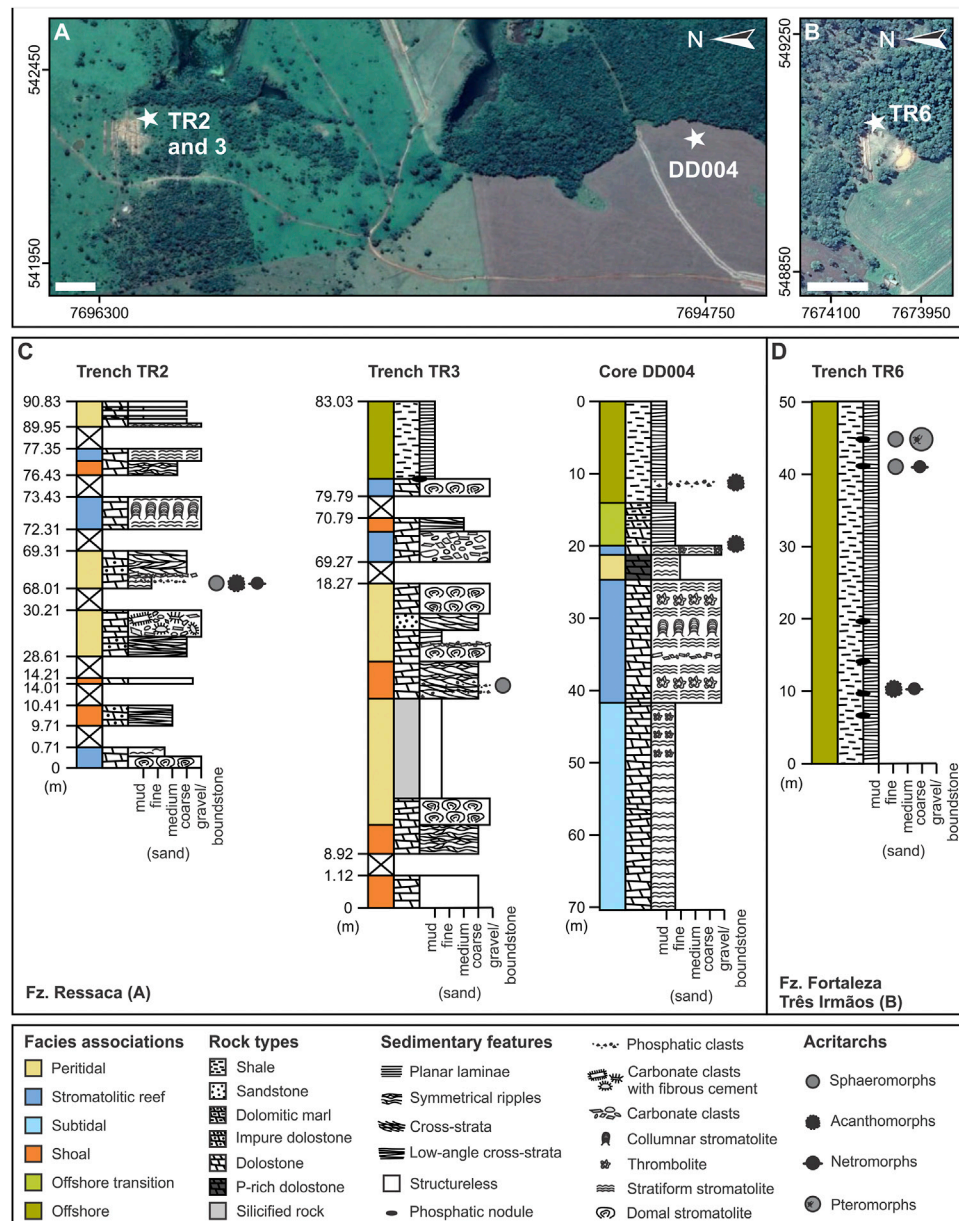


FIGURE 2 | Studied successions. **(A)** Satellite image (Google Earth Pro v. 7.3.4.8248) of Fazenda (Fz.) Ressaca with approximate locations of trenches TR2 and TR3, and drill hole DD004. **(B)** Satellite image (Google Earth Pro v. 7.3.4.8248) of Fazenda Fortaleza Três Irmãos area displaying the approximate location of trench TR6. **(C)** Simplified columnar sections measured along trenches TR2 and TR3, and drill core DD004. **(D)** Simplified columnar section measured along trench TR6. UTM zone: 21K. White scale bars: 100 m.

Irmãos, in areas of phosphate prospection carried out by EDEM mining company in the Serra da Bodoquena. Thirty samples were collected from phosphate-rich intervals mainly composed of dolomitic microbialite and shale in the drill core and trenches, 12 of which yielded the microfossils described here (Table 1).

Samples of P-rich dolomitic microbialite were examined in petrographic thin sections (4FR19-4, 4FR19-17, FL18-5 and 4FR19-36, Table 1) using a Leica DM750 P microscope equipped with a Leica MC 170 HD camera. Some images were obtained using a simplified version of the “white-card” technique of Folk (1987), by placing a small

piece of white paper beneath the thin section to diffuse the incoming light beam, thereby softening the visual effect of carbonate crystal boundaries and permitting a clearer view of individual rock components, especially, those made of or containing organic matter.

Palynological preparations were made from P-rich dolomitic microbialite (samples 1, 2 and 3), P-rich nodules in shale (samples 7, 11, 12 and 17) (Table 1). About 100 g of fresh samples were reacted with HCl (37%) and HF (30%) at the Centro de Pesquisa Leopoldo Américo Miguez de Mello (CENPES—Petrobrás, Rio de Janeiro), initially with HCl for 2 days, neutralized, and then with

TABLE 1 | Summary of basic facts on the size and distribution of acritarchs of the Bocaina Formation recognized in this study.

Group	Taxon	Specimens (N)	Size range (µm)	Sample (n)	Lithology	Level (m)				GP5T
						TR2	TR3	TR6	DD004	
Sphaeromorphs	<i>Leiosphaeridia crassa</i>	3	59–65	12 ^S (3)	P-nod			42.15		2564
	<i>Leiosphaeridia minutissima</i>	8	23–68	1 ^S (2)	P-mic ^a	68.27				2557
				2 ^S (1)	P-mic	68.15				2558
				6 ^S (1)	P-mic ^a		14.81			2561
				17 ^S (4)	P-nod			46.5		2567
	<i>Synsphaeridium</i> sp.	2	12–20	3 ^S (1)	P-mic	68.05				2560
				6 ^S (1)	P-mic ^a		14.81			2561
Acanthomorphs	<i>Megasphaera</i> -like	1	296	4FR19-4 ⁺ (1)	P-mic ^a				12.5	2570
	<i>Tanarium</i> sp.	4	73–90	1 ^S (1)	P-mic ^a	68.27				2557
				2 ^S (1)	P-mic	68.15				2558
				11 ^S (1)	P-nod			10.7		2565
				4FR19-36 ⁺ (1)	P-mic				21	2572
	<i>cf. Eotylotopalla</i>	4	33–113	1 ^S (3)	P-mic ^a	68.27				2557
				FL18-5 ⁺ (1)	P-mic					2574
Pteromorphs	<i>Archaeodiscina umbonulata</i>	3	58–116	17 ^S (3)	P-nod			46.5		2567
Netromorphs	<i>Asseserium fusulentum</i>	5	54–78	3 ^S (1)	P-mic	68.05				2559
				7 ^S (3)	P-nod			10.56		2562; 2563
				12 ^S (1)	P-nod			42.15		2564
Morphotype 1 (unnamed acanthomorph)		2	47–131	3 ^S (1)	P-mic	68.05				2560
				4FR19-17 ⁺ (1)	P-mic				19	2556

N, total number of specimens; n = number of specimens per sample.

^Spalynological slide.

⁺thin section.

^asample collected from an open pit in the same shallow marine facies associations context as observed in trenches TR2 and TR3.

P-nod = phosphate-rich nodule in shale.

P-mic, phosphate-rich microbialite; P-mic^a, reworked clasts of phosphate-rich microbialite; GP5T = catalogue numbers of microfossil-bearing palynological and petrographic slides in collection GP5T, Laboratório de Paleontologia Sistemática, USP.

HF for 1 h on a hot plate, and then repeatedly rinsed with distilled water until neutralized. A portion of the organic slurry was withdrawn with a micropipette under a binocular microscope and preserved as palynological slides.

Also, at CENPES, three-dimensional Confocal Laser Scanning Microscope (CLSM) images were obtained from selected specimens of palynological slides from samples 1, 3 and 5 (Table 1) with lasers of different wavelengths using a ZEISS® Imager.Z1mTM microscope, equipped with a ZEISS® LSM 700TM confocal laser scanning system. ZEISS® Zen® BlackEditionTM software was used to capture images with a ×100 oil immersion lens. The submicron-scale resolution of the fluorescence in the vesicles obtained by CLSM allowed reconstruction of their three-dimensional volume, thereby providing insight into their morphology and fidelity of preservation (Figures 5F,H,S).

Rotatable 3D CLSM images rendered for two specimens are deposited in the public repository Sketchfab profile LMPT (<https://skfb.ly/opV9p>; <https://skfb.ly/opVXX>). Reconstruction by Sketchfab can produce artifacts in these images, such as voids where the surface is deeply shaded. True holes, however, may be seen clearly in the confocal images (Figures 5F,H).

Dark brown to black carbonaceous acritarch vesicles were investigated by Raman spectroscopy at the Brazilian Astrobiology Research Unit (NAP/Astrobio), using a Renishaw inVia micro-Raman, with 532 nm excitation wavelength, diode laser (500 mW) and 2400-groove/mm grating. Spectra were collected with a ×50 objective at 1, 5 or 10% laser power. This technique is broadly used to determine graphitic composition of organic-walled microfossils (Schopf et al., 2005).

The material is identified as “Doushantuo-Pertatataka-Bocaina fossils, Corumbá Group, Brazil,” and deposited in paleontological collection GP5T, Palynology, in the Laboratório de Paleontologia Sistemática, USP, under catalogue numbers GP5T/2556, 2570, 2572 and 2574 (all petrographic thin sections) and GP5T/2557 to 2565, 2567 and 2570 (palynological sections).

RESULTS

Sedimentary Succession

The base of the Bocaina Formation in the study area (Figure 1B) is a sequence boundary truncating siliciclastic-

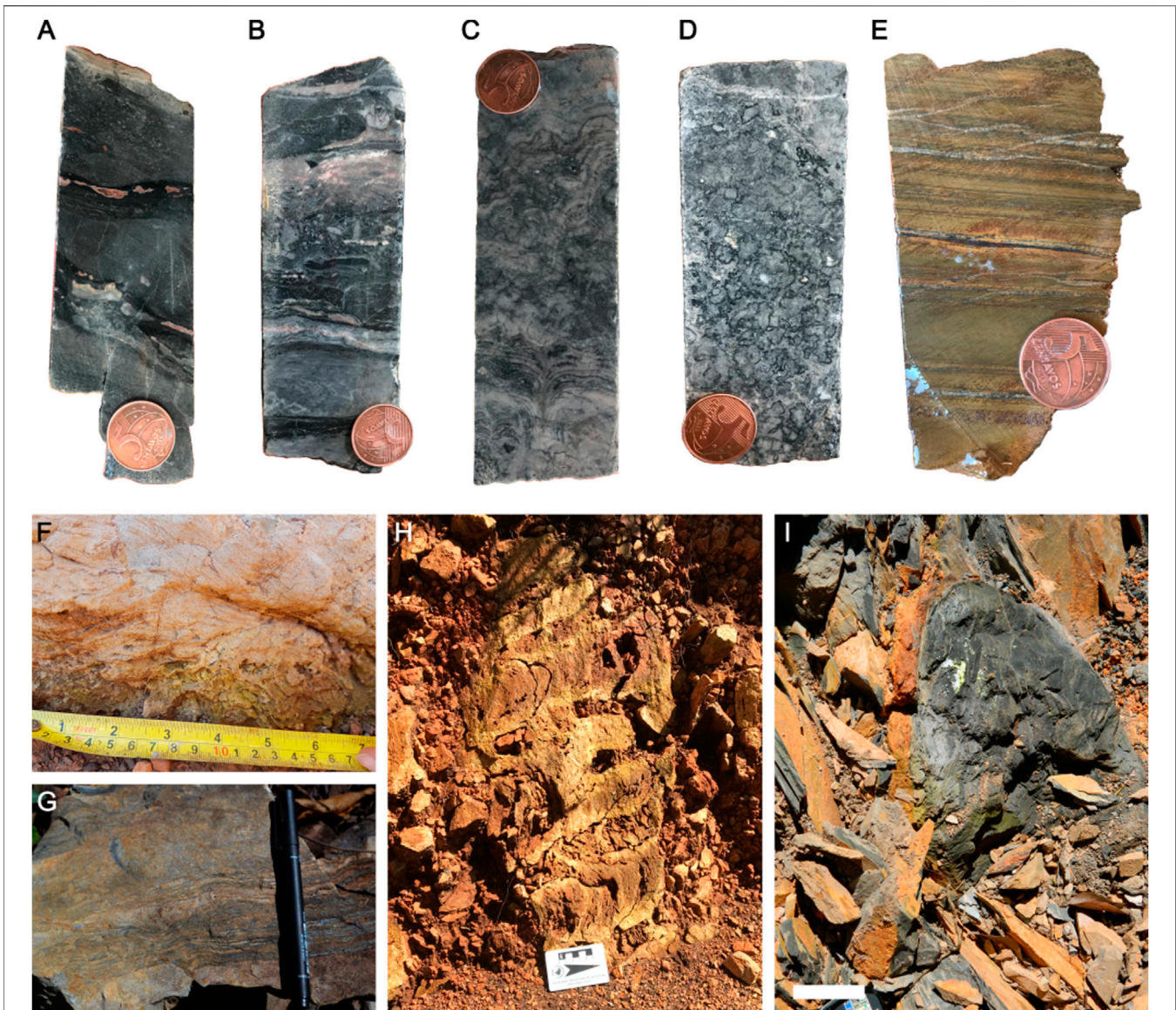


FIGURE 3 | Representative facies examples from the studied successions. **(A)** Dolomitic grainstone and boundstone association, with minor rudstone. Note two P-rich darker beds made up predominantly by irregularly laminated boundstone with dispersed coarse-grained carbonate clasts and irregular vugs. The intermediate grainstone bed appears cross-stratified. **(B)** Fine-grained dolostone, rudstone and grainstone, from base to top, with subordinate boundstone intercalations, locally P-rich (black). **(C)** Columnar to domal stromatolites, from base to top. **(D)** Thrombotic boundstone. **(E)** Incipiently foliated fine-grained siliciclastic facies. **(F)** Cross-section of impure dolomitic grainstone displaying chevron-type upbuilding of bidirectional cross-laminae. **(G)** P-rich stratiform boundstone with subordinate grainstone. **(H)** Cross-section of columnar stromatolites in near vertical altered dolostone bed. **(I)** Cross-section of P-rich nodule in shale. Five-cent piece **(A–E)**: 22 mm; pen **(G)**: 14 cm; White scale bar **(I)**: 10 cm.

dominated deposits of the Cerradinho and Puga Formations, whereas its top is limited by the sequence boundary associated with the basal polymictic breccia of the Tamengo Formation. These units often dip between 20 and 60 degrees to eastern quadrants, comprising the normal flank of asymmetrical folds with westward vergence (Figure 1B). Metamorphism is incipient, and primary sedimentary structures and mineralogy are well preserved. The thickness of the Bocaina Formation in this part of the Serra da Bodoquena (Figure 1B) exceeds 500 m.

More than 70 m of continuous stratigraphic thickness of the upper Bocaina Formation are evident in core DD004, and more than 50 m are exposed in Trench TR6 (Figure 2). Trenches TR2 and TR3 offer sparser, meter-scale exposures scattered over about 80–90 m of stratigraphic thickness of the upper Bocaina Formation (Figure 2). The succession represented by these sections shows an upward transition from dolostone to shale (Figure 2).

The dolostone consists mainly of grainstone (Figures 3A,B,F) and boundstone (Figures 3A–E,G,H) with minor rudstone

(Figures 3A,B,G) and mudstone (Figure 3B). Grainstones are composed of fine to medium ooids and peloids, with symmetrical ripples (Figure 3G), low-angle and trough cross-strata, as well as sparse quartz sand grains and coarse carbonate clasts (Figures 3A,B). This facies is organized in decimeter-thick beds often intercalated with microbial mats associated with centimeter-thick granule to pebble breccia (Figures 3A,B,G). Parts of the succession are dominated by microbialites, including thrombolites (Figure 3D), columnar and domal stromatolites (Figures 3C,H), and breccias. Phosphate-rich horizons are associated with boundstones (Figure 3G) or breccias with phosphate-rich clasts (Figure 3B). Marl and sandstone intercalations also occur along the carbonate-dominated successions, especially near the top of core DD004, below the shales (Figures 2C, 3E,I). The shale-dominated section reaches more than 50 m in thickness and locally displays phosphate-rich nodules (Figure 3I), seams and clasts (Figures 2C,D).

The studied part of the Bocaina Formation presents retrogradational stratigraphic architecture in which shallow-water carbonates are succeeded by offshore shales (Figure 2). Phosphate-rich grainstone deposits predominantly displaying oscillation ripples and rip-up clast concentrations, locally with fibrous cements, comprise peritidal facies associations (Figure 2). Diverse boundstone facies with subordinate breccia are interpreted as stromatolitic reefs, whereas successions dominated by cross-bedded grainstone represent carbonate shoals (Figure 2). Subtidal deposits include fine-grained grainstone intercalated with microbial mats and associated breccia (Figure 2). Intercalated marl and mudstone below the shaly succession mark the offshore transition to thick shale deposits in a deeper offshore setting (Figure 2).

Acritarchs

The Bocaina assemblage consists of moderately to very well-preserved organic-walled microfossils present in 12 of the 30 analyzed samples and represented by acid-released palynomorphs from four samples of shale-hosted phosphatic nodules (samples 7, 11, 12 and 17) and eight samples of phosphatic microbialites (samples 1, 2, 3, 6, 4FR19-4, 4FR19-17, FL18-5, and 4FR19-36) from the upper Bocaina Formation (Figure 1, Table 1).

The Bocaina assemblage is diverse and includes specimens attributed to five known taxa: *Asseserium fusulentum* (Figures 5B,C), *Leiosphaeridia crassa* (Figure 5I), *L. minutissima* (Figure 5J), *Synsphaeridium* sp. (Figure 5L), *Tanarium* sp. (Figures 5M,N), plus three morphotypes comparable to *Archaeodiscina* ? (Figure 5A), *Eotylotopalla* (Figures 5D–H), and *Megasphaera* (Figure 5K). Additionally, one unnamed form described here as Morphotype 1 (unnamed doubled-walled acanthomorphs) is also presented (Figures 5O–Q).

The acritarchs described here vary in diameter from 12 to 296 μm as well as in shape and morphology of processes. They include three species of sphaeromorphs, four taxa of acanthomorphs, including the new morphotype 1 and one each of pteromorphs and netromorphs (Downie et al., 1963). Of the 30 samples examined, 12 were fossiliferous. Of these, six

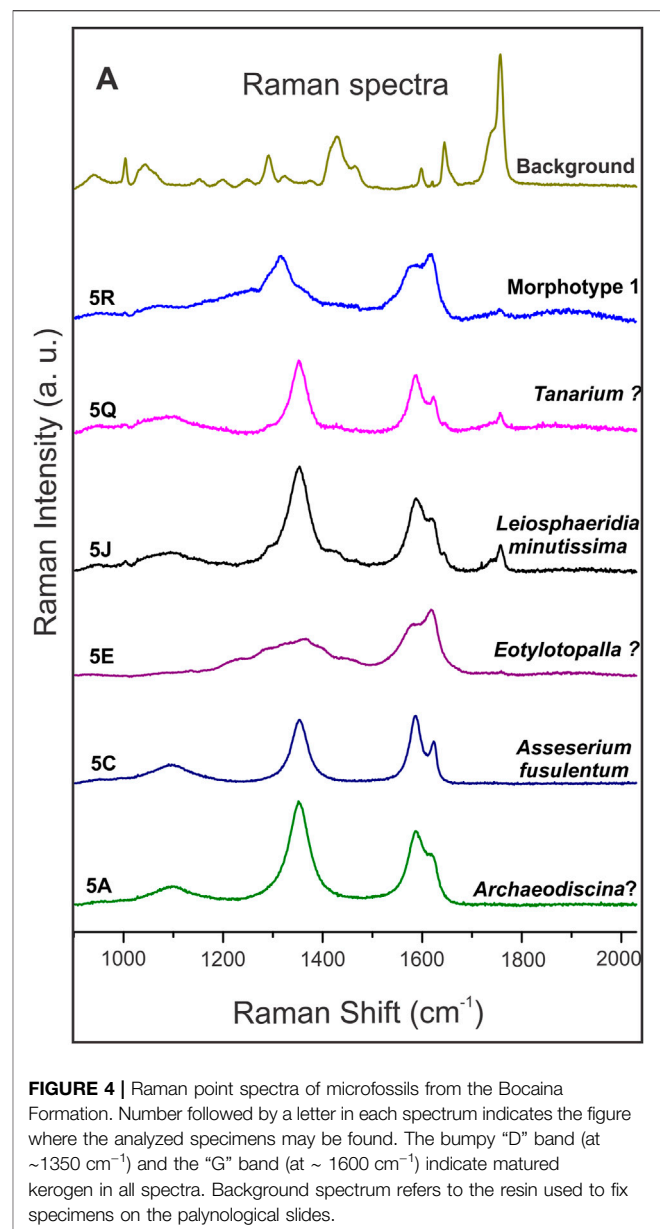


FIGURE 4 | Raman point spectra of microfossils from the Bocaina Formation. Number followed by a letter in each spectrum indicates the figure where the analyzed specimens may be found. The bumpy “D” band (at $\sim 1350\text{ cm}^{-1}$) and the “G” band (at $\sim 1600\text{ cm}^{-1}$) indicate matured kerogen in all spectra. Background spectrum refers to the resin used to fix specimens on the palynological slides.

yielded sphaeromorphs ($n = 13$); eighth, acanthomorphs ($n = 11$); three, netromorphs ($n = 5$) and one, pteromorphs ($n = 3$) (Table 1).

Microfossils vary in color regardless of their facies association. They can be light brown, opaque brown to black or translucent grey. Thick-walled vesicles are usually dark to opaque brown, while thin vesicles are generally translucent grey (Figure 5). Evaluation of the thermal alteration of the organic vesicles by Raman spectroscopy showed D and G bands (at $\sim 1350\text{ cm}^{-1}$ and $\sim 1600\text{ cm}^{-1}$, respectively) indicative of mature kerogen in all microfossils analyzed. The presence of kerogen in all the specimens is consistent with the syngenicity of the microfossils and their host-rocks (Schopf et al., 2005). Raman spectra produced no evidence of co-occurring silica, carbonate, or phosphate in their composition (Figure 4). Detailed

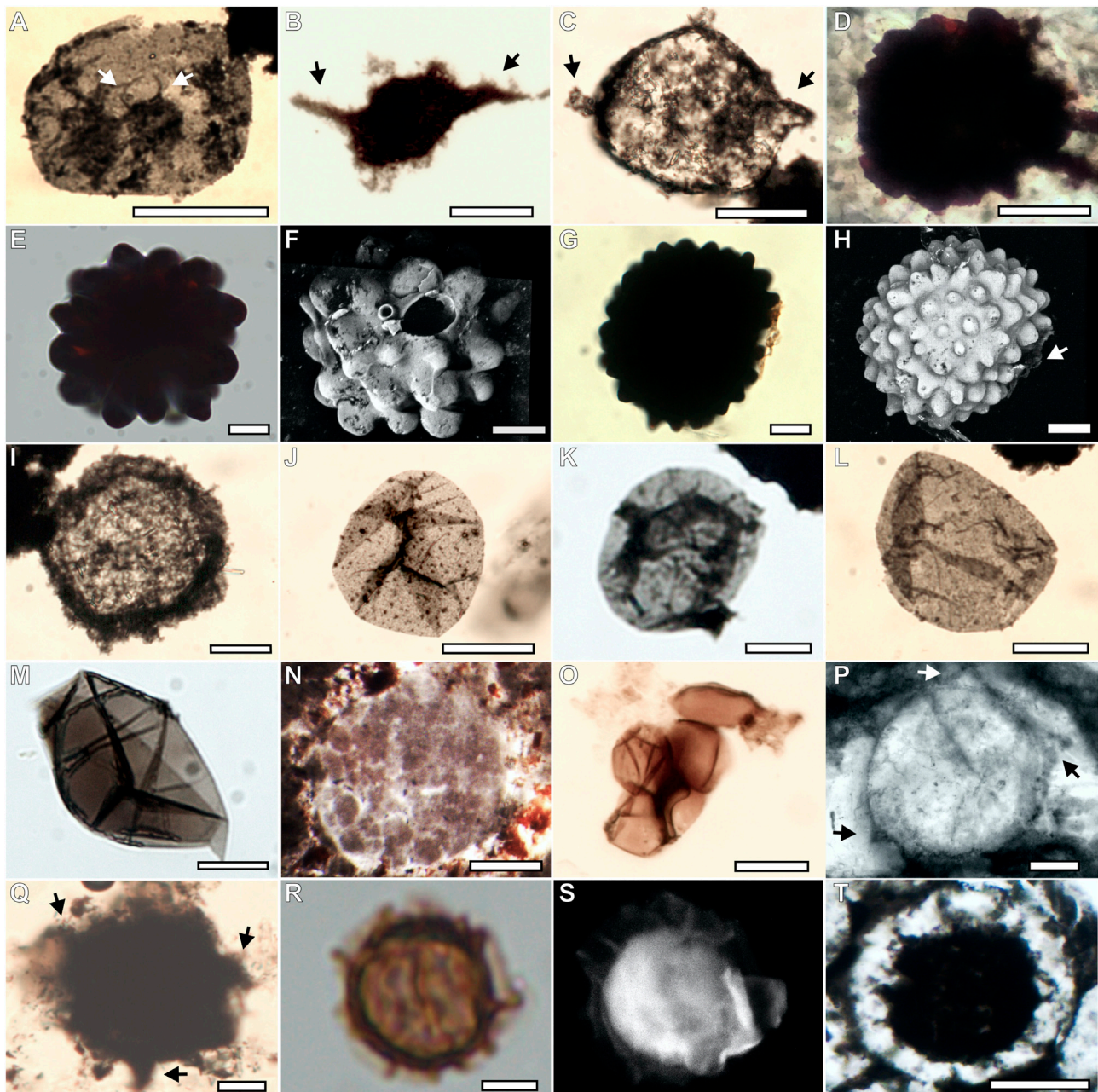


FIGURE 5 | Acritarch assemblage from the Bocaina Formation in palynological slides, confocal 3D reconstructions and thin sections. **(A; GP5T/2567)**

Archaeodiscina ? in a palynological slide, characterized by relatively small central body bearing a few relatively long, very narrow spines (indicated by white arrows) within a thin-walled membrane or vesicle. **(B,C; GP5T/2559, 2562)** Asseserium fusulentum in a palynological slide, showing a roughly fusiform acritarch with irregular opposite spines indicated by black arrows. **(D; GP5T/2574)** cf. Eotylotopalla in thin section, showing a spheroidal acanthomorph vesicle, ornamented with generally broader than high, rounded to conical processes or verrucae. **(E–H; GP5T/2557)** **(E,G)** Cf. Eotylotopalla in palynological slide, showing a spheroidal acanthomorph vesicle, ornamented with generally broader than high, rounded to conical processes or verrucae. **(F)** Confocal image of specimen shown in **(E)**, with large and small elliptical openings. **(H)** Confocal image of specimen shown in **(G)** with white arrow highlighting opening. **(I; GP5T/2564)** Thick walled Leiosphaeridia crassa in palynological slide. **(J–M; GP5T/2561; 2567, 2558, 2570, respectively)** Thin walled Leiosphaeridia minutissima in palynological slide. **(N; GP5T/2570)** Cross-section through a Megasphaera-like acritarch in a thin section. **(O; GP5T/2560)** Thick-walled aggregate of Synsphaeridium sp in palynological slide. **(P; GP5T/2572)** Tanarium sp., spheroidal acanthomorph acritarch ornamented with sparse obtusely conical processes indicated by arrows in thin section. **(Q; GP5T/2565)** Tanarium ? spheroidal acanthomorph acritarch ornamented with sparse conical processes indicated by arrows in palynological slides. **(R; GP5T/2560)** morphotype 1 consisting of a double-walled spheroidal vesicle with processes in the inner wall. Clear area defines original limits of outer membrane. **(S)** Confocal image of specimen shown in **(R)**. **(T; GP5T/2556)** Morphotype 1 consisting of a double-walled spheroidal vesicle with processes in the inner wall in thin section. Scale bars: 5 μm = **R, S**; 20 μm = **A, C–M**; 25 μm = **B**; 100 μm = **N, T**.

descriptions of the microfossils are provided in the Systematic Paleontology section below.

DISCUSSION

The Bocaina Formation has already been tentatively correlated to other Neoproterozoic units by means of litho-, bio- and chemostratigraphy (Gaucher et al., 2003). However, until now, no biozones have been recognized. Here, we present a new diversified acritarch assemblage, including representatives from the Doushantuo-Pertatataka assemblage, as *Asseserium fusulentum*, cf. *Eotylotopalla*, *Tanarium* sp, a *Megasphaera*-like vesicle, *Leiosphaeridia crassa*, *L. minutissima* and *Synsphaeridium* sp, plus the Cambrian representative *Archaeodiscina* ? and one morphotype unknown in the literature (Figure 5).

The microfossils described here present Raman spectra typical of amorphous carbon, consistent with the degradation of organic matter to kerogen. Contemporary organic matter bands (e.g., C–N, N–H, C=O) were not observed (Figure 4). Spectra indicative of carbonate, silica and phosphate were not present at the surface of these specimens (Figure 4).

Of the 12 fossiliferous samples studied from the Bocaina Formation, six were obtained from the shale-dominated succession here interpreted as offshore deposits near the top of the studied interval. Of these six samples, four come from phosphate-rich nodules within the shale succession and one is from reworked phosphatic microbialite clasts within shale (Figure 2; Table 1). Six other fossiliferous samples were collected within the carbonate-dominated succession. Four correspond to *in situ* phosphate-rich microbialites and two to reworked clasts of phosphate rich microbialites within shallow marine facies associations (Figure 2, Table 1). Hence, we interpret that most of the Ediacaran complex acritarchs (ECAP, sensu Zhang et al., 1998; Moczyłowska and Nagovitsin, 2012; Xiao et al., 2014; Moczyłowska, 2016) recognized here were entombed in both shallow proximal ($n = 17$) as well as relatively deeper distal settings ($n = 17$) (Figure 2; Table 1).

Facies interpreted as deposited in shallow water settings host *Synsphaeridium* sp, cf. *Eotylotopalla*, *Megasphaera*-like structures, *Tanarium* sp. and *Asseserium fusulentum*. Distal deposits present *Leiosphaeridia crassa* and *Archaeodiscina* ? as well as rare specimens of *Tanarium* sp. and *Asseserium fusulentum*. *L. minutissima* is the only species common in both settings. Morphotype 1 was found in shallow water settings.

Two unusual new acritarch forms resembling *Eotylotopalla* (Yin, 1987), are designated here as cf. *Eotylotopalla* (Yin, 1987) (Figures 5D–H). Unlike previously described specimens of this species, they possess large openings (more obvious in Figure 5F and less visible in Figure 5H) and just beside them much smaller openings at the top of an unusually small process (only visible in Figure 5F). Either or both may be artifacts of preservation or sample preparation. But we interpret the larger opening as an original feature of the acritarch, because the border of the opening is evenly elevated above the surrounding surface and very even,

neither torn nor irregular. Moreover, no other processes of similar size show signs of breakage.

Accepting that the hole is a biogenic structure, two possible interpretations suggest themselves. The verrucate, aperturate raspberry-like resistant organic vesicle is comparable to tests of the extant testate amoebae *Netzelia muriformis* and *N. tuberculata* (Gauthier-Lièvre and Thomas, 1960; Owen and Jones, 1976). Testate amoebae were already described in Neoproterozoic rocks from Brazil (Morais et al., 2017), however, no similar specimen was described until now. Additionally, tests in *Netzelia muriformis* and *N. tuberculata* are constructed of autogenous siliceous elements and possess a lobate opening with 3–8 indentations (Gomaa et al., 2017). Despite these discrepancies, phylogenomic reconstructions suggest that major lineages of testate amoebae were already diversified during the Neoproterozoic, which may suggest that the specimens reported here could be related to hypothetical ancestors for *Netzelia* (Lahr et al., 2019).

The new acritarch also resembles sexually produced zygospores in fungi of the Zygomycota (Hermann and Podkovyrov, 2006), that is, it could represent a stage in the life cycle of an early multicellular organism. More specifically, the opening may have been the point of insertion of the peduncular hyphae or served as the exit for the germinating fungus. However, structures resembling fungi structures (e.g., peduncular hyphae) were not found until now, which prevented the establishment of this biological affinity. New aperturate raspberry-like resistant organic vesicles can help to answer questions about the biological affinity for cf. *Eotylotopalla*.

Two double-walled acanthomorphic acritarchs described here share similarities with *Distosphaera speciosa* (Zhang et al., 1998), as a spheroidal vesicle characterized by two wall layers (Figures 5O–Q). However, *D. speciosa* hosts processes in both vesicles, while the specimens described here have processes only in the inner vesicle. Due to this fact, they were interpreted in open nomenclature as morphotype 1.

The quality of preservation of the acritarchs described here is due to their preservation in phosphatized microbialites and phosphatic nodules in shales in the study area within the so-called phosphatization taphonomic window (Porter, 2004), best epitomized by the exceptional preservation of Doushantuo microfossil assemblage in phosphate (Xiao et al., 2014). The reduced diversity and size of acritarchs in the overlying Tamengo Formation reflects the general trend for acritarchs worldwide at the end of the Ediacaran (Gaucher et al., 2003), while the closure of the phosphatization window accounts in part for their paucity.

CONCLUSION

Microfossils in the latest Ediacaran Bocaina Formation are diverse, contrasting sharply with the simple, leiosphaerid-dominated assemblage of the overlying *Cloudina*- and *Corumbella*-bearing Tamengo Formation. The Bocaina assemblage hosts acritarch taxa typical of the supposedly older Doushantuo-Pertatataka assemblage, specifically, *Asseserium*,

Leiosphaeridia, *Tanarium*, the acanthomorphic vesicle described here as morphotype 1 and a vesicle resembling *Megasphaera*, yet it also includes forms comparable to younger acritarch genera of Cambrian age *Archaeodiscina*. Moreover, two unusual and important new acritarch taxa are also present. The first, cf. *Eotylotopalla*, possesses a raspberry-like form and distinct opening that permit comparison with some modern testate amoebae *Netzelia* and less with fungal zygospores. The second, Morphotype 1 resembles *Distosphaera speciosa* Zhang et al., 1988. However, the absence of diagnostic features prevents this interpretation, leading us to interpretate these specimens in open nomenclature.

The diversity of the Bocaina acritarch assemblage, with its supposedly “older” Doushantuo-Pertatataka elements, complex new forms, and Cambrian look-alikes, suggests that, at c. 555 Ma, the plankton in the Ediacaran ecosystem, at least in the Bocaina Formation, was stable and thriving. Initiation of the end-Ediacaran plankton crisis responsible for the depauperate acritarch assemblages of the latest Ediacaran may well be lost in the hiatus represented by the erosional unconformity between the Bocaina and Tamengo formations.

The acritarchs reported here bode well for the potential of the c. 555-Ma-old Bocaina phosphorites and phosphate-rich dolostones to provide further important data on paleobiology and biostratigraphy of the latest Ediacaran as the Neoproterozoic biosphere gave way to that of the Phanerozoic.

SYSTEMATIC PALEONTOLOGY

Group Acritarcha Evitt, 1963.

Genus *Archaeodiscina* Naumova, 1960 emend. Volkova, 1968.

Type species.--*Archaeodiscina granulate* Naumova.

Archaeodiscina ? Volkova, 1968 (**Figure 5A**).

Holotype.--*Archaeodiscina umbonulata* Volkova, Volkova, p. 27, pl. 5, **Figures 1–8**; pl. 11, Figure 8 (holotype pl. 5, **Figure 1**).

Material.--Three compressed specimens recovered in the palynological residue of a phosphatic nodule within shale (GP5T/2567).

Description.--Outer membrane irregularly circular to elliptical (compressed), translucent, 58–116 μm in diameter, with few folds; inner body circular to elliptical, 16–36 μm in greatest dimension with a few very narrow ray-like processes or folds 4–14 μm length that give it a “star-like” character.

Occurrence.-- All specimens came from a single phosphatic nodule in shale in TR6 (46.5 m) in the Bocaina Formation (**Table 1**).

Remarks.--*Archaeodiscina* has double membranes. The outer membrane diameter usually ranges from 25 to 50 μm and the inner range from 22 to 42 μm . The inner star-like spheroidal body range from 2 to 7 μm and radial folds length 4–10 μm (Downie, 1982; Moczydlowska, 2011). Specimens from the Bocaina Formation are larger (>50 μm in diameter) than specimens belonging to this genus. As *Archaeodiscina*, they are distinguished from other pteromorphs by the presence of a morphologically regular surficial organic body consisting of a

spheroidal center hosting processes. The illustrated specimen presents a central vesicle with a few very fine processes and also presents opaque organic grains adhered to their surfaces. Other dark features may be interpreted to be linear folds of the outer vesicle. The specimen shown in **Figure 5A** is the most similar to *Archaeodiscina umbonulata* (see Moczydlowska 2011, Plate 1), showing clearly, at least, two processes (indicated by white arrow in **Figure 5A**). However, the other two specimens have organic material adhered to the surface that prevents a clear view of the central body and processes. Due to this fact, specimens described here were interpreted with reservations.

Genus *Asseserium* Moczydlowska and Nagovitsin, 2012.

Type species.--*Asseserium diversum* Moczydlowska and Nagovitsin, 2012.

Asseserium fusulentum Moczydlowska and Nagovitsin, 2012 (**Figures 5B,C**).

Holotype.--PN8/16-3, Moczydlowska and Nagovitsin, 2012, **Figure 5F**, p. 13.

Material.--Five specimens recovered, one recovered in palynological residues from one level of phosphatic microbialites from TR2 (GP5T/2559) and four recovered in two levels of phosphatic nodules within shale (GP5T/2562; 2563; 2564).

Description.--Oval to elongate bipolar vesicles ranging from 54 to 78 μm length and 25–37 μm width. Processes located at opposite sites, conical of varied length (6–27 μm) and basal width or bulbous (**Figures 5B,C**), and may differ in shape at opposite poles.

Occurrence.--In the Bocaina Formation, one specimen occurs in one level of phosphatic microbialites from TR2 (68.05 m) and four occur in two levels of phosphatic nodules from TR6 (10.56 and 42.15 m; **Table 1**). *A. fusulentum* is common in the Ediacaran Vychegda and Doushantuo formations of Russia and China, respectively (Vorob'eva et al., 2007; Liu and Moczydlowska, 2019); early Ediacaran Ura Formation and East Siberia (Moczydlowska and Nagovitsin, 2012).

Remarks.--*A. fusulentum* is characterized by a medium-sized, bipolar in symmetry vesicle and spindle-shaped in outline (originally three-dimensional spindle) with smooth surface and bearing two processes gradually extending from the central portion of the vesicle. The wall of the vesicle and processes is uniform. Processes are conical in shape and taper towards slightly rounded tips, being hollow inside and communicate with the vesicle cavity. Specimens described here fit the original description of *Asseserium fusulentum* described by Moczydlowska and Nagovitsin (2012), which ranges from 60 to 124 μm in length and 24–67 μm in width with processes up to 20 μm long. Organic-walled acritarch with two processes that arise from opposite poles similar to *A. fusulentum* was described in early to middle Ediacaran siliciclastic deposits in northern Russia, in the Vychegda Formation (their **Figure 4I**), and were not attributed to any recognized species (Vorob'eva et al., 2009).

Genus *Eotylotopalla* Yin, 1987.

Type species.--*Eotylotopalla delicata* Yin, 1987, p. 442, pl. 23, Figure 15; pl. 24, Figures 8, 9.
cf. *Eotylotopalla* Yin, 1987 (**Figures 5D–H**).

Material.--Four specimens, one observed in a thin section of a phosphatic microbialite and three recovered in palynological residues from a similar interval (GP5T/2574; 2557).

Description.--Opaque spheroidal vesicles, 33–113 μm in diameter, densely and evenly covered by rounded to bluntly conical processes and verrucae 5–16 μm in diameter and 8–10 μm high. Openings evident in two larger specimens, measurable in one (26 \times 16 μm , **Figures 5E,F**), but unknown in two smaller specimens because of their opacity. A second smaller opening (7 \times 6 μm) of unknown origin (taphonomic?) appears just below the larger one in **Figure 5F**. The larger opening exhibits a uniform, slightly raised border.

Occurrence.--One specimen observed in a thin section of a phosphatic microbialite horizon without stratigraphic control, collected in a pit opened in the area of trenches TR2 and TR3 (**Figure 5D**). Two additional specimens (**Figures 5F–H**) in palynological slides from phosphatic microbialites in TR2 (68.27 m, **Table 1**). This taxon was first described in the upper Doushantuo Formation, China (Yin, 1987; Zhang et al., 1998), and later found in the early Neoproterozoic Wynnian Formation, Canada (Butterfield, 2015, p. 9, **Figure 3E**) and the late Ediacaran Kessyusa Group, Arctic Siberia (Grazhdankin et al., 2020, p. 711, **Figure 4D**).

Remarks.--Specimens from the Bocaina Formation are slightly larger than the type material, which ranges from 35 to 45 μm in diameter (Zhang et al., 1998), and the vesicle described by Grazhdankin et al. (2020), which reaches 83 μm , but are smaller than the vesicles described by Xiao et al. (2014), which reach 200 μm in diameter. Specimens shown in **Figures 5D–F**, resembles *Eotylotopalla dactylos* Zhang et al., 1998, mainly by the regularly spaced cylindrical processes, openly communicating with the interior vesicle. Specimen shown in **Figures 5G,H** is more similar to *E. strobilata* (Faizullin, 1998) Sergeev, Knoll and Vorob'eva, 2011, hosting small, hemispherical, nearly equidimensional processes, densely and evenly distributed over vesicle wall.

Openings differentiate at least two of the Bocaina specimens from previously described material and justify their identification as cf. *Eotylotopalla*, pending further research. The elliptical shape of the openings in the only specimen in which they are clearly visible is likely due to distortion of originally circular structures during compaction.

The two larger specimens are reminiscent of the small hollow aperturate spherical tests of the extant species of testate amoebae *Netzelia muriformis* and *N. tuberculata* (Gauthier-Lièvre and Thomas, 1960; Owen and Jones, 1976), which have small regular rounded protuberances giving them a raspberry-like outline. The extant organisms differ, however, in being composed of endogenous siliceous elements (Gomaa et al., 2017) and having lobate openings with three to eight indentations (Gauthier-Lièvre and Thomas, 1960).

Cf. *Eotylotopalla* is also similar to fungal zygosporangia of multicellular fungi of the Zygomycota (Hermann and

Podkovyrov, 2006), in which case the openings might represent the exit point upon germination or the area of insertion of a peduncular hypha.

Genus *Leiosphaeridia* Eisenack, 1958, emend. Downie and Sarjeant, 1963, emend. Turner, 1984.

Type species.--*Leiosphaeridia baltica* Eisenack, 1958.

Leiosphaeridia crassa (Naumova, 1949); Javaux and Knoll: **Figure 4(4–6)**, 2017 (**Figure 5I**).

Holotype.--No holotype was designated by Naumova (1949). A specimen of *Leiotriletes minutissimus* from Naumova (1949, pl. 1, **Figure 1**) was designated as lectotype by Jankauskas et al. (1989, p. 75), but this was later synonymized with *L. minutissima* (Porter and Riedman, 2016).

Material.--Three specimens found in palynological residues of phosphatic nodules in shale from a single level in TR6 (GP5T/2564).

Description.--*Leiosphaeridia* with thick-walled, relatively dark walls, ranging from 59 to 65 μm in diameter.

Occurrence.--In the Bocaina Formation, *L. crassa* occurs in a single level of phosphatic nodules in shale in TR6 (42.15 m; **Table 1**). *L. crassa* is very widespread in Proterozoic and lower Paleozoic rocks (Knoll et al., 2020).

Remarks.--Jankauskas et al. (1989) proposed species identification within this polyphyletic genus based on size, wall color and texture, which we have adopted here. *Leiosphaeridia crassa* is recognized by the smooth, pliant walls with lanceolate folds and a modal diameter of less than 70 μm .

Leiosphaeridia minutissima (Naumova, 1949), emend. Jankauskas et al., 1989, emend. Javaux and Knoll, 2017 (**Figures 5J–M**).

Lectotype.--No holotype was designated by Naumova (1949). A specimen of *Leiotriletes minutissimus* from Naumova (1949, pl. 1, **Figure 1**) was designated as lectotype by Jankauskas et al. (1989, p. 75).

Emended diagnosis.--Species of *Leiosphaeridia* characterized by thin, smooth walls, with sinuous folds and a modal diameter less than 70 μm .

Material.--Eight specimens, four found in palynological residues of phosphatic microbialites in two levels from TR2 (GP5T/2558; 2570), one found in one level of phosphatic microbialites in TR3 (GP5T/2561) and three from a single level of phosphatic nodules in shale from TR6 (GP5T/2567).

Description.--As for diagnosis. Specimens range from 23 to 68 μm in diameter.

Occurrence.--In the Bocaina Formation, *L. minutissima* occurs in phosphatic microbialites in two levels of TR2 (68.27 and 68.15 m, **Table 1**), one level of phosphatic microbialites in TR3 (14.81 m, **Table 1**) and in one level of phosphatic nodules in shale from TR6 (46.5 m; **Table 1**). *L. minutissima* generally dominates Upper Ediacaran deposits (575–542 Ma) (Grey et al., 2003; Huntley et al., 2006; Gaucher and Sprechmann, 2009). It is also abundant in the overlying Tamengo Formation (Gaucher et al., 2003) and widespread in the Nama

Group (Germs et al., 1986) and Arroyo del Soldado Group (Uruguay) in Western Gondwana.

Remarks.--Species of *Leiosphaeridia minutissima* are characterized by thin, smooth walls, with sinuous folds and a modal diameter less than 70 μm . *L. minutissima* from the Bocaina Formation is more common in phosphatic microbialites in TR2 and TR3 and less common in phosphatic nodules in shale from TR6 (**Table 1**). Specimens from phosphatic nodules in shale have a translucent wall, but dark spots randomly dispersed over the surface that appears to be adherent granular amorphous organic matter (**Figure 5J**).

Genus *Megasphaera* Chen and Liu, 1986, emend. Xiao et al., 2014.

Type species.--*Megasphaera inornata* Chen and Liu, 1986, emend. Xiao et al., 2014.

Megasphaera-like (**Figure 5N**).

Material.--One vesicle classified as aff. *Megasphaera* in a petrographic thin-section of phosphatic microbialite (GP5T/2570).

Description.--A single specimen consisting of a large spheroidal vesicle, 296 μm in diameter, without processes, enclosing well-defined to diffuse spheroidal structures from 35 to 41 μm in diameter interpreted as internal cells.

Occurrence.--In the Bocaina Formation, the specimen occurs only in a phosphatic microbialite in drill-core DD004 (12.5 m, **Table 1**). *Megasphaera inornata* was recognized first in the mid-to late Ediacaran Doushantuo Formation, China (Chen and Liu, 1986; Xiao et al., 2014), and more recently in younger deposits immediately preceding the transition to the Cambrian, in the Khensu Formation, Mongolia (Anderson et al., 2019) and Kessyusa Group, central Arctic Siberia (Grazhdankin et al., 2020).

Remarks.--*Megasphaera* is recognized by the large spherical vesicles, smooth or sculptured, but without long processes. One or more cells may be enclosed within the vesicle. The only specimen in the Bocaina Formation is degraded and found in a thin section of phosphatic microbialite. It would not have survived, had the rock been subjected to acid maceration. While the vesicle margin and several internal cells are well defined at its lower border (**Figure 5K**), the other cells are more diffuse with less clearly defined borders. The poor preservation of the specimen does not permit speculation about its biological affinities.

Genus *Synsphaeridium* Eisenack, 1965.

Synsphaeridium sp. (**Figure 5O**).

Material.--Two well-preserved clusters of five and six specimens each in palynological residues of phosphatic microbialites, one in TR2 and other in TR3 (GP5T/2560; 2561).

Description.--Two small compact clusters of five contiguous psilate cells that range from 12 to 20 μm in diameter. Clusters are 29.6 and 51.8 μm in greatest dimension.

Occurrence.--*Synsphaeridium* is rare in the Bocaina Formation, occurring only in one level of phosphatic

microbialites in TR2 and TR3 (68.05 and 14.1 m, respectively; **Table 1**). They are widespread in Proterozoic deposits from the mid-Neoproterozoic (Knoll et al., 2020) and early to late Cambrian (Prasad et al., 2010; Slater and Willman, 2019).

Remarks.--Individual cells in the cluster are like small *Leiosphaeridia* (18–30 μm), but are smaller than specimens of *L. crassa* and *L. minutissima* described here. The cells are clearly tightly packed, suggesting that they were held tightly together in life.

Genus *Tanarium* Kolosova, 1991, emend. Moczyłowska et al., 1993, emend. Grey, 2005.

Type species.--*Tanarium conoideum* Kolosova, 1991.

Holotype.--PMU-Sib.4-J/30/3, Moczyłowska et al., 1993, Figure 10C–D, p. 514.

Tanarium sp. (**Figures 5P–Q**).

Material.--Four specimens, one in a thin section (GP5T/2572) of phosphatic microbialite from drill-core DD004 (21 m), two from the palynological residues of two levels of phosphatic microbialites in TR2 (GP5T/2557; 2558) and one in a single level of phosphatic nodule in shale from TR6 (GP5T/2565).

Description.--Spheroidal vesicles 73–90 μm in diameter, bearing sparse (3–7 along perimeter) prominent simple processes with hook-like terminations, ranging from 5 to 14 μm long and 11–20 μm wide at base, which may be hidden within degraded granular to amorphous and dark marginal organic matter.

Occurrence.--In the Bocaina Formation, one specimen occurs in a phosphatic microbialite in drill-core DD004 (21 m), two occur in two levels of phosphatic microbialites from TR2 (68.27 and 68.15 m) and one in phosphatic nodules in shale from TR6 (10.07 m). *Tanarium* is widely distributed in the Ediacaran Khamaka Formation, Siberian Platform (Moczyłowska, 2016), lower Ediacaran Ura Formation, East Siberia (Moczyłowska and Nagovitsin, 2012), middle Ediacaran Vychegda Formation, East European Platform, Russia, Ediacaran Ungoolya Group, Australia (Willman et al., 2006), Ediacaran Dey Dey Mudstone and Tanana Formation (Willman and Moczyłowska, 2008), and Ediacaran Doushantuo Formation (Xiao et al., 2014).

Remarks.--The genus *Tanarium* hosts acanthomorphs characterized by generally long (process length 12–50% and typically >20% of vesicle diameter) and more variable or somewhat heteromorphic processes (Moczyłowska et al., 1993; Grey, 2005; Moczyłowska, 2005). Specimens described here are usually dark (**Figure 5Q**), with the exception of the specimen shown in the petrographic thin section (**Figure 5P**). The poor preservation observed in some recovered specimens led us to identify them as *Tanarium* only at the level of the genus. Degraded specimens from the Bocaina Formation are similar to the published figures in Moczyłowska 2016 (Plate 3.1–2). However, the ornamentation of the specimen shown in our **Figure 5N**, preserved in 3 dimensions, clearly resembles specimens of *T. tuberosum* shown in Moczyłowska 2016 (Plate

3.3-6). For these reasons, the specimens described here are identified as *Tanarium* sp. All the specimens recovered *via* palynological maceration are mostly opaque with degraded granular to amorphous, translucent organic matter around the vesicles.

Incertae Sedis

Morphotype 1 (Figures 5R–T).

Material.--Two specimens, one in a thin-section of phosphatic microbialite (GP5T/2556) and the other from a palynological residue of a phosphatic microbialite (GP5T/2560).

Description.--Double-walled spheroidal vesicle. Outer walls are 231 and 16 μm in diameter and the inner walls are 140 and 12.5 μm , respectively. Scattered cylindrical processes from 3 to 22 μm long on the inner wall are recognizable in both palynological slide and petrographic thin section.

Occurrence.--In the Bocaina Formation, one specimen was recovered from a phosphatic microbialite from drill core DD004 (19 m) and the other from a phosphatic microbialite in TR2 (68.05 m) (Table 1).

Remarks.--*Distosphaera speciosa* Zhang et al., 1998 are recognized by the spheroidal vesicles characterized by two wall layers, both of which bear processes. The outer wall has sparsely but evenly distributed conical processes, which are sharply pointed at the apex, hollow and open at the base. The inner wall bears long, slender, solid processes, which connect to and support the outer wall. Specimens from the Bocaina Formation vary in size, but still closely comparable to *D. speciosa* from the Doushantuo Formation (Zhang et al., 1998) having an outer wall, easily visible in a confocal image in Figure 5P. However, scattered sharply conical processes in the outer vesicles in specimens from the Bocaina Formation are not recognizable, preventing this identification. More specimens may help to interpret these specimens within a new genus.

REFERENCES

- Adorno, R. R., do Carmo, D. A., Germs, G., Walde, D. H. G., Denezine, M., Boggiani, P. C., et al. (2017). Cloudina Lucianoi (Beurlen & Sommer, 1957), Tamengo Formation, Ediacaran, Brazil: Taxonomy, Analysis of Stratigraphic Distribution and Biostratigraphy. *Precambrian Res.* 301, 19–35. doi:10.1016/j.precamres.2017.08.023
- Almeida, F. F. M. (1965). Geologia da Serra da Bodoquena (Mato Grosso), Brasil. *Boletim da Divisão de Geologia e Mineralogia, Departamento Nacional de Produção Mineral. DNPM* 219, 1–96.
- Almeida, F. F. M. (1945). Geologia Do sudoeste mato-grossense: Boletim da Divisão de Geologia e Mineralogia, Departamento Nacional de Produção Mineral. *DNPM* 116, 1–118.
- Almeida, F. F. M. (1946). Origem dos minérios de ferro e manganês de Urucum: Boletim da Divisão de Geologia e Mineralogia. *DNPM* 119, 1–58. Departamento Nacional de Produção Mineral.
- Amorim, K. B., Afonso, J. W. L., Leme, J. d. M., Diniz, C. Q. C., Rivera, L. C. M., Gómez-Gutiérrez, J. C., et al. (2020). Sedimentary Facies, Fossil Distribution and Depositional Setting of the Late Ediacaran Tamengo Formation (Brazil). *Sedimentology* 67 (7), 3422–3450. doi:10.1111/sed.12749

DATA AVAILABILITY STATEMENT

The original contributions presented in the study are included in the article/supplementary material, further inquiries can be directed to the corresponding author.

AUTHOR CONTRIBUTIONS

LM: Conceptualization; LM, BF, IR, ES, AM, and EA: Data collection; LM, TF, BF, DL, and JL Data analysis and interpretation; JL and RT: Supervision Funding acquisition and Project administration. All authors discussed the results and contributed to the final manuscript.

FUNDING

The study was funded by the São Paulo Research Foundation (FAPESP) (grants #2015/16235-2; #2016/05937-9; #2016/06114-6; #2017/22099-0) and financed in part by the Coordenação de Aperfeiçoamento de Pessoal de Nível Superior—Brasil (CAPES—Finance Code 001).

ACKNOWLEDGMENTS

The authors thank the EDEM mining company (Empresa de Desenvolvimento em Mineração e Participações Ltda.) for access to the drill-cores and trenches, specially L. Nery, the Research Unit in Astrobiology (NAP/Astrobio-PRP/USP), the Centro de Pesquisas, Desenvolvimento e Inovação Leopoldo Américo Miguez de Mello (CENPES/PETROBRÁS) for support with the Confocal images acquisitions, and the Institute of Geoscience (University of São Paulo) for institutional support. We also thanks the insightful discussion with S. Xiao (Virgínia-Tech University) and the reviewers Q. Ouyang and S. Willman.

- Anderson, R. P., Macdonald, F. A., Jones, D. S., McMahon, S., and Briggs, D. E. G. (2017). Doushantuo-type Microfossils from Latest Ediacaran Phosphorites of Northern Mongolia. *Geology* 45 (12), 1079–1082. doi:10.1130/G39576.1
- Anderson, R. P., McMahon, S., Macdonald, F. A., Jones, D. S., and Briggs, D. E. G. (2019). Palaeobiology of Latest Ediacaran Phosphorites from the Upper Khesen Formation, Khuvsgul Group, Northern Mongolia. *J. Syst. Palaeontology* 17 (6), 501–532. doi:10.1080/14772019.2018.1443977
- Boggiani, P. C., Alvarenga, C. D., and Mantesso-Neto, V. (2004). “Faixa Paraguai. Geologia Do Continente Sul-Americano,” in *Evolução da Obra de Fernando Flávio Marques de Almeida: São Paulo* (São Paulo: Beca), 113–120.
- Boggiani, P. C., Gaucher, C., Sial, A. N., Babinski, M., Simon, C. M., Riccomini, C., et al. (2010). Chemostratigraphy of the Tamengo Formation (Corumbá Group, Brazil): A Contribution to the Calibration of the Ediacaran Carbon-Isotope Curve. *Precambrian Res.* 182 (4), 382–401. doi:10.1016/j.precamres.2010.06.003
- Butterfield, N. J. (2015). Early Evolution of the Eukaryota. *Palaeontology* 58 (1), 5–17. doi:10.1111/pala.12139
- Campanha, G. A. d. C., Boggiani, P. C., Sallun Filho, W., Sá, F. R. d., Zuquim, M. d. P. S., and Piacentini, T. (2011). A faixa de dobramento Paraguai na Serra da Bodoquena e depressão Do Rio Miranda, Mato Grosso Do Sul. *Geol. Usp. Sér. Cient.* 11 (3), 79–96. doi:10.5327/Z1519-874X2011000300005

- Chen, M., and Liu, K. (1986). The Geological Significance of Newly Discovered Microfossils from the Upper Sinian (Doushantuo Age) Phosphorites. *Chin. J. Geology*. 21 (1), 46–53.
- Condon, D., Zhu, M., Bowring, S., Wang, W., Yang, A., and Jin, Y. (2005). U–pb Ages from the Neoproterozoic Doushantuo Formation, China. *Science* 308 (5718), 95–98. doi:10.1126/science.1107765
- Dorr, J. V. N., II (1945). Manganese and Iron Deposits of Morro Do Urucum, Mato Grosso, Brazil. *Bull. United States Geol. Surv.* 946A, 1–47.
- Downie, C., Evitt, R., and Sarjeant, W. A. S. (1963). Dinoflagellates, Hystrichospheres and the Classification of Acritarchs. *Stanford Univ. Publications Geol. Sci.* 7 (3), 1–16.
- Downie, C. (1982). Lower Cambrian Acritarchs from Scotland, Norway, Greenland and Canada. *Trans. R. Soc. Edinb. Earth Sci.* 72 (4), 257–285. doi:10.1017/S0263593300010051
- Downie, C., and Sarjeant, W. A. S. (1963). On the Interpretation and Status of Some Hystrichosphere Genera. *Palaentology* 6 (1), 83–96.
- Eisenack, A. (1965). Mikrofossilien aus dem Silur Gotlands. Hystrichosphären Problematika. *Neues Jahrb. Geol. Paläontol. Abh.* 122, 257–274.
- Eisenack, A. (1958). Tasmanites Newton 1975 und Leiosphaeridia n.g. als Gattungen der Hystrichosphaeridia. *Palaentographica Abt. A*. 110, 1–19.
- Evitt, W. R. (1963). A Discussion and Proposals Concerning Fossil Dinoflagellates, Hystrichospheres, and Acritarchs. *Proc. Natl. Acad. Sci.* 49 (2), 158–164. doi:10.1073/pnas.49.2.158
- Fedonkin, M. A., and Waggoner, B. M. (1997). The Late Precambrian Fossil Kimberella Is a Mollusc-like Bilateral Organism. *Nature* 388 (6645), 868–871. doi:10.1038/42242
- Folk, R. L. (1987). Detection of Organic Matter in Thin-Sections of Carbonate Rocks Using a white Card. *Sediment. Geology*. 54 (3), 193–200. doi:10.1016/0037-0738(87)90022-4
- Frei, R., Dossing, L. N., Gaucher, C., Boggiani, P. C., Frei, K. M., Bech Ártung, T., et al. (2017). Extensive Oxidative Weathering in the Aftermath of a Late Neoproterozoic Glaciation - Evidence from Trace Element and Chromium Isotope Records in the Urucum District (Jacadigo Group) and Puga Iron Formations (Mato Grosso Do Sul, Brazil). *Gondwana Res.* 49, 1–20. doi:10.1016/j.gr.2017.05.003
- Freitas, B. T., Rudnitski, I. D., Morais, L., Campos, M. D. R., Almeida, R. P., Warren, L. V., et al. (2021). Cryogenian Glaciostatic and Eustatic Fluctuations and Massive Marinoan-Related Deposition of Fe and Mn in the Urucum District, Brazil. *Geology* 49, 1478–1483. doi:10.1130/G49134.1
- Freitas, B. T., Warren, L. V., Boggiani, P. C., De Almeida, R. P., and Piacentini, T. (2011). Tectono-sedimentary Evolution of the Neoproterozoic BIF-Bearing Jacadigo Group, SW-Brazil. *Sediment. Geology*. 238 (1–2), 48–70. doi:10.1016/j.sedgeo.2011.04.001
- Gaucher, C., Boggiani, P. C., Sprechmann, P., Sial, A., and Fairchild, T. R. (2003). Integrated correlation of the Vendian to Cambrian Arroyo del Soldado and Corumbá Groups (Uruguay and Brazil): palaeogeographic, palaeoclimatic and palaeobiologic implications. *Precambrian Res.* 120 (3–4), 241–278. doi:10.1016/S0301-9268(02)00140-7
- Gaucher, C., and Sprechmann, P. (2009). Chapter 9.1 Neoproterozoic Acritarch Evolution. *Dev. Precambrian Geology*. 16, 319–326. doi:10.1016/S0166-2635(09)01622-3
- Gauthier-Lièvre, L., and Thomas, R. (1960). Le Genre Cucurbitella Pénard. *Arch. Protistenk* 104, 569–602.
- Germes, G. J. B., Knoll, A. H., and Vidal, G. (1986). Latest Proterozoic Microfossils from the Nama Group, Namibia (South West Africa). *Precambrian Res.* 32 (1), 45–62. doi:10.1016/0301-9268(86)90029-X
- Golubkova, E. Y., Zaitseva, T. S., Kuznetsov, A. B., Dovzhikova, E. G., and Maslov, A. V. (2015). Microfossils and Rb–Sr Age of Glaucinite in the Key Section of the Upper Proterozoic of the Northeastern Part of the Russian Plate (Keltmen-1 Borehole). *Dokl. Earth Sc.* 462 (2), 547–551. ISSN 1028334X. doi:10.1134/S1028334X15060045
- Gomaa, F., Lahr, D. J. G., Todorov, M., Li, J., and Lara, E. (2017). A Contribution to the Phylogeny of Agglutinating Arcellinida (Amoebozoa) Based on SSU rRNA Gene Sequences. *Eur. J. Protistology* 59, 99–107. doi:10.1016/j.ejop.2017.03.005
- Grazhdankin, D., Nagovitsin, K., Golubkova, E., Karlova, G., Kochnev, B., Rogov, V., et al. (2020). Doushantuo-Pertatataka-type Acanthomorphs and Ediacaran Ecosystem Stability. *Geology* 48 (7), 708–712. doi:10.1130/G47467.1
- Grey, K., and Calver, C. R. (2007). Correlating the Ediacaran of Australia. *Geol. Soc. Lond. Spec. Publications* 286 (1), 115–135. doi:10.1144/SP286.8
- Grey, K. (2005). *Ediacaran Palynology of Australia*, 31. (Hornsby: Memoir, Association of Australasian Palaeontologists), 439.
- Grey, K., Walter, M. R., and Calver, C. R. (2003). Neoproterozoic Biotic Diversification: Snowball Earth or Aftermath of the Acraman Impact. *Geol.* 31 (5), 459–462. doi:10.1130/0091-7613(2003)031<0459:nbdseo>2.0.co;2
- Hermann, T. N., and Podkovyrov, V. N. (2006). Fungal Remains from the Late Riphean. *Paleontol. J.* 40 (2), 207–214. ISSN 0031-0301. doi:10.1134/S0031030106020122
- Hofmann, H. J. (1971). Polygonomorph Acritarch from the Gunflint Formation (Precambrian), Ontario. *J. Paleontol.* 45 (3), 522–524. https://www.jstor.org/stable/1302699.
- Huntley, J., Xiao, S., and Kowalewski, M. (2006). 1.3 Billion Years of Acritarch History: An Empirical Morphospace Approach. *Precambrian Res.* 144 (1–2), 52–68. doi:10.1016/j.precamres.2005.11.003
- Jankauskas, T., Mikhailova, N., and Hermann, T. N. (1989). *Precambrian Microfossils of the USSR*. Leningrad: Nauka, 1–191. [in Russian].
- Javaux, E. J., and Knoll, A. H. (2017). Micropaleontology of the Lower Mesoproterozoic Roper Group, Australia, and Implications for Early Eukaryotic Evolution. *J. Paleontol.* 91 (2), 199–229. doi:10.1017/jpa.2016.124
- Knoll, A. H. (2003). Biomineralization and Evolutionary History. *Rev. mineralogy Geochim.* 54 (1), 329–356. doi:10.2113/0540329
- Knoll, A. H., Germes, G. J. B., Tankard, A., and Welsink, H. (2020). Tonian Microfossils from Subsurface Shales in Botswana. *Precambrian Res.* 345, 105779. doi:10.1016/j.precamres.2020.105779
- Kolosova, S. P. (1991). Late Precambrian Spiny Microfossils from the Eastern Part of the Siberian Platform. *Algologia* 1 (1991), 53–59. [in Russian].
- Lahr, D. J. G., Kosakyan, A., Lara, E., Mitchell, E. A. D., Morais, L., Porfirio-Sousa, A. L., et al. (2019). Phylogenomics and Morphological Reconstruction of Arcellinida Testate Amoebae Highlight Diversity of Microbial Eukaryotes in the Neoproterozoic. *Curr. Biol.* 29 (6), 991–1001. doi:10.1016/j.cub.2019.01.078
- Liu, P., and Moczydlowska, M. (2019). *Ediacaran Microfossils from the Doushantuo Formation Chert Nodules in the Yangtze Gorges Area, South China, and New Biozones*. John Wiley & Sons, 172.
- Maciel, P. (1959). Tilito Cambriano (?) no Estado de Mato Grosso. *Boletim da Sociedade Brasileira de Geologia. São Paulo* 8 (1), 31–39.
- McGee, B., Babinski, M., Trindade, R., and Collins, A. S. (2018). Tracing Final Gondwana Assembly: Age and Provenance of Key Stratigraphic Units in the Southern Paraguay Belt, Brazil. *Precambrian Res.* 307, 1–33. doi:10.1016/j.precamres.2017.12.030
- McKirdy, D. M., Webster, L. J., Aroui, K. R., Grey, K., and Gostin, V. A. (2006). Contrasting Sterane Signatures in Neoproterozoic marine Rocks of Australia before and after the Acraman Asteroid Impact. *Org. Geochem.* 37 (2), 189–207. doi:10.1016/j.orggeochem.2005.09.005
- Moczydlowska, M. (1991). Acritarch Biostratigraphy of the Lower Cambrian and the Precambrian–Cambrian Boundary in southeastern Poland. *Fossils and Strata* 29, 127.
- Moczydlowska, M. (2016). Algal Affinities of Ediacaran and Cambrian Organic-Walled Microfossils with Internal Reproductive bodies: Tanarium and Other Morphotypes. *Palynology* 40 (1), 83–121. doi:10.1080/01916122.2015.1006341
- Moczydlowska, M., and Nagovitsin, K. E. (2012). Ediacaran Radiation of Organic-Walled Microbiota Recorded in the Ura Formation, Patom Uplift, East Siberia. *Precambrian Res.* 198, 1–24. doi:10.1016/j.precamres.2011.12.010
- Moczydlowska, M. (2005). Taxonomic Review of Some Ediacaran Acritarchs from the Siberian Platform. *Precambrian Res.* 136, 283–307. doi:10.1016/j.precamres.2004.12.001
- Moczydlowska, M. (2011). The Early Cambrian Phytoplankton Radiation: Acritarch Evidence from the Lükati Formation, Estonia. *Palynology* 35 (1), 103–145. doi:10.1080/01916122.2011.552563
- Moczydlowska, M. (2008). The Ediacaran Microbiota and the Survival of Snowball Earth Conditions. *Precambrian Res.* 167, 1–15. doi:10.1016/j.precamres.2008.06.008
- Moczydlowska, M., Vidal, G., and Rudavskaya, V. A. (1993). Neoproterozoic (Vendian) Phytoplankton from the Siberian Platform, Yakutia. *Palaentology* 36, 495–521.
- Morais, L., Fairchild, T. R., Lahr, D. J. G., Rudnitski, I. D., Schopf, J. W., Garcia, A. K., et al. (2017). Carbonaceous and Siliceous Neoproterozoic Vase-Shaped

- Microfossils (Urucum Formation, Brazil) and the Question of Early Protistan Biomineralization. *J. Paleontol.* 91 (3), 393–406. doi:10.1017/jpa.2017.16
- Naumova, S. N. (1949). Spores of the Lower Cambrian. *Izvestiya Akademii Nauk SSSR, Seriya Geologicheskaya* 4, 49–56.
- Naumova, S. N. (1960). “Sporogo-pyltsevy Kompleksy Rifejskikh I Nizhnemkembrijskikh Otlozhenij SSSR (Spore-Pollen Assemblages of the Riphean and Lower Cambrian Deposits in the USSR),” in *Stratigrafiya Pozdnego Dokembriya I Kembriya, Problem 8 (Stratigraphy of the Late Precambrian and Cambrian, Problem 8, International Geological Congress 21 Session. Reports of the Soviet Geologists)* (Moscow: Akademia Nauk SSSR), 109–117.
- Owen, G., III, and Jones, E. E. (1976). Nebela Tuberculatacomb. Nov. (Arcellinida), its History and Ultrastructure. *The J. Protozoology* 23 (4), 485–487. doi:10.1111/j.1550-7408.1976.tb03819.x
- Pacheco, M. L. A. F., Galante, D., Rodrigues, F., de M. Leme, J., Bidola, P., Hagadorn, W., et al. (2015). Insights into the Skeletonization, Lifestyle, and Affinity of the Unusual Ediacaran Fossil Corumbella. *PLoS One* 10 (3), e0114219. doi:10.1371/journal.pone.0114219
- Parry, L. A., Boggiani, P. C., Condon, D. J., Garwood, R. J., Leme, J. d. M., McIlroy, D., et al. (2017). Ichnological Evidence for Meiofaunal Bilaterians from the Terminal Ediacaran and Earliest Cambrian of Brazil. *Nat. Ecol. Evol.* 1 (10), 1455–1464. doi:10.1038/s41559-017-0301-9
- Porter, S. M. (2004). Closing the Phosphatization Window: Testing for the Influence of Taphonomic Megabias on the Pattern of Small Shelly Fossil Decline. *Palaio* 19, 178–183. doi:10.1669/0883-1351(2004)019<0178:ctpwtf>2.0.co;2
- Porter, S. M., and Riedman, L. A. (2016). Systematics of Organic-Walled Microfossils from the Ca. 780–740 Ma Chuar Group, Grand Canyon, Arizona. *J. Paleontol.* 90 (5), 815–853. doi:10.1017/jpa.2016.57
- Prasad, B., Asher, R., and Borgohai, B. (2010). Late Neoproterozoic (Ediacaran)-Early Paleozoic (Cambrian) Acritarchs from the Marwar Supergroup, Bikaner-Nagaur Basin, Rajasthan. *J. Geol. Soc. India* 75 (2), 415–431. doi:10.1007/s12594-010-0038-4
- Rud'ko, S. V., Petrov, P. Y., Kuznetsov, A. B., Shatsillo, A. V., and Petrov, O. L. (2017). Refined $\delta^{13}\text{C}$ Trend of the Dal'naya Taiga Series of the Ura Uplift (Vendian, Southern Part of Middle Siberia). *Dokl. Earth Sc.* 477 (2), 1449–1453. doi:10.1134/S1028334X17120182
- Schopf, J. W., Kudryavtsev, A. B., Agresti, D. G., Czaja, A. D., and Wdowiak, T. J. (2005). Raman Imagery: a New Approach to Assess the Geochemical Maturity and Biogenicity of Permineralized Precambrian Fossils. *Astrobiology* 5 (3), 333–371. doi:10.1089/ast.2005.5.333
- Slater, B. J., and Willman, S. (2019). Early Cambrian Small Carbonaceous Fossils (SCF S) from an Impact Crater in Western Finland. *Lethaia* 52 (4), 570–582. doi:10.1111/let.12331
- Turner, R. E. (1984). Acritarchs from the Type Area of the Ordovician Caradoc Series, Shropshire, England. *Palaontographica Abteilung B Paläophytologie* 190 (4-6), 87–157.
- Van Iten, H., Burkey, M., Leme, J. D. M., and Marques, A. C. (2014). Cladistics and Mass Extinctions: the Example of Conulariids (Scyphozoa, Cnidaria) and the End Ordovician Extinction Event. *Gff* 136 (1), 275–280. doi:10.1080/11035897.2014.880506
- Vidal, G., and Moczyłowska-Vidal, M. (1997). Biodiversity, Speciation, and Extinction Trends of Proterozoic and Cambrian Phytoplankton. *Paleobiology* 23 (2), 230–246. doi:10.1017/S0094837300016808
- Volkova, N. A. (1968). “Acritarchs from the Precambrian and Lower Cambrian Deposits of Estonia,” in *Problematic Riphean-Cambrian Layers of the Russian Platform, the Urals and Kazakhstan. Trudy Geologicheskogo Instituta*. Editors N. A. Volkova, Z. A. Zhuravleva, V. E. Zabrodin, and B. Klinger (Moscow: Akademia Nauk SSSR, Nauka), 188, 8–36.
- Vorob'eva, N. G., Sergeev, V. N., and Knoll, A. H. (2007). “Microfossil Assemblages from the Vychedga Formation of the East European Platform Passive Margin—A Biostratigraphic Model for the Upper Riphean (Cryogenian)/Vendian (Ediacaran) Boundary,” in *The Rise and Fall of the Vendian (Ediacaran) Biota Origin of the Modern Biosphere Transaction of the International Conference on the IGCP Project, Moscow GEOS*, 493, 42–46.
- Vorob'eva, N. G., Sergeev, V. N., and Knoll, A. H. (2009). Neoproterozoic Microfossils from the Margin of the East European Platform and the Search for a Biostratigraphic Model of Lower Ediacaran Rocks. *Precambrian Res.* 173, 163–169. doi:10.1016/j.precamres.2009.04.001
- Willman, S., and Moczyłowska, M. (2008). Ediacaran Acritarch Biota from the Giles 1 Drillhole, Officer Basin, Australia, and its Potential for Biostratigraphic Correlation. *Precambrian Res.* 162 (3-4), 498–530. doi:10.1016/j.precamres.2007.10.010
- Willman, S., Moczyłowska, M., and Grey, K. (2006). Neoproterozoic (Ediacaran) Diversification of Acritarchs—A New Record from the Murnaroo 1 Drillcore, Eastern Officer Basin, Australia. *Rev. Palaeobotany Palynology* 139 (1-4), 17–39. doi:10.1016/j.revpalbo.2005.07.014
- Xiao, S., and Knoll, A. H. (2000). Phosphatized Animal Embryos from the Neoproterozoic Doushantuo Formation at Weng'an, Guizhou, South China. *J. Paleontol.* 74 (5), 767–788. doi:10.1017/S002233600003300X10.1666/0022-3360(2000)074<0767:paefn>2.0.co;2
- Xiao, S., and Narbonne, G. M. (2020). “The Ediacaran Period,” in *Geologic Time Scale 2020* (Elsevier), 41. doi:10.1016/b978-0-12-824360-2.00018-8
- Xiao, S., Zhou, C., Liu, P., Wang, D., and Yuan, X. (2014). Phosphatized Acanthomorphic Acritarchs and Related Microfossils from the Ediacaran Doushantuo Formation at Weng'an (South China) and Their Implications for Biostratigraphic Correlation. *J. Paleontol.* 88 (1), 1–67. doi:10.1666/12-157R
- Yin, L. (1987). Microbiotas of Latest Precambrian Sequences in China. *Stratigr. Palaeontology Systemic Boundaries China, Precambrian-Cambrian Boundary* 1, 415–494.
- Zaine, M. F., and Fairchild, T. R. (1987). “Novas considerações sobre os fósseis da Formação Tamengo, Grupo Corumbá, SW Brasil,” in *Congresso Brasileiro de Paleontologia, 10, Resumos das comunicações* (Rio de Janeiro: Sociedade Brasileira de Paleontologia), 54. [in Portuguese].
- Zang, Z. W., and Walter, M. R. (1992). *Late Proterozoic and Cambrian Microfossils and Biostratigraphy, Amadeus basin, central Australia*, 12. (Hornsby: Memoir, Association of Australasian Palaeontologists), 132.
- Zhang, Y., Yin, L., Xiao, S., and Knoll, A. H. (1998). Permineralized Fossils from the Terminal Proterozoic Doushantuo Formation, south China. *J. Paleontol.* 72 (4), 1–52. https://www.jstor.org/stable/1315592.

Conflict of Interest: Author EA was employed by EDEM, (Empresa De Desenvolvimento em Mineração e Participações Ltda).

The remaining authors declare that the research was conducted in the absence of any commercial or financial relationships that could be construed as a potential conflict of interest.

Publisher's Note: All claims expressed in this article are solely those of the authors and do not necessarily represent those of their affiliated organizations, or those of the publisher, the editors and the reviewers. Any product that may be evaluated in this article, or claim that may be made by its manufacturer, is not guaranteed or endorsed by the publisher.

Copyright © 2021 Morais, Fairchild, Freitas, Rudnitski, Silva, Lahr, Moreira, Abrahão Filho, Leme and Trindade. This is an open-access article distributed under the terms of the Creative Commons Attribution License (CC BY). The use, distribution or reproduction in other forums is permitted, provided the original author(s) and the copyright owner(s) are credited and that the original publication in this journal is cited, in accordance with accepted academic practice. No use, distribution or reproduction is permitted which does not comply with these terms.



Charniodiscus and Arborea Are Separate Genera Within the Arboreomorpha: Using the Holotype of *C. concentricus* to Resolve a Taphonomic/Taxonomic Tangle

Daniel Pérez-Pinedo^{1*}, Christopher McKean¹, Rod Taylor¹, Robert Nicholls² and Duncan McIlroy¹

¹Department of Earth Sciences, Memorial University of Newfoundland, St. John's, NL, Canada, ²Paleocreations, Bristol, United Kingdom

OPEN ACCESS

Edited by:

Juliana Leme,
University of São Paulo, Brazil

Reviewed by:

B. Runnegar,
University of California, Los Angeles,
United States
Shuhai Xiao,
Virginia Tech, United States

*Correspondence:

Daniel Pérez-Pinedo
dperezpinedo@mun.ca

Specialty section:

This article was submitted to
Paleontology,
a section of the journal
Frontiers in Earth Science

Received: 29 September 2021

Accepted: 20 December 2021

Published: 20 January 2022

Citation:

Pérez-Pinedo D, McKean C, Taylor R,
Nicholls R and McIlroy D (2022)
Charniodiscus and Arborea Are
Separate Genera Within the
Arboreomorpha: Using the Holotype of
C. concentricus to Resolve a
Taphonomic/Taxonomic Tangle.
Front. Earth Sci. 9:785929.
doi: 10.3389/feart.2021.785929

Charniodiscus is one of the most iconic and first described of the Ediacaran frondose taxa. Since the diagnosis of the holotype of *C. concentricus* in 1958, the scarcity and poor preservation of unequivocal specimens has resulted in genus-level taxonomic uncertainty. Since the recent reinterpretation of *C. concentricus* as a multifoliate frond, other *Charniodiscus* species—all of which are bifoliate—have been left in taxonomic limbo, with most authors comparing them to the clade Arboreomorpha and also the Rangeomorpha. Reconsideration of the taphonomy of the holotype of *C. concentricus* has revealed that the frond is bifoliate as first described, and also that the frondose portion was broadly conical rather than planar as previously inferred. The conical frond of *Charniodiscus* is thus morphologically quite different from all other frondose taxa within the Arboreomorpha. Our emendation of the generic diagnosis of *Charniodiscus* to encompass bifoliate arboreomorphs with conical fronds without a backing sheet distinguishes *Charniodiscus concentricus* and *C. procerus* from more planar leaf-like arboreomorphs such as *Arborea arborea*, *A. longa* and *A. spinosa*, all of which have a distinctive backing sheet. Additionally, we find no evidence of rangeomorph-type fractal branching in *Charniodiscus*.

Keywords: *Charniodiscus*, *Arborea*, holotype, taxonomy, taphonomy, Ediacaran, Avalon

INTRODUCTION

Charniodiscus Ford, 1958 was one of the first described fossils from the Ediacaran and is one of the most iconic—and most often illustrated—of the frondose Ediacaran taxa. The type species of the genus, *Charniodiscus concentricus*, was described from Charnwood Forest, UK (Ford, 1958) (Figure 1). *C. concentricus* was originally described as an organ taxon i.e., the disc part of *Charnia masoni* (Ford, 1958), but subsequently as a bifoliate frond with a stem and a basal disc (Ford, 1963). However, more recently consensus has shifted towards it being a multifoliate frond (Dzik, 2002; Brasier and Antcliffe, 2009; Liu et al., 2017). The genus has been compared to both the Rangeomorpha (Brasier et al., 2012) and the Arboreomorpha (Erwin et al., 2011) with current consensus being that most, if not all, *Charniodiscus* species are arboreomorphs (e.g., Laflamme et al., 2018; Dunn et al., 2019). The commonly accepted species of *Charniodiscus* include *C. concentricus*

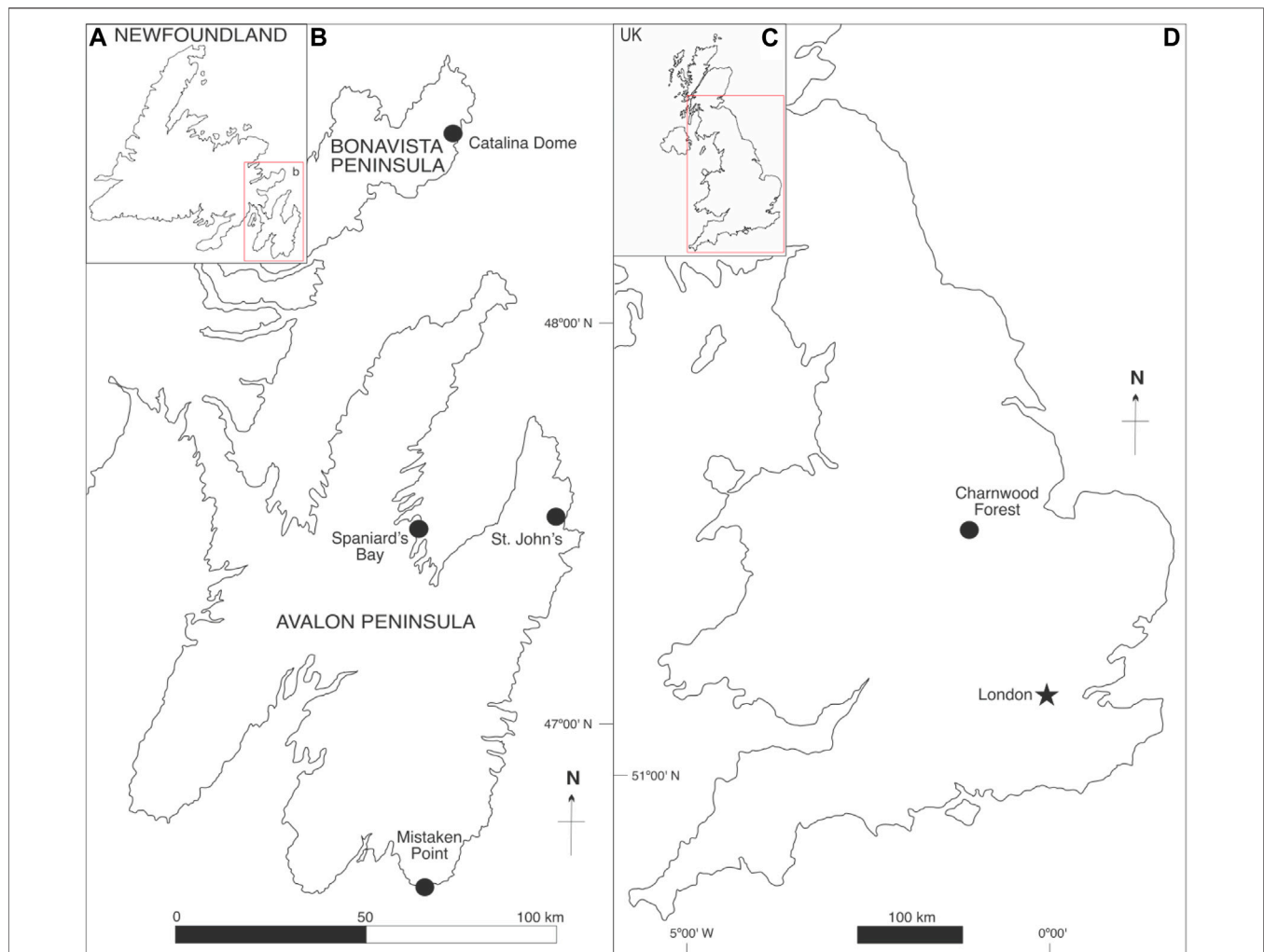


FIGURE 1 | Map of some of the most relevant Avalonian fossil assemblages (black circles). **(A)** General map of Newfoundland, Atlantic Canada. **(B)** Detail of the Avalon and Bonavista Peninsulas. **(C)** General map of the United Kingdom. **(D)** Detail of England.

Ford 1958; *C. longus* Glaessner and Wade, 1966; *C. yorgensis* Borchardt and Nesson, 1999; *C. procerus* Laflamme et al., 2004; and *C. spinosus* Laflamme et al., 2004 (**Figure 2**).

The taxonomy of *Charniodiscus* remains incompletely resolved in large part due to the complex preservation of the type species of *Charniodiscus* (cf. Brasier and Antcliffe, 2009; Brasier et al., 2012; **Figure 3**). While some species previously described as *Charniodiscus* are currently considered to be arboreomorphs (e.g., *Arborea*) (Laflamme et al., 2018; Dunn et al., 2019), those works have not addressed the morphology and taphonomy of the type species of the genus directly. *Charniodiscus* has been reported to have a worldwide distribution from sites in: Charnwood Forest, UK (e.g., Ford, 1958; Ford, 1962; Ford, 1963; Wilby et al., 2011); South Australia (e.g., Glaessner and Daily, 1959; Glaessner and Wade, 1966; Jenkins and Gehling, 1978; Gehling, 1991; Jenkins, 1992—though most of these occurrences are now considered to be *Arborea*); the White Sea region of Russia (Fedonkin, 1985;

Ivantsov, 2016); north-western Canada (Narbonne and Hofmann, 1987); and Newfoundland, Canada (e.g., Jenkins, 1992; Seilacher, 1992; Hofmann et al., 2008). *Charniodiscus* is thus a cosmopolitan taxon whose taxonomy and relationship to the somewhat similar *Arborea* is of global relevance. This study aims to improve palaeobiological understanding of the common species within *Charniodiscus* by reconsideration of the taphonomy and morphology of the type material from Charnwood Forest, UK, and the abundant *Charniodiscus* of the Newfoundland Ediacaran biotas of the Avalon and Bonavista peninsulas.

Preservation in the Avalon Assemblage

During periods of low sedimentation rates or hiatus, Ediacaran seafloors were commonly colonized by microbial matgrounds—likely mainly photosynthetic in shallow marine settings and chemosynthetic or chemoheterotrophic in deep marine settings. Matgrounds in waters of all depths in the

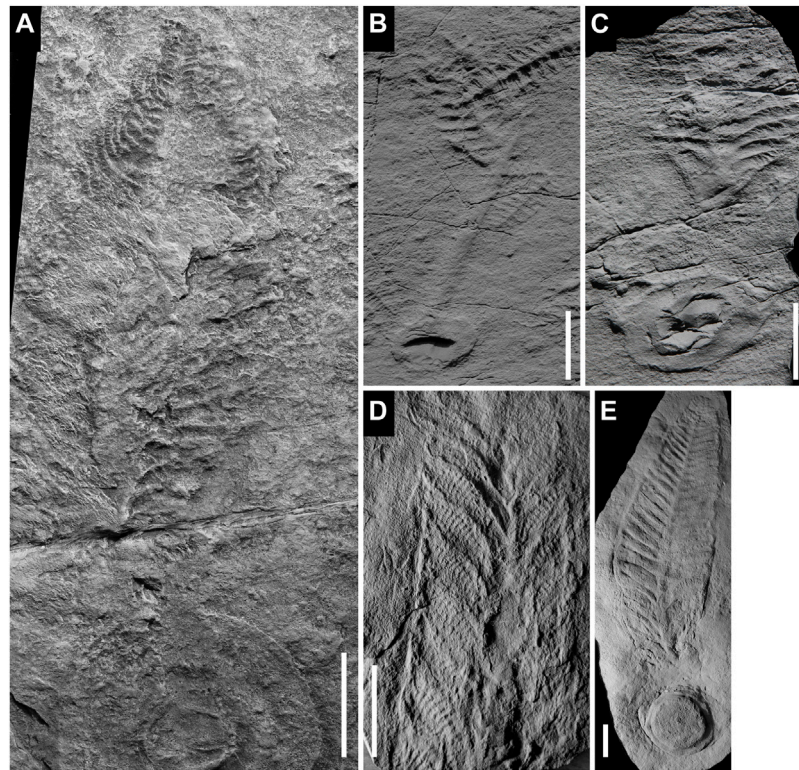
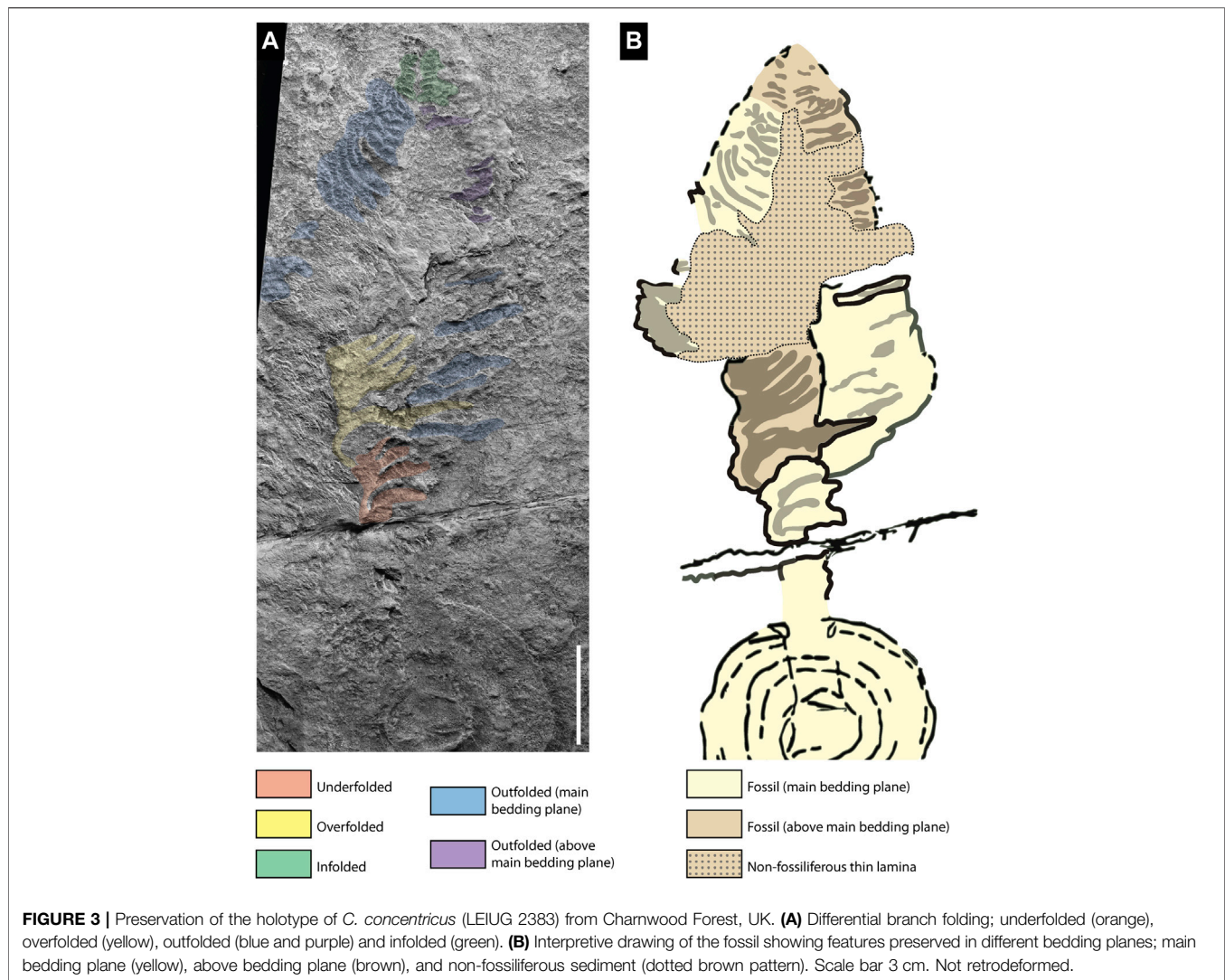


FIGURE 2 | Casts of relevant *Charniodiscus* species. **(A)** *C. concentricus* holotype (LEIUG 2383) from Charnwood Forest, UK. **(B,C)** *C. procerus* and *C. spinosus* respectively from the upper part of the Mistaken Point Formation ("E"-surface) at Mistaken Point, Newfoundland. Jesmonite cast of field specimens. **(D,E)** *C. longus* cast (SAM P13777) and *C. arboreus* (*Arborea*) cast (OUMNH AW.00043/p) respectively from Ediacara, South Australia. Scale bars 3 cm. Not retrodeformed.

Ediacaran were exceptionally well developed and well preserved, owing to the rarity of motile macrobionts (e.g., Liu et al., 2010), macrobioturbation (McIlroy and Logan, 1999), and ecosystem services like scavenging and grazing (Herringshaw et al., 2017); this would also have led to the persistence of abundant seafloor necromass (Liu et al., 2011; McIlroy et al., 2021). The importance of matgrounds for soft bodied preservation of Ediacaran organisms has been extensively explored based around the death mask model of mouldic preservation proposed by Gehling (1999) and extended to encompass aspects of early diagenetic mineralization (Mapstone and McIlroy, 2006; Liu, 2016) and preservation as original carbonaceous compressions (e.g., Steiner and Reitner, 2001; Xiao et al., 2002). The role of sedimentological parameters as they interface with taphonomic processes in taphonomy is pivotal but remains under-studied (Kenchington and Wilby, 2014).

The Avalon Assemblage (Waggoner, 2003) is the oldest of the Ediacaran assemblages. The earliest known Ediacaran fossils are from deep marine volcanoclastic settings of the Avalon Terrane in Newfoundland spanning at least the interval ca. 574–564 Ma (Matthews et al., 2021) and Charnwood Forest, UK, (Noble et al., 2015). These successions form part of the peri-Gondwanan Avalonian volcanic arc system (Murphy et al., 2004; McIlroy and Horák, 2006; Wen et al., 2020) and predominantly consist of

turbidites and laterally extensive tuffites (McIlroy et al., 1998; Wood et al., 2003; Matthews et al., 2021). The soft bodied Ediacaran fossils are typically preserved as impressions on top of volcanoclastic siltstones, particularly where they are overlain by tuffites (Narbonne, 2005; Liu et al., 2015; Matthews et al., 2021). Positive epireliefs are the most common mode of preservation for stems and some basal discs of frondose organisms, which implies that they maintained their integrity long enough for lithification of the overlying tuff. Negative epireliefs are typically associated with the less resistant frondose portions of quasi-infaunal reclining organisms (permanently affixed to the seafloor), produced by smothering of matgrounds by dead/felled erect or recumbent (parallel and elevated above the seafloor in a windsock-like manner) organisms (McIlroy et al., 2009) or by sediment-displacing growth of quasi-infaunal reclining organisms (McIlroy et al., 2020; Taylor et al., 2021; McIlroy et al., 2021) (**Figure 4**). Soft bodied Ediacaran taphonomic style is influenced by a combination of: 1) differential decomposition rates of labile vs relatively refractory body tissues; 2) the influence of currents and related sedimentary processes; 3) body posture in life; and 4) the nature of seafloor microbial matgrounds associated with the organism in life (e.g., Wade, 1968; Gehling, 1999; Narbonne, 2005; McIlroy et al., 2020, McIlroy et al., 2021).



Aside from the holotype of the type species of *Charniodiscus* (Charnwood Forest, UK) most of the specimens of the genus are known from Newfoundland and have been described from either Mistaken Point (Laflamme et al., 2004) or the Catalina Dome (Hofmann et al., 2008). In both locations, the top surfaces of the basal discs and stems—as well as the junction between them—are commonly preserved as positive epireliefs whereas the frondose portions commonly lie beneath the ambient bedding plane. This suggests preservation by matground smothering (McIlroy et al., 2009; **Figure 4**) with sharp ridges occurring due to post-mortem sediment infiltration between frondose elements. In the younger Charnian assemblage of the UK the Ediacaran biotas are typically preserved as very low negative and positive epireliefs on fine-grained surfaces under a thin tuffaceous layer (Brasier and Antcliffe, 2009; Wilby et al., 2011), like the Conception-type preservation (Narbonne, 2005). This assemblage shares some genera with Newfoundland, but like Newfoundland also includes several endemic taxa.

Previous Taphonomic/Morphological Consideration of the *Charniodiscus concentricus* Holotype

The Arboreomorpha (Erwin et al., 2011; cf. the Frondomorpha of Grazhdankin, 2014) encompasses numerous frondose species that lack the fractal-like branching of the Rangeomorpha (Narbonne, 2004; Brasier and Antcliffe, 2004, Brasier and Antcliffe, 2009). Arboreomorphs are characterized by arboreomorph branching architecture in which rows of primary branches project from the central stalk extending to an outer rim and may have transverse structures called second order branches (Laflamme and Narbonne, 2008; Erwin et al., 2011). The clade encompasses two genera, *Charniodiscus* and *Arborea*, whose taxonomic relationship has hitherto been confused. Some authors have considered *Arborea* to be a junior synonym of *Charniodiscus* on the basis of similar gross morphology (Glaessner and Daily, 1959; Jenkins and Gehling, 1978). The Newfoundland *Charniodiscus* species (*C. spinosus*, *C.*

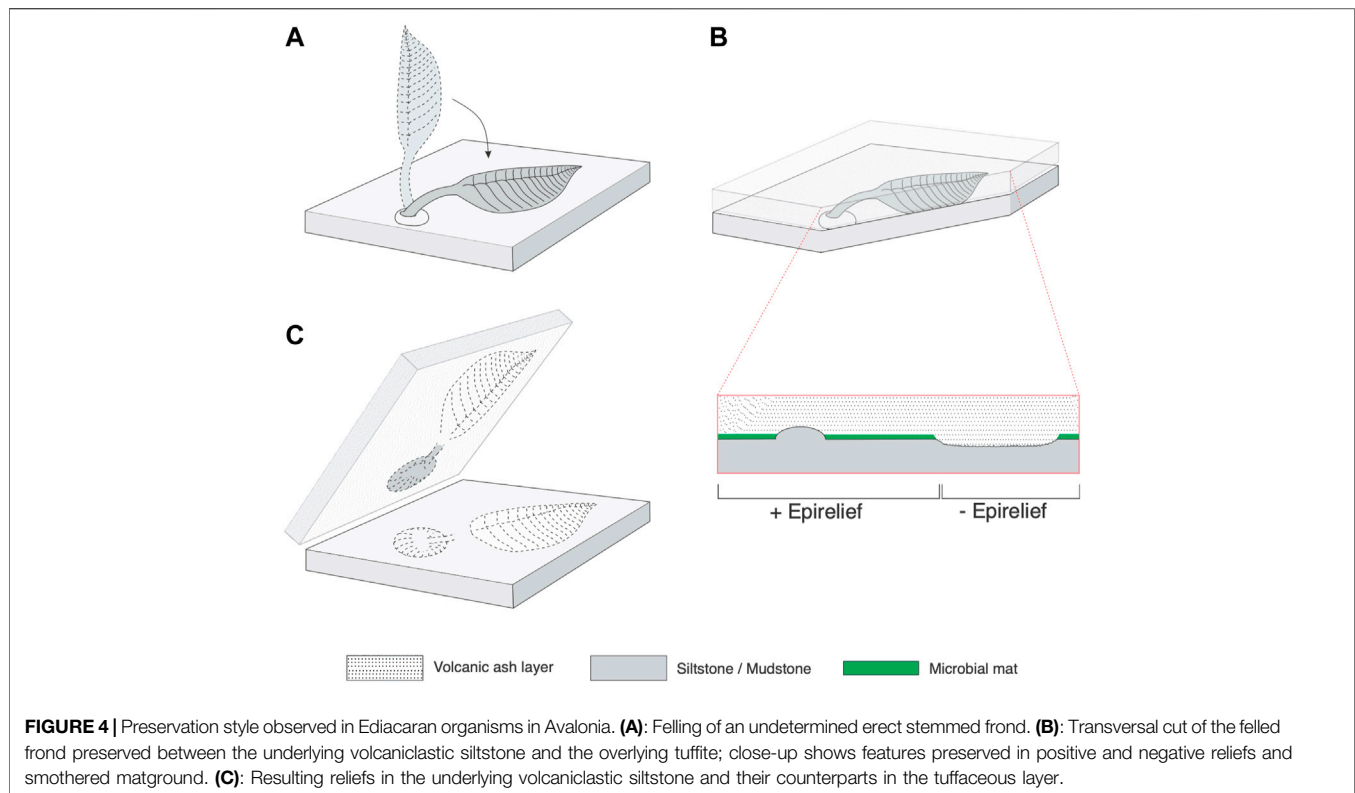


FIGURE 4 | Preservation style observed in Ediacaran organisms in Avalonia. **(A)**: Felling of an undetermined erect stemmed frond. **(B)**: Transversal cut of the felled frond preserved between the underlying volcaniclastic siltstone and the overlying tuffite; close-up shows features preserved in positive and negative reliefs and smothered matground. **(C)**: Resulting reliefs in the underlying volcaniclastic siltstone and their counterparts in the tuffaceous layer.

procerus and *C. arboreus*) have been attributed to the Arboreomorpha, but not closely related to the type species of *Charniodiscus* (e.g., Laflamme et al., 2004; Hofmann et al., 2008; Liu et al., 2015), however, there has been no attempt to formally move these taxa out of *Charniodiscus*. These taxonomic interpretations are further confused by differing opinions on the morphology and taphonomy of the holotype of *Charniodiscus concentricus* (Dzik, 2002; Brasier and Antcliffe, 2009). It has been suggested that *C. concentricus* is a multifoliate rangeomorph rather than an arboreomorph, albeit without observable rangeomorph branching (undivided and furled morphology cf. Brasier and Antcliffe, 2009; Brasier et al., 2012), which we do not consider to be objectively testable.

Charniodiscus concentricus is a soft-bodied unipolar, lanceolate to ovate frondose organism consisting of a segmented frond and a cylindrical stem, which is associated with a basal disc (e.g., Brasier and Antcliffe, 2009; Figure 2A). The term holdfast is not used herein as it implies a biomechanical function that cannot be unequivocally demonstrated. The frond presents 30 to 50 primary branches attached to both sides of the stem in either alternating or opposing arrangements. The primary branches of *C. concentricus* have secondary order bar-like transverse structures (e.g., Laflamme et al., 2004) (Figure 3A). There is also a pronounced curvature to the primary branches, and a notable decrease in branch width and length towards the frond apex (which has been considered a species-level difference between *C. concentricus* and *Arborea* (Jenkins and Gehling, 1978; Laflamme et al., 2004). The widely accepted multifoliate nature of *C. concentricus* (Dzik, 2002; Brasier and Antcliffe, 2009,

Figure 12) is currently considered to be one of the fundamental differences between *Charniodiscus* and *Arborea* spp. (Liu et al., 2017; Dunn et al., 2019).

The holotype of *C. concentricus* combines both positive and negative epirelief impressions and includes some preservation on the tuffaceous siltstone that is at a level slightly above the main microbially-dominated bedding plane associated with the basal disc (Figure 3B). Both the basal disc and the stem are preserved in low positive epirelief, although the latter may be a partially collapsed remnant of what was originally a cylindrical structure. The central and distal-most sections of the frond are preserved in negative relief but at a level slightly above the main bedding plane, while the proximal arcuate subparallel primary branches are in negative epirelief on the same surface as the basal disc and stem (Brasier and Antcliffe, 2009; Figure 3B).

Historical Reasoning for A Multifoliate *Charniodiscus concentricus*

Explanation of the biostratinomy of the *Charniodiscus* type species as a bifoliate frond in which the bottom-left part of the frond was overfolded (Jenkins and Gehling, 1978, Figures 4X,Y) has more recently been superseded by a multifoliate model (Dzik, 2002; Brasier and Antcliffe, 2009, Figure 12). The multifoliate model invokes the presence of at least three foliate sheets of primary branches resembling rangeomorph branching (Brasier and Antcliffe, 2009; Brasier et al., 2012).

The acceptance of the multifoliate nature of the holotype of the type species of *Charniodiscus* resulted in taxonomic

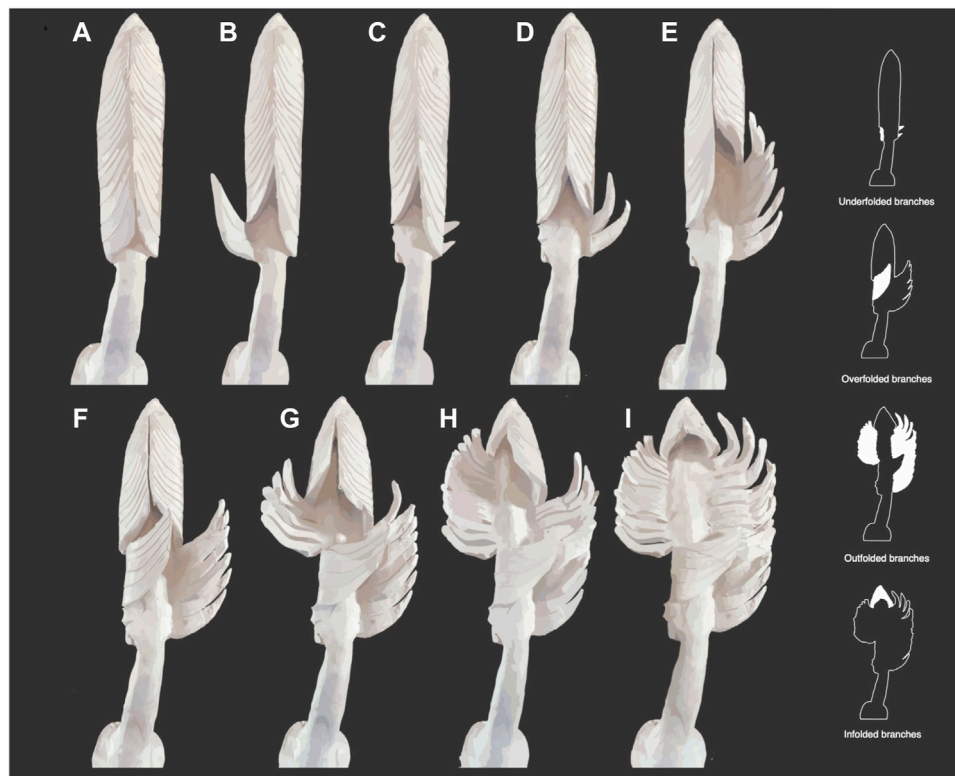


FIGURE 5 | Taphonomic stop-motion model of the holotype of *C. concentricus* showing different branch folding. **(A–C)** underfolding of proximal-most branches. **(A–I)** infolding of distal-most branches. **(D–I)** outfolding of bottom-right and central branches. **(F–I)** overfolding of bottom-left branches.

inconsistencies regarding the other bifoliate species of the genus (Laflamme et al., 2018). Moreover, since there is no evidence to support fractal branching architecture, assignment of the genus to the Rangeomorpha (undivided rangeomorph branching of Brasier et al., 2012) is unsupported. The Newfoundland species of *Charniodiscus* have remained within the genus, despite the inferred multifoliate nature of the type species (Laflamme and Narbonne, 2008), but have also been considered to be separate from *Arborea* based on branching criteria of Brasier et al. (2012). The need to unravel this taphonomic, and taxonomic, tangle has been mentioned in the literature by numerous authors (e.g., Brasier and Antcliffe, 2009; Liu et al., 2015; Laflamme et al., 2018; Wang et al., 2020) but remains unresolved.

A NEW TAPHONOMIC UNDERSTANDING OF THE *CHARNIODISCUS CONCENTRICUS* HOLOTYPE

The 8 or 9 most apical primary branches of the holotype are negative epireliefs that are short, narrow, and rounded close to the axis and are directed slightly towards the frond base. There is no central stem preserved at the tip owing to the fact that the branches are impressed into sediment lying atop the plane of the inferred axial stem (Figure 3A—green). These apical

branches do not have any preserved transverse ornament, which is typical of some branches of the holotype. These transverse branches could have escaped preservation thus their actual existence cannot be ruled out. The arrangement of the branches is consistent with infolding of originally curved branches resulting in the impression of the interior surface of the branch into the sediments overlying the stem. This type of infolding preservation is also common in specimens attributed to *C. arboreus* from the Catalina Dome by Hofmann et al. (2008), (Figure 16 7–8).

The longer arcuate branches immediately adjacent to the apex of the holotype of *C. concentricus* are strongly curved and slightly imbricated towards the tip; there is no evidence of a clearly preserved axial stem, which may also be buried in this portion of the fossil (Figure 3A—blue, purple). We consider that branch curvature is due to the outfolding collapse of a sub-conical frond (Figures 5D–I). The strongly curved branches have sharp transverse ridges formed by sediment infilling the gaps between the transverse second order branches. Since these branches are outfolded, it would suggest that in life the external surfaces of the primary order ridge-like branches are what would be impressed into the sediment, and thus that the external surfaces were covered in transverse ridges. The curved portion of the outfolded set of branches on the right is observed in a slightly higher plane than the ambient plane (Figure 3—purple).

Our study of the holotype supports the interpretation of the bottom-left proximal region of the frond being folded across the central axis (Jenkins and Gehling, 1978, Figures 4X,Y), albeit with some modifications. We interpret the first set of proximal branches (Figures 3A—orange) as being underfolded beneath the stem (Figures 5A–C). Evidence for this underfolding comes from: 1) the underfolded branches being the topographically lowest structures preserved in the holotype; and 2) the absence of a preserved stem, which would have lain above the underfolded branches and could not therefore have been impressed into the sediment.

The presence of underfolding is important for considering the life attitude of the organism because, in order to be able to underfold the branches, the stem cannot have lain upon the sediment surface in life. This leaves an erect or recumbent lifestyle as the only realistic modes of life. Additionally, underfolding would have necessarily occurred prior to the felling of the frond. Of the branches preserved in the proximal part of the frond, these are the only ones to preserve obliquely orientated secondary units in the inner surface of the branches.

The second set of proximal branches on the left-hand side of the fossil are preserved as impressions in sediment that lay at a higher level than the stem (Figures 3A—yellow) and above the ambient bedding plane (Figure 3B). The branches preserved at this higher level are the basis for inferring that *Charniodiscus* was a multifoliate frond (Dzik, 2002; Brasier and Antcliffe, 2009). However, we follow Jenkins and Gehling (1978) in considering that these branches were swept across the axis from left to right such that the bases of the branches are approximately aligned with the position of the stem, which we infer lay at a lower level below the sediment that casts the branches (Figures 5F–I). The sediment on top of the stem was either present inside the subconical frond during life, or shortly after death/felling, but before collapse and complete burial of the frond. In our model the stem is not preserved due to its position at a level below the rock surface (Figure 3B). The apparently smooth surface of the distal branches (Figures 3A—green) suggests that the inner surface of the branches may have been unornamented in the arcuate portion of the sub-conical frond.

EVIDENCE FOR CHARNIODISCUS BEING A COLLAPSED SUB-CONICAL STRUCTURE

The marked curvature of the outfolded branches of *C. concentricus*, the straight basally-directed infolded branches of the tip, and the preservation of sediment atop the central axis of much of the frond is most consistent with the frond being a collapsed sub-conical structure with a more flattened side adjacent to the stem (Figure 2A). The curvature of the branches suggests that the tips of the branches met in an apically-directed zipper-like fashion on the front side of the sub-conical frond. Actualistic modeling of the frond branches as they are preserved in the holotype is consistent with the tips of the branches meeting in a chevron-like seam when reconstructed (Figure 5A). Since the bases of the branches meet the axis at nearly 90° it seems logical that these branches have not been

greatly modified by compression; this suggests that the basal portion of the branches were rather flat, producing a flattened base to the sub-conical frond (Figures 5–7).

The pronounced curvature of the apical branches is a prominent feature of *Charniodiscus concentricus* and a significant difference between it and *Arborea* (Jenkins and Gehling, 1978; Laflamme et al., 2004). Other arboreomorphs with strongly curved branches in the Avalon assemblage include *Charniodiscus procerus* (Laflamme et al., 2004; Figure 6) and another un-named *Charniodiscus* species with broad strongly arcuate branches (Figure 7). We consider all of these forms to be species of *Charniodiscus* and each of them probably had a similar conical frond without a “backing sheet” (*sensu* Dunn et al., 2019).

Arboreomorphs without pronounced branch curvature include: *Charniodiscus arboreus* (*sensu* Hofmann et al., 2008, fig. 16 7–8); *C. longus* (Figure 2D); *C. oppositus*; and *C. spinosus* (Figure 2C). Most if not all of these taxa also have a prominent backing sheet and are thus likely to be species of *Arborea*.

We thus consider that there are two different unipolar bifoliate frond morphologies within the Arboreomorpha: 1) sub-conical fronds with arboreomorph branching and no backing sheet, typical of *Charniodiscus*; and 2) planar fronds with a prominent backing sheet on one side and arboreomorph branching on the other, which are attributable to *Arborea*.

SYSTEMATIC PALAEONTOLOGY

Phylum Indet.

Clade Arboreomorpha.

Genus *Charniodiscus* Ford 1958.

Type species. — *Charniodiscus concentricus*, described from the Charnian Supergroup of the UK (Ford, 1958).

Emended generic diagnosis. — Unipolar frondose arboreomorphs with basal disc, stem, a bifoliate frond without a backing sheet and loosely constrained branches. The bases of the branches are commonly straight and attached to the stem at nearly right angles but are distally curved forming a sub-conical frond in life. Outer surface of the branches of the sub-conical frond has transverse ridges orthogonal to the long axis of the branches. The internal surface of the branch has similar oblique ridges close to the junction with the stem.

Discussion. — The species of *Charniodiscus* considered valid herein are *C. concentricus* and *C. procerus*. The status of *C. yorgensis* requires restudy of the type material that is beyond the scope of this study. All other taxa hitherto attributed to *Charniodiscus* (*C. arboreus*, *C. longus*, *C. oppositus*, and *C. spinosus*) should likely be considered to be species of *Arborea* but require further study and comparison with the type species (cf. Laflamme et al., 2018; Wang et al., 2020). The branches of *C. concentricus* are considered to be homologous with the pea-pod-like units of *Arborea* (cf. Dunn et al., 2019).

Charniodiscus concentricus Ford 1958.

Emended specific diagnosis. — *Charniodiscus* with basal disc, stem, and a bifoliate frond, lacking a supporting backing sheet, composed of approximately 25 independent branches that were

- 1958 *Charniodiscus concentricus* Ford, p. 212 pl. 13, fig. 2-3 (originally as a form taxon, basal disc of *Charnia*)
- 1963 *Charniodiscus concentricus* Ford, pl. 1, fig.1 a-d
- non 1966 *Charniodiscus arboreus* Glaessner and Wade, pl. 102, fig. 1-2
- non 1966 *Charniodiscus longus* Glaessner and Wade, pl. 100, fig. 4
- non 1978 *Charniodiscus oppositus* Jenkins and Gehling, p. 204 pl. 3, fig. 4
- ? 1999 *Charniodiscus yorgensis* Borchardt and Nessov, p. 54, text-fig. 2
- 2004 *Charniodiscus procerus* Laflamme *et al.*, p. 830, fig. 3
- non 2004 *Charniodiscus spinosus* Laflamme *et al.*, p. 830-831, fig. 3-4

Type species. — *Charniodiscus concentricus*, described from the Charnian Supergroup of the UK (Ford, 1958).

strongly curved inward and upward in life to form a sub-conical frond, which becomes lanceolate to ovate upon collapse/compression.

Description. — *Charniodiscus concentricus* has a round basal disc bearing concentric rings without a prominent central boss, from which a broad stem emerges. The stem is short (~4 cm) and relatively poorly preserved in the holotype. The primary arboreomorph branches are attached to the lateral margins of the stem. The impression of the frond is bifoliate and lanceolate to ovate in outline (16.2 cm length: 6.3 cm wide). The external distal portion and the internal proximal section of the primary branches have secondary order transverse bar-like morphology. There is no evidence of fractal branching pattern characteristic of the Rangeomorpha.

Discussion. — The junction between the branches and the stem in the holotype *Charniodiscus concentricus* is not preserved except at the base. The stem of the holotype is poorly preserved, especially in comparison to *C. procerus* from the Newfoundland

Ediacaran biota (**Figure 6**). This may relate to a combination of different tissue composition/resilience and different body postures in life. Curvature of the branches in *C. concentricus* and *C. procerus* is considerably more pronounced than in other species of the genus, occasionally leading to compromised preservation of the branches towards distal sections (**Figure 6**).

Charniodiscus concentricus has parallel transverse ridges preserved in the external distal-most section of certain apical branches and in the internal side of the proximal-most section of certain proximal branches. However, there is no evidence of the fractal branching pattern which would be required to assign the genus to the Rangeomorpha (Brasier *et al.*, 2012). Additionally, the absence of the prominent backing sheet of *Arborea* further distinguishes *Charniodiscus* from *Arborea*. Our reinterpretation of the holotype is significantly different from previous models (Ford, 1958; Jenkins and Gehling, 1978; Dzik,

- 1958 *Charniodiscus concentricus* Ford, p. 212 pl. 13, fig. 2-3 [as a form taxon, basal disc of *Charnia*]
- 1963 *Charniodiscus concentricus* Ford, pl. 1, fig.1 a-d [description of frond associated with basal disc]
- 1978 *Charniodiscus concentricus* Jenkins and Gehling, p. 350-352, fig. 2, 4
- 2002 *Charniodiscus concentricus* Dzik, p. 322 - 323
- 2009 *Charniodiscus concentricus* Brasier and Antcliff, p. 375-377, fig. 12-14
- 2012 *Charniodiscus concentricus* Brasier *et al.*, p. 1109-1114, fig. 3
- 2017 *Charniodiscus concentricus* Liu *et al.* fig. 3 a-c

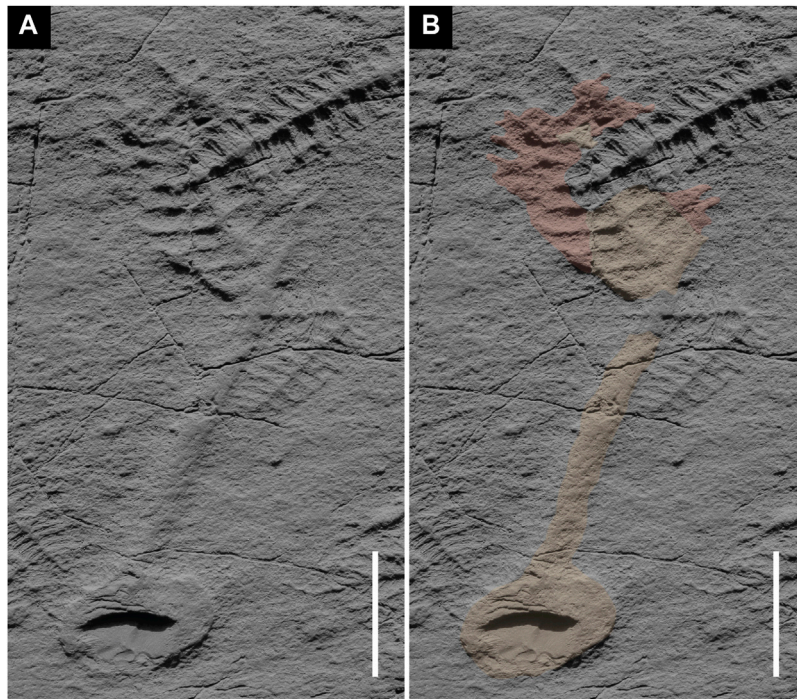


FIGURE 6 | *Charniodiscus procerus* from the so-called “Seilacher’s Corner”, upper part of the Mistaken Point Formation (“E”-surface) at Mistaken Point, Newfoundland. **(A)** cast. **(B)** Basal disc, stem and flat basal section of the branches meeting the central axis at $\sim 90^\circ$ in orange; apical section of the branches showing pronounced curvature in red. Scale bars 3 cm. Jesmonite cast of field specimen. Not retrodeformed.

2002; Brasier and Antcliffe, 2009; Brasier et al., 2012) in that the holotype is herein demonstrated to be bifoliate, non-fractal, lacking the backing sheets characteristic of *Arborea*, and having a conical shape defined by Arboreomorph-type branches (Laflamme and Narbonne, 2008).

MODE OF LIFE OF *CHARNIODISCUS* *CONCENTRICUS*

Reconstructions of most frondose Ediacaran taxa have followed Glaessner (1984) in depicting them as being erect, pennatulacean-

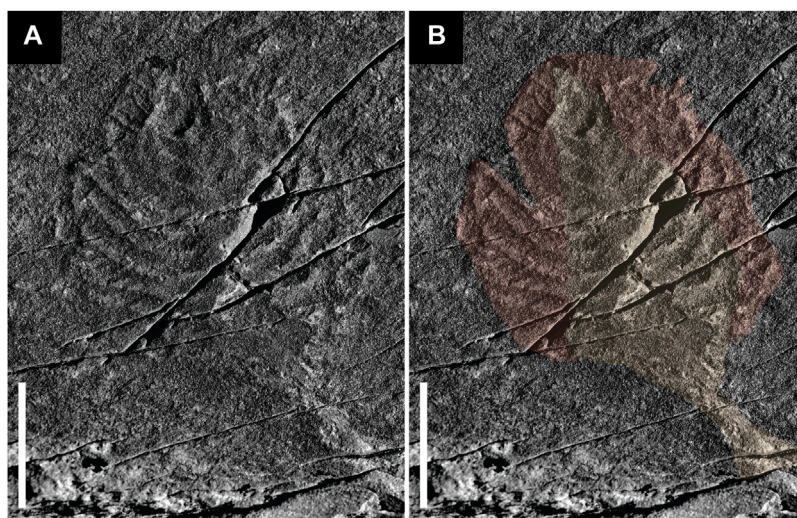


FIGURE 7 | *Charniodiscus* sp. from the Mistaken Point Formation (“D”-surface) at Mistaken Point, Newfoundland. **(A)** field photography of the specimen. **(B)** Stem and flat basal section of the branches meeting the central axis at $\sim 90^\circ$ in orange; apical section of the branches showing pronounced curvature in red. Scale bars 3 cm. Field photography. Not retrodeformed.

like organisms and the coining of descriptive terms such as stems, basal disc, and frondlets belies attempts to draw analogies to extant taxa (e.g., algae). This imparts an implicit bias towards palaeobiological reconstructions presenting many Ediacaran organisms as having an erect mode of life. This standard paradigm has recently been challenged (McIlroy et al., 2020, McIlroy et al., 2021), in an assertion that the null hypothesis for orientation should be the preserved (i.e., reclined on the sediment) position unless there is evidence to the contrary.

Arboreomorphs generally possess well-preserved basal discs, possibly representing anchoring structures that were partially immersed in the sediment (Burzynski and Narbonne, 2015; Tarhan et al., 2015). Some discs have folds consistent with originally inflated bodies that eventually experienced collapse (Dunn et al., 2019; McIlroy et al., 2021) which might imply the presence of some form of cnidarian-like hydrostatic skeleton in life. Since some species of *Charniodiscus* and *Arborea* commonly have poor preservation of the stem, this can be taken to suggest that: 1) the stem did not lie upon the seafloor surface during preservation (i.e., stems arched upward due to the displacement of the frond allowing deposition of sediment between the stem and the bedding plane; **Figure 4**); or 2) stems of some taxa decayed more rapidly than the other tissues. The stem of the *Charniodiscus concentricus* holotype is remarkably flat, and relatively poorly preserved. The stem, as previously interpreted, is apparently offset from the axis of the frond. We consider that this is an artifact of the underfolding of the branches under the stem, which obscures one margin of it (**Figure 3A**). There is no evidence of swing marks associated with the holotype unlike some frondose taxa (Jensen et al., 2018) and only erect (e.g., Glaessner and Daily, 1959; Glaessner, 1984) or recumbent (Laflamme et al., 2018) modes of life are consistent with underfolding and the commonly poor preservation of the stem. The impression of the upper parts of the branches into sediment that lay above the level of the stem strongly suggests the presence of sediment above the stem before post-mortem collapse of the frond. This taphonomic mode is consistent with a curved front surface to the bifoliate frond.

Additional evidence for sub-conical frondose arboreomorphs comes from the recent discovery of a specimen of *Charniodiscus* sp. preserved in full relief in a thin Tc sand unit immediately above the Spaniard's Bay assemblage in Newfoundland (Narbonne et al., 2009; Brasier et al., 2013). The three-dimensional morphology of the *Charniodiscus* frond can be inferred from the well-preserved collapsed sub-conical frond with indication of the transverse cross section (**Figure 8**). The frond is characterized by basally-directed infolding collapse of the frond with the junctions between the tips of opposing primary branches being well preserved. This mode of infolding collapse is also seen in the very tip of the holotype of *C. concentricus* and the partial fill of the originally sub-conical Spaniard's Bay specimen above the level of the stem is similar to that of parts of the holotype (**Figures 3A**—green). The primary branches of the Spaniard's Bay *Charniodiscus* have no evidence for fractal rangeomorph branching, further supporting the non-rangeomorph nature of *Charniodiscus*.

The most common Avalonian arboreomorph with strongly curved broad branches is *Charniodiscus procerus* (Laflamme et al.,

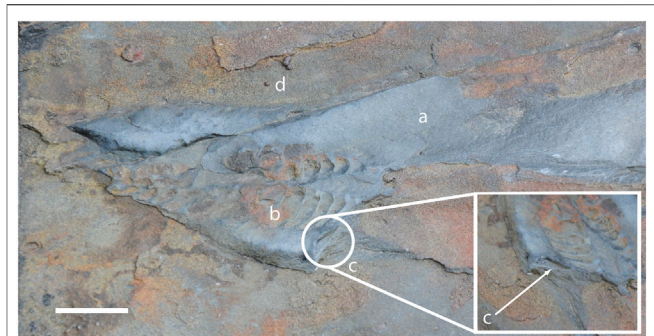


FIGURE 8 | *Charniodiscus* sp. from Spaniard's bay, Newfoundland. **(A)** Overlying siltstone. **(B)** collapsed sub-conical frond preserved in sandstone. **(C)** cross section view. **(D)** underlying siltstone. Scale bar 1 cm. Field photography. Not retrodeformed.

2004, **Figure 3A**) which has a central triangular section adjacent to the stem that is typically well preserved as deep negative epireliefs (**Figures 6**—orange). In well preserved material, the arcuate portion of branches extends from the triangular portion in a manner similar to the more numerous very narrow branches close to the tip of *C. concentricus*. The distal curved portion of the primary branches of *C. procerus* (**Figures 6**—red) are interpreted—by analogy with *C. concentricus* and *C. sp.* from Spaniards Bay—as casts of the impressions made by the external surfaces of the curved portion of the conical frond that we consider to be typical of *Charniodiscus*.

In contrast to the flattened stem of *C. concentricus* and the poorly preserved stem of other Arboreomorphs and Rangeomorphs in the same Newfoundland assemblages (Laflamme et al., 2004; Laflamme et al., 2012), the stem of *C. procerus* is generally well preserved and covered in matground textures (**Figure 6**) and even other reclining taxa such as *Fractofusus*. As such it would seem that *C. procerus* conforms to the null hypothesis of McIlroy et al. (2020), McIlroy et al. (2021) that unless there is positive evidence to support an erect mode of life, the stem of the frond should be considered to have lain on or in the seafloor during life. However, the presence of a specimen of *Fractofusus* below the frond of one specimen may also suggest that the frondose portion may have been erect arising from the end of the reclined stem, only falling post-mortem onto the seafloor on top of the aforementioned *Fractofusus* (**Figure 6**). A second hitherto undescribed *Charniodiscus* with highly curved broad primary branches with transverse ornament is also present in the Newfoundland assemblage (**Figure 7**).

PALAEOBIOLOGICAL MODEL OF CHARNIODISCUS

The original cnidarian affinities of frondose Ediacaran organisms (e.g., *Charnia* and *Bragdatia*) have recently been questioned (e.g., Brasier and Antcliffe, 2004; Narbonne, 2004; Narbonne, 2005;

Antcliffe and Brasier, 2008), though their utility as functional morphological analogs may still be valid (Dunn et al., 2019). If *Charniodiscus* is accepted as a sub-conical stemmed frondose arboreomorph, then it might function biomechanically erect in the water column like most pennatulaceans (cf. Kushida et al., 2020, **Figure 2A**) in which case it might draw water up through the cone by Bernoulli effect. The same morphotype might also be an adaption to funnel water if held in a recumbent or reclined position parallel to the seafloor, either with the cone directed into or away from the current. If held in a recumbent or reclining position the broad end of the cone would face into the current in the manner of a windsock. In erect or seafloor-parallel recumbent positions, the frond would be exposed to the water column as a foliate feeding structure. This could result in ecological benefits from resource partitioning and reduced competition in ecosystems with crowded lower tiers. Both absorption of dissolved matter and filter feeding strategies are congruent with tiered epifaunal models (Clapham and Narbonne, 2002; Ghisalberti et al., 2014).

While presumed erect or recumbent positions are plausible body postures for some taxa, it remains uncertain for some others which pose important challenges to the interpretation of Ediacaran tiering models (McIlroy et al., 2021). The stems that connect holdfasts and fronds in arboreomorphs (e.g. *Arborea*, *C. concentricus*, *C. spinosus*) are poorly preserved (**Figure 2**). This is likely due to the arching of the stem as fronds are felled from their erect or recumbent position onto the seafloor (cf. Glaessner and Daily, 1959; Glaessner, 1984; McIlroy et al., 2021). In contrast, *C. procerus* generally has a long well-preserved stem with a semicircular cross section and no supporting evidence for erect or recumbent stem positions (**Figure 6**). This suggests that in life the stem of *C. procerus* lay flat on the seafloor implying exposure of the lower surface to sedimentary microbial ecosystems and pore water hypoxia (cf. Dufour and McIlroy, 2017). The stem could have therefore had other functions than merely structural support, possibly establishing symbiotic relationships with chemosynthetic, sulphur-oxidising bacteria to mitigate the elevated toxicity (McIlroy et al., 2021). Whether the stem of a *Charniodiscus* was reclined on/in the sediment or held in a recumbent position just above it, there is significant potential for sediment to become trapped inside the sub-conical frondose portion. This is especially true during periods of rapid sediment influx, accumulating at a level above the stem and into which the distal portion of the branches might become impressed (**Figures 3A—green**).

C. procerus shows flat proximal sections of the primary branches meeting the central axis at nearly right angles providing support for the distally curved section of the same branches in a similar fashion to other *Charniodiscus* specimens (**Figures 7, 8**). These branches were curved inward and apically directed, forming a reclined sub-conical or erect frondose portion whose lumen would be exposed to the water column. The sub-conical structure would funnel water in a similar manner as in seafloor-parallel recumbent positions.

It has been considered that Ediacaran fronds with primary branches annexed together or having a “backing sheet” could not have fed like the Pennatulacea, which require water flow between

primary branches (Seilacher, 1992). Our functional morphological understanding of *Charniodiscus concentricus* as a recumbent (sediment-parallel) or erect frond allows funneled flow between the branches of the frond, which was held slightly above the benthic boundary layer. The branches of *C. concentricus* are interpreted as fascicled, loosely constrained branches not supported by a backing sheet of tissue similar to some Shibatan charnids (Xiao et al., 2021, **Figures 5C–E**) or *Arborea* spp. However, due to the lack of preserved specialized zooids or feeding structures, the feeding mechanisms of *Charniodiscus* and other arboreomorphs remain uncertain but may have included osmotrophy and/or filter feeding (Laflamme et al., 2018).

Taxonomic Consideration of Other *Charniodiscus* Species

Throughout the ~35 My of evolutionary history of the Ediacaran biota we observe a contrast between highly unique morphological disparity (Shen et al., 2008) and low taxonomic diversity (Waggoner, 2003). This has led to the creation of numerous monospecific genera, a lack of unified consensus regarding higher taxonomic ranks (Xiao and Laflamme, 2009), and genus and clade-level taxonomic inconsistencies (Brasier and Antcliffe, 2009; Liu et al., 2015; Laflamme et al., 2018; Wang et al., 2020).

Cladistic classification for Ediacaran macrofossils based on branching architecture, body symmetry, and growth parameters (Erwin et al., 2011) recognized the clade Arboreomorpha, which encompasses bifoliate fronds bearing annexed primary branches attached to a dorsal sheet. Those primary branches were considered to have orthogonal teardrop-shaped secondary branches. All species of *Charniodiscus* and *Arborea* were included in this clade except for *C. concentricus*. Dececchi et al. (2017) supported Erwin et al. (2011), using autapomorphically-constructed clades, in the recognition of the clade Arboreomorpha, which was defined as having spherical to hemispherical secondary branches with no further orders of branching and lacking a modular petalodium. We consider these transverse ridges to be semicircular. Arboreomorpha was also reported to show conserved inflating growth patterns and diagnostic numbers of branches (Laflamme et al., 2004).

In the light of our work there are several bifoliate planar arboreomorphs that require further taxonomic revision, including:

- 1) *C. longus* Glaessner and Wade, 1966 (formerly *Rangia longa* and *Glaessnerina longa*; Fedonkin et al., 2007), an elongate and lanceolate frond bearing at least 40 primary branches and uniform secondary subdivisions without a preserved stem or basal disc (Glaessner and Wade, 1966; Laflamme et al., 2004; Wang et al., 2020). The branching is clearly *Arborea*-like and there appears to be a prominent backing sheet (**Figure 2D**), indicating that it should likely be considered as *Arborea longa*.
- 2) The endemic Newfoundland species *C. spinosus*, which has a backing sheet, a stem that is typically poorly preserved, and an apical spine. Careful photography of the branching allows the recognition of *Arborea*-like branches (**Figure 2C**), suggesting that this species should also be included in *Arborea*, as *Arborea spinosa*.

- 3) Material from the Bonavista Peninsula of Newfoundland described as *C. arboreus* and *C. sp.* by Hofmann et al. (2008) bear little resemblance to the type material of *Arborea* (Glaessner and Wade, 1966) in being non-tapering without prominent holdfasts or robust stems. Specimens from Bonavista are commonly preserved in a manner akin to the tip of *C. concentricus* (i.e., collapse infolding) and should likely be retained within *Charniodiscus*, probably as a distinct species with fewer branches than the holotype.

CONCLUSION

The inferred multifoliate nature of the holotype of *Charniodiscus concentricus* (Dzik, 2002; Brasier and Antcliffe, 2009) made it considerably different from all the other (bifoliate) species of the genus. Newfoundland species of *Charniodiscus* have hitherto been retained in the genus, but separated from *Arborea* based on the inferred rangeomorph-like branching architecture of *Charniodiscus* (Brasier and Antcliffe, 2009). Our taphonomic and morphological reinterpretation of *Charniodiscus concentricus* allows the resolution of existing taxonomic inconsistencies. The pronounced curvature of the outfolded branches, taken alongside the straight basally-directed infolded collapsed branches of the tip, the observed differential branch folding, and the preservation of sediment atop the central axis of much of the frond suggests that the frond was a bifoliate collapsed sub-conical structure with apically directed branches meeting in an-echelon fashion characterized by *Arborea*-type branching lacking a continuous sheet of tissue.

Based on the poorly preserved stem in *Charniodiscus concentricus*—likely due to the arching that would occur during the felling of the frond to the seafloor from its erect or recumbent life position—and the underfolding of the branches under the stem we infer an erect or recumbent lifestyle as the only plausible options for life attitude. *C. concentricus* as reconstructed herein (Figure 5) could have functioned biomechanically either erect in the water column like a cone on a stick, similar to the mode of life of many pennatulacean cnidarians, or if held in a recumbent position parallel to the seafloor the cone might have functioned to funnel water over and possibly between the branches.

Charniodiscus procerus generally has high relief well-preserved stems with no additional evidence for erect or recumbent body postures in life. This is likely due to a dominantly reclining position of the organism, which would have had the stem laid upon or even partly embedded within the matground. This challenges the paradigm that all Ediacaran stemmed taxa were erect fronds in the water column (e.g. Vixseboxse et al., 2021). Similarly, the distal curved portions of the primary branches of *C. procerus* are interpreted—by analogy with *C. concentricus* and *C. sp.* from Spaniards Bay—as casts of the impressions made by the external surfaces of the curved portion of the conical frond smothering the surrounding matground due to post-mortem outfolding.

We propose emendation of the generic diagnosis of *Charniodiscus* to encompass bifoliate arboreomorphs with sub-

conical petalodiums, while retaining *Arborea* for the bifoliate planar arboreomorphs with a backing sheet. As such we infer two distinct frond morphologies: 1) sub-conical fronds with arboreomorph branching which we consider to be typical of *Charniodiscus*; versus 2) planar foliate sheets of the genus *Arborea* in which the arboreomorph branching is considered to be on the front surface. Our model supports the retention of both *Charniodiscus* and *Arborea*, solving the existing taxonomic inconsistencies. Additionally, we find no evidence of rangeomorph-type fractal branching in *Charniodiscus* and thus reject its inclusion in the Rangeomorpha.

The non-vertical (recumbent or reclining) life attitude invoked for *Charniodiscus* spp. herein is based on our improved taphonomic understanding of the genus and is consistent with other proposals for Ediacaran fronds (Laflamme and Narbonne, 2008; Laflamme et al., 2018). We also note here that the presence of a backing sheet in *Arborea* spp. would be a significant impediment to flow increasing the aspect ratio of the frond. This suggests that it might also be an adaptation to modify the life attitude of *Arborea* spp. to become recumbent in a current, allowing for current orientation of the frond and increased turbulent flow over the frond surface.

DATA AVAILABILITY STATEMENT

The original contributions presented in the study are included in the article/supplementary material, further inquiries can be directed to the corresponding author.

AUTHOR CONTRIBUTIONS

DP-P and DM conceived the project. DP-P and CM constructed figures. DP-P, CM, RT, RN, and DM analyzed the data and prepared the manuscript.

FUNDING

Funding was provided to D. Mc. by Discovery Grant and Discovery Accelerator Supplement awards from the Natural Sciences and Engineering Research Council, which are acknowledged with thanks.

ACKNOWLEDGMENTS

Jenna Neville and Giovanni Pasinetti are thanked for their assistance through both discussions related to this topic and their support in the field. We acknowledge with thanks the Oxford University Museum of Natural History for access to the Brasier collections. Fieldwork and fossil casting in Newfoundland was conducted under permit from the Parks and Natural Areas Division of the Government of Newfoundland and Labrador. This project was supported by an NSERC Discovery Grant and Discovery Accelerator Supplement to DMc.

REFERENCES

- Antcliffe, J. B., and Brasier, M. D. (2008). *Charnia* at 50: Developmental Analysis of Ediacaran Fronds. *Paleontology* 64 (6), 1753–2284. doi:10.1111/j.1475-4983.2007.00738.x
- Borchardt, D. V., and Nesson, L. A. (1999). New Records of Metaphytes from the Vendian (Precambrian) of Zimnii Bereg of the White Sea. *Tr. Zool. Inst. Ross. Akad. Nauk.* 277, 50–57.
- Brasier, M., and Antcliffe, J. (2004). Decoding the Ediacaran Enigma. *Science* 305, 1115–1117. doi:10.1126/science.1102673
- Brasier, M. D., and Antcliffe, J. B. (2009). Evolutionary Relationships within the Avalonian Ediacara Biota: New Insights from Laser Analysis. *J. Geol. Soc. Lond.* 166 (2), 363–384. doi:10.1144/0016-76492008-011
- Brasier, M. D., Antcliffe, J. B., and Liu, A. G. (2012). The Architecture of Ediacaran Fronds. *Paleontology* 55 (5), 1105–1124. doi:10.1111/j.1475-4983.2012.01164.x
- Brasier, M. D., Liu, A. G., Menon, L., Matthews, J. J., McIlroy, D., and Wacey, D. (2013). Explaining the Exceptional Preservation of Ediacaran Rangeomorphs from Spaniard's Bay, Newfoundland: A Hydraulic Model. *Precambrian Res.* 231, 122–135. doi:10.1016/j.precamres.2013.03.013
- Burzynski, G., and Narbonne, G. M. (2015). The Discs of Avalon: Relating Discoid Fossils to Frondose Organisms in the Ediacaran of Newfoundland. *Can. Palaeogeogr. Palaeocl.* 434, 34–45. doi:10.1016/j.palaeo.2015.01.014
- Clapham, M. E., and Narbonne, G. M. (2002). Ediacaran Epifaunal Tiering. *Geol* 30, 627–630. doi:10.1130/0091-7613(2002)030<0627:eeet>2.0.co;2
- Decocchi, T. A., Narbonne, G. M., Greentree, C., and Laflamme, M. (2017). Relating Ediacaran Fronds. *Paleobiology* 43 (2), 171–180. doi:10.1017/pab.2016.54
- Dufour, S. C., and McIlroy, D. (2017). Ediacaran Pre-placozoan Diploblasts in the Avalonian Biota: The Role of Chemosynthesis in the Evolution of Early Animal Life. *Geol. Soc. Lond. Spec. Publ.* 448, 211–219. doi:10.1144/sp448.5
- Dunn, F. S., Liu, A. G., and Gehling, J. G. (2019). Anatomical and Ontogenetic Reassessment of the Ediacaran Frond *Arborea arborea* and its Placement within Total Group Eumetazoa. *Paleontology* 62, 851–865. doi:10.1111/pala.12431
- Dzik, J. (2002). Possible Ctenophoran Affinities of the Precambrian “sea-pen” *Rangea*. *J. Morphol.* 252, 315–334. doi:10.1002/jmor.1108
- Erwin, D. H., Laflamme, M., Tweedt, S. M., Sperling, E. A., Pisani, D., and Peterson, K. J. (2011). The Cambrian Conundrum: Early Divergence and Later Ecological success in the Early History of Animals. *Science* 334 (6059), 1091–1097. doi:10.1126/science.1206375
- Fedonkin, M. A., Gehling, J. G., Grey, K., Narbonne, G. M., and Vickers-Rich, P. (2007). *The Rise of Animals: Evolution and Diversification of the Kingdom Animalia*. Baltimore, MD, United States: JHU Press.
- Fedonkin, M. A. (1985). “Systematic Description of Vendian Metazoa,” in *The Vendian System: Historic-Geological and Palaeontological Basis*. Editor B. S. Sokolov and A. B. Ivanovskiy (Paleontology/Moscow: Nauka), 1, 70–107.
- Ford, T. D. (1958). Pre-cambrian Fossils from Charnwood Forest. *Proc. Yorkshire Geol. Soc.* 31, 211–217. doi:10.1144/pygs.31.3.211
- Ford, T. D. (1962). The Oldest Fossils. *New Sci.* 15, 191–194.
- Ford, T. D. (1963). The Pre-cambrian Fossils of Charnwood Forest. *Trans. Leicester Lit. Phil. Soc.* 57, 57–62.
- Gehling, J. G. (1999). Microbial Mats in Terminal Proterozoic Siliciclastics: Ediacaran Death Masks. *Palaio* 14, 40–57. doi:10.2307/3515360
- Gehling, J. G. (1991). The Case for Ediacaran Fossil Roots to the Metazoan Tree. *Mem. Geol. Surv. India.* 20, 181–224.
- Ghisalberti, M., Gold, D. A., Laflamme, M., Clapham, M. E., Narbonne, G. M., Summons, R. E., et al. (2014). Canopy Flow Analysis Reveals the Advantage of Size in the Oldest Communities of Multicellular Eukaryotes. *Curr. Biol.* 24, 305–309. doi:10.1016/j.cub.2013.12.017
- Glaessner, M. F., and Daily, B. (1959). The Geology and Late Precambrian Fauna of the Ediacara Fossil reserve. *Rec. Aust. Mus.* 13, 369–401.
- Glaessner, M. F. (1984). *The Dawn of Animal Life: A Biohistorical Study*. Cambridge, United Kingdom: Cambridge University Press.
- Glaessner, M. F., and Wade, M. (1966). The Late Precambrian Fossils from Ediacara, South Australia. *Paleontology* 9, 599–628.
- Grazhdankin, D. (2014). Patterns of Evolution of the Ediacaran Soft-Bodied Biota. *J. Paleontol.* 88, 269–283. doi:10.1666/13-072
- Herringshaw, L. G., Callow, R. H., and McIlroy, D. (2017). Engineering the Cambrian Explosion: the Earliest Bioturbators as Ecosystem Engineers. *Geol. Soc. Lond. Spec. Publ.* 448, 369–382. doi:10.1144/sp448.18
- Hofmann, H. J., O'Brien, S. J., and King, A. F. (2008). Ediacaran Biota on Bonavista Peninsula, Newfoundland, Canada. *J. Paleontol.* 82, 1–36. doi:10.1666/06-087.1
- Ivantsov, A. Y. (2016). Reconstruction of *Charniodiscus yorgensis* (Macrobiota from the Vendian of the White Sea. *Paleontol. J.* 50, 1–12. doi:10.1134/s0031030116010032
- Jenkins, R. J. (1992). “Functional and Ecological Aspects of Ediacaran Assemblages,” in *Origin and Early Evolution of the Metazoa* (Boston, MA: Springer).
- Jenkins, R. J. F., and Gehling, J. G. (1978). A Review of the Frond-like Fossils of the Ediacara Assemblage. *Rec. Aust. Mus.* 17, 347–359.
- Jensen, S., Höglström, A. E. S., Almond, J., Taylor, W. L., Meinhold, G., Høyberget, M., et al. (2018). Scratch Circles from the Ediacaran and Cambrian of Arctic Norway and Southern Africa, with a Review of Scratch circle Occurrences. *Bull. Geosci.* 93, 287–304. doi:10.3140/bull.geosci.1685
- Kennington, C., and Wilby, P. R. (2014). *Of Time and Taphonomy: Preservation in the Ediacaran*. [Bookchapter]. London, United Kingdom: Cambridge University Press. Available at: <https://www.repository.cam.ac.uk/handle/1810/247083>.
- Kushida, Y., Higashiji, T., and Reimer, J. D. (2020). First Observation of Mole-like Burrowing Behavior Observed in a Sea Pen. *Mar. Biodivers.* 50, 1–9. doi:10.1007/s12526-020-01054-y
- Laflamme, M., Flude, L. I., and Narbonne, G. M. (2012). Ecological Tiering and the Evolution of a Stem: the Oldest Stemmed Frond from the Ediacaran of Newfoundland, Canada. *J. Paleontol.* 86, 193–200. doi:10.1666/11-044.1
- Laflamme, M., Gehling, J. G., and Droser, M. L. (2018). Deconstructing an Ediacaran Frond: Three-Dimensional Preservation of *Arborea* from Ediacara, South Australia. *J. Paleontol.* 92, 323–335. doi:10.1017/jpa.2017.128
- Laflamme, M., Narbonne, G. M., and Anderson, M. M. (2004). Morphometric Analysis of the Ediacaran Frond *Charniodiscus* from the Mistaken Point Formation. *Newfoundland. J. Paleontol.* 78, 827–837. doi:10.1666/0022-3360(2004)078<0827:maotef>2.0.co;2
- Laflamme, M., and Narbonne, G. M. (2008). Ediacaran Fronds. *Paleogeogr. Palaeoclimatol. Palaeoecol.* 258, 162–179. doi:10.1016/j.palaeo.2007.05.020
- Liu, A. G. (2016). Framboidal Pyrite Shroud Confirms the ‘death Mask’ Model for Moldic Preservation of Ediacaran Soft-Bodied Organisms. *Palaio* 31, 259–274. doi:10.2110/palo.2015.095
- Liu, A. G., Kennington, C. G., and Mitchell, E. G. (2015). Remarkable Insights into the Paleocology of the Avalonian Ediacaran Macrobiota. *Gondwana Res.* 27, 1355–1380. doi:10.1016/j.gr.2014.11.002
- Liu, A. G., McIlroy, D., Antcliffe, J. B., and Brasier, M. D. (2011). Effaced Preservation in the Ediacara Biota and its Implications for the Early Macrofossil Record. *Paleontology* 54, 607–630. doi:10.1111/j.1475-4983.2010.01024.x
- Liu, A. G., McIlroy, D., and Brasier, M. D. (2010). First Evidence for Locomotion in the Ediacara Biota from the 565 Ma Mistaken Point Formation. *Newfoundland. Geology* 38, 123–126. doi:10.1130/g30368.1
- Liu, A. G., Menon, L. R., Shields, G. A., Callow, R. H., and McIlroy, D. (2017). Martin Brasier's Contribution to the Palaeobiology of the Ediacaran–Cambrian Transition. *Geol. Soc. Lond. Spec. Publ.* 448, 179–193. doi:10.1144/sp448.9
- Mapstone, N. B., and McIlroy, D. (2006). Ediacaran Fossil Preservation: Taphonomy and Diagenesis of a Discoid Biota from the Amadeus Basin, central Australia. *Precambrian Res.* 149, 126–148. doi:10.1016/j.precamres.2006.05.007
- Matthews, J. J., Liu, A. G., Yang, C., McIlroy, D., Levell, B., and Condon, D. J. (2021). Achnostratigraphic Framework for the Rise of the Ediacaran Macrobiota: New Constraints from Mistaken Point Ecological Reserve. *Newfoundland. Bull. Geol. Soc. Am.* 133, 612–624. doi:10.1130/gsab.s.12509984.v1
- McIlroy, D., Brasier, M. D., and Lang, A. S. (2009). Smothering of Microbial Mats: Implications for the Ediacaran Biota. *J. Geol. Soc. Lond.* 166, 1117–1121. doi:10.1144/0016-76492009-073
- McIlroy, D., Brasier, M. D., and Moseley, J. B. (1998). The Proterozoic–Cambrian Transition within the ‘Charnian Supergroup’ of central England and the Antiquity of the Ediacara Fauna. *J. Geol. Soc. Lond.* 155, 401–411. doi:10.1144/gsjgs.155.2.0401
- McIlroy, D., Dufour, S. C., Taylor, R., and Nicholls, R. (2021). The Role of Symbiosis in the First Colonization of the Seafloor by Macrobiota: Insights

- from the Oldest Ediacaran Biota (Newfoundland, Canada). *Biosystems* 205, 104413. doi:10.1016/j.biosystems.2021.104413
- McIlroy, D., Hawco, J., McKean, C., Nicholls, R., Pasinetti, G., and Taylor, R. (2020). Palaeobiology of the Reclining Rangeomorph *Beothukis* from the Ediacaran Mistaken Point Formation of southeastern Newfoundland. *Geol. Mag.*, 1–15. doi:10.1017/s0016756820000941
- McIlroy, D., and Horák, J. M. (2006). “Neoproterozoic: the Late Precambrian Terranes that Formed Eastern Avalonia,” in *The Geology of England and Wales*. Editors P. R. Brechley and P. F. Rawson (Bath, UK: Geological Society Publishing House), 9–25.
- McIlroy, D., and Logan, G. A. (1999). The Impact of Bioturbation on Infaunal Ecology and Evolution during the Proterozoic-Cambrian Transition. *Palaios* 14, 58–72.
- Murphy, J. B., Pisarevsky, S. A., Nance, R. D., and Keppie, J. D. (2004). Neoproterozoic–Early Paleozoic Evolution of Peri-Gondwanan Terranes: Implications for Laurentia-Gondwana Connections. *Int. J. Earth Sci.* 93, 659–682. doi:10.1007/s00531-004-0412-9
- Narbonne, G. M., and Hofmann, H. J. (1987). Ediacaran Biota of the Wernecke Mountains, Yukon, Canada. *Palaeontology* 30, 647–676.
- Narbonne, G. M., Laflamme, M., Greentree, C., and Trusler, P. (2009). Reconstructing a Lost World: Ediacaran Rangeomorphs from Spaniard's Bay, Newfoundland. *J. Paleontol.* 83, 503–523. doi:10.1666/08-072r1.1
- Narbonne, G. M. (2004). Modular Construction of Early Ediacaran Complex Life Forms. *Science* 305, 1141–1144. doi:10.1126/science.1099727
- Narbonne, G. M. (2005). The Ediacara Biota: Neoproterozoic Origin of Animals and Their Ecosystems. *Annu. Rev. Earth Pl. Sc.* 33, 421–442. doi:10.1146/annurev.earth.33.092203.122519
- Noble, S. R., Condon, D. J., Carney, J. N., Wilby, P. R., Pharaoh, T. C., and Ford, T. D. (2015). U–pb Geochronology and Global Context of the Charnian Supergroup, UK: Constraints on the Age of Key Ediacaran Fossil Assemblages. *Bull. Geol. Soc. Am.* 127, 250–265. doi:10.1130/b31013.1
- Seilacher, A. (1992). Vendobionta and Psammocorallia: Lost Constructions of Precambrian Evolution. *J. Geol. Soc. Lond.* 149, 607–613. doi:10.1144/gsjgs.149.4.0607
- Shen, B., Dong, L., Xiao, S., and Kowalewski, M. (2008). The Avalon Explosion: Evolution of Ediacara Morphospace. *Science* 319, 81–84. doi:10.1126/science.1150279
- Steiner, M., and Reitner, J. (2001). Evidence of Organic Structures in Ediacara-type Fossils and Associated Microbial Mats. *Geology* 29, 1119–1122. doi:10.1130/0091-7613(2001)029<1119:eoosie>2.0.co;2
- Tarhan, L. G., Droser, M. L., Gehling, J. G., and Dzaugis, M. P. (2015). Taphonomy and Morphology of the Ediacara Form Genus *Aspidella*. *Precambrian Res.* 257, 124–136. doi:10.1016/j.precamres.2014.11.026
- Taylor, R. S., Matthews, J. J., Nicholls, R., and McIlroy, D. (2021). A Re-assessment of the Taxonomy, Palaeobiology and Taphonomy of the Rangeomorph Organism *Hapsidophyllas flexibilis* from the Ediacaran of Newfoundland, Canada. *Pal. Z.*, 95 (2), 187–207. doi:10.1007/s12542-020-00537-4
- Vixseboxse, P. B., Kenchington, C. G., Dunn, F. S., and Mitchell, E. G. (2021). Orientations of Mistaken Point Fronds Indicate Morphology Impacted Ability to Survive Turbulence. *Front. Earth Sci.* 9, 762824. doi:10.3389/feart.2021.762824
- Wade, M. (1968). Preservation of Soft-bodied Animals in Precambrian Sandstones at Ediacara, South Australia. *Lethaia* 1, 238–267. doi:10.1111/j.1502-3931.1968.tb01740.x
- Waggoner, B. (2003). The Ediacaran Biotas in Space and Time. *Integr. Comp. Biol.* 43, 104–113. doi:10.1093/icb/43.1.104
- Wang, X., Pang, K., Chen, Z., Wan, B., Xiao, S., Zhou, C., et al. (2020). The Ediacaran Frondose Fossil *Arborea* from the Shibantan limestone of South China. *J. Paleontol.* 94, 1034–1050. doi:10.1017/jpa.2020.4
- Wen, B., Evans, D. A., Anderson, R. P., and McCausland, P. J. (2020). Late Ediacaran Paleogeography of Avalonia and the Cambrian Assembly of West Gondwana. *Earth Planet. Sc. Lett.* 552, 116591. doi:10.1016/j.epsl.2020.116591
- Wilby, P. R., Carney, J. N., and Howe, M. P. (2011). A Rich Ediacaran Assemblage from Eastern Avalonia: Evidence of Early Widespread Diversity in the Deep Ocean. *Geology* 39, 655–658. doi:10.1130/g31890.1
- Wood, D. A., Dalrymple, R. W., Narbonne, G. M., Gehling, J. G., and Clapham, M. E. (2003). Paleoenvironmental Analysis of the Late Neoproterozoic Mistaken Point and Trepassy Formations, southeastern Newfoundland. *Can. J. Earth Sci.* 40, 1375–1391. doi:10.1139/e03-048
- Xiao, S., Chen, Z., Pang, K., Zhou, C., and Yuan, X. (2021). The Shibantan Lagerstätte: Insights into the Proterozoic–Phanerozoic Transition. *J. Geol. Soc. Lon* 178 (1), jgs2020–135. doi:10.1144/jgs2020-135
- Xiao, S., and Laflamme, M. (2009). On the Eve of Animal Radiation: Phylogeny, Ecology and Evolution of the Ediacaran Biota. *Trends Ecol. Evol.* 24, 31–40. doi:10.1016/j.tree.2008.07.015
- Xiao, S., Yuan, X., Steiner, M., and Knoll, A. H. (2002). Macroscopic Carbonaceous Compressions in a Terminal Proterozoic Shale: a Systematic Reassessment of the Miaohé Biota, South China. *J. Paleontol.* 76, 347–376. doi:10.1017/s002236000041743

Conflict of Interest: The authors declare that the research was conducted in the absence of any commercial or financial relationships that could be construed as a potential conflict of interest.

Publisher's Note: All claims expressed in this article are solely those of the authors and do not necessarily represent those of their affiliated organizations, or those of the publisher, the editors and the reviewers. Any product that may be evaluated in this article, or claim that may be made by its manufacturer, is not guaranteed or endorsed by the publisher.

Copyright © 2022 Pérez-Pinedo, McKean, Taylor, Nicholls and McIlroy. This is an open-access article distributed under the terms of the Creative Commons Attribution License (CC BY). The use, distribution or reproduction in other forums is permitted, provided the original author(s) and the copyright owner(s) are credited and that the original publication in this journal is cited, in accordance with accepted academic practice. No use, distribution or reproduction is permitted which does not comply with these terms.



What Happens Between Depositional Events, Stays Between Depositional Events: The Significance of Organic Mat Surfaces in the Capture of Ediacara Communities and the Sedimentary Rocks That Preserve Them

Mary L. Droser^{1*}, Scott D. Evans², Lidya G. Tarhan³, Rachel L. Surprenant¹, Ian V. Hughes⁴, Emmy B. Hughes⁵ and James G. Gehling⁶

OPEN ACCESS

Edited by:

Dermeval Aparecido Do Carmo,
University of Brasilia, Brazil

Reviewed by:

Mao Luo,
Nanjing Institute of Geology and
Paleontology (CAS), China
Huan Cui,
Université de Paris, France

*Correspondence:

Mary L. Droser
Mary.droser@ucr.edu

Specialty section:

This article was submitted to
Paleontology,
a section of the journal
Frontiers in Earth Science

Received: 30 November 2021

Accepted: 31 January 2022

Published: 23 February 2022

Citation:

Droser ML, Evans SD, Tarhan LG, Surprenant RL, Hughes IV, Hughes EB and Gehling JG (2022) What Happens Between Depositional Events, Stays Between Depositional Events: The Significance of Organic Mat Surfaces in the Capture of Ediacara Communities and the Sedimentary Rocks That Preserve Them.
Front. Earth Sci. 10:826353.
doi: 10.3389/feart.2022.826353

¹Department of Earth and Planetary Sciences, University of California, Riverside, Riverside, CA, United States, ²Department of Geosciences, Virginia Tech, Blacksburg, VA, United States, ³Department of Earth and Planetary Sciences, Yale University, New Haven, CT, United States, ⁴Section of Ecology, Behavior and Evolution, Division of Biological Sciences, University of California, San Diego, San Diego, CA, United States, ⁵Department of Earth and Atmospheric Sciences, Georgia Institute of Technology, Atlanta, GA, United States, ⁶Department of Palaeontology, South Australia Museum, Adelaide, SA, Australia

In the absence of complex, bioturbating organisms, the seafloor during the Precambrian was covered in widespread organic matgrounds. The greatest diversity and complexity of organic mat textures occur in the Ediacaran fossil record as exemplified by the Ediacara Member of the Rawnsley Quartzite, which crops out in and around the Flinders Ranges, South Australia. This succession unambiguously demonstrates that heterogeneous mats coexisted with and were central to the ecology and biology of the Ediacara Biota. Excavation of 33 fossiliferous beds with varying types and extents of organosedimentary surface textures provide the opportunity to utilize this record to develop criteria to evaluate the maturity or extent of growth of Ediacaran matgrounds and, using these characteristics, to examine the relationship between mat type, mat maturity and Ediacara Biota community structure. Based on the assumption that mat maturity represents an indicator of the duration of time between burial events, we can test predictions about the relationship between mat maturity and community development. We find that mat maturity, rather than the mat type itself, more strongly influenced the distribution of taxa and the development of Ediacara macroorganism communities. Using a ranked Mat Maturity Index, we find that although density of macroscopic body fossils and genus diversity correlate with mat maturity, evenness does not. We additionally find that the sessile taxa *Obolus* and *Coronacollina* are restricted to surfaces with mature mats whereas all other Ediacaran macrobiota show no connection to mat occurrence and maturity. However, we do observe that large *Dickinsonia* are more likely to occur on surfaces recording mature matgrounds. The exceptional record of mat surfaces preserved in the Flinders Ranges area demonstrates that, in addition to the apparent ecological role played by mat surfaces in Ediacaran communities, they were also

likely a significant component of the Ediacara Member biomass and were integral to community function.

Keywords: Ediacara, organic mat, paleoecology, Ediacaran, Ediacara Biota

INTRODUCTION

The history of life on Earth spans at least 3.5 billion years, the first 2.5 billion years of which were almost exclusively characterized by microscopic, single-celled organisms. Therefore, if we were to visit Earth at a random point in time, we would be unlikely to find the diversity and complexity of macroscopic life that characterizes the biosphere today. In the absence of complex, bioturbating organisms, the Precambrian seafloor was covered by widespread organic matgrounds, consisting of aggregates of primarily microscopic forms. These are readily identified in the geologic record as distinct macroscopic sedimentary structures, features

such as “microbially induced sedimentary structures” (MISS; Noffke, 2009)—e.g., microbial laminations and organosedimentary textures preserved on bedding planes—and organic microfossils that together represent definitive evidence of Precambrian life.

The greatest diversity and complexity of organic mat textures in the fossil record occur in successions of Ediacaran age (635–541 Ma; e.g., Bose et al., 2012; Gehling, 1999; Hagadorn and Bottjer, 1999; Porada and Bouougri, 2007; Sarkar et al., 2011). The Ediacaran stratigraphic record is further characterized by textured organic surfaces (TOS; Gehling and Droser, 2009) which consist of organosedimentary textures recording the presence of

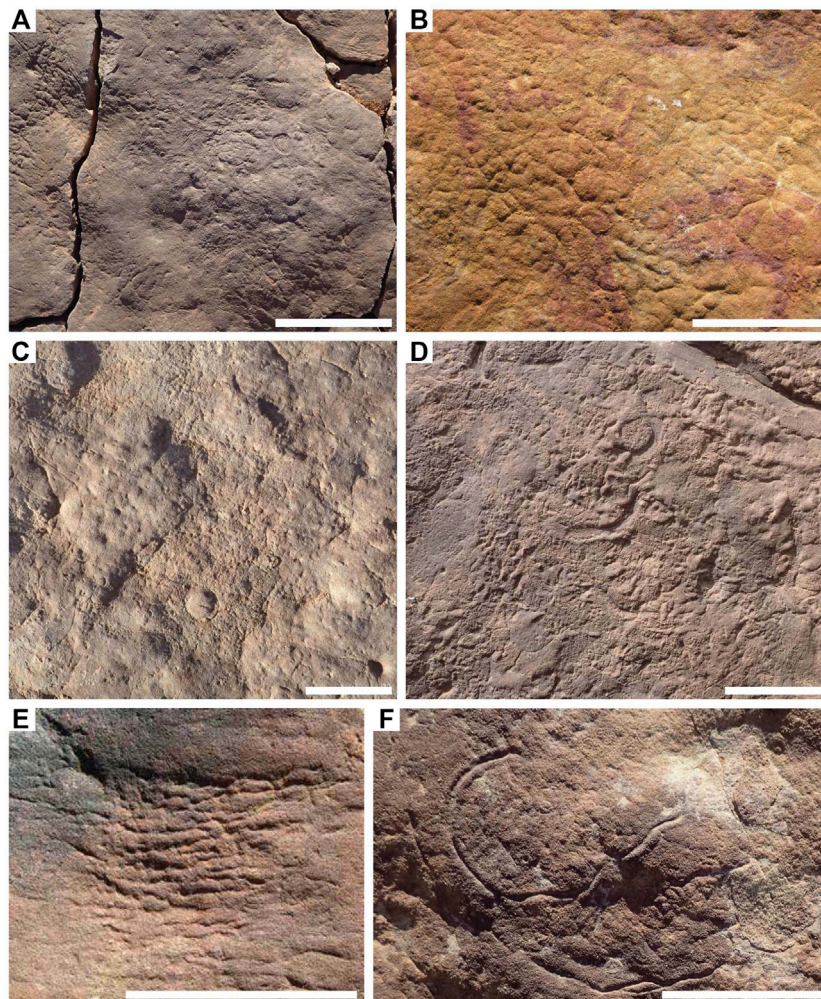


FIGURE 1 | Textured organic surfaces (TOS) on excavated beds from the Ediacara Member and the informal Nilpena Member. **(A)** TOS on bedding plane TB-ARB. **(B)** Elephant skin TOS. **(C)** TOS on bedding plane 1T-F-Annex. **(D)** TOS on bedding plane WS-Sub. **(E)** Weave on TC-MM3 bedding plane. **(F)** *Helminthoidichnites* preserved in hyporelief on the bedding plane of TB-Sh2. Scale bars = 5 cm.

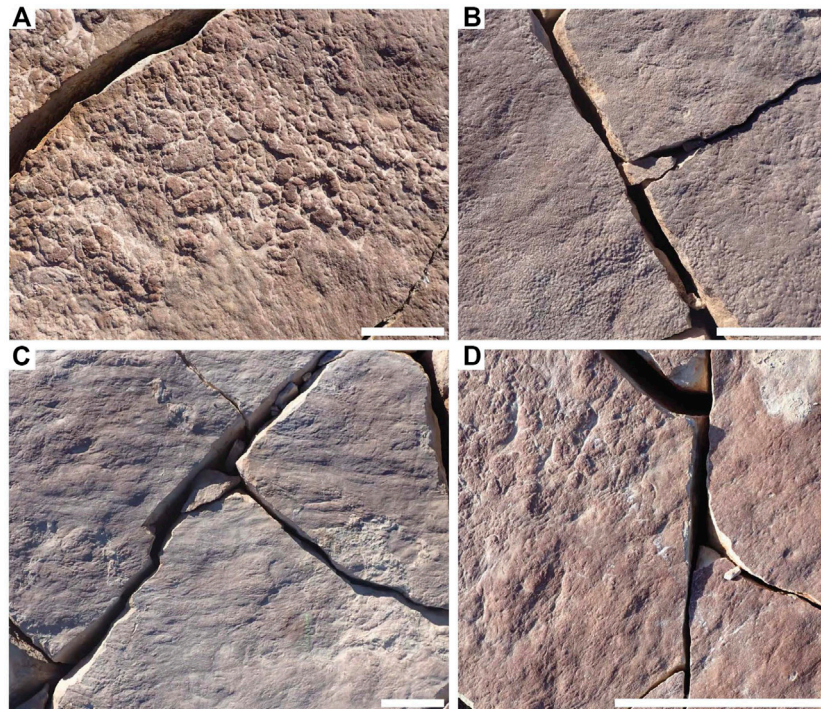


FIGURE 2 | Distinct mat textures preserved in hyporelief on bedding plane LV-Fun. **(A)** Clotted TOS. **(B)** Foam TOS. **(C)** Hair TOS. **(D)** Hair and clotted TOS in distinct patches with sharp transitional boundaries. Scale bars = 5 cm.

not only benthic microbial aggregates but also densely packed communities of macroscopic and multicellular eukaryotic organisms, as well as their interaction with hydrodynamic and sedimentary processes. Multicellular matgrounds included “thickets” of macroscopic, eukaryote-grade tubular organisms such as *Funisia dorothea* (Droser and Gehling, 2008; Surprenant et al., 2020). TOS thus refers to the sedimentological expression of these matgrounds and the processes impacting them.

Heterogenous mats coexisted with and were central to the ecology and biology of the Ediacara Biota, the oldest macroscopic community-forming organisms in the fossil record (e.g., Xiao and Laflamme, 2009; Droser and Gehling, 2015). Thus, the Ediacaran occupies a unique time in Earth history wherein the earliest complex macrofauna and matgrounds are observed occupying the same environments. Such matgrounds played a pivotal role in rendering the seafloor habitable for the Ediacara Biota, by stabilizing seafloor sediments and providing food and potentially oxygen (e.g., Seilacher, 1999; Gingras et al., 2011; Droser et al., 2017; Gehling and Droser, 2018; Evans et al., 2019; Evans et al., 2020). Furthermore, the organically-stabilized substrate also shaped the sedimentologic and stratigraphic expression of Ediacaran successions by binding sediment, which inhibited reworking and erosion and facilitated the capture of a complete sedimentary and stratigraphic record (Noffke, 2009; Tarhan et al., 2017).

The Ediacara Member of the Rawnsley Quartzite, which crops out throughout the Flinders Ranges area (South Australia), contains the most diverse assemblage of the Ediacara Biota

(Droser et al., 2006; Darroch et al., 2015; Droser and Gehling, 2015; Droser et al., 2019) and sedimentary structures indicative of widespread, heterogenous mats (Figures 1–3; Gehling and Droser, 2009). At the Nilpena Ediacara National Park (NENP), excavation of 40 bedding planes, 33 of which preserve >10 individual macroscopic body fossils, reveals an unprecedented abundance and diversity of *in situ* macroorganism communities and associated microbial mats. Many of the bedding-plane features that are central to defining MISS and TOS (e.g., preservational variability, bed-scale diversity, associated macrobiota, grain size, mineralogy, chemical composition, and sedimentary structures) have previously been described (e.g., Bottjer et al., 2007; Bouougri and Porada, 2007; Carbone and Narbonne, 2014; Corenbilt et al., 2019; Elliott et al., 2011; Hill et al., 2016; Kumar and Ahmad, 2014; Laflamme et al., 2012; Liu et al., 2013; Nettle et al., 2014; Noffke, 2015; Noffke et al., 2002; Noffke, 2009; Sarkar et al., 2008, Sarkar et al., 2016; Tarhan et al., 2017; Vago et al., 2017). Here our aim is to use this record to develop criteria to evaluate the maturity or extent of growth of Ediacaran matgrounds and, using these characteristics, to examine the relationship between mat type and maturity and Ediacara Biota community structure.

GEOLOGICAL SETTING

In the Flinders Ranges area of South Australia, the Ediacara Member of the Rawnsley Quartzite consists of 10–300 m of shallow marine deposits that are characterized by dense and

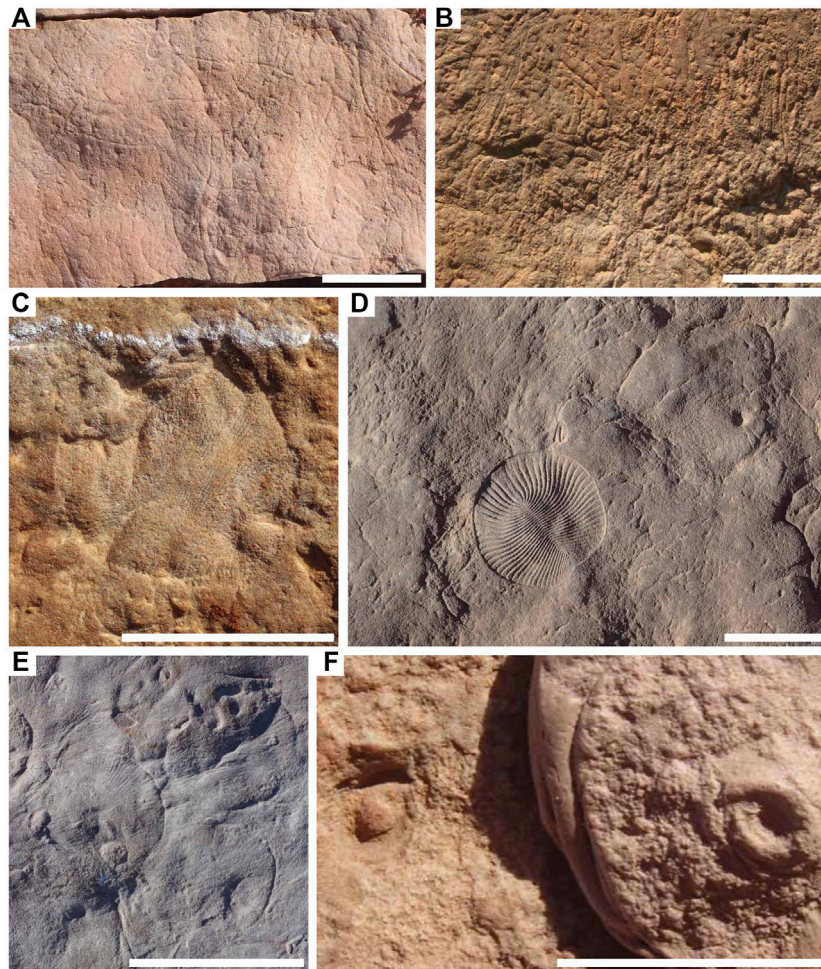


FIGURE 3 | Complex TOS and macrofossils associated with TOS on excavated beds. **(A)** Complex TOS created by *Plexus ricei* aggregates on bed P-SNG1. **(B)** Complex TOS produced by a densely packed population of *Funisia dorothea* on WS-MAB annex surfaces **(C)** *Dickinsonia* body fossil draped over the complex TOS “groove” on STC-X bed. **(D)** *Dickinsonia* body fossil overlying undefined TOS on bedding plane TB-ARB. **(E)** *Dickinsonia* body fossil overlying TOS and associated *Dickinsonia* footprints on TB-BRW bed. **(F)** *Obamius coronatus* fossil (left) and putty mold (right), showing that the organism was embedded within the TOS on LV-Fun bed. Scale bars = 5 cm.

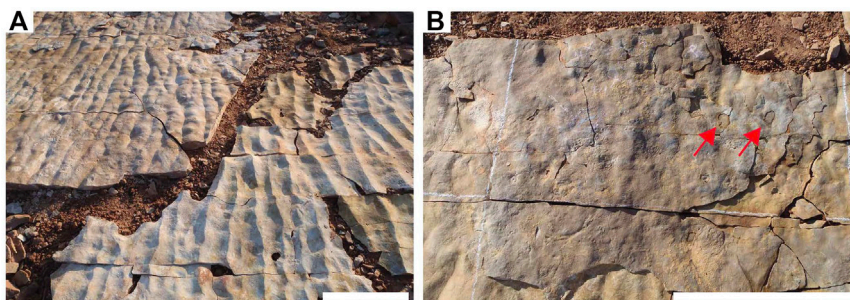
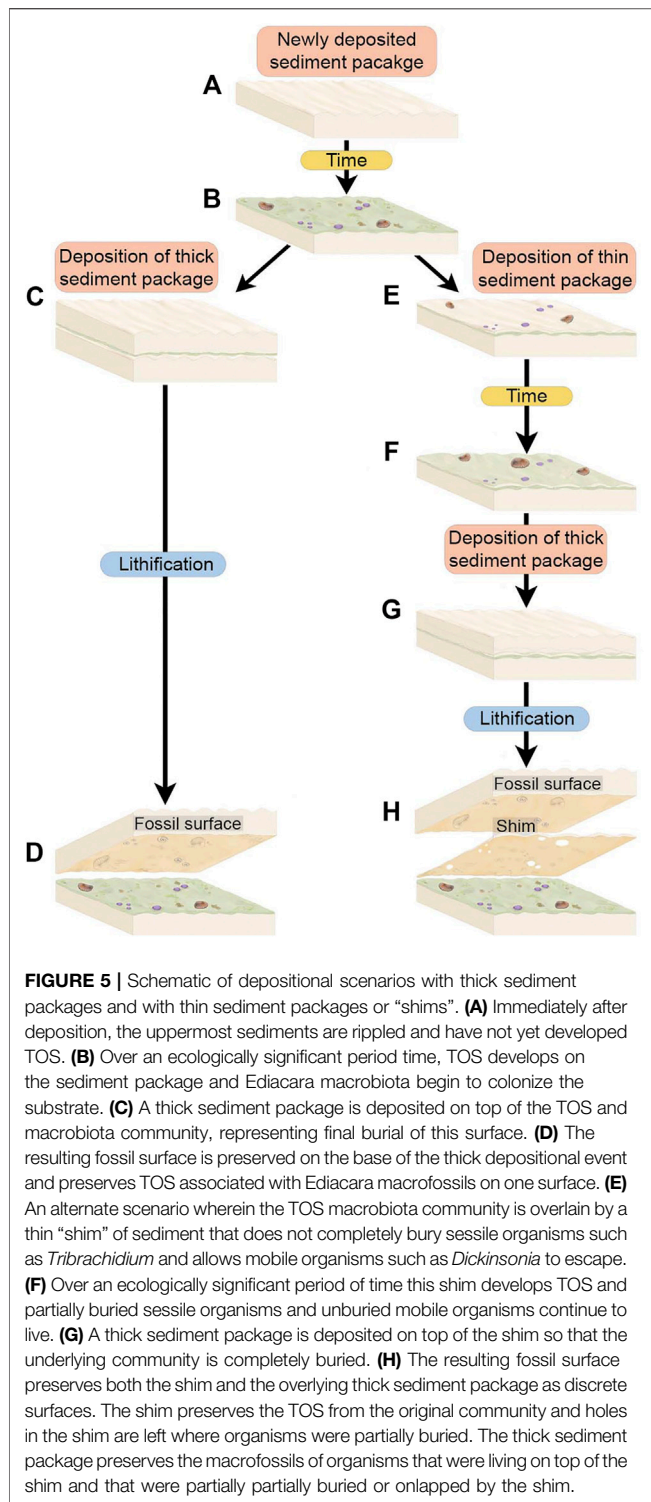


FIGURE 4 | Images of bed STC-G and STC-G Shim. **(A)** Excavated and flipped sole surface of STC-G (left) and top bedding surface of shim underlying STC-G. **(B)** Image of the sole surface of STC-G with STC-G Shim still in place, red arrows denote macrofossils from the underlying bed that were not cast by STC-G Shim but were cast by the thicker STC-G. Scale bars = 50 cm. **(A)** Modified from Tarhan et al. (2017).



well-preserved fossil assemblages of the Ediacara Biota (Gehling, 2000). A new unit, the Nilpena Member, characterized by a basal incision, has been informally described at NENP (Gehling et al., 2019) and includes the upper tens of meters of what was previously included in the Ediacara Member. Within these two

units, benthic communities of the Ediacara Biota and organic matgrounds were preserved by episodic obrution events as casts and molds on the bases of sandstone beds (Gehling, 1999). At NENP, exposures of the Ediacara Member and the informal Nilpena Member have uniquely facilitated the excavation and reconstruction of 40 discrete bedding planes preserving evidence of both macroscopic organisms and widespread organic surfaces. These bedding planes represent, in total, approximately 350 square meters of Ediacaran seafloor, permitting the spatially broad and stratigraphically detailed reconstruction of snapshots of Ediacara communities. Importantly, each bed can be correlated with a cross-sectional reference in outcrop, including bed junctions within a stratigraphic package.

Four facies at NENP are fossil rich and preserve variable depositional environments (Gehling and Droser, 2013; Droser et al., 2019), two of which are readily excavated for bedding-plane analysis. The Oscillation-Rippled Sandstone (ORS) Facies of the Ediacara Member is particularly relevant for deciphering *in situ* relationships between the organic mat and macroscopic organisms of the Ediacara Biota. The ORS Facies consists of mm- to cm-scale beds of symmetrically rippled to interference-rippled, fine- to coarse-grained sandstone representing deposition in relatively shallow water near to above fair-weather wave base (Gehling and Droser, 2013; Tarhan et al., 2017). Over 30 excavated beds at NENP are from this facies and preserve classic members of the Ediacara Biota (e.g., *Dickinsonia*) and abundant, diverse TOS predominantly as external molds on the bases of beds. Within the informal Nilpena Member, the Planar-Laminated and Rip-Up Sandstone (PLRUS) Facies consists of laterally continuous, planar-laminated, fine-grained sandstone beds on which fossils and TOS similarly occur primarily as hyporelief external molds. This facies represents the upper fill of a sub-wave base incision, deposited under unidirectional flow (Gehling and Droser, 2013; Tarhan et al., 2017). There are six excavated beds from this facies. A particularly unusual characteristic of both the ORS and PLRUS Facies is the lack of mud-sized sediment (Gehling, 1999; Gehling and Droser, 2013; Tarhan et al., 2017; Droser et al., 2019); the fossiliferous ORS and PLRUS successions discussed here are completely composed of very fine- to coarse-grained sandstone.

THE SEDIMENTOLOGICAL SIGNATURE OF MATGROUNDS

The Phanerozoic record of marine siliciclastic sedimentary rocks is typically characterized by bed junctions that are erosive, graded (e.g., sandstone overlain by mudstone) or bioturbated. Sequential beds of similar grain size are typically amalgamated. During the Ediacaran, in contrast, sediment mixing by bioturbation was largely absent and the organic binding provided by mats inhibited sediment reworking and erosion, as well as providing a diagenetic interface for authigenic mineralization via the precipitation of silica cements, promoting lithologic separation (Noffke, 2009; Tarhan et al., 2016; Tarhan et al., 2017).

There are a number of distinct sedimentary features that occur within the Ediacara Member and the informal Nilpena Member

TABLE 1 | Criteria for the ranking of original mat maturity.

	Adherence	Ripples	TOS
Mat Maturity Index 1	High	Sharp ripple crests, ripples well preserved	Not visible
Mat Maturity Index 2	None to low	Well-preserved ripples	Visible; may be patchy; little to no topographic relief
Mat Maturity Index 3	None	Muted ripple crests but ripples relatively clear	Visible TOS; may cover entire bed; minimal relief up to 1 mm
Mat Maturity Index 4	None	Muted ripples	Visible TOS; heterogeneity at bed scale; relief up to several mm locally

TABLE 2 | Bed data for taxa and mats. N is the number of discrete body fossils. Dominant TOS type indicated by M micropucker, E elephant skin, W weave, C clotted, F foam, H hair, I complex irregular, *F Funisia*, A algae and *P Plexus*. NA is no visible mat structure. Beds with more than one type of TOS are indicated by the appropriate combination of letters. Mat Maturity Index is based on rankings from **Table 1**. Within each site, beds are listed in stratigraphic order with the younger at the top. The stratigraphic relationship between sites is not known.

Facies	Site	Bed	Area (m ²)	N	Fossil density (indiv/m ²)	Number of genera	Shannon diversity	Simpson (evenness)	TOS type	Mat Maturity Index	
ORS	STC	X	9.0	41	4.6	8	1.56	0.68	F	4	
		J	11.9	54	4.5	6	1.43	0.72	W, I	2	
		I	15.4	90	5.8	7	1.55	0.74	NA	1	
		G	13.2	13	1.0	3	0.83	0.47	NA	1	
		B	10.8	98	9.1	8	0.83	0.36	I, W	2	
		AB	3.4	202	59.4	4	0.14	0.05	F	4	
	TC	Gully	1.1	14	12.7	2	0.26	0.13	NA	2	
		MM5	10.4	80	7.7	8	1.30	0.59	W	3	
		MM4	20.0	214	10.7	7	0.24	0.08	NA	2	
		MM3	19.7	363	18.4	15	1.46	0.63	W	3	
		MM2	10.3	375	36.4	3	0.05	0.02	F	4	
		1T	LS	1.4	51	36.4	8	1.50	0.71	I	3
	NA		4.1	87	21.2	14	2.10	0.81	I	4	
	A		9.5	169	17.8	11	1.67	0.72	I	2	
	F		23.4	302	12.9	14	2.12	0.87	I, E	4	
	T		6.2	252	40.6	9	0.82	0.33	I	4	
	BOF		7.3	440	60.3	9	0.80	0.35	A	4	
	SE	Rugo	3.7	58	15.7	7	1.15	0.56	I	3	
		P	P	2.2	73	33.2	5	1.13	0.63	P	4
			SNG1	1.4	121	86.4	5	0.31	0.13	p	4
			SNG2	1.2	120	100.0	4	0.34	0.16	P	4
	TB		Sh1	4.0	23	5.8	3	0.58	0.30	I, W	2
		BRW	9.3	22	2.4	3	0.85	0.54	I	4	
		ARB	13.1	225	17.2	14	1.94	0.79	I, E, F	4	
PLRUS	West Side (WS)	Parv	7.5	128	17.1	9	1.14	0.62	M	3	
		TBEW	3.5	71	20.3	8	1.46	0.66	M	3	
		Sub	3.9	373	95.6	10	1.12	0.47	M	4	
		MAB	3.3	158	47.9	3	0.14	0.05	F	4	
	LV	Fun ^a	22.4	695 (228)	31.0 (10.2)	15 (14)	1.23 (1.81)	0.53 (0.75)	C, F, H, I	4	

^aData for LV-Fun includes 31 "clusters" of *Funisia* estimated to each contain ~15 individuals, data in () show same analysis without *Funisia*.

as a result of abundant, heterogeneous organic surfaces, as discussed in detail by Tarhan et al. (2017). Widespread organic surfaces, which acted as stabilizing barriers between successive depositional events, also resulted in: 1) the preservation of extremely thin (sub-mm- to mm-scale) beds, which we refer to as shims; 2) textural uniformity, including lack of disparity in grain size, between adjacent beds; 3) lack of Phanerozoic-style amalgamation; 4) lack of erosional bed junctions; and 5) palimpsest ripples or doubly rippled bedforms defined by rippled bed tops and bases which crisply cast the tops of underlying rippled beds (Tarhan et al., 2017; Droser et al., 2019). In particular, the lack of amalgamation between beds of similar grain sizes and lithologies, including

some as thin as a millimeter (Tarhan et al., 2017) as a result of organic mats is a striking feature associated with these widespread organic surfaces, and a sedimentological signature that is rarely found in the Phanerozoic record (Tarhan et al., 2017). Furthermore, in the ORS and PLRUS Facies, because the mats served as organic dividers between events, there is little to no erosional reworking or amalgamation, even between successive beds of similar grain size—resulting in a uniquely high-resolution record of each successive depositional event.

Thus, the unusual paucity of erosional loss or unconformities within these facies facilitates the capture of not only a complete record of depositional events but also of the organic mat and macrobiota ecosystem that developed between these depositional

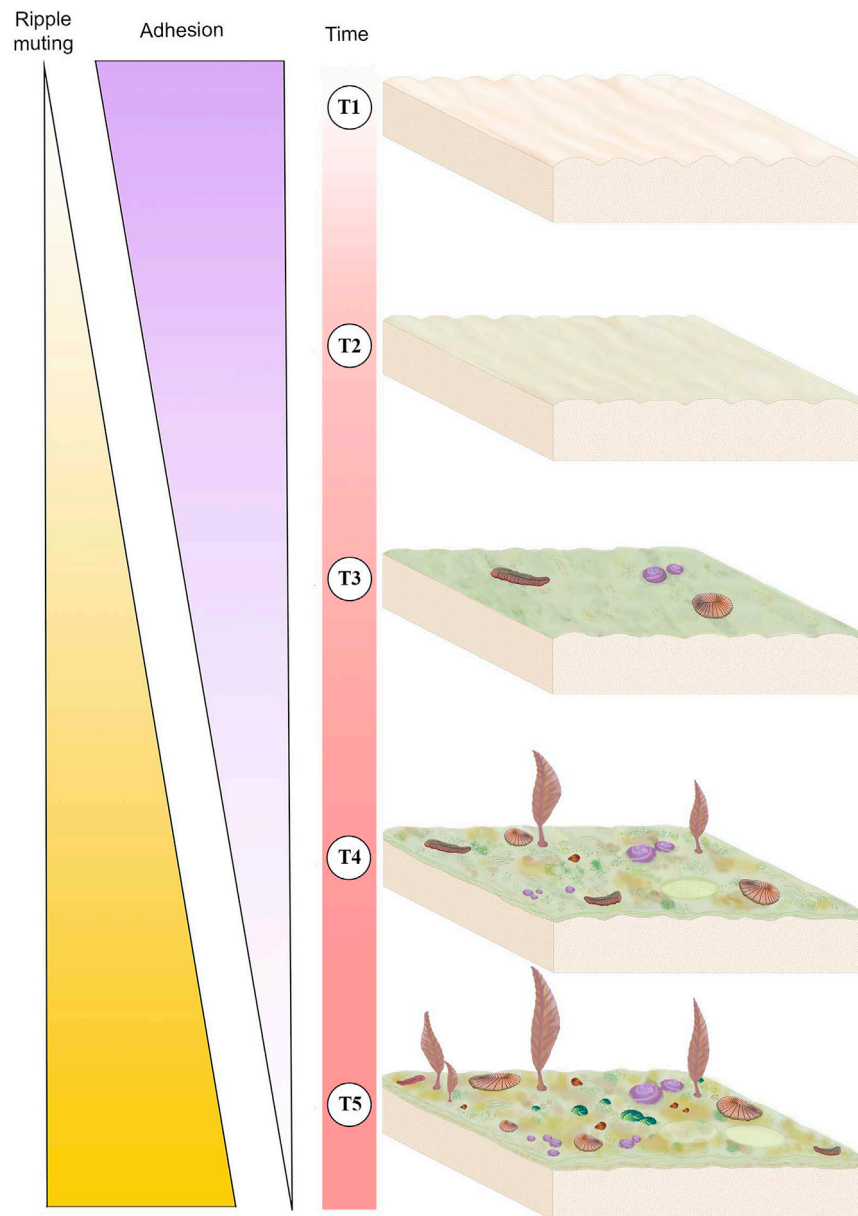


FIGURE 6 | Schematic of mat development over time (T1-T5) and its associated sedimentological and ecological impacts. Thickness of the “Ripple muting” and “Adhesion” triangles corresponds to the intensity of the variable, i.e., the thickest part of each triangle represents strong adhesion or ripple muting whereas the thinnest part represents weak adhesion or rippling muting. T1 represents a newly deposited sediment package with newly formed ripples and no mat, this surface would exhibit high adhesion and no ripple muting. T2 represents the same surface after a short period of time during which it has developed an immature mat, adhesion is moderate and ripples are only slightly muted. The same surface in T3 has a higher maturity mat and has begun to be colonized by mobile and sessile macrobiota, adhesion is moderate-to-weak and ripples are moderately muted. T4 illustrates that mat continues to develop and become more complex in texture and the community of Ediacaran macroorganisms becomes larger and more diverse, adhesion is weak and ripple muting is strong. T5 represents a mature surface that has been exposed for a long period of time, illustrating a thick and texturally diverse mat that is populated by a high-density and high-diversity community of macrobiota, at this stage there is no adhesion and ripple muting is strong.

events. This is fundamentally unlike the Phanerozoic sedimentological record, where upper layers of sediment are commonly reworked, if not eroded, and texturally uniform layers are typically amalgamated, and fossil assemblages are commonly time-averaged. The events—both biological and

physical—that happen between depositional events are likewise typically not preserved.

The majority of individual beds in the ORS Facies are shims of <5 mm (and commonly 1–2 mm) in thickness (Figure 4; Tarhan et al., 2017) and laterally discontinuous. These shims are typically

TABLE 3 | Common types of textured organic surfaces.

Name	Pattern	Hyporelief preservation
Elephant Skin	Regular	Positive relief with very fine networks of sharp reticulating grooves with patterns of triple junctions, sharp grooves, and triangular pits
Weave	Regular	Patches of subparallel and acutely branching rectilinear elements
Micropucker	Regular	Closely spaced, mm-scale, equal-sized, negative-relief pits
Clotted	Irregular	Irregularly sized but aggregated, sub-rounded to oval-shaped high-relief mounds on bed soles with thick grooves
Foam	Regular	Highly regular mm-scale uniformly sized positive-relief domes
Hair	Regular	Sub-mm to mm thick linear strands, commonly bunched
Complex Irregular	Irregular	Positive and negative relief TOS, highly variable at the cm scale

characterized by textured organic surfaces of varying types and stages of development. While we are able to identify and characterize and even excavate these shims, they do not commonly preserve macroscopic body fossils, likely because the extreme thinness of shims relative to Ediacara epimat organisms resulted in onlapping of shims along the margins of macroorganisms rather than complete casting (Tarhan et al., 2017). In some cases, shims contain holes where macroorganisms were present and the macroorganisms are in turn cast by a thicker bed overlying the shim (Figures 4, 5). An example of this is the relationship between STC-G and STC-G Shim (Figures 4, 5). However, shims commonly contain assemblages of the undermat-mining trace fossil *Helminthoidichnites* (Tarhan et al., 2017; Gehling and Droser, 2018). Thus, most depositional events were not lethal for Ediacara macroorganisms but they did commonly smother the mat surface.

The development of the mat surface itself is a function of the time between depositional events, and is unrelated to either the thickness of the underlying bed upon which the mat grew or that of the overlying bed which casted the mat surface. Thus, as would be expected, shims can and do record textural evidence of well-developed mats even where they have no or few body fossils. We are mainly concerned with relationships between mats and discrete macrobiota, and so, because shims do not readily preserve body fossils, the focus of this study is on excavated beds on the order of centimeters in thickness.

MAT MATURITY

Under the unique conditions of the Ediacaran matground-dominated seafloor, the amount of time between depositional events would have had a considerable impact on the matground maturity of each preserved bed as well as the community of organisms that inhabited that surface. Studies of modern matgrounds demonstrate that relatively mature mats can develop on the order of weeks (Doemel and Brock, 1977).

Sedimentological characters, including TOS, provide three main criteria for evaluating mat maturity independent of associated body fossils (Table 1). The primary indicator of organically mediated sedimentology at NENP is the extent of adherence between successive beds (Tarhan et al., 2017; Figure 4). We infer that limited matground development, e.g., the presence of only a very thin biofilm, resulted in moderate adherence of adjacent beds whereas development of a thicker organic surface resulted in very low adherence between adjacent

beds (Tarhan et al., 2017; Droser et al., 2019). Second, in the ORS Facies, beds characterized by a thin biofilm are indicated by relatively sharply defined ripples, whereas surfaces that were colonized by thicker and more mature mats are characterized by muted ripples (Figure 4), presumably due to both overgrowth of previously formed ripples and inhibition of additional reworking and ripple accretion (Tarhan et al., 2017; Droser et al., 2019). As such, the clarity and profile of ripples across a bed surface (both part and counter-part) and in cross-section are a useful measure of mat development. Examination of TOS on these surfaces also provides an indication of maturity. Third, high surface relief of TOS, and the presence of distinct iterative structures likely reflects relatively high matground maturity and duration of growth (Figures 1–3). Maturity does not appear to be associated with a particular type of matground (i.e., a particular type of TOS), but greater maturity may have facilitated more variability in growth morphologies or taphonomic morphologies resulting from matground-sediment and matground-current interactions, as recorded by TOS variability across a given bedding-plane surface. Using these three criteria, we evaluate mat maturity, denoted as Mat Maturity Index (MMI), on all excavated beds containing macroscopic body fossils, on a relative scale from 1 to 4 (Table 2 and Figures 1–3, Figure 6). Beds assigned a MMI value of 1 are considered the least mature, as evidenced by substantial adhesion to underlying beds and the presence of well-defined ripple crests (Figures 4, 6). These beds also contain no visible TOS. Two fossiliferous beds (Table 2) are classified as Mat Maturity Index 1. A MMI ranking of 2 was applied to those beds with clearly defined ripples but no adhesion. While these may include visible TOS, it is typically in discrete, isolated patches and consists of relatively low-relief structures. Beds with a MMI of 3 are characterized by muted ripple crests, no adhesion and visible TOS. MMI 4 is indicated by no adhesion, notably muted ripples and heterogeneous TOS that entirely covers the surface, with locally high relief (Figures 1–3).

NATURE OF TEXTURED ORGANIC SURFACES

Modern microbial mat ecosystems contain diverse consortia of primarily microscopic organisms that vary in composition and texture forming a variety of surface expressions (e.g., Gomes et al., 2020). The physical characteristics, growth rates and community

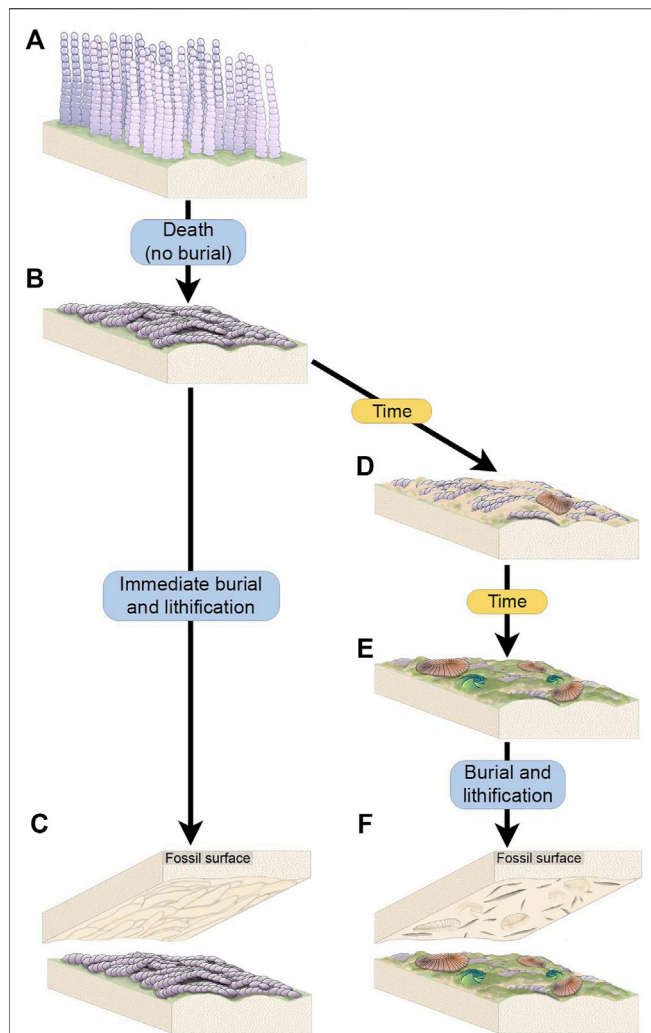


FIGURE 7 | Schematic of the two scenarios through which complex *Funisia dorothea* TOS is hypothesized to have formed. **(A)** A living community of densely packed individuals of *Funisia*. **(B)** Death of the *Funisia* population in the absence of sediment deposition, creating a thick TOS. **(C)** The *Funisia* population is buried soon after death, resulting in the casting of the *Funisia* TOS on the base of the depositional event. **(D)** In an alternate scenario, the dead *Funisia* population remains unburied on the seafloor for an ecologically significant period of time, background sedimentation occurs and mobile organisms begin to colonize the surface. **(E)** The dead *Funisia* population remains exposed on the seafloor and *Funisia* begin to decay while new TOS begins to form on top. More macroorganisms, including sessile taxa, begin to colonize the decaying *Funisia* surface. **(F)** The fossil surface resulting from the burial of this time averaged *Funisia* surface preserves the TOS “Groove”, representing the build up of sediment and TOS between decaying *Funisia* associated with a community of mobile and sessile macroorganisms.

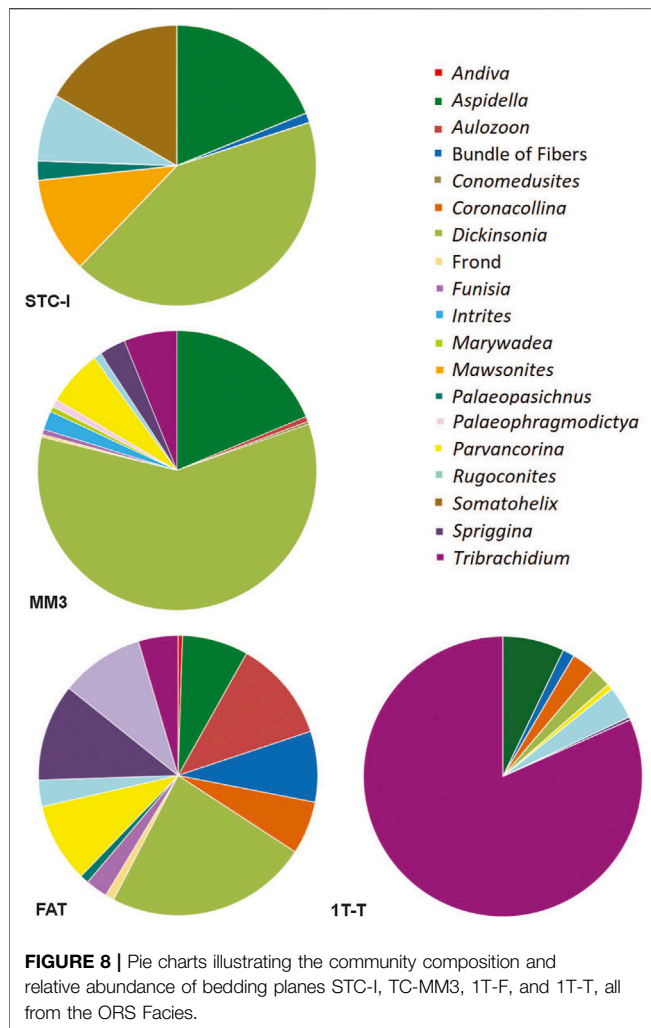
composition of modern microbial mats has been demonstrated to vary significantly based on environmental factors such as irradiance and nutrient concentrations (Hawes et al., 2016; Stal et al., 1985). Examination of TOS from the Ediacara Member and informal Nilpena Member indicates that mat surfaces were remarkably diverse in preserved physical expression, widespread, and heterogeneously distributed across

the Ediacaran seafloor (**Figure 1**; Droser et al., 2006; Droser et al., 2019; Gehling and Droser, 2009; Tarhan et al., 2017). Variation in TOS within and between beds is a function of the composition of the organic surface, the physical energy of the environment and duration of time between episodes of disturbance and final burial. Thus, specific textures do not necessarily correspond to discrete microbial communities or taxa but are also a product of energy, chemistry and both underlying and overlying lithology (Noffke et al., 2002; Sarkar et al., 2008; Bose et al., 2012; Mariotti et al., 2014; Sarkar et al., 2016; Kovalchuck et al., 2017). TOS are preserved on the bases of beds in positive and negative hyporelief, in the same manner as body fossils (Gehling and Droser, 2009; Tarhan et al., 2016).

TOS can be categorized using three primary characteristics: 1) regular or irregular patterning; 2) the size of patterning and 3) relief—largely positive, negative, or mixed (**Table 3**). While many TOS surfaces are not readily categorized into distinct morphotypes, there are a number of recurring TOS fabrics in the Ediacara and Nilpena members (**Figure 1**). A number of textures have been described previously from the Ediacara Member (Gehling and Droser, 2009) and here we describe several more. These are summarized in **Table 3**. The well-known “elephant skin” is preserved as very fine networks of sharp reticulating grooves with patterns of triple-junctions, sharp grooves, and triangular pits (**Figure 1B**). Coarse “elephant skin” may appear like micro-load casts (Gehling and Droser, 2009). “Pucker” is another commonly occurring TOS which consists of closely spaced, equal-sized dimples and pits (Gehling and Droser, 2009)—which, when occurring on the order of a mm, are referred to as “micropucker” (**Figure 1D**). “Weave” consists of subparallel to parallel rectilinear elements branching at acute angles, occurring in patches with minimal relief (**Figure 1E**) (Tarhan et al., 2022).

We add to this list three more distinct textures. Areas of variably sized but aggregated, sub-rounded to oval-shaped high-relief mounds with thick grooves on bed soles are referred to as “clotted” (**Figure 2A**). “Foam” consists of highly regular mm-scale uniformly sized circular positive-relief domes (**Figure 2B**). “Hair” consists of long—up to tens of centimeters—sub-mm- to mm-scale strands commonly occurring in bunches and locally twisted (**Figure 2C**). Elephant skin, clotted and foam are preserved largely in positive hyporelief, reflecting local depressions in the mat surface, at a scale ranging from millimeters to centimeters. These patterns may reflect the presence of a near uniform reticulate pattern in the case of elephant skin, burst bubbles in the case of foam (Eriksson et al., 2007) or pinnacles or tufts in the case of clotted (Gerdes, 2007).

Many TOS surfaces likely represent multiple generations of “microbial” mats and/or local patchiness in mat community composition. These mats commonly co-occurred with (and may have also hosted) multicellular organisms such as algae. Definition of distinct morphotypes for these TOS is challenging but they appear to typically record the most mature mats, as indicated by the Mat Maturity Index criteria outlined above and in **Table 1** and are therefore instead grouped together as “irregular complex TOS” (but likely represent a range of organisms and communities, as well as interactions with



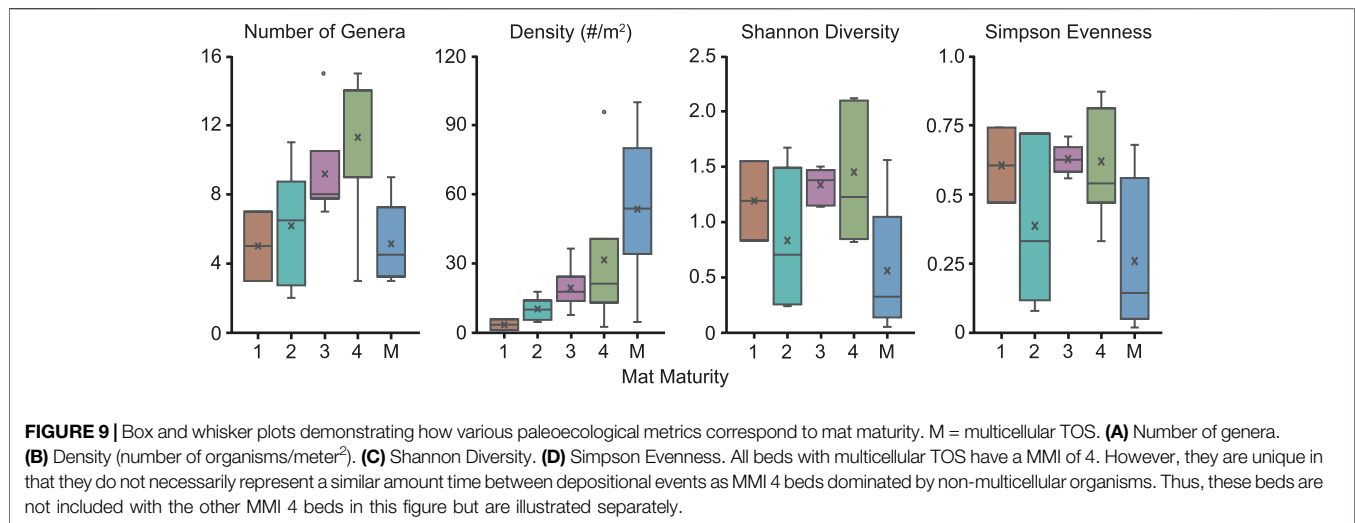
hydrodynamic and sedimentary processes). These types of TOS are exhibited on beds 1T-F and TB-ARB (Figures 1B,C). The rheology of the upper sediment surface and mat may also have impacted the expression of resulting TOS. This is exemplified by bed WS-Sub where micropucker (Gehling and Droser, 2009) appears to have been formed on a malleable rather than stiff upper mat surface (Figure 1D). Many beds exhibit variable TOS across the surface, particularly those beds that have a MMI ranking of 3 or 4. LV-Fun exemplifies this with distinct patches of clotted and foam as well as hair TOS (Figure 2), in places demarcated by very sharp boundaries (Figure 2D). Additionally, LV-Fun is also locally characterized by irregular complex TOS.

TEXTURED ORGANIC SURFACES FORMED BY MULTICELLULAR ORGANISMS

The organic substrates inferred to have covered vast stretches of the Ediacaran seafloor are commonly referred to as “microbial mats” because modern mats typically consist of microscopic,

predominantly single-celled organisms. However, modern organic substrates comprised of macroscopic, multicellular taxa have also been described (e.g., “spicule mats” such as that described by Morganti et al., 2021) and densely aggregated multicellular organisms formed widespread matgrounds in the past (Gehling and Droser, 2009) (Figures 3A,B). While multicellular organisms likely comprised part of the consortia recorded by many varieties of TOS at NENP, fossiliferous surfaces also contain TOS that are dominated by the textural remnants of specific macroscopic multicellular taxa. The most widespread example of these is *Funisia*—a straight or curved hollow tubular macrofossil up to 30 cm long and 12 mm wide with a circular cross-section and uniform diameter, consisting of sub-rectangular modules ranging from 6 to 8 mm long (Droser and Gehling, 2008). *Funisia* stood upright on the seafloor in great density, estimated to be as high as 6,000/m² and is, by an order of magnitude, the most abundant fossil at NENP (Surprenant et al., 2020). Upon death, *Funisia* fell to the seafloor, commonly in loosely oriented aggregations, potentially as a result of lethal perturbation by high-energy currents. In some cases, these felled tubes were buried without further colonization of the surrounding seafloor, whereas in others the *Funisia* organic surface was subsequently colonized by another community of Ediacara macroorganisms (Figure 7).

Funisia completely covers four of the excavated beds (WS-MAB, TC-MM2, STC-AB and STC-X) and is very common on two additional beds (LV-Fun, TB-BRW). On three of these surfaces (WS-MAB, TC-MM2, STC-AB), *Funisia* is distinctively associated with dense assemblages of *Aspidella*, the discoidal holdfast of a frondose organism such as *Arborea*. These *Aspidella*-*Funisia* assemblages are so distinctive of the Ediacara and Nilpena members (occurring in both the ORS and PLRUS Facies) that they have been inferred to reflect an ecological association or biofacies (Tarhan et al., 2015). Moreover, the presence of *Funisia* aggregations appears to have also directly influenced the preservation of associated *Aspidella* and thus represents a taphofacies—where the latter occur with *Funisia* aggregations, they are characteristically preserved along bed bases as convex internal molds of the pedal (basal) surface of the holdfast, whereas *Aspidella* occurring in the absence of *Funisia* aggregations are characteristically preserved along bed bases as external and composite molds of variable relief of the upper surface of the holdfast and, in cases, the associated stem (Tarhan et al., 2015) or are entirely removed, leaving the biogenic tool mark described as mop (Tarhan et al., 2010; Tarhan et al., 2015). Bed STC-X, in contrast, contains abundant *Funisia* associated with a more variable macrofossil assemblage. The pervasive *Funisia* TOS on this bed indicates that a dense assemblage of *Funisia* once populated this surface. However, following the death and collapse of the *Funisia* community, this patch of seafloor presumably remained unburied on the surface for a sufficiently long period of time that *Dickinsonia*, *Tribrachidium* and other epimat macroorganisms began to colonize the organic substrate provided by dead and decaying *Funisia* (Figure 3B, Figures 7D–F). The draping and distortion of *Dickinsonia* overlying palimpsests of toppled



Funisia on this surface (Figure 3C) reveal that a dense community of *Funisia* initially populated this surface and, once toppled, created a unique albeit topographically irregular organic substrate that allowed *Dickinsonia* and other taxa to colonize the area. STC-X provides an example of time-averaging of two distinct communities preserved on an individual bed. Critically, however, this time-averaging occurred on an ecological (and likely sub-annual) time scale. Even on beds where *Funisia* does not cover the bed surface and was simply a component of the local community, it still appears to have contributed significantly to matground and organic substrate development, and would have provided an organic interface separating successive sandy deposits and was thus not only ecologically but also sedimentologically and taphonomically important (Tarhan et al., 2015; Droser et al., 2019).

Plexus was a broadly curved, elongate tubular organism that resided in a prone orientation on the Ediacaran seafloor. *Plexus* individuals range in size from 5 to 80 cm long and 5–20 mm wide, and have two main components: a rigid median structure and a fragile, commonly collapsed outer wall (Joel et al., 2014). *Plexus* is preserved as an external mold on bed soles, and as a counterpart cast on bed tops in sandstones of the ORS Facies. While *Plexus* is recognized as isolated individuals elsewhere, on three successive beds at NENP it covers the surface and dead or decaying *Plexus* served as an organic mat base-layer that was subsequently colonized by other organisms. Similar to *Funisia* on bed STC-X, these likely represent two ecologically time-averaged communities (Figure 3A; Joel et al., 2014), for example on P-P bed, where abundant *Plexus* are overlain by *Dickinsonia*, *Aulozoon* and *Phyllozoon*.

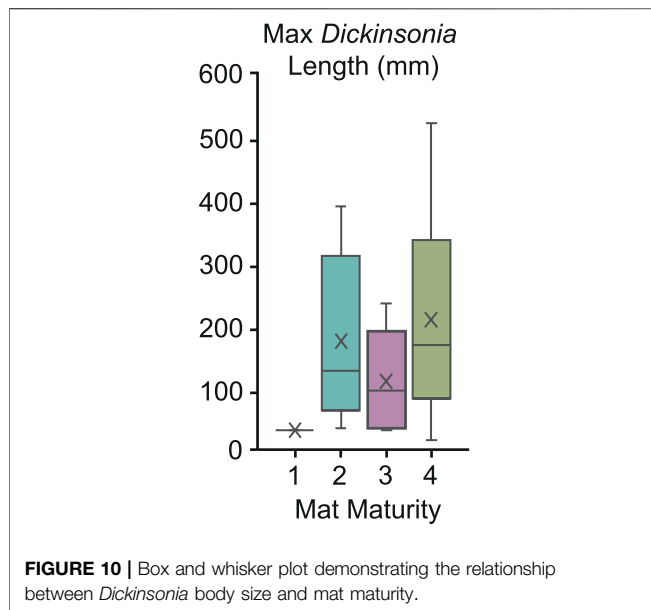
Densely aggregated fossil algae produced an organic surface on 1T-BOF. In this case, several genera and species of algae (Xiao et al., 2020) cover the bed. The association of particularly small individuals of *Dickinsonia* and *Spriggina* with algal macrofossil aggregations on 1T-BOF suggests that these dense and diverse

algae served as a nursery preferentially colonized by juvenile macrobiota (Droser et al., 2019).

All of the beds with a TOS composed of multicellular organisms exhibit a MMI of 4 based on the criteria described above; these surfaces are characterized by bed-covering, commonly high-relief TOS; ripples are present but muted and successively excavated beds are not characterized by adhesion (Figures 3A–C).

THE ROLE OF MATS IN THE ECOLOGY OF THE EDIACARA BIOTA

The environments created by widespread matgrounds in the Ediacaran played a significant role in the distribution of early animals. Fossil evidence suggests that Ediacaran organisms were specifically adapted to these substrates, living in and relying upon resources provided by matgrounds (Seilacher, 1999; Gehling and Droser, 2009; Gehling and Droser, 2018; Gehling et al., 2005; Gehling et al., 2014; Sperling and Vinther, 2010; Evans et al., 2019; Evans et al., 2020). Oxygen concentrations are thought to have been highly variable throughout the Ediacaran, and estimates suggest that they were typically much lower than in similarly energetic, shallow marine modern environments (e.g., Sperling et al., 2015; Reinhard et al., 2016; also reviewed by; Droser et al., 2017; Evans et al., 2018a; Cole et al., 2020; Reinhard and Planavsky, 2021). The activity of photosynthetic organisms living in mat communities would have produced oxygen and pockets of oxygen trapped along mat interfaces may have thus created more habitable microenvironments (e.g., Gingras et al., 2011). Although less stringently limited by oxygen, similar ecological patterns are observed in the modern in communities where photosynthetic microbial mats are responsible for a large percentage of local primary production (Almela et al., 2019). In short, the ecologies of the oldest fossil animals were intimately linked to the unique substrates of the Ediacaran (Droser et al., 2017).



The majority of Ediacara Biota macroorganisms were sessile taxa living on or embedded in the mat. For example, *Obamus* and *Coronacollina* both lived embedded in the upper surface of the mat rendering the outer edge of the organism, in places, indistinguishable from the mat (Clites et al., 2012; Dzaugis et al., 2019). *Tribrachidium* specimens have relatively distinct edges but lived slightly embedded in the mat as demonstrated by the preservation of their basal surfaces as slight divots where specimens had been removed by current or death (Fedonkin, 1985; Hall et al., 2015). The frond holdfast *Aspidella* provides the best example of anchoring within the mat as discussed above.

Trace fossil evidence suggests that several Ediacaran organisms fed on abundant organic matter found in these matgrounds (Gehling et al., 2005, 2014; Sperling and Vinther, 2010; Gehling and Droser, 2018; Evans et al., 2019, Evans et al., 2020; Xiao et al., 2019). Four Ediacara taxa—*Dickinsonia*, *Ikaria*, *Kimberella* and *Yorgia*—left trace fossil evidence of their grazing and mobility (Gehling et al., 2005, Gehling et al., 2014; Ivantsov, 2009, Ivantsov, 2011; Evans et al., 2018b, Evans et al., 2019, Evans et al., 2020). Because Ediacaran matgrounds were widespread and interlaminated with sediment (and may have also been rich in sediment), in order to produce a preservable trace fossil these organisms had to actively disrupt the mat surface (Droser et al., 2017; Evans et al., 2019). In order for these traces to be successfully preserved as trace fossils, this excavated area would then need to be buried and molded by the overlying sand before re-growth of the mat obscured the traces of these organisms' activities. Indeed, a comparison of *Dickinsonia* body fossil and "footprint" sizes reveals that footprints are, on average, significantly larger than body fossils, suggesting that, at least in part, small footprints were more readily obscured by mat growth (Evans et al., 2019). The close association between the leveed trace fossil *Helminthoidichnites* (preserved in both concave and convex relief, even along individual traces, and both bed tops and bases) and particularly thin shims and thinner portions of shims

(Gehling and Droser, 2018) suggests that the *Helminthoidichnites* tracemaker or tracemakers (e.g., *Ikaria*, cf. Evans et al., 2020) grazed not only on exposed upper surfaces of the mat, but also traced nutrient-rich mats underlying thin sand veneers (Figure 1F). Other taxa, including *Andiva* and *Spriggina*, may have also been mobile but are not associated with evidence of disruption of the local organic mat surface, potentially suggesting a different feeding mode (Evans et al., 2019). Assemblages of aligned *Parvancorina* (themselves aligned with other paleocurrent indicators) have been interpreted to reflect a rheotactic lifestyle for *Parvancorina* (Coutts et al., 2018; Paterson et al., 2017) but these organisms do not appear to have visibly impacted the underlying mat during such activity.

The large number of beds and distribution of different types of TOS provide an opportunity to examine the potential association of specific TOS types and certain macrofossil taxa. Surprisingly, there is only one example of such an association: *Funisia* matgrounds and the holdfast form genus *Aspidella*, as discussed above. Other common taxa such as *Dickinsonia*, *Tribrachidium*, *Spriggina*, *Rugoconites* and *Parvancorina* do not preferentially occur with specific TOS types.

Mat maturity, rather than the mat type itself, however, may have more strongly influenced the distribution of taxa and the development of Ediacara macroorganism communities. Based on the assumption that mat maturity represents an indicator of the duration of time between burial events, we can test several predictions about the relationship between MMI and community development: 1) diversity, evenness and macrofossil density should correlate with mat maturity and 2) the range of body sizes within a species on individual beds should increase with mat maturity.

Distribution of Taxa, Density, Species Richness, and Evenness

Of common taxa that occur on more than three beds, only two, *Obamus* and *Coronacollina*, are restricted to surfaces with a high MMI ranking. *Obamus* occurs only on LV-Fun, TB-ARB, 1T-F and 1T-NA, all with MMI values of 4. *Coronacollina* similarly occurs on beds with MMI values of 4 and only a single bed with an MMI of 3, 1T-LS. All other common taxa occur on beds with MMI values of 2, 3 and 4. Because there are only two fossiliferous beds (i.e., beds containing macroscopic body fossils) with an MMI value of 1, it is difficult to evaluate the significance of low mat maturity for the distribution of taxa. However, STC-I contains a number of common taxa, including *Dickinsonia*, *Rugoconites* and *Aspidella* (Figure 8). Thus, with the exception of *Obamus* and *Coronacollina*, mat maturity does not appear to have dictated the distribution of taxa.

Fossil density appears to be the metric that is most robustly correlated with mat maturity. Fossil density in non-multicellular TOS surfaces across all taxa, including taxonomically diverse assemblages, ranges from 2.5 to 95 individuals per square meter (Table 2 and Figure 9B). Fossil density does not take into account body size. However, with the notable exception of *Dickinsonia*, discussed below, the range of body sizes—millimeters to <5 cm in

length—observed in most individuals of the most common taxa is small enough to have had minimally impacted density.

The number of described genera on individual beds excavated at Nilpena range from 2 to 15 (Table 2 and Figure 9A). Overall, the highest number of genera occur on beds with an MMI of 3 or 4 (excluding those TOS formed by aggregated macroscopic multicellular organisms) (Figure 9A). We also calculated Shannon diversity indices (H) which incorporate both the number of species and also the evenness of their abundance. The distribution of Shannon diversity indices does not appear to correlate with MMI, regardless of whether only “microbial”-grade TOS or all TOS types, including aggregations of multicellular organisms such as *Funisia*, are considered (Figure 9C).

For typical surfaces of the ORS Facies (i.e., excluding those with multicellular-grade TOS), STC-I and TC-MM3 provide contrasting examples (Figure 8). *Dickinsonia* is the most common macrofossil on each of these two beds. The base of TC-MM3 is characterized by muted but still readily distinguishable ripples, no adherence to the underlying bed and visible TOS (MMI of 3) with a fossil density of 18.4 individuals/m². We interpret TC-MM3 to record a relatively mature community. TC-MM3 is also characterized by relatively high taxonomic diversity with 15 described genera (Figure 9 and Table 2). In contrast, bed STC-I is characterized by sharp-crested ripples, no visible TOS and was underlain by a shim that strongly adhered to STC-I, indicating that the mat colonizing that shim (and preserved on the base of STC-I) was immature. This bed has 7 macrofossil genera, a fossil density of 5.8 individuals/m² and a Shannon diversity index of 1.55, just slightly higher than TC-MM3 (Table 2).

1T-F, also from the ORS Facies with common *Dickinsonia*, exemplifies a mature mat (MMI 4) (Figure 8). 1T-F does not adhere to the underlying bed and ripples are strongly muted. Furthermore, 1T-F is characterized by spatially heterogeneous TOS with local areas of relatively high (mm-scale) relief (Figure 1C). 1T-F records 16 genera and the highest Shannon diversity index recorded at NENP ($H = 2.12$). Although *Dickinsonia* is common, 1T-F exhibits higher evenness than either TC-MM3 or STC-I (Table 1).

In contrast, Bed 1T-T has a MMI of 4 and, although it is characterized by a high macrofossil density (40.6 individuals/m²) and a relatively high number of genera, it is dominated by *Tribrachidium* (Figure 8), resulting in a low Shannon diversity index ($H = 0.82$).

Bedding planes characterized by multicellular TOS are among the most mature beds (Table 1). These beds reflect densely packed communities of *Funisia*, *Plexus* or macroalgae that would have required a relatively longer duration between depositional events to develop, grow and experience macroorganism recruitment and colonization. They have a generic diversity ranging from 3 to 7 taxa and Shannon indices ranging from 0.05 to 1.56, depending on whether death of the mat-forming community was closely followed by burial or instead remained unburied at the sediment-water interface for a sufficiently long duration for a new community to develop, thus recording an ecologically time-averaged surface. Those surfaces that were not buried immediately (i.e., time-averaged surfaces) generally have higher generic diversity and Shannon indices because they represent multiple communities.

STC-X exhibits such a situation with a community that lived on top of unburied *Funisia*, as reflected by its eight genera and Shannon diversity index of 1.56 (Figure 3C).

Distribution of Body Sizes

Body size is positively correlated with changes in nutrient availability in modern ecosystems (e.g., Woodward et al., 2005), and variable oxygen concentrations produce size limitations on aerobic organisms (e.g., Payne et al., 2011). Greater time of exposure, as represented by more mature mats, would have increased the probability of growth of macroorganisms to more extreme sizes (Droser et al., 2017). Thus, we might expect mature mats to exhibit a greater range of body sizes, including both juvenile and adult forms. However, advanced maturity would not limit the ability of settlement by juvenile forms and these nutrient-rich organic substrates may even have been preferred by some taxa. Indeed, *Obamus* is limited to beds characterized by mature mats (e.g., TB-ARB and LV-Fun), suggesting that larvae preferentially colonized these settings (Dzaugis et al., 2019). Body size does appear to be related to TOS recording densely packed fossil algae communities on 1T-BOF, where particularly small specimens of *Dickinsonia* and *Spriggina* occur, suggesting that these dense and diverse algae served as a nursery preferentially colonized by juvenile macrobiota (Xiao et al., 2013; Droser et al., 2019).

Dickinsonia was mobile and fed directly on the organic mat (Ivantsov and Malakhovskaya, 2002; Gehling et al., 2005; Sperling and Vinther, 2010; Evans et al., 2019). It occurs on nearly every bed and is the third most common genus, behind *Funisia* and the holdfast *Aspidella*, at NENP (Droser et al., 2019). *Dickinsonia* is the most abundant fossil on seven beds, dominating (>50% of all fossils) four of them. These beds vary in mat maturity, and *Dickinsonia* is therefore an ideal candidate to investigate potential trends between body size and mat maturity. This fossil is less common on beds characterized by multicellular TOS, potentially due to the difficulty of navigating these high-relief surfaces (Droser et al., 2019) and so we exclude those beds from this evaluation.

Dickinsonia dominates bed TC-MM3 and is the most abundant fossil on 1T-F, both characterized by mature mats (Table 2). However, it also dominates STC-I, one of the least mature mats from the ORS Facies. Trace fossil evidence suggests that a large *Yorgia* was also present for some period on bed STC-I, although lack of body fossil preservation suggests it moved on prior to burial. Thus, very low mat maturities did not limit the distribution of large, mobile taxa that fed directly on the organic mat, such as *Dickinsonia* and *Yorgia*, but it is unclear for what duration they would have been able to support larger forms, especially of those organisms that activity fed upon matgrounds. The ability of these taxa to move into and out of a community (Evans et al., 2019) may complicate the observed impacts of overall low benthic nutrient availability.

To test for potential relationships, we compare the MMI of beds at NENP with the maximum body size of associated *Dickinsonia* and preserved footprints. Despite the mobility and resultant transient nature of occupation within an environment, we find that mature mats are more likely to contain large *Dickinsonia* (Figure 10). This supports the hypothesis that greater time of exposure and/or increased nutrient availability on these surfaces supported a greater range of body sizes, at least

among mobile and mat-feeding macroorganisms. Although this includes different species of *Dickinsonia* that may grow at variable rates, all fed in the same manner.

Body size data for sessile organisms is more limited, largely because they are less common and typically occupy a smaller range of body sizes than *Dickinsonia* at NENP. Although *Aspidella* is more abundant, this form genus could represent the holdfast of multiple different taxa, potentially belonging to distinct morphogroups (Rangeomorpha and Arboreomorpha) (Tarhan et al., 2015). However, the preservation of *Aspidella* assemblages characterized by right-skewed size distributions on individual fossiliferous bedding planes on which it is the most abundant macrofossil is more parsimoniously interpreted as populations of a single taxon (Tarhan et al., 2015). Nonetheless, preservation of *Aspidella* is intimately linked to mat development (Tarhan et al., 2015; Surprenant et al., 2020). Similarly, as noted here, *Funisia* most commonly occurs in dense aggregates, often to the exclusion of other taxa and representing a distinct TOS in and of itself (Droser and Gehling, 2008; Gehling and Droser, 2009). Thus, despite their abundance, *Aspidella* and *Funisia* are less ideally suited than *Dickinsonia* as indicators of macroorganism responses to mat maturity.

Tribrachidium is potentially the best sessile taxon for investigating relationships with mat maturity because it occurs on numerous beds (and, like *Aspidella* and *Funisia*, spans multiple facies), dominating two (Hall et al., 2015; Droser et al., 2019). The body size distribution of *Tribrachidium*, however, does not match trends observed for *Dickinsonia*. *Tribrachidium* occurs in clusters of similar-sized specimens, with the smallest and largest cohorts preserved on beds TC-MM3 and WS-TBEW (Hall et al., 2015), respectively, both with an MMI of 3. A third cohort of intermediate size occurs on bed 1T-T, likewise characterized by high MMI. Millimeter-scale *Tribrachidium* also occur on the newly excavated LV-Fun, one of the surfaces with the highest MMI at NENP. Thus, the size of *Tribrachidium* cohorts does not appear to be correlated with mat maturity and is more likely a random result of the time of colonization relative to burial.

DISCUSSION

Though there is little evidence of interactions between Ediacara taxa, there are abundant indications that several Ediacara taxa interacted with the organically bound seafloor. Widespread organic surfaces served as a source of food for a number of organisms, particularly mobile taxa, and others lived in close proximity to the mat, embedded or “stuck” within it. However, most of the Ediacara taxa recorded on fossiliferous bedding planes at NENP do not appear to be preferentially associated with particular types of TOS. The most remarkable aspect of the textured organic surfaces at NENP is the variability of morphotypes and the heterogeneity of these surfaces within and between beds. While many of the TOS occurring on these beds are regular in morphology and readily distinguishable, certain textures—particularly on beds with an MMI of 4—consist of irregular complex TOS. This level of heterogeneity is consistent with that characterizing some modern well-developed mats (Stal et al., 1985; Hawes et al., 2016; Gomes et al., 2020).

Based on biomarker data, cyanobacteria may have been the primary constituents of many Proterozoic photosynthetic mats (Gomes et al., 2020). However, other taxa clearly contributed to these communities (Gomes et al., 2020). This is obvious in the case of multicellular TOS but it also likely true of even “microbial-grade” TOS. In particular, variability within an individual bed, such as LV-Fun (Figure 2) on the scale of centimeters and decimeters likely reflects compositional differences in that environmental differences on such a small scale can be largely discounted. This is consistent with modern mats that are heterogeneous on micro and macro scales, reflecting a variety of environmental and compositional differences.

Time between depositional events was irregular as indicated by the range of mat maturities. As predicted, fossil density and number of genera appear to be positive correlated with MMI. Regions of the seafloor characterized by longer “hiatal” intervals between depositional events experienced greater matground growth and maturity and fostered the colonization of more macroorganisms representing different genera. However, with the exception of *Obamus* and *Coronacollina*, the distribution of individual taxa does not appear to have been dictated by mat maturity. The distribution of these two taxa is consistent with larval settlement preferences.

Individual beds of the Ediacara Member exhibit a wide range of evenness values (Table 2; Droser and Gehling, 2015). There are beds with evenness values on par with those of the Phanerozoic, such as 1T-F (Droser and Gehling, 2015; Droser et al., 2019; Finnegan et al., 2019). However, those data currently available suggest that, following Powell and Kowalewski (2002), on the whole, evenness may have increased through time (Droser and Gehling, 2015). The prevalence of lower evenness values in general in the Ediacaran as compared with the Phanerozoic likely impacts the potential correlation of MMI with fossil assemblage evenness. In other words, a high-dominance community is not necessarily “immature”. For example, 1T-T has an MMI of 4 with a relatively high number of genera and high fossil density—but is dominated by a cohort of *Tribrachidium* (Hall et al., 2015). It would be difficult to interpret this bed as recording anything other than a relatively mature macroorganism community. For most beds at NENP, the same taxa are present across beds but not in equivalent abundances; it is the varying relative abundances of each bed that distinctively characterize these fossil assemblages. High dominance by an individual taxon is not uncommon (Droser et al., 2019). For example, *Dickinsonia* and the frond holdfast *Aspidella* each occur on nearly all of the beds at NENP. *Dickinsonia* dominates some beds and *Aspidella*-associated frondose organisms presumably dominated others. Thus, although these metrics are directly related, the lack of correlation of Shannon diversity indices and evenness in fossilized Ediacara communities should perhaps not be surprising.

Mats have long been recognized to be significant components of Ediacaran ecosystems. They form an integral part of the actual communities as sources of food, providing a suitable and stabilized substrate and potentially a source of oxygen in a low-oxygen world. While it is not possible to evaluate biomass from these fossil communities, given the widespread nature of these mats and the maturity and complexity of mats with sufficient time to develop, it is very likely that mats constituted a significant component of Ediacaran

biomass as they do in certain environments today (e.g., Sutherland, 2009). Interestingly, the type of mat does not appear to be a controlling factor in the distribution of taxa. However, the maturity of mats, reflecting the duration of time between events is not surprisingly correlated with both density and generic diversity.

DATA AVAILABILITY STATEMENT

The raw data supporting the conclusion of this article will be made available by the authors, without undue reservation.

AUTHOR CONTRIBUTIONS

MD and SE wrote the first draft of the paper. SE and IH did the data analysis. Concepts and subsequent drafts were developed by all of the authors.

REFERENCES

- Almela, P., Velázquez, D., Rico, E., Justel, A., and Quesada, A. (2019). Carbon Pathways through the Food Web of a Microbial Mat from Byers Peninsula, Antarctica. *Front. Microbiol.* 10, 628. doi:10.3389/fmicb.2019.00628
- Bose, P. K., Eriksson, P. G., Sarkar, S., Wright, D. T., Samanta, P., Mukhopadhyay, S., et al. (2012). Sedimentation Patterns during the Precambrian: a Unique Record? *Mar. Pet. Geology* 33, 34–68. doi:10.1016/j.marpetgeo.2010.11.002
- Bottjer, D. J., Hagadorn, J. W., Schieber, J., Bose, P. K., Eriksson, P. G., Banerjee, S., et al. (2007). “Mat-growth Features,” in *Atlas of Microbial Mat Features Preserved within the Clastic Rock Record* (Amsterdam, New York: Elsevier), 53–71.
- Bouougri, E. H., and Porada, H. (2007). Siliciclastic Biolaminites Indicative of Widespread Microbial Mats in the Neoproterozoic Nama Group of Namibia. *J. Afr. Earth Sci.* 48, 38–48. doi:10.1016/j.jafrearsci.2007.03.004
- Carbone, C., and Narbonne, G. M. (2014). When Life Got Smart: The Evolution of Behavioral Complexity through the Ediacaran and Early Cambrian of NW Canada. *J. Paleontol.* 88, 309–330. doi:10.1666/13-066
- Clites, E. C., Droser, M. L., and Gehling, J. G. (2012). The Advent of Hard-Part Structural Support Among the Ediacara Biota: Ediacaran harbinger of a Cambrian Mode of Body Construction. *Geology* 40, 307–310. doi:10.1130/g32828.1
- Cole, D. B., Mills, D. B., Erwin, D. H., Sperling, E. A., Porter, S. M., Reinhard, C. T., et al. (2020). On the Co-evolution of Surface Oxygen Levels and Animals. *Geobiology* 18, 260–281. doi:10.1111/gbi.12382
- Corenbilt, D., Darrozes, J., Julien, F., Otto, T., Roussel, E., Steiger, J., et al. (2019). The Search for a Signature of Life on Mars: A Biogeomorphological Approach. *Astrobiol.* 19, 1279–1291. doi:10.1089/ast.2018.1969
- Coutts, F. J., Bradshaw, C. J. A., García-Bellido, D. C., and Gehling, J. G. (2018). Evidence of Sensory-Driven Behavior in the Ediacaran Organism *Parvancorina*: Implications and Autecological Interpretations. *Gondwana Res.* 55, 21–29. doi:10.1016/j.gr.2017.10.009
- Darroch, S. A. F., Sperling, E. A., Boag, T. H., Racicot, R. A., Mason, S. J., Morgan, A. S., et al. (2015). Biotic Replacement and Mass Extinction of the Ediacara Biota. *Proc. R. Soc. B.* 282, 20151003. doi:10.1098/rspb.2015.1003
- Doemel, W. N., and Brock, T. D. (1977). Structure, Growth, and Decomposition of Laminated Algal-Bacterial Mats in Alkaline hot springs. *Appl. Environ. Microbiol.* 34 (4), 433–452. doi:10.1128/aem.34.4.433-452.1977
- Droser, M. L., Gehling, J. G., and Jensen, S. R. (2006). Assemblage Palaeoecology of the Ediacara Biota: The Unabridged Edition? *Palaeogeogr. Palaeoclimatol. Palaeoecol.* 232, 131–147. doi:10.1016/j.palaeo.2005.12.015
- Droser, M. L., and Gehling, J. G. (2008). Synchronous Aggregate Growth in an Abundant New Ediacaran Tubular Organism. *Science* 319, 1660–1662. doi:10.1126/science.1152595

FUNDING

This work was supported by a NASA Exobiology grant (80NSSC19K0472 to MD, LT, and SE) and NASA Earth and Space Science Fellowships (grant PLANET17F-0124 to SE and 20-PLANET20-0015 to RS).

ACKNOWLEDGMENTS

We are grateful to Ross and Jane Fargher for access to the National Heritage Nilpena Ediacara fossil site on their property, acknowledging that this land lies within the Adnyamathanha Traditional Lands. We are also grateful to the South Australia Department of the Environment and Water for facilitating field work. We thank P. Dzaugis, M. Dzaugis and J. Irving for field assistance. H. McCandless aided in the preparation of this manuscript.

- Droser, M. L., Gehling, J. G., Tarhan, L. G., Evans, S. D., Hall, C. M. S., Hughes, I. V., et al. (2019). Piecing Together the Puzzle of the Ediacara Biota: Excavation and Reconstruction at the Ediacara National Heritage Site Nilpena (South Australia). *Palaeogeogr. Palaeoclimatol. Palaeoecol.* 513, 132–145. doi:10.1016/j.palaeo.2017.09.007
- Droser, M. L., and Gehling, J. G. (2015). The Advent of Animals: The View from the Ediacaran. *Proc. Natl. Acad. Sci. USA* 112, 4865–4870. doi:10.1073/pnas.1403669112
- Droser, M. L., Tarhan, L. G., and Gehling, J. G. (2017). The Rise of Animals in a Changing Environment: Global Ecological Innovation in the Late Ediacaran. *Annu. Rev. Earth Planet. Sci.* 45, 593–617. doi:10.1146/annurev-earth-063016-015645
- Dzaugis, P. W., Evans, S. D., Droser, M. L., Gehling, J. G., and Hughes, I. V. (2019). Stuck in the Mat: *Obamus Coronatus*, a New Benthic Organism from the Ediacara Member, Rawnsley Quartzite, South Australia. *Aust. J. Earth Sci.* 67, 1440–0952. doi:10.1080/08120099.2018.1479306
- Elliott, D. A., Vickers-Rich, P., Trusler, P., and Hall, M. (2011). New Evidence on the Taphonomic Context of the Ediacaran *Pteridinium*. *Acta Palaeontologica Pol.* 56, 641–650. doi:10.4202/app.2010.0060
- Eriksson, P. G., Schieber, J., Bouougri, E., Gerdes, G., Porada, H., Banerjee, S., et al. (2007). CHAPTER THREE CLASSIFICATION OF STRUCTURES LEFT BY MICROBIAL MATS IN THEIR HOST SEDIMENTS.
- Evans, S. D., Diamond, C. W., Droser, M. L., and Lyons, T. W. (2018a). Dynamic Oxygen and Coupled Biological and Ecological Innovation during the Second Wave of the Ediacara Biota. *Emerging Top. Life Sci.* 2, 223–233. doi:10.1042/etls20170148
- Evans, S. D., Dzaugis, P. W., Droser, M. L., and Gehling, J. G. (2018b). You Can Get Anything You Want from Alice’s Restaurant Bed: Exceptional Preservation and an Unusual Fossil Assemblage from a Newly Excavated Bed (Ediacara Member, Nilpena, South Australia). *Aust. J. Earth Sci.* 67, 1440–0952. doi:10.1080/08120099.2018.1470110
- Evans, S. D., Gehling, J. G., and Droser, M. L. (2019). Slime Travelers: Early Evidence of Animal Mobility and Feeding in an Organic Mat World. *Geobiology* 17, 490–509. doi:10.1111/gbi.12351
- Evans, S. D., Hughes, I. V., Gehling, J. G., and Droser, M. L. (2020). Discovery of the Oldest Bilaterian from the Ediacaran of South Australia. *Proc. Natl. Acad. Sci. USA* 117, 7845–7850. doi:10.1073/pnas.2001045117
- Fedonkin, M. A. (1985). “Systematic Description of Vencian Metazoans,” in *The Vendian System. Paleontology. 1*. Editors B. S. Sokolov and A. B. Iwanowski (Berlin: Springer-Verlag), 71–120.
- Finnegan, S., Gehling, J. G., and Droser, M. L. (2019). Unusually Variable Paleocommunity Composition in the Oldest Metazoan Fossil Assemblages. *Paleobiology* 45 (2), 235–245. doi:10.1017/pab.2019.1
- Gehling, J. G., and Droser, M. L. (2009). Textured Organic Surfaces Associated with the Ediacara Biota in South Australia. *Earth Sci. Revs.* 96, 196–206. doi:10.1016/j.earscirev.2009.03.002

- Gehling, J. G., and Droser, M. L. (2013). How Well Do Fossil Assemblages of the Ediacara Biota Tell Time. *Geology* 41, 447–450. doi:10.1130/g33881.1
- Gehling, J. G., and Droser, M. L. (2018). Ediacaran Scavenging as a Prelude to Predation. *Emerg. Top. Life Sci.* 2, 213–222. doi:10.1042/etls20170166
- Gehling, J. G. (1999). Microbial Mats in Terminal Proterozoic Siliciclastics: Ediacaran Death Masks. *Palaio* 14, 40–57. doi:10.2307/3515360
- Gehling, J. G. (2000). Environmental Interpretation and a Sequence Stratigraphic Framework for the Terminal Proterozoic Ediacara Member within the Rawnsley Quartzite, South Australia. *Precambrian Res.* 100, 65–95. doi:10.1016/s0301-9268(99)00069-8
- Gehling, J. G., Droser, M. L., Jensen, S., and Runnegar, B. N. (2005). “Ediacara Organisms: Relating Form to Function,” in *Evolving Form and Function: Fossils and Development*. Editor D. E. G. Briggs (New Haven, CT: Yale Univ. Press), 43–66.
- Gehling, J. G., Runnegar, B. N., and Droser, M. L. (2014). Scratch Traces of Large Ediacara Bilateral Animals. *J. Paleontol.* 88, 284–298. doi:10.1666/13-054
- Gehling, J. G., García-Bellido, D. C., Droser, M. L., Tarhan, L. G., and Runnegar, B. (2019). The Ediacaran-Cambrian Transition: Sedimentary Facies versus Extinction. *Estud. Geol.* 75, e099. doi:10.3989/egol.43601.554
- Gerdes, G. (2007). *Chapter Two Structures Left by Modern Microbial Mats in Their Host Sediments*.
- Gingras, M., Hagadorn, J. W., Seilacher, A., Lalonde, S. V., Pecoits, E., Petrash, D., et al. (2011). Possible Evolution of mobile Animals in Association with Microbial Mats. *Nat. Geosci.* 4, 372–375. doi:10.1038/ngeo1142
- Gomes, M. L., Riedman, L. A., O'Reilly, S., Lingappa, U., Metcalfe, K., Fike, D. A., et al. (2020). Taphonomy of Biosignatures in Microbial Mats on Little Ambergis Cay, Turks and Caicos Islands. *Front. Earth Sci.* 8, 576712. doi:10.3389/feart.2020.576712
- Hagadorn, J. W., and Bottjer, D. J. (1999). Restriction of a Late Neoproterozoic Biotope: Suspect-Microbial Structures and Trace Fossils at the Vendian-Cambrian Transition. *Palaio* 14, 73–85. doi:10.2307/3515362
- Hall, C. M. S., Droser, M. L., Gehling, J. G., and Dzaugis, M. E. (2015). Paleocology of the Enigmatic Tribrachidium: New Data from the Ediacaran of South Australia. *Precambrian Res.* 269, 183–194. doi:10.1016/j.precamres.2015.08.009
- Hawes, I., Jungblut, A. D., Obryk, M. K., and Doran, P. T. (2016). Growth Dynamics of a Laminated Microbial Mat in Response to Variable Irradiance in an Antarctic lake. *Freshw. Biol.* 61 (4), 396–410. doi:10.1111/fwb.12715
- Hill, C., Corcoran, P. L., Aranha, R., and Longstaffe, F. J. (2016). Microbially Induced Sedimentary Structures in the Paleoproterozoic, Upper Huronian Supergroup, Canada. *Precambrian Res.* 281, 155–165. doi:10.1016/j.precamres.2016.05.010
- Ivantsov, A. Y. (2009). New Reconstruction of *Kimberella*, Problematic Vendian Metazoan. *Paleontolog. J.* 43, 3–12. doi:10.1134/s003103010906001x
- Ivantsov, A. Y. (2011). Feeding Traces of Proarticulata-The Vendian Metazoa. *Paleontol. J.* 45, 237–248. doi:10.1134/s0031030111030063
- Ivantsov, A. Y., and Malakhovskaya, Y. E. (2002). Giant Traces of Vendian Animals. In *Doklady Earth Sciences C/C of Doklady-Akademiia Nauk. INTERPERIODICA PUBLISHING*. 385, 618–622.
- Joel, L. V., Droser, M. L., and Gehling, J. G. (2014). A New Enigmatic, Tubular Organism from the Ediacara Member, Rawnsley Quartzite, South Australia. *J. Paleontol.* 88 (2), 253–262. doi:10.1666/13-058
- Kovalchuk, O., Owttrim, G. W., Konhauser, K. O., and Gingras, M. K. (2017). Desiccation Cracks in Siliciclastic Deposits: Microbial Mat-Related Compared to Abiotic Sedimentary Origin. *Sediment. Geol.* 347, 67–68. doi:10.1016/j.sedgeo.2016.11.002
- Kumar, S., and Ahmad, S. (2014). Microbially Induced Sedimentary Structures (MISS) from the Ediacaran Jodhpur Sandstone, Marwar Supergroup, Western Rajasthan. *J. Asian Earth Sci.* 91, 352–361. doi:10.1016/j.jseas.2014.01.009
- Laflamme, M., Schiffbauer, J. D., and Narbonne, G. M. (2012). “Deep-water Microbially Induced Sedimentary Structures (MISS) in Deep Time: The Ediacaran Fossil Ivesheadia,”. *Microbial Mats in Siliciclastic Depositional Systems through Time*. Editors N. Noffke and H. Chafetz (Tulsa: SEPM Special Publication), 101, 111–123.
- Liu, A. G., Brasier, M. D., Bogolepova, O. K., Raevskaya, E. G., and Gubanov, A. P. (2013). First Report of a Newly Discovered Ediacaran Biota from the Irkineeva Uplift, East Siberia. *Newsletters Stratigr.* 46, 95–110. doi:10.1127/0078-0421/2013/0031
- Mariotti, G., Pruss, S. B., Perron, J. T., and Bosak, T. (2014). Microbial Shaping of Sedimentary Wrinkle Structures. *Nat. Geosci.* 7, 736–740. doi:10.1038/ngeo2229
- Morganti, T. M., Purser, A., Rapp, H. T., German, C. R., Jakuba, M. V., Hehemann, L., et al. (2021). *In Situ* observation of Sponge Trails Suggests Common Sponge Locomotion in the Deep central Arctic. *Curr. Biol.* 31 (8), R368–R370. doi:10.1016/j.cub.2021.03.014
- Nettle, D., Halverson, G. P., Cox, G. M., Collins, A. S., Schmitz, M., Gehling, J., et al. (2014). A Middle-Late Ediacaran Volcano-Sedimentary Record from the Eastern Arabian-Nubian Shield. *Terra Nova* 26, 120–129. doi:10.1111/ter.12077
- Noffke, N. (2009). The Criteria for the Biogenicity of Microbially Induced Sedimentary Structures (MISS) in Archean and Younger, sandy Deposits. *Earth-Science Rev.* 96, 173–180. doi:10.1016/j.earscirev.2008.08.002
- Noffke, N. (2015). Ancient Sedimentary Structures in the <3.7 Ga Gillespie Lake Member, Mars, that Resemble Macroscopic Morphology, Spatial Associations, and Temporal Succession in Terrestrial Microbialites. *Astrobiology* 15, 169–192. doi:10.1089/ast.2014.1218
- Noffke, N., Knoll, A., and Grotzinger, J. (2002). Sedimentary Controls on the Formation and Preservation of Microbial Mats in Siliciclastic Deposits: A Case Study from the Upper Neoproterozoic Nama Group, Namibia. *Palaio* 17, 533–544. doi:10.1669/0883-1351(2002)017<0533:scotfa>2.0.co;2
- Paterson, J. R., Gehling, J. G., Droser, M. L., and Bicknell, R. D. C. (2017). Rheotaxis in the Ediacaran Epibenthic Organism *Parvancorina* from South Australia. *Sci. Rep.* 7, 45539. doi:10.1038/srep45539
- Payne, J. L., McClain, C. R., Boyer, A. G., Brown, J. H., Finnegan, S., Kowalewski, M., et al. (2011). The Evolutionary Consequences of Oxygenic Photosynthesis: A Body Size Perspective. *Photosynth. Res.* 107, 37–57. doi:10.1007/s11120-010-9593-1
- Porada, H., and Bouougri, E. H. (2007). Wrinkle Structures-A Critical Review. *Earth-Science Rev.* 81, 199–215. doi:10.1016/j.earscirev.2006.12.001
- Powell, M. G., and Kowalewski, M. (2002). Increase in Evenness and Sampled Alpha Diversity through the Phanerozoic: Comparison of Early Paleozoic and Cenozoic marine Fossil Assemblages. *Geol.* 30 (4), 331–334. doi:10.1130/0091-7613(2002)030<0331:ieasa>2.0.co;2
- Reinhard, C. T., and Planavsky, N. J. (2021). The History of Ocean Oxygenation. *Annu. Rev. Mar. Sci.* 14, 331–353. doi:10.1146/annurev-marine-031721-104005
- Reinhard, C. T., Planavsky, N. J., Olson, S. L., Lyons, T. W., and Erwin, D. H. (2016). Earth's Oxygen Cycle and the Evolution of Animal Life. *Proc. Natl. Acad. Sci. USA* 113, 8933–8938. doi:10.1073/pnas.1521544113
- Sarkar, S., Bose, P., Samanta, P., Sengupta, P., and Eriksson, P. (2008). Microbial Mat Mediated Structures in the Ediacaran Sonia Sandstone, Rajasthan, India, and Their Implications for Proterozoic Sedimentation. *Precambrian Res.* 162, 248–263. doi:10.1016/j.precamres.2007.07.019
- Sarkar, S., Samanta, P., and Altermann, W. (2011). Setulfs, Modern and Ancient: Formative Mechanism, Preservation Bias and Palaeoenvironmental Implications. *Sediment. Geology*. 238, 71–78. doi:10.1016/j.sedgeo.2011.04.003
- Sarkar, S., Choudhuri, A., Mandal, S., and Eriksson, P. G. (2016). Microbial Mat-Related Structures Shared by Both Siliciclastic and Carbonate Formations. *J. Palaeogeogr.* 5, 278–291. doi:10.1016/j.jop.2016.05.001
- Seilacher, A. (1999). Biomat-Related Lifestyles in the Precambrian. *PALAIOS* 14 (1), 86–93. doi:10.2307/3515363
- Sperling, E. A., and Vinther, J. (2010). A Placozoan Affinity for *Dickinsonia* and the Evolution of Late Proterozoic Metazoan Feeding Modes. *Evol. Dev.* 12, 201–209. doi:10.1111/j.1525-142x.2010.00404.x
- Sperling, E. A., Wolock, C. J., Morgan, A. S., Gill, B. C., Kunzmann, M., Halverson, G. P., et al. (2015). Statistical Analysis of Iron Geochemical Data Suggests Limited Late Proterozoic Oxygenation. *Nature* 523, 451–454. doi:10.1038/nature14589
- Stal, L. J., Gernerden, H., and Krumbein, W. E. (1985). Structure and Development of a Benthic marine Microbial Mat. *FEMS Microbiol. Ecol.* 31 (2), 111–125. doi:10.1111/j.1574-6968.1985.tb01138.x
- Surprenant, R. L., Gehling, J. G., and Droser, M. L. (2020). Biological and Ecological Insights from the Preservation Variability of *Funisia Dorothea*, Ediacara Member, South Australia. *PALAIOS* 35, 359–376. doi:10.2110/palo.2020.014
- Sutherland, D. L. (2009). Microbial Mat Communities in Response to Recent Changes in the Physicochemical Environment of the Meltwater Ponds on the McMurdo Ice Shelf, Antarctica. *Polar Biol.* 32, 1023–1032. doi:10.1007/s00300-009-0601-x

- Tarhan, L. G., Droser, M. L., and Gehling, J. G. (2010). Taphonomic Controls on Ediacaran Diversity: Uncovering the Holdfast Origin of Morphologically Variable Enigmatic Structures. *Palaio* 25, 823–830. doi:10.2110/palo.2010.p10-074r
- Tarhan, L. G., Droser, M. L., Gehling, J. G., and Dzaugis, M. P. (2015). Taphonomy and Morphology of the Ediacara Form Genus *Aspidella*. *Precambrian Res.* 257, 124–136. doi:10.1016/j.precamres.2014.11.026
- Tarhan, L. G., Hood, A. V. S., Droser, M. L., Gehling, J. G., and Briggs, D. E. G. (2016). Exceptional Preservation of Soft-Bodied Ediacara Biota Promoted by Silica-Rich Oceans. *Geology* 44, 951–954. doi:10.1130/g38542.1
- Tarhan, L. G., Droser, M. L., Gehling, J. G., and Dzaugis, M. P. (2017). Microbial Mat Sandwiches and Other Anactolistic Sedimentary Features of the Ediacara Member (Rawnsley Quartzite, South Australia): Implications for Interpretation of the Ediacaran Sedimentary Record. *Palaio* 32, 181–194. doi:10.2110/palo.2016.060
- Tarhan, L. G., Droser, M. L., and Gehling, J. G. (2022). Picking Out the Warp and Weft of the Ediacaran Seafloor: Paleoenvironment and Paleocology of an Ediacara Textured Organic Surface. *Precambrian Res.* 369, 106539. doi:10.1016/j.precamres.2021.106539
- Vago, J. L., and Westall, F. (2017). Pasteur Instrument Teams, Landing Site Selection Working Group, and; Other Contributors (2017). Habitability on Early Mars and the Search for Biosignatures with the ExoMars Rover. *Astrobiol.* 17, 471509. doi:10.1089/ast.2016.1533
- Woodward, G., Ebenman, B., Emmerson, M., Montoya, J., Olesen, J., Valido, A., et al. (2005). Body Size in Ecological Networks. *Trends Ecol. Evol.* 20, 402–409. doi:10.1016/j.tree.2005.04.005
- Xiao, S., Droser, M., Gehling, J. G., Hughes, I. V., Wan, B., Chen, Z., et al. (2013). Affirming Life Aquatic for the Ediacara Biota in China and Australia. *Geology* 41 (10), 1095–1098. doi:10.1130/G34691.1
- Xiao, S., Chen, Z., Zhou, C., and Yuan, X. (2019). Surfing in and on Microbial Mats: Oxygen-Related Behavior of a Terminal Ediacaran Bilaterian Animal. *Geology* 47 (11), 1054–1058. doi:10.1130/g46474.1
- Xiao, S., Chen, Z., Pang, K., Zhou, C., and Yuan, X. (2020). The Shibantan Lagerstätte: Insights into the Proterozoic–Phanerozoic Transition. *Jol. Geol. Soc.* 178, jgs2020 135. doi:10.1144/jgs2020-135
- Xiao, S., and Laflamme, M. (2009). On the Eve of Animal Radiation: Phylogeny, Ecology and Evolution of the Ediacara Biota. *Trends Ecol. Evol.* 24, 31–40. doi:10.1016/j.tree.2008.07.015

Conflict of Interest: The authors declare that the research was conducted in the absence of any commercial or financial relationships that could be construed as a potential conflict of interest.

Publisher's Note: All claims expressed in this article are solely those of the authors and do not necessarily represent those of their affiliated organizations, or those of the publisher, the editors and the reviewers. Any product that may be evaluated in this article, or claim that may be made by its manufacturer, is not guaranteed or endorsed by the publisher.

Copyright © 2022 Droser, Evans, Tarhan, Surprenant, Hughes, Hughes and Gehling. This is an open-access article distributed under the terms of the Creative Commons Attribution License (CC BY). The use, distribution or reproduction in other forums is permitted, provided the original author(s) and the copyright owner(s) are credited and that the original publication in this journal is cited, in accordance with accepted academic practice. No use, distribution or reproduction is permitted which does not comply with these terms.



Methodological Development of a Combined Preparation for Micropaleontological and Sedimentological Studies of Samples From the Proterozoic Record

Matheus Denezine^{1*}, Rodrigo Rodrigues Adôrno^{1,2}, Dermeval Aparecido Do Carmo¹, Edi Mendes Guimarães¹, Detlef Hans Gert Walde¹, Carlos José Souza De Alvarenga¹, Gerard Germs³, Lucas Silveira Antonietto¹, Christian Gianfranco Valdivia Rodríguez⁴ and Osvaldo De Oliveira Nunes Junior¹

¹Institute of Geosciences, University of Brasília, Brasília, Brazil, ²Geological Survey of Brazil, Brasília, Brazil, ³Department of Geology, University of the Free State, Bloemfontein, South Africa, ⁴Institute of Chemistry, University of Brasília, Brasília, Brazil

OPEN ACCESS

Edited by:

Juliana Leme,
University of São Paulo, Brazil

Reviewed by:

Luana Morais,
University of São Paulo, Brazil
Clive Francis Burrett,
Mahasarakham University, Thailand

*Correspondence:

Matheus Denezine
matheusdenezine@gmail.com

Specialty section:

This article was submitted to
Paleontology,
a section of the journal
Frontiers in Earth Science

Received: 06 November 2021

Accepted: 18 January 2022

Published: 30 March 2022

Citation:

Denezine M, Adôrno RR, Do Carmo DA, Guimarães EM, Walde DHG, De Alvarenga CJS, Germs G, Antonietto LS, Valdivia Rodríguez CG and Nunes Junior ODO (2022) Methodological Development of a Combined Preparation for Micropaleontological and Sedimentological Studies of Samples From the Proterozoic Record. *Front. Earth Sci.* 10:810406. doi: 10.3389/feart.2022.810406

The recovery of microfossils from Proterozoic rocks is commonly challenging because of metamorphism. In this study, an application of different methods usually applied on Phanerozoic rocks to test efficiency on recovering microfossil from Proterozoic units is presented. Chemical, physical, and biological factors can influence the recovery of microfossils, thereby becoming a barrier for biostratigraphic and paleoecological studies. Furthermore, low-cost projects with a reduced amount of sample collected, such as drill core sampling, need to optimize the preparation time and sample needed for different analyses. To overcome this challenge, the classical procedure of mineralized microfossil preparation, the palynological technique, and the study of clay mineralogy with the analyses of diagenetic alteration and the search for possible microfossils in thin sections were combined. Three Proterozoic lithostratigraphic units were selected to develop an integrated procedure for preparing samples for micropaleontologic and sedimentologic studies: the Paranoá Group, Mesoproterozoic, and the Bambuí Group, Ediacarian-Cambrian, Brazil, and Nama Group, Ediacaran-Cambrian, Namibia. Recovering individual microfossils from the Paranoá and Bambuí groups has been a challenge for paleontologists. Therefore, most micropaleontological studies have been done as a part of microfossils analyses in thin sections. All sediment fractions were studied in trial for the examination (and picking) of mineralized microfossils, even the finest ones. The microfossil picking was conducted using a stereomicroscope. Three species were recovered following this procedure: *Vetronostocale* aff *V. amoenum* Schopf and Blacic, 1971, *Myxococcoides* sp., and *Melanocyrrillium* sp. Analyses in whole rock samples of residues from water (H₂O) and hydrogen peroxide 30% (H₂O₂) procedures showed similar results when the clay fraction studied was obtained as part of micropaleontological preparation compared with the results from the standard clay mineral preparation method. The clay fraction diffractograms showed that the micropaleontological preparation with H₂O and H₂O₂ caused an increase in the intensity of the quartz reflections compared with

untreated samples. Moreover, detailed protocols for organic-walled microfossil preparation and low concentrated acetic and formic acids attacks for mineralized microfossil extraction were presented.

Keywords: micropaleontological preparation, sedimentological preparation, proterozoic microfossils, clay minerals, curatorship protocol

INTRODUCTION

The diversity and preservation of fossil specimens from the Precambrian have been considered rare compared with those recovered from the Phanerozoic (Knoll, 1985; Schopf, 1995). Among other causes, such as taphonomic alterations, which greatly influence the fossil record, the preparation methodology also plays an essential role in recovering. Therefore, this barrier in the study of the Precambrian strata requires methodological considerations because, depending on the method applied, the fossil record may be lost. The present study proposes a protocol to increase microfossil recovery based on a combined methodology focused on micropaleontological and sedimentological analysis integration (Alves, 1987; Campos, 2012; Horne and Siveter, 2016; Leite et al., 2018). Samples from Paranoá and Bambuí groups, Brazil, and Nama Group, Namibia, were analyzed to assess all methods presented in this study.

Because of distinctive micropaleontological recoveries procedures on samples from Phanerozoic to other strata, it is necessary to formalize preparation methodologies for recovery of organic-walled and mineralized microfossils from Precambrian lithostratigraphic units. With mineralized micropaleontological analyses, the residues from the same preparation can be used for clay mineral analyses. This combination accelerates the whole research besides reducing the costs of preparation procedures. The application of this protocol could improve the recovery of microfossils from Precambrian units and, consequently, improve biostratigraphic studies besides combining analyses for micropaleontology and sedimentology for integration and reduction of costs. In the present case, at least three laboratories are working together, Laboratory of Mineralized Microfossils, Laboratory of Organic-walled Microfossils, and Laboratory of X-ray Diffraction, so curatorial procedures must be shared and followed to promote efficiency on data acquisition and analysis integration.

Moreover, it also detailed the curatorship procedures, identification, allocation by collection category, packaging, and housing samples under the policy of the Museum of Geosciences, University of Brasília. In addition to the management methodology, rules for the transit of samples between laboratories are also described.

GEOLOGICAL SETTINGS

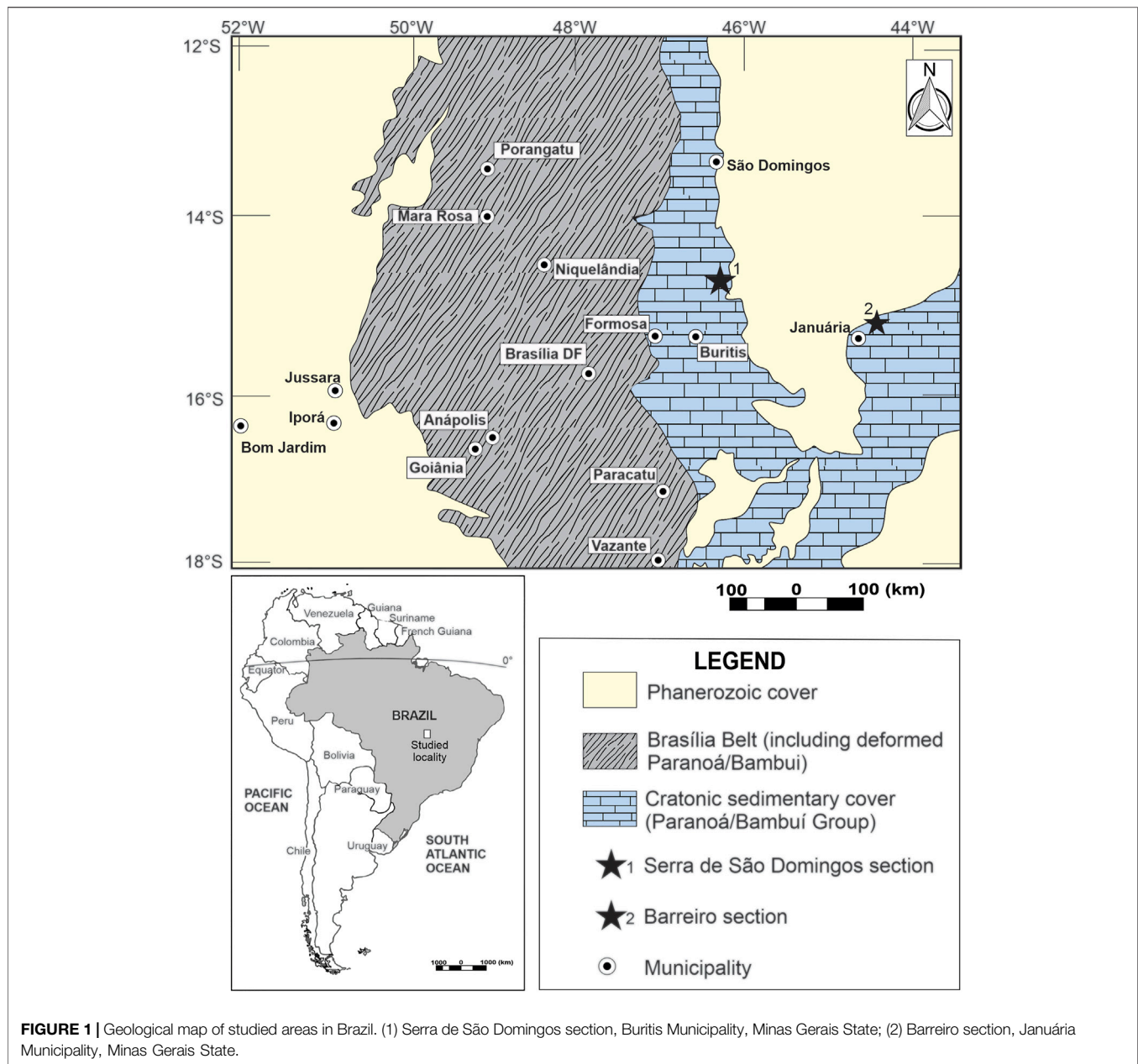
Two localities in Minas Gerais State, Brazil, were studied: the Buritis Municipality, which is part of the Brasília belt within the Tocantins province, and the Januária Municipality, which is located in a nondeformed domain of the São Francisco craton (Figure 1). A thick interval of Meso-Neoproterozoic sedimentary rocks was

deposited along the west portion of the San Francisco craton. These rocks were separated into three stratigraphic units, from bottom to top: Paranoá Group, Jequitai Formation, and Bambuí Group.

The deposition of terrigenous and chemical sedimentary rocks belonging to the Paranoá Group dates from the Mesoproterozoic when the separation of the Rodinia supercontinent generated a passive rift-margin basin, West of the São Francisco craton (Alvarenga et al., 2014). Faria (1995) studied the stratigraphy of the Paranoá Group in the type locality of Alto Paraíso de Goiás and São João D'Aliança municipalities, Goiás State, Brazil; however, the study did not formalize the units according to any stratigraphic code. Thereafter, Campos et al. (2013) formalized 11 stratigraphic units within the Paranoá Group according to the Brazilian Code of Stratigraphic Nomenclature in order to adjust the informal units proposed by Faria (1995). The Paranoá Group consists of, in ascending stratigraphic order, the Ribeirão São Miguel, Córrego Cordovil, Serra da Boa Vista, Serra Almécegas, Serra do Paranã, Ribeirão Piçarrão, Ribeirão do Torto, Serra da Meia Noite, Ribeirão Contagem, Córrego do Sansão, and Córrego do Barreiro formations (Campos et al., 2013) (Figure 3).

After the deposition of the Paranoá Group, because of climatic changes, the Jequitai Formation was deposited under glacial conditions, and their records remain in erosional contact with the Paranoá Group (unconformity) (Uhlein et al., 1995; Caxito et al., 2012). Right above in conformable contact, the carbonated-terrigenous Bambuí Group was deposited in a foreland-type basin generated from the flexure caused by tectonics in the Brasília belt. The Bambuí Group consists of five lithostratigraphic units, from base to top, the Sete Lagoas, Serra de Santa Helena, Lagoa do Jacaré, Serra da Saudade, and Três Marias formations (Dardenne, 1978) (Figure 3). Lately, the Bambuí Group has been attributed to the Ediacaran/Cambrian interval (Pimentel et al., 2011; Warren et al., 2014; Paula-Santos et al., 2015; Moreira et al., 2020; Sanchez et al., 2021).

The Nama Group, Namibia (Figure 2), represents the deposition in a shallow water foreland system; the deposition of the basal portion started around 550 Ma, followed by the deposition of siliciclastic Molasse sediments from the upper portion deposited in 540 Ma (Germs, 1983; Germs and Gresse, 1991). In the central and southern part of Namibia, the Nama Group rests discordantly on the crystalline basement. Its basal portion is represented by a succession of siliciclastic and carbonate rocks with occurrences of skeletal fossils of *Cloudina lucianoi* and other fossils with carbonate skeletons, as well as ichnofossils and palynomorphs in the Kuibis Formation (Germs, 1995; Gaucher et al., 2005). The upper portion of the Nama Group is represented by the Schwarzrand subgroup, which contains the ichnofossil *Phycodes pedom*, *Cloudina*, and palynomorphs (Figure 3) (Germs, 1983; Germs and Gresse, 1991; Gaucher et al., 2005).

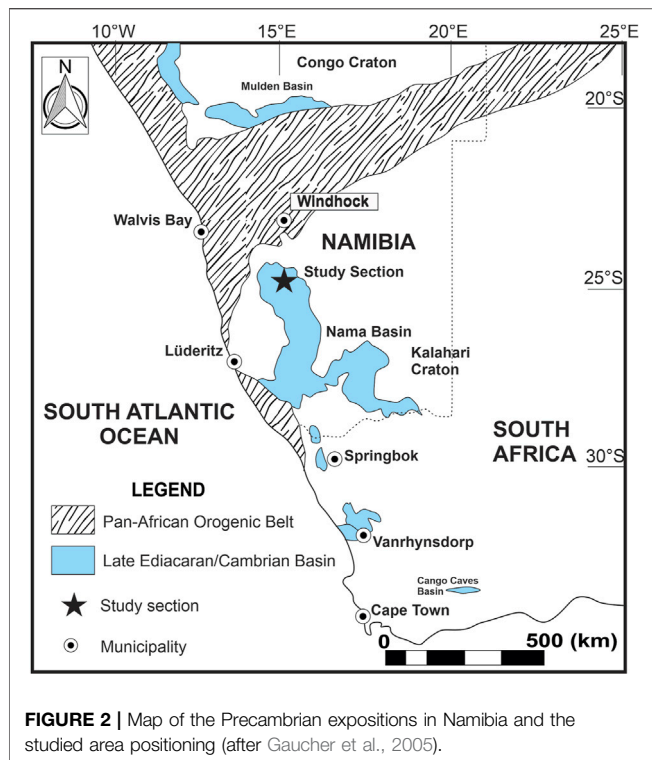


MATERIALS AND METHODS

The studied material is from three Precambrian units: Paranoá (Mesoproterozoic) and Bambuí (Ediacaran-Cambrian) groups, São Francisco craton, Brazil, and Nama Group (Ediacaran-Cambrian), Namibia. The samples from Brazil were collected in outcrops from Buritis and Januária municipalities, Minas Gerais State (Table 1). Detailed methodological processes for microfossiliferous recovery are discussed in *Preparation Methodologies*.

The same sample was analyzed through different ways to obtain clay minerals information: (1) using the residues from water (H_2O) and hydrogen peroxide 30% (H_2O_2) micropaleontological preparations; (2) using the standard clay preparation, which initially included material disaggregation with a hammer and

powdering in the Planetary Mill pulverisette by Fritsch for 5 min with 400 revolutions/min. X-ray powder diffraction was carried out on clay fractions. Clay fractions ($<2\ \mu m$) were separated by centrifugation routine at LARIX described by Campos (2012) and modified from Alves (1987). The measurements were undertaken in oriented clay fractions in air-dried conditions. Analyses were performed in a RIGAKU Ultima IV diffractometer equipped with $CuK\alpha$ radiation, Ni filter, under 35 kV and 15 mA. The samples were scanned at $5^\circ/\text{min}$ velocity, 0.05 stepping ranging from 2 to $40^\circ 2\theta$ for clay fraction. Mineral phases were identified using Jade XRD 9.0 (Materials Data) with PC-PDF (Powder Diffraction File—PDF for PC—ICDD). Major (M), minor (m), and trace (tr) components were established by comparing the reflection intensities in d: $4.26\ \text{\AA}$ for quartz, $10\ \text{\AA}$ for illite, and $7\ \text{\AA}$ for chlorite.



CURATORSHIP PROTOCOL

Curatorship procedures must rule the studied material (rocks and fossils samples) management when multiple analysis is performed in different laboratories. This procedure aims to share information about samples, data acquisition, and analysis integration. In this study, the protocol used at the Micropaleontology Laboratory of the University of Brasília (LabMicro), on curatorship of geological and paleontological samples that become housed at the Museum of Geosciences, was presented. The LabMicro is currently responsible for the Paleontological Collection of the Museum of Geosciences of the University of Brasília (MGeo), which is subdivided into seven collections: (1) field collection, (2) residual samples, (3) recovered collection, (4) research collection, (5) special collection, (6) didactical collection, and (7) macrofossil collection (**Table 2**).

Sample curatorship starts during fieldwork. Field sampling is always accompanied by labeling to identify collected samples once they arrive at the laboratory. This is guaranteed by the mandatory completion of an individual sample tag containing data about their recollection site (**Figure 4**). The field collection comprises materials that have recently arrived at the LabMicro through fieldwork, independent of its immediate use (or not) as research, teaching, and/or training material. If they generate such interest, samples are due to be processed through laboratory work, which will result in both a residual sample and possible recovered fossil assemblage. The residual sample left from preparation is stored in the residual collection in field bags inside storage cabinets, whereas the recovered fossil assemblage is encased in micropaleontological slides to be held

in specific fossil cabinets, consisting of the recovered collection. Research macrofossil and microfossil specimens, used to illustrate taxa in publications such as articles, theses, and reports, are isolated from others either in macrofossil cabinets or microslides that will be deposited at their specific fossil cabinets. In this case, the specimen is relocated into the research collection and recoded with a CP prefix.

Special collection covers fossil material of scientific interest donated or temporarily transferred to the MGeo by partner institutions such as universities, private companies, and other museums. The didactical collection is used in undergraduate and graduate courses given by the Institute of Geosciences, University of Brasília (IG); it comprises fossil material from other collections at the LabMicro and those collected by professors and students at the IG, as well as third-party direct donations. Finally, the macrofossil collection comprises macrofossil samples that require special conditions for safekeeping because of their size; therefore, they are stored in a cabinet of their own.

Samples arriving at the LabMicro initially get separated into three collections: field, macrofossils, or residual collections (the latter to be prepared for possible microfossil recovery). Once the fossil content is recovered from analyzed samples by picking, it is deposited either on multicelled micropaleontological slides (carbonate/siliceous fossils separated from rock through sieving) or glass microscope slides (organic-walled microfossils concentrated through organic preparation). The possible use of any microfossils on publications requires their relocation into single-celled micropaleontological slides to be stored in the research collection cabinet or the relocation of the entire glass microscope slide (with microfossils of scientific relevance properly marked) into the same space.

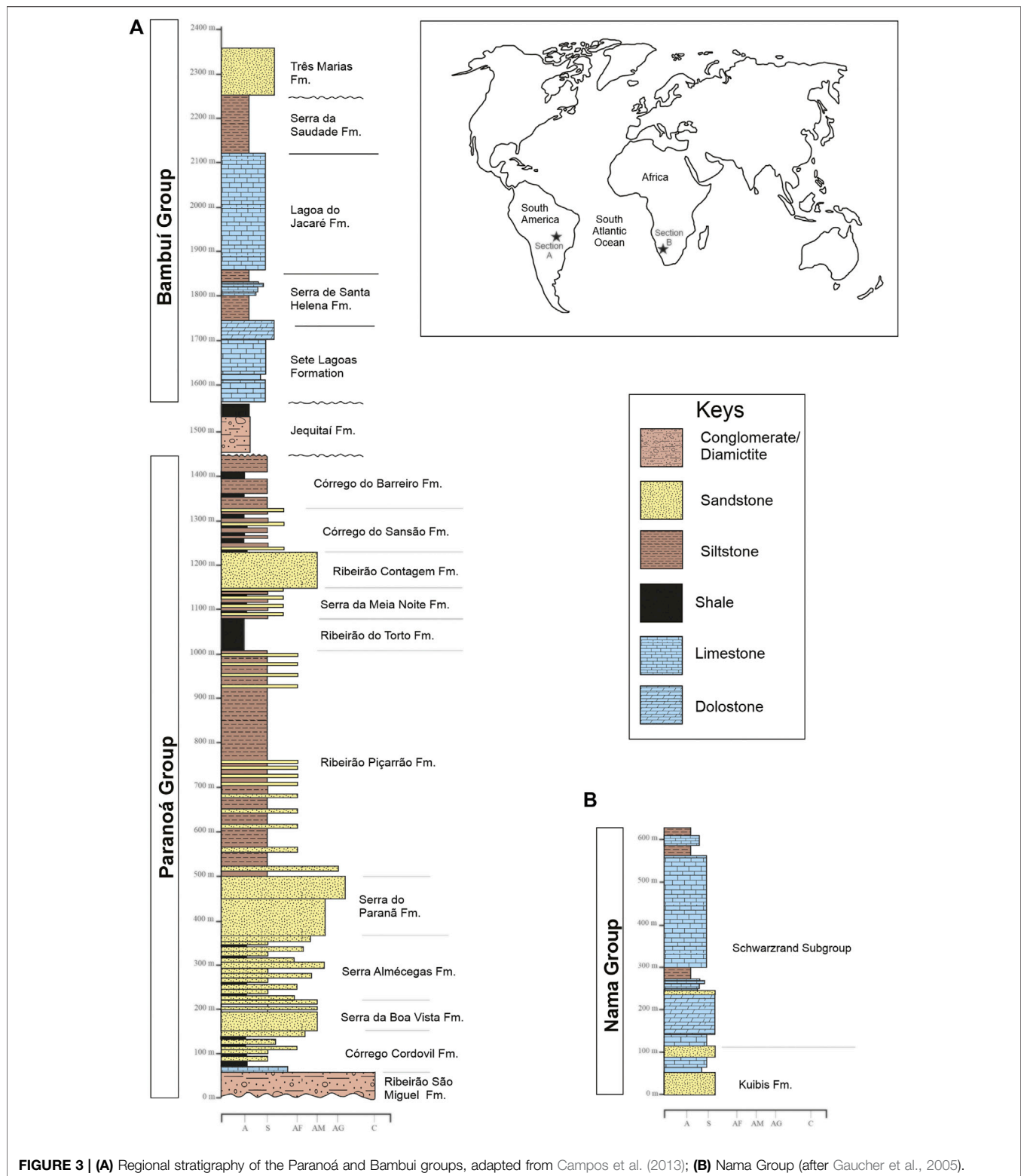
PREPARATION METHODOLOGIES

Once the initial steps of the curatorial procedure are completed, thin-section slides of the samples are produced for sedimentological/paleontological studies. Subsequently, a mechanical fragmentation of samples can be performed by using several possible methodologies, including soaking them in H₂O and/or chemical attack with H₂O₂, acetic acid 4%–10%, formic acid 10%, hydrochloric acid 36% (HCl), and hydrofluoric acid 40% (HF).

In the present work, both water and oxygen peroxide preparations were performed for mineralized microfossiliferous recovery. After washing both preparations on a sieve set (composed of 630-, 250-, 120-, 80-, and 50- μ m mesh sieves plus a collecting bucket underneath), each fraction was analyzed on a stereoscopic microscope to pick for mineralized fossil remains.

Combined Preparation for Mineralized Microfossils and Clay Minerals (H₂O or H₂O₂)

The preparation presented herein aims to recover mineralized fossiliferous remains from disaggregating 30 g of sedimentary



rock samples. This method is commonly used with Quaternary and Cretaceous units (Horne and Siveter, 2016; Leite et al., 2018; Machado et al., 2020). Two distinct sieving procedures were conducted on the same sample for mineralized microfossil


recovery and clay mineral analyses: (1) treatment with water before sieving and (2) attack with hydrogen peroxide before sieving. Both methods aim to disaggregate the rock sample. After sieving both products from the water treatment and

TABLE 1 | Samples from Ediacaran units analyzed for specific preparations.

Sample	Fossils recovered	Lithotype	Stratigraphic unit	Locality	Applied methods
MP1203	CP965; CP966; CP967; CP968; CP969	Siltstone	Paranoá Group	Serra de São Domingos section, Buritis, Brazil	H ₂ O and H ₂ O ₂ analyses
MP1221	CP970	Siltstone	Bambuï Group, Sete Lagoas Formation	Rio de São Domingos section, Buritis, Brazil	H ₂ O, H ₂ O ₂ , and clay mineral analyses
MP1226	—	Siltstone	Bambuï Group, Serra de Santa Helena Formation	Rio de São Domingos section, Buritis, Brazil	H ₂ O, H ₂ O ₂ , and clay mineral analyses
MP1231	CP971; CP972; CP 973	Siltstone	Bambuï Group, Serra de Santa Helena Formation	Rio de São Domingos section, Buritis, Brazil	H ₂ O, H ₂ O ₂ , and clay mineral analyses
MP2289	CP974	Limestone	Nama Group, Kuibis Subgroup	Namibia	Low concentrated acetic acid
MP2995	CP961	Limestone	Bambuï Group, Sete Lagoas Formation	Barreiro section, Januária, Brazil	H ₂ O, H ₂ O ₂ , HCl, and HF attacks
MP3013	CP914	Limestone	Bambuï Group, Sete Lagoas Formation	Barreiro section, Januária, Brazil	H ₂ O, H ₂ O ₂ , HCl, and HF attacks
MP3034	CP963	Limestone	Bambuï Group, Sete Lagoas Formation	Barreiro section, Januária, Brazil	H ₂ O, H ₂ O ₂ , HCl, and HF attacks
MP3710	CP916	Limestone	Bambuï Group, Sete Lagoas Formation	Barreiro section, Januária, Brazil	H ₂ O, H ₂ O ₂ , HCl, and HF attacks
MP3714	CP917	Limestone	Bambuï Group, Sete Lagoas Formation	Barreiro section, Januária, Brazil	H ₂ O, H ₂ O ₂ , HCl, and HF attacks

TABLE 2 | Collections into the paleontological collection of the Museum of Geosciences, University of Brasília.

Collection	Code	Material
Field collection	Code gave during fieldwork	Rock sample
Residual collection	MP	Residual rock and organic fractions
Recovered collection	MP (same as the residual collection)	Microfossils recovered but not illustrated in publications
Research collection	CP	Microfossils illustrated in publications
Special collection	Coded according to their previous repository	Microfossils donated and loaned from another institution
Didactical collection	CD	Rock, microfossils, and macrofossils for didactical purposes
Macrofossil collection	MAF	Macrofossils


SAMPLE FORM - IG/UnB
SAMPLE P _____ Am _____
P = GPS point (arabic); Am = sampling sequence by point

Special Collection nº UnB-GEO-E _____

City _____

Objective of the fieldwork _____

Participantes _____

Sampling date ____/____/____

Group/Formation/Member/Suite/Complex _____

Geographic location _____

Lithotype _____

Column level _____

GPS point _____ Zone _____ Datum _____ Altitude _____

Coord UTM _____ mL _____ mN, _____

Obs: _____ MP: _____

FIGURE 4 | Sample datasheet used to identify samples during the Laboratory of Micropaleontology fieldwork, University of Brasília, Brazil. The datasheet contains all information needed for further curatorship.

hydrogen peroxide attack, the sedimentary fractions were dried in a laboratory drying oven, and then analyses were performed under a stereoscope microscope to pick microfossils.

After mechanical disaggregation, a single sample followed two preparation routes: (1) left in beaker for 48 h with H₂O and (2) left in beaker for 48 h with H₂O₂ 30% (PV). After these procedures, the samples were washed in a battery of sieves (630, 250, 160, 80, and 50 µm) (**Figure 5**). The fraction smaller than 50 µm were kept in an appropriate container. All fractions were dried in a laboratory drying oven at 60°C and then examined under a stereoscope microscope to pick microfossils. This drying temperature prevents unwanted fragmentation of microfossils. The finest fraction (>50 µm) from both preparations was also analyzed through X-ray diffraction for clay minerals studies.

Mineralized Microfossiliferous Recovery (Acetic and Formic Acid Attacks)

The traditional study of *Cloudina* species and other tubular carbonate fossils hosted in limestone is performed preferably in two-dimensional (2D) views. This analysis uses polish or thin sections due to the ease of this methodology and quick

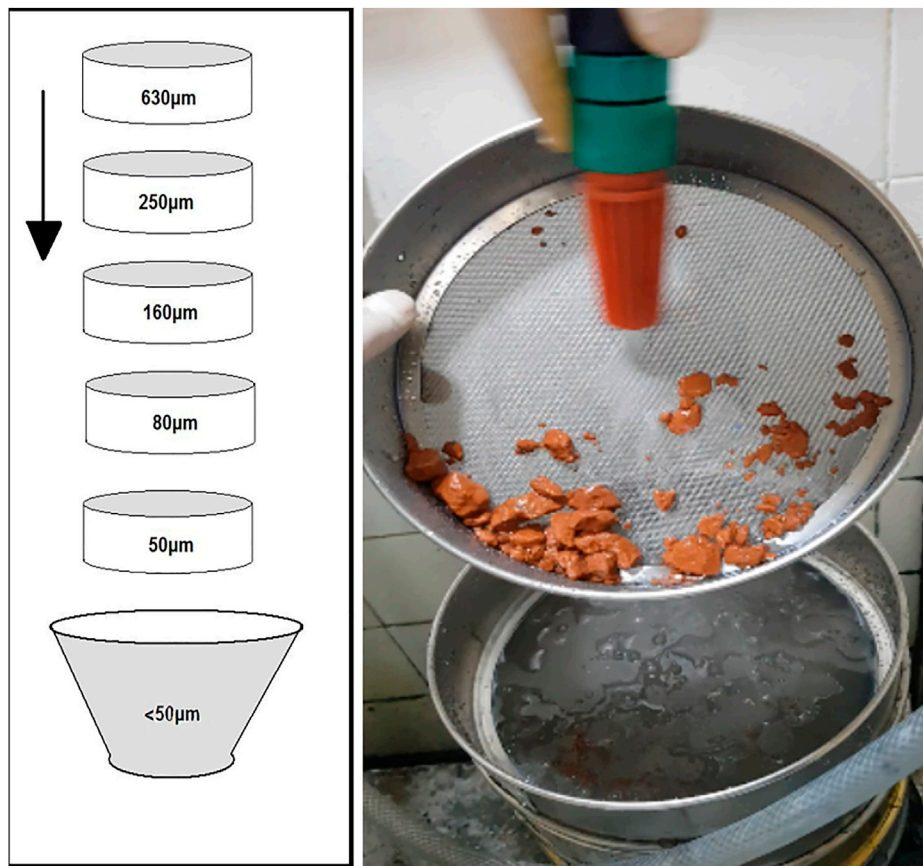


FIGURE 5 | Battery of sieves (630, 250, 160, 80, and 50 μm) and final recipient to store sediments smaller than 50 μm.

preparation, although studying fossils in 2D views make the 3D morphology reconstruction more complex and less accurate. In some cases, phosphatization processes offer an opportunity to know more about its morphology. The fossil can be easily isolated from the rock matrix by acid attack without destroying the specimen (Hua et al., 2003). In contrast, when the composition of the fossil and that of the matrix are both carbonates, it becomes a challenge to separate the specimen from the rock. This work shows a new methodology of fossil extraction using a low concentrated acetic acid such as vinegar (~4% acetic acid).

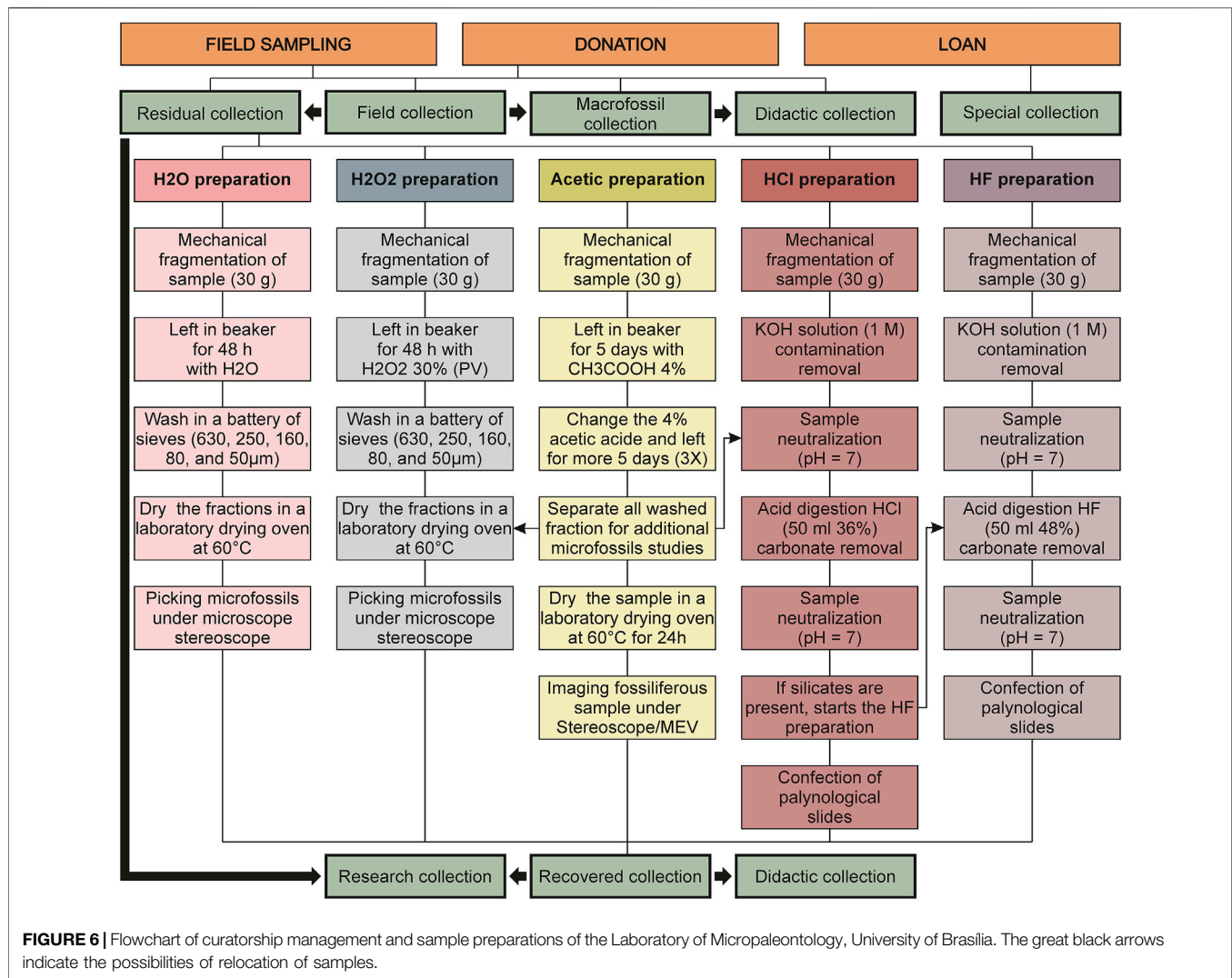
The preparation returned a positive result because acetic acid (4%) attacks the carbonate matrix preferentially, to the detriment of the carapace. Its slightly larger magnesium content is dissolved more slowly than the carbonate matrix. The dissolved fraction of the sample can be separated to analyze the palynological content (Figure 6).

The methodology consists of selecting a fossiliferous sample and introducing acetic acid solution 4% concentration. As the shell composition varies slightly from the matrix's, it allows the acid to act differently, releasing the specimens following the reaction: $\text{CaCO}_{3(s)} + 2\text{CH}_3\text{COOH}_{(aq)} \rightarrow \text{Ca}(\text{CH}_3\text{-COO})_{2(aq)} + \text{H}_2\text{O}_{(l)} + \text{CO}_{2(g)}$. A similar, but slower, process occurs in the outcrops of these carbonate fossiliferous rocks, where the

carbonic acid (H_2CO_3) of the rain erodes the matrix resulting in the eventual exposition of the skeleton. The reaction can be controlled daily by observing the acid's reaction on the fossiliferous sample. The entire preparation cycle takes approximately 15–20 days. The acid must be replaced every 3 days. At the end of the preparation, the sample must be gently and thoroughly washed with running water for approximately 5 min.

After the preparation mentioned previously, the fragments retained in sieves with mesh equal to or greater than 160 μm undergo a new preparation, this time using weak acids, such as acetic acid, to attack limestone, and formic acid, to attack dolomites, both at 10% concentration, with the aim of disaggregating the sample. For each sample to be prepared, it is recommended to use 1 L of 10% diluted acid solution for 200 g of sample. The sample is then placed in a hood, where it will remain until the chemical reaction is complete.

Periodically, after every 24 h of acid attack, it is recommended to change this acidic solution, as it loses its reaction power as the limestone is attacked. The solution that would initially be discarded during the exchange process, as it is a methodological evaluation, is separated for testing in micropaleontology. These tests are carried out with an emphasis on permineralized palynomorphs and for those



microfossils that may be sorted with the aid of a stereoscopic microscope (any particle in suspension).

When weak acids are used, the preparation can take up to 2 months to be completed, but instead, the risk of destruction of mineralized microfossils is reduced. After being disaggregated, the material is washed in a battery of sieves. The fraction retained in each sieve is dried in an oven at 60°C and then examined under a stereoscopic microscope.

Organic-Walled Microfossils Preparation (Hydrochloric and Hydrofluoric Acid Attacks)

Approximately 30 g of sample is used for preparation to recover organic microfossils. Here, the mineral components of the rock are dissolved using two acids: HCl and HF (Figure 6). First, fragmented samples are put in a 400-mL beaker, adding 50 mL of HCl at 36% concentration during 24 h to dissolve carbonates. The next step is to bring the sample solution to a neutral pH value, using distilled water in periodic washings. The neutralization

procedure involves the addition of distilled water to beaker capacity, waiting for the decantation of the organic extract, carefully removing the acid solution; the process is repeated until neutral pH is reached. Then 50 mL of HF at 40% concentration is added to dissolve silicates for 48 h. Then, the washing procedure is repeated. All recovered organic residues are placed in polypropylene tubes and distilled water at pH 7 to further conserve these residues.

After the acid attack process, the final remains are named palynological extract. This material is kept in water solution and, sometimes, when following the classic procedure, needs to be sieved before preparing palynological slides. In synthesis, this traditional procedure uses aleatory organic remains distributed in this solution to prepare palynological slides. Nevertheless, an approach to this classic procedure on picking palynological remains under a stereoscope microscope is presented. Using a very liner brush (000), it is possible to select specimens to prepare palynological slides with this procedure. There are two ways of making palynological slides: (1) palynological slides created after picking microfossils under a stereoscope microscope; (2)

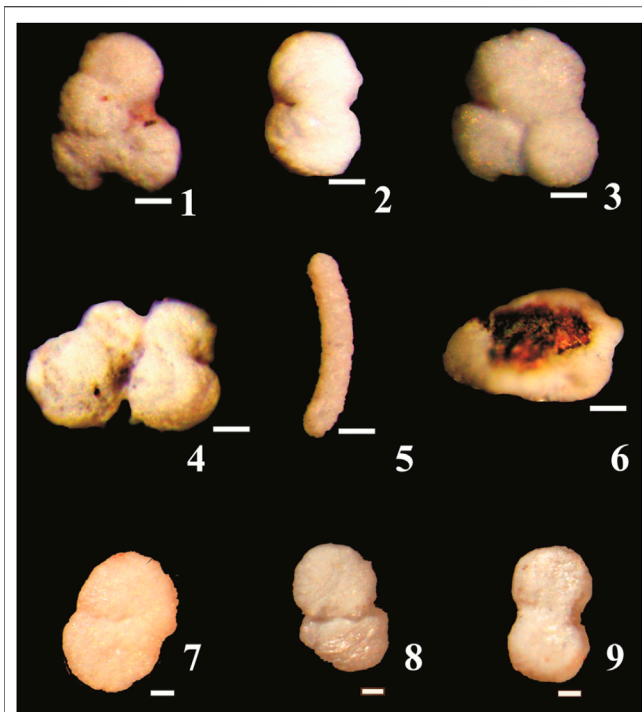


FIGURE 7 | Recovered specimens from the Proterozoic units of the São Francisco craton, São Domingos River section (samples from the Sete Lagoas, MP1221, and Serra de Santa Helena, MP1231, formations) and from São Domingos Hill section (sample from the Paranoá Group, MP1203), Municipality of Buritis, Minas Gerais State, Brazil. **(1–5)** Specimens from the Paranoá Group; **(6)** Specimens from the Sete Lagoas Formation, Bambuí Group; **(7–9)** Specimens from the Serra de Santa Helena, Bambuí Group. **(1–4, 7–9)** *Myxococcoides* sp., respectively, CP965, CP966, CP967, CP968, CP971, CP972, CP 973; **(5)** *Vetronostocale* aff. *V. amoenum* Schopf and Blacic, 1971, CP969; **(6)** *Melanocyrrillium* sp., CP970. Scale bar: 10 μ m.

palynological slides without preanalyses under stereoscope microscope, which involves placing a few drops of the recovered organic residue and distilled water on a glass cover. Both types of slides are prepared after putting on a heating plate at 30°C. After the water had evaporated, a few drops of Entellan® resin were added to the coverslip to be completely sealed after contact with the blade. The resin used has the function of drying together with the material mounted on the blade and preventing oxidation of the organic matter and its degradation.

RESULTS AND REMARKS

The results presented comprehend micropaleontological, mineralized, organic-walled microfossils, and sedimentological data, specifically clay mineral analyses. The oxidation attack was conducted to promote the complete or partial disaggregation of sedimentary rock. When sedimentary rock is composed of organic matrix, the H_2O_2 reacts with it and may result in a full or partial disaggregation. In this case, it is possible to recover microfossils in the H_2O_2 preparation, even in samples with oxidation considered ineffective (MP1226) and low efficiency (MP1203,

MP1221, and MP1231). After the chemical reaction, the sedimentary material was sieved and by picking finest fractions. The coccoidal structures, as well as tubular and vase-shaped structures, recovered (**Figure 7**) were recognized as fossil content due to their similar morphological and size features assigned to well-described species and genus commonly found in Precambrian units. Besides that, they are very distinct from other grain particles analyzed from the same sample. The species recovered from the Paranoá Group, Mesoproterozoic, from sample MP1203, comprehends *Myxococcoides* sp. (CP965, CP966, CP967, CP968) (**Figures 7.1–4**) and *Vetronostocale* aff. *V. amoenum* Schopf and Blacic, 1971 (CP969) (**Figure 7.5**). One species was recovered in the Sete Lagoas Formation, Bambuí Group, from sample MP1221: *Melanocyrrillium* sp. (CP970) (**Figure 7.6**), and one species was recovered from the Serra de Santa Helena Formation, Bambuí Group, from sample MP1231: *Myxococcoides* sp. (CP971, CP972, CP973) (**Figures 7.7–9**).

The limestone samples of Sete Lagoas Formation, Januária Municipality, did not show a considerable disaggregation effectiveness. The H_2O_2 disaggregation method shows more effectiveness on siliciclastic rocks when compared with carbonate rocks. This could be due to the difference in permeability of those two lithotypes. The more permeable the rock, the easier the H_2O_2 reacts with the organic matter content. In this context, metamorphism can also affect the H_2O_2 disaggregation process as, depending on the metamorphic grade, it could change the rock permeability because of rock compaction.

The finest fraction (>50 μ m) sieved from samples MP1226, MP1221, and MP1231 from three distinct micropaleontological preparations procedures were analyzed: (1) treatment with tap water before sieving, (2) treatment with deionized water before sieving, and (3) hydrogen peroxide attack before sieving. Analyses in whole rock from all three procedures showed similar results when the clay fraction studied was obtained as part of micropaleontological preparation compared with the results from the standard clay mineral preparation method. The total similarities between diffractograms could be verified when both oxidized (H_2O_2) and nonoxidized (tap water and deionized water) preparations of the same sample (**Table 3**) are compared. The mineral composition of the whole rock sample, determined by X-ray diffraction, shows that all samples have quartz as their major constituent, besides the sample MP1221, which also has calcite as the major component. Illite and albite are minor constituents of all samples.

The standard clay mineral preparation results present changes in reflection intensities compared with the whole rock: the phyllosilicates have higher reflection intensity, which becomes major constituents, whereas the quartz reflection intensity decreases, which becomes a minor constituent. When the standard clay mineral preparation results are analyzed, the clay fraction shows the same composition as the whole rock, but (except for calcite in MP1221) the reflection intensities are opposite to those of the whole rock. Chlorite and illite are major constituents in the clay fraction, whereas quartz and albite are minor constituents (**Figure 8**). The diffractograms of samples MP1226 and MP1221 show a low and ill-defined band at the d~28 position that expands slightly under treatment with

TABLE 3 | Mineral composition of siltstones in whole rock and clay fraction, indicating the major constituents (M), minor (m), and trace (tr).

Sample	Preparation	Identified minerals	Whole rock	Clay fraction
MP1226	Standard clay mineral preparation	Clinochlore (chlorite)	m or tr	M
		Illite (muscovite)	m or tr	M
		Quartz	M	M
		Albite (feldspar)	m	M
	Micropaleontological residues	H ₂ O	Clinochlore (chlorite)	m
			Illite (muscovite)	m
			Quartz	M
			Albite (feldspar)	m
		H ₂ O ₂	Clinochlore (chlorite)	m or tr
			Illite (muscovite)	m
			Quartz	M
			Albite (feldspar)	m
MP 1221	Standard clay mineral preparation	Clinochlore (chlorite)	m	M
		Illite (muscovite)	m	M
		Quartz	M	m
		Albite (feldspar)	M	m
		Calcite	M	M
	Micropaleontological residues	H ₂ O	Clinochlore (chlorite)	M
			Illite (muscovite)	M
			Quartz	M
			Albite (feldspar)	m
			Calcite	M
		H ₂ O ₂	Clinochlore (chlorite)	m or tr
			Illite (muscovite)	m
			Quartz	M
			Albite (feldspar)	m
			Calcite	M
MP 1231	Standard clay mineral preparation	Clinochlore (chlorite)	M	M
		Illite (muscovite)	M	M
		Quartz	M	m or tr
		Albite (feldspar)	m	m or tr
	Micropaleontological residues	H ₂ O	Clinochlore (chlorite)	M
			Illite (muscovite)	m
			Quartz	M
			Albite (feldspar)	M
		H ₂ O ₂	Clinochlore (chlorite)	M
			Illite (muscovite)	m
			Quartz	M
			Albite (feldspar)	M

glycerol, indicating the presence of interstratified clay mineral, possibly illite/vermiculite. Clay residues obtained from samples treated with H₂O and H₂O₂ during the micropaleontological preparation do not maintain this trend. The clay fraction maintains the same intensities as the total sample: quartz remains a major constituent, whereas phyllosilicates are presented as minor or trace constituents (**Figure 9**). This effect can be explained as the effect of disaggregation, dispersion, or release of quartz particles during micropaleontological treatment.

The procedure of analyzing the same sample residue for both micropaleontological and sedimentological approaches as a combined preparation reduces time of maceration and costs, besides being sure that both analyses comprehend the

same depositional interval. This association leads to a more precise paleoenvironmental interpretation. In addition, it can save samples when a small amount is available for multiple analyses.

The acetic acid preparation was conducted on a sample from the Nama Group, Namibia; it showed efficient extraction of carbonate *C. luciano* skeleton within a carbonate matrix. This extraction technique allowed 3D imaging of the carbonate skeleton (**Figure 10**). This preparation shows similar results compared with phosphatized skeleton preparations from Dengying Formation in China (Hua et al., 2005). Researchers might use this easy, accessible, and environmentally friendly method to conduct 3D studies on carbonate skeleton fossils within limestone rocks. This

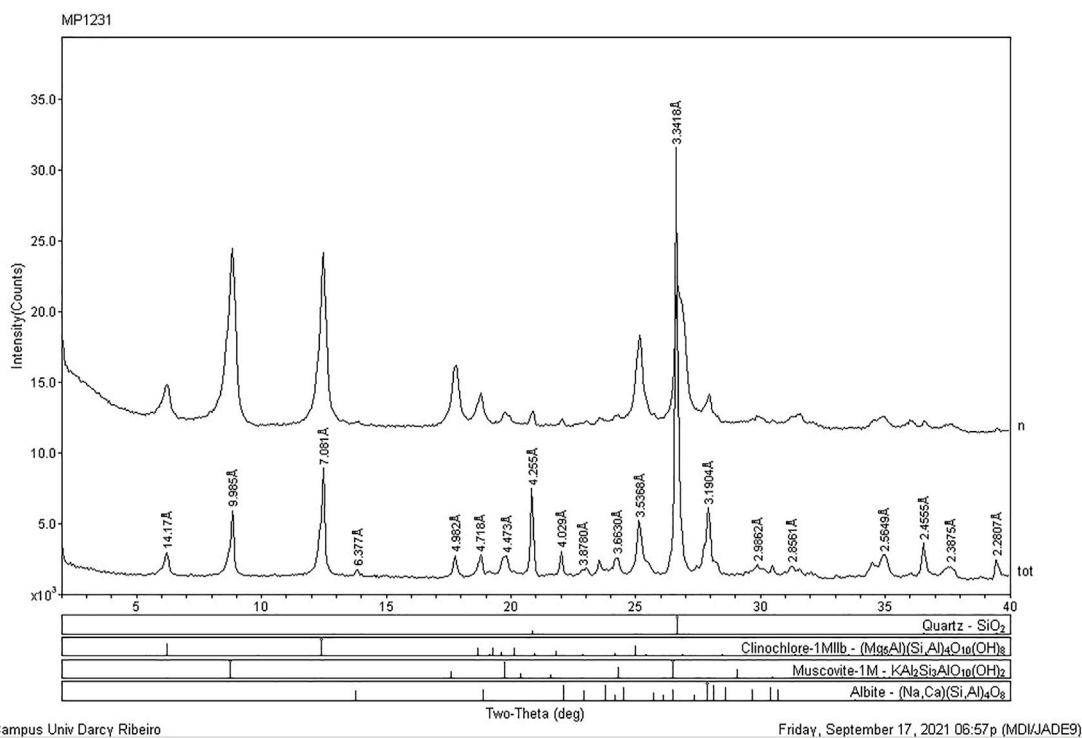


FIGURE 8 | Diffractograms of sample MP1231 from Bambuí Group, Municipality of Buritis, Minas Gerais State, Brazil. Whole rock (tot) and clay fraction (n); note the variation in reflection intensities.

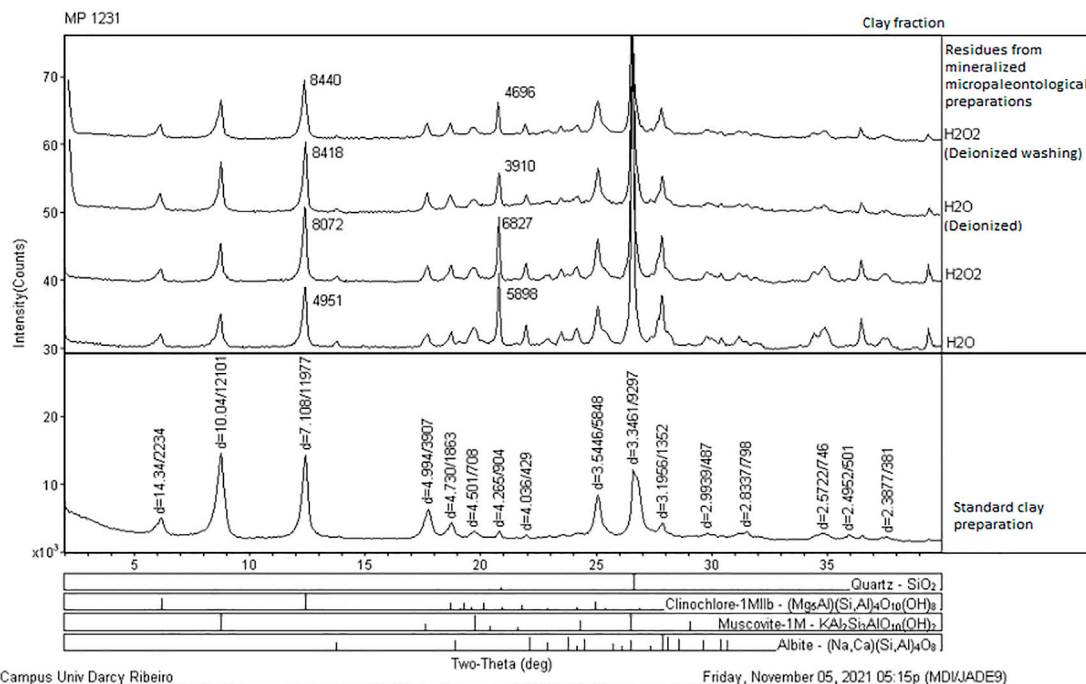


FIGURE 9 | Diffractogram of the sample MP1231 from Bambuí Group, Municipality of Buritis, Minas Gerais State, Brazil. Clay fraction (n); note the variation in reflection intensities between the diffractogram of untreated sample (base) and treated samples; note that all treatments have the same effect on the clay fraction.

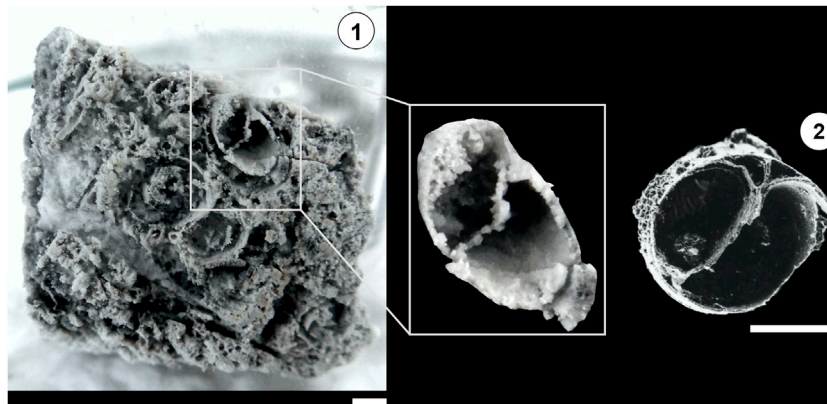


FIGURE 10 | Comparison between results of different preparations. **(1)** *Cloudina lucianoi* (Beurlen and Sommer, 1957), CP974. Sample MP2289, carbonate from the type-section of *Cloudina riemkeae* Germs, 1972, Nomtsas Formation, Namibia, (UTM Coord. 33 k 0667883 7358829); **(2)** Phosphatized skeleton of *Cloudina lucianoi* from Dengying Formation, China (Hua et al., 2005). Scale bars: 400 µm.

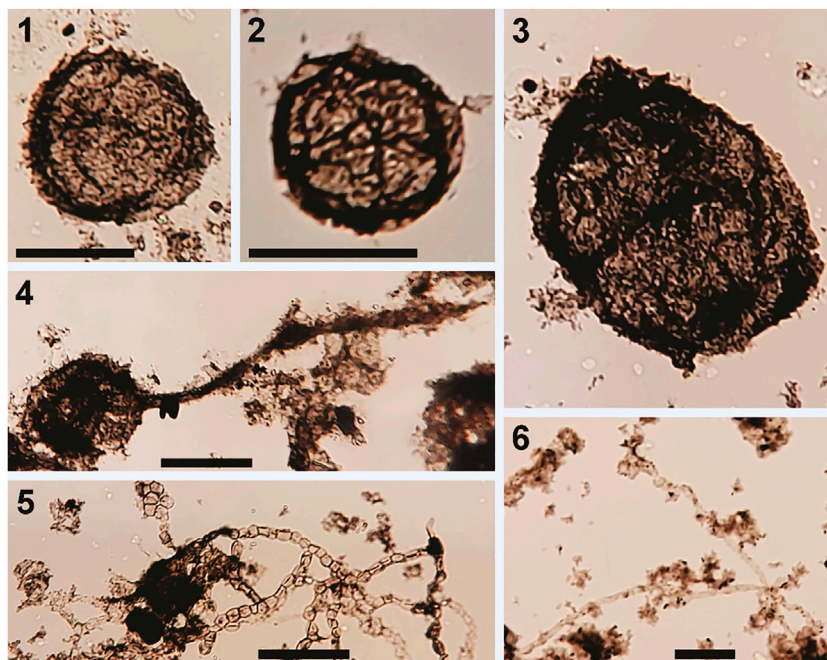


FIGURE 11 | Organic-walled microfossils recovered from Sete Lagoas Formation, Bambuí Group, Januária Municipality. **(1–2)** *Leiosphaeridia minutissima* (Naumova, 1949)—CP963; **(3)** *Leiosphaeridia tenuissima* Eisenack, 1958—CP914; **(4)** *Germinosphaera bispinosa* Mikhailova, 1986 - CP917; **(5)** *Ghoshia* sp.—CP916; **(6)** *Siphonophycus robustum* (Schopf, 1968)—CP961. Scale bars: 25 µm.

extraction is possible when the skeleton composition is slightly or entirely different compared with the host carbonate matrix, such as the case of (1) the slightly richer magnesium *C. lucianoi* skeleton from Namibia and (2) the complete different composition of the phosphatized *C. lucianoi* skeleton from Dengying Formation, China (Hua et al., 2005).

The organic-walled microfossil preparation of limestones from Sete Lagoas Formation, Bambuí Group, Januária Municipality, Minas Gerais State, Brazil (Table 1), which

followed the protocol presented in this work, led to the recovery of exquisitely specimens of organic-walled microfossils. The recovered assemblage comprises *Leiosphaeridia minutissima* (Naumova, 1949), CP963 (Figures 11.1, 2) and *Leiosphaeridia tenuissima* Eisenack, 1958, CP914 (Figure 11.3), one acritarch: *Germinosphaera bispinosa* Mikhailova, 1986, CP917 (Figure 11.4), and two cyanobacteria species: *Ghoshia* sp., CP916 (Figure 11.5), and *Siphonophycus robustum* (Schopf, 1968), CP961 (Figure 11.6).

CONCLUSION

- (1) Efficiency of mineralized microfossiliferous disaggregation using H_2O_2 : differences in disaggregation efficiency were observed, varying from ineffective (MP1226) to low efficiency (MP1203, MP1221, and MP1231). The lithotype, the amount of organic matter within the matrix, and the metamorphic grade can influence the disaggregation efficacy. The H_2O_2 disaggregation method shows more effectiveness on siliciclastic rocks when compared with carbonate rocks. This could be due to the difference in permeability of those two lithotypes. The more permeable the rock, the easier the H_2O_2 reacts with the organic matter content. In this context, metamorphism can also affect the H_2O_2 disaggregation process as, depending on the metamorphic grade, it could change the rock permeability due to rock compaction.
- (2) Mineralized microfossils recovered using the H_2O_2 preparation: three permineralized species were recovered: *Vetronostocale* aff *V. amoenum* Schopf and Blacic, 1971 (from Paranoá Group), *Myxococcoides* sp. (from Paranoá Group and Lagoa do Jacaré Formation, Bambuí Group), and *Melanocyrrillium* sp. (from Sete Lagoas Formation, Bambuí Group).
- (3) Organic-walled microfossils recovered from Sete Lagoas Formation, Bambuí Group, using HCl and HF preparation: *L. minutissima* (Naumova, 1949), *L. tenuissima* Eisenack, 1958, *G. bispinosa* Mikhailova, 1986, *Ghoshia* sp., *S. robustum* (Schopf, 1968). The organic residue can integrate organic carbon isotopic studies.
- (4) Mineralized microfossils recovered using acetic acid preparation: *C. luciano* (Beurlen and Sommer, 1957).
- (5) Integration of clay mineral and micropaleontology preparations methods: the whole rock diffractograms of siltstones without treatments (standard preparation for clay mineral analyses) or treated in micropaleontological preparation with H_2O (tap water or deionized water) and H_2O_2 did not show differences and allow the determination of mineral composition.
- (6) Clay fraction diffractograms of residues from micropaleontological preparation: The clay fraction diffractograms showed that the micropaleontological preparation caused an increase in the intensity of the quartz reflections compared with untreated samples. Samples obtained after micropaleontological treatment may not be suitable for assessing the intensity of diagenesis using the Kübler Index, but they are useful for identifying the mineral assemblage.
- (7) 3D extraction of a skeletal fossil can be possible even when the skeleton is carbonate in a carbonate matrix using weak acetic acid dissolution. This extraction is possible when the skeleton composition is slightly or entirely different from the host carbonate matrix. The organic material released by this preparation can be integrated into palynology studies.

DATA AVAILABILITY STATEMENT

The original contributions presented in the study are included in the article/Supplementary Material, further inquiries can be directed to the corresponding author.

AUTHOR CONTRIBUTIONS

MD—Fieldwork, data collection and interpretation, drawing of the figures and writing of the manuscript. RA—Fieldwork, data collection and interpretation, drawing of the figures and writing of the manuscript. DC—Ph.D. supervisor of MD, fieldwork, data interpretation and writing of the manuscript. EG—Data interpretation, drawing of the figures and writing of the manuscript. DW—Fieldwork and review of the paleontological and stratigraphic aspects of the manuscript. CA—Fieldwork and review of the stratigraphic aspects of the manuscript. GG—Fieldwork, data collection. LA—Curator of the Paleontology Collection of the Museum of Geosciences, University of Brasília, review the curatorship protocol and the mineralized microfossiliferous preparation protocol. CV—Data interpretation and review of the manuscript. OJ—Data collection and interpretation of the mineralized microfossils.

FUNDING

This study was financed in part by the Coordination for the Improvement of Higher Education Personnel—Brazil (CAPES)—Finance Code 001. Part of the studied samples was obtained from the Ediacarian Project, funded by the National Agency for Petroleum, Gas, and Biofuels (ANP) and the Brazilian Petroleum Corporation (PETROBRAS).

ACKNOWLEDGMENTS

We want to thank all institutions that participated in the development of this research: the National Council for Scientific and Technological Development (CNPq), the Coordination for the Improvement of Higher Education Personnel (CAPES), CAPES/IODP—Brazil Program via project 88887.091704/2014-01, the Brazilian Petroleum Corporation (PETROBRAS), the National Agency for Petroleum, Gas, and Biofuels (ANP) and the University of Brasília (UnB). We thank FINATEC for assistance in administrative affairs supporting scientific projects in Brasília. We would like to specially thank Dr. Norma Maria da Costa Cruz for approaching and sharing the palynological preparation method with students. We thank the two reviewers whose comments and suggestions helped improve and clarify this manuscript.

REFERENCES

- Alvarenga, C. J. S., Santos, R. V., Vieira, L. C., Lima, B. A. F., and Mancini, L. H. (2014). Meso-Neoproterozoic Isotope Stratigraphy on Carbonates Platforms in the Brasília Belt of Brazil. *Precambrian Res.* 251, 164–180. doi:10.1016/j.precamres.2014.06.011
- Alves, D. B. (1987). Desenvolvimento da metodologia de preparação de amostras para análise difratométrica de argilominerais no Centro de Pesquisas da Petrobrás. *Bol. Geociências da Petrobras* 1, 157–175.
- Beurlen, K., and Sommer, F. W. (1957). *Observações estratigráficas e paleontológicas sobre o calcário Corumbá*. Rio de Janeiro: Departamento Nacional de Produção Mineral, Divisão de Geologia e Mineralogia, Boletim, Vol. 168, 1–35.
- Campos, J. E. G., Dardenne, M. A., Freitas-Silva, F. H., and Martins-Ferreira, M. A. C. (2013). Geologia Do Grupo Paranoá na porção externa da Faixa Brasília. *Braz. J. Geol.* 43, 461–476. doi:10.5327/Z2317-48892013000300004
- Campos, L. F. B. (2012). *Diagênese das seqüências Proterozóicas com base na caracterização de argilominerais – topo do Grupo Paranoá e base do Grupo Bambuí – Norte do Distrito Federal* Masters Dissertation. Brasília: Institute of Geosciences, University of Brasília, 145.
- Caxito, F. d. A., Halverson, G. P., Uhlein, A., Stevenson, R., Gonçalves Dias, T., and Uhlein, G. J. (2012). Marinoan Glaciation in East central Brazil. *Precambrian Res.* 200–203, 38–58. doi:10.1016/j.precamres.2012.01.005
- Dardenne, M. A. (1978). “Síntese sobre a estratigrafia Do Grupo Bambuí no Brasil Central,” in *XXX Congresso Brasileiro de Geologia* (Recife: Trabalho completo), 597–610.
- Eisenack, A. (1958). Microfossilien aus dem Ordovizium des Baltikums, 1, Markasitschicht, Dictyonema-Scheifer, Glaukonitsand, Glaukonitkalk. *Senckenbergian Lethaea* 39, 389–404.
- Faria, A. (1995). *Estratigrafia e sistemas deposicionais do Grupo Paranoá nas áreas de Cristalina. Distrito Federal e São João D’aliança-Alto Paraíso de Goiás*. Doctoral Thesis. Brasília: Institute of Geosciences, University of Brasília, 199.
- Gaucher, C., Frimmel, H. E., and Germs, G. J. B. (2005). Organic-walled Microfossils and Biostratigraphy of the Upper Port Nolloth Group (Namibia): Implications for Latest Neoproterozoic Glaciations. *Geol. Mag.* 142, 539–559. doi:10.1017/S0016756805001123
- Germs, G. J. B., and Gresse, P. G. (1991). The Foreland basin of the Damara and Gariep Orogens in Namaqualand and Southern Namibia: Stratigraphic Correlations and basin Dynamics. *South Afr. J. Geol.* 94, 159–169.
- Germs, G. J. B. (1983). “Implications of a Sedimentary Facies and Depositional Environmental Analysis of the Nama Group in South West Africa/Namibia,” in *Evolution of the Damara Orogen of South Africa/Namibia*. Editor R. M. Miller (South Africa: Geological Society of South Africa), 89–114.
- Germs, G. J. B. (1972). New Shelly Fossils from Nama Group, South West Africa. *Am. J. Sci.* 272, 752–761. doi:10.2475/ajs.272.8.752
- Germs, G. (1995). The Neoproterozoic of Southwestern Africa, with Emphasis on Platform Stratigraphy and Paleontology. *Precambrian Res.* 73, 137–151. doi:10.1016/0301-9268(94)00075-3
- Horne, D. J., and Siveter, D. J. (2016). Collecting and Processing Fossil Ostracods. *J. Crustac. Biol.* 36, 841–848. doi:10.1163/1937240X-00002487
- Hua, H., Chen, Z., Yuan, X., Zhang, L., and Xiao, S. (2005). Skeletogenesis and Asexual Reproduction in the Earliest Biomineralizing Animal Cloudina. *Geol.* 33, 277–280. doi:10.1130/G21198.1
- Hua, H., Pratt, B. R., and Zhang, L.-Y. (2003). Borings in Cloudina Shells: Complex Predator-Prey Dynamics in the Terminal Neoproterozoic. *Palaios* 18, 454–459. doi:10.1669/0883-1351(2003)018<0454:bicscp>2.0.co;2
- Knoll, A. H. (1985). Patterns of Evolution in the Archean and Proterozoic Eons. *Paleobiology* 11, 53–64. doi:10.1017/s0094837300011398
- Leite, A. M., Do Carmo, D. A., Ress, C. B., Pessoa, M., Caixeta, G. M., Denezine, M., et al. (2018). Taxonomy of Limnic Ostracoda (Crustacea) from the Quiricó Formation, Lower Cretaceous, São Francisco basin, Minas Gerais State, Southeast Brazil. *J. Paleontol.* 92, 661–680. doi:10.1017/jpa.2018.1
- Machado, C. P., Coimbra, J. C., and Bergue, C. T. (2020). Provinciality of Ostracoda (Crustacea) in the Northeastern and Eastern Brazilian Shelves Based on Neontological and Paleontological Analyses. *Rev. Bras. Paleontol.* 23, 3–31. doi:10.4072/rbp.2020.1.01
- Mikhailova, N. S. (1986). “Novye Nakhodki Mikrofotofossilij Iz Otlozhenij Verkhnego Rifeya Krasnoyarskogo Kraya,” in *Aktual’nye Voprosy Sovremennoj, Naukova Dumka*. Editor B. S. Sokolov (Kiev: Nauka), 31–37.
- Moreira, D. S., Uhlein, A., Dussin, I. A., Uhlein, G. J., and Pimentel Misuzaki, A. M. (2020). A Cambrian Age for the Upper Bambuí Group, Brazil, Supported by the First U-Pb Dating of Volcaniclastic Bed. *J. South Am. Earth Sci.* 99, 102503–102515. doi:10.1016/j.jsames.2020.102503
- Naumova, S. N. (1949). Spores of the Lower Cambrian. *Izv. Akad. Nauk SSSR* 4, 49–56.
- Paula-Santos, G. M., Babinski, M., Kuchenbecker, M., Caetano-Filho, S., Trindade, R. I., and Pedrosa-Soares, A. C. (2015). New Evidence of an Ediacaran Age for the Bambuí Group in Southern São Francisco Craton (Eastern Brazil) from Zircon U-Pb Data and Isotope Chemostratigraphy. *Gondwana Res.* 28, 702–720. doi:10.1016/j.gr.2014.07.012
- Pimentel, M. M., Rodrigues, J. B., DellaGiustina, M. E. S., Junges, S., Matteini, M., and Armstrong, R. (2011). The Tectonic Evolution of the Neoproterozoic Brasília Belt, central Brazil, Based on SHRIMP and LA-ICPMS U-Pb Sedimentary Provenance Data: A Review. *J. South Am. Earth Sci.* 31, 345–357. doi:10.1016/j.jsames.2011.02.011
- Sanchez, E. A. M., Uhlein, A., and Fairchild, T. R. (2021). Treptichnus Pedum in the Três Marias Formation, South-central Brazil, and its Implications for the Ediacaran-Cambrian Transition in South America. *J. South Am. Earth Sci.* 105, 102983–102989. doi:10.1016/j.jsames.2020.102983
- Schopf, J. W., and Blacic, J. M. (1971). New Microorganisms from the Bitter Springs Formation (Late Precambrian) of the north-central Amadeus Basin, Australia. *J. Paleontol.* 45, 105–114.
- Schopf, J. W. (1995). “Disparate Rates, Differing Fates: Tempo and Mode of Evolution Changed from the Precambrian to the Phanerozoic,” in *Tempo and Mode in Evolution*. Editors W. M. Fitch and F. J. Ayala (Washington, D.C.: National Academy of Sciences), 41–62. Available at: <https://www.ncbi.nlm.nih.gov/books/NBK232208/>
- Schopf, J. W. (1968). Microflora of the Bitter Springs Formation, Late Precambrian, Central Australia. *J. Paleontol.* 42, 651–688.
- Uhlein, A., Trompette, R., and Egydio-Silva, M. (1995). Rifeamentos Superpostos E Tectônica De Inversão Na Borda Sudeste Do Cráton Do São Francisco. *Revista Geonomos* 3, 99–107. doi:10.18285/geonomos.v3i1.219
- Warren, L. V., Quaglio, F., Riccomini, C., Simões, M. G., Poiré, D. G., Strikis, N. M., et al. (2014). The Puzzle Assembled: Ediacaran Guide Fossil Cloudina Reveals an Old Proto-Gondwana Seaway. *Geology* 42, 391–394. doi:10.1130/G35304.1

Conflict of Interest: The authors declare that the research was conducted in the absence of any commercial or financial relationships that could be construed as a potential conflict of interest.

Publisher’s Note: All claims expressed in this article are solely those of the authors and do not necessarily represent those of their affiliated organizations, or those of the publisher, the editors and the reviewers. Any product that may be evaluated in this article, or claim that may be made by its manufacturer, is not guaranteed or endorsed by the publisher.

Copyright © 2022 Denezine, Adôrno, Do Carmo, Guimarães, Walde, De Alvarenga, Germs, Antonietto, Valdivia Rodríguez and Nunes Junior. This is an open-access article distributed under the terms of the Creative Commons Attribution License (CC BY). The use, distribution or reproduction in other forums is permitted, provided the original author(s) and the copyright owner(s) are credited and that the original publication in this journal is cited, in accordance with accepted academic practice. No use, distribution or reproduction is permitted which does not comply with these terms.



A New Conulariid (Cnidaria, Scyphozoa) From the Terminal Ediacaran of Brazil

Juliana M. Leme^{1*}, Heyo Van Iten^{2,3} and Marcello G. Simões⁴

¹Department of Sedimentary and Environmental Geology, Geosciences Institute, Universidade de São Paulo, São Paulo, Brazil,

²Department of Geology, Hanover College, Hanover, IN, United States, ³Department of Invertebrate Paleontology, Research Associate, Cincinnati Museum Center, Cincinnati, OH, United States, ⁴Sector of Zoology, Universidade Estadual Paulista, IB, UNESP, Botucatu, Brazil

OPEN ACCESS

Edited by:

Simon Darroch,
Vanderbilt University, United States

Reviewed by:

Marc Laflamme,
University of Toronto Mississauga,
Canada
Ross Anderson,
University of Oxford, United Kingdom
Frankie Dunn,
University of Oxford, United Kingdom

*Correspondence:

Juliana M. Leme
leme@usp.br

Specialty section:

This article was submitted to
Paleontology,
a section of the journal
Frontiers in Earth Science

Received: 15 September 2021

Accepted: 18 March 2022

Published: 08 June 2022

Citation:

Leme JM, Van Iten H and Simões MG
(2022) A New Conulariid (Cnidaria,
Scyphozoa) From the Terminal
Ediacaran of Brazil.
Front. Earth Sci. 10:777746.
doi: 10.3389/feart.2022.777746

Paraconularia ediacara n. sp., the oldest documented conulariid cnidarian, is described based on a compressed thin specimen from the terminal Ediacaran Tamengo Formation near Corumbá, Mato Grosso do Sul State, Brazil. The conulariid was collected from a laminated silty shale bed also containing *Corumbella weneri* and vendotaenid algae. The specimen consists of four partial faces, two of which are mostly covered, and one exposed corner sulcus. The two exposed faces exhibit 32 bell-curve-shaped, nodose transverse ribs, with some nodes preserving a short, adaperturally directed interspace ridge (spine). The transverse ribs bend adapertureward on the shoulders of the corner sulcus, within which the ribs terminate, with the end portions of the ribs from one face alternating with and slightly overlapping those from the adjoining face. This is the first Ediacaran body fossil showing compelling evidence of homology with a particular conulariid genus. However, unlike the periderm of Phanerozoic conulariids, the periderm of *P. ediacara* lacks calcium phosphate, a difference which may be original or an artifact of diagenesis or weathering. The discovery of *P. ediacara* in the Tamengo Formation corroborates the hypothesis, based in part on molecular clock studies, that cnidarians originated during mid-late Proterozoic times, and serves as a new internal calibration point, dating the split between scyphozoan and cubozoan cnidarians at no later than 542 Ma. Furthermore, *P. ediacara* reinforces the argument that the final phase of Ediacaran biotic evolution featured the advent of large-bodied eumetazoans, including, possibly, predators.

Keywords: conulariids, systematics, Ediacaran, Tamengo Formation, Paleocology

INTRODUCTION

One of the fundamental problems in the study of the history of life is the timing of the origins of the major groups of metazoans. Molecular clock studies (Runnegar, 1982; Hedges et al., 2004; Peterson et al., 1979; Erwin et al., 2011; dos Reis et al., 2015; Dohrmann and Wörheide, 2017) have placed the origins of the metazoan phyla within the Tonian (max.) to Ediacaran (min.) interval, dating key branching events, including the protostome-deuterostome split and the split between cnidarians and other eumetazoans, at various points within this broad time span. Standing in contrast to the results of molecular clock studies is present understanding of the Neoproterozoic fossil record. Specifically, Ediacaran body fossils currently interpreted as skeletonized or soft-bodied eumetazoans, for example *Cloudina*, *Corumbella*, and *Kimberella* (Fedonkin and Waggoner, 1997; Fedonkin et al., 2007;

Bobrovskiy et al., 2018; Dunn et al., 2021), are less than 600 million years old, and thus at present there is a substantial gap between the ages of the apparent first appearances of eumetazoans in the body fossil record and the oldest molecular clock estimates of their times of origin.

Described in this article is the first documented Neoproterozoic conulariid, *Paraconularia ediacara* n. sp. from the terminal Ediacaran Tamengo Formation (upper Corumbá Group) of west-central Brazil. This conulariid, currently represented by a flattened partial periderm preserving such anatomical features as transverse ribs, nodes, and microlamellae, was originally identified (Van Iten et al., 2014a; Van Iten et al., 2016) as *Paraconularia* sp. Previously, the oldest known occurrences of *Paraconularia* were in strata of Middle Devonian age (Hergarten, 1985; Babcock and Feldmann, 1986), and therefore the presence of this genus in the topmost part of the Ediacaran System is truly noteworthy.

Conulariids in general are an extinct order (Conulariida) of marine cnidarians, last occurring in the topmost Triassic (Norian) Stage (Lucas, 2012; Barth et al., 2013), that may have been most closely related to scyphozoan cnidarians of the extant order Coronata (Van Iten et al., 2006a). Conulariids and coronates are united by the possession of a prominent, sessile polyp stage that produced/produces a multi-lamellar, steeply pyramidal or conical periderm bearing (in some species) internal projections along the perradii and interradii (Werner, 1966; Van Iten et al., 1996). Conulariids also exhibit similarities to staurozoans, including tetramorous radial symmetry and prominent gastric septa (Van Iten, 1992; Jerre, 1994; Marques and Collins, 2004; Van Iten et al., 2006a), and thus the hypothesis of a sister group relationship between conulariids and staurozoans (Marques and Collins, 2004) may merit further investigation. The oldest previously known conulariids are *Baccaconularia meyeri* and *B. robinsoni* from the Furongian (late Cambrian) Saint Lawrence Formation of southwestern Wisconsin and southeastern Minnesota, United States (Hughes et al., 2000; Van Iten et al., 2006b). Two other Ediacaran fossils, *Vendoconularia triradiata* (late Ediacaran, White Sea Coast, Russia) (Ivantsov and Fedonkin, 2002; Van Iten et al., 2005; Ivantsov et al., 2019), preserved as molds and casts, and conulariid-like carbonaceous compression fossils from the early Ediacaran Lantian Formation of South China (Yuan et al., 2011; Van Iten et al., 2013), have been interpreted as conulariids or have been compared with this group (Ivantsov and Fedonkin, 2000; Van Iten et al., 2005; Ivantsov et al., 2019). However, hypotheses of homology between these Ediacaran fossils and conulariids have been challenged (Grazhdankin, 2014; Wan et al., 2016; Dzik et al., 2017). In contrast, conulariids exhibit detailed similarities in gross morphology to carinacitiids and hexangulaconulariids, two families of small shelly fossils (SSFs) from the basal (Fortunian) stage of the Cambrian System (Morris and Menge, 1992), and at present there seems to be no better candidate for the nearest relatives of these SSF taxa than conulariids (Guo et al., 2020a; Guo et al., 2020b; Guo et al., 2021). Importantly, the possible presence of Cambrian conulariids or closely related forms immediately above

the Ediacaran-Cambrian boundary itself suggests that conulariids may have originated during Neoproterozoic times.

The terminal Ediacaran genus *Corumbella*, currently known from localities in North and South America and Iran (Pacheco et al., 2015; Walde et al., 2015; Vaziri et al., 2018; Walde et al., 2019; Amorim et al., 2020), has also been interpreted as a polypoid scyphozoan closely related to conulariids (Van Iten et al., 2014a; Van Iten et al., 2016; Pacheco et al., 2015). It should be noted, however, that Walde et al. (2019, p. 335) hypothesized that *Corumbella* was a worm-like bilaterian.

The discovery of *Paraconularia* in strata of latest Ediacaran age not only demonstrates that conulariids crossed the crucial Ediacaran-Cambrian boundary, but it also corroborates the hypothesis that phylum Cnidaria originated during the Neoproterozoic. Additionally, the existence of this ancient scyphozoan, extant species of which engage in predation (Pearse et al., 1987), may provide additional support for the hypothesis (e.g., Hua et al., 2003; Schiffbauer et al., 2016) that the origin of predation and complex food webs predated the beginning of the Phanerozoic Eon and the Cambrian Explosion.

GEOLOGICAL SETTING

The late Ediacaran to earliest Cambrian (ca. 565–539 Ma; see Linnemann et al., 2019) Corumbá Group, named after the city of Corumbá in Mato Grosso do Sul State (west-central Brazil), crops out at the junction of the Amazon Craton, the northern Rio Apa Block, and the folded southern Paraguay Belt (Amorim et al., 2020) (**Figure 1**). It was initially deposited in an elongate rift basin that evolved into a passive continental margin hosting shallow to deep marine environments. The basin was deformed during the Brazilian Orogeny, which resulted in the formation of the southern part of the Paraguay Belt in southwestern Brazil (Almeida, 1968; Gaucher et al., 2003; Alvarenga et al., 2009; Boggiani et al., 2010; Warren et al., 2014; Amorim et al., 2020). The Corumbá Group exhibits a maximum thickness of about 400 m and is subdivided into five formations (**Figure 2**). The lowermost, or Cadiueus Formation, consists of conglomerate, sandstone, and shale, while the overlying Cerradinho Formation is composed of sandstone, shale, and carbonates (limestone and dolostone). Above this unit, the Bocaina Formation, composed of dolomite and subordinate shale, directly underlies the Tamengo Formation, which ranges from 80 to 100 m thick and consists predominantly of dark gray carbonaceous limestone and subordinate silty shale (Amorim et al., 2020). Both lithologies yield macroscopic body fossils, the most conspicuous of which are the skeletonized eumetazoans *Cloudina luciano* (in limestone) and *Corumbella werneri* (in silty shale). The Corumbá Group terminates with the Guaicurus Formation, a thick package of uniform shale which has yielded trace fossils of meiofaunal bilaterians (Parry et al., 2017).

High-precision dating of two volcanic tuffs situated a few meters below the top of the Tamengo Formation yielded mean

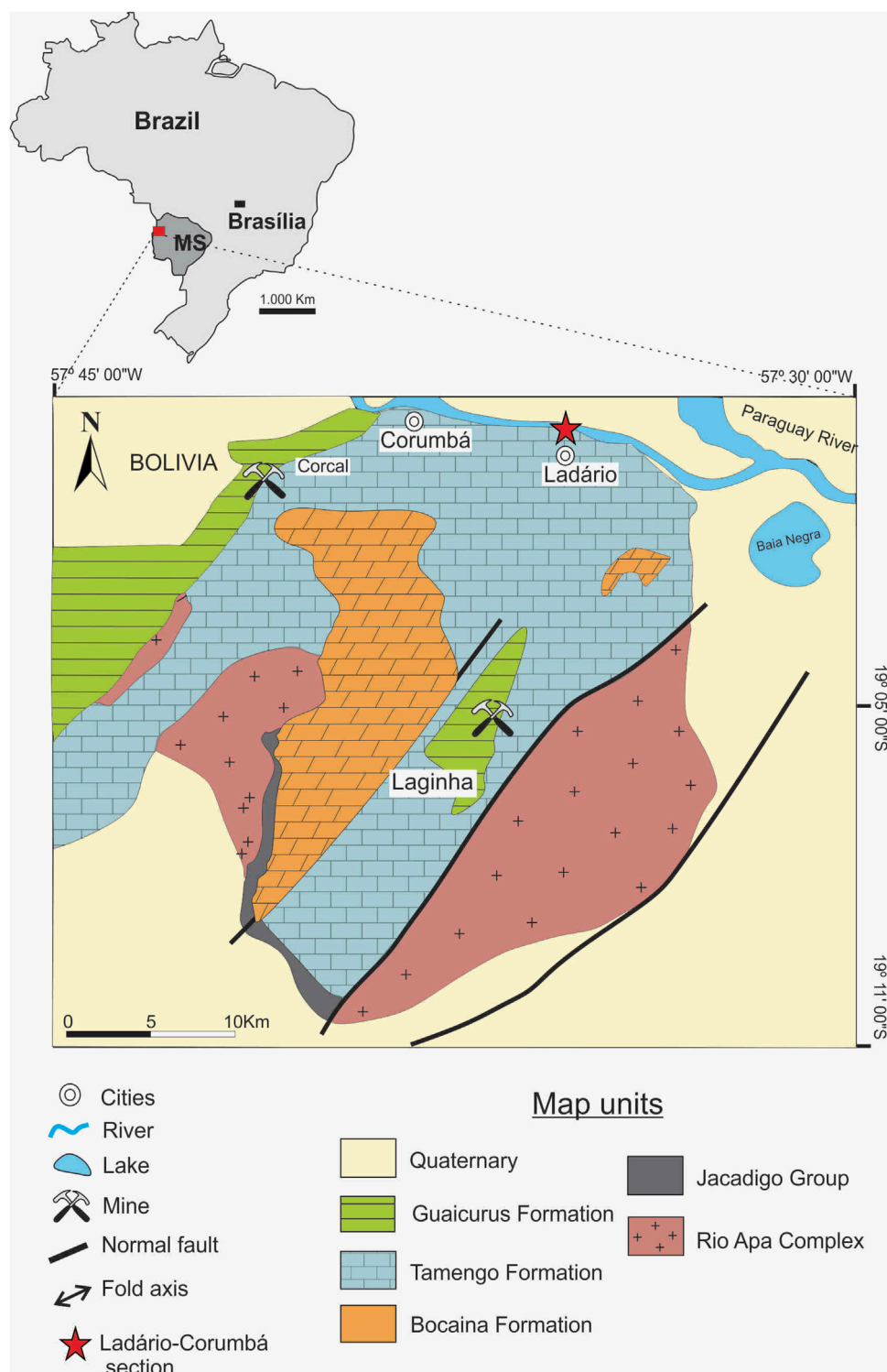


FIGURE 1 | Geological map of the Paraguay Belt in South America, showing the location of the Corumbá (Brazil) area, the Ladário-Corumbá section (red star), and the geology of the Corumbá Group.

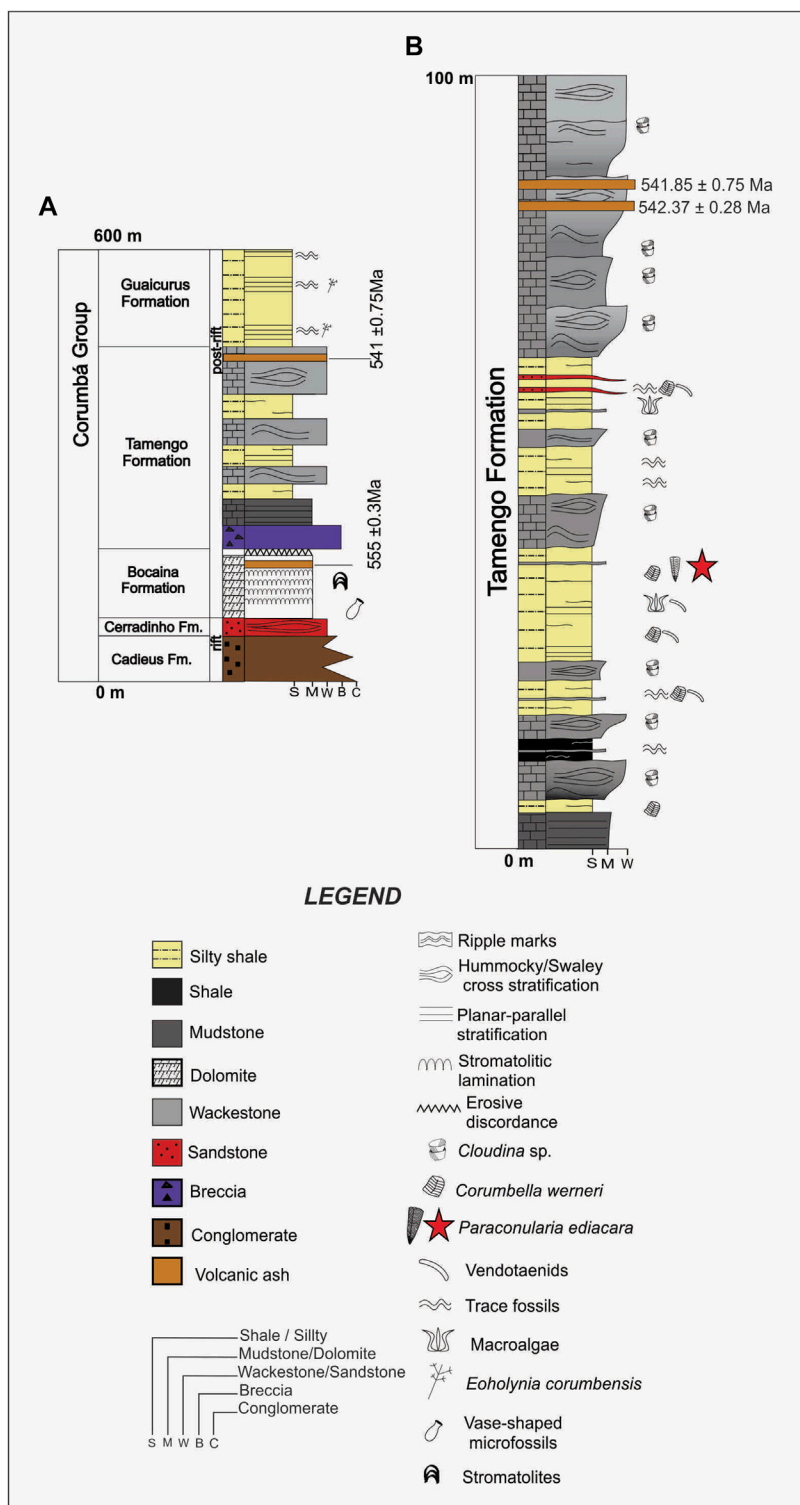


FIGURE 2 | Measured stratigraphic columns for **(A)** the Corumbá Group and **(B)** the Tamengo Formation, showing in **(B)** the levels of occurrence of *Cloudina*, *Corumbella*, vendotaenids, macroalgae, and *Paraconularia ediacara* n. sp. (red star). Modified from Amorim et al. (2020).

U-Pb ages of 541.85 ± 0.75 Ma and 542.27 ± 0.38 Ma, respectively (Parry et al., 2017). Combined with an age of 555.18 ± 0.30 Ma for a tuff bed near the top of the underlying Bocaina Formation (Parry et al., 2017), these two dates indicate that the entire Tamengo Formation is latest Ediacaran in age. This conclusion is corroborated by the presence throughout the Tamengo Formation of *Cloudina* (Figure 2), a likely index fossil for the latest Ediacaran (Xiao et al., 2016). Importantly, *Paraconularia ediacara* occurred at a level situated well below the top of the Tamengo Formation, and therefore its age may be several million years older than 542 Ma, the approximate age of the second oldest tuff layer mentioned above.

MATERIALS AND METHODS

The Tamengo Formation conulariid, formally diagnosed and described below, was collected from an outcrop designated as ELC (Ladário/Corumbá Escarpment) IV (Amorim et al., 2020) and located on the south bank of the Paraguay River near the village of Ladário (Figures 1, 2). The conulariid occurred within a 1.5-m-thick, non-bioturbated, finely laminated silty shale bed, at a level approximately 45 m below the top of the Tamengo Formation (Figure 2). The same bed, including the bedding plane on which the conulariid occurred, also yields *Corumbella*, vendotaenids, and macroalgae. The conulariid was revealed by splitting a hand-sized slab into two pieces, one bearing the part and the other the counterpart. Both are housed in the paleontological collections of the Department of Sedimentary and Environmental Geology of the Geosciences Institute of the University of São Paulo, under collection number 1T/2301a, b.

Assignment of the conulariid to a new species of *Paraconularia* is based on two lines of evidence: (1) recognition of a set of gross morphological features uniquely exhibited by conulariids in general (e.g., Hughes et al., 2000; Van Iten et al., 2008); and (2) comparisons with illustrations and reposit specimens of previously described *Paraconularia* from Devonian through Triassic rocks in North and South America (Driscoll, 1963; Babcock and Feldmann, 1986; Babcock et al., 1987; Babcock, 1993; Leme et al., 2004; Escalante-Ruiz et al., 2014), Africa (Van Iten et al., 2008), Europe (de Koninck, 1883; Slater, 1907; Hergarten, 1985; Barth et al., 2013; Lukševičs, 2020), Asia (Xu and Li, 1979; Zhu, 1985; Swami et al., 2017; Min et al., 2021), and Australia/New Zealand/Tasmania (Thomas, 1969; Waterhouse, 1979; Parfrey, 1982; Waterhouse, 1986). Imaging and Raman compositional analysis of the new conulariid were carried out in the Department of Sedimentary and Environmental Geology of the Geosciences Institute of the University of São Paulo, São Paulo State, Brazil. Low magnification optical examination and light photography were conducted using an OLYMPUS DSX stereomicroscope under low angle illumination. A small fragment of the periderm was coated with gold and examined using a LEO 440 scanning electron microscope (SEM).

SYSTEMATIC PALEONTOLOGY

Phylum Cnidaria Verrill, 1865
Subphylum Medusozoa Peterson, 1979
Class Scyphozoa Götze, 1887
Order Conulariida Miller and Gurley, 1896
Genus *Paraconularia* Sinclair, 1940

Type species: *Conularia inaequicostata* de Koninck, 1883, p. 223, pl. LIV, figs. 9-11.
Paraconularia ediacara n. sp.

(Plate I)

Paraconularia sp. Van Iten, Marques, Leme, and Simões, 2014a, p. 683, fig. 3c,d.
P. sp. Van Iten, Leme, Pacheco, Simões, Fairchild, Rodrigues, Galante, Boggiani, and Marques, 2016, p. 34-37, fig. 3.3.

Diagnosis: Large *Paraconularia* with circular nodes that are moderately coarse, widely spaced (10-11 per 5 mm), and extended adapertureward as a short, adaperturally tapered interspace ridge. Faces approximately equal in width. Transverse ribs in the apertural/upper middle region of the periderm low bell-curve-shaped and uninterrupted at the facial midline, numbering 10-11 per 10 mm. Apical angle approximately 10°. Corner sulcus subangular; corners and facial midline without internal thickening or carina.

Description: Part and counterpart of a thin (~0.2–0.5 mm), strongly compressed (transversely) fragment of a steeply pyramidal, four-sided periderm measuring approximately 34 mm long and 24 mm wide and lying parallel to bedding. Exposed portion of the periderm consists primarily of two mutually adjacent, very gently tapered partial faces and the corner sulcus between them (Plate I, Figures 1, 2). Faces originally about equal in width. Nearly smooth inner surface of small portions of the two mostly covered faces visible at the broken apical end of the part (Plate I, Figure 1). Apical region entirely missing. Apertural margin may be partially preserved. Apical angles ~10°. Length of the complete periderm exceeded 100 mm (as indicated by adapical extension of the truncated facial midlines). External surface of the two exposed faces exhibits 32 trochoidal, thickened, node-bearing transverse ribs separated by broad interspaces and numbering 10-11 per 10 mm. Transverse ribs adaperturally arcuate, approximately bell-curve-shaped (inflected circular curve geometry; Babcock and Feldmann, 1986), crossing both faces without interruption or diminution at the facial midline (Plate I, Figures 1, 2, 5, 7). Transverse ribs bent adapertureward on the shoulders of the subangular corner sulcus, within which they terminate, with the end portions of the transverse ribs from one face alternating with and slightly overlapping those from the adjoining face (Plate I, Figures 1, 3–6). Nodes moderately coarse, separated from each other by a gap that measures approximately 0.5–1.5 (rarely 2.0) node diameters in length, numbering from 10 to 11 per 5 mm (Plate I, Figures 5, 8). Many nodes extended adapertureward as a short, spine-like interspace ridge (adapertural spine; Babcock and Feldmann, 1986) (Plate I, Figure 5). Nodes of every other transverse rib form rectilinear files that are nearly parallel to the facial midline or the nearest corner. Corners and facial midlines without internal thickening or carina. Schott (apical wall) absent. Periderm very finely lamellar (Plate I, Figures 9, 10), apparently organic, though possibly with originally phosphatic microlamellae lost secondarily.

Derivation of name: *ediacara*, from Ediacaran, the age of the conulariid occurrence.

Type material: The holotype, reposited in the palaeontological collections of the Department of Sedimentary and Environmental Geology, University of São Paulo, São Paulo State, Brazil (IT/2301 a, b).

Occurrence: Thick silty shale bed in the middle part of the Tamengo Formation (upper Corumbá Group) at Locality ELC (Ladário/Corumbá Escarpment) IV (Amorim et al., 2020) on the south bank of the Paraguay River near the village of Ladário in Mato Grosso do Sul State, southwestern Brazil.

Age and horizon: Latest Ediacaran (no younger than 542 Ma), approximately 45 m below the top of the Tamengo Formation (upper Corumbá Group) (Parry et al., 2017).

Remarks and comparisons: Together with previously published anatomical data and illustrations (e.g., Babcock and Feldmann, 1986), the photographic illustrations here presented (**Plate I**, Figures 1, 2, 4, 5, 8–10; **Figure 3**) show that *P. ediacara* exhibits a complex suite of gross anatomical features that is shared only with Devonian-Triassic conulariids that have been placed in the genus *Paraconularia*. To be sure, there has been some divergence of opinion regarding the diagnostic characters of *Paraconularia* (e.g., Babcock and Feldmann, 1986; Van Iten et al., 2008; Min et al., 2021), and there is also some uncertainty surrounding the diagnostic characters and taxonomic composition of Conulariida itself (e.g., Hughes et al., 2000). Be that as it may, in recent years it has generally been assumed (e.g., Van Iten et al., 2006b; 2014b) that *Paraconularia* and similar genera such as *Conularia* are members of a single, monophyletic group that excludes medusozoan taxa lacking a finely lamellar, steeply pyramidal, organo-phosphatic or (possibly) organic periderm with (usually) sulcate corners bounding four faces bearing regularly arrayed small nodes and/or transverse ribs. Among previously known genera from the terminal Ediacaran and basal Cambrian, only *Corumbella* (terminal Ediacaran) and *Carinachites* (basal Cambrian, ca. 535 Ma, Han et al., 2017) are similar to *P. ediacara* and many other conulariids in having an originally quadrate skeleton showing regular corrugation of the gently tapered sides or faces. Absent in these two genera, however, are the fine details and pattern of arrangement of the transverse ribs of *Paraconularia*. As discussed in part by Van Iten et al. (2016), the faces of *Paraconularia*, including the type species, are crossed by aperturally arcuate or angulated, generally node-bearing transverse ribs which terminate within the corner sulcus. There, the end portions of the transverse ribs trend obliquely apertureward, with the end portions of the transverse ribs from one face alternating with and partially overlapping those from the adjoining face. Apertural bending of the transverse ribs on the shoulders of the corner sulcus can be subtle, and it has been reported (Min et al., 2021) that in some species such bending is absent. Along the facial midline, the transverse ribs may be interrupted, with the ends of the ribs on one half face arranged in alternation with those on the other half face, or they may be continuous, as in both *P. ediacara* and the type species (see de Koninck, 1883, pl. LIV, Figure 9). As in most conulariids having trochoidal (longitudinally) transverse ribs, the periderm thickens from the center line of the interspaces to the axial plane of the fold-like transverse ribs, in such a way as to reduce the

relief of the transverse ribs on the inner surface of the periderm (see for example Ford et al., 2016, Figure 3E). In many of the species bearing nodes, including *P. ediacara*, the apertural half of each node is developed into a short, spine-like ridge (apertural spine; Babcock and Feldmann, 1986) that extends part way across the interspaces. Finally, the pattern of arrangement of the nodes on the faces is such that the nodes of every other transverse rib are collinear, forming longitudinal series that are approximately parallel to the facial midline or nearest corner.

In addition to being far older geologically than other described species in *Paraconularia*, *P. ediacara* is also distinguishable from them morphologically, being characterized by the following unique set of gross anatomical features: (1) transverse ribs in the apertural/upper middle region low bell-curve-shaped (angulated circular curve geometry; Babcock and Feldmann, 1986), continuous across the facial midline, numbering from 10 to 11 per 10 mm; and (2) rib nodes moderately large, clearly separated from each other and developed aperturally into a short, spine-like interspace ridge. It is perhaps the second item that is most important, though, as in nearly all other known species the transverse ribs are either smooth (nodes are absent) or the nodes are very small and mutually contiguous or nearly so (**Figure 3**; see also illustrations in Babcock and Feldmann, 1986). Further grounds for assigning the Tamengo Formation *Paraconularia* to a new species are provided by the fact that the difference in absolute age between it and Devonian *Paraconularia* is roughly 130 million years, which is about an order of magnitude greater than the estimated life spans of the longest-lived invertebrate/cnidarian species (Valentine, 1970; Raup, 1978, 1991; Sepkoski, 1992; Lawton and May, 1995).

Preservation and taphonomy: The holotype and only known specimen of *P. ediacara* n. sp. is a fragment of an elongate pyramidal periderm, the faces of which lie parallel to bedding and probably measured at least 100 mm long when complete. It consists of a combination of skeletal material, possibly altered, and external molds of the same. The periderm does not react with dilute HCl and therefore is not calcareous, as expected given that the periderm of Phanerozoic conulariids is organo-phosphatic (Ford et al., 2016). It should be noted here that Van Iten et al. (2016) incorrectly reported the length of the fragment as 26 mm, which is close to its maximum width. The incompleteness of the fossil, which lacks the apical third and probably part of the middle region, is not an artifact of collecting, as the margins of the specimen are fully bordered by silty shale, and the specimen itself was revealed by splitting the host rock slab. The present distorted state of the specimen, with the two exposed faces and corner sulcus nearly touching the relatively smooth, mostly hidden facial pair/corner beneath them (**Plate I**, Figure 1), is typical of thin-walled conulariids preserved parallel to bedding in shale (see for example Babcock and Feldmann, 1986, figures. 18.5 and 26.4). The smoothness of the hidden faces, the broken edges of which are nevertheless sharp, also is typical of conulariids and reflects inward thickening and consequent diminution of the relief of the transverse ribs on the inner surface of the periderm. Owing possibly to having been restricted to the exteriormost levels in the periderm, which can undergo exfoliation during splitting of the host rock, the short interspace ridges are not evident at all

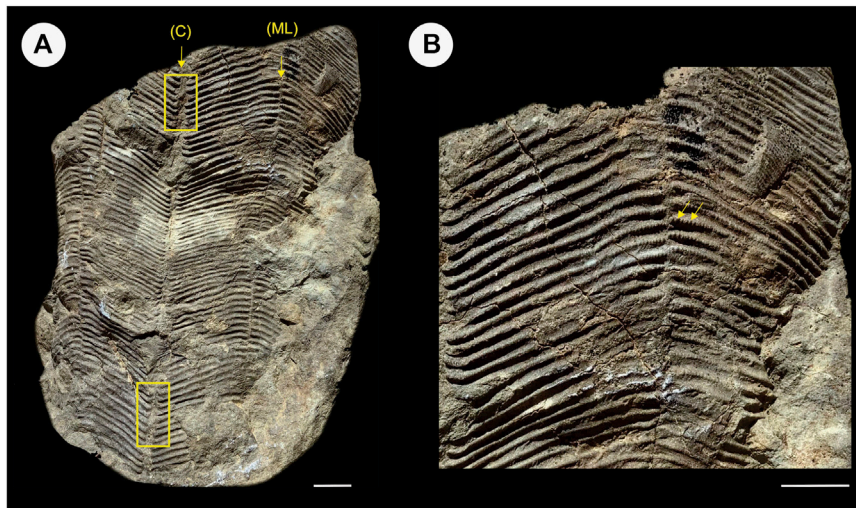


FIGURE 3 | *Paraconularia* sp. (Mississippian, Kentucky, United States; GP-1E 11672). **(A)** compressed partial specimen displaying two faces and the corner sulcus between them (photograph oriented with the apertural end of the fossil at the top). Yellow open rectangles highlight stretches of the corner sulcus (C) in which adapertural bending and alternation of the ends of the transverse ribs, which alternate as well along the facial midline (ML), are best displayed. **(B)** detail of the right face just below the apertural end of the fossil. Yellow arrows immediately to the right of the facial midline highlight some of the minute nodes. Scale bar: 10 mm.

places on the fossil and are easiest to discern on external molds. Finally, the presence of imbricated fragments of *Corumbella* in the same silty shale bed that yielded *P. ediacara* (Rodrigues et al., 2003; Amorim et al., 2020) suggests that the specimen was transported and fragmented prior to final burial.

The high magnification SEM images (Plate I, Figures 9, 10) reveal that the periderm of *P. ediacara* is composed of extremely thin (< 5 µm), mutually parallel microlamellae. This is the basic microstructure of Phanerozoic conulariids preserving the periderm, which is a bi-composite material consisting of apatitic and organic microlamellae arranged in alternation (Ford et al., 2016). Color images (Plate I, Figures 1, 2, 4, 5) of *P. ediacara* show that it is variegated, with irregularly bounded areas of pale tan-brown periderm occurring alongside patches of darker-colored periderm. Similar color variation is exhibited by the host silty shale and may reflect post-burial diagenesis and/or chemical weathering. In other words, the original periderm probably was uniform in color, as is the periderm of Phanerozoic conulariids, which however may bear pigmented lines or bands corresponding to internal carinae at the corners and/or facial midlines (Van Iten, 1992). Lastly, and as reported previously by Van Iten et al. (2016), Raman analysis of portions of the periderm failed to yield any lines diagnostic of phosphorous, one of the elemental constituents of apatite; instead, it appears that the periderm is now, and may originally have been, entirely or predominantly organic in composition. This hypothesis can potentially be tested by imaging broken edges of the periderm at very high magnifications. If in fact originally apatitic microlamellae have been lost secondarily, then there might still be an extremely narrow gap between the preserved, organic microlamellae. Otherwise, all microlamellae should be in direct contact with each other. Our photomicrographs (Plate I, Figures 9, 10) show no clear evidence of microscopic gaps, and thus, at this point, we are inclined to think that originally apatitic microlamellae were not present.

DISCUSSION

Significance

The discovery of *Paraconularia* in strata of terminal Ediacaran age is significant for several reasons. First, the new conulariid expands the list of skeletonized or tubular Ediacaran genera, including *Cloudina*, *Namacalathus*, *Namapoikia*, and *Sinotubulites*, which are generally regarded as eumetazoans (e.g., Fedonkin, 1992; Fedonkin and Waggoner, 1997; Grazhdankin, 2014; Grazhdankin, 2016; Becker-Kerber et al., 2017).

Second, and as noted above, conulariids were scyphozoan cnidarians or close medusozoan relatives of this group. Moreover, even though other Ediacaran taxa, most notably *Corumbella* and *Vendoconularia*, have been interpreted as scyphopolyps, the hypothesis of a scyphozoan affinity for *P. ediacara* enjoys a substantially stronger basis in comparative anatomy. It should be noted here that *Bjarmia cycloplerusa*, described by Grazhdankin, (2016) from the late Ediacaran Erga Formation (southeastern White Sea area, Russia), was classified by this author as a coronate scyphomedusa (jellyfish). However, this occurrence was not included by Young and Hagadorn, (2020, p. 185) among their “thirteen confirmed medusa-bearing deposits”, the oldest of which (the Chengjiang Lagerstätte) is early Cambrian (Stage 3) in age. Thus, either singly or together with certain other body fossils, *P. ediacara* now constitutes the strongest paleontological evidence of the presence of scyphozoans or any cnidarians during Neoproterozoic times.

Third, *Paraconularia* is now one of the longest lived eumetazoan genera, ranging downward from the Upper Triassic into the topmost Ediacaran, or through about 340 million years of geological time. Conulariids and *Paraconularia* are established (respectively) as a eumetazoan order and genus that survived the end-Ediacaran extinction event, a status currently shared with the agglutinated foraminiferan *Platysolenites* (Kontorovich et al., 2009), certain

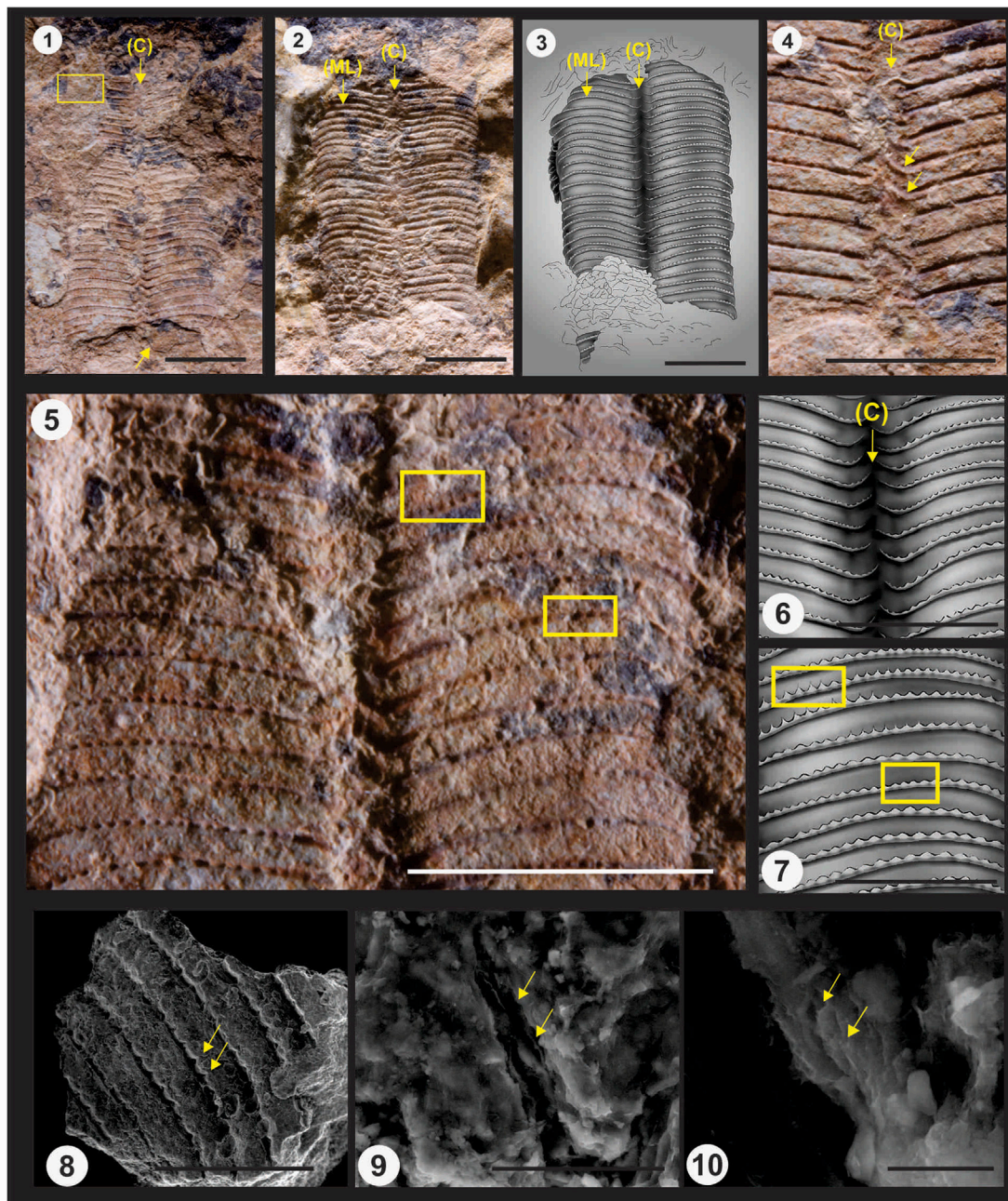


PLATE 1 | *Paraconularia ediacara* n. sp. (terminal Ediacaran, middle Tamengo Formation, upper Corumbá Group, Mato Grosso do Sul, Brazil; specimen GP-IT 2301, Geosciences Institute, University of São Paulo). 1, 2, color light photographs (both oriented with the apertural end of the fossil at the top); 1, the part, showing the two exposed partial faces and corner sulcus (indicated by the arrow labelled C) between them. The truncated apical ends of the two mostly covered faces project slightly from underneath the truncated apical ends of the two exposed faces (bottom arrow). Open yellow rectangle outlines the area from which the small fragment of periderm for SEM imaging (Figures 8–10 below) was extracted; 2, the counterpart (again with the corner indicated by an arrow labelled C, and with one of the facial midlines indicated by an arrow labelled ML); 3, schematic drawing of the part, highlighting the alternation of the nodose transverse ribs in the corner sulcus (C) and the continuation of the transverse ribs across the facial midline (ML). 4, 5, color light photographs (both oriented with the apertural end of the fossil at the top); 4, detail of the exposed corner sulcus of the counterpart. Note the pronounced adapertural deflection and alternation of the end portions of the transverse ribs within the corner sulcus (yellow arrows); 5, detail of the lower (apical) portion of the two exposed faces of the part, showing the widely spaced nodes. Upper rectangle highlights several nodes preserving the short interspace ridges in positive relief, while the lower rectangle highlights several nodes showing much shorter interspace ridges; 6, schematic drawing of a portion of the corner sulcus (C) shown in 5; 7, schematic drawing of the facial area with rectangles shown in 5; 8–10, SEM photomicrographs (secondary electron mode) of a small fragment of the periderm; 8, exterior surface of the periderm, showing several transverse ribs, widely spaced nodes, and very short, spine-like interspace ridges (pointing toward the apertural end of the periderm, yellow arrows); 9, detail of the fragment shown in 8, with canyon-like fractures exposing the edges of several microlamellae (yellow arrows); 10, detail of one of the fractures shown in 9 and exposing microlamellae (yellow arrows). Scale bar: 5 to 8 mm (Figures 1–3, 5); 7 mm (Figure 4); 5 mm (Figures 6, 7); 3 mm (Figure 8); 40 μ m (Figure 9); 5 μ m (Figure 10).

microfossils (Anderson et al., 2017; Grazhdankin et al., 2020), and three skeletonized metazoan genera, namely *Anabarites*, *Cambrotubulus*, and *Cloudina* (Zhu et al., 2017). Furthermore, cladistic analyses of phylogenetic relationships among genera within Conulariida (De Moraes Leme et al., 2008; Van Iten et al., 2014b) suggest that *Paraconularia* is a relatively apical branch, thus pushing the origin of conulariids even farther into the deep past.

Fourth, conulariids are now known from a level below that of the first occurrence of most SFFs (Zhu et al., 2017), in other words before the putative onset of the Cambrian Explosion of eumetazoan (mainly bilaterian) diversity. If in fact there was such an event (Blair and Hedges, 2005; Wood et al., 2019), then conulariids were around well before it started, and they were an order of magnitude larger than early Cambrian small shelly fossils. Put another way, the discovery of conulariids in the Tamengo Formation adds to a growing body of evidence (e.g., Darroch et al., 2015; Darroch et al., 2016; Zhu et al., 2017; Darroch et al., 2018b) of some degree of phylogenetic and ecological continuity across the Ediacaran-Cambrian boundary.

Fifth, the apparent organic composition of the Tamengo Formation periderm raises the intriguing possibility that the earliest conulariids were non-mineralizing, with production of phosphatic micro-lamellae within the clade having originated after the end of the Ediacaran but before the end of the Cambrian, as indicated by the presence of mineralized *Baccaconularia* in the Furongian of the north-central United States (Hughes et al., 2000; Van Iten et al., 2005). Conulariids in certain Phanerozoic strata, for example *Anaconularia anomala* from the Upper Ordovician Letná and Zahorany formations of Bohemia (Bruthansová and Van Iten, 2020), are known only from molds and casts, and thus post-mortem loss of the entire periderm has occurred in some cases, though the causes of this phenomenon in conulariids have yet to be determined. In the present case, the hypothesis of complete or partial loss of an apatitic skeletal component can potentially be tested through the discovery and microstructural analysis of additional conulariid specimens from the Tamengo and other Ediacaran formations.

Sixth, by analogy with extant scyphozoans, *P. ediacara* was a predator. Using elongate tentacles armed with nematocysts, modern scyphozoans prey primarily on meso-zooplankton (Grazhdankin, 2016). To date, no such soft-part structures have been detected in conulariids. Nevertheless, if *P. ediacara* was a predator, it seems likely that its prey were microscopic, possibly single-celled organisms living in the water column or even on the seafloor (see also discussions in the sections below). Again, by analogy with modern scyphozoans, *P. ediacara* may also have had the ability to assimilate dissolved organic matter (Arai, 1997).

Finally, the presence of conulariids in latest Ediacaran strata implies that Cnidaria has an even deeper Proterozoic evolutionary history. According to a previous cladistic analysis of the phylogenetic relationships among major groups within the phylum (Van Iten et al., 2006a; 2014a), conulariids (Conulariida) originated after Scyphozoa and Cubozoa split from each other, and after the most recent common ancestor of these two classes split from its most recent common ancestor with Hydrozoa. Still earlier, medusozoans (Scyphozoa, Cubozoa, Hydrozoa, and Staurozoa) split from their most recent common ancestor with Anthozoa. It should be noted, however, that certain more recent studies of cnidarian phylogeny (e.g., Zhao et al., 2019) have concluded that Scyphozoa is

paraphyletic. Be that as it may, the origin of Conulariida, now placed on the basis of body fossil evidence within the Neoproterozoic, was preceded by multiple branching events in the evolutionary history of Cnidaria. Moreover, and in accordance with the phylogenetic trees of Van Iten et al. (2006a) and Van Iten et al. (2014a), Cubozoa and Scyphozoa diverged from their most recent common ancestor no later than 542 Ma, the minimum absolute age of *P. ediacara*, which may therefore serve as a new internal calibration point for molecular clock studies of the evolution of Cnidaria.

Ediacaran Marine Paleoeecology

Together with the presence of the putative cnidarian polyps *Corumbella* and *Cloudina* in late Ediacaran rocks in Africa and North and South America (e.g., Kouchinsky et al., 2012; Pacheco et al., 2015; see however Yang et al., 2020 for a discussion of the possible annelid affinities of *Cloudina*), the presence of *P. ediacara* in the Tamengo Formation of Brazil may lend additional weight to the hypothesis (e.g., Hua et al., 2003; Schiffbauer et al., 2016) that the feeding strategy of predation, exhibited by extant medusozoans in general (Arai, 1997), originated before the close of the Neoproterozoic. Additionally, the existence of other late Ediacaran organisms capable of skeletogenesis or tube construction, including *Namacalathus*, *Namapoikia*, and *Sinotubulites* (e.g., Fedonkin, 1992; Fedonkin and Waggoner, 1997; Grotzinger et al., 2000; Hofmann and Mountjoy, 2001; Wood et al., 2002; Hua et al., 2003; Grazhdankin, 2014; Grazhdankin, 2016), further signals an increase in ecological complexity near the end of the Proterozoic. Indeed, some authors (e.g., Narbonne, 2005) have argued that terminal Ediacaran marine communities were comparable in productivity and trophic structure to modern marine ecosystems, and it is becoming increasingly likely that terminal Ediacaran ecosystems featured complex food chains composed of herbivores, filter feeders, and predators (Vermeij, 1989; Lipps and Culver, 2002; Babcock et al., 2005; Xiao and Laflamme, 2009; Laflamme et al., 2013; Droser and Gehling, 2015; Schiffbauer et al., 2016; Gibson et al., 2019; Muscente et al., 2019; Wood et al., 2019; Cracknell et al., 2021). Animals in these ecosystems developed a variety of foraging strategies based on microorganisms (picoplankton, microplankton, and microbial mats) as the primary producers (Vidal and Moczyłowska-Vidal, 1997; Gehling, 1999; Seilacher, 1999; Lipps and Culver, 2002; Darroch et al., 2016; Darroch et al., 2018a; Darroch et al., 2018b; Darroch et al., 2020), though with certain modern elements such as bioturbating infauna also present. In short, then, the occurrence of *P. ediacara* and other, possible predators (*Corumbella* and *Cloudina*) in the latest Ediacaran Tamengo Formation lends additional plausibility to the hypothesis of increasing complexity of ecosystems just prior to the beginning of the Phanerozoic.

Taphonomy and Epifaunal Tiering of the Tamengo Formation Biota

Paraconularia ediacara, *Corumbella*, and *Cloudina* in the Tamengo Formation were components of a marine macrobenthic ecosystem developed in a mixed carbonate-siliciclastic ramp setting (Amorim et al., 2020). Together with vendotaenids (*Vendotaenia* sp.), macroalgae, and the ichnofossil *Multina minima* (Parry et al., 2017), *P. ediacara* and *Corumbella* occur on bedding planes in silty shales deposited in the outer to distal mid-ramp facies (Amorim

et al., 2020). Both taxa are represented by comminuted, flattened, loosely packed remains that are randomly arranged in the sedimentary matrix. Therefore, these fossils probably are parautochthonous to allochthonous elements that settled from suspension on a deep (below storm wave base), low-energy fine-grained bottom. Shallower, more proximal parts of the ramp were frequently affected by storms, and the skeletons of *P. ediacara* and *Corumbella* may have been transported basinward over hundreds of meters, a taphonomic condition well exemplified by Devonian conulariids preserved in distal shale facies (Rodrigues et al., 2003). The occurrence of *Corumbella* as imbricated bioclasts at the base of lens-shaped deposits of very fine sand (Amorim et al., 2020) suggests further that these skeletons were sturdy enough to survive tractive transport. Importantly, *in situ* (i.e., preserved in life position) occurrences of *P. ediacara* and *Corumbella* have not been found in the Tamengo Formation. However, dense accumulations of *in situ* *Cloudina* shells are known from the shallow water, microbially-induced carbonates making up the bulk of the formation. Although single bedding planes bearing *in situ* associations of all three benthic invertebrates are unknown, their frequent co-occurrence (particularly *Corumbella* and *Cloudina*) in polytypical assemblages suggest that they may have colonized the same bottoms or at least mutually adjacent ones. Indeed, *in situ* *Cloudina*–*Corumbella*–*Namacalathus* associations are known from inner ramp carbonate deposits of the Ediacaran Itapucumi Group in Paraguay (Warren et al., 2012; Warren et al., 2017).

The three macrobenthic invertebrate taxa present in the Tamengo Formation seem to have been sessile epifaunal members of a low-to high-density, tiered community that flourished in a ramp setting subjected to intermittent burial events. The occurrence of these fossils together with meiofaunal ichnofossils (Parry et al., 2017) suggests a relatively complex tiering structure with distinct epifaunal guilds and even a shallow infaunal one. Based on estimates of the maximum original height of the best-preserved fossil specimens, at least two and possibly three nonoverlapping tiers extended from 0 to 10 cm above the seafloor. The lowest level from 0 to 1 cm was dominated by *Cloudina*, which grew at a subhorizontal to oblique (occasionally vertical) attitude relative to the seafloor (Becker-Kerber et al., 2017). This animal was largely prone, having only one or two of its nested funnel-like segments oriented slightly oblique to bedding (Becker-Kerber et al., 2017) to benefit from bottom currents. *Corumbella weneri* had a resistant but flexible carapace (Pacheco et al., 2015) which grew to an estimated 80 mm in length (Babcock et al., 2005). This species lived with the apical end embedded in muddy sediment (Pacheco et al., 2011; Pacheco et al., 2015), a condition also observed in specimens from the Ediacaran Itapucumi Group of Paraguay (Warren et al., 2012; Warren et al., 2017). Thus, *C. weneri* occupied a substantially higher tiering level than that of *Cloudina*, while *P. ediacara*, which appears to have been somewhat longer than *C. weneri*, may have occupied an even higher tiering level. As was the case for other Ediacaran assemblages (see Clapham and Narbonne, 2002, p. 630), the biomass of the Tamengo Formation community was concentrated in the basal 10 cm above the seafloor. The tiering structure of this community appears to

have been controlled both by constructional differences between taxa and by feeding behavior, possibly with *Cloudina* being a passive filter feeder (Becker-Kerber et al., 2017) and both *C. weneri* and *P. ediacara* engaging, possibly, in active predation.

CONCLUDING STATEMENT

The first known Ediacaran conulariid, *Paraconularia ediacara* n. sp., is diagnosed and described based on an incomplete but otherwise well-preserved specimen from the terminal Ediacaran Tamengo Formation of southern Brazil. The discovery of this body fossil has important implications for studies of the origins of the major groups of animal phyla and the early evolution of marine ecosystems. It is hoped that further collecting at the Ladário localities near Corumbá (Mato Grosso do Sul State) will yield additional material of this conulariid, which provides further support for the hypothesis of a relatively deep Neoproterozoic origin for phylum Cnidaria and therefore, possibly, of predation as well.

DATA AVAILABILITY STATEMENT

The raw data supporting the conclusions of this article will be made available by the authors, without undue reservation.

AUTHOR CONTRIBUTIONS

JL and HV performed laboratory work and taxonomical identification. All three co-authors worked together in the field to search for additional specimens of *P. ediacara*, participated in the formulation of interpretations and hypotheses in the discussion section of the paper, and approved the submitted version.

FUNDING

JL was supported by the FAPESP (proc. 13/17835-8; 16/06114-6) and HV was supported in part by a research grant from the Hanover College Faculty Development Committee.

ACKNOWLEDGMENTS

T. R. Fairchild (University of São Paulo, Brazil) is gratefully acknowledged as the collector of the Tamengo Formation *Paraconularia* specimen. Engineer I. J. Sayeg is thanked for assistance with scanning electron microscopy, and L. E. Anelli is thanked for assistance with light photography. Permission to examine repositied specimens of Phanerozoic species of *Paraconularia* was granted by M. Coyne (Geological Survey of Canada, Ottawa), A. Howell (Redpath Museum, McGill University, Montreal, Canada), J. Miller-Camp (Indiana University, Bloomington, United States), J. Darrell and C.

Sendino (Natural History Museum, London, United Kingdom), Lisa Amati (New York State Museum, Albany, United States), D. Erwin (United States National Museum, Washington, D. C.), and T. Adrain (University of Iowa, Iowa City, United States). The comparison

specimen of *Paraconularia* sp. from the Mississippian of Kentucky (United States) was photographed by T. V. Van Iten. Finally, the thoughtful and constructive reviews of the three referees are greatly appreciated.

REFERENCES

- Almeida, F. F. (1968). Evolução Tectônica Do Centro Oeste Brasileiro No Proterozoico Superior. *An. Acad. Bras. ciência Supl. simpósio manto Super.* 40, 285–296.
- Alvarenga, C. J. S., Boggiani, P. C., Babinski, M., Dardenne, M. A., Figueiredo, M. F., Santos, R. V., et al. (2009). “The Amazonian Palecontinent,” in *Neoproterozoic-Cambrian Tectonics, Global Change and Evolution: A Focus on Southwest Gondwana*. Editors C. Gaucher, A. N. Sial, G. P. Halverson, and H. E. Frimmel (Amsterdam: Elsevier), 498.
- Amorim, K. B., Afonso, J. W. L., Leme, J. d. M., Diniz, C. Q. C., Rivera, L. C. M., Gómez-Gutiérrez, J. C., et al. (2020). Sedimentary Facies, Fossil Distribution and Depositional Setting of the Late Ediacaran Tamengo Formation (Brazil). *Sedimentology* 67 (7), 3422–3450. doi:10.1111/sed.12749
- Anderson, R. P., Macdonald, F. A., Jones, D. S., McMahon, S., and Briggs, D. E. G. (2017). Doushantuo-type Microfossils from Latest Ediacaran Phosphorites of Northern Mongolia. *Geology* 45 (12), 1079–1082. doi:10.1130/G39576.1
- Arai, M. N. (1997). *A Functional Biology of Scyphozoa*. Dordrecht: Springer Netherlands, 316.
- Babcock, L. E. (1993). “Exceptionally Preserved Conulariids from the *Conularienschichten*, Fossil-Lagerstätten in the Devonian of Brazil,” in *Fosiles y Facies de Bolivia – Vol. II Invertebrados y Paleobotanica*. Editor R. Suarez-Soruco (Revista Tecnica de YPF), 13–14, 77–91.
- Babcock, L. E., and Feldmann, R. M. (1986). Devonian and Mississippian Conulariids of North America. Part B. *Paraconularia*, *Reticulaconularia*, New Genus and Organisms Rejected from Conulariida. *Ann. Carnegie Mus.* 55, 411–479.
- Babcock, L. E., Feldmann, R. M., Wilson, M. T., and Suárez-Riglos, M. (1987). Devonian Conulariids of Bolivia. *Natl. Geogr. Res.* 3, 210–231.
- Babcock, L. E., Grunow, A. M., Sadowski, G. R., and Leslie, S. A. (2005). Corumbella, an Ediacaran-Grade Organism from the Late Neoproterozoic of Brazil. *Palaeogeogr. Palaeoclimatol. Palaeoecol.* 220 (1–2), 7–18. doi:10.1016/j.palaeo.2003.01.001
- Barth, G., Kozur, H. W., Franz, M., and Weems, R. E. (2013). “*Paraconularia Bachmanni* N. Sp. From the Germanic Upper Triassic, the First Fresh-Water Occurrence of a Conulariid,” in *The Triassic System*. Editors L. H. Tanner, J. A. Spielmann, and S. G. Lucas (New Mexico Museum of Natural History and Science, Bulletin), 61, 42–47.
- Becker-Kerber, B., Pacheco, M. L. A. F., Rudnitzki, I. D., Galante, D., Rodrigues, F., and Leme, J. d. M. (2017). Ecological Interactions in *Cloudina* from the Ediacaran of Brazil: Implications for the Rise of Animal Biomineralization. *Sci. Rep.* 7, 5482. doi:10.1038/s41598-017-05753-8
- Blair, J. E., and Hedges, S. B. (2005). Molecular Clocks Do Not Support the Cambrian Explosion. *Mol. Biol. Evol.* 22 (3), 387–390. doi:10.1093/molbev/msi039
- Bobrovskiy, I., Hope, J. M., Ivantsov, A., Nettersheim, B. J., Hallmann, C., and Brocks, J. J. (2018). Ancient Steroids Establish the Ediacaran Fossil *Dickinsonia* as One of the Earliest Animals. *Science* 361 (6408), 1246–1249. doi:10.1126/science.aat7228
- Boero, F., Bouillon, J., and Piraino, S. (2005). The Role of Cnidaria in Evolution and Ecology. *Italian J. Zoology* 72, 65–71. doi:10.1080/11250000509356654
- Boggiani, P. C., Gaucher, C., Sial, A. N., Babinski, M., Simon, C. M., Riccomini, C., et al. (2010). Chemostratigraphy of the Tamengo Formation (Corumbá Group, Brazil): A Contribution to the Calibration of the Ediacaran Carbon-Isotope Curve. *Precambrian Res.* 182, 382–401. doi:10.1016/j.precamres.2010.06.003
- Bruthansová, J., and Van Iten, H. (2020). Invertebrate Epibionts on Ordovician Conulariids from the Prague Basin (Czech Republic, Bohemia). *Palaeogeogr. Palaeoclimatol. Palaeoecol.* 558, 109963. doi:10.1016/j.palaeo.2020.109963
- Clapham, M. E., and Narbonne, G. M. (2002). Ediacaran Epifaunal Tiering. *Geol* 30 (7), 627–630. doi:10.1130/0091-7613(2002)030<0627:eet>2.0.co;2
- Cracknell, K., Garcia-Bellido, J. G., Gehling, M. J., Ankor, S. A. F., García-Bellido, D. C., Gehling, J. G., et al. (2021). Pentaradial Eukaryote Suggests Expansion of Suspension Feeding in White Sea-Aged Ediacaran Communities. *Sci. Rep.* 11, 4121. doi:10.1038/s41598-021-83452-1
- Darroch, S. A. F., Boag, T. H., Racicot, R. A., Tweedt, S., Mason, S. J., Erwin, D. H., et al. (2016). A Mixed Ediacaran-Metazoan Assemblage from the Zaris Sub-Basin, Namibia. *Palaeogeogr. Palaeoclimatol. Palaeoecol.* 459, 198–208. doi:10.1016/j.palaeo.2016.07.003
- Darroch, S. A. F., Cribb, A. T., Buatois, L. A., Germs, G. J. B., Kenchington, C. G., Smith, E. F., et al. (2020). The Trace Fossil Record of the Nama Group, Namibia: Exploring the Terminal Ediacaran Roots of the Cambrian Explosion. *Earth-Science Rev.* 212, 103435. doi:10.1016/j.earscirev.2020.103435
- Darroch, S. A. F., Smith, E. F., Laflamme, M., and Erwin, D. H. (2018a). Ediacaran Extinction and Cambrian Explosion. *Trends Ecol. Evol.* 33, 653–663. doi:10.1016/j.tree.2018.06.003
- Darroch, S. A. F., Laflamme, M., and Wagner, P. J. (2018b). High Ecological Complexity in Benthic Ediacaran Communities. *Nat. Ecol. Evol.* 2, 1541–1547. doi:10.1038/s41559-018-0663-7
- Darroch, S. A. F., Sperling, E. A., Boag, T. H., Racicot, R. A., Mason, S. J., Morgan, A. S., et al. (2015). Biotic Replacement and Mass Extinction of the Ediacara Biota. *Proc. R. Soc. B* 282 (1814), 20151003. doi:10.1098/rspb.2015.1003
- de Koninck, L. G. (1883). Faune du calcaires carbonifère de la Belgique, Partie 4, Gasteropodes. *Ann. Musée R. d'Histoire Nat. Belg. Ser. Paleontol.* 8, 193–213.
- Dohrmann, M., and Wörheide, G. (2017). Dating Early Animal Evolution Using Phylogenomic Data. *Sci. Rep.* 7, 3599. doi:10.1038/s41598-017-03791-w
- De Moraes Leme, J., Guimarães Simões, M., Carlos Marques, A., Van Iten, H., and Marques, A. C. (2008). Cladistic Analysis of the Suborder Conulariina Miller and Gurley, 1896 (Cnidaria, Scyphozoa; Vendian-Triassic). *Palaeontology* 51 (3), 649–662. doi:10.1111/j.1475-4983.2008.00775.x
- dos Reis, M., Thawornwattana, Y., Angelis, K., Telford, M. J., Donoghue, P. C. J., and Yang, Z. (2015). Uncertainty in the Timing of Origin of Animals and the Limits of Precision in Molecular Timescales. *Curr. Biol.* 25 (22), 2939–2950. doi:10.1016/j.cub.2015.09.066
- Driscoll, E. G. (1963). *Paraconularia Newberryi (Winchell) and Other Lower Mississippian Conulariids from Michigan, Ohio, Indiana, and Iowa*, 18. Michigan: Contributions from the Museum of Paleontology of the University of Michigan, 33–46.
- Droser, M. L., and Gehling, J. G. (2015). The Advent of Animals: The View from the Ediacaran. *Proc. Natl. Acad. Sci. U.S.A.* 112, 4865–4870. doi:10.1073/pnas.1403669112
- Dunn, F. S., Liu, A. G., Grazhdankin, D. V., Vixseboxse, P., Flannery-Sutherland, J., Green, E., et al. (2021). The Developmental Biology of *Charnia* and the Eumetazoan Affinity of the Ediacaran Rangeomorphs. *Sci. Adv.* 7 (30), 1–13. doi:10.1126/sciadv.abe0291
- Dzik, J., Baliński, A., and Sun, Y. (2017). The Origin of Tetradial Symmetry in Cnidarians. *Lethaia* 50, 306–321. doi:10.1111/let.12199
- Erwin, D. H., Laflamme, M., Tweedt, S. M., Sperling, E. A., Pisani, D., and Peterson, K. J. (2011). The Cambrian Conundrum: Early Divergence and Later Ecological Success in the Early History of Animals. *Science* 334, 1091–1097. doi:10.1126/science.1206375
- Escalante-Ruiz, A. R., Quiroz-Barroso, S. A., and Tovar, F. S. (2014). Conulariids misisipicos de Nochistlán, Oaxaca, México: consideraciones sistemáticas, estratigráficas y paleobiogeográficas. *Rev. Bras. Paleontol.* 17 (2), 195–206. doi:10.4072/rbp.2014.2.07
- Fedonkin, M. A., Gehling, J. G., Grey, K., Narbonne, G. M., and Vickers Rich, P. (2007). *The Rise of Animals: Evolution and Diversification of the Kingdom Animalia*. Baltimore: The Johns Hopkins University Press, 326.
- Fedonkin, M. A. (1992). “Vendian Faunas and the Early Evolution of Metazoa,” in *Origin and Early Evolution of the Metazoa. Topics in Geobiology*. Editors J. H. Lipps and P. W. Signor (Boston, MA: Springer), 10. doi:10.1007/978-1-4899-2427-8_4

- Fedonkin, M. A., and Waggoner, B. M. (1997). The Late Precambrian Fossil *Kimberella* Is a Mollusc-like Bilaterian Organism. *Nature* 388, 868–871. doi:10.1038/42242
- Ford, R. C., Van Iten, H., and Clark, G. R. (2016). Microstructure and Composition of the Periderm of Conulariids. *J. Paleontol.* 90 (3), 389–399. doi:10.1017/jpa.2016.63
- Gaucher, C., Boggiani, P. C., Sprechmann, P., Sial, A. N., and Fairchild, T. R. (2003). Integrated correlation of the Vendian to Cambrian Arroyo del Soldado and Corumbá Groups (Uruguay and Brazil): palaeogeographic, palaeoclimatic and palaeobiologic implications. *Precambrian Res.* 120, 241–278. doi:10.1016/s0301-9268(02)00140-7
- Gehling, J. G. (1999). Microbial Mats in Terminal Proterozoic Siliciclastics: Ediacaran Death Masks. *Palaio* 14 (1), 40–57. doi:10.2307/3515360
- Gibson, B. M., Rahman, I. A., Maloney, K. M., Racicot, R. A., Mocke, H., LaflammeDarroch, M. S. A. F., et al. (2019). Gregarious Suspension Feeding in a Modular Ediacaran Organism. *Sci. Adv.* 5, eaaw0260. doi:10.1126/sciadv.aaw0260
- Götte, A. (1887). Entwicklungs Geschichte der *Aurelia aurita* und *Cotylorhiza tuberculata*. *Abh. Entwicklungsgeschichte Tiere* 4, 1–79.
- Grazhdankin, D. (2016). Forbidden Fruits in the Garden of Ediacara. *Paläontologische Z.* 90, 649–657. doi:10.1007/s12542-016-0327-3
- Grazhdankin, D., Nagovitsin, K., Golubkova, E., Karlova, G., Kochnev, B., Rogov, V., et al. (2020). Doushantuo-Pertatataka-type Acanthomorphs and Ediacaran Ecosystem Stability. *Geology* 48 (7), 708–712. doi:10.1130/G47467.1
- Grazhdankin, D. (2014). Patterns of Evolution of the Ediacaran Soft-Bodied Biota. *J. Paleontol.* 88, 269–283. doi:10.1666/13-072
- Grotzinger, J. P., Watters, W. A., and Knoll, A. H. (2000). Calcified Metazoans in Thrombolite-Stromatolite Reefs of the Terminal Proterozoic Nama Group, Namibia. *Paleobiology* 26 (3), 334–359. doi:10.1666/0094-8373(2000)026<0334:cmitsr>2.0.co;2
- Guo, J., Han, J., Iten, H. V., Wang, X., Qiang, Y., Song, Z., et al. (2020a). A Fourteen-Faced Hexangulaconulariid from the Early Cambrian (Stage 2) Yanjiahe Formation, South China. *J. Paleontol.* 94 (1), 45–55. doi:10.1017/jpa.2019.56
- Guo, J., Han, J., Van Iten, H., Song, Z., Qiang, Y., Wang, W., et al. (2020b). A New Tetradial Olivoid (Medusozoa) from the Lower Cambrian (Stage 2) Yanjiahe Formation, South China. *J. Paleontol.* 94 (3), 457–466. doi:10.1017/jpa.2019.101
- Guo, J., Han, J., Van Iten, H., Song, Z., Qiang, Y., Wang, W., et al. (2021). A Ten-Faced Hexangulaconulariid from Cambrian Stage 2 of South China. *J. Paleontol.* 95 (5), 957–964. doi:10.1017/jpa.2021.25
- Han, J., Li, G., Wang, X., Yang, X., Guo, J., Sasaki, O., et al. (2017). *Olivoides*-like Tube Aperture in Early Cambrian Carinacitids (Medusozoa, Cnidaria). *J. Paleontol.* 92, 3–13. doi:10.1017/jpa.2017.10
- Hedges, S., Blair, J. E., Venturi, M. L., and Shoe, J. L. (2004). A Molecular Timescale of Eukaryote Evolution and the Rise of Complex Multicellular Life. *BMC Evol. Biol.* 4, 2. doi:10.1186/1471-2148-4-2
- Hergarten, B. (1985). Die Conularien des Rheinischen Devons. *Senckenberg. Lethaea* 66, 269–297.
- Hofmann, H. J., and Mountjoy, E. W. (2001). *Namacalathus-Cloudina* Assemblage in Neoproterozoic Miette Group (Byng Formation), British Columbia: Canada's Oldest Shelly Fossils. *Geology* 29 (12), 1091–1094. doi:10.1130/0091-7613(2001)029<1091:ncainm>2.0.co;2
- Hua, H., Pratt, B. R., and Zhang, L.-Y. (2003). Borings in *Cloudina* Shells: Complex Predator-Prey Dynamics in the Terminal Neoproterozoic. *Palaio* 18, 454–459. doi:10.1669/0883-1351(2003)018<0454:bicscp>2.0.co;2
- Hughes, N. C., Gunderson, G. O., and Weedon, M. J. (2000). Late Cambrian Conulariids from Wisconsin and Minnesota. *J. Paleontology* 74, 828–838. doi:10.1666/0022-3360(2000)074<0828:lccfwa>2.0.co;2
- Ivantsov, A. Y., and Fedonkin, M. A. (2002). Conulariid-like Fossil from the Vendian of Russia: a Metazoan Clade across the Proterozoic/Palaeozoic Boundary. *Palaontology* 45, 1219–1229. doi:10.1111/1475-4983.00283
- Ivantsov, A. Y., Vickers-Rich, P., Zakrevskaya, M. A., and Hall, M. (2019). Conical Thecae of Precambrian Macroorganisms. *Paleontol. J.* 53, 1134–1146. doi:10.1134/s0031030119110054
- Jerre, F. (1994). Anatomy and Phylogenetic Significance of *Eoconularia Loculata*, a Conulariid from the Silurian of Gotland. *Lethaia* 27, 97–109. doi:10.1111/j.1502-3931.1994.tb01562.x
- Kontorovich, A. E., Sokolov, B. S., Kontorovich, V. A., Varlamov, A. I., GrazhdankinEfimov, D. V. A. S., Efimov, A. S., et al. (2009). The First Section of Vendian Deposits in the Basement Complex of the West Siberian Petroleum Megabasin (Resulting from the Drilling of the Vostok-3 Parametric Borehole in the Eastern Tomsk Region). *Dokl. Earth Sc.* 425 (1), 219–222. doi:10.1134/s1028334x09020093
- Kouchinsky, A., Bengtson, S., Runnegar, B., Skovsted, C., Steiner, M., and Vendrasco, M. (2012). Chronology of Early Cambrian Biomineralization. *Geol. Mag.* 149, 221–251. doi:10.1017/s0016756811000720
- Laflamme, M., Darroch, S. A. F., Tweedt, S. M., Peterson, K. J., and Erwin, D. H. (2013). The End of the Ediacara Biota: Extinction, Biotic Replacement, or Cheshire Cat? *Gondwana Res.* 23, 558–573. doi:10.1016/j.jgr.2012.11.004
- Leme, J., Rodrigues, S. C., Simões, M. G., and Van Iten, H. (2004). Sistemática dos conulários (Cnidaria) da Formação Ponta Grossa (Devoniano), Estado Do Paraná, bacia Do Paraná, Brasil. *Rev. Bras. Paleontol.* 7 (2), 213–222. doi:10.4072/rbp.2004.2.14
- Linnemann, U., Ovtcharova, M., Schaltegger, U., Gärtner, A., Hautmann, M., Geyer, G., et al. (2019). New High-Resolution Age Data from the Ediacaran-Cambrian Boundary Indicate Rapid, Ecologically Driven Onset of the Cambrian Explosion. *Terra nova*. 31 (1), 49–58. doi:10.1111/ter.12368
- Lipps, J. H., and Culver, S. J. (2002). The Trophic Role of Marine Microorganisms Through Time. *Paleontol. Soc. Pap.* 8, 69–92. doi:10.1017/S1089332600001066
- Lucas, S. G. (2012). The Extinction of the Conulariids. *Geosciences* 2, 1–10. doi:10.3390/geosciences2010001
- Lukševičs, E. (2020). First Record of Conulariids from the Tērvete Formation, Upper Devonian of Latvia. *Est. J. Earth Sci.* 69, 262–268. doi:10.3176/earth.2020.21
- Marques, A. C., and Collins, A. G. (2004). Cladistic Analysis of Medusozoa and Cnidarian Evolution. *Invertebr. Biol.* 123, 23–42. doi:10.1111/j.1744-7410.2004.tb00139.x
- Miller, S. A., and Gurley, W. F. E. (1896). New Species of Paleozoic Invertebrates from Illinois and Other States. *Ill. State Mus. Nat. Hist.* 11, 1–50.
- Min, H., Wang, X.-L., and Wang, H. (2021). A New Permian Species of *Paraconularia* from Abaga Banner, Inner Mongolia. *Palaeoworld*. doi:10.1016/j.palwor.2021.10.002
- Morris, S. C., and Menge, C. (1992). Carinacitids, Hexangulaconulariids, and *Punctatus*: Problematic Metazoans from the Early Cambrian of South China. *J. Paleontol.* 66 (3), 384–406. doi:10.1017/s0022336000033953
- Muscente, A. D., Bykova, N., Boag, T. H., Buatois, L. A., Mángano, M. G., Eleish, A., et al. (2019). Ediacaran Biozones Identified with Network Analysis Provide Evidence for Pulsed Extinctions of Early Complex Life. *Nat. Commun.* 10, 911. doi:10.1038/s41467-019-08837-3
- Narbonne, G. M. (2005). The Ediacara Biota: Neoproterozoic Origin of Animals and Their Ecosystems. *Annu. Rev. Earth Planet. Sci.* 33 (1), 421–442. doi:10.1146/annurev.earth.33.092203.122519
- Pacheco, M. L. A. F., Leme, J. M., and Machado, A. F. (2011). Taphonomic analysis and geometric modelling for the reconstitution of the Ediacaran metazoan *Corumbella wernerii* Hahn et al. 1982 (Tamengo Formation, Corumbá Basin, Brazil). *Journal of Taphonomy* 9 (4), 269–283.
- Pacheco, M. L. A. F., Galante, D., Rodrigues, F., de M. Leme, J., Bidola, P., Hagadorn, W., et al. (2015). Insights into the Skeletonization, Lifestyle, and Affinity of the Unusual Ediacaran Fossil *Corumbella*. *Plos One* 10, e0114219. doi:10.1371/journal.pone.0114219
- Parfrey, S. M. (1982). Palaeozoic Conulariids from Tasmania. *Alcheringa An Australas. J. Paleontol.* 6, 69–77. doi:10.1080/03115518208565421
- Parry, L. A., Boggiani, P. C., Condon, D. J., Garwood, R. J., Leme, J. d. M., McIlroy, D., et al. (2017). Ichnological Evidence for Meiofaunal Bilaterians from the Terminal Ediacaran and Earliest Cambrian of Brazil. *Nat. Ecol. Evol.* 1, 1455–1464. doi:10.1038/s41559-017-0301-9
- Pearse, V., Pearse, J., Buchsbaum, M., and Buchsbaum, R. (1987). *Living Invertebrates*. Pacific Grove, California: Boxwood Press, 848.
- Peterson, K. W. (1979). “Development of Coloniality in Hydrozoa,” in *Biology and Systematics of Colonial Organism*. Editors G. Larwood and B. R. Rosen (New York: Academic Press).
- Rodrigues, S., Simões, M., and Leme, J. M. (2003). Tafonomia Comparada Dos Conulatae (Cnidaria), Formação Ponta Grossa (Devoniano), Bacia Do Paraná, Estado Do Paraná. *Rev. Bras. Geociências* 33, 165–186. doi:10.25249/0375-7536.2003334379388
- Runnegar, B. (1982). The Cambrian Explosion: Animals or Fossils? *J. Geol. Soc. Aust.* 29 (3-4), 395–411. doi:10.1080/00167618208729222

- Schiffbauer, J. D., Huntley, J. W., O'Neil, G. R., Darroch, S. A. F., Laflamme, M., and Cai, Y. (2016). The Latest Ediacaran Wormworld Fauna: Setting the Ecological Stage for the Cambrian Explosion. *GSA Today* 26 (11), 4–11. doi:10.1130/gsatg265a.1
- Seilacher, A. (1999). Biomat-related Lifestyles in the Precambrian. *Palaio* 14, 86–93. doi:10.2307/3515363
- Sinclair, G. W. (1940). The Genotype of *Conularia*. *Can. Field-Naturalist* 54, 72–74.
- Slater, I. L. (1907). A Monograph of the British Conulariae. *Palaeontogr. Soc.* 61, 1–41.
- Swami, N., Satish, S. C., Laishram, R., and Dharwadkar, A. (2017). First Record of Extinct Paraconularia (Cnidaria, Scyphozoa) from Tethyan Sequence (Upper Permian) of Spiti Valley, Himachal Himalaya, India. *Palaeontol. Electron.* 2042A (3), 1–6. doi:10.26879/736
- Thomas, G. A. (1969). *Notoconularia*, a New Conularid Genus from the Permian of Eastern Australia. *J. Paleontology* 43 (5), 1283–1290.
- Van Iten, H., Leme, J. M., Marques, A. C., and Simões, M. G. (2013). Alternative interpretations of some earliest Ediacaran fossils from China. *Acta Palaeontologica Polonica* 51 (1), 111–113. doi:10.4202/app.2011.0096
- Van Iten, H., Marques, A. C., Leme, J. d. M., Pacheco, M. L. A. F., and Simões, M. G. (2014a). Origin and Early Diversification of the Phylum Cnidaria Verrill: Major Developments in the Analysis of the Taxon's Proterozoic-Cambrian History. *Palaeontology* 57, 677–690. doi:10.1111/pala.12116
- Van Iten, H., Burkey, M. H., Leme, J. M., and Marques, A. C. (2014b). Cladistics and Mass Extinctions: the Example of Conulariids (Scyphozoa, Cnidaria) and the End Ordovician Extinction Event. *GFF* 136, 275–280. doi:10.1080/11035897.2014.880506
- Van Iten, H., Fitzke, J. A., and Cox, R. S. (1996). Problematical Fossil Cnidarians from the Upper Ordovician of the North-Central USA. *Palaeontology* 39, 1037–1064.
- Van Iten, H., Leme, J. M., Simões, M. G., Marques, A. C., and Collins, A. G. (2006a). Reassessment of the Phylogenetic Position of Conulariids (?Vendian-Triassic) within the Subphylum Medusozoa (Phylum Cnidaria). *J. Syst. Palaeontol.* 4 (1), 109–118. doi:10.1017/s1477201905001793
- Van Iten, H., Leme, J. d. M., and Simões, M. G. (2006b). Additional observations on the gross morphology and microstructure of Baccacconularia Hughes, Gunderson et Weedon, 2000, a Cambrian (Furongian) conulariid from the north-central USA. *Palaeoworld* 15, 294–306. doi:10.1016/j.palwor.2006.10.006
- Van Iten, H., Leme, J. M., De Moraes Leme, J., Coelho Rodrigues, S., and Guimaraes Simoes, M. (2005). Reinterpretation of a Conulariid-like Fossil from the Vendian of Russia. *Palaeontology* 48 (3), 619–622. doi:10.1111/j.1475-4983.2005.00471.x
- Van Iten, H., Leme, J. M., Pacheco, M. L. A. F., Simões, M. G., Fairchild, T. R., Rodrigues, F., et al. (2016). “Origin and Early Diversification of Phylum Cnidaria: Key Macrofossils from the Ediacaran System of North and South America,” in *The Cnidaria, Past, Present and Future*. Editors S. Goffredo and Z. Dubinsky (Cham: Springer International Publishing), 31–40. doi:10.1007/978-3-319-31305-4_3
- Van Iten, H. (1992). Morphology and Phylogenetic Significance of the Corners and Midlines of the Conulariid Test. *Paleontology* 35, 335–358.
- Van Iten, H., Moussa, K., and Yahaya, M. (2008). Conulariids of the Upper Talak Formation (Mississippian, Visean) of Northern Niger (West Africa). *J. Paleontology* 82, 178–182. doi:10.1666/06-083.1
- Vaziri, S. H., Majidifard, M. R., and Laflamme, M. (2018). Diverse Assemblage of Ediacaran Fossils from Central Iran. *Sci. Rep.* 8, 5060. doi:10.1038/s41598-018-23442-y
- Vermeij, G. J. (1989). The Origin of Skeletons. *Palaio* 4, 585–589. doi:10.2307/3514748
- Verrill, A. E. (1865). Classification of Polyps (Extract Condensed from Synopsis of the Polyps and Corals of the North Pacific Exploring Expedition under Commodore C. Ringgold and Captain John Rogers, U.S.N.). *Commun. Essex Inst.* 4, 145–152.
- Vidal, G., and Moczyłowska-Vidal, M. (1997). Biodiversity, Speciation, and Extinction Trends of Proterozoic and Cambrian Phytoplankton. *Paleobiology* 23 (2), 230–246. doi:10.1017/s0094837300016808
- Walde, D. H.-G., Weber, B., Erdtmann, B. D., and Steiner, M. (2019). Taphonomy of *Corumbella Werner* from the Ediacaran of Brazil: Sinotubulitid Tube or Conulariid Test? *Alcheringa An Australas. J. Palaeontol.* 43, 335–350. doi:10.1080/03115518.2019.1615551
- Walde, D. H. G., do Carmo, D. A., Guimarães, E. M., Vieira, L. C., Erdtmann, B.-D., Sanchez, E. A. M., et al. (2015). New Aspects of Neoproterozoic-Cambrian Transition in the Corumbá Region (State of Mato Grosso do Sul, Brazil). *Ann. Paléontologie* 101, 213–224. doi:10.1016/j.annpal.2015.07.002
- Wan, B., Yuan, X., Chen, Z., Guan, C., Pang, K., Tang, Q., et al. (2016). Systematic Description of Putative Animal Fossils from the Early E Diacaran L Antian F Ormation of S Outh C Hina. *Palaeontology* 59, 515–532. doi:10.1111/pala.12242
- Warren, L. V., Pacheco, M. L. A. F., Fairchild, T. R., Simões, M. G., Riccomini, C., Boggiani, P. C., et al. (2012). The Dawn of Animal Skeletogenesis: Ultrastructural Analysis of the Ediacaran Metazoan *Corumbella Werner*. *Geology* 40, 691–694. doi:10.1130/g33005.1
- Warren, L. V., Quaglio, F., Riccomini, C., Simões, M. G., Poiré, D. G., Strikis, N. M., et al. (2014). The Puzzle Assembled: Ediacaran Guide Fossil *Cloudina* Reveals an Old Proto-Gondwana Seaway. *Geology* 42, 391–394. doi:10.1130/g35304.1
- Warren, L. V., QuaglioSimões, F. M. G., SimõesRiccomini, M. G. C., Gaucher, C., Riccomini, C., Poiré, D. G., et al. (2017). *Cloudina-Corumbella-Namacalathus* Association from the Itapucumi Group, Paraguay: Increasing Ecosystem Complexity and Tiering at the End of the Ediacaran. *Precambrian Res.* 298, 79–87. doi:10.1016/j.precamres.2017.05.003
- Waterhouse, J. B. (1986). Late Palaeozoic Scyphozoa and Brachiopoda (Inarticulata, Strophomenida, Productata and Rhynchonellida) from the Southeast Bower Basin, Australia. *Palaeontographica* 193, 1–77.
- Waterhouse, J. B. (1979). Permian and Triassic Conulariid Species from New Zealand. *J. R. Soc. N. Z.* 9 (4), 475–489. doi:10.1080/03036758.1979.10421833
- Werner, B. (1966). *Stephanoscyphus* (Scyphozoa, Coronatae) und seine direkte Abstammung von den fossilen Conulata. *Helgol. Wiss. Meeresunters* 13, 317–347. doi:10.1007/bf01611953
- Wood, R. A., Grotzinger, J. P., and Dickson, J. A. D. (2002). Proterozoic Modular Biomineralized Metazoan from the Nama Group, Namibia. *Science* 296, 2383–2386. doi:10.1126/science.1071599
- Wood, R., Liu, A. G., Bowyer, F., Wilby, P. R., Dunn, F. S., Kenchington, C. G., et al. (2019). Integrated Records of Environmental Change and Evolution Challenge the Cambrian Explosion. *Nat. Ecol. Evol.* 3, 528–538. doi:10.1038/s41559-019-0821-6
- Xiao, S., and Laflamme, M. (2009). On the Eve of Animal Radiation: Phylogeny, Ecology and Evolution of the Ediacara Biota. *Trends Ecol. Evol.* 24 (1), 31–40. doi:10.1016/j.tree.2008.07.015
- Xiao, S., Narbonne, G. M., Zhou, C., Laflamme, M., Grazhdankin, D. V., Moczyłowska-Vidal, M., et al. (2016). Towards an Ediacaran Time Scale: Problems, Protocols, and Prospects. *Episodes* 39 (4), 540–555. doi:10.18814/epiuiugs/2016/v39i4/103886
- Xu, G., and Li, F. (1979). New Conulariid Genera and Species in China. *Acta Geol. Sin.* 53 (2), 91–98.
- Young, G. A., and Hagadorn, J. W. (2020). Evolving Preservation and Facies Distribution of Fossil Jellyfish: a Slowly Closing Taphonomic Window. *Boll. della Soc. Paleontol. Ital.* 59, 185–203. doi:10.4435/BSPI.2020.22
- Yuan, X., Chen, Z., Xiao, S., Zhou, C., and Hua, H. (2011). An Early Ediacaran Assemblage of Macroscopic and Morphologically Differentiated Eukaryotes. *Nature* 470, 390–393. doi:10.1038/nature09810
- Zhao, Y., Vinther, J., Parry, L. A., Wei, F., Green, E., Pisani, D., et al. (2019). Cambrian Sessile, Suspension Feeding Stem-Group Ctenophores and Evolution of the Comb Jelly Body Plan. *Curr. Biol.* 29, 1112–1125. doi:10.1016/j.cub.2019.02.036
- Zhu, M., Zhuravlev, A. Y., Wood, R. A., Zhao, F., and Sukhov, S. S. (2017). A Deep Root for the Cambrian Explosion: Implications of New Bio- and Chemostratigraphy from the Siberian Platform. *Geology* 45, 459–462. doi:10.1130/g38865.1
- Zhu, Z. K. (1985). New Devonian and Permian Conulariids from China. *Acta Palaeontol. Sin.* 24 (5), 528–538.

Conflict of Interest: The authors declare that the research was conducted in the absence of any commercial or financial relationships that could be construed as a potential conflict of interest.

Publisher's Note: All claims expressed in this article are solely those of the authors and do not necessarily represent those of their affiliated organizations, or those of the publisher, the editors and the reviewers. Any product that may be evaluated in this article, or claim that may be made by its manufacturer, is not guaranteed or endorsed by the publisher.

Copyright © 2022 Leme, Van Iten and Simões. This is an open-access article distributed under the terms of the Creative Commons Attribution License (CC BY). The use, distribution or reproduction in other forums is permitted, provided the original author(s) and the copyright owner(s) are credited and that the original publication in this journal is cited, in accordance with accepted academic practice. No use, distribution or reproduction is permitted which does not comply with these terms.



New Facies Model and Carbon Isotope Stratigraphy for an Ediacaran Carbonate Platform From South America (Tamengo Formation—Corumbá Group, SW Brazil)

Maria E. A. F. Ramos¹, Martino Giorgioni^{1*}, Detlef H. G. Walde¹, Dermeval A. do Carmo¹, Gabriella Fazio¹, Lucieth C. Vieira¹, Matheus Denezine¹, Roberto V. Santos¹, Rodrigo R. Adorno^{1,2} and Lucas Lage Guida¹

OPEN ACCESS

Edited by:

Michael Andrew Clare,
University of Southampton,
United Kingdom

Reviewed by:

Sabatino Ciarcia,
University of Sannio, Italy
Luca Basilone,
University of São Paulo, Brazil
Aram Bayet-Goll,
Institute for Advanced Studies in Basic
Sciences (IASBS), Iran

*Correspondence:

Martino Giorgioni
gmartino@unb.br

Specialty section:

This article was submitted to
Sedimentology, Stratigraphy and
Diagenesis,
a section of the journal
Frontiers in Earth Science

Received: 28 July 2021

Accepted: 17 May 2022

Published: 27 June 2022

Citation:

Ramos MEAF, Giorgioni M,
Walde DHG, do Carmo DA, Fazio G,
Vieira LC, Denezine M, V. Santos R,
R. Adorno R and Lage Guida L (2022)
New Facies Model and Carbon Isotope
Stratigraphy for an Ediacaran
Carbonate Platform From South
America (Tamengo
Formation—Corumbá
Group, SW Brazil).
Front. Earth Sci. 10:749066.
doi: 10.3389/feart.2022.749066

¹Geosciences Institute, University of Brasília, Brasília, Brazil, ²Center for Technological Development-CEDES, Geological Survey of Brazil, Brasília, Brazil

The Ediacaran is a period characterized by the diversification of early animals and extensive neritic carbonate deposits. These deposits are still not well understood in terms of facies and carbon isotope composition ($\delta^{13}\text{C}$). In this study we focus on the Tamengo Formation, in southwestern Brazil, which constitutes one of the most continuous and well-preserved sedimentary record of the late Ediacaran in South America. We present new detailed lithofacies and stable isotopes data from two representative sections (Corcal and Laginha) and revise the paleoenvironmental and stratigraphic interpretation of the Tamengo Formation. The Corcal section consists of neritic deposits including shallow-water limestone beds, alternated with shale and subordinate marl beds. These facies yield specimens of the Ediacaran fossils *Cloudina lucianoi* and *Corumbella weneri*. On the other hand, the Laginha section shows more heterogeneous facies, such as impure carbonates, breccias, marls, and subordinate mudstone beds, as well as no evidence of *Corumbella weneri*. The stable carbon isotope record is also different between the two sections, despite belonging to the same unit. The Corcal section displays higher and more homogeneous $\delta^{13}\text{C}$ values, consistent with those of Ediacaran successions worldwide. The Laginha section, instead, displays more variable $\delta^{13}\text{C}$ values, which suggest the influence of local and post depositional processes. The difference between the two sections was attributed to the different distance from the shore. We propose that the difference is due to topographic variations of the continental platform, which, at the Laginha site, was steeper and controlled by extensional faults. Therefore, the Corcal section is a better reference for the Tamengo Formation, whereas the Laginha is more particular and influenced by local factors. Besides, the lithofacies associations of the Tamengo Formation are like those of the Doushantuo and Dengying formations, in South China, with no significant biogenic carbonate buildups, and different from those of other important Ediacaran units, such as the Nama Group in Namibia and the Buah Formation in Oman. Our work highlights the complexity and heterogeneity of Ediacaran carbonate

platforms and of their carbon isotopic composition. In addition, we characterize the Corcal section as a possible reference for the Ediacaran in South America.

Keywords: neoproterozoic, C and O isotopes, Paraguay Belt, Corcal, Laginha, carbonate ramp

1 INTRODUCTION

The Neoproterozoic geological record discloses a period of remarkable tectonic, climatic, and evolutionary changes on Earth. The paleogeographic modifications, related to Rodinia fragmentation followed by Gondwana assembly, are accompanied by glaciations and extensive volcanism, as well as major oceanic and climatic perturbations (e.g., Hoffman et al., 1998; Fike et al., 2006; Och and Shields-Zhou, 2012; Li et al., 2013; Gernon et al., 2016; Thallner et al., 2021). Furthermore, the fossil record reveals a noteworthy radiation of metazoans during the Ediacaran Period (e.g., Knoll and Carroll, 1999; Penny et al., 2014; Xiao et al., 2016; Kaufman, 2018; Gan et al., 2021).

The Ediacaran in general is characterized by climate warming and sea level rise following the major glaciations of the Cryogenian (e.g., Jiang et al., 2003a; Canfield et al., 2007; Kennedy et al., 2008; Le Heron and Craig, 2012; Lenton et al., 2014; Hohl et al., 2015; Wei et al., 2019). These conditions prompted the growing of carbonate platforms onto the inundated continental margins, as well as major perturbations in the carbon and sulfur cycles (e.g., Gorjan et al., 2000; Hurtgen et al., 2005; Elie et al., 2007; Halverson and Hurtgen, 2007; Ries et al., 2009; Johnston et al., 2012; Loyd et al., 2012; Crockford et al., 2016; Delpomdor et al., 2016; Tostevin et al., 2017; Zhang et al., 2018; Laakso et al., 2020; Yu et al., 2020). Therefore, Ediacaran carbonate sediments provide key information about the environmental and climatic conditions of this period, due to their high potential of preservation (e.g., Grotzinger and James, 2000). However, sedimentological studies on Ediacaran carbonates are challenging since they display several features with no analogues in the present-day, or even in the entire Phanerozoic (e.g., Grotzinger and Knoll, 1995; Chen et al., 2019; Hu et al., 2020; Riding and Virgone, 2020). This is true especially for the isotopic composition of carbon ($\delta^{13}\text{C}$), which yields values extremely anomalous, both positively and negatively (e.g., Kaufman and Knoll, 1995; Halverson et al., 2010; Grotzinger et al., 2011; Cui et al., 2018).

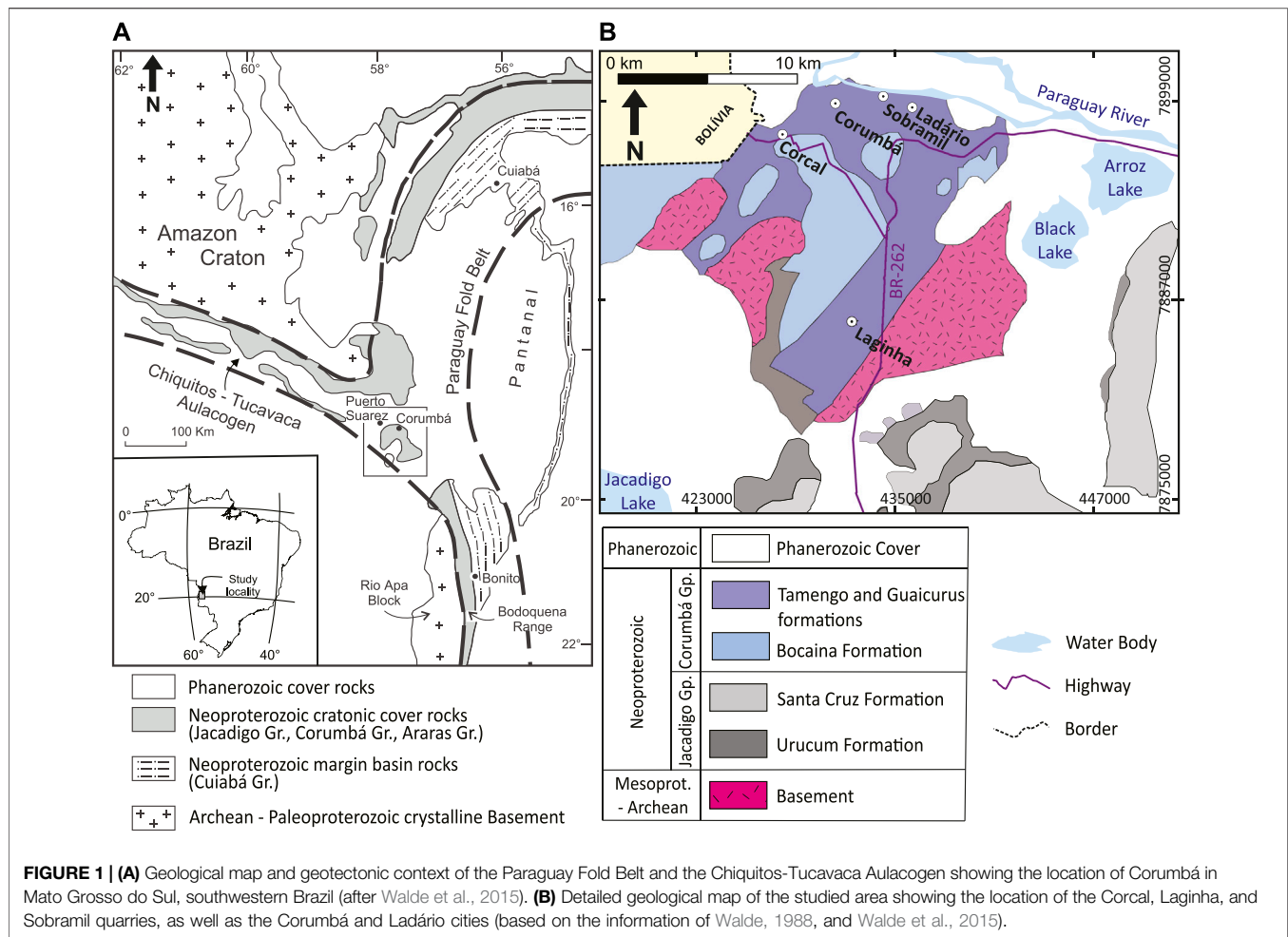
The origin of the Ediacaran $\delta^{13}\text{C}$ anomalies is still controversial, as they cannot be completely explained neither by primary nor by post depositional processes with the current state of knowledge. Indeed, there is evidence supporting either of the two possibilities (e.g., Fike et al., 2006; Bristow and Kennedy, 2008; Derry, 2010; Frimmel, 2010; Grotzinger et al., 2011; Shields et al., 2019; Husson et al., 2020; Xiao et al., 2020; Cui et al., 2021). This constitutes a major problem, as Ediacaran stratigraphic calibration is based mainly on carbon isotope chemostratigraphy (e.g., Narbonne et al., 2012; Xiao et al., 2016). Therefore, more detailed studies on Ediacaran carbonates are necessary to unravel the enigmatic origin of their carbon isotopic composition, as well as the

paleoenvironmental conditions in which the rise of the early animals on Earth occurred.

In Brazil, the most important Ediacaran geological record is the Tamengo Formation, of the Corumbá Group (Boggiani et al., 2010; Walde et al., 2015; Amorim et al., 2020). The importance of this unit comes mainly from the occurrence of upper Ediacaran guide fossils, such as *Cloudina lucianoi* and *Corumbella werneri* (e.g., Hahn et al., 1982; Adorno et al., 2017). However, this unit still lacks a detailed characterization of its depositional system, when compared with the main references for the Ediacaran period. Therefore, our main hypothesis is to test the potential of the Tamengo Fm. as a representative Ediacaran archive. In this work, we present new detailed stratigraphic sections and facies analyses of the Tamengo Formation, which provide an enhanced characterization of this Ediacaran carbonate paleoenvironment. The results reveal a heterogeneous ramp, deposited onto an irregular topography, in some parts influenced by extensional tectonics. In addition, we present new carbon and oxygen isotopes data that contribute to the validation of the Tamengo Formation's $\delta^{13}\text{C}$ curve as a possible chemostratigraphic reference for the Ediacaran in South America.

2 GEOLOGICAL SETTING AND LITHOSTRATIGRAPHY

The carbonate and associated siliciclastic sedimentary rocks of the Tamengo Formation (Corumbá Group) are exposed near the city of Corumbá, Mato Grosso do Sul, in western Brazil, close to the Bolivian border. These units are part of the succession of the southern portion of the Paraguay Belt, a thrust-and-fold belt generated during the Pan-African-Brasiliano orogenic cycle (de Alvarenga and Trompette, 1992; Boggiani et al., 1993; Trompette et al., 1998; Boggiani and Alvarenga 2004; Campanha et al., 2011; Meira, 2011). The Paraguay Belt extends for about 1,000 km with an approximate N-S orientation and is surrounded by the Amazon Craton to the North, the Pantanal Basin to the East, the Rio Apa Block to the South, and the Tucavaca-Chiquitos Aulacogen to the West. Jones (1985) and Walde (1988) consider that the Corumbá region sits on a tectonic triple junction, where the southern and northern branches of the Paraguay Belt intersect with the Tucavaca-Chiquitos Aulacogen (**Figure 1**). These basins formed after extensional tectonics related to the breakup of the Rodinia supercontinent, between 650 and 540 Ma (Babinski et al., 2013). This led to the evolution of a rift system, which formed the southern Paraguay Basin, filled with the sediments of the Jacadigo and Corumbá Groups of Neoproterozoic age (Trompette et al., 1998; De Alvarenga et al., 2009; **Figures 1, 2**). In the Early Paleozoic, the tectonic regime inverted, and these sequences were affected by the Brasiliano Orogeny, with ductile to brittle

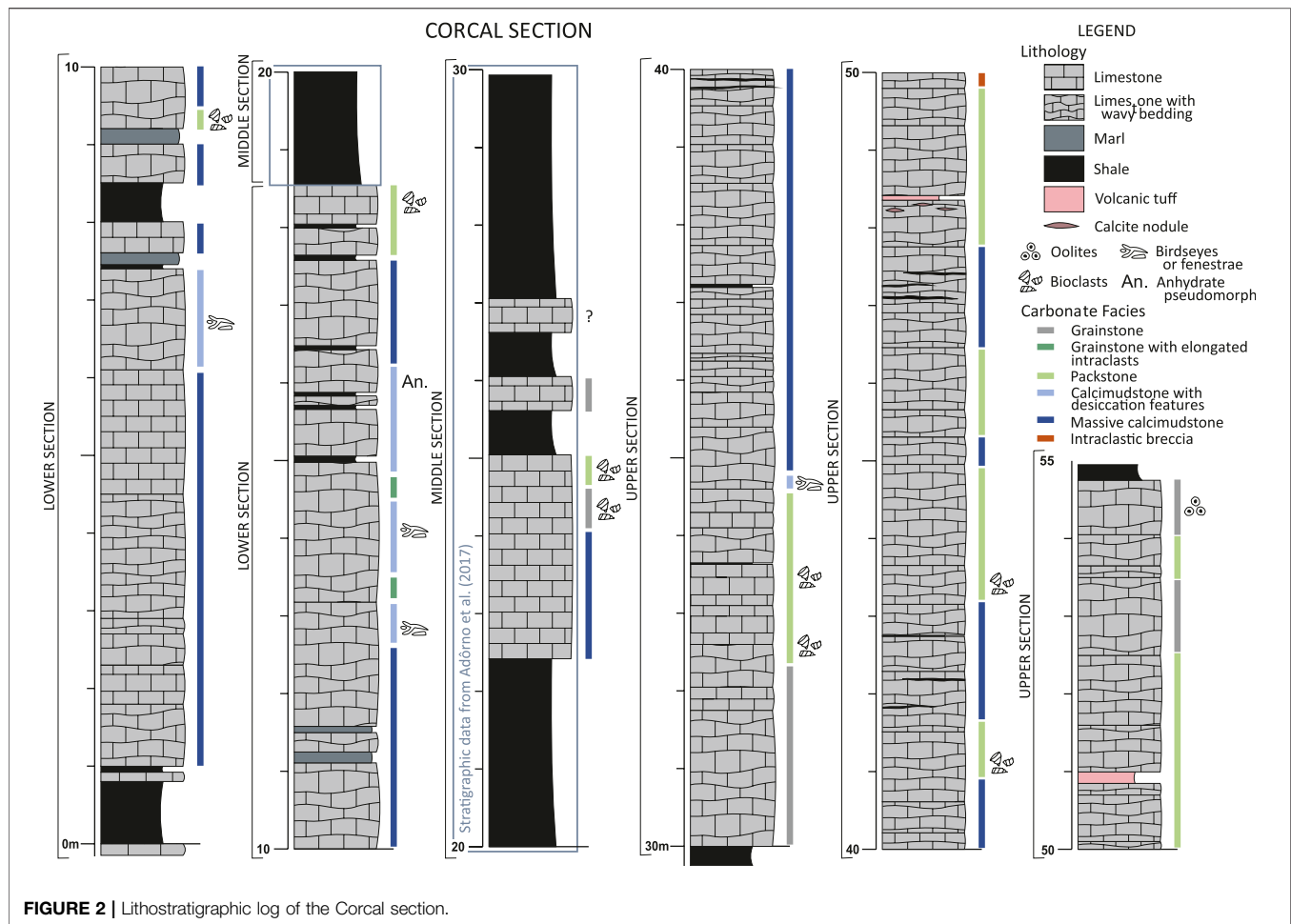


deformation and low-grade metamorphism, in greenschist facies (Trompette et al., 1998; D'el-Rey Silva et al., 2016).

The Jacadigo Group comprises diamictites, arkosic sandstones, and volcanic rocks of the Urucum Formation, at the base, followed by hematite-jaspilites with manganese rich horizons and dropstones of the Santa Cruz Formation, with minimum depositional age of 587 ± 7 Ma ($^{40}\text{Ar}/^{39}\text{Ar}$ in cryptomelane; Piacentini et al., 2013). The Corumbá Group includes carbonate and siliciclastic facies arranged in five units (Almeida, 1964; Almeida, 1965; Almeida, 1984; Boggiani, 1998; **Figure 1**). The Cadiueus and Cerradinho Formations form the lower part and consist of conglomerates, arkoses, siltstones, and occasionally limestones. These units of the lower Corumbá Group do not outcrop in the region of Corumbá. The overlying Bocaina Formation consists of stromatolitic dolostones and subordinate phosphorite levels, occurring with a wider spatial extent. These units are interpreted as a transgressive sequence, beginning with alluvial fan deposits (Cadiueus and Cerradinho Formations) followed by a vast tidal (Bocaina Fm.) flat with high evaporation rates (Boggiani, 1998; Oliveira, 2010; Fontanela, 2012; Sial et al., 2016). The upper part of the Corumbá Group is represented by the Tamengo and Guaicurus Formations. The former includes basal breccias and sandstones, followed by sets of dark fossil-rich limestones, alternated with marls and shales (e.g.,

Ramos et al., 2019). Dolostones and phosphorites occur locally. The paleontological content of the Tamengo Formation includes skeletal macrofossils, especially *C. lucianoi* (Beurlen and Sommer, 1957) an index species for the late Ediacaran (e.g., Grant, 1990; Adórno et al., 2017), and *C. werneri* (Hahn et al., 1982). Recently, a rich assemblage of ichnofossils, vendotaenids, and organic-walled microfossils was also described (e.g., Adórno, 2019). These fossil assemblages have drawn most part of the attention in the studies on the Tamengo Formation (Fairchild, 1978; Walde et al., 1982; Zaine and Fairchild, 1985; Zaine, 1991; Hidalgo, 2002; Gaucher et al., 2003; Kerber et al., 2013; Tobias, 2014; Walde et al., 2015; Adórno et al., 2017; Becker-Kerber et al., 2017; Parry et al., 2017; Walde et al., 2019; Diniz et al., 2021). *C. lucianoi* is usually found in limestones, whereas *C. werneri* occurs in shales (Adórno et al., 2017; Oliveira et al., 2019; Adórno, 2019; Amorim et al., 2020).

Boggiani (1998) suggests that the Tamengo Formation formed above the Bocaina Formation during a transgression, establishing a slope-break ramp system marked by reworking of the shallower sediment. On the other hand, Oliveira et al. (2019) and Amorim et al. (2020) propose a shallower setting, with oolitic bars and storm-derived deposits. The overlying Guaicurus Formation consists of laminated siltstones, which mark the end of carbonate deposition, related to climatic or tectonic changes. This unit was probably



deposited in a deeper environment, below the storm wave base (Boggiani, 1998; Gaucher et al., 2003; Oliveira, 2010). The boundary between the Tamengo and Guaicurus formations is still controversial, as it probably contains a hiatus and then the transition to the Cambrian (Adorno et al., 2019a; Fazio et al., 2019).

Concerning the age of the Corumbá Group, U-Pb dating of zircons from volcanic ash by Parry et al. (2017) provide ages of 555.18 ± 0.7 Ma for the top of the Bocaina Formation and $\sim 542.37 \pm 0.7$ Ma for the top of the Tamengo Formation. These ages agree with the 543 ± 3 Ma provided before by Babinski et al. (2008). Furthermore, the presence of the index-fossils *C. luciano* and *Cloudina carinata* in the Tamengo Formation supports an upper Ediacaran age (Adorno et al., 2017; Adorno et al., 2019b).

3 METHODOLOGY

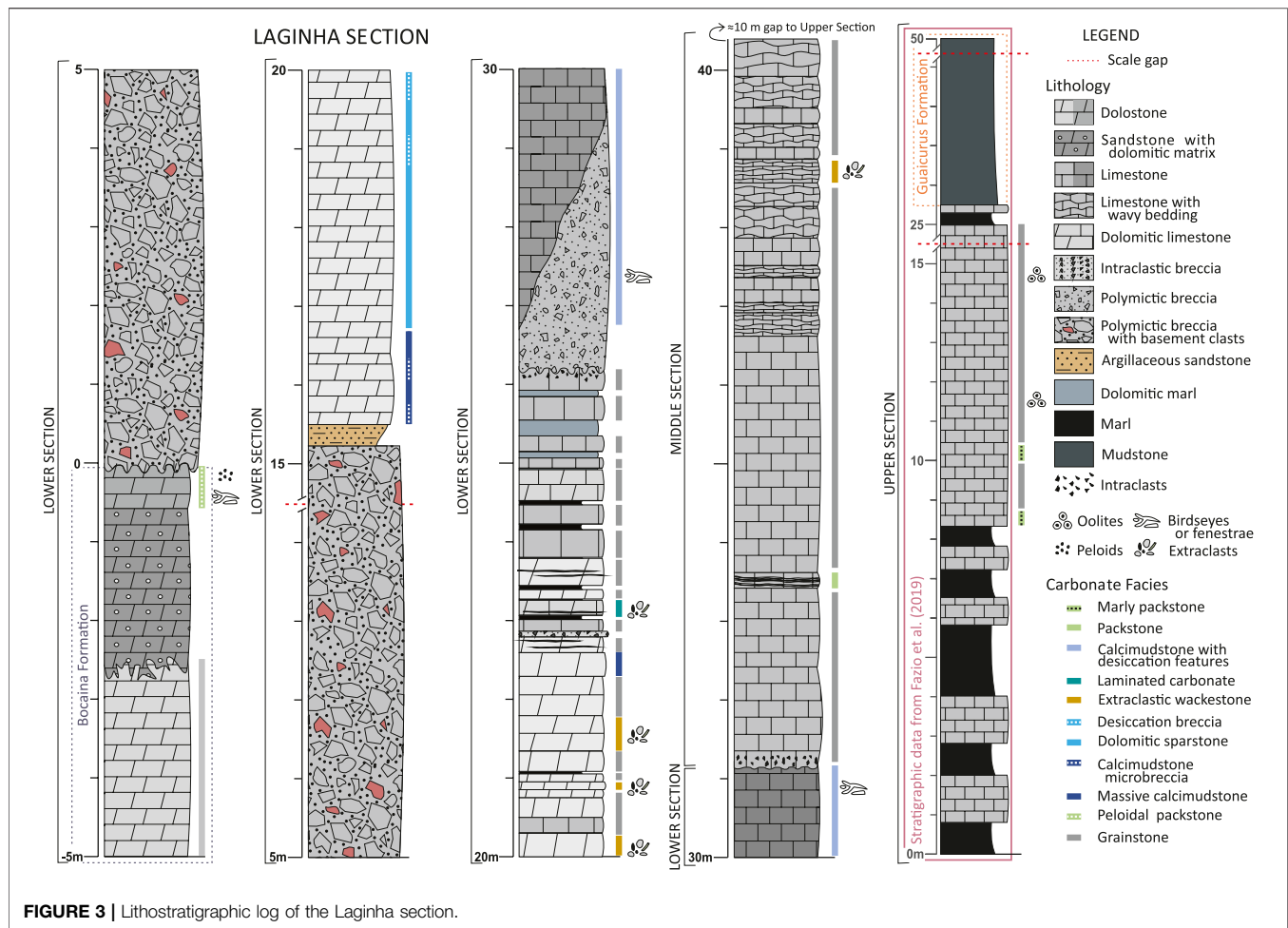
3.1 Fieldwork and Lithostratigraphy

The studied outcrops are in two limestone quarries near the city of Corumbá, in western Brazil. The Corcal and Laginha sections were selected for their vertical continuity, fresh rock exposures, accessibility, and availability of previous studies.

These sites were visited in June 2018 and detailed lithostratigraphic logs were measured and described with a cm to dm resolution (Figures 2, 3). A total of 225 samples were collected for petrographic characterization and geochemical analyses. Outcrops conditions allowed for collecting samples bed by bed. In case of lenticular or amalgamated beds, the samples were collected considering a thicker interval, in order not to confuse the stratigraphic relationships. The average sample spacing resulted of ~ 20 cm. Some intervals were completed using the lithostratigraphic logs of Adorno et al. (2017) and Fazio et al. (2019), as highlighted in Figures 2, 3. This choice was taken for intervals that were already sufficiently detailed in these previous studies, or that were not possible to access.

3.2 Petrography

Petrographic characterization was performed using a ZEISS petrographic microscope at the University of Brasília (UnB). Seventy-nine thin sections were studied, being 40 from the Corcal and 36 from the Laginha section (Supplementary Material). A plain white paper was placed underneath the thin section and used as a light diffuser to clarify textural features under the microscope (Delgado, 1977).



The classification of the carbonate lithofacies was done according to Wright (1992) and Flügel (2004) on the base of: 1) texture, considering the amount of matrix respect to other constituents; 2) composition, based on the mineralogy and the type of grains; 3) sedimentary structures. Therefore, the name represents the main textural features, and the adjectives refer to composition and structures (i.e., “massive calcimudstone”, “dolomitic sparstone”, “intraclastic breccia”).

The Wentworth (1922) grain size classification was used for the siliciclastic facies. Besides, “shale” and “mudstone” were differentiated, as the former displayed fissile or foliated structure and calcite filled veins, which were absent in the latter. Facies associations were defined according to the carbonate ramp model of Burchette and Wright (1992).

3.3 Scanning Electron Microscopy

After the analysis at the optical petrographic microscope, which allowed for identifying constituents that needed a more detailed characterization, nine thin sections were selected among the representative lithofacies for SEM analyses. Prior to the analysis the sections were coated with carbon, and then analyzed at the University of Brasília (UnB) using a FEI QUANTA 450 scanning electron microscope with

a BSE detector, 20 kV accelerating voltage, working distance of 10–12 mm, and in high-vacuum mode.

3.4 Carbon and Oxygen Isotopes Geochemistry

For carbon and oxygen isotopes analysis in carbonate ($\delta^{13}\text{C}$ and $\delta^{18}\text{O}$), 116 samples from Corcal and 54 from Lágina were collected with 20–40 cm spacing. The respective lithofacies was always annotated alongside each sample, to constrain the interpretation of the results. Additionally, areas containing veins, fractures, and other post-depositional features, likely to interfere with the primary isotopic signal, were avoided. Fresh rock samples were powdered using a drill with a 3 mm-diameter bit. Prior to the analysis about 300 μg of material were put in glass vials, acclimatized at 72°C, and flushed with He to eliminate atmospheric gases. Afterwards, carbonate samples were reacted with concentrated phosphoric acid during 1 h, and the released CO_2 was analyzed with a Thermo® Gasbench II connected to a Thermo® Delta V^{Plus} mass spectrometer at the University of Brasília (UnB). The isotopic ratios are reported in per mil (‰), using the conventional δ notation, relative to the Vienna Pee Dee Belemnite (VPDB) standard. The analytical precision is $\pm 0.1\text{‰}$ for both $\delta^{13}\text{C}$ and $\delta^{18}\text{O}$.

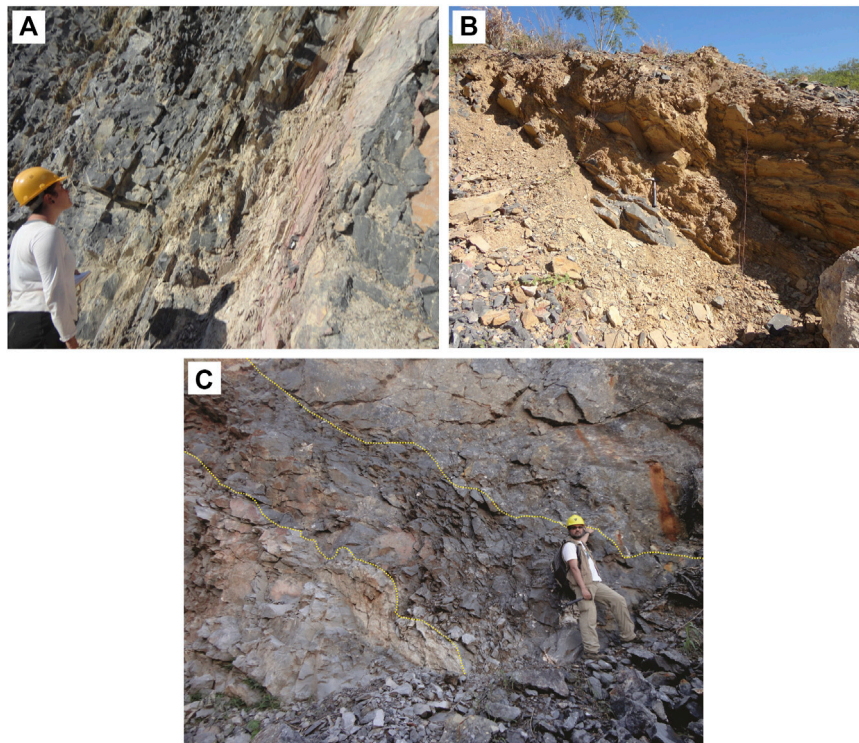


FIGURE 4 | (A) Limestones and marls in the lower part of the Corcal section. **(B)** Shale layer in the middle part of the Corcal section. **(C)** Basal part of Laginha section displaying the contact between the Bocaina and Tamengo formations. From bottom to top: light gray dolomitic grainstone, first erosional contact, dark gray sandstone with dolomitic matrix grading upward into dark gray peloidal packstone, second erosional contact, homogeneous polymictic breccia with basement clasts. Erosional contacts are highlighted by yellow dotted lines.

4 RESULTS

4.1 Corcal Section

The Corcal section is 55 m thick and consists of m-thick bundles of shallow-water limestone with tabular to wavy amalgamated beds and cm-thick beds of mudstone and marl, alternating with m-thick intervals of shales (Figures 2, 4). Neither the base nor the top of the Tamengo Formation is exposed at this site. The lower and upper parts of the section were logged in the northern and southern side of the quarry, respectively. On the other hand, the middle part was completed using the log by Adôrno et al. (2017), as it was considered sufficiently detailed after verification in the field. The split of the profile in these three sub-sections was done to avoid parts that occurred tectonically disturbed by faults and folds, which deformed especially the most ductile shale beds. However, the stratigraphy was adequately exposed for allowing the recognition of the entire succession in continuity.

The lower part of the section (from 0 to 18.60 m) consists of shallow-water limestones organized in 1–2 m thick bundles of wavy and amalgamated beds alternated with bundles of cm- to dm-thick tabular beds (Figures 2, 4). At the microscopic scale, the limestones in this interval consist mainly of calcimudstones, often recrystallized, with some extraclasts of quartz and mica, bioclasts, and intraclasts (Figure 5). Generally, they display a

massive structure, but locally evidence of desiccation can be observed, such as birdseyes, anhydrate pseudomorphs, silicification, dolomitization, and micritization (Figures 5B,C,G). Alongside the calcimudstones, there are minor occurrences of packstones and grainstones formed by bioclasts, intraclasts, and siliciclastic extraclasts (Figures 5D,H–J). Grain size is from sand to granule and the intergranular space is filled with micrite or calcite cement. Occasionally recrystallization or dolomitization is present. The structure is massive, with lenticular veins and calcite-filled fractures. In few cases the grainstones display angular and variously elongated intraclasts, sometimes with combining edge, and local ferruginous matrix, suggesting possible brecciation by desiccation. The limestone succession is interrupted by few centimeter to decimeter thick beds of shales and marls, formed by clay to silt-size detrital grains, especially quartz, with massive to finely laminated structures and variable carbonate, occurring as cement or microscopic nodules (Figure 5E). Fazio et al. (2019) noted also the presence of gypsum pseudomorphs.

The middle part of the section (from 18.60 to 29.90 m) consists mainly of massive shales, interrupted by a 2.25 m thick and two decimeter thick limestone beds. The shales are siliciclastic mudstone, sometimes thinly laminated, with minor quartz grains and carbonate cement (Figure 4B). There are rare

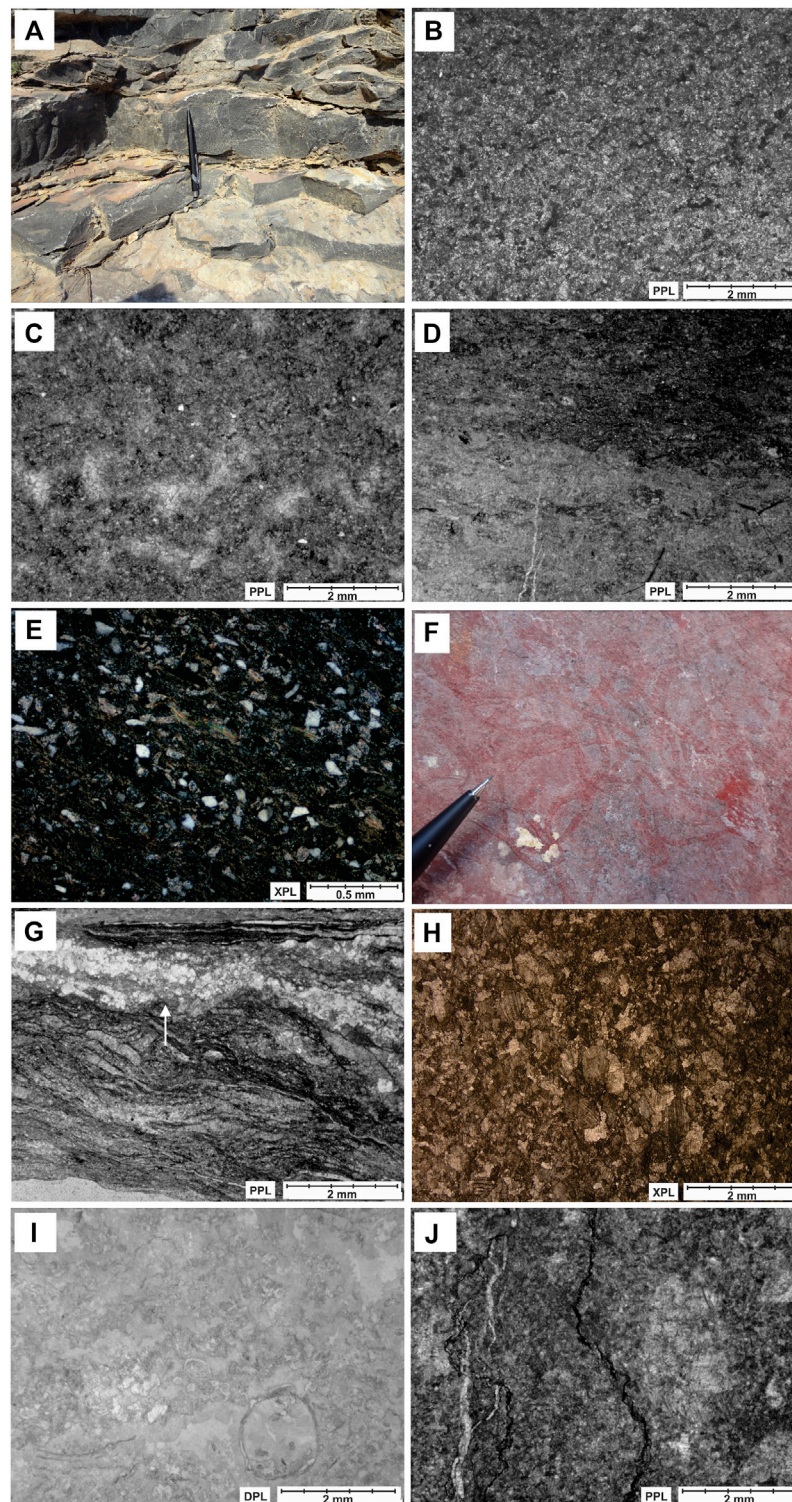


FIGURE 5 | Lithofacies of the Corral section: **(A)** Limestone beds in the upper part of the section (scale object is 13 cm). **(B)** Thin section view of a massive calcimudstone (b/w; Sample C1 2,62). **(C)** Fenestral structures filled with calcite cement (b/w; Sample MP 2118). **(D)** Thin section view of an intraclastic grainstone with local ferruginous matrix (b/w; Sample MP 2119). **(E)** Thin section view of a marl (Sample MP 2115). **(F)** Specimens of *C. wernerii* preserved along a surface in a shale bed (scale object is 2 cm). **(G)** Calcimudstone with elongated intraclasts and silicified anhydrite pseudomorphs, indicated by arrow (b/w; Sample MP 2123). **(H)** Recrystallized grainstone (Sample C3 24,60). **(I)** Grainstone with bioclasts of *Cloudina* (b/w; Sample MP 2128). **(J)** Recrystallized packstone (b/w; Sample MP 2132).

opaque grains, compaction-related segregation structures, calcite and quartz-filled fractures, and silicified nodules. These are also the lithological intervals yielding the fossils of *C. werneri*, indicating the upper Ediacaran age of the Tamengo Formation (Figure 5F; Adorno et al., 2017). The limestone beds consist of calcimudstones and grainstones, similar to those in the lower part of the section.

The upper part of the section (from 29.90 to 54.40 m) consists of limestone arranged in sets of centimeter to decimeter thick beds, varying from tabular to wavy, interchanged with rare millimeter to centimeter thick shale beds, and, occasionally centimeter thick mudstone lenses (Figure 5A). Amorim et al. (2020) also described hummocky cross stratification in correlative outcrops of this interval. As this kind of sedimentary structure is generally highlighted by weathering on the surface of the rock, it is not visible in the Corcal section because the surface of the outcrop is too fresh, being it in an active quarry. At microscopic scale the limestones consist of calcimudstone and grainstone with intraclasts and bioclasts of *Cloudina* type organisms, as suggested by the tubular shapes (Figures 5H,I). At 34.65 m birdseye porosity was noted, and at 48.00 and 50.50 m there are tabular centimeter thick beds of light, greenish to whitish, clayey sediment, different from the other mudstones, described as possible volcanic tuffs. In addition, at 48.13 m there are pinkish centimetric calcite nodules, and a layer of intraclastic breccia was observed at 49.66 m. The uppermost limestone bed is a massive oolitic grainstone and, above, starts a massive interval of shales with carbonate lenses, described in detail by Fazio et al. (2019). SEM analysis revealed also the presence of fluorapatite in 4 different levels of the Corcal section: 6.50, 10.40, 2.55, and 18.42 m.

4.2 Laginha Section

The Laginha section is about 100 m thick and displays both the lower and the upper boundaries of the Tamengo Formation. The succession yields a higher variety of lithofacies than the Corcal section (Figure 3).

The lower part of the section (from ~5 to 30 m) starts with a dolomitic interval, formed by 2.50 m thick massive bed of light grey grainstone, followed by ~2.00 m of massive dark gray sandstone with dolomitic matrix mostly composed of very well-rounded quartz grains with approximately equal amounts of grains and matrix. Above, there is ~0.5 m thick peloidal packstone with fenestral pores, filled with spathic calcite. The contact between the latter two beds is very irregular, indicating an erosional and possibly karstified unconformity (Figure 4C). This interval represents the uppermost part of the Bocaina Formation (Boggiani, 1998). The Tamengo Formation starts with a ~15 m thick bed of massive polymictic breccia containing various types of intraclasts and extraclasts with composition of quartz, dolostone, limestone, chert, phosphorite, and granite type rocks. They are poorly sorted, with chaotic distribution and with a rounded to very angular shape. The matrix is dolomitic and dark gray, there are irregular voids filled with white spathic calcite (Figure 6A). The contact at the base is erosional. Above the thick polymictic

breccia there is a 25 cm thick friable yellowish-brown, massive argillaceous sandstone, with sand-size quartz grains and lithoclasts within an argillaceous matrix (Figures 6B, 7A, 8A,B).

Upwards occurs a mainly carbonate succession, starting with 4.5 m of massive dolostones with numerous randomly oriented fractures, with millimeters to centimeters size and filled with white sparry calcite (Figure 8C). Above, there are 2.80 m of sparstones, arranged in sets of centimeter to decimeter thick tabular beds, dolomitic to calcitic, massive to laminated, containing stylolites and calcite-filled veins, locally brecciated and associated with fluorite (Figures 6C,D, 7D). The succession continues with alternating dolostones and limestones, consisting of laminated facies, with alternating crystalline and sandy laminae, the formers are calcitic to dolomitic, with sparse extraclasts of quartz and mica; and the latter are grain-supported, with calcitic to dolomitic matrix and sand-size extraclasts varying in composition from quartz to k-feldspar (Figures 6E,F, 7B, 8D–G). Authigenic pyrite and phosphatized grains are present, and SEM-EDS analyses revealed traces of zircon and possible anatase. Late compaction structures, such as stylolites and calcite-filled veins, occur frequently. In addition, there are massive wackestones with micritic matrix and abundant extraclasts, especially quartz and muscovite, ranging from fine to coarse sand-size; and grainstones formed predominantly by concentric ooids, occurring as single or composite, often micritized or completely recrystallized, with rare aggregate grains and cemented by calcite. At 22.75 m there is a 7 cm thick bed of intraclastic breccia, grain-supported, with micritic matrix and angular intraclasts, ranging in size from fine sand to granule, with the larger grains of tabular shape, and with abundant fine quartz grains (Figure 7C).

At 26.40 m occurs an irregular massive polymictic breccia, with maximum thickness of 5 m and erosional contact at the base, which laterally meets a light gray limestone in angular unconformity (Figure 7E). It is grain-supported, with limestone intraclasts and grains varying from quartz to dolomite, phosphorite, mudstone, k-feldspar, and pyrite, with micritic matrix. It is worth noting the absence of coarse granitoid clasts from the basement, observed in the breccia at the base of this unit (Figure 6G).

The middle part of the section (from 30 to ~44 m) starts with 5.35 m of dark gray limestone, overlying the breccia with a very irregular, erosional, and perhaps karstified contact. This interval is massive, consisting of calcimudstones micritized to recrystallized, with fenestral pores and chert nodules; alternatively, they occur mottled, dolomitized, with quartz and opaque extraclasts, and calcite-filled fractures. Sometimes they are brecciated, with fractures and very angular intraclasts, with isopachous or dog tooth cement at the margins and syntaxial cement at the center (Figures 8H–L). The last 3.75 m thick interval of the middle section consists of dark gray limestones arranged in sets of centimeters to decimeters thick beds, varying from tabular to wavy. Microscopically they are oolitic grainstones, with local occurrences of micritic matrix and extraclasts (Figures 7F, 8M–O).

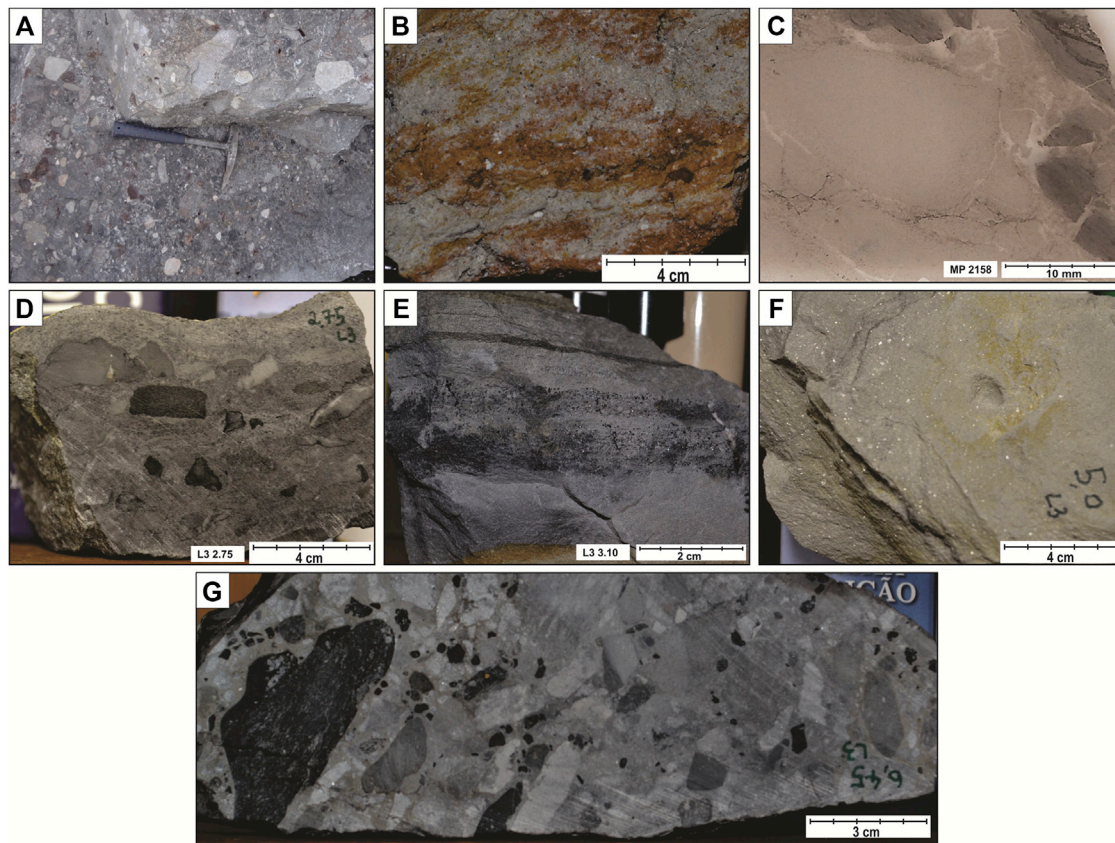


FIGURE 6 | Macroscopic view of sedimentary facies in the lower part of the Laginha section. Sample identification and scale at the right-hand bottom corner of each picture. **(A)** Basal polymictic breccia with basement clasts, poorly sorted and with micritic matrix. **(B)** Muddy sandstone with quartz grains and lithoclasts. **(C)** Thin section photograph of a dolomitized desiccation breccia. Note the broken dark grains still positioned next to each other counterparts. **(D)** Intraclastic breccia with square, angular clasts. **(E)** Laminated carbonate with alternated finer and coarser layers. **(F)** Dolomitic marl displaying mica extraclasts. **(G)** Polymictic intraclastic breccia with homogeneous structure.

During the fieldwork we could not access to the upper part of the section, and thus we completed the log with that of Fazio et al. (2019). However, with the stratigraphic information available it was not possible to precisely link the middle to the upper part of the section and a 10 m gap is estimated between the two. According to Fazio et al. (2019), the upper part of the section comprises 30 m, with the lower half consisting of alternating limestones and laminated mudrocks, with a composition ranging from carbonate to siliciclastic. Above this interval, in conformable or para conformable contact, there are ~24 m of pure siltstone, with millimeters to centimeters thick, plane parallel to wavy lamination, belonging to the Guaicurus Formation. The contact between the two formations in the Laginha section presents 1 m-thick non-cohesive yellowish beige siltstone with kaolinite and gypsum among its mineralogy (Fazio et al., 2019).

4.3 Carbon and Oxygen Stable Isotopes Geochemistry

The Corcal section displays little dispersed $\delta^{13}\text{C}$ values (Figure 9), ranging from 0.70‰ to 6.97‰. In the lower part

of the section, the values increase gradually from ~3.5‰ to ~5‰, and then persist through the middle and upper part. There are minor positive peaks of 5.33‰, 6.97‰, and 5.75‰ at 10, 12.95, and 15.95 m, respectively, and a negative peak of 4.16‰ at 32.85 m, as well as few outliers. $\delta^{18}\text{O}$ values range from -10.47‰ to -4.75‰. In the lower part of the section values are more dispersed but become steadier in the middle and upper part. The cross-plot between $\delta^{13}\text{C}$ and $\delta^{18}\text{O}$ shows no linear correlation or facies-related clustering (Figure 10).

The Laginha section yields $\delta^{13}\text{C}$ values from -3.11‰ to 4.92‰ (Figure 9). In the Bocaina Formation the values show a linear increase from 1.53‰ to 3.14‰. Above the polymictic breccia, which was not analyzed for stable isotopes, values start at 0.79‰ and decrease to -3.00‰ at 21 m, then increase again to 0.13‰ at 27.35 m and 1.92‰ at 30.75 m. In this last interval the values are scattered, showing no clear trend. The middle part of the section has values around -1.00‰, with a distinct negative peak of -2.14‰ at 34.8 m. The upper part of the section has a lower sampling resolution, however, a rough trend can be observed with values starting around 4‰, increasing to 4.80‰ at 12 m, and then decreasing to around 2‰ from 17 m to the top of the Tamengo

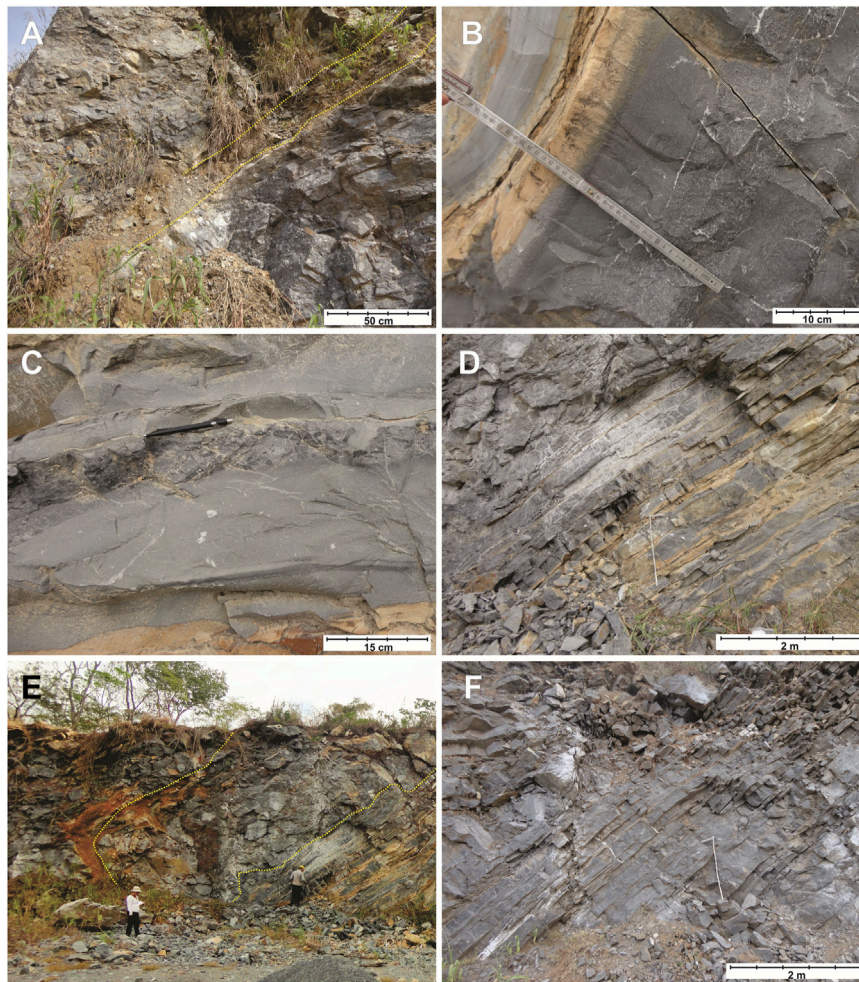


FIGURE 7 | Macroscopic lithofacies of the Laginha section. **(A)** Polymictic breccia overlaid by muddy sandstone and then carbonate beds. **(B)** Sequence of dark gray fine grainstone, dark gray coarse lithic sandstone with carbonate matrix, and light gray dolomitic wackestone. **(C)** Cm thick layer of intraclastic breccia in the lower section. **(D)** Limestones with dm thick tabular bedding in the lower section. **(E)** Homogeneous, polymictic intraclastic breccia within dark gray limestones. **(F)** Limestones with dm thick tabular bedding in the upper part of the lower section, with chaotic bedding towards the top.

Formation. The average is -1.01‰ in the lower and middle part of the section, and 3.29‰ in the upper part. $\delta^{18}\text{O}$ values range from -10.09‰ to -2.12‰ , with average of -6.84‰ . They are dispersed, showing no clear trend, within the lower and middle part of the section, and range between -8‰ and -6‰ in the upper part. The cross-plot between $\delta^{13}\text{C}$ and $\delta^{18}\text{O}$ shows no linear correlation or facies-related clustering (**Figure 10**).

5 DISCUSSION

5.1 Facies Interpretation

5.1.1 Corcal Section

In the Corcal section were recognized nine sedimentary facies, listed in **Table 1**. The lower part is dominated by the facies C1, alternated with C4, with the occurrence of C2 and C3. This facies association suggests a shallow low-energy environment, dominated by the settling of fine-grain sediments, with the

supply of coarser carbonate grains reworked by waves or currents. Episodic influx of siliciclastic material and of emersion and desiccation also occurred (Tucker and Wright, 1990; Schlager, 2005; Łabaj and Pratt, 2016). Silicification, observed in some levels, also supports this interpretation, as silica is supplied by continental runoff and then, during diagenesis, gets mobilized and fills the cracks opened by the desiccation (Laschet, 1984 in Flügel, 2004). This evidence suggests a back to inner ramp environment for the lower part of the Corcal section (Burchette and Wright, 1992).

The shales dominating the middle part of the Corcal, facies C8, represent a significant decreasing of the energy and of the carbonate input. They can be attributed to episodes of relative sea level rise, in which the flooded carbonate factory decreased its productivity, and the environment reached higher depths, below the storm wave base (Walker, 1984; Łabaj and Pratt, 2016; Oliveira et al., 2019; Amorim et al., 2020; Ding et al., 2021). The limestone intervals within the shales display facies C1, C5,

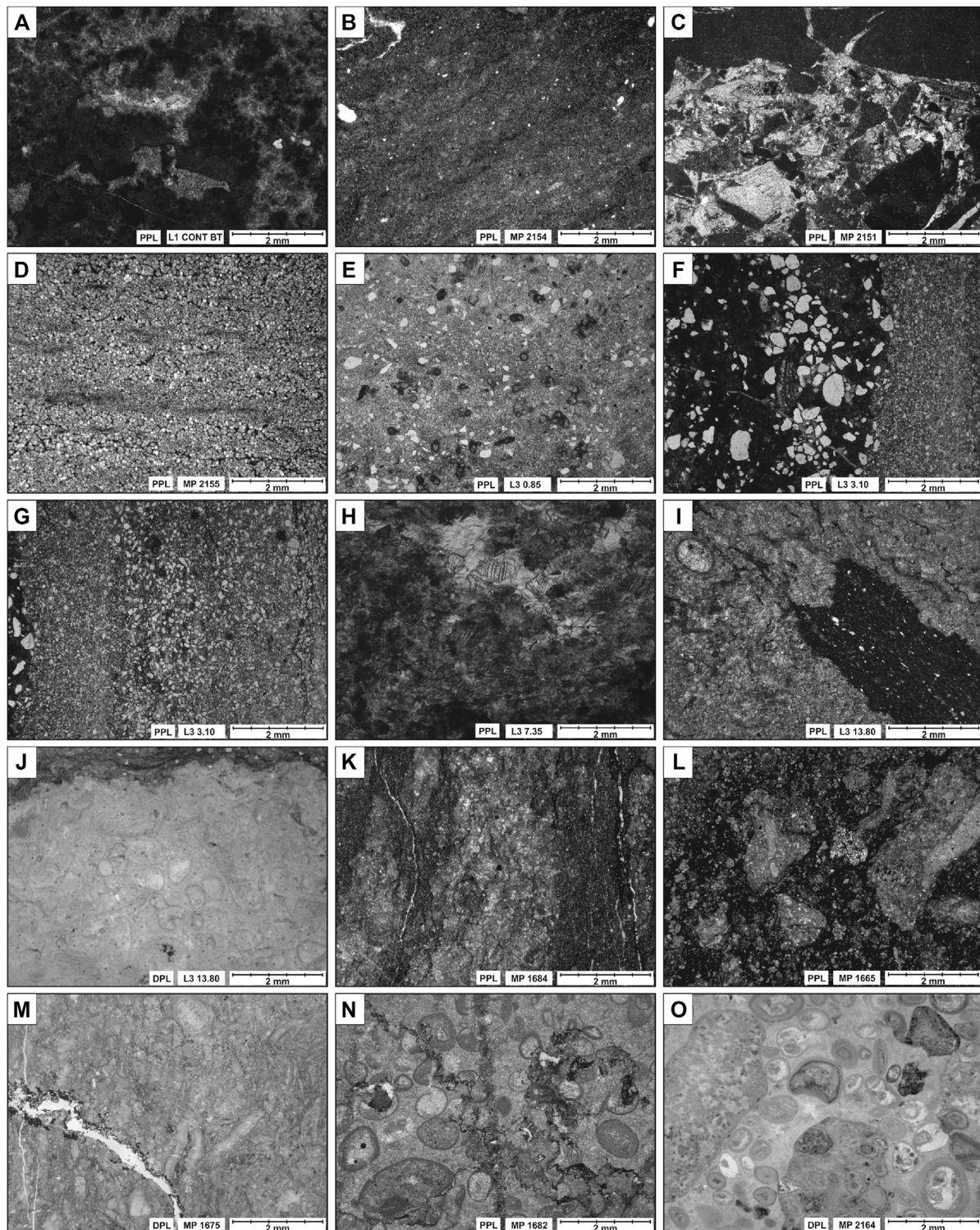
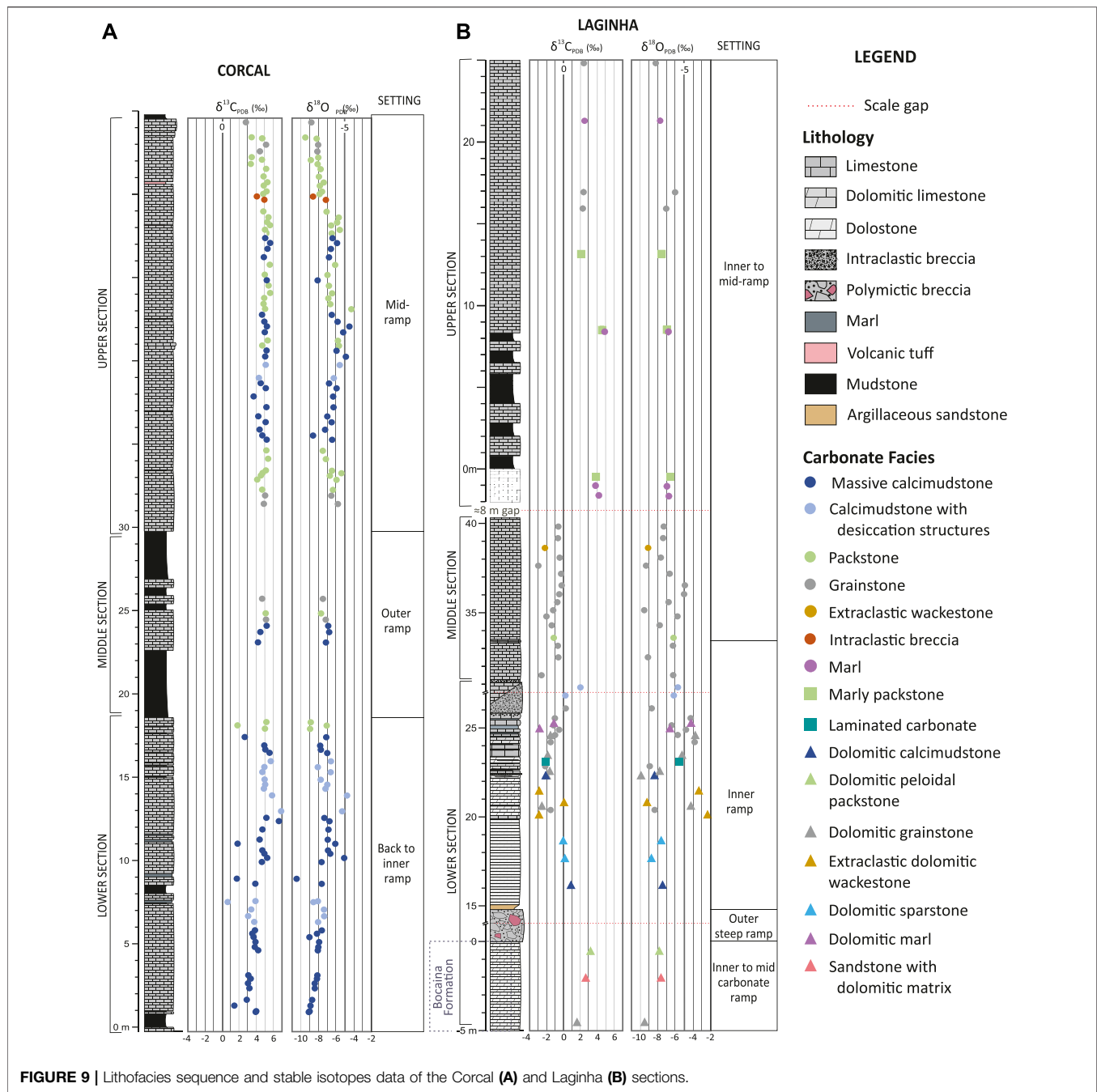


FIGURE 8 | Microfacies in the Laginha section (all in b/w). Light type, sample identification, and scale at the right-hand bottom corner of each picture.

(A)—Dolomitized peloidal packstone with fenestral porosity. **(B)** Massive calcimudstone with quartz extracasts. **(C)** Calcimudstone microbreccia with sparite cement. **(D)** Dolomitic sparstone. **(E)** Extraclastic wackestone. **(F,G)** Laminated carbonate showing alternate layers of pure and impure dolostone and limestone with extracasts. **(H)** Calcimudstone with fenestral porosity. **(I,J)** Intraclastic packstone with sub-rounded intraclasts or bioclasts. **(K)** Marl with local clay seams. **(L,M)**—Marly packstone with angular intraclasts. **(N,O)**—Oolitic grainstone with stylolites.

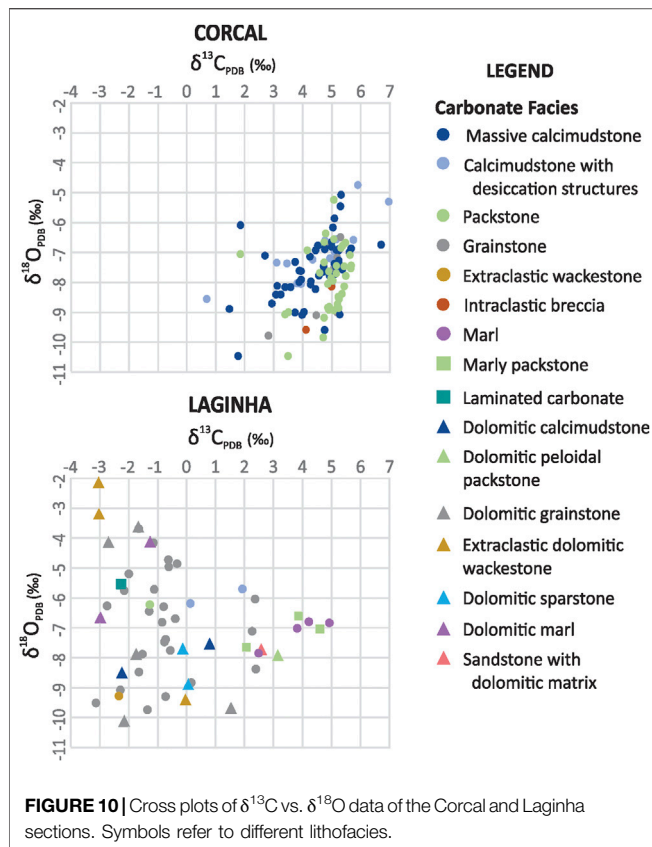


and C6, indicative of higher energy conditions that can be attributed to a mid-ramp setting (Burchette and Wright, 1992; Schlager, 2005). Therefore, they can represent higher frequency cycles of carbonate platform recovery and progradation during the transgressive phase.

The facies succession in the upper part of the Corcal section consists of facies C5, C6, C7, with local occurrence of C2 and C9. It indicates an active carbonate factory and higher energy conditions than the underlying sequence. It can be related to a mid-ramp carbonate platform environment, with depth mainly below and sometimes above the fair-weather wave base (Burchette and

Wright, 1992). This interval may represent the carbonate platform recovery and progradation during the sea level high stand, after the rise (Schlager, 2005; Łabaj and Pratt, 2016).

The volcanic tuff beds of facies C9 might be related to a nearby volcanic eruption. The ashes could have been transported by winds and currents and redeposited by settling or low-density gravity flows (Nichols, 2009). The volcanic activity could be related to the extensional tectonics occurring in the Corumbá region during the Ediacaran (Alvarenga et al., 2011; Warren et al., 2019). These, volcanic tuff beds were described in previous studies, such as Boggiani et al. (2010) and Amorim et al. (2020),



and dated by Babinski et al. (2008) and Parry et al. (2017) providing ages of 543 ± 3 Ma and 541.85 ± 0.75 Ma, respectively.

5.1.2 Lagenha Section

The Lagenha section displays a greater variety of lithofacies than the Corcal, as 18 were recognized and listed in **Table 2**. The karstified surface above the dolomitic grainstone (facies L1) in the upper Bocaina Formation can be evidence of emersion, and the very well rounded and sorted grains of the overlaying sandstone bed (facies L2) suggest long distance transport and possible reworking by beach waves (Tucker and Wright, 1990). Besides, peloids occurring in the overlaying facies L3 are typical of shallow, low energy restricted marine conditions (Tucker and Wright, 1990; Flügel, 2004). Hence, these units can represent a peritidal environment developed after a local regression, as suggested also by Boggiani (1998) and Oliveira (2010).

The thick polymictic breccia with basement clasts at the base of the Tamengo Formation constitutes the facies L4 (**Figure 3**). Breccia facies in carbonate platforms may be due to multiple factors. Storm episodes can produce breccias, however, in this case they are clast supported and occur in beds with maximum thickness of few meters and interbedded with fine offshore facies (e.g., Seguret et al., 2001; Wang et al., 2019). The breccia at the base of the Tamengo Formation is very poorly sorted, contains abundant matrix and basement clasts, indicating continental erosion occurring nearby the carbonate platform. Its thickness higher than 10 m and massive structure resemble the breccias

described in the Otavi Group in Namibia (Eyles and Januszczak, 2007). This is one of the most studied successions of the Neoproterozoic and the breccias are interpreted as related to extensional tectonic (Eyles and Januszczak, 2007). The same interpretation was given to similar breccia deposits of Cretaceous age in the Northern Calcareous Alps (Sanders and Höfling, 2000). Considering that the Corumbá Group is interpreted as part of a rift filling sequence, this polymictic breccia might be related to a rapid graben infill, with material supplied in part by exposed structural highs, mixed with reworked carbonate coming from the platform growing along the surrounding margin. In this context, the argillaceous sandstone above the breccia (facies L5) can be attributed to a later stage of the graben infill, probably in more distal conditions (Jiang et al., 2003b; Łabaj and Pratt, 2016). Therefore, such sequence of facies might represent a phase of intense continental erosion, alongside a steep topography related to extensional faulting, which triggered massive flows of sediments and their redeposition downslope. Here we revise the interpretation of Boggiani (1998), Fernandes and Boggiani (2021), who interpreted this deposit as associated to a regressive phase. Even though a relatively low sea level might have favored continental erosion, a steep topography and sufficient depth were necessary to accommodate such a thick sediment bed.

Carbonate deposition in the Lagenha section begins with a sequence of facies L6 and L7, followed by L8 alternated with L9, L10, and L11. These facies can indicate a low energy environment, however, the presence of syn-sedimentary fractures and occasional brecciation suggests post depositional destabilization, possibly related to the still ongoing opening of the rift or to the gravitational slides onto a steep substrate (e.g., Sanders and Höfling, 2000; Basilone et al., 2016). The absence of fluidification and slumping structures makes more likely a gravitational than a seismic trigger (Audemard and Michetti, 2011). Consequently, the lenticular massive breccia devoid of basement clasts (facies L12), occurring between 5 and 10 m, can be related to a local sediment slide, with reworking of intraclasts, forming a small fan downdip (Ding et al., 2021). Besides, the calcimudstones with bird-eyes structures, occurring repeatedly above (facies L13), indicate shallow tidal or peritidal conditions, reached after the rapid filling of the graben in a still relatively low sea level phase (**Figures 6, 9**; Tucker and Wright, 1990; Burchette and Wright, 1992; Flügel, 2004; Ding et al., 2021).

The rhythmic marls and limestones (facies L14, L15) in the middle part of the Lagenha section, show changes in the content of mud respect to skeletal grains (Oliveira, 2010; Fazio et al., 2019). The shifts between carbonate and siliciclastic deposition could have been driven by high frequency variation in relative sea level or climate in a mid-ramp environment (e.g., Schlager, 2005; Harper et al., 2015; Łabaj and Pratt, 2016). These alternating facies change gradually upward to marly intraclastic packstones (facies L16), representing a small shift back to inner ramp (Burchette and Wright, 1992).

The upper segment of the section consists of oolitic grainstones (facies L17), up until the contact with the mudstones of the Guaicurus Formation. The oolites are cemented by calcite and range in size from mid to coarse

TABLE 1 | Lithofacies and facies associations of the Corcal section.

Facies asociacion	Facies	Description	Process
Back-ramp to inner ramp carbonate platform	C1—Massive calcimudstone	Sets of decimeters thick wavy to tabular beds composed of massive dark gray carbonate mudstone. Local occurrence of bioclasts, intraclasts, interstitial concentration of clay and extraclasts (Qz, Op).	Settling of suspended micrite with episodic wave reworking and continental input.
	C2—Calcimudstone with desiccation features	Sets of centimetres to decimetres thick beds with wavy to tabular bedding, composed of massive, dark gray, carbonate mudstone with bird-eyes structures or chert filled cracks. Local occurrence of bioclasts, intraclasts and extraclasts (Qz, Ap, Bt, Op).	Settling of suspended micrite with episodic wave reworking, continental input, and emersion and desiccation.
	C3—Grainstone with elongated intraclasts	Grainstone in centimeters thick tabular beds composed of elongated micritic intraclasts and blocky calcite cement.	Micrite indurated and fragmented by desiccation and episodic wave reworking.
	C4—Marl	Centimeters to decimeters thick tabular beds with mixed siliciclastic and carbonate mud. From brown to light gray in color, massive to fissile.	Settling of suspended micrite and siliciclastic mud in shallow low-energy conditions.
Mid-ramp carbonate platform	C5—Packstone	Sets of centimeters to decimeters thick tabular to wavy beds of massive, dark gray packstone composed of intraclasts and bioclasts, mainly of <i>Cloudina</i> type organisms, in a micritic matrix. Local occurrence of sparse extraclasts, clay seams, nodules, and mild dolomitization.	Transport and reworking of sediments below the fair-weather wave base.
	C6—Grainstone	Sets of centimeters to decimeters thick tabular to wavy beds of massive dark gray grainstone composed of bioclasts, mainly of <i>Cloudina</i> type organisms, intraclasts, and oolites cemented by sparite.	Transport and reworking of sediments above the fair-weather wave base.
	C7—Intraclastic breccia	Centimeters thick tabular bed of recrystallized breccia composed of rounded, poorly sorted intraclasts in micritic matrix.	Highly reworked micritic or micritized grains redeposited below the fair-weather wave base.
Outer ramp carbonate platform	C8—Shale	Centimeters to metres thick tabular beds composed of massive to fissile siliciclastic mudstone, beige to gray, with calcite filled veins. Local occurrence of <i>C. werneri</i> specimens and ichnofossils	Settling of suspended mud below the storm wave base.
Volcanic pulse	C9—Volcanic tuff	Centimeters thick tabular beds of whitish to yellowish claystone, very friable.	Volcanic ashes transported by winds and currents after the eruption and redeposited by settling or gravity flows.

sand, with a relatively thick carbonate coating, indicating a shallow, warm, high-energy environment (Sumner and Grotzinger, 1993). This facies can represent oolitic sand shoals in an inner ramp environment during a relatively high sea level phase, similar to the upper Corcal section (Figure 6; Tucker and Wright, 1990; Amorim et al., 2020; Ding et al., 2021).

Finally, the grayish mudstones of the Guaicurus Formation represent the facies L18. The fine grains size and the absence of carbonate constituents indicate very low energy condition and no carbonate input, similar to the facies C8 in the Corcal section. However, Fazio et al. (2019) noticed a different mineralogical composition and the absence of post burial deformation structures in the mudstone of the Guaicurus Formation, respect to the shales of the Corcal section. Besides, the yellowish beige siltstone with kaolinite and gypsum at the base of the Guaicurus Formation can indicate alteration by connate fluids or by post-depositional meteoric water interaction. All this evidence suggests a period of non-deposition prior to the onset of the Guaicurus Formation, during which the sediments of the Tamengo formation became altered (Fazio et al., 2019). This highlights the possibility of a hiatus occurring between the Tamengo and the Guaicurus formations.

5.2 Lateral and Temporal Variation in $\delta^{13}\text{C}$

The $\delta^{13}\text{C}$ values have no clear correlation with $\delta^{18}\text{O}$ in both studied sections, which indicates no significant alteration by early burial diagenesis even though some samples are recrystallized (Kaufman and Knoll, 1995; Derry, 2010). In addition, the isotopic values are not clustered according to the sedimentary facies. In the Corcal section there is little point-to-point variation and a clear increasing trend within the lower part, reaching values between 4‰ and 6‰ that occur steadily in the upper part. Overall, the $\delta^{13}\text{C}$ record of the Corcal section is consistent with that of Boggiani et al. (2010), Rivera (2019), and the values agree with those of upper Ediacaran sections worldwide, such as in Northwester Canada (Macdonald et al., 2013), South China (Jiang et al., 2007; Ding et al., 2020), Namibia (Halverson et al., 2005), and Oman (Cozzi et al., 2004). In general, the $\delta^{18}\text{O}$ values in the Corcal section are relatively heavier in the upper part of the section, as well as the $\delta^{13}\text{C}$. These general increasing trends are consistent with the interpretation of a relative rise in sea level from the lower to the upper section, suggested in Section 5.1.1, since a more active carbonate factory and a higher distance from the shore might increase the $\delta^{13}\text{C}$ and the $\delta^{18}\text{O}$ values (Immenhauser et al., 2003).

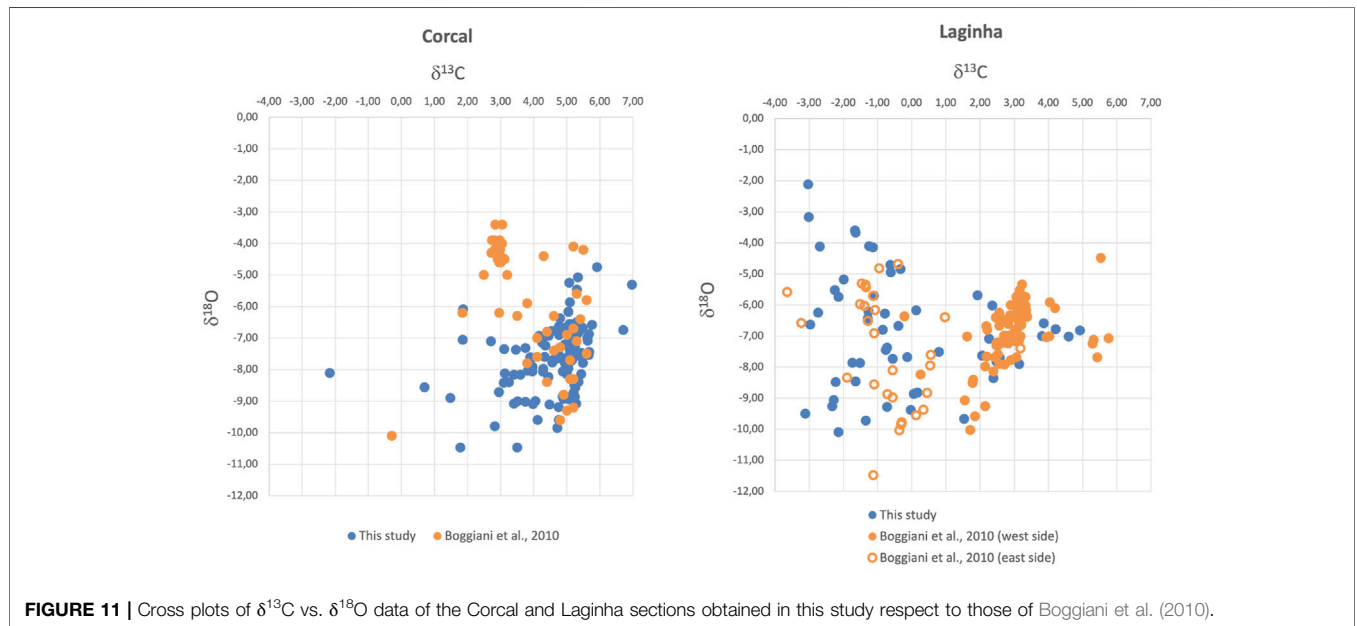
TABLE 2 | Lithofacies and facies associations of the Laginha section.

Facies association	Facies	Description	Process
Inner to mid-ramp carbonate platform	L1—Dolomitic grainstone	Meters thick tabular bed composed of massive light gray dolomitic grainstone.	Wave reworked sediment above the fair-weather wave base.
	L2—Sandstone with dolomitic matrix	Meters thick tabular bed composed of massive dark gray sandstone with dolomitic matrix. The grains are coarse sand sized, very well rounded, predominantly of quartz, with few lithoclasts.	Wave reworked sediment within the shoreface.
	L3—Peloidal packstone	~50 cm tabular bed composed of massive dark gray peloidal packstone with bird-eyes structures.	Low energy reworking in a shallow lagoon with episodic exposure.
Extensional tectonic and rapid accommodation space opening	L4—Polymictic breccia with basement clasts	Ten meters thick bed of massive polymictic breccia. The matrix is dark gray and dolomitic. Clasts range in size from sand to boulder, varying from rounded to very angular, and include limestones, dolostones, cherts, phosphorites, and granitoid rocks.	Rapid massive sediment flow onto a steep topography.
	L5—Argillaceous sandstone	Centimeters thick tabular bed composed of massive muddy sandstone, yellowish-brown when weathered, containing poorly sorted grains of quartz and lithoclast within an argillaceous matrix.	Massive siliciclastic sediment flow in deep and low energy conditions.
Inner ramp carbonate platform in a relatively steep and tectonically active setting	L6—Massive calcimudstone	Centimeters to decimeters thick tabular beds of massive gray carbonate mudstone, with sporadic extraclasts of quartz.	Settling of suspended micrite in shallow and restricted conditions with sporadic continental input.
	L7—Calcimudstone microbreccia	Centimeters thick beds of brecciated grey carbonate mudstone, with very angular clasts ranging in size from fine sand to gravel and cemented by syntaxial and eventually dog tooth calcite cement	Tectonic brecciation of micritic layers and subsequent early diagenetic cementation.
	L8—Dolomitic sparstone	Centimeters to decimetres thick tabular beds of massive to laminated, gray, crystalline dolostone, with extraclasts of quartz. Locally occurring fractures.	Sedimentation in shallow and restricted conditions with sporadic low energy currents reworking and continental input
	L9—Extraclastic wackestone	Centimeters to decimetres thick beds of light gray massive wackestone with poorly sorted quartz, mica, and phosphate grains, within a micritic matrix	Sedimentation in shallow and restricted conditions with continental input.
	L10—Intraclastic breccia	Centimeters thick weavy bed of massive breccia with poorly sorted and angular grains, with abundant extraclasts of quartz	Pulse of resedimented material with mixed (carbonate and siliciclastic) composition.
	L11—Laminated carbonate	Centimeters thick bed of gray fine crystalline, dolomitic to calcitic, carbonate laminae, alternated with poorly sorted siliciclastic laminae.	Settling of suspended micrite with pulses of siliciclastic material from the continent.
	L12—Polymictic intraclastic breccia	Meters thick lenticular bed of polymictic breccia with micritic, dark gray matrix. Clasts range in size from sand to pebble, vary in shape from rounded to angular, and include quartz, limestones, dolostones, siliciclastic mudstones, and phosphorites	Massive flow of reworked sediment from the shore, probably deposited as a local fan.
	L13—Calcimudstone with desiccation features	Centimeters to decimetres thick tabular beds composed of massive, gray, recrystallized carbonate mudstone with fenestral pores filled with spatic mosaic calcite, with local occurrence of micritization and silicified nodules.	Settling of micrite in very shallow conditions with episodes of emersion and desiccation.
Inner to mid-ramp carbonate platform	L14—Packstone	Decimeters thick bed of dark gray packstone with irregular intraclasts and <i>Cloudina</i> type bioclasts.	Transport and reworking of sediments below the fair-weather wave base.
	L15—Marl	Centimeters to decimetres thick beds with mixed siliciclastic and carbonate mud, occurring as thin layers within carbonate beds or as thick massive tabular beds.	Settling of suspended micrite and siliciclastic mud in shallow low-energy conditions.
	L16—Marly packstone	Decimeters thick bed of dark gray, massive marly intraclastic packstone, quite recrystallized,	

(Continued on following page)

TABLE 2 | (Continued) Lithofacies and facies associations of the Lágina section.

Facies asociación	Facies	Description	Process
	L17—Grainstone	with irregular intraclasts and possibly few <i>Cloudina</i> type bioclasts. Sets of decimeters thick beds of dark gray massive grainstone, mainly formed by oolites, and showing microstylolites.	Settling of suspended micrite with input of reworked carbonate grains from the surroundings. Transport and reworking of sediments above the fair-weather wave base.
Offshore siliciclastic setting	L18—Mudstone	Centimeters thick beds of laminated, beige mudstone.	Settling of siliciclastic mud in low energy conditions.

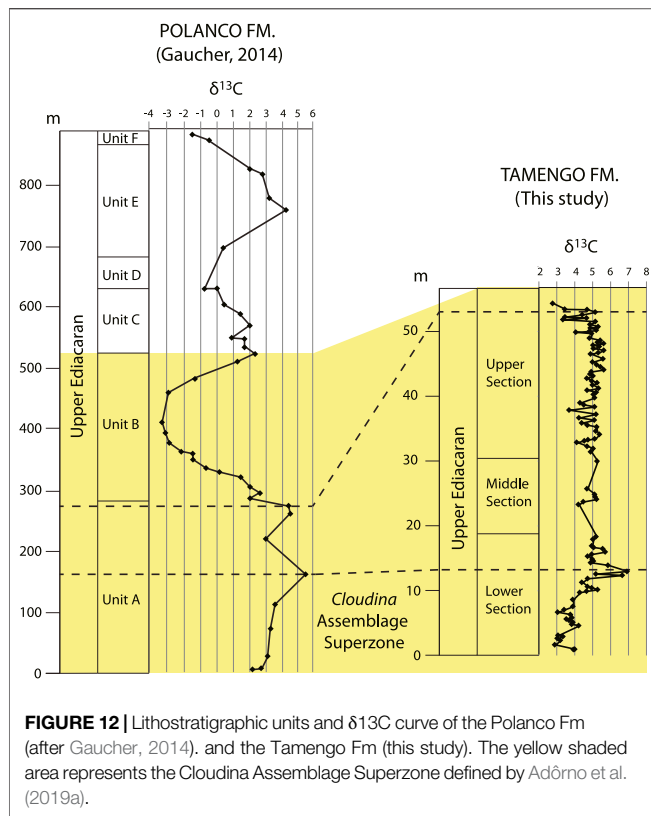
**FIGURE 11 |** Cross plots of $\delta^{13}\text{C}$ vs. $\delta^{18}\text{O}$ data of the Corcal and Lágina sections obtained in this study respect to those of Boggiani et al. (2010).

On the other hand, the Lágina section displays $\delta^{13}\text{C}$ values more variable and generally 1‰–2‰ lower than those in the Corcal, especially in the lower and middle parts. However, there is no distinct relationship between $\delta^{13}\text{C}$ and sedimentary facies, lithology, or diagenetic features. Moreover, this variability can be observed laterally, as well as vertically. Boggiani et al. (2010) measured two profiles, one on the East and one on the West side of the Lágina quarry, which yielded significantly different values, despite representing the same stratigraphic interval (Figure 12). The profile of the Lágina section in this study corresponds to the West side of Boggiani et al. (2010), however, the data overlap with both profiles (Figure 11).

The different facies and $\delta^{13}\text{C}$ values of the Tamengo Formation in the two studied sections make also difficult to correlate them precisely. This becomes even more difficult as Ediacaran guide fossils, such as *C. lucianoi* and *C. werneri*, were found only in the Corcal section, but lack in the Lágina (Adórno et al., 2017). This is due, in part, to the fact that the lower part of the Tamengo Fm. occurs only in the Lágina section, however, the upper part of this section should display $\delta^{13}\text{C}$ values that match those of the Corcal, which is not the case. The greater variability of $\delta^{13}\text{C}$ values in the Lágina section indicates a stronger influence by local environmental

or diagenetic factors in this section, respect to Corcal (Klein et al., 1999; Frank and Bernet, 2000; Spangenberg et al., 2014; Swart and Oehlert, 2018). Unraveling these factors is a complex work, which is beyond the goal of this study. However, it is important to stress that the $\delta^{13}\text{C}$ signal of the Lágina section is not representative of the general Ediacaran seawater and thus this section is not suitable for chemostratigraphic correlations. Previous studies chose the Lágina as reference section for correlation since it displays the entire Tamengo Formation, from the base to the top (Boggiani et al., 2010; Oliveira et al., 2019; Amorim et al., 2020). Our results show that the validity of these correlations must be re-assessed and that the Corcal section is a more suitable reference for stratigraphic correlation, despite not encompassing the entire unit.

The new $\delta^{13}\text{C}$ record of the Corcal section allows for enhancing the correlation of the Corumbá Group with the Arroyo del Soldado Group in Uruguay, which presumably deposited along the same continental margin (Gaucher et al., 2003). Considering the facies similarity, Gaucher et al. (2003) proposed that the Tamengo Formation could be correlated with the Polanco Formation of the Arroyo del Soldado Group. Adórno et al. (2019a) revised this correlation with a biostratigraphic



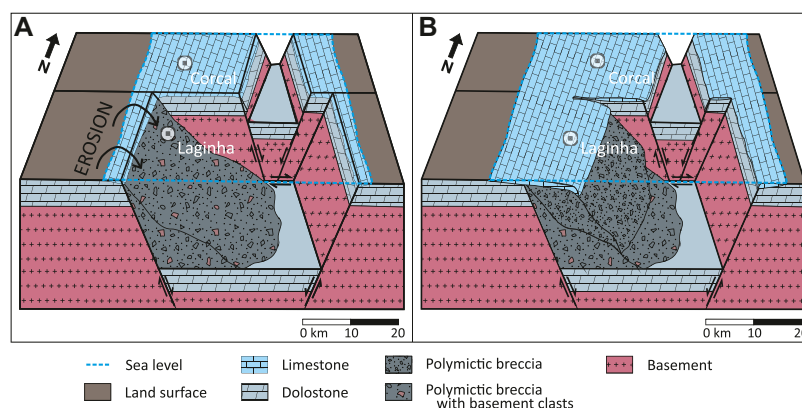
approach and showed that the Tamengo Formation is equivalent to the upper part of the Yermal Formation and the lower to middle part of the Polanco Formation. The $\delta^{13}\text{C}$ curve of the Polanco Formation shows three positive excursions, one in the lower and two in the upper part (Figure 12; Gaucher, 2014). By integrating the biostratigraphic data of Adôrno et al. (2019a) with the $\delta^{13}\text{C}$ data of Gaucher (2014) and of the Corcal section, the upper part of the Tamengo Formation turns

equivalent to the lower part of the Polanco Formation (Figure 12). According to this correlation, the upper Polanco, the Barriga Negra, and the Cerro Espulitas formations of the Arroyo del Soldado Group should be equivalent to the uppermost part of the Tamengo Formation and to the lower part of the Guaicurus Formation, suggesting that the uppermost part of the Ediacaran is very condensed in the Corumbá Group. However, it is also possible that an unconformity occurs between the Tamengo and the Guaicurus formations (Adôrno et al., 2019a; Fazio et al., 2019).

5.3 Tamengo Formation Depositional Model

Previous studies proposed that the Tamengo Formation deposited as a ramp carbonate platform onto a passive margin (Boggiani et al., 2010; Oliveira et al., 2019; Amorim et al., 2020). According to this model the Laginha section represents the shallower part of the carbonate platform, whereas the Corcal section the mid- and outer parts. The clastic lithofacies and the cross and hummocky stratification indicate an environment controlled mainly by waves and storms (Dott and Bourgeois, 1982; Seguret et al., 2001; Dumas and Arnott, 2006; Amorim et al., 2020). However, here we identified desiccation features in the lower part of the Corcal section, indicating that the environment reached also back- to inner ramp conditions (Tucker and Wright, 1990; Burchette and Wright, 1992; Tucker and Dias-Brito, 2017). Consequently, the carbonate ramp of the Tamengo Formation shifted from a back-ramp to an outer ramp setting, represented by the C2 and C8 facies, respectively (Table 1). This implies an environment more dynamic than previously thought, strongly controlled by sea level fluctuations, as well as by waves and storms.

This has also important implications for constraining the dwelling conditions of the Ediacaran organisms *C. luciano* and *C. werner*, of which fossils have been recovered in the Corcal and in the correlative Sobramil section (Adôrno et al., 2017; Walde et al., 2015; Oliveira et al., 2019; Amorim et al.,



2020). The occurrence of these fossils is strongly facies dependent, as *Cloudina* type fragments have been observed in the packstone and grainstone facies, whereas *C. weneri* occurs only in the shales. This indicates shifting ecological conditions in response to sea level variations, with *C. weneri* proliferating in a deeper environment, with lower energy and a softer and finer substrate, during transgressive phases. On the other hand, *C. luciano* became dominant in shallower and higher energy conditions, therefore with more light and nutrients availability, during high stands (Sanders and Pons, 1999; Walde et al., 2015; Oliveira et al., 2019; Amorim et al., 2020; Li et al., 2021).

The “classical” facies of the Tamengo Formation are those observed in the Corcal section, which occur also in other outcrops of the region along the Paraguay river, such as in the sections of Porto Sobramil (also known as Claudio or Saladeiro), Cacimba, Porto Figueiras, Goldfish, Ladario-Corumbá escarpment, and Horii mine (Boggiani et al., 2010; Walde et al., 2015; Adorno et al., 2019b; Oliveira et al., 2019; Rivera, 2019; Amorim et al., 2020). Alongside the same lithofacies, these sections display also consistent and rather homogenous $\delta^{13}\text{C}$ values (Boggiani et al., 2010; Rivera, 2019; Caetano Filho, 2020; and this work). These facies are different from those observed in the Laginha section, and therefore the Laginha was considered from a more proximal setting than the Corcal and other sections along the Paraguay river (Boggiani et al., 2010; Oliveira et al., 2019; Amorim et al., 2020). However, previous studies focus only on the upper part of the Tamengo Formation and do not consider the thick breccia layers in the Laginha section. In fact, as discussed in the facies interpretation, these breccias, are meters to tens of meters thick, homogeneous, and polymictic, indicating a deposition by mass sediment flows. Therefore, it was necessary a steep topography for triggering the flow and sufficient space to accommodate tens of meters of sediment at once. These conditions contrast with a shallow inner carbonate ramp. Besides, the more variable facies sequence of the Laginha section indicates a more dynamic environment, influenced by other factors alongside waves and sea level variations.

A steep topography and a rapidly opening accommodation space can be found in setting dominated by extensional tectonic (e.g., Sanders and Höfling, 2000; Eyles and Januszczak, 2007). In this context can occur also basement uplift, which provides coarse, angular, and fresh clasts such as those occurring in the lower part of the Laginha section. Warren et al. (2019) propose a model for the basin evolution of the Itapucumi Group, in Paraguay, which outcrops about 250 km to the South of Corumbá and is correlative to the Corumbá Group. According to this model, at the time of deposition of the Tamengo Fm (ca 555 to 542 Ma) the basin was in a thermal subsidence regime, during a post-rift stage, but still influenced by extensional tectonic. Therefore, the carbonate platform of the Tamengo Formation formed onto an irregular margin, with a complex topography, controlled by extensional faults (i.e., Figure 13A, Sanders and Höfling, 2000; Ding et al., 2021). In this context, the Corcal section corresponds to a more stable portion of the ramp, not significantly influenced by the tectonic. On the other hand, the Laginha section sat close to or into the margin of a graben,

with a steep topography, and next to a horst that provided the terrigenous supply. Therefore, the Corcal section was not necessarily further from the shore than the Laginha, but just laid onto a flatter and smoother topography (Figure 13A). The upper part of the Tamengo Formation consists of mid-ramp carbonate facies in both studied sections. Consequently, according to this interpretation, it can represent a period of tectonic quiescence, during which the relative sea level rose. This could have favored the progradation of the carbonate platform, which leveled the topography (e.g., Figure 13B, Tucker and Wright, 1990; Sanders and Pons, 1999; Schlager, 2005; Łabaj and Pratt, 2016).

This interpretation can explain the more variable facies and stable isotopes records of the Laginha section. A steep and tectonically active setting can be more susceptible to changes in input of continental material, local currents, and even burial fluids, which might have contributed to the dolomitization of the lower part of the section (Caetano Filho, 2020). It can also explain the absence of *C. weneri* remains in the Laginha section, as a steep topography and the input of coarse material might have precluded the installation of quite conditions and fine substrate necessary for these organisms. Therefore, the Laginha section represents an exceptional setting for the Tamengo Formation, strongly influenced by local factors both in the lithological and in the stable isotopes' records.

5.4 Implications for Ediacaran Paleoenvironments

The Tamengo Formation contains allochemical and bioclastic constituents typical of Ediacaran carbonate ramps (e.g., Sumner and Grotzinger, 1993; Narbonne et al., 1994; Walter et al., 1995; Grotzinger and James, 2000; Gaucher et al., 2003; Jiang et al., 2003b; Lindsay et al., 2005; Jiang et al., 2011; Xiao et al., 2016; Vaziri and Laflamme, 2018; Warren et al., 2019; Álvaro et al., 2020). On the other hand, the detail facies analysis presented here allows for unraveling more specific characteristics of its depositional environment.

Differently from some of the most renowned coeval carbonate successions, such as the Nama Group in Namibia, the Little Dal Group in northwestern Canada, the Buah Formation in Oman, and even the closest Bambuí Group in Brazil, the Tamengo Formation consists of totally clastic lithofacies, with no biogenic buildups (Batten et al., 2004; Cozzi et al., 2004; Grotzinger et al., 2005; Alvarenga et al., 2014; Uhlein et al., 2019). Microbial laminations have been observed only sporadically as reworked intraclasts in the breccia facies. *Cloudina* type skeletal fragments are frequent, but no specimens have been found in place. However, the abundance of micritic matrix and intraclasts indicates the presence of a developed biogenic carbonate factory. Moreover, recent evidence of microalgae, preserved in shale facies, indicate a diversified biotic assemblage (Diniz et al., 2021). Amorim et al. (2020) explain this apparent paradox suggesting that frequent storms and currents might have prevented the formation of extensive biogenic carbonate buildups, or that the shallower part, in which the carbonate producers dwelled, was not preserved. We agree that the high energy might have contributed, but consider unlikely the non-preservation of carbonate reefs and buildups, as they generally

have the higher potential of preservation (e.g., Tucker and Wright, 1990; Schlager, 2005).

The Tamengo Formation yields lithofacies like those of the Doushantuo and Dengying formations, which form an extensive, well preserved, and well-studied Ediacaran carbonate platforms system onto the Yangtze block, in South China. There, the sediments of the carbonate ramp are preserved with lateral continuity, from the inner shelf to the basin (Jiang et al., 2011; Ding et al., 2019; Ding et al., 2021). This indicates that Ediacaran carbonate platforms were heterogeneous and the presence of subtidal stromatolites, thrombolites, or even metazoan reefs is not necessarily a prerogative. Even though the availability of the outcrops in the Corumbá region is not as high as that in South China, we can infer that the Tamengo Formation was a “Doushantuo- Dengying type” carbonate platform, characterized by a productive carbonate factory, but with environmental conditions that did not allow the deposition of significant buildups with a biogenic framework. This could be due to particularly high energy, but also to temperature, salinity, or nutrients conditions (Tucker and Wright, 1990; Schlager, 2005). In the case of the Tamengo Formation, the presence of extraclasts in several layers suggest the possibility of runoff that episodically decreased the salinity and increased the trophic level of the environment. Besides, especially in the Laginha section, a steep topography might have limited the space with favorable ecological conditions for growing biogenic reefs. It is interesting to note that also the upper Ediacaran Dengying Fm. formed in a setting controlled by extensional tectonic (Ding et al., 2021).

6 CONCLUSION

In this work we present new evidence from two representative sections of the Tamengo Formation. This unit consists of carbonate and subordinate siliciclastic lithofacies, deposited onto a continental platform during the Ediacaran. The two studied sections display different lithofacies and carbonate carbon isotope values, despite belonging to the same lithostratigraphic unit. The previously proposed depositional model attributed this difference to the distance from the shoreline, considering the Laginha section more proximal than the Corcal. Here, we propose that the Laginha site was not necessarily more proximal, but characterized by a steeper topography, which provided the accommodation for the thick breccia bed in the lower part of the section. Such context could have been due to active normal faults at the time of the deposition, indicating that the platform laid on a tectonically active margin. If this were true, then the Laginha section could provide indirect evidence that the Corumbá Graben System was still active at the time of the Tamengo Formation.

We show that the Laginha section is more heterogeneous and discontinuous than the Corcal section, despite displaying both the base and the top of the Tamengo Formation. The $\delta^{13}\text{C}$ record is also more dispersed, suggesting a major influence by local and post depositional factors. On the other hand, the Corcal section yields a more continuous $\delta^{13}\text{C}$ record, with typical Ediacaran values, as well as Ediacaran guide fossils, which allow for a more accurate stratigraphic calibration. Therefore, despite not

encompassing the entire unit, the Corcal section is a more suitable reference for stratigraphic correlations.

By comparing the Tamengo Formation with other Ediacaran carbonate platforms, we observe the absence of biogenic carbonate buildups, which, instead, are common in other coeval units. The facies of the Tamengo Formation are like those of the Doushantuo and Dengying formations, in South China, suggesting that the Ediacaran carbonate platforms could have been more heterogeneous than previously thought. These differences might have been due to different ecological conditions, such as energy, temperature, salinity, or nutrients.

Our results advance in the characterization of the Ediacaran in South America, which is still at a lower level compared to other regions, and highlight the Tamengo Formation as a possible reference unit. Moreover, we show the importance of detailed petrographic and geochemical characterization, alongside facies analyses, to unravel the still enigmatic Ediacaran carbonate paleoenvironments and their significance at regional to global scale.

DATA AVAILABILITY STATEMENT

The original contributions presented in the study are included in the article/**Supplementary Material**, further inquiries can be directed to the corresponding author.

AUTHOR CONTRIBUTIONS

MR—Fieldwork, data collection and interpretation, drawing of the figures and writing of the manuscript. MG—Master supervisor of MR fieldwork, data interpretation, drawing of the figures and writing of the manuscript. DW—Fieldwork and access to the studied sites, data interpretation, review of the manuscript for the regional and stratigraphic context. DC—Access to the thin sections of the Ediacariano project and to the optical microscope laboratory, review of the paleontological and stratigraphic aspects of the manuscript. GF—Fieldwork, review of the diagenetic aspects of the manuscript. LV—Part of the stable isotopes measurements, review of the geochemical aspects of the manuscript. MD—Fieldwork, samples organization, review of the paleontological and stratigraphic aspects of the manuscript. RS—Chief of the stable isotope geochemistry laboratory, assistance with the stable isotopes measurements and data interpretation, review of the geochemical aspects of the manuscript. RA—Fieldwork, assistance with the fossils' data, review of the paleontological and stratigraphic aspects of the manuscript. LG—Bachelor student supervised by MG review of the stratigraphic correlation of the Tamengo Formation with the Arroyo del Soldado Group.

FUNDING

Main funding came from the Research Foundation of the Federal District (FAPDF)—process no. 0193.001609/2017, and the FUNDECT/CNPq/DCR—process no. 59/300.349/2016. This study was financed in part by the Coordenação de

Aperfeiçoamento de Pessoal de Nível Superior—Brasil (CAPES)—Finance Code 001. Part of the studied samples were obtained from the project “Arcabouço cronobioestratigráfico do Ediacariano do Brasil através do desenvolvimento metodológico em paleontologia – EDIACARIANO”, funded by ANP & PETROBRAS, N. PETROBRAS/FUB-IG-2012/5005.

ACKNOWLEDGMENTS

The authors thank André Pullen of the Stable Isotopes Laboratory of the University of Brasília for the technical support with stable isotope analysis; the administration and personnel of the Corcal and Votorantin that allowed the access to the Corcal and Laginha

quarries, respectively; Bernie D. Erdtmann for the helpful discussions and assistance during fieldwork; Aguinaldo Silva of the Federal University of Mato Grosso do Sul and CEPAN for the logistical support in Corumbá. We are also thankful to the associate editor MC and to four reviewers, who contributed with insightful and constructive comments.

SUPPLEMENTARY MATERIAL

The Supplementary Material for this article can be found online at: <https://www.frontiersin.org/articles/10.3389/feart.2022.749066/full#supplementary-material>

REFERENCES

- Adórno, R. R., do Carmo, D. A., Germs, G., Walde, D. H. G., Denezine, M., Boggiani, P. C., et al. (2017). *Cloudina Lucianoi* (Beurlen & Sommer, 1957), Tamengo Formation, Ediacaran, Brazil: Taxonomy, Analysis of Stratigraphic Distribution and Biostratigraphy. *Precambrian Res.* 301, 19–35. doi:10.1016/j.precamres.2017.08.023
- Adórno, R. R. (2019). Taxonomy, Paleocology and Chronobiostratigraphy across the Ediacaran-Cambrian Boundary: Tamengo and Guaicurus Formations. Doctoral thesis. Brasília: University of Brasília, 130.
- Adórno, R. R., Walde, D. H. G., Do Carmo, D. A., Denezine, M., Cortijo, I., Sanchez, E. A. M., et al. (2019a). Análisis Paleontológicos a Través Limite Ediacárico-Cámbrico, Grupo Alto Corumbá, Brasil. *Estud. Geol.* 75 (2), 094. doi:10.3989/egol.43586.549
- Adórno, R. R., Walde, D. H. G., Erdtmann, B. D., Denezine, M., Cortijo, I., Do Carmo, D. A., et al. (2019b). First Occurrence of *Cloudina* Carinata Cortijo et al., 2010 in South America, Tamengo Formation, Corumbá Group, Upper Ediacaran of Midwestern. *Estud. Geol.* 75 (2), 095. doi:10.3989/egol.43587.550
- Almeida, F. F. M. (1965). Geologia da Serra da Bodoquena (Mato Grosso), Brasil. *Bol. Geol. Mineral. DNPM* 219, 1–96.
- Almeida, F. F. M. (1964). Geologia Do Sudoeste Mato-Grossense. *Bol. Div. Geol. Mineral. DNPM* 116, 1–18.
- Almeida, F. F. M. (1984). “Província Tocantins, Setor Sudoeste,” in *O Pré-Cambriano Do Brasil*. Editors F.F.M. de Almeida and Y. Hasui (São Paulo: Edgard Blücher), 265–281.
- Alvarenga, C. J., Boggiani, P. C., Babinski, M., Dardenne, M. A., Figueiredo, M. F., Dantas, E. L., et al. (2011). *Glacially Influenced Sedimentation of the Puga Formation, Cuiabá Group and Jacadigo Group, and Associated Carbonates of the Araras and Corumbá Groups, Paraguay Belt, Brazil*. London, Memoirs: Geological Society 36 (1), 487–497. doi:10.1144/M36.45
- Alvarenga, C. J. S., Santos, R. V., Vieira, L. C., Lima, B. A. F., and Mancini, L. H. (2014). Meso-Neoproterozoic Isotope Stratigraphy on Carbonates Platforms in the Brasília Belt of Brazil. *Precambrian Res.* 251, 164–180. doi:10.1016/j.precamres.2014.06.011
- Álvoro, J. J., Cortijo, I., Jensen, S., Mus, M. M., and Palacios, T. (2020). *Cloudina*-Microbial Reef Resilience to Substrate Instability in a Cadomian Retro-Arc Basin of the Iberian Peninsula. *Precambrian Res.* 336, 105479. doi:10.1016/j.precamres.2019.105479
- Amorim, K. B., Afonso, J. W. L., Leme, J. d. M., Diniz, C. Q. C., Rivera, L. C. M., Gómez-Gutiérrez, J. C., et al. (2020). Sedimentary Facies, Fossil Distribution and Depositional Setting of the Late Ediacaran Tamengo Formation (Brazil). *Sedimentology* 67 (7), 3422–3450. doi:10.1111/sed.12749
- Audemard, F. A. M., and Michetti, A. M. (2011). Geological Criteria for Evaluating Seismicity Revisited: Forty Years of Paleoseismic Investigations and the Natural Record of Past Earthquakes. *Geol. Soc. Am. Special Pap.* 479, 1–21. doi:10.1130/2011.2479(00)
- Babinski, M., Boggiani, P. C., Fanning, M., Simon, C. M., and Sial, A. N. (2008). “U–Pb Shrimp Geochronology and Isotope Chemostratigraphy (C, O, Sr) of the Tamengo Formation, Southern Paraguay Belt,” in 6th South American Symposium on Isotope Geology San Carlos de Bariloche, San Carlos de Bariloche, 2008 160.
- Babinski, M., Boggiani, P. C., Trindade, R. I. F., and Fanning, C. M. (2013). Detrital Zircon Ages and Geochronological Constraints on the Neoproterozoic Puga Diamictites and Associated BIFs in the Southern Paraguay Belt, Brazil. *Gondwana Res.* 23, 988–997. doi:10.1016/j.gr.2012.06.011
- Basilone, L., Sulli, A., and Gasparo Morticelli, M. (2016). The Relationships Between Soft-Sediment Deformation Structures and Syndimentary Extensional Tectonics in Upper Triassic Deep-Water Carbonate Succession (Southern Tethyan Rifted Continental Margin - Central Sicily). *Sediment. Geol.* 344, 310–322. doi:10.1016/j.sedgeo.2016.01.010
- Batten, K. L., Narbonne, G. M., and James, N. P. (2004). Paleoenvironments and Growth of Early Neoproterozoic Calcimicrobial Reefs: Platform Little Dal Group, Northwestern Canada. *Precambrian Res.* 133 (3–4), 249–269. doi:10.1016/j.precamres.2004.05.003
- Becker-Kerber, B., Pacheco, M. L. A. F., Rudnitzki, I. D., Galante, D., Rodrigues, F., and Leme, J. d. M. (2017). Ecological Interactions in *Cloudina* from the Ediacaran of Brazil: Implications for the Rise of Animal Biomineralization. *Sci. Rep.* 7, 5482. doi:10.1038/s41598-017-05753-8
- Beurlen, K., and Sommer, F. W. (1957). Observações estratigráficas e paleontológicas sobre o calcário de Corumbá. *Bol. Geol. Mineral.-DNPM* 168, 1–35.
- Boggiani, P. C., and Alvarenga, C. J. S. (2004). “Faixa Paraguai,” in *Geologia do Continente Sul-Americano: Evolução da Obra de Fernando Flávio Marques de Almeida*. Editors V. Mantesso-Neto, A. Bartorelli, C.D.R. Carneiro, and B.B.B. Neves (São Paulo: Beca Produções Culturais Ltda), 113–120.
- Boggiani, P. C. (1998). Análise Estratigráfica da Bacia Corumbá (Neoproterozoico) – Mato Grosso do Sul. Ph.D. Thesis. Brasil: Universidade de São Paulo, 1–181.
- Boggiani, P. C., Fairchild, T. R., and Coimbra, A. M. (1993). O Grupo Corumbá (Neoproterozoico-Cambriano) Na Região Central Da Serra Da Bodoquena (Faixa Paraguai), Mato Grosso Do Sul. *Rbg* 23, 301–305. doi:10.25249/0375-7536.1993233301305
- Boggiani, P. C., Gaucher, C., Sial, A. N., Babinski, M., Simon, C. M., Riccomini, C., et al. (2010). Chemostratigraphy of the Tamengo Formation (Corumbá Group, Brazil): A Contribution to the Calibration of the Ediacaran Carbon-Isotope Curve. *Precambrian Res.* 182, 382–401. doi:10.1016/j.precamres.2010.06.003
- Bristow, T. F., and Kennedy, M. J. (2008). Carbon Isotope Excursions and the Oxidant Budget of the Ediacaran Atmosphere and Ocean. *Geol.* 36 (11), 863–866. doi:10.1130/g24968a.1
- Burchette, T. P., and Wright, V. P. (1992). Carbonate Ramp Depositional Systems. *Sediment. Geol.* 79, 3–57. doi:10.1016/0037-0738(92)90003-a
- Caetano Filho, S. (2020). Carbon and Sulfur Biogeochemical Cycles in the Brazilian Ediacaran Record. Doctoral dissertation. São Paulo: Universidade de São Paulo, 629.
- Campanha, G. A. d. C., Boggiani, P. C., Sallun Filho, W., Sá, F. R. d., Zuquim, M. d. P. S., and Piacentini, T. (2011). A faixa de dobramento Paraguai na Serra da Bodoquena e depressão Do Rio Miranda, Mato Grosso Do Sul. *Geol. Usp. Sér. Cient.* 11, 79–96. doi:10.5327/z1519-874x2011000300005

- Canfield, D. E., Poulton, S. W., and Narbonne, G. M. (2007). Late-Neoproterozoic Deep-Ocean Oxygenation and the Rise of Animal Life. *Science* 315 (5808), 92–95. doi:10.1126/science.1135013
- Chen, Z.-Q., Tu, C., Pei, Y., Ogg, J., Fang, Y., Wu, S., et al. (2019). Biosedimentological Features of Major Microbe-Metazoan Transitions (MMTs) from Precambrian to Cenozoic. *Earth-Science Rev.* 189, 21–50. doi:10.1016/j.earscirev.2019.01.015
- Cozzi, A., Grotzinger, J. P., and Allen, P. A. (2004). Evolution of a Terminal Neoproterozoic Carbonate Ramp System (Buah Formation, Sultanate of Oman): Effects of Basement Paleotopography. *Geol. Soc. Am. Bull.* 116 (11–12), 1367–1384. doi:10.1130/b25387.1
- Crockford, P. W., Cowie, B. R., Johnston, D. T., Hoffman, P. F., Sugiyama, I., Pellerin, A., et al. (2016). Triple Oxygen and Multiple Sulfur Isotope Constraints on the Evolution of the Post-Marinoan Sulfur Cycle. *Earth Planet. Sci. Lett.* 435, 74–83. doi:10.1016/j.epsl.2015.12.017
- Cui, H., Kaufman, A. J., Peng, Y., Liu, X.-M., Plummer, R. E., and Lee, E. I. (2018). The Neoproterozoic Hüttenberg $\delta^{13}\text{C}$ Anomaly: Genesis and Global Implications. *Precambrian Res.* 313, 242–262. doi:10.1016/j.precamres.2018.05.024
- Cui, H., Kitajima, K., Orland, I. J., Xiao, S., Baele, J.-M., Kaufman, A. J., et al. (2021). Deposition or Diagenesis? Probing the Ediacaran Shuram Excursion in South China by SIMS. *Glob. Planet. Change* 206, 103591. doi:10.1016/j.gloplacha.2021.103591
- D'el-Rey Silva, L. J. H., Walde, D. H.-G., and Saldanha, D. O. (2016). The Neoproterozoic-Cambrian Paraguay Belt, Central Brazil: Part I - New Structural Data and a New Approach on the Regional Implications. *Tectonophysics* 676, 20–41. doi:10.1016/j.tecto.2016.03.019
- De Alvarenga, C. J. S., Boggiani, P. C., Babinski, M., Dardenne, M. A., Figueiredo, M., Santos, R. V., et al. (2009). "Chapter 2 the Amazonian Palaeocontinent," in *Neoproterozoic-Cambrian Tectonics, Global Changes and Evolution: A Focus on Southwestern Gondwana*. Editors C. Gaucher, A.N. Sial, H. Frimmel, and G.P. Halverson (Amsterdam: Elsevier), 15–28. doi:10.1016/s0166-2635(09)01602-8
- de Alvarenga, C. J. S., and Trompette, R. (1992). Glacially Influenced Sedimentation in the Later Proterozoic of the Paraguay Belt (Mato Grosso, Brazil). *Palaeogeogr. Palaeoclimatol. Palaeoecol.* 92, 85–105. doi:10.1016/0031-0182(92)90136-s
- Delgado, F. (1977). Primary Textures in Dolostones and Recrystallized Limestones: a Technique for Their Microscopy Study. *J. Sediment. Petrology* 47, 1339–1341.
- Delpomdor, F., Eyles, N., Tack, L., and Pr  at, A. (2016). Pre- and Post-Marinoan Carbonate Facies of the Democratic Republic of the Congo: Glacially- or Tectonically-Influenced Deep-Water Sediments? *Palaeogeogr. Palaeoclimatol. Palaeoecol.* 457, 144–157. doi:10.1016/j.palaeo.2016.06.014
- Derry, L. A. (2010). A Burial Diagenesis Origin for the Ediacaran Shuram-Wonoka Carbon Isotope Anomaly. *Earth Planet. Sci. Lett.* 294, 152–162. doi:10.1016/j.epsl.2010.03.022
- Ding, Y., Chen, D., Zhou, X., Guo, C., Huang, T., and Zhang, G. (2019). Tectono-Depositional Pattern and Evolution of the Middle Yangtze Platform (South China) During the Late Ediacaran. *Precambrian Res.* 333, 105426. doi:10.1016/j.precamres.2019.105426
- Ding, Y., Chen, D., Zhou, X., Huang, T., Guo, C., and Yeasmin, R. (2020). Paired $\delta^{13}\text{C}_{\text{carb}}\text{-}\delta^{13}\text{C}_{\text{org}}$ Evolution of the Dengying Formation from Northeastern Guizhou and Implications for Stratigraphic Correlation and the Late Ediacaran Carbon Cycle. *J. Earth Sci.* 31 (2), 342–353. doi:10.1007/s12583-018-0886-1
- Ding, Y., Li, Z., Liu, S., Song, J., Zhou, X., Sun, W., et al. (2021). Sequence Stratigraphy and Tectono-Depositional Evolution of a Late Ediacaran Epeiric Platform in the Upper Yangtze Area, South China. *Precambrian Res.* 354, 106077. doi:10.1016/j.precamres.2020.106077
- Diniz, C., Leme, J., and Boggiani, P. C. (2021). New Species of Macroalgae from Tamengo Formation, Ediacaran, Brazil. *Front. Earth Sci.* 9, 884. doi:10.3389/feart.2021.748876
- Dott, R. H., Jr, and Bourgeois, J. (1982). Hummocky Stratification: Significance of its Variable Bedding Sequences. *Geol. Soc. Am. Bull.* 93 (8), 663–680. doi:10.1130/0016-7606(1982)93<663:hssoiv>2.0.co;2
- Dumas, S., and Arnott, R. W. C. (2006). Origin of Hummocky and Swaley Cross-Stratification- the Controlling Influence of Unidirectional Current Strength and Aggradation Rate. *Geol.* 34 (12), 1073–1076. doi:10.1130/g22930a.1
- Elie, M., Nogueira, A. C. R., N  delec, A., Trindade, R. I. F., and Kenig, F. (2007). A Red Algal Bloom in the Aftermath of the Marinoan Snowball Earth. *Terra nova.* 19 (5), 303–308. doi:10.1111/j.1365-3121.2007.00754.x
- Eyles, N., and Januszczak, N. (2007). Syntectonic Subaqueous Mass Flows of the Neoproterozoic Otavi Group, Namibia: Where Is the Evidence of Global Glaciation? *Basin Res.* 19 (2), 179–198. doi:10.1111/j.1365-2117.2007.00319.x
- Fairchild, T. R. (1978). "Evid  ncias paleontol  gicas de uma poss  vel idade Ediacariana ou Cambriana Inferior, para a parte leste Do Grupo Corumb   (Mato Grosso Do Sul)," in *30   Congresso Brasileiro de Geologia, Recife, 1978*, 181. Resumo das Comunica  es.
- Fazio, G., Guimar  es, E. M., Walde, D. W. G., Do Carmo, D. A., Adorno, R. R., Vieira, L. C., et al. (2019). Mineralogical and Chemical Composition of Ediacaran-Cambrian Pelitic Rocks of the Tamengo and Guaicurus Formations, (Corumb   Group - MS, Brazil): Stratigraphic Positioning and Paleoenvironmental Interpretations. *J. S. Am. Earth Sci.* 90, 487–503. doi:10.1016/j.jsames.2018.11.025
- Fernandes, H. A., and Boggiani, P. C. (2021). "Brecha polim  tica basal da Forma  o Tamengo (Grupo Corumb  ): Sedimentologia, proveni  ncia e correla  o com outras unidades ediacaranas," in *Anais 50 CBG-Congresso Brasileiro de Geologia, 2020, June 28–30, 2021*, 1.
- Fike, D. A., Grotzinger, J. P., Pratt, L. M., and Summons, R. E. (2006). Oxidation of the Ediacaran Ocean. *Nature* 444, 744–747. doi:10.1038/nature05345
- Fl  gel, E. (2004). *Microfacies of Carbonate Rocks: Analysis, Interpretation and Application*. Germany: Springer-Verlag Berlin Heidelberg, 976.
- Fontanela, G. T. (2012). Dolomitiza  o e Fosfog  nese na Forma  o Bocaina, Grupo Corumb   (Ediacarano). Disserta  o (Mestrado). S  o Paulo: Instituto de Geoci  ncias, Universidade de S  o Paulo, 148.
- Frank, T. D., and Bernert, K. (2000). Isotopic Signature of Burial Diagenesis and Primary Lithological Contrasts in Periplatform Carbonates (Miocene, Great Bahama Bank). *Sedimentology* 47 (6), 1119–1134. doi:10.1046/j.1365-3091.2000.00344.x
- Frimmel, H. E. (2010). On the Reliability of Stable Carbon Isotopes for Neoproterozoic Chemostratigraphic Correlation. *Precambrian Res.* 182 (4), 239–253. doi:10.1016/j.precamres.2010.01.003
- Gan, T., Luo, T., Pang, K., Zhou, C., Zhou, G., Wan, B., et al. (2021). Cryptic Terrestrial Fungus-Like Fossils of the Early Ediacaran Period. *Nat. Commun.* 12 (1), 1–12. doi:10.1038/s41467-021-20975-1
- Gaucher, C., Boggiani, P. C., Sprechmann, P., Sial, A. N., and Fairchild, T. R. (2003). Integrated correlation of the Vendian to Cambrian Arroyo del Soldado and Corumb   Groups (Uruguay and Brazil): Palaeogeographic, Palaeoclimatic and Palaeobiologic Implications. *Precambrian Res.* 120, 241–278. doi:10.1016/s0301-9268(02)00140-7
- Gaucher, C. (2014). Grupo Arroyo del Soldado. *Geol. del Urug.* 1 (16), 313–339.
- Gernon, T. M., Hincks, T. K., Tyrrell, T., Rohling, E. J., and Palmer, M. R. (2016). Snowball Earth Ocean Chemistry Driven by Extensive Ridge Volcanism During Rodinia Breakup. *Nat. Geosci.* 9, 242–248. doi:10.1038/ngeo2632
- Gorjan, P., Veevers, J. J., and Walter, M. R. (2000). Neoproterozoic Sulfur-Isotope Variation in Australia and Global Implications. *Precambrian Res.* 100 (1–3), 151–179. doi:10.1016/s0301-9268(99)00073-x
- Grant, V. J. (1990). Maternal Personality and Sex of Infant. *Am. J. Sci.* 63, 261–266. doi:10.1111/j.2044-8341.1990.tb01618.x
- Grotzinger, J., Adams, E. W., and Schr  der, S. (2005). Microbial-Metazoan Reefs of the Terminal Proterozoic Nama Group (C. 550–543 Ma), Namibia. *Geol. Mag.* 142 (5), 499–517. doi:10.1017/s0016756805000907
- Grotzinger, J. P., Fike, D. A., and Fischer, W. W. (2011). Enigmatic Origin of the Largest-Known Carbon Isotope Excursion in Earth's History. *Nat. Geosci.* 4, 285–292. doi:10.1038/ngeo1138
- Grotzinger, J. P., and James, N. P. (2000). "Precambrian Carbonates: Evolution of Understanding," in *Carbonate Sedimentation and Diagenesis in the Evolving Precambrian World* (Tulsa, OK: SEPM Special Publication), 67. doi:10.2110/pec.00.67.0003
- Grotzinger, J. P., and Knoll, A. H. (1995). Anomalous Carbonate Precipitates: Is the Precambrian the Key to the Permian? *Palaio* 10, 578–596. doi:10.2307/3515096
- Hahn, G., Hahn, R., Leonardos, O. H., Pflug, H. D., and Walde, D. H. G. (1982). Korperlich Erhaltene Scyphozoen-Reste aus dem Jungpr  kambrium Brasiliens. *Geol. Palaeontol.* 16, 1–18.
- Halverson, G. P., Hoffman, P. F., Schrag, D. P., Maloof, A. C., and Rice, A. H. N. (2005). Toward a Neoproterozoic Composite Carbon-Isotope Record. *Geol. Soc. Am. Bull.* 117, 1181–1207. doi:10.1130/b25630.1
- Halverson, G. P., and Hurtgen, M. T. (2007). Ediacaran Growth of the Marine Sulfate Reservoir. *Earth Planet. Sci. Lett.* 263 (1–2), 32–44. doi:10.1016/j.epsl.2007.08.022

- Halverson, G. P., Wade, B. P., Hurtgen, M. T., and Barovich, K. M. (2010). Neoproterozoic Chemostratigraphy. *Precambrian Res.* 182, 337–350. doi:10.1016/j.precamres.2010.04.007
- Harper, B. B., Puga-Bernabéu, Á., Droxler, A. W., Webster, J. M., Gischler, E., Tiwari, M., et al. (2015). Mixed Carbonate-Siliciclastic Sedimentation Along the Great Barrier Reef Upper Slope: A Challenge to the Reciprocal Sedimentation Model. *J. Sediment. Res.* 85 (9), 1019–1036. doi:10.2110/jsr.2015.58.1
- Hidalgo, R. L. L. (2002). Análise micropaleontológica das formações Tamengo e Guaiacurus, Grupo Corumbá (MS), e Formação Araras (MT), transição do Neoproterozóico-Fanerozóico. Dissertação (Mestrado). São Paulo: Instituto de Geociências, Universidade de São Paulo.
- Hoffman, P. F., Kaufman, A. J., Halverson, G. P., and Schrag, D. P. (1998). A Neoproterozoic Snowball Earth. *Science* 281, 1342–1346. doi:10.1126/science.281.5381.1342
- Hohl, S. V., Becker, H., Herzlieb, S., and Guo, Q. (2015). Multiproxy Constraints on Alteration and Primary Compositions of Ediacaran Deep-Water Carbonate Rocks, Yangtze Platform, South China. *Geochimica Cosmochimica Acta* 163, 262–278. doi:10.1016/j.gca.2015.04.037
- Hu, Y., Cai, C., Liu, D., Pederson, C. L., Jiang, L., Shen, A., et al. (2020). Formation, Diagenesis and Palaeoenvironmental Significance of Upper Ediacaran Fibrous Dolomite Cements. *Sedimentology* 67 (2), 1161–1187. doi:10.1111/sed.12683
- Hurtgen, M. T., Arthur, M. A., and Halverson, G. P. (2005). Neoproterozoic Sulfur Isotopes, the Evolution of Microbial Sulfur Species, and the Burial Efficiency of Sulfide as Sedimentary Pyrite. *Geol.* 33 (1), 41–44. doi:10.1130/g20923.1
- Husson, J. M., Linzmeier, B. J., Kitajima, K., Ishida, A., Maloof, A. C., Schoene, B., et al. (2020). Large Isotopic Variability at the Micron-Scale in ‘Shuram’ Excursion Carbonates from South Australia. *Earth Planet. Sci. Lett.* 538, 116211. doi:10.1016/j.epsl.2020.116211
- Immenhauser, A., Della Porta, G., Kenter, J. A. M., and Bahamonde, J. R. (2003). An Alternative Model for Positive Shifts in Shallow-Marine Carbonate $\delta^{13}\text{C}$ and $\delta^{18}\text{O}$. *Sedimentology* 50 (5), 953–959. doi:10.1046/j.1365-3091.2003.00590.x
- Jiang, G., Christie-Blick, N., Kaufman, A. J., Banerjee, D. M., and Rai, V. (2003b). Carbonate Platform Growth and Cyclicity at a Terminal Proterozoic Passive Margin, Infra Krol Formation and Krol Group, Lesser Himalaya, India. *Sedimentology* 50 (5), 921–952. doi:10.1046/j.1365-3091.2003.00589.x
- Jiang, G., Kaufman, A. J., Christie-Blick, N., Zhang, S., and Wu, H. (2007). Carbon Isotope Variability Across the Ediacaran Yangtze Platform in South China: Implications for a Large Surface-To-Deep Ocean $\delta^{13}\text{C}$ Gradient. *Earth Planet. Sci. Lett.* 261 (1–2), 303–320. doi:10.1016/j.epsl.2007.07.009
- Jiang, G., Kennedy, M. J., and Christie-Blick, N. (2003a). Stable Isotopic Evidence for Methane Seeps in Neoproterozoic Postglacial Cap Carbonates. *Nature* 426 (6968), 822–826. doi:10.1038/nature02201
- Jiang, G., Shi, X., Zhang, S., Wang, Y., and Xiao, S. (2011). Stratigraphy and Paleogeography of the Ediacaran Doushantuo Formation (Ca. 635–551Ma) in South China. *Gondwana Res.* 19 (4), 831–849. doi:10.1016/j.gr.2011.01.006
- Johnston, D. T., Macdonald, F. A., Gill, B. C., Hoffman, P. F., and Schrag, D. P. (2012). Uncovering the Neoproterozoic Carbon Cycle. *Nature* 483 (7389), 320–323. doi:10.1038/nature10854
- Jones, J. P. (1985). The Southern Border of the Guaporé Shield in Western Brazil and Bolivia: An Interpretation of its Geologic Evolution. *Precambrian Res.* 28, 111–135. doi:10.1016/0301-9268(85)90076-2
- Kaufman, A. J. (2018). “The Ediacaran-Cambrian Transition: A Resource-Based Hypothesis for the Rise and Fall of the Ediacara Biota,” in *Chemostratigraphy Across Major Chronological Boundaries*. Editors A. N. Sial, C. Gaucher, M. Ramkumar, and V. Pinto Ferreira. First Edition, 115–142. *Geophysical Monograph* 240 (Washington, DC: John Wiley & Sons, Inc.). doi:10.1002/9781119382508.ch7
- Kaufman, A., and Knoll, A. (1995). Neoproterozoic Variations in the C-Isotopic Composition of Seawater: Stratigraphic and Biogeochemical Implications. *Precambrian Res.* 73, 27–49. doi:10.1016/0301-9268(94)00070-8
- Kennedy, M., Mrofka, D., and Von Der Borch, C. (2008). Snowball Earth Termination by Destabilization of Equatorial Permafrost Methane Clathrate. *Nature* 453 (7195), 642–645. doi:10.1038/nature06961
- Kerber, B. B., Rosa, A. L. Z. d., Gabas, S. G., Leme, J. d. M., and Pacheco, M. L. A. F. (2013). O registro fóssilífero de metazoários ediacaranos na América Do Sul e suas implicações nos estudos sobre origem e complexificação da vida animal. *Geol. Usp. Sér. Cient.* 13 (3), 51–64. doi:10.5327/z1519-874x201300030006
- Klein, J. S., Mozley, P., Campbell, A. R., and Cole, R. (1999). Spatial Distribution of Carbon and Oxygen Isotopes in Laterally Extensive Carbonate-Cemented Layers; Implications for Mode of Growth and Subsurface Identification. *J. Sediment. Res.* 69 (1), 184–201. doi:10.2110/jsr.69.184
- Knoll, A. H., and Carroll, S. B. (1999). Early Animal Evolution: Emerging Views from Comparative Biology and Geology. *Science* 284, 2129–2137. doi:10.1126/science.284.5423.2129
- Laakso, T. A., Sperling, E. A., Johnston, D. T., and Knoll, A. H. (2020). Ediacaran Reorganization of the Marine Phosphorus Cycle. *Proc. Natl. Acad. Sci. U.S.A.* 117 (22), 11961–11967. doi:10.1073/pnas.1916738117
- Łabaj, M. A., and Pratt, B. R. (2016). Depositional Dynamics in A Mixed Carbonate-Siliciclastic System: Middle-Upper Cambrian Abrigo Formation, Southeastern Arizona, U.S.A. *J. Sediment. Res.* 86 (1), 11–37. doi:10.2110/jsr.2015.96
- Laschet, C. (1984). On the Origin of Cherts. *Facies* 10, 257–289. doi:10.1007/bf02536693
- Le Heron, D. P., and Craig, J. (2012). Neoproterozoic Deglacial Sediments and Their Hydrocarbon Source Rock Potential. *Geol. Soc. Lond. Spec. Publ.* 368 (1), 381–393. doi:10.1144/sp368.16
- Lenton, T. M., Boyle, R. A., Poulton, S. W., Shields-Zhou, G. A., and Butterfield, N. J. (2014). Co-Evolution of Eukaryotes and Ocean Oxygenation in the Neoproterozoic Era. *Nat. Geosci.* 7 (4), 257–265. doi:10.1038/ngeo2108
- Li, H., Li, F., Li, X., Zeng, K., Gong, Q., Yi, C., et al. (2021). Development and Collapse of the Early Cambrian Shallow-Water Carbonate Factories in the Hannan-Micangshan Area, South China. *Palaeogeogr. Palaeoclimatol. Palaeoecol.* 583, 110665. doi:10.1016/j.palaeo.2021.110665
- Li, Z.-X., Evans, D. A. D., and Halverson, G. P. (2013). Neoproterozoic Glaciations in a Revised Global Palaeogeography from the Breakup of Rodinia to the Assembly of Gondwanaland. *Sediment. Geol.* 294, 219–232. doi:10.1016/j.sedgeo.2013.05.016
- Lindsay, J. F., Kruse, P. D., Green, O. R., Hawkins, E., Brasier, M. D., Cartlidge, J., et al. (2005). The Neoproterozoic–Cambrian Record in Australia: A Stable Isotope Study. *Precambrian Res.* 143 (1–4), 113–133. doi:10.1016/j.precamres.2005.10.002
- Lloyd, S. J., Marenco, P. J., Hagadorn, J. W., Lyons, T. W., Kaufman, A. J., Sour-Tovar, F., et al. (2012). Sustained Low Marine Sulfate Concentrations from the Neoproterozoic to the Cambrian: Insights from Carbonates of Northwestern Mexico and Eastern California. *Earth Planet. Sci. Lett.* 339–340, 79–94. doi:10.1016/j.epsl.2012.05.032
- Macdonald, F. A., Strauss, J. V., Sperling, E. A., Halverson, G. P., Narbonne, G. M., Johnston, D. T., et al. (2013). The Stratigraphic Relationship Between the Shuram Carbon Isotope Excursion, the Oxygenation of Neoproterozoic Oceans, and the First Appearance of the Ediacara Biota and Bilaterian Trace Fossils in Northwestern Canada. *Chem. Geol.* 362, 250–272. doi:10.1016/j.chemgeo.2013.05.032
- Meira, F. V. E. (2011). Caracterização tafonômica e estratigráfica de *Cloudina lucianoi* (Beurlen e Sommer, 1957) Zaine e Fairchild, 1985, no Grupo Corumbá, Ediacarano do Brasil. Dissertação (Mestrado). São Paulo: Instituto de Geociências, Universidade de São Paulo.
- Narbonne, G. M., Kaufman, A. J., and Knoll, A. H. (1994). Integrated Chemostratigraphy and Biostratigraphy of the Windermere Supergroup, Northwestern Canada: Implications for Neoproterozoic Correlations and the Early Evolution of Animals. *Geol. Soc. Am. Bull.* 106 (10), 1281–1292. doi:10.1130/0016-7606(1994)106<1281:icabot>2.3.co;2
- Narbonne, G. M., Xiao, S., Shields, G. A., and Gehling, J. G. (2012). The Ediacaran Period. *Geol. Time Scale* 1, 413–435. doi:10.1016/b978-0-444-59425-9.00018-4
- Nichols, G. (2009). *Sedimentology and Stratigraphy*. Oxford: John Wiley & Sons.
- Och, L. M., and Shields-Zhou, G. A. (2012). The Neoproterozoic Oxygenation Event: Environmental Perturbations and Biogeochemical Cycling. *Earth-Science Rev.* 110, 26–57. doi:10.1016/j.earscirev.2011.09.004
- Oliveira, R. S. (2010). Depósitos de rampa carbonática Ediacarana do Grupo Corumbá, região de Corumbá, Mato Grosso do Sul. Dissertação (Mestrado). Belém: Instituto de Geociências, Universidade Federal do Pará.
- Oliveira, R. S. d., Nogueira, A. C. R., Romero, G. R., Truckenbrodt, W., and da Silva Bandeira, J. C. (2019). Ediacaran Ramp Depositional Model of the Tamengo Formation, Brazil. *J. S. Am. Earth Sci.* 96, 102348. doi:10.1016/j.jsames.2019.102348

- Parry, L. A., Boggiani, P. C., Condon, D. J., Garwood, R. J., Leme, J. d. M., McIlroy, D., et al. (2017). Ichnological Evidence for Meiofaunal Bilaterians from the Terminal Ediacaran and Earliest Cambrian of Brazil. *Nat. Ecol. Evol.* 1, 1455–1464. doi:10.1038/s41559-017-0301-9
- Penny, A. M., Wood, R., Curtis, A., Bowyer, F., Tostevin, R., and Hoffman, K.-H. (2014). Ediacaran Metazoan Reefs from the Nama Group, Namibia. *Science* 344, 1504–1506. doi:10.1126/science.1253393
- Piacentini, T., Vasconcelos, P. M., and Farley, K. A. (2013). $^{40}\text{Ar}/^{39}\text{Ar}$ Constraints on the Age and Thermal History of the Urucum Neoproterozoic Banded Iron-Formation, Brazil. *Precambrian Res.* 228, 48–62. doi:10.1016/j.precamres.2013.01.002
- Ramos, M. E. A. F., Giorgioni, M., do Carmo, D. A., Walde, D. H. G., Guimarães, E. M., Fazio, G., et al. (2019). Chemostratigraphic and Facies Characterization of Ediacaran Platform Carbonates (Tamengo Formation, Corumbá Group): Preliminary Results. *Estudios Geológicos* 75 (2), e111. doi:10.3989/egcol.43589.566
- Riding, R., and Virgone, A. (2020). Hybrid Carbonates: *In Situ* Abiotic, Microbial and Skeletal Co-Precipitates. *Earth-Science Rev.* 208, 103300. doi:10.1016/j.earscirev.2020.103300
- Ries, J. B., Fike, D. A., Pratt, L. M., Lyons, T. W., and Grotzinger, J. P. (2009). Superheavy Pyrite ($\delta 34\text{S}_{\text{pyr}} > \delta 34\text{S}_{\text{CAS}}$) in the Terminal Proterozoic Nama Group, Southern Namibia: A Consequence of Low Seawater Sulfate at the Dawn of Animal Life. *Geology* 37 (8), 743–746. doi:10.1130/g25775a.1
- Rivera, L. C. M. (2019). C and O Isotopes of the Middle and Upper Tamengo Formation (Corumbá Group-Upper Ediacaran): Effects of the Sedimentary Facies and Diagenesis. Master dissertation. Universidade de São Paulo, 824.
- Sanders, D., and Höfling, R. (2000). Carbonate Deposition in Mixed Siliciclastic–Carbonate Environments on Top of an Orogenic Wedge (Late Cretaceous, Northern Calcareous Alps, Austria). *Sediment. Geol.* 137 (3–4), 127–146. doi:10.1016/s0037-0738(00)00084-1
- Sanders, D., and Pons, J. M. (1999). Rudist Formations in Mixed Siliciclastic–Carbonate Depositional Environments, Upper Cretaceous, Austria: Stratigraphy, Sedimentology, and Models of Development. *Palaeogeogr. Palaeoclimatol. Palaeoecol.* 148 (4), 249–284. doi:10.1016/s0031-0182(98)00186-2
- Schlager, W. (2005). *Carbonate Sedimentology and Sequence Stratigraphy* (No. 8). Tulsa, OK: SEPM Society for Sedimentary Geology.
- Seguret, M., Moussine-Pouchkine, A., Gabaglia, G. R., and Bouchette, F. (2001). Storm Deposits and Storm-Generated Coarse Carbonate Breccias on a Pelagic Outer Shelf (South-East Basin, France). *Sedimentology* 48 (2), 231–254. doi:10.1046/j.1365-3091.2001.00358.x
- Shields, G. A., Mills, B. J. W., Zhu, M., Raub, T. D., Daines, S. J., and Lenton, T. M. (2019). Unique Neoproterozoic Carbon Isotope Excursions Sustained by Coupled Evaporite Dissolution and Pyrite Burial. *Nat. Geosci.* 12 (10), 823–827. doi:10.1038/s41561-019-0434-3
- Sial, A. N., Gaucher, C., Misi, A., Boggiani, P. C., Alvarenga, C. J. S. d., Ferreira, V. P., et al. (2016). Correlations of Some Neoproterozoic Carbonate-Dominated Successions in South America Based on High-Resolution Chemostratigraphy. *Braz. J. Geol.* 46 (3), 439–488. doi:10.1590/2317-4889201620160079
- Spangenberg, J. E., Bagnoud-Velásquez, M., Boggiani, P. C., and Gaucher, C. (2014). Redox Variations and Bioproductivity in the Ediacaran: Evidence from Inorganic and Organic Geochemistry of the Corumbá Group, Brazil. *Gondwana Res.* 26, 1186–1207. doi:10.1016/j.gr.2013.08.014
- Sumner, D. Y., and Grotzinger, J. P. (1993). Numerical Modeling of Ooid Size and the Problem of Neoproterozoic Giant Ooids. *J. Sediment. Pet.* 63 (5), 974–982. doi:10.1306/d4267c5d-2b26-11d7-8648000102c1865d
- Swart, P. K., and Oehlert, A. M. (2018). Revised Interpretations of Stable C and O Patterns in Carbonate Rocks Resulting from Meteoric Diagenesis. *Sediment. Geol.* 364, 14–23. doi:10.1016/j.sedgeo.2017.12.005
- Thallner, D., Biggin, A. J., and Halls, H. C. (2021). An Extended Period of Extremely Weak Geomagnetic Field Suggested by Palaeointensities from the Ediacaran Grenville Dykes (SE Canada). *Earth Planet. Sci. Lett.* 568, 117025. doi:10.1016/j.epsl.2021.117025
- Tobias, T. C. (2014). Micropaleontologia da Formação Tamengo, Eco Parque Cacimba da Saúde, Ediacarano, Grupo Corumbá, Estado de Mato Grosso do Sul. Dissertação (Mestrado). Brasília: Instituto de Geociências, Universidade de Brasília, 88.
- Tostevin, R., He, T., Turchyn, A. V., Wood, R. A., Penny, A. M., Bowyer, F., et al. (2017). Constraints on the Late Ediacaran Sulfur Cycle from Carbonate Associated Sulfate. *Precambrian Res.* 290, 113–125. doi:10.1016/j.precamres.2017.01.004
- Trompette, R., de Alvarenga, C. J. S., and Walde, D. (1998). Geological Evolution of the Neoproterozoic Corumbágraben System (Brazil). Depositional Context of the Stratified Fe and Mn Ores of the Jacadigo Group. *J. S. Am. Earth Sci.* 11, 587–597. doi:10.1016/s0895-9811(98)00036-4
- Tucker, M. E., and Dias-Brito, D. (2017). *Petrologia Sedimentar Carbonática: Iniciação Com Base No Registro Geológico Do Brasil*, 3. Rio Claro, Obra: UNESP-IGCE-Unispetro, 208.
- Tucker, M. E., and Wright, V. P. (1990). *Carbonate Sedimentology*. Oxford: Blackwell Science.
- Uhlein, G. J., Uhlein, A., Pereira, E., Caxito, F. A., Okubo, J., Warren, L. V., et al. (2019). Ediacaran Paleoenvironmental Changes Recorded in the Mixed Carbonate–Siliciclastic Bambuí Basin, Brazil. *Palaeogeogr. Palaeoclimatol. Palaeoecol.* 517, 39–51. doi:10.1016/j.palaeo.2018.12.022
- Vaziri, S. H., and Laflamme, M. (2018). Lithostratigraphy and Sedimentary Environment of the Precambrian Kushk Series of Central Iran. *Can. J. Earth Sci.* 55 (11), 1284–1296. doi:10.1139/cjes-2017-0234
- Walde, D. H.-G., Weber, B., Erdtmann, B. D., and Steiner, M. (2019). Taphonomy of Corumbella Wernerii from the Ediacaran of Brazil: Sinotubulitid Tube or Conulariid Test? *Alcheringa Australas. J. Palaeontol.* 43, 335–350. doi:10.1080/03115518.2019.1615551
- Walde, D. H. G. (1988). *Das Proterozoische Paraguay-Araguaia Orogen in West-Brasilien, Ausgehend von Untersuchungen im Raum Corumbá*. Habil. Schrift. Freiburg: Albert-Ludwigs-Universität, 122.
- Walde, D. H. G., Do Carmo, D. A., Guimarães, E. M., Vieira, L. C., Erdtmann, B.-D., Sanchez, E. A. M., et al. (2015). New Aspects of Neoproterozoic–Cambrian Transition in the Corumbá Region (State of Mato Grosso do Sul, Brazil). *Ann. Paléontologie* 101, 213–224. doi:10.1016/j.annpal.2015.07.002
- Walde, D. H. G., Leonardos, O. H., Hahn, G., Hahn, R., and Pflug, H. (1982). The First Precambrian Megafossil from South America, *Corumbella Wernerii*. *An. Acad. Bras. Ciências* 54, 461.
- Walker, R. G. (1984). “Shelf and Shallow Marine Sands,” in *Facies Models*. Editor R.G. Walker (Canada: Geological Association of Canada), 141–170.
- Walter, M. R., Veevers, J. J., Calver, C. R., and Grey, K. (1995). Neoproterozoic Stratigraphy of the Centralian Superbasin, Australia. *Precambrian Res.* 73 (1–4), 173–195. doi:10.1016/0301-9268(94)00077-5
- Wang, J., La Croix, A. D., Wang, H., Guo, F., and Ren, B. (2019). Linkage Between Calcirudite Lithofacies and Storm-Generated Depositional Processes in the Upper Cambrian Series, Shandong Province, Eastern China. *Sediment. Geol.* 391, 105518. doi:10.1016/j.sedgeo.2019.105518
- Warren, L. V., Freitas, B. T., Riccomini, C., Boggiani, P. C., Quaglio, F., Simões, M. G., et al. (2019). Sedimentary Evolution and Tectonic Setting of the Itapucumi Group, Ediacaran, Northern Paraguay: From Rodinia Break-Up to West Gondwana Amalgamation. *Precambrian Res.* 322, 99–121. doi:10.1016/j.precamres.2018.12.022
- Wei, G.-Y., Hood, A. v. S., Chen, X., Li, D., Wei, W., Wen, B., et al. (2019). Ca and Sr Isotope Constraints on the Formation of the Marinoan Cap Dolostones. *Earth Planet. Sci. Lett.* 511, 202–212. doi:10.1016/j.epsl.2019.01.024
- Wentworth, C. K. (1922). A Scale of Grade and Class Terms for Clastic Sediments. *J. Geol.* 30 (5), 377–392. doi:10.1086/622910
- Wright, V. P. (1992). A Revised Classification of Limestones. *Sediment. Geol.* 76, 177–185. doi:10.1016/0037-0738(92)90082-3
- Xiao, S., Cui, H., Kang, J., McFadden, K. A., Kaufman, A. J., Kitajima, K., et al. (2020). Using SIMS to Decode Noisy Stratigraphic $\delta^{13}\text{C}$ Variations in Ediacaran Carbonates. *Precambrian Res.* 343, 105686. doi:10.1016/j.precamres.2020.105686
- Xiao, S., Narbonne, G. M., Zhou, C., Laflamme, G. R., and D. V., Grazhdankin, D. V., Moczydlowska-Vidal, M., et al. (2016). Towards an Ediacaran Time Scale: Problems, Protocols, and Prospects. *Episodes* 39 (4), 540–555. doi:10.18814/epiugs/2016/v39i4/103886
- Yu, W., Algeo, T. J., Zhou, Q., Du, Y., and Wang, P. (2020). Cryogenian Cap Carbonate Models: A Review and Critical Assessment. *Palaeogeogr. Palaeoclimatol. Palaeoecol.* 552, 109727. doi:10.1016/j.palaeo.2020.109727

- Zaine, M. F. (1991). Análise dos fósseis de parte da Faixa Paraguai (MS, MT) e seu contexto temporal e paleoambiental. Ph.D. Thesis. Brazil: University of São Paulo, 218.
- Zaine, M. F., and Fairchild, T. R. (1985). Comparison of *Aulophycus Lucianoi* Beurlen & Sommer from Ladário (MS) and the Genus *Cloudina* Germs, Ediacaran of Namibia. *An. Acad. Bras. Ciências* 57, 1.
- Zhang, F., Xiao, S., Kendall, B., Romaniello, S. J., Cui, H., Meyer, M., et al. (2018). Extensive Marine Anoxia During the Terminal Ediacaran Period. *Sci. Adv.* 4 (6), eaan8983. doi:10.1126/sciadv.aan8983

Conflict of Interest: The authors declare that the research was conducted in the absence of any commercial or financial relationships that could be construed as a potential conflict of interest.

Publisher's Note: All claims expressed in this article are solely those of the authors and do not necessarily represent those of their affiliated organizations, or those of the publisher, the editors and the reviewers. Any product that may be evaluated in this article, or claim that may be made by its manufacturer, is not guaranteed or endorsed by the publisher.

Copyright © 2022 Ramos, Giorgioni, Walde, do Carmo, Fazio, Vieira, Denezine, V. Santos, R. Adorno and Lage Guida. This is an open-access article distributed under the terms of the Creative Commons Attribution License (CC BY). The use, distribution or reproduction in other forums is permitted, provided the original author(s) and the copyright owner(s) are credited and that the original publication in this journal is cited, in accordance with accepted academic practice. No use, distribution or reproduction is permitted which does not comply with these terms.



New Material of Carbonaceous Compressions from the ~1.5 Ga Singhora Group, Chhattisgarh Supergroup, India, and their Interpretation as Benthic Algae

Veeru Kant Singh* and Mukund Sharma

Birbal Sahni Institute of Palaeosciences, Lucknow, India

OPEN ACCESS

Edited by:

Shuhai Xiao,
Virginia Tech, United States

Reviewed by:

Qin Ye,
China University of Geosciences,
China
Ke Pang,
State Key Laboratory of Palaeobiology
and Stratigraphy, Nanjing Institute of
Geology and Palaeontology (CAS),
China

*Correspondence:

Veeru Kant Singh
veerukantsingh@bsip.res.in

Specialty section:

This article was submitted to
Paleontology,
a section of the journal
Frontiers in Earth Science

Received: 30 November 2021

Accepted: 06 June 2022

Published: 21 July 2022

Citation:

Singh VK and Sharma M (2022) New
Material of Carbonaceous
Compressions from the ~1.5 Ga
Singhora Group, Chhattisgarh
Supergroup, India, and their
Interpretation as Benthic Algae.
Front. Earth Sci. 10:825430.
doi: 10.3389/feart.2022.825430

The origin, antiquity, and affinity of benthic seaweeds (multicellular algae) in the geological past are shrouded in mystery due to their preservation bias. In this study, we present a new material of well-preserved carbonaceous compression fossils in shale horizons of the Mesoproterozoic (ca. ~1,500–1,300 Ma) Singhora Group of the Chhattisgarh Supergroup. Eleven distinct taxa, including one new taxon, *Palaeoscytosiphon shuklaii*, n. gen. et. sp., and one new species, *Jiuqunaoella sergeevii*, n. sp., are established. Four unidentified morphologies are also reported. Morphologically, the carbonaceous fossils are fan-shaped, palmate, elongated, leaf-like algal thalli with/without holdfast at the base, isolated or dichotomously branched long filaments, along with multicellular reproductive structures. The results of laser Raman spectroscopy and energy dispersive X-ray spectroscopy (EDX) are also presented in support of their biogenicity. Collectively, the preservation mode of the Singhora carbonaceous fossils suggests multicellular algal affinity and adds to a Burgess Shale-type (BST) taphonomic window in the Pre-Ediacaran biosphere.

Keywords: multicellular, eukaryotes, macroalgae, carbonaceous compressions, Mesoproterozoic, Chhattisgarh Supergroup, India

INTRODUCTION

Macroalgae (seaweeds) are multicellular marine algae easily observed by the unaided eye, whose “thallus” is characterized by holdfasts for attachment, and by “laminae,” reproductive “sori,” gas bladders, and stipes (Xiao and Dong, 2006; Brodie and Lewis, 2007). They are considered macroscopic photosynthetic eukaryotes in the Precambrian biosphere (Xiao and Dong, 2006; Bykova et al., 2020). Gray to black shales in Ediacaran sedimentary rocks contain unusually well-preserved Burgess Shale-type preservation of carbonaceous compressions (macroalga) (Yuan et al., 1999; Xiao et al., 2002; Dornbos et al., 2016; Ye et al., 2019) and cast and mold preservation (Laflamme et al., 2013). Notable carbonaceous fossils are known from the Lantian, Doushantuo, and Liuchapo Formations in South China (Steiner, 1994; Xiao et al., 2002; Zhao et al., 2004; Yuan et al., 2011; Ye et al., 2019); the Perevalok Formation in the Central Urals (Grazhdankin et al., 2007; Marusin et al., 2011); the Khatyspyt Formation in Siberia (Grazhdankin et al., 2008); the Deep Spring Formation in the United States (Rowland and Rodriguez, 2014); and the Zuun-Arts Formation in Western Mongolia (Dornbos et al., 2016). Most of these assemblages are characterized by low

taxonomic diversity and are dominated by multicellular benthic algae (Xiao et al., 2002), and some are identified as putative macro-metazoans (Wan et al., 2016; Yuan et al., 2016; Ye et al., 2019). These records have gradually contributed to our comprehensive understanding of the evolution, emergence, and diversification of macroalgae before the Cambrian explosion. Globally, they are considered ecologically important primary producers in marine benthic ecosystems and have played an important role in the evolution of eukaryotic organisms in the late Proterozoic biosphere (Ediacaran) (Brocks et al., 2017; Isson et al., 2018).

In recent years, considerable progress has been made in understanding the evolution and diversification of Proterozoic macroalgal fossils preserved on the surface of siliciclastic sediments. However, their evolutionary timing and recognition in deep time is crucial due to preservational factors (taphonomy) in both palaeontological data and molecular clock analyses (Xiao and Dong, 2006; Parfrey et al., 2011). Geographically, the Proterozoic macroalgal fossils (*Chuarial-Tawuia* assemblage) and multicellular metaphyte fossils have been extensively documented from the sedimentary successions of Africa (Amard, 1992), Antarctica (Cooper et al., 1982), Australia (Haines, 1998), Canada (Hofmann and Rainbird, 1994), China (Xiao et al., 2002; Tang et al., 2017; Ye et al., 2019; Tang et al., 2020; Tang et al., 2021), Namibia (Leonov et al., 2009), Russia (Gnilovskaya, 1971; Gnilovskaya et al., 2000), Spain (Amard, 1992; Jensen et al., 2007), Spitsbergen (Butterfield et al., 1994), Siberia (Grazhdankin et al., 2008), Ukraine (Gnilovskaya et al., 1988; Steiner, 1997), Ural (Marusin et al., 2011), United States (Ford and Breed, 1973; Rowland and Rodriguez, 2014), Yakutia (Vidal et al., 1993), and India (Sharma et al., 1991, 2009; Sharma, 2006; Sharma and Shukla, 2009a, 2009b; Singh et al., 2009; Sharma and Singh, 2019). These carbonaceous megascopic fossils have drawn the attention of various researchers seeking to understand their affinity, taxonomic position (both debatable) (Hofmann, 1992; Xiao and Dong, 2006; Lamb et al., 2007; Wan et al., 2016; Sharma and Singh, 2019; Ye et al., 2019) and possible natural experimentation in response to the advent of oxygen in the palaeoenvironment (Lenton et al., 2014; Lyons et al., 2014; Tang et al., 2017; Muscente et al., 2019; Tang et al., 2020; Zhang F. et al., 2021; Maloney et al., 2021).

Such fossils are also recorded from the Palaeoproterozoic to Mesoproterozoic sediments of the United States: the ca. 1.87 Ga Negaunee Iron-Formation (Tyler et al., 1957; Han and Runnegar, 1992) and the ca. 1.4 Ga Greyson Formation (Walter et al., 1990); China, including the ca. 1.65 Ga Changzhongou Formation (Zhu et al., 2000), the ca. 1.63 Ga Tuanshanzi Formation (Zhu and Chen, 1995; Yan and Liu, 1997; Qu et al., 2018), the ca. 1.56 Ga Gaoyuzhuang Formation (Du et al., 1986; Zhu et al., 2016), the ca. 1.4 Ga Xiamling Formation (Zhang F. et al., 2021) and the ca. 1.0 Ga Nanfen Formation (Tang et al., 2020); and India, including the ca. 1.63 Ga Olive Shale (Rai and Singh, 2006; Sharma, 2006), and the ca. ~1.5 Ga Saraipali Shale (Babu and Singh, 2011; Babu and Singh, 2013). Although the Palaeo- and Mesoproterozoic fossil record of macroalgae (eukaryotes) is infrequent, they play an important role in the evolution of multicellular life in the Precambrian Era. The cellular structures and phylogenetic

affinities of these fossil remains are uncertain, due to the preservation of limited morphological details (Kumar, 2001; Bykova et al., 2020), modes of preservation (Lamb et al., 2007), broad taphonomic variability (Samuelsson and Butterfield, 2001), and the current paucity of biochemical information (Arouri et al., 1999; Dutta et al., 2006; Sharma et al., 2009). A few demonstrate cyanobacterial affinity (Sharma and Shukla, 2009b). Recently, a coenocytic eukaryotic and macroalgal affinity has been assigned to tomaculate fossil *Tawuia* based on recalcitrant cell walls, asexual reproduction through asymmetric constrictions, and possible abscission structures (Tang et al., 2021). Their evolutionary patterns and ecological influences have been mostly disregarded (Bykova et al., 2020). To improve our understanding of macroalgal evolution in the Mesoproterozoic biosphere, the present study systematically describes and discusses the biogenicity, antiquity, and affinity of new material from carbonaceous megascopic fossils found in the rocks of the Singhora Group, Chhattisgarh Supergroup, India.

Geology and Age of the Singhora Group

In the peninsular region of central India, the Palaeoproterozoic–Mesoproterozoic succession of unmetamorphosed, less-deformed sedimentary succession of the Chhattisgarh Supergroup lies over the crystalline rocks of the Bastar Craton (Mukherjee et al., 2014; Chakraborty et al., 2020). Lithostratigraphically, it is divided into four groups, viz., the Singhora, the Chandarpur, the Raipur, and the Kharsia, in ascending order (Das et al., 1992; Mukherjee et al., 2014; Chakraborty et al., 2015). In the ~2,300 m thick litho package of the Chhattisgarh Supergroup, the Singhora Group is designated as the lowermost stratigraphic unit, containing mixed siliciclastic and carbonate litho-associations (Das et al., 2003; Mukherjee et al., 2014). The Singhora Group of rocks is located in the southeastern and western parts of the Chhattisgarh Basin (Figure 1.1). It is well-exposed in the Singhora Township, situated in parts of the Mahasamund District in Chhattisgarh State and the Barapahar area of the Bargarh District, Odisha (Das et al., 2003). With ~400 m thickness, the litho package of the Singhora Group (200 km² in aerial extent) is further subdivided into four Formations, viz., the Rehatikhol, the Saraipali, the Bhalukona, and the Chhuipali, in order of superposition (Figure 1.2) (Table 1).

With ~20 m maximum thickness, the Rehatikhol Formation of the Singhora Group marks the initiation of sedimentation in the Baradwar Subbasin, resting over the granitic/gneissic basement of Bastar Craton. It is represented by the repetitive sequence of conglomerate and arkose with minor intercalations of siltstone and shale. More than ~60 m thick, the Saraipali Formation is the second unit of the Singhora Group (Mukherjee et al., 2014). The finely-laminated shale, siltstone, volcanoclastic tuffs, and limestone-dominated Saraipali Formation overlie the basal Rehatikhol Formation. The arenaceous sediment dominated Bhalukona Formation (~20 m) overlies the Saraipali Formation. It is constituted of quartz arenite with minor shale and siltstone intercalations in its basal part representing a coarsening upward sequence. The shale and carbonate-dominated Chhuipali Formation is the topmost unit of the

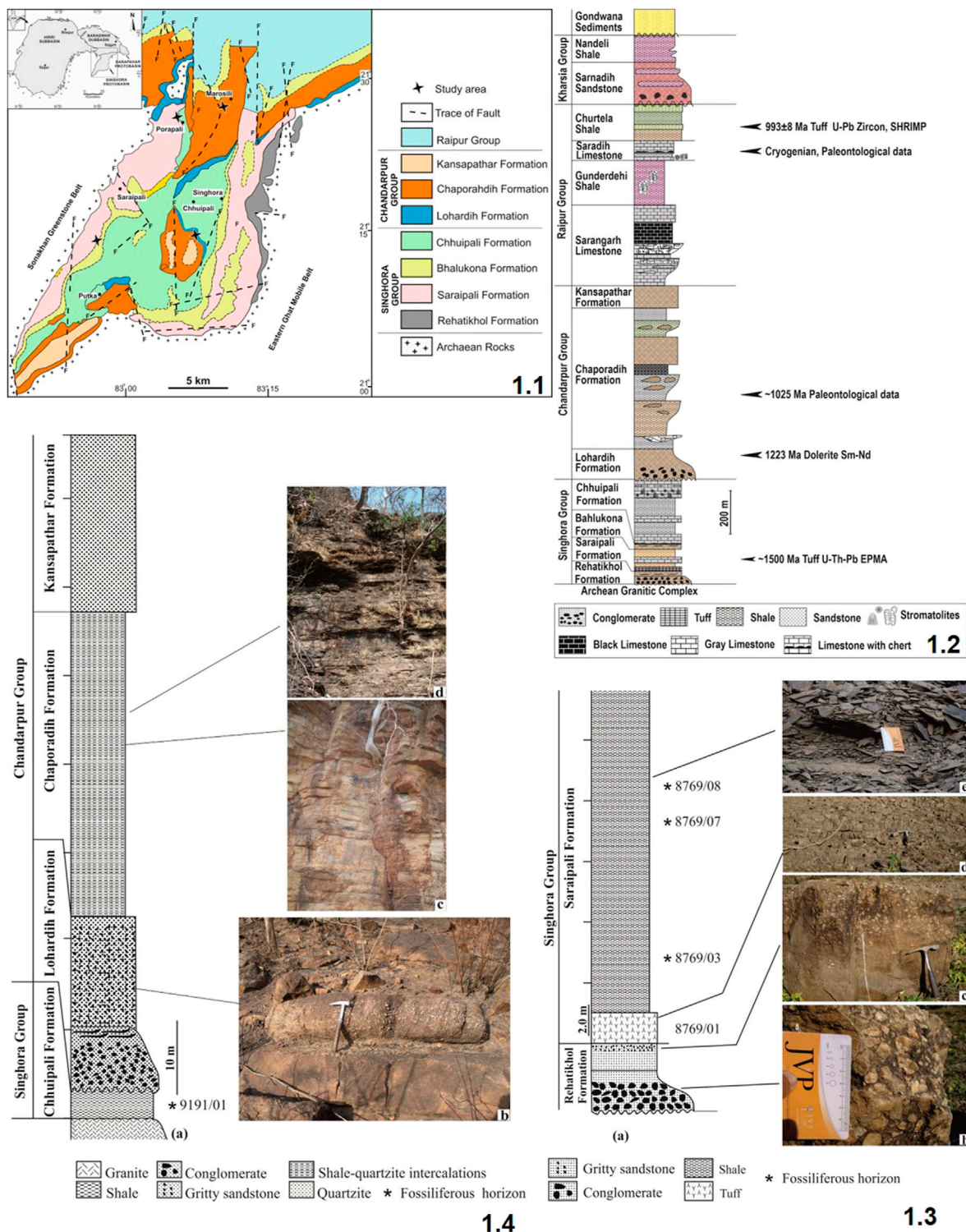


FIGURE 1 | Generalized geological map of the Baradwar Subbasin in and around the Singhora and Sarangarh areas, Chhattisgarh (after Das et al., 2001); 1.2: Lithostratigraphic succession of the Chhattisgarh Supergroup in the Baradwar Subbasin (modified after Das et al., 1992; Patranabis deb and Chaudhury, 2008); 1.3: (A) Generalized lithology of the Singhora Group, Surangi River section; (B) Conglomerate of the Rehatikhol Formation; (C) Gritty sandstone of the Rehatikhol Formation; (D) Tuff/porcellanite of the Saraipali Formation; (E) Fossil bearing carbonaceous shale of the Saraipali Formation. Card and geological hammer used for scale; 1.4: (A) Generalized lithology of Bendla Dongar section; (B) Gritty sandstone of the Lohardi Formation; (C, D) Shale-quartzite intercalation heterolithic of the Chaporadhi Formation. Hammer is used for scale.

TABLE 1 | Generalized lithostratigraphic succession of the Chhattisgarh Supergroup (Das et al., 1992; Patranabis-Deb and Chaudhuri, 2008; Mukherjee and Ray, 2010) Age data source: 1. Bickford et al., (2011), 2. Pandey et al., (2012), 3. Das et al., (2009). * Fossiliferous unit.

	Group	Formation	Lithology	AGE
Chhattisgarh Supergroup	Kharsia	Nandeli shale	Gypsiferous purple shale and dolomite	
		Samadih sandstone	Sandstone and conglomerate	
	~~~~~Unconformity~~~~~			
	Raipur	Churtela shale	Purple shale and Tuff	1,000 Ma (Tuff) ¹
		Saradih limestone	Dolomite/Stromatolitic limestone	
		Gunderdehi shale	Calcareous shale with stromatolitic limestone	
		Sarangarh limestone	Flaggy limestone and shale	
	Chandarpur	Kansapathar formation	Quartz arenite	1,641 ± 120 Ma (Dolerite Intrusive) ²
		Chaporadih formation	Glaucconitic sandstone/siltstone, black shale	
		Lohardih formation	Subarkose with basal conglomerate	1223 ± 140 Ma (Sm-Nd) ²
	~~~~~Unconformity~~~~~			
Archean Basement (Sonakhan and Sambalpur Granites)	Singhora	Chhuipali formation*	Stromatolitic limestone and Variegated shale	c.1500 Ma (Tuff) ³
		Bhalukona formation	Quartz arenite and minor shale	
		Saraipali formation*	Variegated shale/siltstone, tuff/porcellanite	
		Rehatikhol formation	Sandstone with conglomerate at the base	

Singhora Group, resting over the Bhalukona Formation. It is about ~300 m thick in the central part of the basin. Rocks of this unit are characterized by variegated shale with intercalations of siltstone, minor sandstone, chert, and stromatolitic limestone/dolomite. It is both bedded and stromatolitic and occurs as pockets as well as lenses. The limestone is light gray to dark gray and is composed of sparry calcite forming a mosaic with patches of micritic carbonate. In places, it is associated with ferruginous arenite. Chertified limestone is further overlain by low-dipping variegated shale which dominates without (>100 m thick), which is laminated and highly friable; 5–20 m thick stromatolitic limestone and dolomite comprise the upper part of this formation and occur as pockets and lenses. The limestone is light gray, impure, and bedded, characterized by the presence of thin chert partings. Stromatolite sections are conspicuous on the horizontal surface parallel to the bedding. Available studies suggest alluvial fan, braid plain, shelf (storm infested), shallow marine, and shelf depositional conditions for the Singhora Group of rocks in stratigraphic order (Das et al., 1992; Chakraborty et al., 2010; Chakraborty et al., 2012; Chakraborty et al., 2015). Carbonaceous fossils are documented from the Saraipali and Chhuipali Formations of the Singhora Group.

The age of the Singhora Group of rocks is constrained by U-Th-Pb SHRIMP EPMA dating of monazite and zircon in the Khariar and Shingora tuffs, which provide a minimum age around ~1,500 Ma (Das et al., 2009; Bickford et al., 2011; Chakraborty and Barkat, 2020). About ~80 Ma of depositional timeframe has been suggested after Sm-Nd isochron dating (~1,420 Ma) of dibasic intrusives piercing the Saraipali Formation. SHRIMP II and LA-ICP-MS zircon dating from the different stratigraphic units of the Singhora Group yields the youngest age population, between c. 1,619 Ma and c. 2,543 Ma, implying sedimentation initiation of >1,600 Ma (Das et al., 2017). However, Babu and Singh (2011) have suggested the latest Palaeoproterozoic (~1750 Ma) age based on the carbonaceous remains of eukaryotic affinity from the Saraipali Formation of the Singhora Group. The occurrence of

acanthomorphic acritarch *Tappania plana* in the Saraipali Formation also suggest an early Mesoproterozoic age for the Singhora Group of rocks (Singh et al., 2019).

MATERIAL AND METHODS

The fossils described here were collected from the siliciclastic unit of the Saraipali Formation and the Chhuipali Formation of the Singhora Group, Mahasamund District, Chhattisgarh State, India.

The Surangi River section (Latitude: N21°14'30.53"; Longitude: E82°58'05.25") is situated 25 km southwest of Saraipali Township in the Mahasamund District. The sedimentary succession of this section is characterized by up to 2.0 m thick low-dipping dark grey to black fine-grained porcellanite/tuffs followed by ~ 20 m thick black and gray shale with minor sandy intercalations at places (Das et al., 1992; Mukherjee et al., 2014). Shale with a gentle dip is the dominant lithology of this formation. Most shale horizons from this unit contain Saraipali preserved as carbonaceous compressions within and on the surface. Specimens described here come from the lower part of this section, as illustrated in **Figure 1.3**.

The Bendla Dongar section (Latitude: N21°26'3.45"; Longitude: E83°05'5.44") is situated 18.5 km north of Saraipali Township near Porapali Village in the Mahasamund District. This hill is about 150 m high (**Figure 1.4**). The sedimentary succession in this section is characterized by the low-dipping khaki-coloured fine-grained shale of the Chhuipali Formation in the Singhora Group. The sequence is further characterized by the Chandarpur Group rocks, represented by the bedded quartzite with glauconite and thin arkosic conglomerate of the Lohardih Formation at the base (**Figure 1.4B**), shale-mudstone—sandstone lower heterolithics more than 20 m thick (**Figures 1.4C, D**) and about 10–15 m thick brown-coloured ferruginous sandstone at the top, which distinctly

belongs to the Chaporadih Formation. Khaki shale of this unit contains carbonaceous remains preserved as compressions/impressions on the bedding plane (**Figure 1.4**). More than 200 carbonaceous films (compressions/impressions) hosted in shale slabs were collected for the present study from the Saraipali Shale and Chhuipali Shale. All illustrated specimens, photomicrographs, and associated samples have been repositied in the Museum at Birbal Sahni Institute of Palaeosciences, Lucknow. These can be retrieved vide statement no. BSIP 1584.

Fossil Measurements and Analytical Microscopy

All fossiliferous slabs were thoroughly cleaned and prepared before morphological studies. Megascopic carbonaceous fossils were analyzed and morphologically identified on an OLYMPUS SZ61 Stereoscopic microscope and were photographed and measured on a software-supported OLYMPUS SC50 digital camera. Digital Photographic images were further processed on Olympus Cell Sense Standard software version 2.1 for detailed linear measurements. Approximately 20 samples of carbonaceous films were analyzed with Energy Dispersive X-ray Spectroscopy (EDX) to make elemental mapping and Laser Raman Spectroscopy (LRS) analyzing the macroalgae's chemical characterization.

Laser Raman Spectroscopy (LRS)

Selected specimens were analyzed for chemical characterization using a RENISHAW inVia Reflex Raman Microscope at BSIP, which permits the acquisition of both point spectra and Raman images, which display the two-dimensional spatial distribution of molecular-structural components of the specimens and their associated mineral matrix. The optics of the Raman system are based on a Leica DM-2700M REN RL/TL microscope. The instrument was calibrated against the Raman signal for Si obtained from an internal silicon wafer reference at 521 cm^{-1} . Spectral acquisition was performed over an extended range from ~ 200 to $\sim 2000\text{ cm}^{-1}$. On each point of the specimen, Raman spectra were collected by using 0.5% laser power with 20 s of exposure time. The samples were exposed to a Coherent Infrared (IR) laser, which provided excitation at a 785-nm wavelength at a power of $\sim 1\text{--}5\text{ mW}$ over $1.5\text{ }\mu\text{m}$, to obtain a good signal-to-noise ratio, avoid radiation damage, and minimize laser-induced heating (Schopf et al., 2006). In these conditions, the analysis time was a few minutes (an accumulated time of 30 s and 10 scans). A $\times 50$ objective lens (with an extended working distance of 10.6 mm and a numerical aperture of 0.5) was used to obtain a horizontal spectral resolution of $1.5\text{ }\mu\text{m}$.

Energy Dispersive X-ray Spectroscopy (EDX)

To determine the elemental constitution of carbonaceous fossils, selected specimens were analyzed under the JEOL JSM-7610F Field Emission Scanning Electron Microscope with Energy Dispersive X-ray Spectroscopy (FESEM-EDX) instrument at 7.05 keV with a platinum coating. The instrument, equipped with Gentle Beam (GB) mode, provides high-resolution images

even at a low accelerating voltage from 100 V to 3.9 kV without damaging the specimen surface. The EDX documents the quantitative and qualitative elemental analysis of fossil materials, such as C, O, P, S, Si, Fe, Al, O, K, and many others present in Mendeleev's Periodic Table.

RESULTS

Systematic Palaeontology

Systematic descriptions, interpretations, and affinities of identified macrofossils of carbonaceous remains are typically based on gross morphological characteristics, as in most treatment of fossil taxa. Distinct morphological characters are an essential tool to establish the taxonomy of any fossils at the genus and species level. Morphologically, they vary in size (from millimeters to a few centimeters), orientation, their degree of twisting/folding, and, in general, appear to be *in situ* remains. The carbonaceous fossils are fan-shaped, palmate, elongated, leaf-like, ribbon-like, algal thalli with/without holdfast at the base, with rounded and angular distal ends, isolated or dichotomously branched long tubular filaments with a cylindrical axis, along with multicellular reproductive structures (**Supplementary Figures S1, S2**). New taxa are described following the rules of the International Code of Nomenclatures established for Algae, Fungi, and Plants (Shenzhen Code 2018). The taxonomic details of the identified fossils have been provided at the genus and species level based on characteristics and descriptions proposed by Xiao et al. (2002) and Ye et al. (2019).

Genus: Palaeoscytosiphon n. gen.

Type species: Palaeoscytosiphon shuklaii n. sp.

Etymology: With reference to the *Scytosiphon*-a modern phaeophyte.

Diagnosis: It is a branched and compressed thallus comprised of long multiple ribbons, with a holdfast at the base. The holdfast is occasionally rhizoidal (root-like). Ribbons are long and gradually taper to the distal end. Tapering angles are $2\text{--}3^\circ$. Ribbons are 1.0–6.0 mm long and 0.1–0.3 mm wide. Edges of the ribbons are parallel and sharp; each thallus contains 4–12 stalks arising from the holdfast. Filaments are often branched, more or less symmetrically dichotomous in a few specimens. Ribbons in some of the specimens are curved and twisted, perhaps due to taphonomic processes (**Figures 3.1, 3.3**).

Comparison: The morphological characteristics of described carbonaceous fossils can be compared to the brown alga *Scytosiphon lomentaria*—an irregularly arranged weed with a tubular, hollow, unbranched thallus growing on a rhizoid-like holdfast (**Figure 4**). It is a member of the order *Scytosiphonales* of the algal group *Phaeophyceae*.

Palaeoscytosiphonella shuklaii n. sp.

Figures 2, 3.

Stratigraphic position: The Saraipali Formation, the Singhora Group.

Derivation of Name: In honour of the Late Dr. Manoj Shukla, a Precambrian palaeobiologist from India.

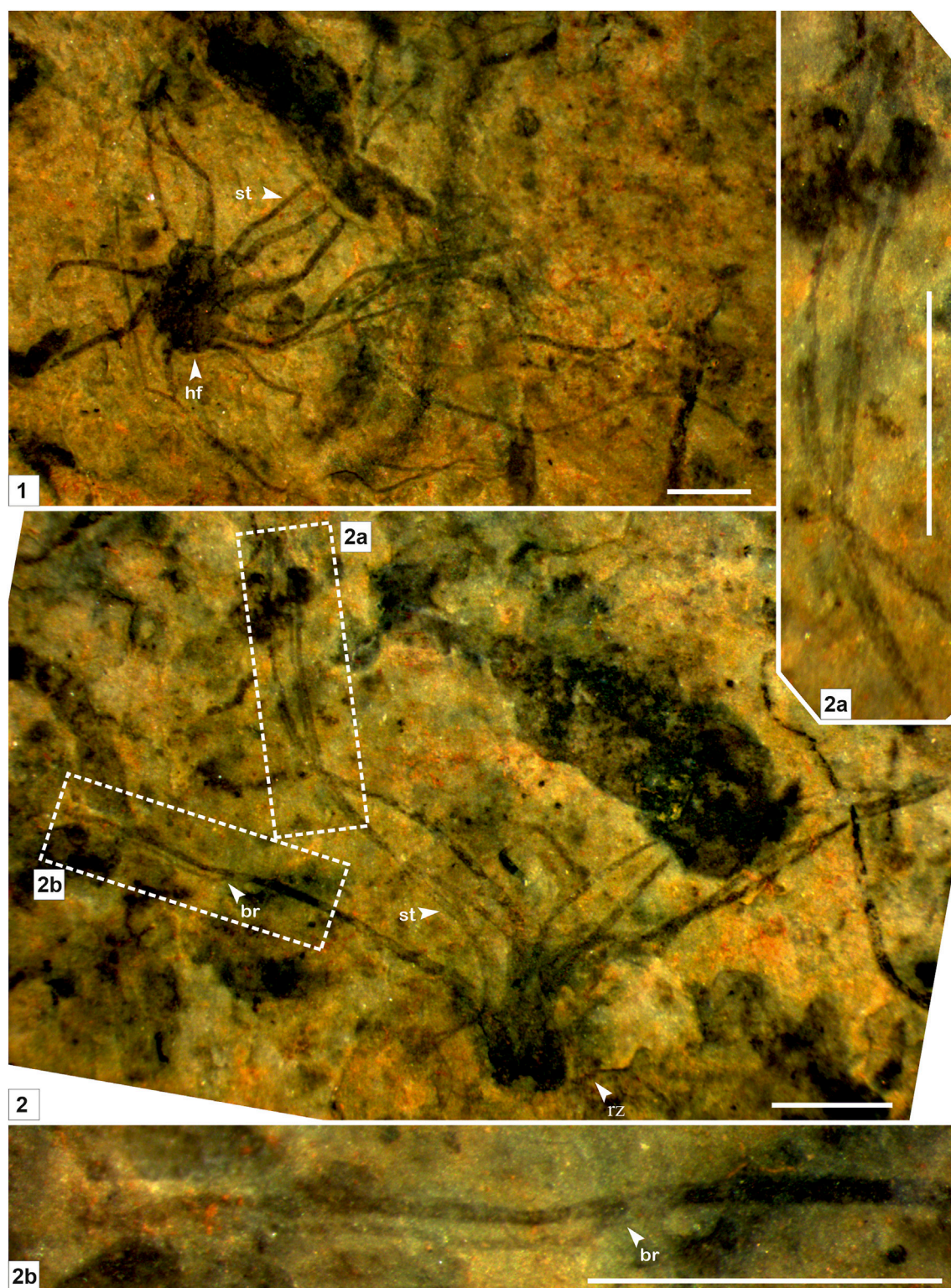


FIGURE 2 | Macroscopic fossil *Palaeoscytosiphon shuklaji* n. gen., n. sp. from the Saraipali Formation. (Arrow indicates the prominent features: st. stalk; br. branching; hf. holdfast; rz. rhizoid.) **(1–2).** **1.** Type specimen comprised of compressed thallus with long multiple tubular stalks attached with a discoidal holdfast at the base; **2.** Longitudinal preservation of *Palaeoscytosiphon shuklaji*; **2.a, 2.b.** Enlarged view of Panel 2 showing secondary branching in stalks. **1.** Specimen no. BSIP 41897; **2.** Specimen no. BSIP 42022. Scale bar is 2 mm for each specimen.

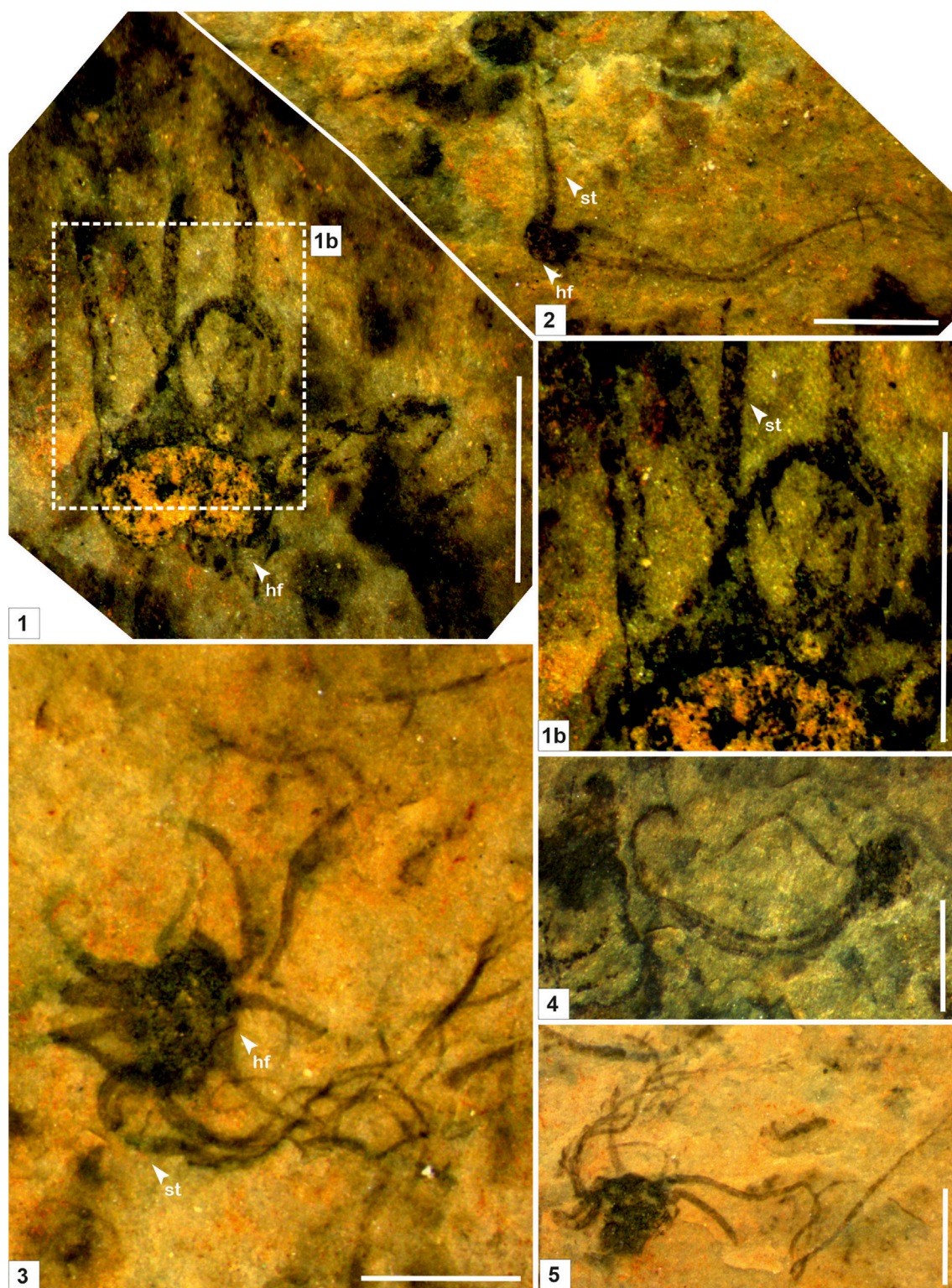
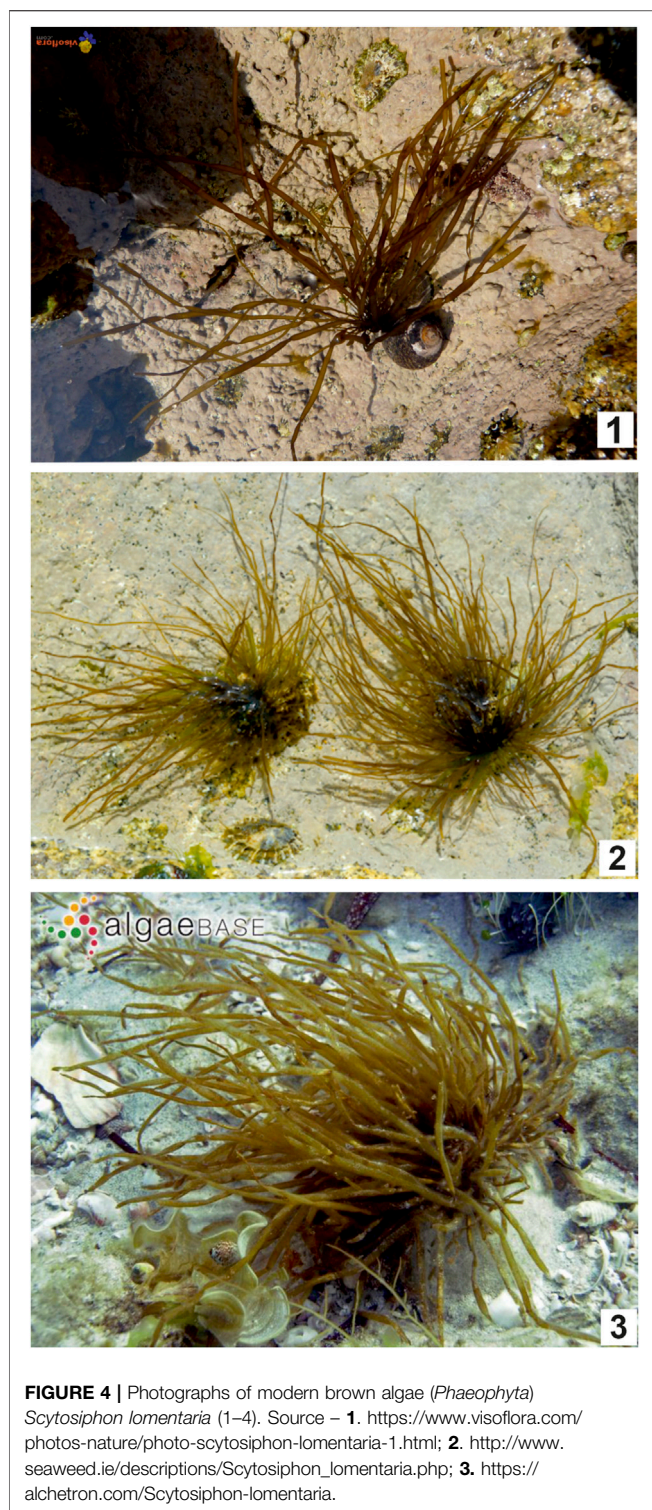


FIGURE 3 | Macroscopic fossil *Palaeoscytosiphon shuklaji* n. gen., n. sp. from the Saraipali Formation (arrow indicates the prominent features: st. stalk; br. branching; hf. holdfast) (1–5). **1b.** Enlarged view of connection between stalk and holdfast. **1, 2.** Specimen no. BSIP 42022; **3.** Specimen no. BSIP 42023; **4.** Specimen no. BSIP 42021; **5.** Specimen no. BSIP 42024. Scale bar is 2.0 mm for each specimen.



Type Specimen: **Figure 2.1**, Specimen No. 8769/82, BSIP Museum.

Material: 10 well-preserved specimens from the Surangi River section, southwest of Saraipali Township, Mahasamund District, Chhattisgarh, India.

Description: As for genus/type species.

Remarks: Stalks of modern *Scytosiphons* are up to 400 mm long and 3–10 mm wide. Generally, it grows on stones and hard mud in shallow rock pools (up to 17 m deep), the mid-to-low tide region of exposed shores, and in tide pools (**Figure 4**). Specimens assigned to *Palaeoscytosiphon shuklaii* are well-preserved, constituting multiple carbonaceous ribbons (**Figures 2.1, 2.2; Figure 3.1**). A rhizoid-like holdfast (**Figure 2.2, Figure 3.3**) and dichotomous branching in ribbons (**Figures 2.2A, 2.2B**) can be distinctly seen in specimens. Carbonaceous ribbons in some specimens are broken and ill-preserved (**Figures 3.2–3.5**). The mode of preservation of *P. shuklaii* is illustrated in **Supplementary Figure S2**. Additionally, the thread-like elongated filamentous compression fossil form *Proterotaenia montana*, known from the Palaeoproterozoic (~1,637 Ma) Tuanshanzi Formation of China, has also been compared with the tubular filaments of the extant brown algae *Scytosiphon lomentaria* (Yan and Liu, 1997). Singh et al. (2009) have reported specimens such as *Palaeochorda vindhyansis* from the Neoproterozoic Bhandar Group of the Vindhyan Supergroup, India. *Palaeochorda vindhyansis* is characterized by smooth, hollow, unbranched long tubular cord-like ribbons attached by a holdfast-like structure similar to *Chorda* in morphology. In modern morphology, the Chordafilum is characterized by hollow, unbranched, long cord-like ribbons attached by a small discoid holdfast. However, in *Palaeochorda vindhyansis*, the discoidal holdfast is absent. In this case, *P. vindhyansis* can be considered a junior synonym of *Palaeoscytosiphon shuklaii*. Conversely, the specimens of *P. shuklaii* have a distinct rhizoidal holdfast (**Figure 2.2**).

Genus: *Baculiphyca*. Yuan, Li, and Chen, 1995, emend. Xiao et al. 2002.

Type species: *Baculiphyca taeniata*. Yuan, Li, and Chen, 1995, emend. Xiao et al. 2002.

Baculiphyca taeniata. Yuan, Li, and Chen, 1995, emend. Xiao et al. 2002.

Figures 5.1, 5.1.1.

Stratigraphic position: Mesoproterozoic Chhuipali Formation, the Singhara Group.

Material: One specimen from the Bendla Dongar section, north of Saraipali Township, Mahasamund District, Chhattisgarh, India.

Description: Elongate, unbranched clavate algal thallus, attached to the substrate by a basal rhizoidal holdfast. The holdfast typically bears fine (ca. 0.1–0.3 mm in diameter) filamentous rhizoids at its base. The thallus expands gradually to the distal end at an apical divergence angle of 2°–6°. The upper portion is more or less blade-like. The terminus is straight. Elongated thalli are 2.5 mm long and 0.2 mm thick.

Remarks: Yuan et al. (1995) instituted the genus *Baculiphyca* with its type species *Baculiphyca taeniata* assigned to carbonaceous fossils composed of a clavate, bent and folded thallus attached with a rhizoidal holdfast. Later, in a taxonomic assessment, Xiao et al. (2002) emended the diagnosis of *Baculiphyca* based on both rhizoidal and globose holdfasts. Subsequently, based on complex morphology, Xiao et al. (2002) have also suggested possible eukaryotic algal affinity for the genus *Baculiphyca*. Recently, Ye et al. (2019) established a

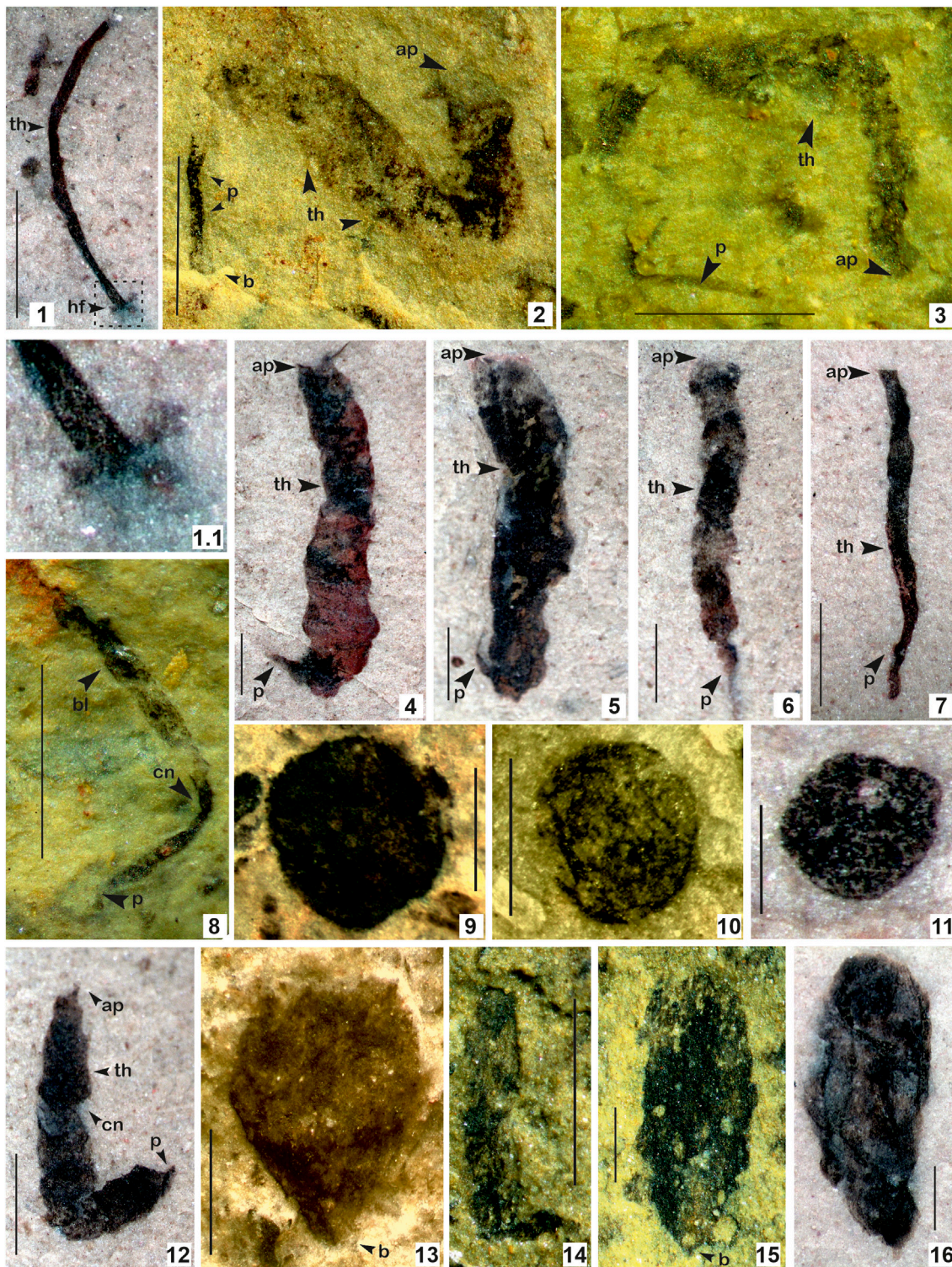


FIGURE 5 | 1. *Baculiphyca taeniata* Yuan et al., 1995, emend. Xiao et al., 2002; **1.1.** Enlarged view of **(B)** *taeniata* holdfast; **2–8, 12. *Changchengia stipitata*** Yan, 1997 in Yan and Liu, 1997 with distinct parastem ate base; **9–11. *Chuaria circularis*** Walcott, 1899; Vidal and Ford, 1985; **13–15. *Eopalmaria pristina*** Yan, 1995. (Arrow indicates the prominent features: ap. apex; b. base; bd. bead; th. thallus; cn. constrictions, p. parastem; hf. holdfast). 1. Specimen no. BSIP 418983; 2. Specimen no. BSIP 39782; 3. Specimen no. BSIP 39779; 4. Specimen no. BSIP 42026; 5. Specimen no. BSIP 41899. 6. Specimen no. BSIP 42038; 7. Specimen no. BSIP 42033a; 8. Specimen no. BSIP 39776; 9. Specimen no. BSIP 42022; 10. Specimen no. BSIP 41897; 11. Specimen no. BSIP 42042; 12. Specimen no. BSIP 42036; 13. Specimen no. BSIP 42040; 14. Specimen no. BSIP 39774; 15. Specimen no. BSIP 39778; 16. Specimen no. BSIP 42030. Specimens 1, 4–7, 11, 12, 16 from the Bendla Dongar section and 2, 3, 8–10, 13–15 from the Surangi River section. Scale bar is 1.0 mm for each specimen.

new species, *Baculiphyca brevistipitata*, from the upper Ediacaran Doushantuo Formation, China. A specimen from the Chhuipali Formation is characterized by a dark black elongated stipe with a globose holdfast, showing a close resemblance to Miaohu specimens (Xiao et al., 2002; Ye et al., 2019), but is comparatively smaller (Figure 5.1). The presence of a holdfast in *Baculiphyca* proves their benthic habit as microorganisms. Holdfasts may play an important role, anchoring them to strengthen *Baculiphyca* in mud and making their thallus/stipe flexible for movement according to currents.

In the fossil records, *Baculiphyca* is widely known in the Ediacaran carbonaceous assemblages, specifically in China and India (Singh et al., 2009; Ye et al., 2019). This is the first report of *Baculiphyca* from the Mesoproterozoic succession and suggests their antiquity is possibly ~400 Ma deeper in the Proterozoic biosphere.

Genus: Changchengia Yan. Yan and Liu, 1997.

Type species: Changchengia stipitata. Yan and Liu, 1997.

Changchengia stipitata Yan. Yan and Liu, 1997.

Figures 5.2–5.8, 5.12

Stratigraphic position: The Saraipali and Chhuipali Formations, the Singhora Group.

Material: Twenty (20) specimens from the Surangi River section, southwest of Saraipali Township; and fifteen (15) specimens from the Bendla Dongar section, north of Saraipali Township, Mahasamund District, Chhattisgarh, India.

Description: Unbranched, lanceolate, broad ribbon-like thalli, widest at the middle, wider toward the apex, narrowing toward the base. Algal thalli are folded and twisted with depressed margins, smooth and prominent. A distinct differential type parastem-like structure (Figures 5.2–5.8) is present at the base of the thalli. The measured thallus is 3.0–8.0 mm in length, and up to 1.0 mm wide. The parastem is up to 0.5 mm long. In one specimen, the parastem-like structure is attached to a disc-like base (Figure 5.8).

Remarks: Specimens described here are morphologically similar to, but relatively smaller than, the *C. stipitata* known from the Tuanshanzi Formation (~1,637 Ma) of Yanshan Basin in Jinxian, Hubei, China (Yan and Liu, 1997). Specimens with similar morphologies have been documented from the Palaeoproterozoic Olive Shale of the Vindhyan Supergroup, India (Rai and Singh, 2006; Sharma, 2006). Based on the preservation mode of *C. stipitata*, Sharma (2006) has suggested their growth in a lagoonal environment.

A parastem is the main morphological characteristic feature of *Changchengia stipitata*, occurring at the base of the thalli. Such structures are well-preserved in both Saraipali (Figures 5.2, 5.3, 5.8) and Chhuipali specimens (Figures 5.4–5.7). The presence of a disc-like structure at the parastem base suggests *C. stipitata* belonged to a benthic habitat. Our interpretation for the parastem of *Changchengia stipitata* is that it helped to anchor the algal thalli on the bottom, protecting it from current movement in the water.

Genus: Chuaria. Walcott, 1899; Vidal and Ford, 1985.

Type species: Chuaria circularis. Walcott, 1899; Vidal and Ford, 1985.

Chuarua circularis. Walcott, 1899; Vidal and Ford, 1985.

Figures 5.9–5.11

Stratigraphic position: The Saraipali and Chhuipali Formations, the Singhora Group.

Material: Twenty (20) specimens from the Surangi River section, southwest of Saraipali Township; and fifteen (15) specimens from the Bendla Dongar section, north of Saraipali Township, Mahasamund District, Chhattisgarh, India.

Description: Isolated, flattened, smooth, circular to subcircular black carbonaceous compressions or impressions. Two-dimensionally preserved discs, ranging from 0.5 to 0.8 mm in diameter.

Remarks: Specimens of *Chuarua circularis* recorded from the Chhattisgarh Supergroup are morphologically similar in type and material to those from China, Canada, Russia, and other localities, including India. The specimens consist of impressions and compressions of carbonized material, deposited and compacted between the bedding planes or parallel to the laminations of rock. It is one of the few globally-distributed carbonaceous specimens extensively reported from Palaeoproterozoic to Neoproterozoic sediments (Hofmann, 1994; Dutta et al., 2006; Sharma et al., 2009). Carbonaceous discs without wrinkles, documented by the Uinta Mountain Group, were also designated as *Chuarua circularis* (Hofmann, 1977). In later reports, carbonaceous discs with or without wrinkles were globally demonstrated as *Chuarua circularis* (Yuan et al., 2001; Kumar and Srivastava, 2003; Sharma et al., 2009; Ye et al., 2019). It has also been interpreted as a colonial cyanobacterium, based on its putative association with Nostoc-like filaments (Sun, 1987; Steiner, 1997); or as a multicellular eukaryote because of its excystment opening and a potentially complex life cycle (Kumar, 2001; Sharma et al., 2009; Wang et al., 2011; Tang et al., 2017). Specimens with medial structures are demonstrated as polyphyletic in origin (Butterfield et al., 1994; Sharma et al., 2009). Sharma et al. (2009) proposed a hybrid model for the *Chuarua-Tawuia* association and suggested that the biogeopolymer of *Chuarua* is similar to the algaenan macromolecules of many algae species. Recent analysis using backscattered-electron scanning electron microscopy (BSE-SEM) revealed that *Chuarua* may have had a multicellular vegetative stage in its life cycle (Tang et al., 2017).

Genus: Eopalmaria. Yan, 1995.

Type species: Eopalmaria pristina. Yan, 1995.

Eopalmaria pristina. Yan, 1995.

Figures 5.13–5.16

Stratigraphic position: The Saraipali and Chhuipali Formations, the Singhora Group.

Material: Eight (08) specimens from the Surangi River section, southwest of Saraipali Township, and five (05) specimens from the Bendla Dongar section, north of Saraipali Township, Mahasamund District, Chhattisgarh, India.

Description: Unbranched elongate, flat, sheet-like algal thalli, with a wide and uneven apex, foliate, angular to subangular at the base. The measured specimens range between 0.5–6.0 mm long and 0.5–1.50 mm wide. Parastem-like stipes are absent at its base.

Remarks: *Eopalmaria pristina* was originally described as a palmate-shaped carbonaceous compression from the ca.

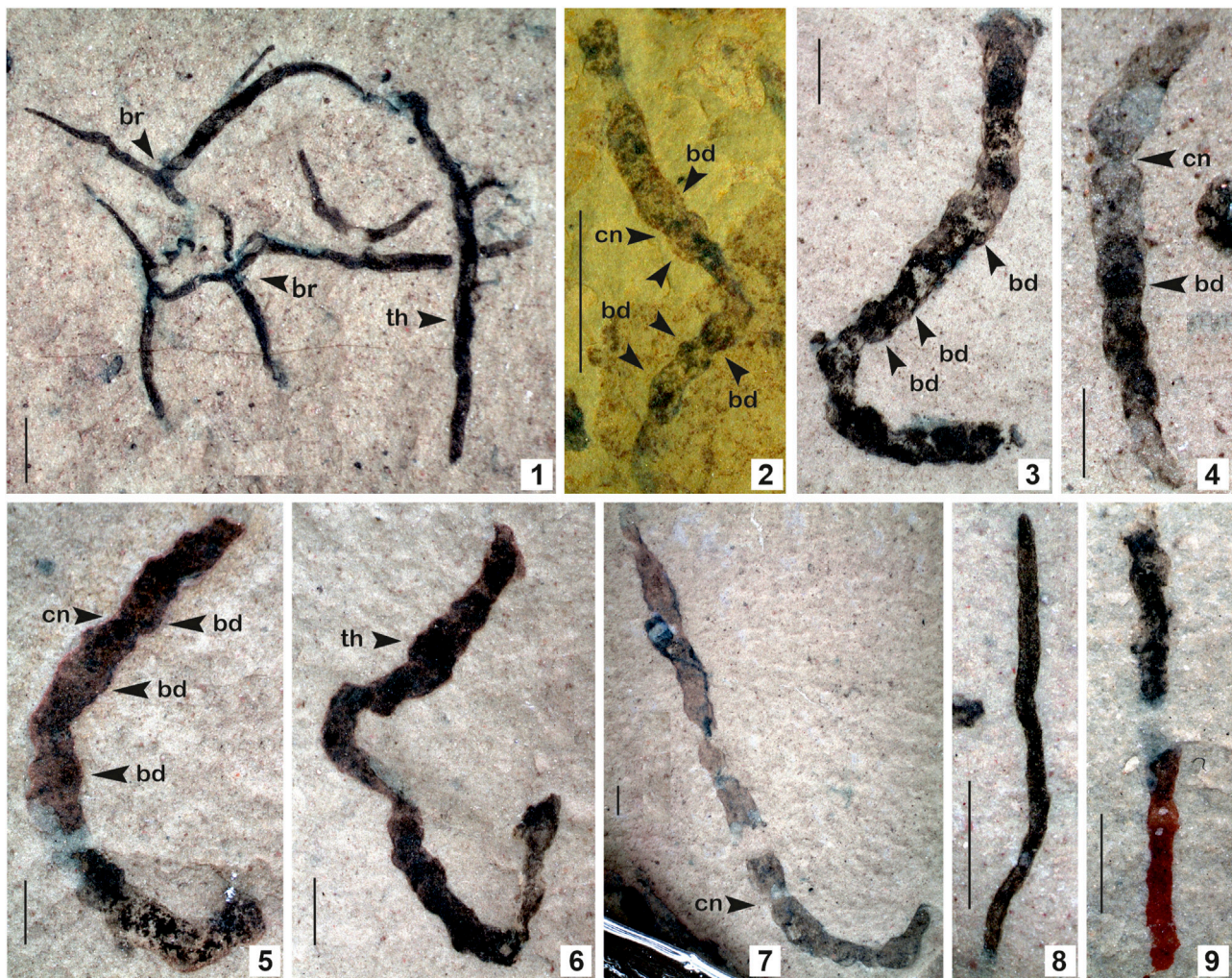


FIGURE 6 | 1. *Eoholynia corumbensis* Gaucher et al., 2003; **2–7.** *Jiuqunaoella sergeevii* n. sp.; **8–9.** *Synocylindra yunnanensis* Chen and Erdtmann, 1991. (Arrow indicates the prominent features: br. branching; bd. bead; cn. constriction; th. thallus). 1. Specimen no. BSIP 42028; 2. Specimen no. BSIP 39782; 3. Specimen no. BSIP 42032; 4. Specimen no. BSIP 41898; 5. Specimen no. BSIP 42029; 6. Specimen no. BSIP 42035; 7. Specimen no. BSIP 42027; 8. Specimens no. BSIP 42037; 9. Specimens no. BSIP 42041. Specimens 1, 3–9 from the Bendla Dongar section and 2 from the Surangi River section. Scale bar is 1.0 mm for each specimen.

1,637 Ma Tuanshanzi Formation of the Changcheng Group of China (Yan, 1995). In size and morphological characteristics, the present specimens are similar to the biota known from the latest Palaeoproterozoic Olive Shale, Semri Group, Vindhyan Supergroup, India (Sharma, 2006). *E. pristina* is morphologically comparable to the modern algae *Rhodomenia palmata* of the algal group *Rhodophyta*, *Spathoglossum* of the *Phaeophyta*, and *Monostroma* among the *Chlorophyta* (Yan and Liu, 1997).

Genus: *Eoholynia*. Gnilovskaya, 1975.

Type species: *Eoholynia mosquensis*. Gnilovskaya, 1975.

Eoholynia corumbensis. Gaucher et al., 2003.

Figure 6.1.

Stratigraphic position: The Chhuipali Formation, the Singhora Group.

Material: Single specimen from the Bendla Dongar section, north of Saraipali Township, Mahasamund District, Chhattisgarh, India.

Description: Dichotomously branched, non-septate, ribbon-like carbonaceous thallus, 05–06 branches in the thallus. Primary branches give rise to secondary branches. Secondary branches are sharply tapered at the end. The length of the complete specimen is 3–18 mm, approximately 0.1–0.4 mm wide.

Remarks: Similar carbonaceous compressions have been documented from the Neoproterozoic Guaicurus Formation of the Corumba Group, Brazil (Gaucher et al., 2003). Branches of *E. corumbensis* are wider than *E. mosquensis* (Gnilovskaya, 1979). Based on morphological characters, the biological affinity of *Eoholynia* is assigned to eukaryotic algae, probably of *Phaeophyta* or *Rhodophyta* (Hofmann, 1994; Burzin, 1996). *E. corumbensis* is considered probably benthic, as has been suggested for *E. mosquensis* (Gnilovskaya, 1975). *Miaohephyton bifurcatum* Steiner (1994)—a morphologically similar fossil to *E. corumbensis*—has also been placed among the brown algae (*Phaeophyta*) (Xiao et al., 1998). Subsequently,

Eoholynia was placed among the vendotaenid algae (Gaucher et al., 2003).

Genus: *Jiuqunaoella* Chen. Chen and Xiao, 1991, emend. Xiao in Xiao et al., 2002.

Type species: *Jiuqunaoella simplicis* Chen. Chen and Xiao, 1991, emend. Xiao et al., 2002.

Jiuqunaoella sergeevii n. sp.

Figures 6.2–6.7.

Type locality: Surangi River section, southwest of Saraipali Township, Mahasamund District, Chhattisgarh, India.

Type specimen: **Figure 6.2**, Specimen No. BSIP 39782.

Stratigraphic position: Carbonaceous shale of the Saraipali and Chhuipali Formations, the Singhora Group.

Material: 10 specimens: two (02) specimens from the Surangi River section, southwest of Saraipali Township; and eight (08) specimens from the Bendla Dongar section, north of Saraipali Township, Mahasamund District, Chhattisgarh, India.

Derivation of species name: In honour of the Late Prof. Vladimir N. Sergeev, Russian Academy of Sciences, Moscow, for his significant contribution to the field of Precambrian Palaeobiology.

Diagnosis: Ribbon-like carbonaceous compressions consist of a regular series of distinct chamber-like segments arranged in a beaded manner. Filaments are twisted and folded, having more or less parallel margins.

Description: Refer to the diagnosis. Ribbons are 4.0–11.0 mm long and 0.5–1.0 mm wide. The diameter of the chamber ranges from 0.5 to 1.0 mm.

Remarks: Chen (in Chen and Xiao, 1991) established the genus *Jiuqunaoella* with its type species *Jiuqunaoella simplicis*, from the Ediacaran Doushantuo Formation, Miaohu Village, in Hubei Province, China. In the absence of a type repository for the species, it was considered an invalid taxon. Later, Chen (in Xiao et al., 2002) revised the diagnosis of this genus and retained it as a genuine fossil in the Ediacaran Miaohu biota, assigned and compared with coenocytic green algae. The carbonaceous compression assigned to the new species *Jiuqunaoella sergeevii* in the Lower Mesoproterozoic Saraipali Formation differs from the type species *Jiuqunaoella simplicis* by its chamber-like segments arranged in a beaded manner (**Figure 6.2**). Such morphotypes are also known as *Eosolenides* from upper Mesoproterozoic Lakhanda mudstone. Morphologically, *Eosolenides* fossils are fragments of an elongate, benthic, apparently soft-bodied, double-walled, tubular organism attached to its underlying substrate (German and Podkovyrov, 2009). A possible interpretation is that the ribbons of *J. sergeevii* may be a remnant of *Eosolenides*. In size, it is different from other ribbon-like carbonaceous compressions, such as *Tyrasotaenia* and *Cyanocylindra*. We assigned it to coenocytic green algae, as suggested by Xiao et al. (2002). Carbonaceous ribbons with similar features are recorded from the Chhuipali Formation of the Singhora Group exposed at the Bendla Dongar section of the study area (**Figures 6.3–6.7**).

Genus: *Sinocylindra*. Chen and Erdtmann, 1991.

Type species: *Sinocylindra yunnanensis*. Chen and Erdtmann, 1991.

Sinocylindra yunnanensis. Chen and Erdtmann, 1991.

Stratigraphic position: The Chhuipali Formations, the Singhora Group.

Material: Two specimens from the Bendla Dongar section, north of Saraipali Township, Mahasamund District, Chhattisgarh, India.

Description: Smooth, ribbon-like carbonaceous compression, twisted and folded. Both margins are more or less parallel. Specimens bear uneven and closely-spaced transverse nodes. Terminus ends of the ribbon are rounded. The ribbons are 3.0–4.0 mm long and up to 0.2 mm wide.

Remarks: The genus *Sinocylindra* differs from other ribbon-like carbonaceous compressions, such as *Tyrasotaenia* and *Jiuqunaoella* in the Chhuipali biota, by its rounded terminus and more or less parallel wall margins. The carbonaceous ribbons assigned to *Sinocylindra yunnanensis* show a close resemblance to Miaohu specimens of China (Xiao et al., 2002). Chen and Erdtmann (1991) established the genus *Sinocylindra* with its species *Sinocylindra yunnanensis* from the Ediacaran Doushantuo Formation of China (Chen and Erdtmann, 1991). Xiao et al. (2002) suggested that it may be part of multicellular algae such as *Chaetomorpha* (green), *Nemalion* (red), or *Chorda* (brown), and also suggested an individual status rather than the cyanobacterial sheath *Siphonophycus*. *Sinocylindra* is well-known in the carbonaceous fossil assemblages of the Ediacaran to Cambrian periods. Its occurrence in the Mesoproterozoic Chhuipali Formation (1.3 Ga) indicates its antiquity is ~400 Ma earlier in the Proterozoic biosphere.

Genus: *Tuanshanzia*. Yan, 1995.

Type species: *Tuanshanzia fasciaria* (Yan). Yan and Liu, 1997.

Tuanshanzia fasciaria (Yan). Yan and Liu, 1997.

Figures 7.1–7.6.

Stratigraphic position: The Saraipali and Chhuipali Formations, the Singhora Group.

Material: Twenty-five (25) specimens from the Surangi River section, southwest of Saraipali Township, and ten (10) specimens from the Bendla Dongar section, north of Saraipali Township, Mahasamund District, Chhattisgarh, India.

Description: Unbranched, taeniote algal thallus, with rotundate apex, slightly tapering toward its base, smooth margins, thin, parastem absent. The thallus is moderately folded or twisted. Measured specimens are 4.0–18.5 mm in length and 0.25–0.5 mm in width.

Remarks: The specimens of the present species in Singhora macroalgae are smaller than those from the Tuanshanzi Formation of the Changcheng Group (~1,637 Ma) in Jinxian, Hubei, China (Yan and Liu, 1997). In size, they are similar to specimens of the Olive Shale, Semri Group, Vindhyan Supergroup (Sharma, 2006). Parastem-like structures are absent in both the algal thalli of *T. fasciaria* and *T. lanceolata*. Yan and Liu (1997) emended the genus *Tuanshanzia*, pointing out it can be distinguished from *Changchengia* by its lack of stalk-like parastem structure. They suggested that its species can be differentiated by their distinct morphology. It represents sessile

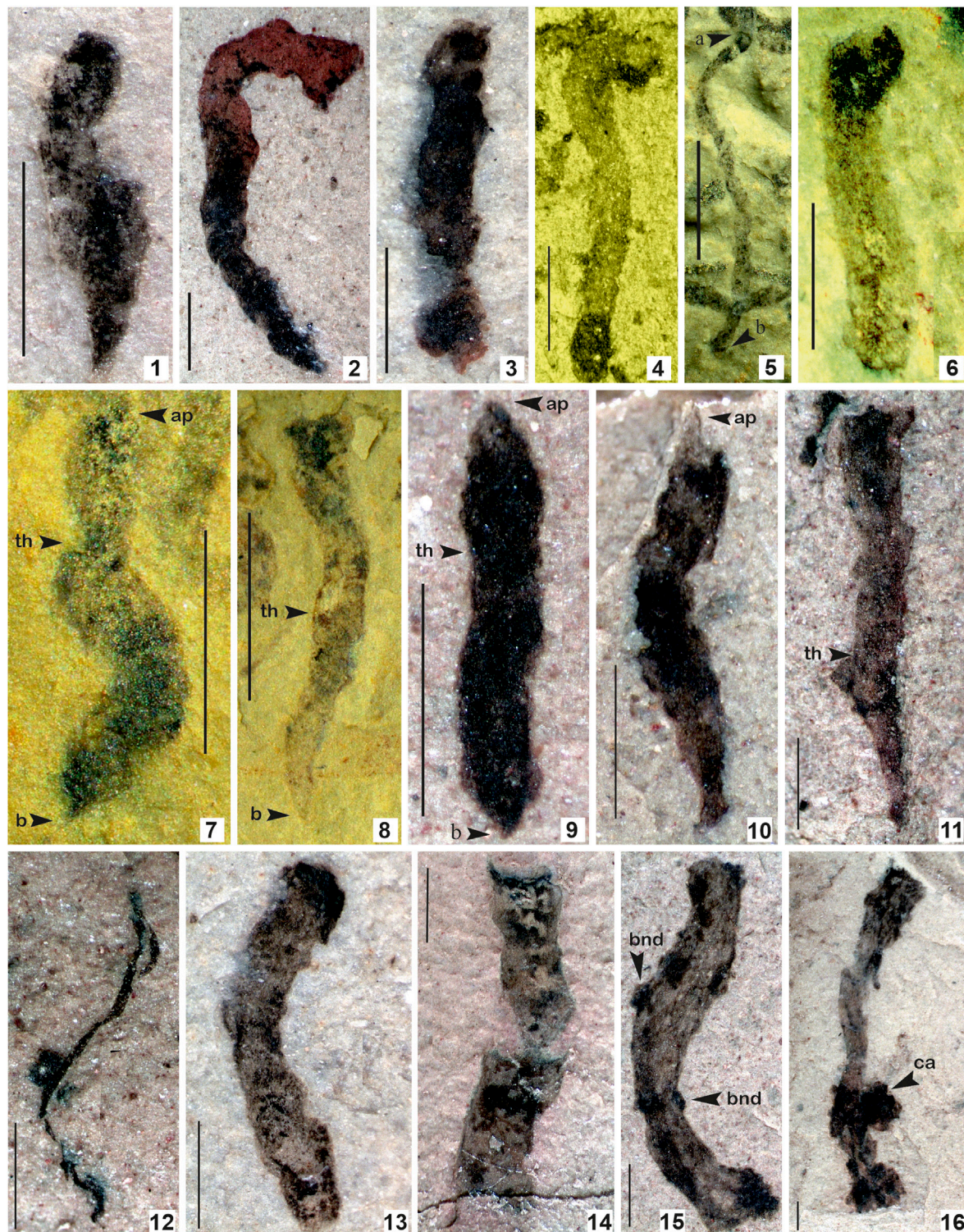


FIGURE 7 | 1–6. *Tuanshanzia fasciaria* (Yan) Yan and Liu, 1997; **7–11.** *Tuanshanzia lanceolata* Yan, 1995; **12.** *Tyrasotaenia podolica* Gnilevskaya, 1971; **13–16.** Unnamed ribbon-like film comprised of small conical/circular projection on the surface. (Arrow indicates the prominent features: bnd. Branching node; ca. colonial aggregates; th. thallus) 1. Specimen no. BSIP 42040; 2. Specimen no. BSIP 42039; 3. Specimens no. BSIP 42041; 4. Specimen no. BSIP 39777; 5. Specimen no. BSIP 39780; 6. Specimen no. BSIP 39769; 7. Specimen no. BSIP 39769; 8. Specimen no. BSIP 39782; 9. Specimen no. BSIP 42028; 10. Specimen no. BSIP 42036; 11. Specimen no. BSIP 42043; 12. Specimen no. BSIP 42025; 13. Specimen no. BSIP 42033b; 14. Specimen no. BSIP 42031; 15. Specimen no. BSIP 42045a; 16. Specimen no. BSIP 42044. Specimens 1–3, 9–16 from the Bendla Dongar section and 4–8 from the Surangi River section. Scale bar is 1.0 mm for each specimen.

frond-like algal thalli with bilaterally symmetrical and flat structures.

Tuanshanzia lanceolata. Yan, 1995.

Figures 7.7–7.11

Stratigraphic position: The Saraipali and Chhuipali Formations, the Singhora Group.

Material: Ten specimens from the Surangi River section, southwest of Saraipali Township, and fifteen specimens from the Bendla Dongar section, north of Saraipali Township, Mahasamund District, Chhattisgarh, India.

Description: Broad sheet-like lanceolate algal thallus, moderately folded, smooth edges, widest in the middle, twisted, narrowing, and tapering toward both ends (Figures 7.7, 7.9, 7.10). The distal end of the thallus is incomplete in some specimens (Figures 7.8, 7.11), its parastem absent. Sheets are 3.0–8.0 mm long and 0.25–0.8 mm wide.

Remarks: The present form is morphologically comparable to known specimens of the Tuanshanzi Formation (~1637 Ma) of the Changcheng Group, China (Yan, 1995), the Olive Shale Semri Group, and the Vindhyan Supergroup (Sharma, 2006). It is comparatively smaller than original specimens. Flattened sheet-like compression resembles the tubular thallus of some of the Phaeophyta, viz., *Siphonales* (*Dictyosiphonales*) and green algae Ulvales. Some specimens in the Bendla Dongar section are characterized by a rusty color, probably resulting from oxidation or removal of organic matter.

Genus: *Tyrasotaenia*. Gnilovskaya 1971.

Type species: *Tyrasotaenia podolica*. Gnilovskaya, 1971.

Tyrasotaenia podolica. Gnilovskaya, 1971.

Figure 7.12.

Stratigraphic position: The Chhuipali Formations, the Singhora Group.

Material: Only six (6) specimens from the Bendla Dongar section, north of Saraipali Township, Mahasamund District, Chhattisgarh, India.

Description: Solitary, unbranched, long cylindrical filaments, more or less straight and parallel, occasionally folded and curved. Measured specimens are 2–4 mm long and 0.1–0.2 mm thick.

Remarks: The ribbon-like carbonaceous fossil *Tyrasotaenia* was initially recorded from the fine-grained clastic sediments of the 900 Ma Russian Platform (Gnilovskaya, 1971) and later from the 1,300 Ma Belt Supergroup, Montana (Walter et al., 1976); Little Dal Group, Mackenzie Mountains, Northwestern Canada (Hofmann and Aitken, 1979). In India, such types of carbonaceous filaments are known from the Proterozoic Vindhyan Supergroup (Shukla and Sharma, 1990; Sharma, 2006; Sharma et al., 2016). Based on its morphological similarity to stalks of Chorda and Scytosiphon belonging to the Phaeophyta, *Tyrasotaenia podolica* may be a remnant of benthic macroalga/seaweeds.

Unnamed Forms

Figures 7.13–7.16.

Stratigraphic position: The Chhuipali Formation, the Singhora Group.

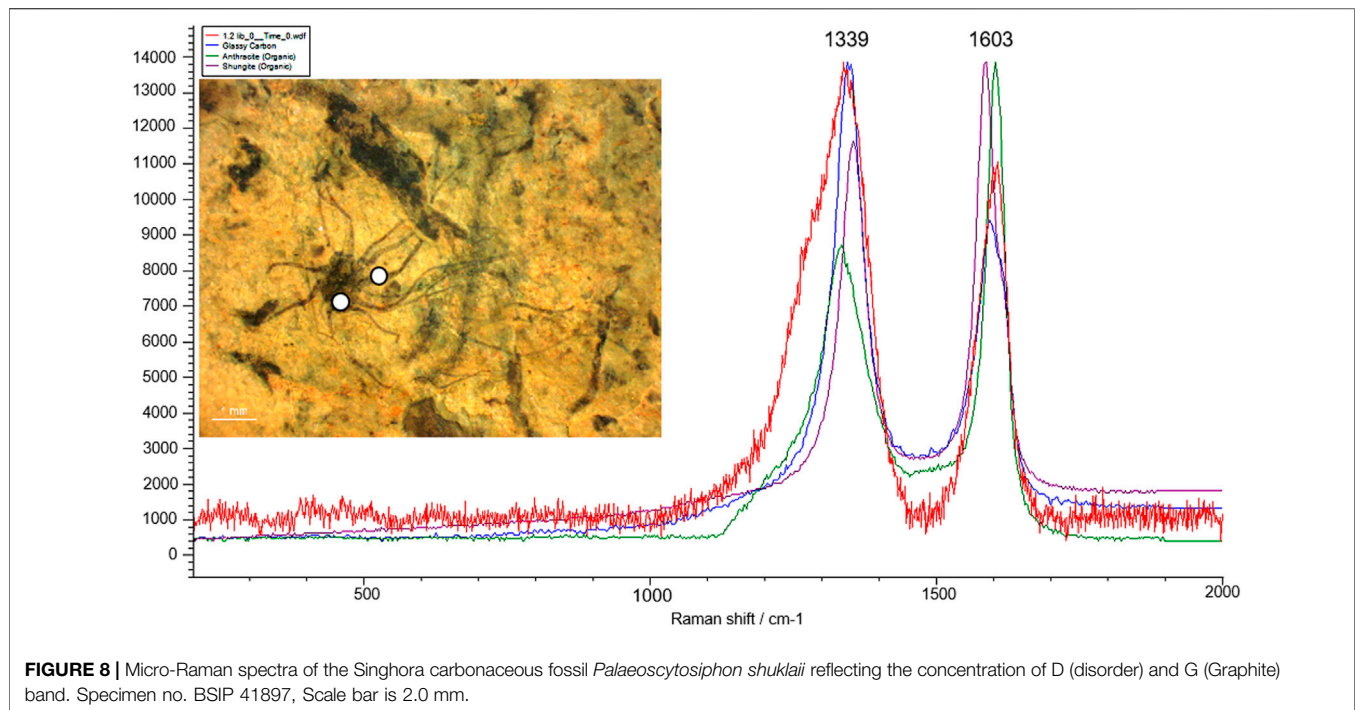
Material: Five incomplete specimens from the Bendla Dongar section, north of Saraipali Township, Mahasamund District, Chhattisgarh, India.

Description: Compressed ribbon-like tubular structures with more or less parallel sidewalls, comprised of small protrusions projected and evenly distributed over the ribbon. Terminal margins of ribbon are straight. Projections in Figure 7.15 seem to be broken nodes of branching. Protrusions seem to be colonial aggregates of small coccoids (Figure 7.16). The thickness of the ribbon is up to 1.0 mm and the protrusion is up to 0.2 mm in diameter. Specimens are incomplete.

Remarks: The Bendla Dongar section contains many incompletely preserved ribbon-like tubular compressions. Some ribbons are comprised of more or less parallel margins similar to filamentous cyanobacteria *Siphonophycus*. However, ribbons are much larger than the *Siphonophycus* (Figures 7.13, 7.14). Some ribbon-like compressions comprise small protrusions projected and evenly distributed over the ribbon (Figure 7.15). These seem to be a node of further branching in the organism. The terminal margins of the ribbons are straight. Some specimens hold bunches of carbonaceous aggregates projected on the terminal end or sometimes in the middle (Figure 7.16).

Raman Spectroscopy

Over the last few decades, *in situ* techniques, including Laser Raman Spectroscopy (LRS), Fourier Transform Infrared Spectroscopy (FTIR), Secondary Ion Mass Spectroscopy (SIMS), and Atomic Force Microscopy (AFM) have been employed to understand the cellular morphology, ultrastructure, and chemical composition of organic matter preserved in these carbonaceous compressions (Javaux and Marshall, 2006; Oehler et al., 2006; Marshall et al., 2007; Schopf et al., 2010; Kilburn and Wacey, 2015; Delarue et al., 2018; Wacey et al., 2019). To understand the biogenicity and geochemical maturity of the carbonaceous films, selected specimens were analyzed using Laser Raman Spectroscopy. Laser Raman Spectroscopy is a non-intrusive, non-destructive analytical approach to investigate carbon compounds in Precambrian carbonaceous matter (Schopf et al., 2005). *In situ* Raman analysis on fossil materials at different targeted regions revealed the presence of 1,322 cm⁻¹–1,356 cm⁻¹ and 1,599 cm⁻¹–1,608 cm⁻¹ spectral bands, which indicate the level of graphitization in the form of D (Disordered peak) and G (Graphite peak) bands of organic carbon. Additionally, micro-Raman spectra of newly instituted carbonaceous fossil *P. shuklaii* included the D-band (Disordered band) at 1,339 cm⁻¹ and G-band (Graphite band) at 1,603 cm⁻¹ (Figure 8). This variation in the spectral band is caused by due vibration of complex carbon molecular structures, uneven surfaces, and dangling bonds (Qu et al., 2018). The obtained spectra and the positions and width of the D and G bands are characteristic of organic carbon, as revealed in Figure 8. The other best-matched minerals are glassy carbon and Shungite. Shungite is an elementary noncrystalline mineraloid of biogenic origin comprised of 98% carbon. The Raman spectra analysis and comparisons with available records (Noffke et al., 2013; Qu et al.,



2018; Shukla et al., 2019) show that the Singhora films are typically carbonaceous and have a biogenic origin. The carbonaceous fossil composition is also corroborated by Raman first-order spectra organic-walled microfossils (OWMs) embedded in the host rock, which are dominated by distinct D and G bands of carbon (**Supplementary Figure S3**) supporting the syngeneity of cellular remains within the host rock. On the basis of fossil colour preservation fidelity, the Raman Index of Preservation (RIP) value of kerogen is 8.5 (Schopf et al., 2005).

Energy Dispersive X-ray Spectroscopy (EDX) in the SEM

The Energy Dispersive X-ray Spectroscopy (EDX) technique was applied to understand the chemical composition of the carbonaceous macroalgae. The results of EDX elemental mapping conducted on the Saraipali macroscopic carbonaceous fossils are illustrated in **Figure 9**. Elemental mapping reveals distinctive differences in composition between the matrix and the fossils. Analysis of the fossiliferous shale matrix demonstrates consistently high concentrations of aluminum (Al-11.28%), oxygen (O-50.98%), and silicon (Si-26.27%) relative to other elements (K-3.01% and Fe-1.93%). However, the concentration of carbon (C-6.54%) in shale matrix silicon (Si) is not enriched relative to the matrix (**Figure 9.2**). On the other hand, EDX analysis of carbonaceous fossil material demonstrates strong carbon enrichment (C-63.40%) relative to other elements, viz., oxygen (O-32.33%), silicon (Si-2.54%), aluminum (Al-1.06%), potassium (K-0.32%) and iron (Fe-0.36%) (**Figure 9.1**). Similarly, the Chhuipali macrofossils are preserved on a khaki shale bedding surface and are easily distinguishable from the shale matrix by

their darker colour. The elemental composition of the shale matrix is the same as Saraipali Shale (**Figure 9.2**). Most of the fossils preserved are robust, continuous carbonaceous films as compressions/impressions.

EDX results reveal that the studied fossil material of macroalgae are typically composed of carbon, and indicates *in situ* preservation in aluminosilicate clay mineral-bearing rocks. Weathered macrofossils are easily visible due to the strong contrast between the dark fossils and the buff-coloured shale matrix. Aluminosilicate clay elements (Si and Al) are exhausted in the fossils relative to the matrix. Both the acid maceration and EDX elemental mapping analyses show elevated organic carbon enrichment in the fossils relative to the rock matrix. Further, this mode of preservation suggests Burgess Shale-type preservation for these macroscopic fossils (Butterfield, 1995; Gaines et al., 2008; Orr et al., 2009; Wang et al., 2014). Recently, based on morphological and EDX studies, Dornbos et al. (2016) have also suggested Burgess Shale-type fossil preservation for macroscopic filaments *Chinggiskhaania bifurcata* and *Zuunartsphyton delicatum* recorded from the upper Ediacaran and Cambrian Zuun-Arts Formations, Mongolia.

DISCUSSION

Biogenicity of the Singhora Carbonaceous Fossils

In the present study, the extensively well-preserved Singhora carbonaceous compressions and impressions show distinct ribbon-shaped, leaf-shaped, fan-shaped morphology with putative stipes and/or holdfast structures preserved on the bedding surface of the host rock. These carbonaceous remains are found preserved in

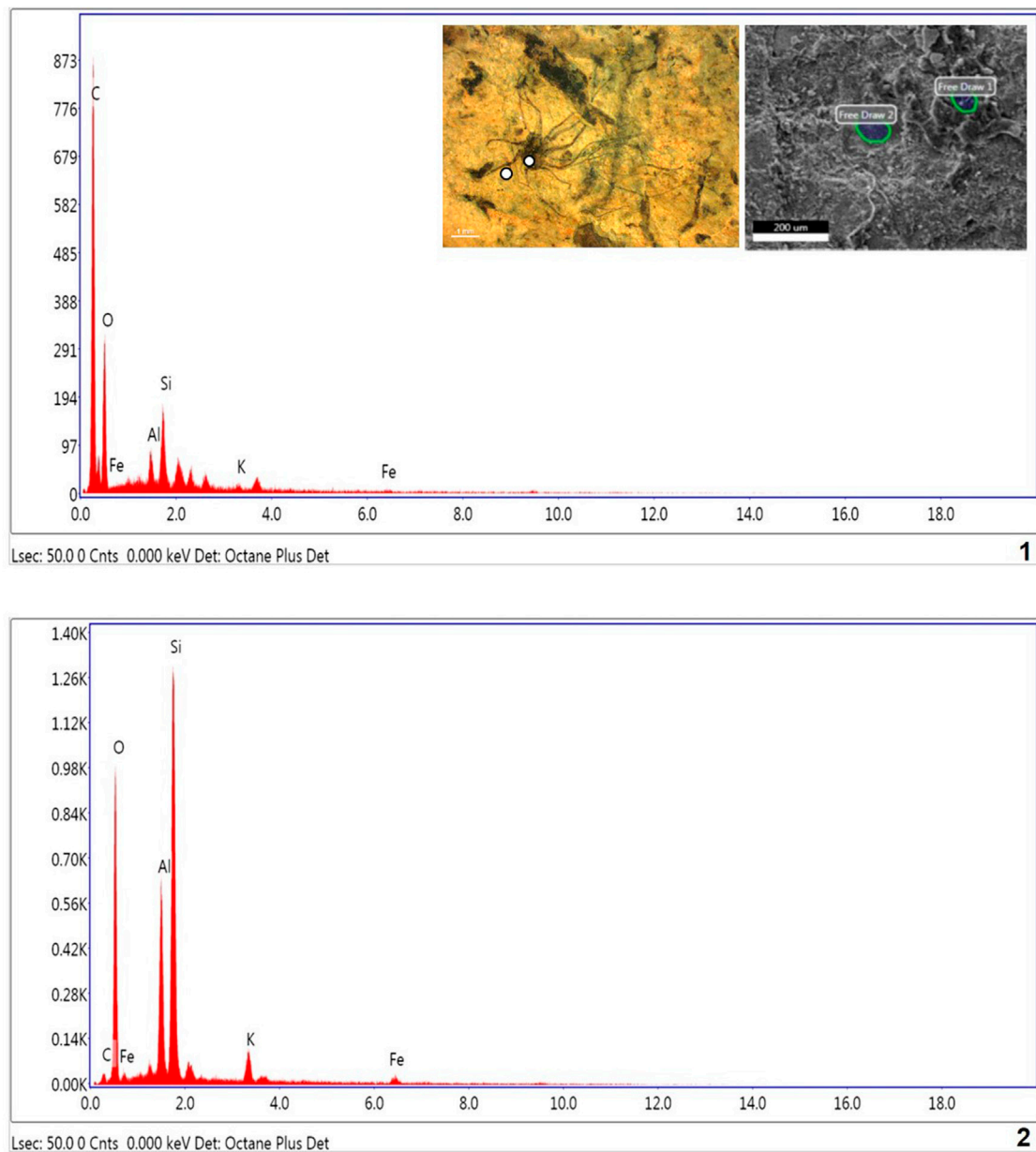


FIGURE 9 | EDX spectra of Singhara carbonaceous compressions and host rock. **1.** Macroscopic film shows high concentration of C and low concentration of other elements respectively. Presence of high carbon in fossils indicated carbonaceous and organic nature of fossils.; **2.** Shale matrix: showing high concentration of Al, Si, O, K, and Fe elements and partial concentration of Si, indicating host rock is aluminosilicate clay.

multiple layers in regularly repeated forms (see **Supplementary Figures S4–S6**). Gross morphology and preservation behaviour of the Singhara assemblage show close resemblance to ~1,637 Ma Tuanshanzi and ~1,560 Ma Gaoyuzhuang carbonaceous assemblages of China (Zhu and Chen 1995; Yan and Liu, 1997; Zhu et al., 2016). The Tuanshanzi Formation in Northern China is characterized by millimeter to centimeter-sized scattered carbonaceous compressions of irregular or indeterminate shape (ribbons and blades), interpreted as seaweed specifically attributed to Phaeophyta (Yan 1995; Zhu and Chen 1995; Yan and Liu, 1997)

mainly based on varied morphology. The Gaoyuzhuang carbonaceous fossils are decimeter sized, regular, and strongly elongated (Zhu et al., 2016). Based on their size, shape, and chemical structure investigation, both the Chinese assemblages are considered benthic multicellular eukaryotes (Zhu et al, 2016; Qu et al., 2018).

Due to the lack of well-preserved cellular structures, carbonaceous compression fossils are often challenged for their biogenicity (Zhu et al., 2016). Among them, the Tuanshanzi carbonaceous fossils are the most debated. Knoll et al. (2006) have

questioned the seaweed affinity proposed for the Tuanshanzi fossils, interpreting them as rare, fortuitously-shaped fragments re-deposited among irregular mat shards. They have also been interpreted as macroalgae with holdfast-stipe-blade differentiation, but their variable morphologies appear to suggest that some of them may be fragmented algal mats (Xiao and Dong, 2006). Butterfield (2009), based on their lack of regularly repeated forms and angular margins, considered the carbonaceous films a part of the fragmented microbial mats. Likewise, the biogenicity of the Singhora carbonaceous compression fossils can also be questioned. But due care was applied in recovering the Singhora fossil material. The Singhora carbonaceous compressions have rounded algal thalli (Figures 5.14–5.16; Figure 7.1), angular distal ends (Figures 5.4–5.7, 5.12; Figures 7.9–7.11) and twisted and folded sheets (Figures 5.2, 5.3, 5.8; Figure 7.7). These features make the Singhora carbonaceous fossils true Phaeophytic fossils. Two possible interpretations of the Tuanshanzi fossils' angular margins are that they either represent the original shape of the algae, or their distal ends were twisted and overlapped during or after the burial process. The same interpretation may hold for the Singhora carbonaceous fossils.

A substantial number of macroscopic compressions, impressions, and casts are globally known in rocks of the latest Palaeoproterozoic and early Mesoproterozoic ages (Hofmann and Chen, 1981; Han and Runnegar, 1992; Kumar, 1995; Zhu and Chen, 1995; Yan and Liu, 1997; Zhu et al., 2000; Rai and Singh, 2006; Sharma, 2006; Zhu et al., 2016). Millimeter to centimeter-sized carbonaceous compressions with a diverse range of shapes, varying from circular, elongate, filamentous, to complex branching, recorded on the bedding plane surfaces of the Proterozoic successions, are reviewed by Hofmann (1992). Most of them are claimed as “multicellular eukaryotes” (Xiao et al., 2002; Knoll et al., 2006; Xiao and Dong, 2006; Zhu et al., 2016; Sharma and Singh, 2019; Bykova et al., 2020). Palaeoproterozoic carbonaceous macroscopic fossils, including the circular, elliptical, elongate, and irregularly shaped carbonaceous compressions often described as *Chuaria*, *Shouhsienia*, and *Tawuia* from the ca. 1,800 Ma Changzhongou and Chuanlinggou Formations in northern China (Hofmann and Chen 1981; Zhu et al., 2000), were claimed as megascopic eukaryotes and the oldest representatives of multicellular organisms (Zhu et al., 2000). Further investigations of the original material, including plane light investigations of thin sections and acid maceration, the petrographic study of thin sections, SEM, EDS, CHN, XRD, and biomarker analyses, indicate that Changzhongou compressions are clasts composed of clays or phosphates with little carbon, as typically found in pseudo-fossils instead of multicellular structures (Lamb et al., 2007). However, interpreting biogenic origins and affinities for many of these carbonaceous fossils remains relatively controversial because they lack well-preserved pigments and cellular structures (Hofmann, 1994; Knoll et al., 2006; Xiao and Dong, 2006; Lamb et al., 2007; Butterfield, 2009; El Albani et al., 2010; Knoll, 2011).

Recently, Qu et al. (2018) have reinvestigated chemical, isotopic, and molecular-structural features of organic matter

from the carbonaceous films of the Tuanshanzi Formation, using *in situ* Raman Spectroscopy, FTIR, and organic carbon isotopic composition, to determine the affinity of carbonaceous compressions. These were interpreted as the oldest putative macroscopic multicellular eukaryotes by Zhu and Chen (1995). The results of Raman Spectroscopy and carbon isotopic composition of organic remains from the Tuanshanzi carbonaceous compressions demonstrate unambiguous benthic eukaryotic macroalgae and have experienced only advanced diagenesis (Qu et al., 2018). They further suggest that the Tuanshanzi Formation carbonaceous compressions imply higher oceanic oxygen concentrations during the Palaeo- and Mesoproterozoic than previously estimated. Similarly, well-preserved sheets of organic fragments extracted through acid maceration of the fossiliferous samples infer organized multicellularity for the Singhora fossils (Supplementary Figure S3). The organic fragments are dark brown, show various optical densities under transmitted light microscopy, demonstrating thermally-altered organic matter composition (anthracitic carbon). Further, the Raman spectra (D and G bands) of the carbonaceous material approximately equate organic fragments within the host rock. The Singhora carbonaceous compressions record a modest diversity of macroscopic photosynthetic multicellular eukaryotes syngeneic in nature.

Mode of Preservation and Taphonomy of Singhora Carbonaceous Fossils

Several different modes of preservation, specifically silicification, pyritization, phosphatization, carbonaceous compressions/impressions, and cast and mold preservation are established for most exceptionally-preserved micro and macroorganisms. Carbonaceous compressions/impressions are mainly responsible for preserving most macroalgae and organic-walled microfossils (OWMs) embedded in shales and siltstone of the Proterozoic successions. Our understanding of carbonaceous compression fossil preservation from the Palaeo- and Mesoproterozoic strata is inadequate due to limited records of macroalgae, particularly non-calcified macroalgae, unusual taphonomic conditions, and conflicts in taxonomic assignments (Lamb et al., 2007). The taphonomic biases contribute to the scanty fossil record of Proterozoic macroalgae.

We analyzed more than 200 specimens of macrofossils of the Singhora Group of rocks containing various branched and unbranched carbonaceous films with two-dimensional to three-dimensional morphological details (Table 2). Taphonomically, the Singhora macroalgal fossils described here are typically preserved as two-dimensional compressional elements (i.e., branches and stipes). Many of them have an elevated concentration of organic carbon, attesting to their preservation as carbonaceous compressions. Both the Saraipali and Chhuipali specimens are also enriched in aluminosilicates. Framboidal pyrite is conspicuously missing in both assemblages. Some specimens in the Chhuipali Shale show a reddish colour from where the carbon film has been detached, but they are easily distinguished from the rock matrix (Figure 5.4, Figure 6.9,

TABLE 2 | Megascopic carbonaceous macroalgae from the Saraipali and Chhuipali Formations of the Singhora Group.

Mega fossils/Species	Overall morphology	Interpretation
<i>Baculiphyca taeniata</i>	Algal thallus with rhizoidal or globose holdfast	Eukaryotic alga
<i>Palaeoscytosiphon shuklaji</i> n. gen., n. sp.	Numerous ribbons attached with rhizoidal holdfast	Eukaryotic alga
<i>Changchengia stipitata</i>	Algal thallus with prominent parastem	Eukaryotic alga
<i>Eopalmaria pristina</i>	Palmate shape algal thallus with wide uneven apex	Eukaryotic alga
<i>Tuanshanzia fasciaria</i>	Algal thallus with rotundate apex and tapered base, parastem absent	Eukaryotic alga
<i>Tuanshanzia lanceolata</i>	Lanceolate algal thallus, both ends tapered	Eukaryotic alga
<i>Tyrasotaenia podolica</i>	Thin ribbon-like thallus, fragment of macroalgae	Eukaryotic alga?
<i>Eoholynia corumbensis</i>	Dichotomously branched, ribbon-like thallus	Eukaryotic alga
<i>Jiuqunaoella sergeevii</i> n. sp.	Ribbon-like thallus with chamber-like segments arranged in a beaded manner	Green alga
<i>Synocylindra yunnanensis</i>	Ribbon-like carbonaceous compression with uneven and closely-spaced transverse nodes	Eukaryotic alga?

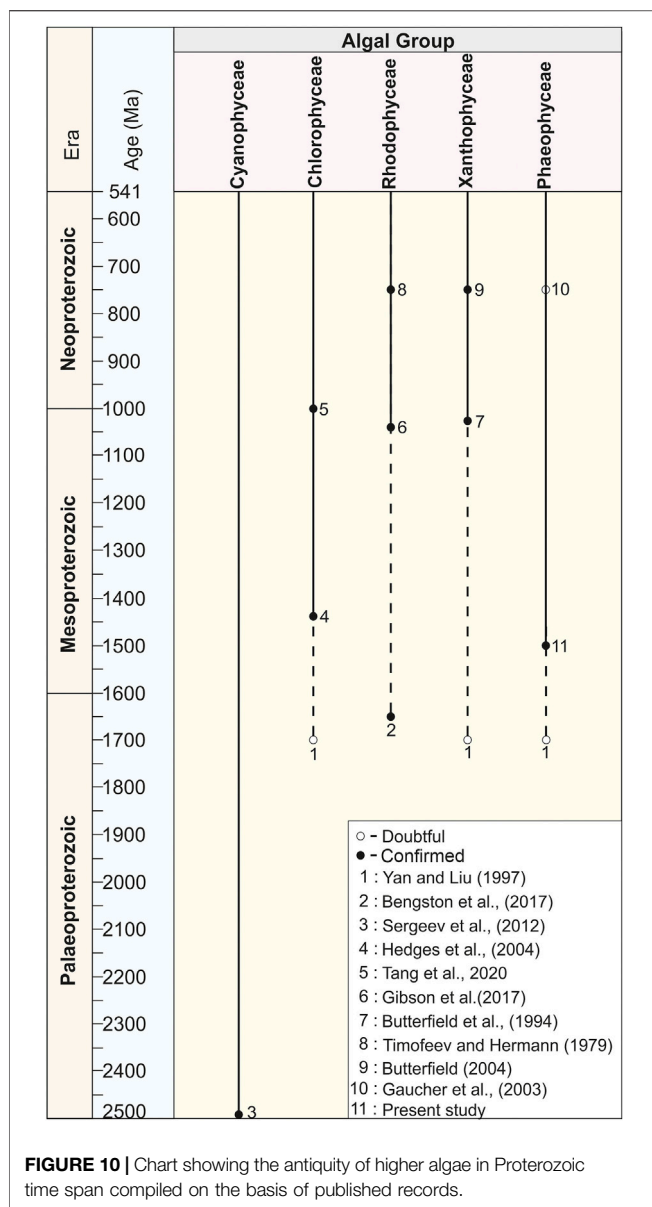
Figure 7.2). Most macrofossils in the Singhora assemblage are preserved as carbonaceous compressions through kerogenization, as confirmed by acid macerations, Laser Raman Spectroscopy (Singh et al., 2019) and Energy Dispersive X-ray Spectroscopy elemental mapping analysis, which resulted in high organic carbon enrichment in the fossils compared to the rock matrix (discussed in the text). EDX results revealed that the studied macroalgae fossil material from the Singhora Group is typically composed of carbon and indicates *in situ* preservation in aluminosilicate clay mineral-bearing rocks. Additionally, Singhora carbonaceous compression macrofossils are characterized by mixed kerogenization and aluminosilicification. Overall, this mode of preservation meets the requirements of Burgess Shale-type (BST) preservation for the carbonaceous compressions of the Singhora Group (Butterfield, 1995; Gaines et al., 2008; Orr et al., 2009; Wang et al., 2014; Ye et al., 2019). Globally, BST is considered exemplary of non-mineralizing organism preservation in fully marine siliciclastic sediments (Butterfield, 1995; Anderson et al., 2011). Several hypotheses for taphonomic pathways, viz., kerogenization, pyritization, and aluminosilicification provide insights to understanding BST preservation in most recorded fossil assemblages. However, in many cases, these processes are found in the same fossil assemblage and sometimes even in the same specimen (Cai et al., 2012).

Affinity and Biostratigraphic Significance

An extensively well-preserved variety of macroscopic carbonaceous compressions and impressions are recorded from the Saraipali and Chhuipali Formations of the Mesoproterozoic Singhora Group. These are demonstrably macroalgal fossils and provide information about a new level of algal evolution in the Proterozoic biosphere. Similar megascopic carbonaceous fossils were recorded earlier, from the ca. 1,637 Ma Ma Tuanshanzi Formation from the Changcheng Group of Jixian, China, and termed Tuanshanzian Macroscopic Algae (Yan, 1995; Yan and Liu, 1997; Knoll et al., 2006; Xiao and Dong, 2006; Butterfield, 2009). Based on their considerably large size and varied shapes, they were considered the oldest benthic and eukaryotic multicellular algae (Yan, 1995). The lanceolate thalli of *Tuanshanzia lanceolata* and *Tuanshanzia fasciaria* were described as sessile frond-like algal thalli with bilaterally

symmetrical and flat structures compared to certain species of *Petalomia* among the *Phaeophyta* and *Enteromorpha* or *Monostroma* among the *Chlorophyta* (Yan and Liu, 1997). Similarly, the palmate shape thallus of *Eopalmaria pristina* was linked with *Palmaria/Porphyra/Rhodymenia* among the *Rhodophyta* (Yan and Liu, 1997) and also with *Monostroma* among the *Chlorophyta* (Yan, 1995) and *Spathoglossum* among the *Phaeophyta* (Yan and Liu, 1997). The affinity of broad ribbon-like thallus with short parastem *Changchengia stipitata* was interpreted as a benthic metaphyte (Yan and Liu, 1997). Based on diversification, Yan and Liu (1997) have suggested a neritic, lagoon-like environment under a brackish-water habitat for the Tuanshanzian assemblage. The Saraipali and Chhuipali megascopic algae closely resemble Tuanshanzian specimens, but are relatively smaller in size. The ribbon-like thin tubular films of *Tyrasotaenia podolica* are also considered benthic remnants of *Scytosiphon* among the *Phaeophyta* (Yan and Liu, 1997). Based on megascopic size, thallus nature, and possible parastem-like features, carbonaceous films recorded from the Late Palaeoproterozoic to Early Mesoproterozoic Olive Shale were attributed to eukaryotic algae (Sharma, 2006). Based on its thallus, Steiner (1994) has placed *Tyrasotaenia* in synonymy with *Vendotaenia*.

The Saraipali and Chhuipali assemblages also contain taxonomically well-established megascopic carbonaceous films: namely, *Baculiphyca taeniata* (Yuan et al., 1995), *Cyanocylindra yunnanensis* (Chen and Erdtmann, 1991), and *Eoholynia corumbensis* (Gaucher et al., 2003), primarily known from the Ediacaran successions. A rhizoidal holdfast-bearing carbonaceous film, *Baculiphyca taeniata*, was compared with remnants of green algae, including the *Siphonocladales* and *Dasycladales*. However, due to their simple tubular morphology, Xiao et al. (2002) interpreted the ribbon-like tubular films of *Cyanocylindra yunnanensis* as filamentous cyanobacteria, although they have also placed this form under eukaryotic algae based on a size larger than the *Siphonophycus Schopf*. Similarly, the multi-branched carbonaceous film *Eoholynia corumbensis* is considered an eukaryotic algae, probably remnants of *Phaeophyta* or *Rhodophyta* (Hofmann 1994; Burzin, 1996). The occurrence of such Neoproterozoic complex morphologies in the Mesoproterozoic shales of the Singhora Group of the Chhattisgarh Supergroup predates their antiquity to earlier in time.



Apart from these fossils, the Saraipali Shale contains two new carbonaceous fossil taxa, namely *Palaeoscytosiphon shuklaii* n. gen., n. sp., and *Jiuqunaoella sergeevii*, n. sp. Preservation behaviour suggests that *P. shuklaii* is attributed to benthic multicellular algae *Scytosiphon lomentaria* belonging to family *Scytosiphonaceae* among the class *Phaeophyceae* (brown algae) (Figure 4). *Scytosiphon lomentaria* is a yellowish-brown or dark brown alga, comprised of hollow unbranched cylindrical stipes, up to 400 mm long and 3–10 mm wide. Stalks narrow at the end, with a wider base attached by a rhizoid-like short holdfast (Figure 2). *Scytosiphon lomentaria* most commonly occurs in the upper shore pool and grows on limpets, rocks, and wave-exposed shores. It is considered a model species for life history and molecular studies of brown algae.

The ribbon-like carbonaceous film *Jiuqunaoella sergeevii* consists of many bladder-shaped cells arranged in a beaded

manner. In its global occurrence, *Jiuqunaoella* is widely known for the Ediacaran successions of China (Xiao et al., 2002; Ye et al., 2019). Its bladder-shaped beaded arrangement distinguishes *Jiuqunaoella sergeevii*. These bladder-like structures occur in the thallus, which enable it to receive more light for photosynthesis. In the Miaohu assemblage of the Doushantuo Formation, *Jiuqunaoella simplicis* was reconstructed as a sausage-like cylindrical tube, similar to some coenocytic green algae (Xiao et al., 2002; Ye et al., 2019). The specimens of *Jiuqunaoella* in the Singhara carbonaceous compressions are also characterized by ribbon-like structures with distinct chamber-like circular segments arranged in a beaded manner. Such complex morphological characteristics, including cell-to-cell connections, qualify *J. sergeevii* as a multicellular microorganism. Its degree of morphological differentiation and preservation behaviour reveals that the Saraipali and Chhuipali carbonaceous fossils are attributed to multicellular eukaryotes, similar to Palaeoproterozoic–Mesoproterozoic Tuanshanzi and Gaoyuzhuang carbonaceous fossil assemblages (Yan and Liu, 1997; Zhu et al., 2016), although their exact phylogenetic affinities are comparable to benthic seaweeds belonging to modern algae *Phaeophyceae* and *Chlorophyceae* (Xiao and Dong, 2006; Ye et al., 2019).

In this study, the Singhara carbonaceous compressions exhibit various morphologies, including fan-shaped, palmate, elongated, leaf-like, and ribbon-like, their algal thalli with/without holdfast at the base, with rounded and angular distal ends, isolated or dichotomously branched long tube-like cylindrical axis, along with multicellular reproductive structures. The holdfast's role is to anchor the algal thallus on a hard substrate, protecting it from the currents that qualify their benthic habit, which is also consistent with brown algae (Zhu and Chen, 1995; Qu et al., 2018). Furthermore, their micro-macro morphologies and the results of Laser Raman Spectroscopy of the Singhara carbonaceous compressions share similarities with previously-known fossil materials, which are interpreted as multicellular eukaryotes (Xiao et al., 2002; Zhu et al., 2016; Qu et al., 2018; Zhang S. et al., 2021) and biogenic. Assignment to the multicellular eukaryotic fossils for the Singhara macroalgal carbonaceous compression also supports interpretations of early macroscopic multicellular eukaryote evolution in sulphidic and low-oxygenated Palaeo- and Mesoproterozoic oceans (Zhu et al., 2016; Qu et al., 2018; Bykova et al., 2020).

Antiquity of Carbonaceous Films

Our understanding of eukaryotes's early evolution and diversification in Precambrian Palaeobiology, specifically multicellular macroalgae, is meager in both fossil and biomarker records. It is difficult to define the antiquity and evolution of fossilized remains in deep time, due to the rare occurrence of morphological and anatomical characters with those found in living forms (Butterfield, 2007). Available phylogenetic records suggest that eukaryotes may have first evolved in freshwater environments at the Palaeoproterozoic–Mesoproterozoic transition (Blank, 2013). However, most of the fossil record supports their evolution in marine

environments (Yan and Liu, 1997; Rai and Singh, 2006; Sharma, 2006; Bengtson et al., 2017; Qu et al., 2018). They extended into marine environments in the Tonian Period due to dramatic changes in the marine biological pump, food webs, and benthic habitats (Sanchez-Baracaldo et al., 2017; Del Cortona et al., 2020; Tang et al., 2020; Maloney et al., 2021).

The antiquity of macroalgae in deep time has also been discussed in several publications (Butterfield, 2001; Knoll et al., 2006; Butterfield, 2009, 2015; Knoll, 2015; Zhu et al., 2016; Bengtson et al., 2017; Tang et al., 2020; Zhang F. et al., 2021; Zhang S. et al., 2021; Tang et al., 2021). Globally, there are only a handful of published Proterozoic records of higher multicellular algae, as illustrated in **Figure 10**. Of these, the antiquity of some reports is considered confirmed (genuine) on the basis of distinct morphological and ultrastructural studies. Whereas the antiquity of a few macroalgae is unclear (doubtful) in the absence of distinct skeleton and taphonomic biases.

Several distinct types of micro and macro fossils are recorded after the Great Oxidation Event (GOE) from the Proterozoic succession and claimed as eukaryotes of the oldest antiquity (Retallack et al., 2013; Singh and Sharma, 2014). Eukaryotic fossils recorded from different formations of the world trace their antiquity from ~2,200 Ma to ~1800 Ma, such as the urn-shaped discoidal body of the *Diskagma buttonii* from the ~2,200 Ma Palaeosols of South Africa (Retallack et al., 2013); the coiled carbonaceous megascopic fossil *Grypania* from the ~1870 Ma Negaunee Iron-Formation, Michigan (Han and Runnegar, 1992; Schneider et al., 2002) and the string-of-beads morphology of *Horodyskia* from the 1,500 Ma Backdoor Formation of the Collier Group, Australia are assigned as the Oldest Known Tissue-Grade Colonial Eukaryote (Fedonkin and Yochelson, 2002; Grey et al., 2010). However, Sharma and Shukla (2009b) have established that *Grypania* was prokaryotic. Later, in a review, Knoll et al. (2006) considered the *Horodyskia* as a problematic macrofossil whose eukaryotic affinity is probable but not beyond debate. Similarly, decimeter to millimeter-scale carbonaceous ribbons and blades were recorded from the ~1700 Ma to ~1,600 Ma shales of the Changcheng Group, China (Yan and Liu, 1997; Gao et al., 2011; Zhu et al., 2016) and ~1,600 Ma Olive Shale Formation, India (Sharma, 2006), and ~1,500 Ma Singhora Group, India (Babu and Singh, 2013) were also claimed as eukaryotic fossils. However, their affinity with green, brown, and red algae is not confirmed in the absence of favorable diagnostics (**Figure 10**). Existing compilations of global taxonomic diversity suggest that eukaryotic fossils with complex morphology began to appear in the late Palaeoproterozoic. An eukaryotic nature has also been claimed for the large (>100 µm) sphaeromorphic acritarchs documented from the ~1800 Ma Changzhougou Formation, North China (Lamb et al., 2009). Singh and Sharma (2014) have documented the oldest eukaryotic body fossil, *Shuiyousphaeridium*, from the latest Palaeoproterozoic-early Mesoproterozoic (>1,600 Ma) succession of the Chitrakoot Formation of the Vindhyan Supergroup, India. Similar fossils were known from younger sequences (1744 Ma–1,639 Ma) of the Ruyang Group, China (Yin, 1997; Pang et al., 2020), and (1,500 Ma – 1,400 Ma)

Roper Group, Australia (Javaux, 2007; Javaux and Knoll, 2017). Therefore, at present, the Chitrakoot acritarchs are possibly the oldest eukaryotic remains in the world. Attempts have been made in this direction after the first record of extant Bangiophyte red algae *Bangiomorpha pubescens* from the late Mesoproterozoic (~1,200 Ma) Hunting Formation of Canada (Butterfield, 2000; Gibson et al., 2018). In the fossil records before the Cryogenian (c. 800 Ma), the *Bangiomorpha pubescens* was the only taxonomically unresolved crown-group eukaryote considered the earliest known expression of extant multicellular forms and eukaryotic photosynthesis (Butterfield, 2000; Cohen and Macdonald, 2015). Recently, based on Re-Os geochronology, a precise ~1,047 Ma age has been set for the origin of *Bangiomorpha pubescens* (Gibson et al., 2018) (**Figure 10**). In addition, Bengtson et al. (2017) have reported uniquely well-preserved fossils interpreted as probable crown-group rhodophytes from the ~1,650 Ma Tirohan Dolomite of the lower Vindhyan (Semri Group) sediments of Son Valley in the Chitrakoot region (**Figure 10**). This report includes the discovery of two new fossils: namely, *Rafatazmia chitrakootensis*, *Denaricion mendox* and lobate form *Ramathallus lobatus*. Demonstrably, *Rafatazmia* is a non-branching filamentous thallus that has uniserial rows of large cells, which grow through diffusely distributed septation. This report predated the minimum age of the last eukaryotic common ancestor (LECA) and increased the antiquity of rhodophytes by about 400 Ma (Butterfield, 2015). However, in the absence of distinct pit plugs within the cells, red algae's affinity with the fossil *Rafatazmia* is questionable (Carlisle et al., 2021). Recently, Tang et al. (2020) have predated the antiquity of chlorophyte algae (green algae) ~200 Ma after reporting the multicellular macroscopic carbonaceous compression filamentous fossil *Proterocladus antiquus* from the ~1,000 Ma Nanfen Formation of the Xihe Group, China (**Figure 10**). The *Proterocladus* was originally known from the early Neoproterozoic (Tonian) Swanbergfjellet Formation, Spitsbergen (Butterfield et al., 1994) (**Figure 10**). Together with its large size and morphology, integrated isotopic, geochemical, and ultrastructural studies on carbonaceous compressions of the ~1,630 Ma Tuanshanzi Formation of North China support that the early benthic macroscopic multicellular eukaryotes evolved and prevailed in the sulphidic and low-oxygenated Palaeo- and Mesoproterozoic oceans (Qu et al., 2018). Cyanobacteria is long-ranging and considered a primary producer in Proterozoic Photosynthetic microorganisms (Sergeev et al., 2012) (**Figure 10**).

The fossil records of *Phaeophyta* (brown algae) evolution in the Precambrian successions are not well established. This is due to a generally soft-bodied nature and little occurrence of calcified taxa. A few millimeters of long carbonaceous compressions, typically preserved as flattened outlines or fragments, have been described from Ediacaran successions and their possible affinity as *Phaeophyta* claimed. The carbonaceous macroalga *Eoholynia* (Gnilovskaya, 1975)—a cord or ribbon-like branched thallus, known from Vendian deposits in Russia, was considered eukaryotic algae remains. Its possible affinity was assigned as *Phaeophyta* or *Rhodophyta*

(Gaucher et al., 2003). Similarly, based on the morphological and taphonomic assessment of *Miaohephyton bifurcatum* carbonaceous compressions—dichotomously branched multicellular thalli, known from the Ediacaran Doushantuo Formation, China—Steiner placed them among the brown algae (Xiao et al., 1998). Available records suggest that Phaeophytes may have diverged much later (the Mesozoic) in the geological past compared with red and green algae. In previous publications, claims have been made for many carbonaceous compressions as *Phaeophyta*, documented from the Mesozoic, Palaeozoic, and Ediacaran successions (Loeblich, 1974; Fry, 1983). However, the taxonomic affinity of these impression fossils is far from certain and has been discarded in the absence of key morphological characteristics (Kawai and Henry, 2016).

In the present study, two well-preserved macroscopic carbonaceous compression fossils: namely, *Palaeoscytosiphon shuklaii* n. gen., n. sp., and *Jiuqunaoella sergeevii*, n. sp., are described for the first time from the Saraipali Formation of the Singhora Group. Carbonaceous compressions of the fossil *P. shuklaii* represent all morphological characters in a single specimen, characterized by ribbon/tubular filaments with a distinct holdfast, sharing a similar morphology to the modern brown algae *Scytosiphon lomentaria* (Figure 7). Nevertheless, our present observations on *Palaeoscytosiphon*'s palaeobiologic affinities require a more detailed study that would exceed the scope of this study.

Similarly, carbonaceous compressions of *Eoholynia corumbensis* Gaucher et al. assigned as remains of eukaryotic algae are probably the class *Phaeophyceae* (brown algae)/*Rhodophyceae* (red algae) and considered as benthic seaweeds (Gnilovskaya, 1979; Gnilovskaya et al., 1988; Hofmann, 1994). Further, the present findings also suggest that the *Phaeophyta* evolved during the early Mesoproterozoic Era (~1,500 Ma) instead of the previously suggested late Neoproterozoic (Gnilovskaya, 1975) (Figure 10). In addition, these studies also support the molecular clock analyses that suggest the divergence of *Phaeophyta*, *Rhodophyta*, and *Viridiplantae* in the Palaeoproterozoic–Mesoproterozoic Eras. Further, the crown-group Chlorophyta diverged during the late Mesoproterozoic to early Neoproterozoic eras; however, siphonous, multicellular, and siphonocladous chlorophytes evolved repeatedly in the late Neoproterozoic and Palaeozoic (Tang et al., 2020; Maloney et al., 2021).

CONCLUSIONS

In summary, abundant macroscopic carbonaceous compressions and impressions of macroalgal fossils, attributed to benthic seaweeds, are recorded from the shales and siltstone of the Saraipali and Chhuipali Formations of the Mesoproterozoic Singhora Group, Chhattisgarh Supergroup, India. The presence of exceptionally well-preserved distinct complex morphological features, including holdfasts, parastem, and thalli of different shapes and sizes suggest that

the Singhora carbonaceous compressions are derived from the stem group of eukaryotic macroalgae. Two new taxa, *Palaeoscytosiphon shuklaii* n. gen., n. sp. (*Phaeophyta*), and *Jiuqunaoella sergeevii* n. sp. are established for the first time in the present finding. *P. shuklaii* n. gen., n. sp., *Eoholynia corumbensis* and *Tyrasotaenia podolica* most likely belong to brown algae (*Phaeophyceae*). If our interpretations are correct, both forms may predate the antiquity of *Phaeophyta* in the early Mesoproterozoic Era (~1,500 Ma). Analysis using Laser Raman Spectroscopy (LRS) and Energy Dispersive X-ray Spectroscopy (EDX) of fossiliferous material demonstrate that the Singhora carbonaceous compressions of macroalgae are typically made up of organic carbon. Additionally, high carbon enrichment and depletion of Al, Si, K, and O in the carbonaceous compressions, as well as high enrichment of Al, Si, Fe, O, and K and low carbon in the shale matrix qualifies Burgess Shale-type preservation (BST) for the studied carbonaceous remains. Further, the carbonaceous macrofossils from the rocks of the Singhora Group provide evidence of benthic macroalgae inhabited in the shallow water of the low-oxygenated Mesoproterozoic Ocean.

DATA AVAILABILITY STATEMENT

The original contributions presented in the study are included in the article/Supplementary Material. Further inquiries can be directed to the corresponding author.

AUTHOR CONTRIBUTIONS

VS and MS conceived and designed the project. VS undertook multiple field visits in different localities for the collection of samples, placed them in the proper stratigraphic order, completed the initial scanning of the carbonaceous films from the rock slab. Both authors discussed the implications of the data and finalized the manuscript.

FUNDING

The field and laboratory work of the authors was supported by the Birbal Sahni Institute of Palaeosciences.

ACKNOWLEDGMENTS

The authors are indebted to the Director of the Birbal Sahni Institute of Palaeosciences (BSIP) for providing necessary laboratory and library facilities and giving permission to publish this study (BSIP/RDCC/03/2022–23). Archana Sonker, Shivalee Srivastava, and Subodh Kumar are acknowledged for their assistance during geochemical characterization. The authors are grateful to reviewers for providing critical reviews and suggestions.

SUPPLEMENTARY MATERIAL

The Supplementary Material for this article can be found online at: <https://www.frontiersin.org/articles/10.3389/feart.2022.825430/full#supplementary-material>

Supplementary Figure S1 | Schematic drawings showing carbonaceous remains described from the Chhattisgarh Supergroup. **1–3, 5.** *Tuanshanzia lanceolata*; **4.** *Tuanshanzia fasciaria*; **6.** *Baculiphyca taeniata*; **7, 8.** *Changchengia stipitata*; **9.** *Chuarina circularis*; **10.** *Eopalmaria pristina*; **11.** *Tyrasotaenia podolica*; **12, 17.** *Jiuqunaella sergeevii* n. sp.; **13.** *Eoholynia corumbensis*; **14, 15.** Unnamed forms; **16.** *Synocylindra yunnanensis*. Scale bar is 1.0 mm for each.

Supplementary Figure S2 | Schematic drawing showing mode of preservation of *Palaeoscytosiphon shuklailai* at different stages (1–4). Scale bar is 2.0 mm for each.

REFERENCES

- Albani, A. E., Bengtson, S., Canfield, D. E., Bekker, A., Macchiarelli, R., Mazurier, A., et al. (2010/2002). Large Colonial Organisms with Coordinated Growth in Oxygenated Environments 2.1 Gyr ago Middle Proterozoic (1.5 Ga) *Horodyskia Moniliformis* Yochelson and Fedonkin, the Oldest Known Tissue Grade Colonial Eukaryote. *NatureSmithsonian Contributions Paleobiology* 46694 (73021–29), 100–104. doi:10.1038/nature09166
- Amard, B. (1992). Ultrastructure of *Chuarina* (Walcott) Vidal and Ford (Acritarcha) from the Late Proterozoic Pendjari Formation, Benin and Burkina-Faso, West Africa. *Precambrian Res.* 57, 121–133. doi:10.1016/0301-9268(92)90096-7
- Anderson, E. P., Schiffbauer, J. D., and Xiao, S. (2011). Taphonomic Study of Ediacaran Organic-Walled Fossils Confirms the Importance of Clay Minerals and Pyrite in Burgess Shale-type Preservation. *Geology* 39 (7), 643–646. doi:10.1130/G31969.1
- Arouri, K., Greenwood, P. F., and Walter, M. R. (1999). A Possible Chlorophycean Affinity of Some Neoproterozoic Acritarchs. *Org. Geochem.* 30 (10), 1323–1337. doi:10.1016/S0146-6380(99)00105-9
- Babu, R., and Singh, V. K. (2013). An Evaluation of Carbonaceous Metaphytic Remains from the Proterozoic Singhora Group of Chhattisgarh Supergroup, India. *Special Publication- Geol. Soc. India* 2013, 325–338.
- Babu, R., and Singh, V. K. (2011). Record of Aquatic Carbonaceous Metaphytic Remains from the Proterozoic Singhora Group of Chhattisgarh Supergroup, India and Their Significance. *J. Evol. Res.* 3 (5), 47–66.
- Bengtson, S., Sallstedt, T., Belivanova, V., and Whitehouse, M. (2017). Three-dimensional Preservation of Cellular and Subcellular Structures Suggests 1.6 Billion-Year-Old Crown-Group Red Algae. *PLoS Biol.* 15 (3), e2000735. doi:10.1371/journal.pbio.2000735
- Bickford, M. E., Basu, A., Patranabis-Deb, S., Dhang, P. C., and Schieber, J. (2011). Depositional History of the Chhattisgarh Basin, Central India: Constraints from New SHRIMP Zircon Ages. *J. Geol.* 119 (1), 33–50. doi:10.1086/657300
- Blank, C. E. (2013). Origin and Early Evolution of Photosynthetic Eukaryotes in Freshwater Environments: Reinterpreting Proterozoic Paleobiology and Biogeochemical Processes in Light of Trait Evolution. *J. Phycol.* 49 (6), 1040–1055. doi:10.1111/jpy.12111
- Brocks, J. J., Jarrett, A. J. M., Sirantoine, E., Hallmann, C., Hoshino, Y., and Liyanage, T. (2017). The Rise of Algae in Cryogenian Oceans and the Emergence of Animals. *Nature* 548 (7669), 578–581. doi:10.1038/nature23457
- Brodie, J., and Lewis, J. (2007). *Unravelling the Algae: The Past, Present, and Future of Algal Systematic*. 1st ed. Florida, US: CRC Press.
- Burzin, M. B. (1996). Late Vendian (Neoproterozoic III) Microbial and Algal Communities of the Russian Platform: Models of Facies-dependent Distribution, Evolution and Reflection of Basin Development. *Riv. Ital. Paleontol. Stratigr.* 102 (3), 307–316.
- Butterfield, N. J. (2001). Bias and Bonus: Fossil Preservation through the Precambrian-Cambrian Transition. *Am. Zoologist* 41 (6), 1404.
- Butterfield, N. J. (2000). Bangiomorpha Pubescens. gen., N. sp.: Implications for the Evolution of Sex, Multicellularity, and the Mesoproterozoic/Neoproterozoic Radiation of Eukaryotes. *Paleobiology* 26 (3), 386–404. doi:10.1666/0094-8373(2000)026<0386:bpngns>2.0.co;2
- Butterfield, N. J. (2015). Early Evolution of the Eukaryota. *Palaeontology* 58 (1), 5–17. doi:10.1111/pala.12139
- Butterfield, N. J., Knoll, A. H., and Swett, K. (1994). Paleobiology of the Neoproterozoic Svanbergfjellet Formation, Spitsbergen. *Fossils Strata* 34, 84. doi:10.1111/j.1502-3931.1994.tb01558.x
- Butterfield, N. J. (2007). Macroevolution and Macroecology through Deep Time. *Palaeontology* 50 (1), 41–55. doi:10.1186/1741-7007-2-1310.1111/j.1475-4983.2006.00613.x
- Butterfield, N. J. (2009). Modes of Pre-Ediacaran Multicellularity. *Precambrian Res.* 173 (1–4), 201–211. doi:10.1016/j.precamres.2009.01.008
- Butterfield, N. J. (1995). Secular Distribution of Burgess Shale-type Preservation. *Lethaia* 28 (1), 1–13. doi:10.1111/j.1502-3931.1995.tb01587.x
- Bykova, N., LoDuca, S. T., Ye, Q., Marusin, V., Grazhdankin, D., and Xiao, S. (2020). Seaweeds through Time: Morphological and Ecological Analysis of Proterozoic and Early Paleozoic Benthic Macroalgae. *Precambrian Res.* 350, 105875. doi:10.1016/j.precamres.2020.105875
- Cai, Y., Schiffbauer, J. D., Hua, H., and Xiao, S. (2012). Preservational Modes in the Ediacaran Gaojiazhan Lagerstätte: Pyritization, Aluminosilicification, and Carbonaceous Compression. *Palaeogeogr. Palaeoclimatol. Palaeoecol.* 326–328, 109–117. doi:10.1016/j.palaeo.2012.02.009
- Carlisle, E. M., Jobbins, M., Pankhania, V., Cunningham, J. A., and Donoghue, P. C. J. (2021). Experimental Taphonomy of Organelles and the Fossil Record of Early Eukaryote Evolution. *Sci. Adv.* 7 (5), eabe9487. doi:10.1126/sciadv.abe9487
- Chakraborty, P. P., and Barkat, R. (2020). A Status Report on Age, Depositional Motif and Stratigraphy of Chhattisgarh, Indravati, Kurnool and Bhima Basins, Peninsular India. *Pinsa* 86. doi:10.16943/ptinsa/2020/49801
- Chakraborty, P. P., Dey, S., and Mohanty, S. P. (2010). Proterozoic Platform Sequences of Peninsular India: Implications towards Basin Evolution and Supercontinent Assembly. *J. Asian Earth Sci.* 39 (6), 589–607. doi:10.1016/j.jseae.2010.04.030
- Chakraborty, P. P., Saha, S., and Das, P. (2015). Chapter 13 Geology of Mesoproterozoic Chhattisgarh Basin, Central India: Current Status and Future Goals. *Geol. Soc. Lond. Memoirs* 43, 185–205. doi:10.1144/M43.13
- Chakraborty, P. P., Sarkar, S., and Patranabis-Deb, S. (2012). Tectonics and Sedimentation of Proterozoic Basins of Peninsular India. *Proc. Indian Natl. Sci. Acad.* 78 (3), 393–400.
- Chakraborty, P. P., Tandon, S. K., Roy, S. B., Saha, S., and Paul, P. P. (2020). "Proterozoic Sedimentary Basins of India," in *Geodynamics of the Indian Plate* (Berlin, Germany: Springer), 145–177. doi:10.1007/978-3-030-15989-4_4
- Chen, J., and Erdtmann, B. D. (1991). *The Early Evolution of Metazoa and the Significance of Problematic Taxa*. Cambridge, UK: Cambridge University Press.
- Chen, M., and Xiao, Z. (1991). Discovery of the Macrofossils in the Upper Sinian Doushantuo Formation at Miaohu, Eastern Yangtze Gorges. *Sci. Geol. Sin.* 4, 317–324.
- Cohen, P. A., and Macdonald, F. A. (2015). The Proterozoic Record of Eukaryotes. *Paleobiology* 41 (4), 610–632. doi:10.1017/pab.2015.25
- Cooper, R. A., Jago, J. B., Mackinnon, D. I., Shergold, J. H., and Vidal, G. (1982). "Late Precambrian and Cambrian Fossils from Northern Victoria Land and

- Their Stratigraphic Implications," in *Antarctic Geoscience. 3rd Symposium on Antarctic Geology and Geophysics* (Madison: University of Wisconsin Press), 629–633.
- Das, D. P., Dutta, N. K., Dutta, D. R., Thanavellu, C., and Baburao, K. (2003). Singhora Group - the Oldest Proterozoic Lithopackage of Eastern Bastar Craton and its Significance. *Indian Miner.* 57 (3–4), 127–138.
- Das, D. P., Kundu, A., Das, N., Dutta, D. R., Kumaran, K., Ramamurthy, S., et al. (1992). Lithostratigraphy and Sedimentation of Chhattisgarh Basin. *Indian Miner.* 46 (3–4), 271–288.
- Das, K., Chakraborty, P. P., Horie, K., Tsutsumi, Y., Saha, S., and Balakrishnan, S. (2017). "Detrital Zircon U-Pb Geochronology, Nd Isotope Mapping, and Sediment Geochemistry from the Singhora Group, Central India," in *Sediment Provenance*. Editor R. Mazumder (Amsterdam, Netherlands: Elsevier), 403–451. doi:10.1016/b978-0-12-803386-9.00015-0
- Das, K., Yokoyama, K., Chakraborty, P. P., and Sarkar, A. (2009). Basal Tuffs and Contemporaneity of the Chhattisgarh and Khariar Basins Based on New Dates and Geochemistry. *J. Geol.* 117 (1), 88–102. doi:10.1086/593323
- Del Cortona, A., Jackson, C. J., Bucchini, F., Van Bel, M., D'hondt, S., Škaloud, P., et al. (2020). Neoproterozoic Origin and Multiple Transitions to Macroscopic Growth in Green Seaweeds. *Proc. Natl. Acad. Sci. U.S.A.* 117 (5), 2551–2559. doi:10.1073/pnas.1910060117
- Delarue, F., Robert, F., Tartèse, R., Sugitani, K., Tang, Q., Duhamel, R., et al. (2018). Can NanoSIMS Probe Quantitatively the Geochemical Composition of Ancient Organic-Walled Microfossils? A Case Study from the Early Neoproterozoic Liulaobei Formation. *Precambrian Res.* 311, 65–73. doi:10.1016/j.precamres.2018.03.003
- Dornbos, S. Q., Oji, T., Kanayama, A., and Gonchigdorj, S. (2016). A New Burgess Shale-type Deposit from the Ediacaran of Western Mongolia. *Sci. Rep.* 6, 23438. doi:10.1038/srep23438
- Du, R., Tian, L., and Li, H. (1986). Discovery of Megafossils in the Gaoyuzhuang Formation of the Chancheng System, Jixian. *Acta Geol. Sin.* 60, 115–119.
- Dutta, S., Steiner, M., Banerjee, S., Erdtmann, B.-D., Jeevankumar, S., and Mann, U. (2006). Chuaria Circularis from the Early Mesoproterozoic Suket Shale, Vindhyan Supergroup, India: Insights from Light and Electron Microscopy and Pyrolysis-Gas Chromatography. *J. Earth Syst. Sci.* 115 (1), 99–112. doi:10.1007/BF02703028
- Ford, T. D., and Breed, W. J. (1973). *probretical Precambrian fossils Chuaria Palaeontol.* 16, 533–550.
- Fry, W. L. (1983). An Algal Flora from the Upper Ordovician of the Lake Winnipeg Region, Manitoba, Canada. *Rev. Palaeobot. Palynology* 39 (3), 313–341. doi:10.1016/0034-6667(83)90018-0
- Gaines, R. R., Briggs, D. E. G., and Yuanlong, Z. (2008). Cambrian Burgess Shale-type Deposits Share a Common Mode of Fossilization. *Geol.* 36 (10), 755–758. doi:10.1130/g24961a.1
- Gao, L., Liu, P., Yin, C., Zhang, C., Ding, X., Liu, Y., et al. (2011). Detrital Zircon Dating of Meso- and Neoproterozoic Rocks in North China and its Implications. *Acta Geol. Sin. Engl. Ed.* 85, 271–282. doi:10.1111/j.1755-6724.2011.00397.x
- Gaucher, C., Boggiani, P., Sprechmann, P., Sial, A., and Fairchild, T. (2003). Integrated correlation of the Vendian to Cambrian Arroyo del Soldado and Corumbá Groups (Uruguay and Brazil): palaeogeographic, palaeoclimatic and palaeobiologic implications. *Precambrian Res.* 120 (3–4), 241–278. doi:10.1016/S0301-9268(02)00140-7
- German, T. N., and Podkovyrov, V. N. (2009). New Insights into the Nature of the Late Riphean Eosolenides. *Precambrian Res.* 173 (1–4), 154–162. doi:10.1016/j.precamres.2009.03.018
- Gibson, T. M., Shih, P. M., Cumming, V. M., Fischer, W. W., Crockford, P. W., Hodgskiss, M. S. W., et al. (2018). Precise Age of Bangiomorpha Pubescens Dates the Origin of Eukaryotic Photosynthesis. *Geology* 46 (2), 135–138. doi:10.1130/G39829.1
- Gnilovskaya, M. B. (1971). Drevnejšie Vodnye Rasteniya Venda Russkoj Platformy (The Oldest Vendian Aquatic Plants on the Russian Platform). *Palaeontol. Zhurnal* 3, 101–107.
- Gnilovskaya, M. B., Istchenko, A. A., Kolesniko, C. M., Korenchuk, L. V., and Udaltsov, A. P. (1988). *Vendotaenids of the East European Platform*.
- Gnilovskaya, M. B. (1975). Novye Dannye O Prirode Vendotenid (New Data on the Nature of Vendotaenids). *Dokl. Akad. Nauk. SSSR* 221 (4), 953–955.
- Gnilovskaya, M. B. (1979). The Vendian Metaphyta. *Bull. Centres Rech. Exploration-Production Elf-Aquitaine* 3 (2), 611–618.
- Gnilovskaya, M. B., Veis, A. F., Bekker, Y. R., Olovyanishnikov, V. G., and Raaben, M. E. (2000). Pre-Ediacarian Fauna from Timan (Annelidomorphs of the Late Riphean). *Stratigr. Geol. Correl.* 8 (4), 327–352.
- Grazhdankin, D. V., Balthasar, U., Nagovitsin, K. E., and Kochnev, B. B. (2008). Carbonate-hosted Avalon-type Fossils in Arctic Siberia. *Geol.* 36 (10), 803–806. doi:10.1130/G24946A.1
- Grazhdankin, D. V., Nagovitsin, K. E., and Maslov, A. V. (2007). Late Vendian Miaohe-type Ecological Assemblage of the East European Platform. *Dokl. Earth Sc.* 417 (1), 1183–1187. doi:10.1134/s1028334x07080107
- Grey, K., Yochelson, E. L., Fedonkin, M. A., and Martin, D. M. (2010). Horodyskia Williamsii New Species, a Mesoproterozoic Macrofossil from Western Australia. *Precambrian Res.* 180 (1–2), 1–17. doi:10.1016/j.precamres.2010.02.006
- Haines, P. W. (1998). Chuaria Walcott, 1899 in the Lower Wessel Group, Arafura Basin, Northern Australia. *Alcheringa Australas. J. Palaeontol.* 22 (1), 1–8. doi:10.1080/03115519808619235
- Han, T.-M., and Runnegar, B. (1992). Megascopic Eukaryotic Algae from the 2.1-Billion-Year-Old Negaunee Iron-Formation, Michigan. *Science* 257 (5067), 232–235. doi:10.1126/science.1631544
- Hofmann, H. J., and Altken, J. D. (1979). Precambrian Biota from the Little Dal Group, Mackenzie Mountains, Northwestern Canada. *Can. J. Earth Sci.* 16 (1), 150–166. doi:10.1139/e79-014
- Hofmann, H. J., and Jinbiao, C. (1981). Carbonaceous Megafossils from the Precambrian (1800 Ma) Near Jixian, Northern China. *Can. J. Earth Sci.* 18 (3), 443–447. doi:10.1139/e81-038
- Hofmann, H. J. (1992). "Proterozoic and Selected Cambrian Megascopic Carbonaceous Films," in *The Proterozoic Biosphere, a Multidisciplinary Study*. Editors J. W. Schopf and C. Klein (Cambridge: Cambridge University Press), 957–998.
- Hofmann, H. J. (1994). Proterozoic Carbonaceous Compressions ("metaphytes" and "worms"). *Early life earth* 84, 342–357.
- Hofmann, H. J., and Rainbird, R. H. (1994). Carbonaceous Megafossils from the Neoproterozoic Shaler Supergroup of Arctic Canada. *Palaeontology* 37 (4), 721–731.
- Hofmann, H. J. (1977). The Problematic Fossil Chuaria from the Late Precambrian Uinta Mountain Group, Utah. *Precambrian Res.* 4 (1), 1–11. doi:10.1016/0301-9268(77)90009-2
- Isson, T. T., Love, G. D., Dupont, C. L., Reinhard, C. T., Zumbeke, A. J., Asael, D., et al. (2018). Tracking the Rise of Eukaryotes to Ecological Dominance with Zinc Isotopes. *Geobiology* 16 (4), 341–352. doi:10.1111/gbi.12289
- Javaux, E. J., and Marshal, C. P. (2006). A New Approach in Deciphering Early Protist Paleobiology and Evolution: Combined Microscopy and Microchemistry of Single Proterozoic Acritarchs. *Rev. Palaeobot. Palynology* 139 (1–4), 1–15. doi:10.1016/j.revpalbo.2006.01.005
- Jensen, S., Palacios, T., and Martí Mus, M. (2007). A brief review of the fossil record of the Ediacaran-Cambrian transition in the area of Montes de Toledo-Guadalupe, Spain. *Geol. Soc. Lond. Spec. Publ.* 286, 223–235. doi:10.1144/SP286.16
- Kawai, H., and Henry, E. C. (2016). "Phaeophyta," in *Handbook of the Protists*. Editors J. M. Archibald, A. G. B. Simpson, C. H. Slamovits, L. Margulis, M. Melkonian, D. J. Chapman, et al. (Cham: Springer International Publishing), 267–304. doi:10.1007/978-3-319-32669-6_31-1
- Kilburn, M., and Wacey, D. (2015). Nanoscale Secondary Ion Mass Spectrometry (NanoSIMS) as an Analytical Tool in the Geosciences. *RSC Detect. Sci.* 2015, 1–34.
- Knoll, A. H., Javaux, E. J., Hewitt, D., and Cohen, P. (2006). Eukaryotic Organisms in Proterozoic Oceans. *Phil. Trans. R. Soc. B* 361 (1470), 1023–1038. doi:10.1098/rstb.2006.1843
- Knoll, A. H. (2015). Paleobiological Perspectives on Early Microbial Evolution. *Cold Spring Harb. Perspect. Biol.* 7 (7), a018093. doi:10.1101/cshperspect.a018093
- Knoll, A. H. (2011). The Multiple Origins of Complex Multicellularity. *Annu. Rev. Earth Planet. Sci.* 39, 217–239. doi:10.1146/annurev.earth.031208.100209
- Kumar, S. (1995). Megafossils from the Mesoproterozoic Rohtas Formation (The Vindhyan Supergroup), Katni Area, Central India. *Precambrian Res.* 72 (3–4), 171–184. doi:10.1016/0301-9268(94)00085-6
- Kumar, S. (2001). Mesoproterozoic Megafossil Chuaria-Tawuia Association May Represent Parts of a Multicellular Plant, Vindhyan Supergroup, Central India. *Precambrian Res.* 106 (3–4), 187–211. doi:10.1016/S0301-9268(00)00093-0

- Kumar, S., and Srivastava, P. (2003). Carbonaceous Megafossils from the Neoproterozoic Bhandar Group, Central India. *J. Palaeontol. Soc. India* 48, 139–154.
- Laflamme, M., Darroch, S. A. F., Tweedt, S. M., Peterson, K. J., and Erwin, D. H. (2013). The End of the Ediacara Biota: Extinction, Biotic Replacement, or Cheshire Cat? *Gondwana Res.* 23 (2), 558–573. doi:10.1016/j.gr.2012.11.004
- Lamb, D. M., Awramik, S. M., Chapman, D. J., and Zhu, S. (2009). Evidence for Eukaryotic Diversification in the ~1800 Million-Year-Old Changzhougou Formation, North China. *Precambrian Res.* 173 (1–4), 93–104. doi:10.1016/j.precamres.2009.05.005
- Lamb, D. M., Awramik, S. M., and Zhu, S. (2007). Paleoproterozoic Compression-like Structures from the Changzhougou Formation, China: Eukaryotes or Clasts? *Precambrian Res.* 154 (3–4), 236–247. doi:10.1016/j.precamres.2006.12.012
- Lenton, T. M., Boyle, R. A., Poulton, S. W., Shields-Zhou, G. A., and Butterfield, N. J. (2014). Co-evolution of Eukaryotes and Ocean Oxygenation in the Neoproterozoic Era. *Nat. Geosci.* 7 (4), 257–265. doi:10.1038/ngeo2108
- Leonov, M., Fedonkin, M., Vickers-Rich, P., Ivantsov, A. Y., and Trusler, P. (2009). Discovery of the First Macroscopic Algal Assemblage in the Terminal Proterozoic of Namibia, Southwest Africa. *Commun. Geol. Surv. Namib.* 14 (null), 87–93.
- Loeblich, A. R. (1974). Protistan Phylogeny as Indicated by the Fossil Record. *TAXON* 23 (2–3), 277–290. doi:10.2307/1218707
- Lyons, T. W., Reinhard, C. T., and Planavsky, N. J. (2014). The Rise of Oxygen in Earth's Early Ocean and Atmosphere. *Nature* 506 (7488), 307–315. doi:10.1038/nature13068
- Maloney, K. M., Halverson, G. P., Schiffbauer, J. D., Xiao, S., Gibson, T. M., Lechte, M. A., et al. (2021). New Multicellular Marine Macroalgae from the Early Tonian of Northwestern Canada. *Geology* 49 (6), 743–747. doi:10.1130/g48508.1
- Marshall, C. P., Love, G. D., Snape, C. E., Hill, A. C., Allwood, A. C., Walter, M. R., et al. (2007). Structural Characterization of Kerogen in 3.4Ga Archaeal Cherts from the Pilbara Craton, Western Australia. *Precambrian Res.* 155 (1–2), 1–23. doi:10.1016/j.precamres.2006.12.014
- Marusin, V. V., Grazhdankin, D. V., and Maslov, A. V. (2011). Redkino Stage in Evolution of Vendian Macrophytes. *Dokl. Earth Sci.* 436 (2), 197–202. doi:10.1134/S1028334X11020176
- Mukherjee, A., and Ray, R. K. (2010). An Alternate View on the Stratigraphic Position of the ~1-Ga Sukhda Tuff Vis-à-vis Chronostratigraphy of the Precambrians of the Central Indian Craton. *J. Geol.* 118 (3), 325–332. doi:10.1086/651502
- Mukherjee, A., Ray, R. K., Tewari, D., Ingle, V. K., Sahoo, B. K., and Y Khan, M. W. (2014). Revisiting the Stratigraphy of the Mesoproterozoic Chhattisgarh Supergroup, Bastar Craton, India Based on Subsurface Litho-information. *J. Earth Syst. Sci.* 123 (3), 617–632. doi:10.1007/s12040-014-0418-z
- Muscente, A. D., Bykova, N., Boag, T. H., Buatois, L. A., Mángano, M. G., Eleish, A., et al. (2019). Ediacaran Biozones Identified with Network Analysis Provide Evidence for Pulsed Extinctions of Early Complex Life. *Nat. Commun.* 10 (1), 911. doi:10.1038/s41467-019-08837-3
- Noffke, N., Christian, D., Wacey, D., and Hazen, R. M. (2013). Microbially Induced Sedimentary Structures Recording an Ancient Ecosystem in theca.348 Billion-Year-Old Dresser Formation, Pilbara, Western Australia. *Astrobiology* 13 (12), 1103–1124. doi:10.1089/ast.2013.1030
- Oehler, D. Z., Robert, F., Mostefaoui, S., Meibom, A., Selo, M., and McKay, D. S. (2006). Chemical Mapping of Proterozoic Organic Matter at Submicron Spatial Resolution. *Astrobiology* 6 (6), 838–850. doi:10.1089/ast.2006.6.838
- Orr, P. J., Kearns, S. L., and Briggs, D. E. G. (2009). Elemental Mapping of Exceptionally Preserved 'carbonaceous Compression' Fossils. *Palaeogeogr. Palaeoclimatol. Palaeoecol.* 277 (1), 1–8. doi:10.1016/j.palaeo.2009.02.009
- Pang, K., Tang, Q., Wu, C., Li, G., Chen, L., Wan, B., et al. (2020). Raman Spectroscopy and Structural Heterogeneity of Carbonaceous Material in Proterozoic Organic-Walled Microfossils in the North China Craton. *Precambrian Res.* 346, 105818. doi:10.1016/j.precamres.2020.105818
- Parfrey, L. W., Lahr, D. J. G., Knoll, A. H., and Katz, L. A. (2011). Estimating the Timing of Early Eukaryotic Diversification with Multigene Molecular Clocks. *Proc. Natl. Acad. Sci. U.S.A.* 108 (33), 13624–13629. doi:10.1073/pnas.1110633108
- Patranabis-Deb, S., and Chaudhuri, A. K. (2008). Sequence Evolution in the Eastern Chhattisgarh Basin; Constraints on Correlation and Stratigraphic Analysis. *Palaeobotanist* 57 (1–2), 15–32.
- Qu, Y., Zhu, S., Whitehouse, M., Engdahl, A., and McLoughlin, N. (2018). Carbonaceous Biosignatures of the Earliest Putative Macroscopic Multicellular Eukaryotes from 1630 Ma Tuanshanzi Formation, North China. *Precambrian Res.* 304, 99–109. doi:10.1016/j.precamres.2017.11.004
- Rai, V., and Singh, V. K. (2006). Discovery of Megascopic Multicellularity in Deep Time: New Evidences from the ~1.63 Billion Years Old Lower Vindhyan Succession, Vindhyan Supergroup, Uttar Pradesh, India. *J. Appl. Biosci.* 32 (2), 196–203.
- Retallack, G. J., Krull, E. S., Thackray, G. D., and Parkinson, D. (2013). Problematic Urn-Shaped Fossils from a Paleoproterozoic (2.2Ga) Paleosol in South Africa. *Precambrian Res.* 235, 71–87. doi:10.1016/j.precamres.2013.05.015
- Rowland, S. M., and Rodriguez, M. G. (2014). A Multicellular Alga with Exceptional Preservation from the Ediacaran of Nevada. *J. Paleontol.* 88 (2), 263–268. doi:10.1666/13-075
- Samuelsson, J., and Butterfield, N. J. (2001). Neoproterozoic Fossils from the Franklin Mountains, Northwestern Canada: Stratigraphic and Palaeobiological Implications. *Precambrian Res.* 107 (3–4), 235–251. doi:10.1016/S0301-9268(00)00142-X
- Sánchez-Baracaldo, P., Raven, J. A., Pisani, D., and Knoll, A. H. (2017). Early Photosynthetic Eukaryotes Inhabited Low-Salinity Habitats. *Proc. Natl. Acad. Sci. U.S.A.* 114 (37), E7737–E7745. doi:10.1073/pnas.1620089114
- Schneider, D. A., Bickford, M. E., Cannon, W. F., Schulz, K. J., and Hamilton, M. A. (2002). Age of Volcanic Rocks and Syndepositional Iron Formations, Marquette Range Supergroup: Implications for the Tectonic Setting of Paleoproterozoic Iron Formations of the Lake Superior Region. *Can. J. Earth Sci.* 39 (6), 999–1012. doi:10.1139/e02-016
- Schopf, J. W., Kudryavtsev, A. B., Agresti, D. G., Czaja, A. D., and Wdowiak, T. J. (2005). Raman Imagery: A New Approach to Assess the Geochemical Maturity and Biogenicity of Permineralized Precambrian Fossils. *Astrobiology* 5 (3), 333–371. doi:10.1089/ast.2005.5.333
- Schopf, J. W., Kudryavtsev, A. B., and Sergeev, V. N. (2010). Confocal Laser Scanning Microscopy and Raman Imagery of the Late Neoproterozoic Chichkan Microbiota of South Kazakhstan. *J. Paleontol.* 84 (3), 402–416. doi:10.1666/09-134.1
- Schopf, J. W., Tripathi, A. B., and Kudryavtsev, A. B. (2006). Three-dimensional Confocal Optical Imagery of Precambrian Microscopic Organisms. *Astrobiology* 6 (1), 1–16. doi:10.1089/ast.2006.6.1
- Sergeev, V. N., Sharma, M., and Shukla, Y. (2012). Proterozoic Fossil Cyanobacteria. *Palaeobotanist* 61 (2), 189–358.
- Sharma, M. (2006). Late Palaeoproterozoic (Statherian) Carbonaceous Films from the Olive Shale (Koldaha Shale), Semri Group, Vindhyan Supergroup, India. *J. Palaeontol. Soc. India* 51 (2), 27–35.
- Sharma, M., Mishra, S., Dutta, S., Banerjee, S., and Shukla, Y. (2009). On the Affinity of Chuaria-Tawuia Complex: A Multidisciplinary Study. *Precambrian Res.* 173 (1–4), 123–136. doi:10.1016/j.precamres.2009.04.003
- Sharma, M., Shukla, M., and Venkatachala, B. S. (1991). Metaphyte and Metazoan Fossils from Precambrian Sediments of India; a Critique. *Palaeobotanist* 40, 8–51.
- Sharma, M., and Shukla, Y. (2009a). Mesoproterozoic Coiled Megascopic Fossil Grypania Spiralis from the Rohtas Formation, Semri Group, Bihar, India. *Curr. Sci.* 96, 1636–1640.
- Sharma, M., and Shukla, Y. (2009b). Taxonomy and Affinity of Early Mesoproterozoic Megascopic Helically Coiled and Related Fossils from the Rohtas Formation, the Vindhyan Supergroup, India. *Precambrian Res.* 173 (1–4), 105–122. doi:10.1016/j.precamres.2009.05.002
- Sharma, M., and Singh, V. K. (2019). "Megascopic Carbonaceous Remains from Proterozoic Basins of India," in *Geological Evolution of the Precambrian Indian Shield*. Editor M. E. A. Mondal (Cham: Springer International Publishing), 725–749. doi:10.1007/978-3-319-89698-4_27
- Sharma, M., Tiwari, M., Ahmad, S., Shukla, R., Shukla, B., Singh, V. K., et al. (2016). Palaeobiology of Indian Proterozoic and Early Cambrian Successions- Recent Developments. *Proc. Indian Natl. Sci. Acad.* 82 (3), 559–579. doi:10.16943/ptinsa/2016/48468
- Shukla, M., and Sharma, M. (1990). Palaeobiology of Suket Shale, Vindhyan Supergroup; Age Implications. *Special Publ. Geol. Surv. India* 28, 411–434.
- Shukla, Y., Sharma, M., Noffke, N., and Callego, F. (2019). Biofilm Microfacies in Phosphoritic Units of the Neoproterozoic Halkal Shale, Bhima Basin, South India. *Precambrian Res.* doi:10.1016/j.precamres.2019.105501

- Singh, V. K., Babu, R., and Shukla, M. (2009). Discovery of Carbonaceous Remains from the Neoproterozoic Shales of Vindhyan Supergroup, India. *J. Evol. Biology Res.* 1 (1), 001–017.
- Singh, V. K., and Sharma, M. (2014). Morphologically Complex Organic-Walled Microfossils (OWM) from the Late Palaeoproterozoic - Early Mesoproterozoic Chitrakut Formation, Vindhyan Supergroup, Central India and Their Implications on the Antiquity of Eukaryotes. *J. Palaeontol. Soc. India* 59 (1), 89–102.
- Singh, V. K., Sharma, M., and Sergeev, V. N. (2019). A New Record of Acanthomorphic Acritarch Tappania Yin from the Early Mesoproterozoic Saraipali Formation, Singhara Group, Chhattisgarh Supergroup, India and its Biostratigraphic Significance. *J. Geol. Soc. India* 94 (5), 471–479. doi:10.1007/s12594-019-1343-1
- Steiner, M. (1997). Chuaria Circularis Walcott 1899 – ‘megaspheeromorph Acritarch’ or Prokaryotic Colony? *Acta Univ. Carol. Geol.* 40 (null), 645–665.
- Steiner, R. (1994). “Einführung,” in *Die Neoproterozoischen Megaalgen Sudchinas* (Berlin: Fachbereich Geowissenschaften), 1–4. doi:10.1007/978-3-322-84265-7_1
- Sun, W. (1987). Palaeontology and Biostratigraphy of Late Precambrian Macroscopic Colonial Algae: Chuaria Walcott and Tawuia Hofmann. *Palaeontogr. Abt. A* 203 (null), 109–134.
- Tang, Q., Pang, K., Li, G., Chen, L., Yuan, X., Sharma, M., et al. (2021). The Proterozoic Macrofossil Tawuia as a Coenocytic Eukaryote and a Possible Macroalga. *Palaeogeogr. Palaeoclimatol. Palaeoecol.* 576, 110485. doi:10.1016/j.palaeo.2021.110485
- Tang, Q., Pang, K., Yuan, X., and Xiao, S. (2020). A One-Billion-Year-Old Multicellular Chlorophyte. *Nat. Ecol. Evol.* 4 (4), 543–549. doi:10.1038/s41559-020-1122-9
- Tang, Q., Pang, K., Yuan, X., and Xiao, S. (2017). Electron Microscopy Reveals Evidence for Simple Multicellularity in the Proterozoic fossil Chuaria. *Geology* 45 (1), 75–78. doi:10.1130/G38680.1
- Tyler, S. A., Barghoorn, E. S., and Barrett, L. P. (1957). Anthracitic Coal from Precambrian Upper Huronian Black Shale of the Iron River District, Northern Michigan. *Geol. Soc. Am. Bull.* 68 (10), 1293–1304. doi:10.1130/0016-7606(1957)68[1293:ACFPUH]2.0.CO;2
- Vidal, G., and Ford, T. D. (1985). Microbiotas from the Late Proterozoic Chuaria Group (Northern Arizona) and Uinta Mountain Group (Utah) and Their Chronostratigraphic Implications. *Precambrian Res.* 28 (3–4), 349–389. doi:10.1016/0301-9268(85)90038-5
- Vidal, G., Moczydlowska, M., and Rudavskaya, V. A. (1993). Biostratigraphical Implications of a Chuaria-Tawuia Assemblage and Associated Acritarchs from the Neoproterozoic of Yakutia. *Palaeontology* 36 (2), 387–402.
- Wacey, D., Saunders, M., McPherson, A., Gain, S., Sirantoine, E., and Eiloart, K. (2019). Correlative Microscopy of Diverse Filamentous Microfossils from 850 Ma Rocks. *Microsc. Microanal.* 25 (S2), 2466–2467. doi:10.1017/S1431927619013060
- Walcott, C. D. (1899). Pre-Cambrian Fossiliferous Formations. *Geol. Soc. Am. Bull.* 10, 199–244. doi:10.1130/gsab-10-199
- Walter, M., Oehler, J. H., and Oehler, D. Z. (1976). Megascopic Algae 1300 Million Years Old from the Belt Supergroup, Montana: a Reinterpretation of Walcott’s Helminthoidichnites. *J. Paleontology* 50 (5), 872–881.
- Walter, M. R., Du, R., and Horodyski, R. J. (1990). Coiled Carbonaceous Megafossils from the Middle Proterozoic of Jixian (Tianjin) and Montana. *Am. J. Sci.* 290 A, 133–148.
- Wan, B., Yuan, X., Chen, Z., Guan, C., Pang, K., Tang, Q., et al. (2016). Systematic Description of Putative Animal Fossils from the Early E Diacaran L Antian F Ormation of S Outh C Hina. *Palaeontology* 59 (4), 515–532. doi:10.1111/pala.12242
- Wang, W. E. I., Guan, C., Zhou, C., Wan, B. I. N., Tang, Q., Chen, X., et al. (2014). Exceptional Preservation of Macrofossils from the Ediacaran Lantian and Miaohu Biotas, South China. *PALAIOS* 29 (3/4), 129–136. doi:10.2110/palo.2013.085
- Wang, X., Yuan, X., Zhou, C., Du, K., and Gong, M. (2011). Anatomy and Plant Affinity of Chuaria. *Chin. Sci. Bull.* 56 (null), 693–699. doi:10.1007/s11434-011-4370-x
- Xiao, S., and Dong, L. (2006). On the Morphological and Ecological History of Proterozoic Macroalgae. *Top. Geobiol.* 27, 57–90.
- Xiao, S., Knoll, A. H., and Yuan, X. (1998). Morphological Reconstruction of *Miaohephyton Bifurcatum*, a Possible Brown Alga from the Neoproterozoic Doushantuo Formation, South China. *J. Paleontol.* 72 (6), 1072–1086. doi:10.1017/s0022336000027414
- Xiao, S., Yuan, X., Steiner, M., and Knoll, A. H. (2002). Macroscopic Carbonaceous Compressions in a Terminal Proterozoic Shale: A Systematic Reassessment of the Miaohu Biota, South China. *J. Paleontol.* 76 (2), 347–376. doi:10.1666/0022-3360(2002)076<0347:Mcciat>2.0.CO;2
- Yan, Y. (1995). Discovery and Preliminary Study of Megascopic Algae (1700 Ma) from the Tuanshanzi Formation in Jixian, Hebei. *Acta Micropalaeontologica Sin.* 12, 107–126.
- Yan, Y., and Liu, Z. (1997). Tuanshanzi Macroscopic Algae of 1700 Ma B. P. From Changcheng System of Jixian, China. *Acta Palaeontol. Sin.* 36, 18–41.
- Ye, Q., Tong, J., An, Z., Hu, J., Tian, L., Guan, K., et al. (2019). A Systematic Description of New Macrofossil Material from the Upper Ediacaran Miaohu Member in South China. *J. Syst. Palaeontol.* 17 (3), 183–238. doi:10.1080/14772019.2017.1404499
- Yuan, X., Chen, Z., Xiao, S., Zhou, C., and Hua, H. (2011). An Early Ediacaran Assemblage of Macroscopic and Morphologically Differentiated Eukaryotes. *Nature* 470 (7334), 390–393. doi:10.1038/nature09810
- Yuan, X., Li, J., and Cao, R. (1999). A Diverse Metaphyte Assemblage from the Neoproterozoic Black Shales of South China. *Lethaia* 32 (null), 143–155.
- Yuan, X., Li, J., and Chen, M. (1995). Development and Their Fossil Records of Metaphytes from Late Precambrian. *Acta Palaeontol. Sin.* 34 (null), 90–102.
- Yuan, X., Wan, B., Guan, C., Chen, Z., Zhou, C., Xiao, S., et al. (2016). *The Lantian Biota*. Shanghai: Shanghai Science and Technology Press, 138.
- Yuan, X., Xiao, S., Li, J., Yin, L., and Cao, R. (2001). Pyritized Chuariids with Excystment Structures from the Late Neoproterozoic Lantian Formation in Anhui, South China. *Precambrian Res.* 107 (3–4), 253–263. doi:10.1016/S0301-9268(00)00144-3
- Zhang, F., Wang, H., Ye, Y., Deng, Y., Lyu, Y., Wang, X., et al. (2021a). The Environmental Context of Carbonaceous Compressions and Implications for Organism Preservation 1.40 Ga and 0.63 Ga. *Palaeogeogr. Palaeoclimatol. Palaeoecol.* 573, 110449. doi:10.1016/j.palaeo.2021.110449
- Zhang, S., Su, J., Ma, S., Wang, H., Wang, X., He, K., et al. (2021b). Eukaryotic Red and Green Algae Populated the Tropical Ocean 1400 Million Years Ago. *Precambrian Res.* 357, 106166. doi:10.1016/j.precamres.2021.106166
- Zhao, Y., Chen, M. e., Peng, J., Yu, M., He, M., Wang, Y., et al. (2004). Discovery of a Miaohu-type Biota from the Neoproterozoic Doushantuo Formation in Jiangkou County, Guizhou Province, China. *Chin. Sci. Bull.* 49 (20), 2224–2226. doi:10.1360/982004-4710.1007/bf03185792
- Zhu, S., and Chen, H. (1995). Megascopic Multicellular Organisms from the 1700-Million-Year-Old Tuanshanzi Formation in the Jixian Area, North China. *Science* 270 (5236), 620–622.
- Zhu, S., Zhu, G., Sun, S., Sun, L., Huang, X., Zhang, K., et al. (2000). Discovery of Carbonaceous Compressions and Their Multicellular Tissues from the Changzhougou Formation (1 800 Ma) in the Yanshan Range, North China. *Chin. Sci. Bull.* 45 (9), 541–547. doi:10.1007/bf02887415
- Zhu, S., Zhu, M., Knoll, A. H., Yin, Z., Zhao, F., Sun, S., et al. (2016). Decimetre-scale Multicellular Eukaryotes from the 1.56-Billion-Year-Old Gaoyuzhuang Formation in North China. *Nat. Commun.* 7, 1–8. doi:10.1038/ncomms11500

Conflict of Interest: The authors declare that the research was conducted in the absence of any commercial or financial relationships that could be construed as a potential conflict of interest.

Publisher’s Note: All claims expressed in this article are solely those of the authors and do not necessarily represent those of their affiliated organizations, or those of the publisher, the editors, and the reviewers. Any product that may be evaluated in this article, or claim that may be made by its manufacturer, is not guaranteed or endorsed by the publisher.

Copyright © 2022 Singh and Sharma. This is an open-access article distributed under the terms of the Creative Commons Attribution License (CC BY). The use, distribution or reproduction in other forums is permitted, provided the original author(s) and the copyright owner(s) are credited and that the original publication in this journal is cited, in accordance with accepted academic practice. No use, distribution or reproduction is permitted which does not comply with these terms.



OPEN ACCESS

EDITED BY

Juliana Leme,
University of São Paulo, Brazil

REVIEWED BY

Francisca Martinez-Ruiz,
Spanish National Research Council
(CSIC), Spain
Jeffrey M. Dick,
Central South University, China

*CORRESPONDENCE

Douglas Galante,
douglas.galante@lnls.br

SPECIALTY SECTION

This article was submitted to
Paleontology,
a section of the journal
Frontiers in Earth Science

RECEIVED 29 October 2021

ACCEPTED 30 June 2022

PUBLISHED 22 July 2022

CITATION

Callefo F, Ricardi-Branco F,
Alves Forancelli Pacheco ML,
Cardoso AR, Noffke N,
de Carvalho Teixeira V, Neckel IT,
Maldanis L, Bullock E, Bower D,
Moreira Silva A, Ferreira Sanchez D,
Rodrigues F and Galante D (2022),
Evidence for metabolic diversity in
Meso-Neoproterozoic stromatolites
(Vazante Group, Brazil).
Front. Earth Sci. 10:804194.
doi: 10.3389/feart.2022.804194

COPYRIGHT

© 2022 Callefo, Ricardi-Branco, Alves
Forancelli Pacheco, Cardoso, Noffke, de
Carvalho Teixeira, Neckel, Maldanis,
Bullock, Bower, Moreira Silva, Ferreira
Sanchez, Rodrigues and Galante. This is
an open-access article distributed
under the terms of the [Creative
Commons Attribution License \(CC BY\)](#).
The use, distribution or reproduction in
other forums is permitted, provided the
original author(s) and the copyright
owner(s) are credited and that the
original publication in this journal is
cited, in accordance with accepted
academic practice. No use, distribution
or reproduction is permitted which does
not comply with these terms.

Evidence for metabolic diversity in Meso-Neoproterozoic stromatolites (Vazante Group, Brazil)

Flavia Callefo¹, Fresia Ricardi-Branco²,
Mírian Liza Alves Forancelli Pacheco³,
Alexandre Ribeiro Cardoso², Nora Noffke⁴,
Verônica de Carvalho Teixeira¹, Itamar Tomio Neckel¹,
Lara Maldanis⁵, Emma Bullock⁶, Dina Bower^{7,8},
Adalene Moreira Silva⁹, Dario Ferreira Sanchez¹⁰,
Fabio Rodrigues¹¹ and Douglas Galante^{1*}

¹Brazilian Synchrotron Light Laboratory, Brazilian Center for Research in Energy and Materials, Campinas, Brazil, ²Department of Geology and Natural Resources, Institute of Geosciences, Universidade Estadual de Campinas (UNICAMP), Campinas, Brazil, ³Laboratório de Estudos Paleobiológicos (LEPBio), Departamento de Biologia, Universidade Federal de São Carlos (UFSCar), Sorocaba, Brazil, ⁴Department of Ocean, Earth and Atmospheric Sciences, Old Dominion University, Norfolk, VA, United States, ⁵Université Grenoble Alpes, Université Savoie Mont Blanc, CNRS, IRD, Université Gustave Eiffel, ISTerre, Grenoble, France, ⁶Earth and Planets Laboratory, Carnegie Institution for Science, Washington D.C., DC, United States, ⁷Department of Astronomy, University of Maryland, College Park, MD, United States, ⁸NASA Goddard Space Flight Center, Greenbelt, MD, United States, ⁹Institute of Geosciences—University of Brasília, Brasília, Brazil, ¹⁰Swiss Light Source (SLS), Paul Scherrer Institut (PSI), Villigen, Switzerland, ¹¹Department of Fundamental Chemistry, Institute of Chemistry, Universidade de São Paulo, São Paulo, Brazil

Deciphering the evolution of ecological interactions among the metabolic types during the early diversification of life on Earth is crucial for our understanding of the ancient biosphere. The stromatolites from the genus *Conophyton cylindricus* represent a datum for the Proterozoic (Meso to Neoproterozoic) on Earth. Their typical conical shape has been considered a result of a competition between microorganisms for space, light and nutrients. Well-preserved records of this genus from the “Paleontological Site of Cabeludo”, Vazante Group, São Francisco Craton (Southern Brazil) present *in situ* fossilized biofilms, containing preserved carbonaceous matter. Petrographic and geochemical analyses revealed an alternation between mineral laminae (light grey laminae) and fossilized biofilms (dark grey laminae). The dark grey laminae comprise three different biofilms recording a stratified microstructure of microbial communities. These three biofilms composing the dark grey laminae tend to be organized in a specific pattern that repeats through the stromatolite vertical section. Iron and manganese are distributed differently along the dark and light grey laminae; X-ray absorption and luminescence data showed possible different areas with authigenic iron and iron provided from diagenetic infiltration. Cryptocrystalline apatite in the lowermost biofilms in each dark grey laminae may suggest past metabolic activity of sulfide-oxidizing bacteria. These findings suggest that the microorganisms reached a complex metabolic diversification in order to

maintain an equilibrium situation between the three different biofilms along the vertical section of the structures, thus benefiting the whole microbial community. This means that the stromatolites from the *Conophyton* genus may have formed as a result of a greater complexity of interactions between microorganisms, and not only from competition between photosynthesizers.

KEYWORDS

Conophyton, Proterozoic, microbial metabolism, sulfide-oxidizing bacteria, biomineral, biofilm

1 Introduction

Since the Archean microorganisms were able to adjust themselves to external factors by developing the ability of organization into a complex consortium of single or multiple species called a biofilm (Neu 1994; Neu 1996; Davey and O'Toole 2000). Biofilms are made up of secreted extracellular polymeric substances (EPS) that serve as protection for the cells, provide the exchange of metabolites, and work as a buffer against environmental factors, such as sudden changes in salinity, mechanical stresses, radiation and many others (Decho, 1999). By the trapping and binding of sedimentary particles and *in situ* mineral precipitation, the biofilms may construct organosedimentary structures called stromatolites (Hofmann, 1969; Walter, 1976; Burne and Moore, 1987; Riding, 2011; Noffke and Awramik, 2013). These are the result of biologically induced precipitation of minerals, especially carbonate, in a laminated form, whose process of mineral precipitation and bacterial growth is repeated until the structure grows vertically (Burne and Moore, 1987; Riding, 2011; Noffke and Awramik, 2013). These structures can follow different morphologies such as domical, stratiform, flat layered, columnar, branched, conical, among others, generally reflecting the environmental parameters in which the structure grew up (Hoffman, 1976; Walter, 1976; Grotzinger, 1989; Awramik, 1992; Hofmann, 2000; Zhang et al., 2021). However, conical stromatolites, such as those of the *Conophyton* and *Jacutophyton* genus, are known to reflect biological control in their morphology (Schopf, 1975; Bertrand-Sarfati and Moussine-Pouchkine, 1985; Kah et al., 2009). This means that its morphology results from the predominance of intrinsic factors (how the biota behaves and induces mineral precipitation) over extrinsic factors (how external parameters influence the shape of the structures, such as physical depositional factors as water currents and energy involved).

Stromatolitic structures of the *Conophyton* genus were generated in several locations around the world during the interval between the Meso and Neoproterozoic (approximately from 1.2 Ga to 900 Ma). Generally, they develop in specific conditions such as a marine subtidal environment, high water depth (up to tens of meters, but still within the photic zone) and low energy (without wave action, for example) (Moeri, 1972; Dardenne, 2000; Dardenne, 2005; Sallun Filho and Fairchild,

2005). These stromatolites have a characteristic morphology of a columnar structure without branches; in the vertical section, *Conophyton* is built up by conical laminae that were developed around a central axis (Sallun Filho and Fairchild, 2005). This type of stromatolite only occurs in between Meso to Neoproterozoic in records worldwide, although the reasons for this temporal restriction remain unknown. Therefore, *Conophyton* are considered a datum for this geological time interval (Preiss, 1976). There are several examples of *Conophyton* occurrence around the world, such as Vendian *Conophyton gaubitzia* Krylov from Chichkan Formation (Karoy Group), South Kazakhstan (Schopf, 1976); Mesoproterozoic Atar Group, Mauritania (Bertrand-Sarfati, 1972; Bertrand-Sarfati and Moussine-Pouchkine, 1985; Kah et al., 2009; Burne, 2022); Mesoproterozoic in several units from Brazil: Paranoá, Itaiacoca, Bambuí and Vazante Group (Moeri, 1972; Cloud and Dardenne, 1973; Cloud and Moeri, 1973; Sallun Filho and Fairchild, 2005); Neoproterozoic *Conophytons* from Mina Verdun Group (El Calabozo Formation), Uruguay (Gaucher et al., 2004); Mesoproterozoic *Conophytons* from Helena Formation, Belt Supergroup, Montana, United States (Horodyski, 1985), among others.

It is hypothesized that the typical conical shape of *Conophyton* is a result of a competition for sunlight and space among microorganisms which formed the structures (Walter, 1977; Sallun Filho and Fairchild, 2005). The competition for sunlight and for nutrients in the same space would induce the biofilms to grow in greater volume towards the apical region of the stromatolite in formation. This is corroborated by the preservation of accumulated carbonaceous matter in the apical region of each laminae of fossilized stromatolites.

Stromatolites of subgroup *Conophyton cylindricus* Maslov 1937 are exposed at the "Paleontological Site of Cabeludo" belonging to the Sumidouro Member, Lagamar Formation, Upper Vazante Group, São Francisco Craton (Southeastern Brazil) (Moeri, 1972; Cloud and Moeri, 1973; Sallun Filho and Fairchild, 2005; Fairchild et al., 2015). These structures are remarkably well preserved despite their age of 1.350 Ma to 950 Ma (Cloud and Dardenne, 1973; Cloud and Moeri, 1973; Dardenne, 2005). Fossilized biofilms can be observed in its microscopic texture, intermingled with minerals. This opens a window for possibilities of exploration of possible biosignatures preserved in order to better understand the biological controls that exert a role in the conical formation.

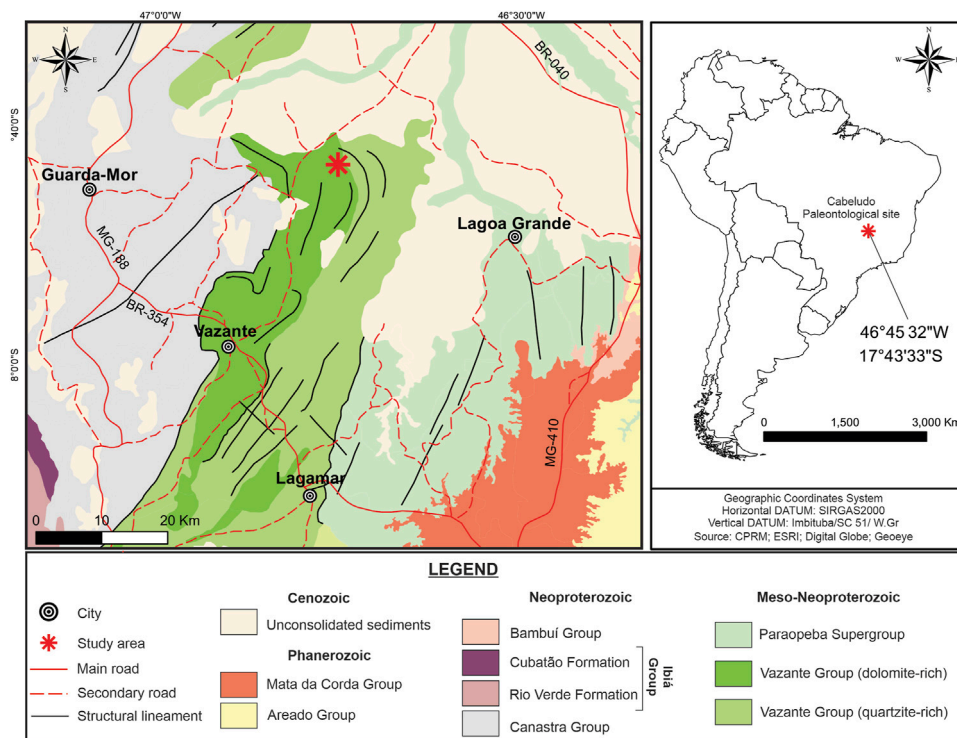


TABLE 1 Studied samples and applied techniques.

Sample	Macroscopic analysis	Petrology	EPMA imaging	Raman spectroscopy	XANES	XEOL	XRF	XRD
CP6/194	x	x						
CP6/195	x	x						
CP6/196	x	x	x	x	x	x	x	x
CP6/197	x	x						
CP6/198	x	x						
CP6/199	x	x						
CP6/200	x	x						
CP6/201	x	x						
CP6/202	x	x						
CP6/203a	x	x	x	x	x		x	
CP6/203b	x	x	x	x	x		x	

Petrographic thin-sections of the *Conophyton*s from the Paleontological Site of Cabeludo revealed an alternation between dark-light laminated build-up composed mostly of

amorphous silica (chert), quartz grains and dolomite, and dark-gray laminae composed of preserved organic matter (kerogen). These darker regions have been interpreted as

preserved biofilms (Dardenne, 2005). However, we observed a stratification within these preserved biofilms, which suggests a more complex construction of these stromatolites during the Meso-Neoproterozoic.

Here we propose the existence of more than one type of preserved biofilm in these *Conophyton*s, besides an organization trend according to their metabolic needs responsive to environmental factors, similar to modern microbial mats. For that, we investigated the internal build-up of the ancient preserved biofilms in order to assess the development of the biofilm from its initial to mature stage. Our approach consisted of combining different methods at microscopic scales for understanding the microscopic textures and resolving the inorganic and organic phases. Petrographic analysis was used for preliminary inspection of the microscopic textures. Electron probe microanalysis (EPMA) provided us higher resolution information of the superficial textures, including the low Z elements present (e.g., C, O). For deeper investigation of the elements present at microns of depths and down to trace concentrations, we did synchrotron X-ray fluorescence (XRF) maps. Raman spectroscopy was used for mapping the presence of kerogen and some mineral phases, the last further corroborated by synchrotron-based X-ray diffraction (XRD). X-ray absorption (XANES) allowed us to deepen the chemical investigation by revealing the chemical species of Fe and Mn present in the samples, and X-ray excited optical luminescence (XEOL) added to this comprehension by providing maps of luminescent areas, signal of specific element valences. Together, these methods provided us with ways of deeper understanding of the geochemistry of the different *Conophyton* textures, and finding patterns that pointed to the presence of different metabolisms. These are represented by a differentiated geochemistry along the distinct preserved biofilms, which could mean biosignatures indicative of non-photosynthetic activities, and also biominerals resulting from the alternative metabolisms to photosynthesis, such as cryptocrystalline apatite (suggesting the past sulfide-oxidizing bacteria metabolic activity). The findings may indicate a greater complexity of microbial interactions between co-habitant microorganisms which formed the *Conophyton*s, showing that these microorganisms developed other strategies of survival instead of competition by space and sunlight.

2 Geological setting

The orogenic belt of the Tocantins Province was formed by fusion of the Amazon Craton, the São Francisco Craton and the Paranapanema Craton (Dardenne, 2000), composing the Gondwana supercontinent (Almeida, 1977). The Vazante Group is part of the Brasília Fold Belt, located in the west portion of the São Francisco

Craton, and extended along approximately 250 km. It consists of low-grade metamorphic sequences of carbonates (dolomite) and pelites, whose deposition is attributed to a shallow marine platform setting (Falci et al., 2018). Late Mesoproterozoic age is indicated by the occurrence of conical stromatolites of the genus *Conophyton* in some stratigraphic units (Dardenne, 2000; Dardenne, 2005; Vasconcelos et al., 2020), and Re-Os dating that yielded $1,304 \pm 210$ Ma (Bertoni et al., 2014). Chronological constraints are established by U-Pb dating of detrital zircon grains from the Upper Vazante Group (Rocinha Formation), which provided 935 ± 14 Ma (Rodrigues et al., 2012). According to Dardenne (2000), the Vazante Group is stratigraphically divided into seven formations (from the bottom to the top): Retiro, Rocinha, Lagamar, Serra do Garrote, Serra do Poço Verde, Morro do Calcário and Serra da Lapa. The study site is located in the east portion of Lagamar Formation, which is subdivided in quartzite-dominated deposits (Arrependido Member) and carbonate-dominated deposits (Sumidouro Member). The Sumidouro Member consists of stromatolitic bioherm dolomites, breccias and dark gray limestones (Dardenne, 2000). Geographically, the fossil site is close to the city of Vazante, Minas Gerais State, in the southeast region of Brazil. The area was called “Paleontological Site of Cabeludo” in the description by Dardenne et al. (1972). The geographic coordinates are $17^{\circ} 43' 33''\text{S}$ and $46^{\circ} 45' 32''\text{W}$ (Figure 1).

3 Material and methods

3.1 Field work

We collected eleven sets of samples of stromatolites from different points inside the paleontological site. Each one was taken from basal, middle, and top portions of the stromatolites, totalizing 33 samples. The samples are deposited in the paleontological collection of the Geosciences Institute, University of Campinas (IG - UNICAMP), receiving the denomination “CP” (paleontological collection) following the number of registry in the collection. Table 1 shows the samples and the method of investigation applied to each one. Those samples which presented better preservation of biofilms in thin section analysis were chosen to be explored with the techniques described subsequently.

3.2 Petrographic thin sections analysis

We prepared eleven thin sections of 30 μm thickness (without glass coverslip to allow compositional analysis). They were analyzed at the Paleohydrogeology Laboratory of the University of Campinas (UNICAMP), with a Carl Zeiss petrographic microscope Scope A1 ZEISS. The images were recorded with a ZEISS AxioCam camera and processed with ZEISS AxioVision® 4.8.2.0. (2006) software.

3.3 Electron probe microanalysis and energy dispersive spectroscopy

We obtained compositional analyses and secondary electron images using the JEOL 8530F electron probe at the Carnegie Institution for Science (Washington, DC). The images and maps were recorded in nine areas of interest within the CP6/196 thin section, sampling each putative kind of biofilm, besides areas of hydrothermal incursion, cracks and recrystallization areas. The probe was operated at 15 kV and 20 nA. We also performed quantitative analyses in each chosen point using the Thermo Scientific Energy Dispersive System (EDS), utilizing the Pathfinder software. Samples were coated with iridium to mitigate charging and to facilitate the analysis of carbon.

3.4 Raman spectroscopy

The Raman Spectroscopy analyses were performed at Carnegie Institution of Science (Washington, DC). The Raman images were acquired with the WITec Scanning Near-Field Optical Microscope, with a camera system coupled to the microscope. The excitation source was a frequency-doubled solid-state YAG laser (532 nm) operating between 0.01 and 5 mW output power. Spectra were collected on a Peltier-cooled Marconi 40-11 CCD chip, after passing through a $f/4,300$ mm focal length imaging spectrometer using a 600 lines/mm grating. We used the WITec Project Plus software to map peaks of interest across the sample and compute peak intensity maps.

3.5 Synchrotron-based μ -X-ray fluorescence and X-ray diffraction

Petrographic thin sections (30 μm thickness) mounted on glass slides were evaluated for their chemical and mineralogical composition using X-ray Fluorescence and X-ray diffraction. μ -XRF elemental maps were first acquired using the XRF beamline at the Brazilian Synchrotron Light Laboratory (LNLS), Brazil. The beamline was used in micro-beam mode with the KB focusing system in order to reach a beam size of 12 $\mu\text{m} \times 25 \mu\text{m}$ diameter. 2D measurements were performed at room temperature in continuous scan mode (fly scan), with step sizes of 30 μm and integrations of 300 ms per pixel. The excitation was made in white-beam mode. Further higher spatial resolution elemental maps were obtained at the microXAS beamline at the Swiss Light Source (SLS), Paul Scherrer Institut (PSI), Switzerland. The silicon drift detector (SDD) was placed at 70° with the incident beam in order to acquire the data, and the X-ray beam was focused down to 1 $\mu\text{m}^2 \times 1 \mu\text{m}^2$ using KB mirrors. The measurements were carried out using a monochromatic beam at energy of 17.2 keV in order

to excite the elements of interest. The step size was 30 μm for the overview area, and 3 μm for selected areas in the preserved biofilms, in order to acquire more details. All elemental maps were analysed using the PyMCA 4.6.0 software (developed by European Synchrotron Radiation Facility—ESRF, Solé et al., 2007).

The mineralogical composition was explored with X-ray diffraction in co-located measurements with X-ray fluorescence at the microXAS beamline. The measurements were made in three specific areas containing each type of biofilm separately. The angle between the X-ray beam and the sample was kept at $\Theta = 20^\circ$ meanwhile the diffraction patterns were acquired using an area detector (Eiger 4 M) covering roughly $2\Theta = 35^\circ$. The output data is composed of several 2D diffraction patterns where the presence of rings indicates a polycrystalline sample (Supplementary Figures S1A–C—top). To obtain the conventional Intensity vs. 2Θ diffractogram, an azimuthal integration was required and shown in Supplementary Figures S1A–C bottom. The main phases were identified using the software XRDUA (De Nolf et al., 2014).

3.6 X-ray absorption near edge structure

The micro XANES measurements were firstly performed using the XRF beamline (LNLS—UVX) around Fe K edge, and posteriorly using the Carnáuba beamline (LNLS - Sirius) around the Mn K edge. The XRF beamline was used in monochromatic beam mode, provided by the Si (111) crystal and a microbeam provided by the KB system (12 $\mu\text{m} \times 25 \mu\text{m}$). Samples were measured in air and at room temperature, without sample-environment controls. The XANES spectra were collected in fluorescence mode, using the SDD detector available at the beamline (Ketek, GmbH). The higher spectral resolution was 0.3 eV. The Fe K-edge data from the sample was compared with synthetic standards (measured at the XAFS1 and XAFS2 beamlines of LNLS) and natural standards (measured with micro-beam in the XRF beamline). These mentioned studies were performed at LNLS UVX storage ring that is now decommissioned.

The Mn-K edges were also measured in the Carnáuba beamline (LNLS—Sirius), in order to have more accuracy in the obtained results, due to its resolution (beam size down to 150 nm \times 400 nm, obtained with KB mirrors) and higher flux, once the new accelerator (Sirius) is a 4th generation machine and the beamline uses a 4-channel monochromator developed in-house (Tolentino et al., 2021). The measurements were acquired in fluorescence mode using Vortex®ME4 SSD detectors (Hitachi) on the energy range of 6,500–6,600 eV, with a step energy of 0.3 eV, accumulation time 0.5 s, in air and room temperature. The data was compared with that of synthetic standards of MnO (Mn²⁺) and Mn₂O₃ (Mn³⁺) measured in transmission mode with an Alibava (AS04-105A) photodiode.

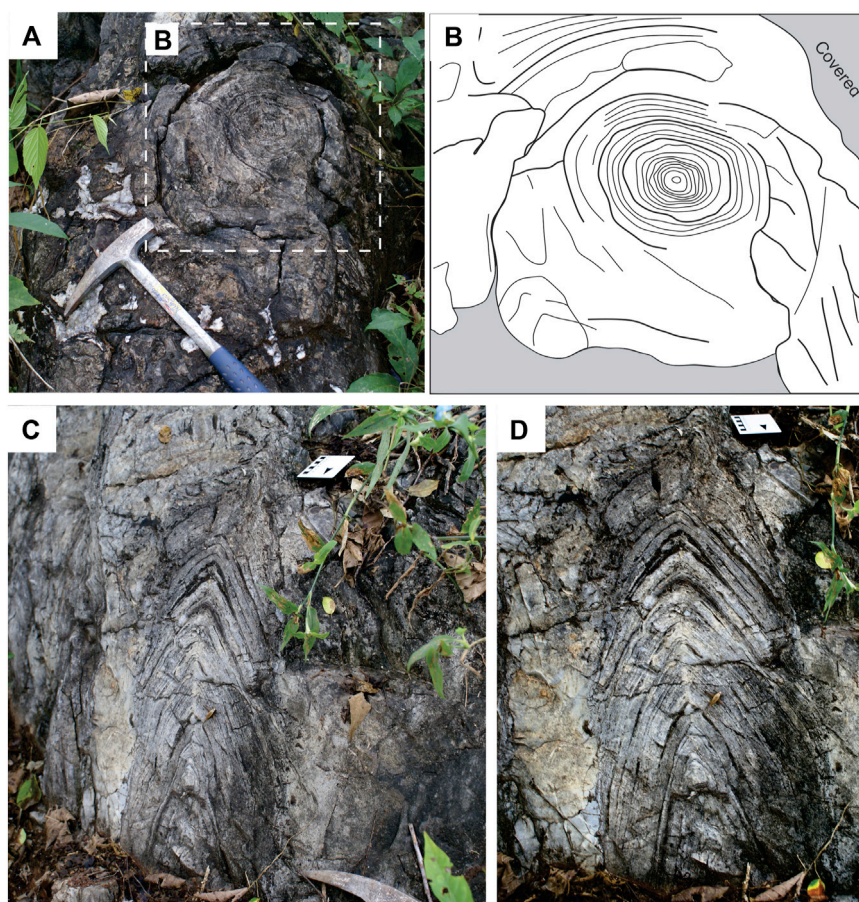


FIGURE 2

Morphology and internal build-up of *Conophyton* in outcrop; Paleontological Site of Cabeludo. (A) regularly-spaced concentric laminae in plan view (Scale: geological hammer—35 cm); (B) sketch of the concentric laminae, preservation degree increases toward the center of the structure; (C) conical laminae in profile view of the outcrop. Note closed angulation of the laminae and vertical alignment of the apex (Scale: 10 cm); (D) close-up view highlighting the planar contact between conical-shaped laminae and the host lithology (Scale: 10 cm).

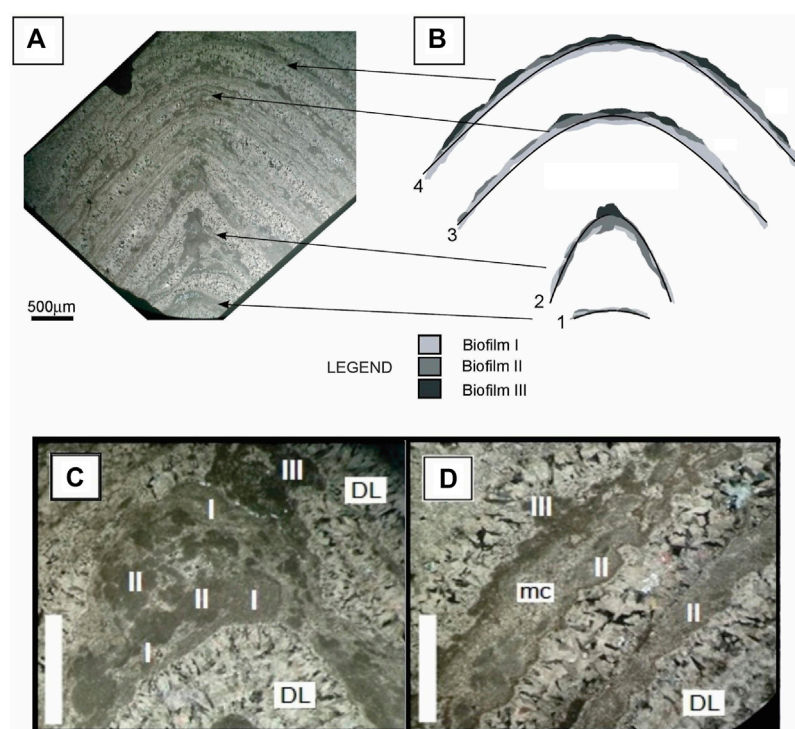
3.7 X-ray excited optical luminescence

X-ray excited optical luminescence (XEOL) experiments were performed at the XRF beamline from the Brazilian Synchrotron Light Laboratory (LNLS), using the setup for microXEOL. This setup is composed of an Al-coated 15X objective reflexive lens (ThorLabs), with a working distance of 23 mm that is used to collect the light emitted by the sample after the interaction with X-rays. This light was collimated in a parabolic collimator (ThorLabs) also Al coated, and focalized in an optical fiber (UV-Vis, Ocean Optics) that was coupled to a spectrometer (QEPro, Ocean Optics). For exciting the samples, the white beam mode was used, with spot size of $12\ \mu\text{m} \times 25\ \mu\text{m}$. The optical signal was acquired in emission mode, with integration of 1 s in each point, monitoring the range from 200–950 nm. The hyperspectral image was analyzed using the PyMCA software in 2D mapping.

4 Results

4.1 Morphology and internal build-up of the stromatolites

The stromatolites of the genus *Conophyton* at the Paleontological Site of Cabeludo occur as solitary units and arranged in clusters. The stromatolites range from 0.5 to 4 m high and are columnar in external morphology. As also observed by Sallun Filho and Fairchild (2005), the horizontal section through a stromatolite reveals its elliptical contour around the central axis, with diameters ranging from approximately 15–70 cm (Figures 2A,B). The conical laminae show high inheritance with each laminae presenting the same size, curvature and morphology of the previous laminae, as well apical areas of each lamination being well aligned to each other. As also pointed out by Moeri (1972), there is an

**FIGURE 3**

(A) Thin section overview showing alternating dark grey laminae and light grey to white laminae (scale bar: 500 µm); (B) sketch of the distribution pattern of the biofilms along four stages of development, forming the *Conophyton*'s organization; (C) Petrographic images of *Conophyton* showing three different organic-rich laminae. Cut in vertical section in the apical zone of organic-rich laminae of the *Conophyton* (scale bar: 500 µm), intermediate part of *Conophyton*; DL- dolomite; (D) cut in vertical section, top part of the *Conophyton*, lateral zone of organic-rich laminae (scale bar: 500 µm); DL—dolomite; mc - micrite. All images are from sample CP6/196.

elongation of the plan outlined in the stromatolites. In the vertical section from the base to the top, a vertical axis serves as support structure, and also present macroscopic layers, ranging from 0.5 to 1 cm. These stromatolites are conical-shaped with closed angulation in the bottom opening towards the top (Figures 2C,D). Whereas the apex of the young stromatolite was initially more conical (as recorded by the laminae close to the base), the apex increasingly became more pointed towards the top (Figures 2C,D). The angle of the laminae at the apex is 50° on average, but it can reach 30° in the basal laminae.

4.2 Microscopic texture in the stromatolites

We observed distinguishable alternations of dark grey laminae (400–600 µm thickness) and light grey to white laminae (700 µm–1 mm thickness) in petrographic analysis (Figure 3). Despite the overall good preservation of these *Conophyton* from the Vazante Group, post depositional modifications also occur, including mechanical compaction,

ductile deformation (e.g., folding) and fractures filled with silica. However, these post depositional changes were not harmful to the evaluation of the original microscopic texture of the stromatolites.

The light grey to white laminae consist of rhombohedral coarse dolomite crystals with secondary recrystallization and scattered quartz grains, while the dark grey laminae consist of fine-grained dolomite crystals. In these laminae, organic matter was identified and preserved as brown-colored, opaque spots with no pleochroism. Rarely, dispersed fine-grained quartz grains occur. In close-up view, it is possible to observe that the dark grey laminae show three different organic-rich laminae, which were defined here as biofilm I, biofilm II and biofilm III (In Figure 3, shown as I, II and III, distributed in 4 stages of development of the *Conophyton*). The meaning of this division is explained in Section 5.2 of the discussions, as well as the division into the four stages of development of dark-grey laminae. The laminae differ in coloration from each other and they have a distinct mottled appearance related to varying carbon content. Notably, the vertical organization of the three different biofilms in each dark grey laminae is repetitive in all analyzed samples. The main visual aspect that differentiates the three biofilms is the

TABLE 2 Comparison of the main observed characteristics of the three biofilms comprising each dark grey laminae.

Biofilm	Color	Mineralogy	Crystal Size	Organic matter	Main elemental composition	Fe and Mn speciation
I	Darker grey	Dolomite, scattered quartz grains, apatite crystals	Fine-grained crystals	Diffusely distributed, high content, kerogen (D and G bands)	Ca, Fe, Mn, P	Fe ²⁺ and Fe ³⁺ Mn ²⁺
II	Intermediate grey	Dolomite, dispersed quartz grains	Fine-grained crystals	Diffusely distributed, high content, kerogen (D and G bands)	Ca, Fe, Mn, Sr, S	Fe ²⁺ and Fe ³⁺ Mn ²⁺
III	Lighter grey	Dolomite	Fine-grained crystals	Diffusely distributed, high content, kerogen (D and G bands)	Ca, Fe, Mn, Sr, S	Fe ²⁺ and Fe ³⁺ Mn ²⁺

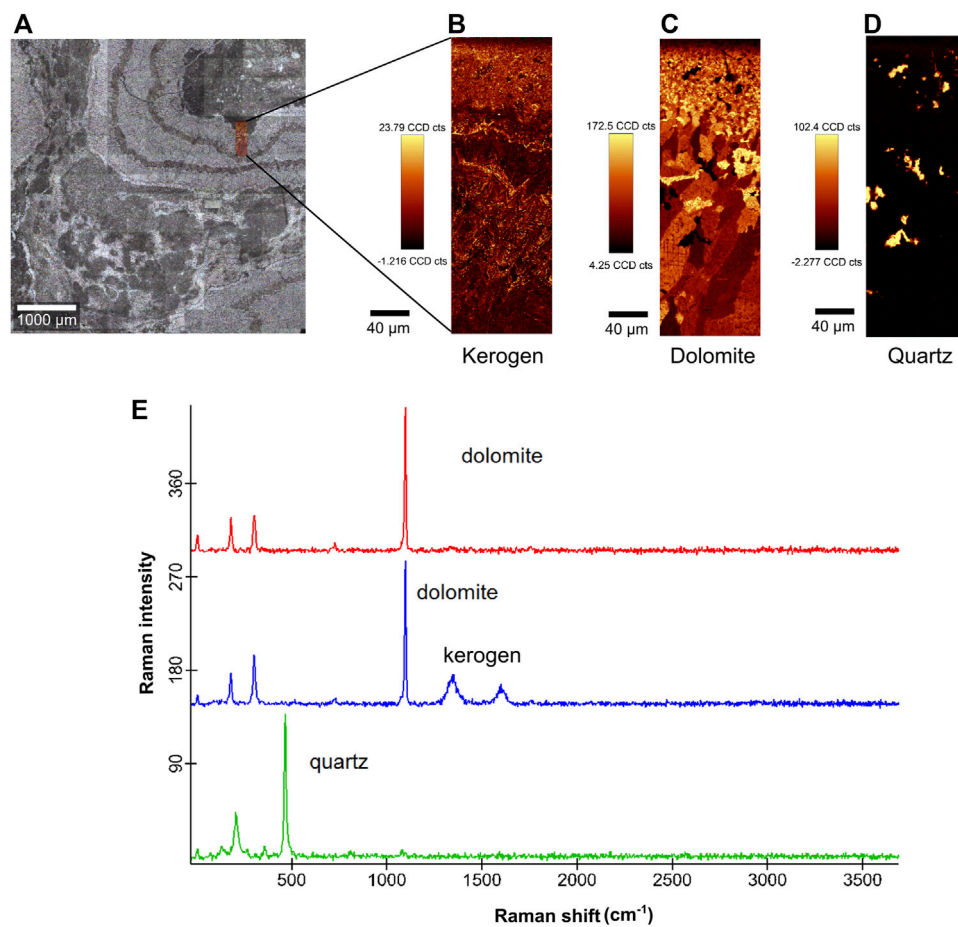


FIGURE 4

Raman spectroscopy analysis of the CP6/196 sample. (A) thin section with mapped area (0.2 mm × 0.6 mm), covering both dark grey laminae (biofilms) and light grey laminae (dolomite and quartz crystals); (B) map of quantitative distribution of kerogen showing higher counts for kerogen in the biofilm area; (C) map of quantitative distribution of dolomite showing homogeneous distribution in the two laminae; (D) sparse quartz grains distributed in both laminae; (E) Raman spectra of dolomite at 1,098 cm⁻¹ (red and blue), carbon (kerogen) with D band at 1,366 cm⁻¹ and G band at 1,583 cm⁻¹ (blue) and quartz at 464 cm⁻¹ and 203 cm⁻¹ (green).

color, while the grain size and texture appear to be the same when looking at petrographic thin sections. However, the biofilm I showed exclusively microcrystalline apatite (Section 4.4), while

the biofilm II and III showed highest intensity in fluorescence signal of Sr in comparison with biofilm I (Supplementary Figure S2). The Table 2 summarizes some main textural and

geochemical aspects which may be used to differentiate the three biofilms which comprises the dark grey laminae.

4.3 Petrological composition in Raman spectroscopy and X-ray diffraction

The Raman semi-quantitative peak intensity maps were acquired in an area covering both dark and light grey laminae (Figure 4A). The maps showed that in the biofilm area (dark grey laminae) had the highest counts of carbon (kerogen, D band—ca. $1,366\text{ cm}^{-1}$ and G band—ca. $1,583\text{ cm}^{-1}$) in comparison with the light grey laminae (Figure 4B). Dolomite is the main component in light-grey laminae, except in areas with high counts of quartz (Figure 4C). The quartz is sparsely dispersed in the dark grey laminae and between the dolomite crystals in the light grey laminae (Figure 4D). Comparing the maps of quantitative distribution of kerogen (Figure 4B) and dolomite (Figure 4C), it is possible to observe that the kerogen is diffusely distributed between the microcrystalline dolomite in the dark-grey laminae, while in light-grey laminae, the kerogen is distributed near to the grain boundaries. The Raman spectra for each component are in Figure 4E: dolomite ($1,098\text{ cm}^{-1}$), kerogen (D band at $1,366\text{ cm}^{-1}$ and G band at $1,583\text{ cm}^{-1}$) and quartz (464 cm^{-1} and 203 cm^{-1}).

The XRD data showed that the main mineral phase present in the *Conophyton* is dolomite. All Bragg reflexions (indexed according to the AMCSD 0000108, Graf 1961), correspond to dolomite (Supplementary Figure S1). However, the presence of discontinuous rings and isolated spots on the 2D diffraction patterns indicates that the beam is illuminating a small amount of crystallites. As a consequence, phases in a small fraction remain undetermined.

4.4 Petrology and composition using EPMA and EDS

In higher resolution analyses, the light grey/white laminae are composed of coarse components (approximately $100\text{ }\mu\text{m}$ – $500\text{ }\mu\text{m}$) including dolomite and scattered quartz grains. Dolomite commonly forms mosaics of euhedral to anhedral crystals, composing an idiomorphic texture. The darker laminae are composed of microcrystalline dolomite with dissipated carbonaceous matter (ancient EPS and cell materials of the stromatolite). The apatite crystals measure from less than $1\text{--}10\text{ }\mu\text{m}$ (maximum). EDS and EPMA analysis show that the small crystals in the ancient biofilms (dark grey laminae; Figures 5A,B) are composed of Ca, Mg, C and O (Figure 5D), corroborating with the dolomite detected by Raman spectroscopy and XRD. Exclusively within the biofilms of the dark grey laminae (biofilm I) very small crystals composed of P, Ca, O and F (compatible with apatite ($\text{Ca}_5(\text{PO}_4)_3$ —general formula) are distributed, Figure 5C.

4.5 Elemental composition of the textures in μ -XRF

Semi quantitative elemental maps with the spatial resolution of $30\text{ }\mu\text{m}$ were acquired in the surface area of $7\text{ cm} \times 8\text{ cm}$ of the samples CP6/203a and CP6/203b (yellow square in Figures 6A,B). The maps were made covering all areas of interest (light and dark grey laminae, and region of hydrothermal vein) in order to compare the compositions. Ca is distributed all over the mapped area, related to dolomite crystals (Figures 6D,E). Si and K are present in some spots, the first one in spots containing authigenic quartz areas in light grey laminae. In the biofilm areas, the analyses showed the predominance of Ca and Fe (Figures 6D,E). The Mn is widespread all over the mapped area, but is present at higher concentration (intensity) in the region with hydrothermal veins, co-occurring with Fe (Figure 6D). Especially in the biofilm III area, Mn, Fe, S and Sr present in higher intensity than in the regions containing other biofilms (Figures 1, 6E, Supplementary Material). Signals from low Z elements such as Si, K and Al are more absorbed within the rock or by the air, making their detection harder than heavier elements. The lack of detection, therefore, does not imply the absence of these elements in our samples.

4.6 Chemical speciation of Fe and Mn contained in *Conophyton*

μ -XANES was applied to evaluate the Fe and Mn chemical speciation (Figure 7). Mn was also investigated with nano-XANES. Fe synthetic references based on iron oxides (Fe_3O_4 , Fe_2O_3 and FeO), and Fe metallic (Fe^0) are compared to the *Conophyton* X-ray absorption spectrum, measured around the Fe K-edge. By qualitative analyses of the absorption spectra (Figure 7A) and the first derivative curves (Supplementary Figure S3), the results suggest Fe is present in a mix of 2+ and 3+ valences. Similar analysis was made to evaluate the Mn oxidizing state (Figure 7B). Even though the signal-to-noise is high due to the low concentration of Mn, it is clear, by qualitative analysis, the predominance of Mn^{2+} . It is noticeable that both measurements (biofilm I and II, and biofilm III) present edges position compatible with the one observed in MnO, which is a reference for Mn^{2+} indicating the predominance of Mn in 2+ form in both biofilms.

4.7 X-ray excited optical luminescence

The 2D map was made in an area of the *Conophyton* (sample CP6/196) covering the dark grey and light grey laminae and also the region containing a hydrothermal vein, in order to evaluate the difference in composition of original laminae and thermally modified areas (Figure 8A) through optical emission. The X-ray

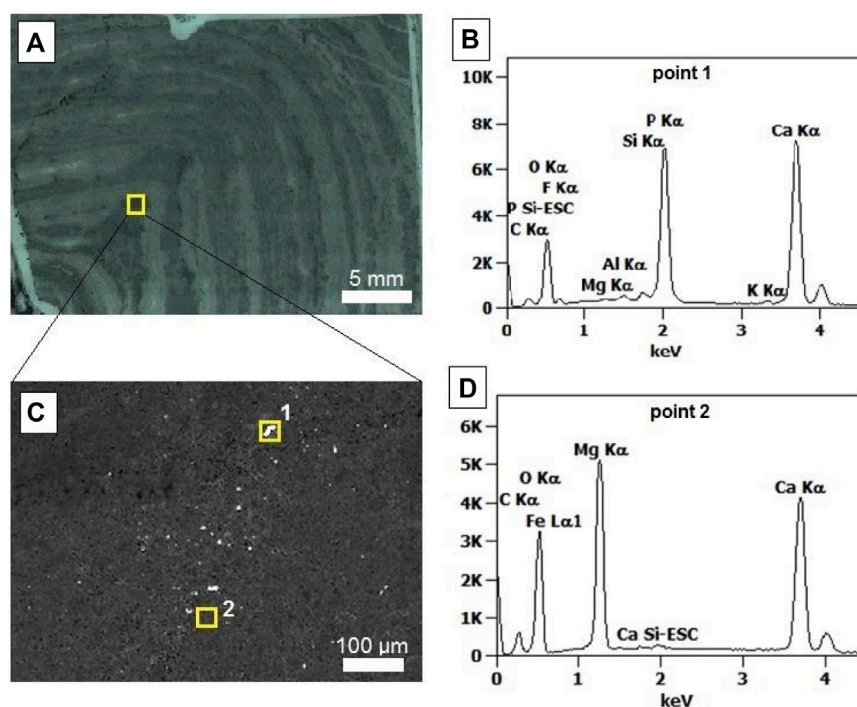


FIGURE 5

EDS spectra (sample CP6/196). (A) thin section showing the analyzed area (dark grey laminae, biofilm; indicated by square); (B) point 1 EDS spectra, compatible with apatite; (C) analyzed area with square 1 (mineral in biofilm II) and square 2 (matrix); (D) point 2 EDS spectra, indicating dolomite composition.

excited optical luminescence image (Figure 8B) shows the regions of more intense luminescence in the sample (yellow to red region, with corresponding general emission spectra with a broadband at the orange-red wavelength range at 650 nm). This area coincides with the diagenetic hydrothermal vein in *Conophyton*. Considering the co-location of Ca, Fe and Mn (XRF maps, Figure 6), the presence of dolomite (Raman—Figure 4; and XRD analysis—Supplementary Figure S1) and the presence of the chemical species showed in XANES analysis (Figure 7), the interpretation of the broadband in the general emission spectra (Figure 8C) leads to the conclusion that the Mn^{2+} within the dolomite lattice as the responsible for the luminescence emission.

5 Discussion

5.1 Preservation of biofilms

There is no evidence for bacterial cells and filaments preserved in the fossilized biofilms from the *Conophyton* of the Paleontological Site of Cabeludo. However, the biofilms are well preserved in both macro and microstructure. Here, we support that these biofilms have been partially preserved as

organic matter (OM) diffused in a dolomitic matrix in regions considered to be authigenic (observed in petrographic thin sections as dark gray laminae) (Figure 3).

Contrary to what is assumed for the paleoenvironment of the stromatolites of the *Conophyton* genus, Moeri (1972) suggested a highly energetic subtidal basin as the most probable environment during the development of the *Conophyton* of the Cabeludo site. The main lines of evidences for the author's interpretation are 1) the great rate of carbonate supply and the early and rapid lithification required for the considerable height of the stromatolites; 2) the absence of subaerial exposure features (that explains the lack of signals of desiccation in the outcrop) which may exclude the possibility of supratidal or intertidal conditions; 3) the absence of micritic matrix; 4) the elongation of the plan outlines in most columns of the stromatolites, which may point to an influence of strong permanent water currents. According to Dardenne (2005), the early lithification was penecontemporaneous with dolomitization. Additionally, the sedimentary environment was described as a subtidal and deep marine setting, with the influence of sporadic tidal currents (that explains the existence of extremely dense bioherms isolated from each other, in addition to the deposition of micritic mud in the intercolumnar space, according Dardenne (2005).

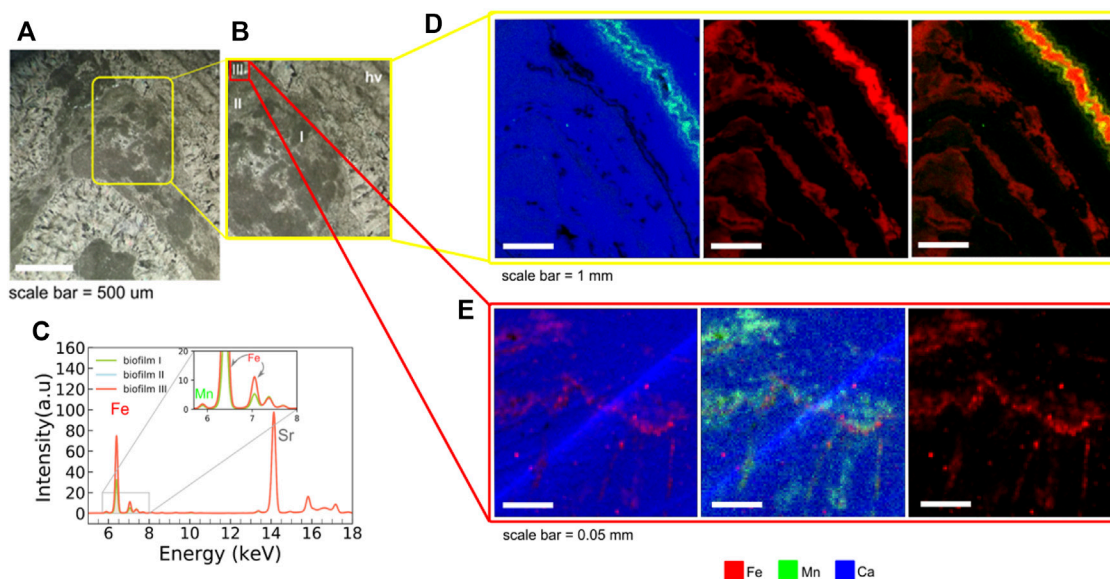


FIGURE 6

μ -X-Ray fluorescence elemental maps from the sample CP6/203b. (A) Petrographic image (scale bar = 500 μ m) showing the area analyzed, containing the three types of biofilms (dark grey laminae) and light grey laminae. The yellow square represents the mapped area mapped with 30 μ m step size; (B) Analyzed area (yellow square) with biofilm I, II and III and hydrothermal vein (hv) mapped in 30 μ m steps (LNLS) and area of biofilm III selected to be mapped with higher resolution at microXAS beamline, SLS (red square); (C) X-ray fluorescence spectra of Fe, Mn and Sr, obtained in the mapped areas from biofilm I, II and III; (D) elemental maps with 30 μ m of step size (XRF beamline, LNLS) in area covering the three types of biofilms, plus an area with hydrothermal vein (with highest intensity of Mn), scale bar = 1 mm; (E) elemental maps with 3 μ m of step size (microXAS beamline, SLS) of area covering the biofilm III. All maps of the figure show the composition of Ca (blue), Mn (green) and Fe (red).

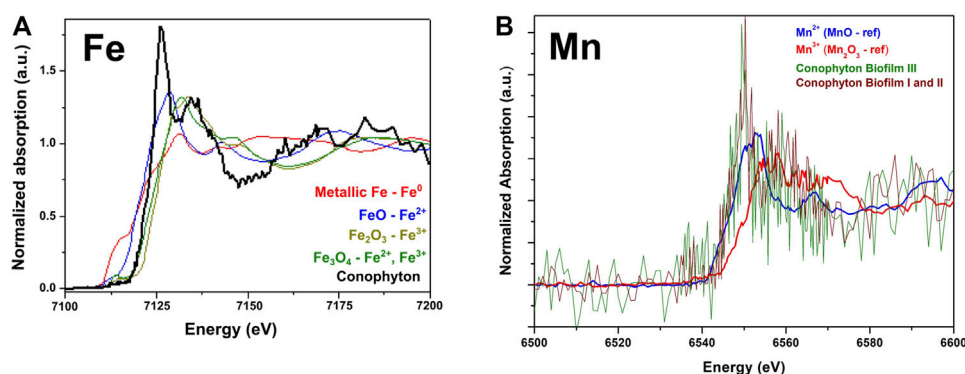


FIGURE 7

XANES absorption spectra of the sample CP6/196. (A) Normalized absorption curves and comparison between the synthetic Fe standards and the *Conophyton* sample; (B) Normalized absorption curves of synthetic Mn standards and *Conophyton* sample.

The early and rapid lithification plus the high rate of sedimentation may have prevented and/or delayed the degradation of the biofilms by aerobic microorganisms. In fact, Raman data acquired in this study shows the preservation of OM, as evidenced by the D and G bands (1,366 and 1,583 cm^{-1}) of kerogen. The quantitative maps (Figures 4B,C) show that kerogen is distributed in a diffuse

way in the dark-gray laminae, while in the light-grey laminae it is limited to the grain boundaries. This can mean that in the dark-grey laminae the OM could be preserved *in situ*, even with the post-diagenetic events. In contrast, in the light-grey laminae, the kerogen was moved to the grain boundaries or in between regions of overgrowth of grains (Figure 4B) due to the secondary dolomitization. The dolomitization can make the preservation of

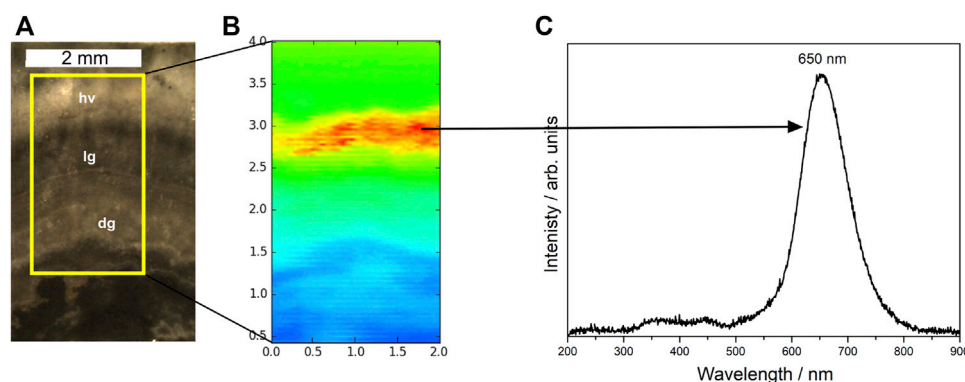


FIGURE 8

X-ray excited optical luminescence (XEOL) image with respective emission spectra under X-ray irradiation. (A) Selected area to be mapped (scale bar: 2 mm), covering areas with dark (biofilms, dg) and light grey laminae (lg), and region with hydrothermal vein (hv); (B) X-ray excited optical luminescence (XEOL) temperature scale image (2 mm × 4 mm), acquired at the X-ray Fluorescence (XRF) beamline at the LNLS with step size of 30 μm; (C) general emission spectra showing a broadband at the orange-red wavelength range at 650 nm.

the microbial morphology difficult (Bartley et al., 2000), but OM can be preserved even after secondary dolomitization, mainly as organic matter particles trapped within dolomite crystals (Murphy et al., 2020).

This sedimentological context also supports a mineral-associated organic matter (MAOM) hypothesis. By studying different types of carbonates of microbial origin in different environmental contexts, Melim et al. (2016) indicated that the entombment of microbes and EPS in carbonates is more widespread than previously thought: it does not occur in travertines, for example, because of the photolytic degradation by sunlight, elevated temperatures, and aerobic microbial degradation. Hence, considering the environmental and physical conditions mentioned for the good preservation of the microbial signatures mentioned above, the paleoenvironmental context of *Conophyton* from the Cabeludo could have favored biofilm preservation due to the fast mineralization.

As observed in XRF elemental maps (Figure 6), it is remarkable that iron is co-located exclusively with the biofilm preserved laminae and in some post-diagenetic features, such as fractures with incursion of hydrothermal fluids. Mineral-associated organic matter (MAOM) in sediments is commonly adsorbed or co-precipitated with the iron minerals (Lalonde et al., 2012). MAOM is thought to persist because OM can form strong chemical bonds to minerals and can be physically protected in microaggregates or co-precipitates (Kögel-Knabner et al., 2008). The association of OM with minerals can restrict the diffusion of oxygen, slowing down natural degradation and protecting it from decomposers. According to our XANES data there is a mix of valencies of iron in the biofilm preserved laminae of *Conophyton*, consisting of Fe^{2+} and Fe^{3+} . The Fe^{3+} , exerting a structural role, may serve as a connective

cement allowing the formation of aggregates of OM and minerals. Also, the Fe^{3+} may serve as a sorbent in which the OM adsorb or co-precipitate with the Fe^{3+} minerals (Chen et al., 2020). In this sense, the Fe^{3+} detected in the region of preserved biofilms may also have been another factor that helped the preservation of OM in *Conophyton*.

5.2 Distribution of different biofilms inside the *Conophyton*

Modern microbial mats can be considered relevant analogues to understand the ecology and the formation of stromatolites, (Dupraz et al., 2009; Foster and Mobberley, 2010; Saghai et al., 2017). The microbiota of a well-developed and stratified microbial mat is very diverse (Des Marais, 1990), composed of microorganisms that form a biogeochemical gradient according to the metabolic needs of their functional groups (Dupraz and Visscher, 2005; Dupraz et al., 2009).

In fact, even in Archean time, microbial mats could already exhibit structural and biological complexity in their ecosystems (Nisbet and Fowler, 1999). Hickman-Lewis et al. (2020) showed evidence of coexistence between Bacteria and Archaea on microbial mats dated 3.5–3.3 Ga based on fossilized biopolymers detected by Fourier transform infrared spectroscopy (FTIR). The microbially induced sedimentary structures (MISS) in the 3.48 Ga Dresser Formation record that benthic microorganisms could already assemble biofilm communities to biofilm forming geomorphologically controlled catenae in response to environmental conditions (Noffke et al., 2013). The more different kinds of microorganisms compose a biofilm, the more complex its internal build-up becomes. Biofilm development integrates

growth conditions and the microbial composition in such a way that the available resources have an optimal exploitation (Tolker-Nielsen and Molin, 2000). An early stage of biofilm includes few microbial groups and a simple internal build-up (often just a few layers); a more mature biofilm, however, has a higher degree of organization and may show a mottled structure (Stoodley et al., 2002; Stolyar et al., 2007; Pernthaler et al., 2008).

Stromatolites are formed initially by microorganisms in a microbial mat and their metabolic activity and geochemistry leads to induction of calcium carbonate precipitation (Reid and MacIntyre, 2000; Dupraz et al., 2009). But not all microbial mats develop a stromatolite; it depends on the microbiota composition, the dominant metabolisms and the surrounding geochemical environment (Havemann and Foster, 2008; Foster and Green, 2011). Stromatolites, in general, are formed mainly by photosynthesizing microorganisms, especially filamentous cyanobacteria (Awramik and Margulis, 1974; Burne and Moore, 1987; Riding, 2011; Noffke and Awramik, 2013), but its microbial diversity may be greater, depending on the environmental parameters. Foster and Green (2011), in an experiment with cultivation-independent molecular techniques in several modern stromatolites, attested to a greater microbial diversity in marine and hypersaline stromatolites. Based on the complexity of the ecosystems that gave rise to some of the stromatolites and microbial mats in the Precambrian, comparing them with their modern representatives, and based on the evidence showed here, we suggest the possibility of greater complexity in the formation of Conophyton from the Paleontological Site of Cabeludo.

According to Walter (1977) and also Sallun Filho and Fairchild (2005), the conical shape typical of *Conophyton* denotes the competition for space, nutrients, and light between microorganisms. This would cause an accumulation of biomass at the apex of the forming stromatolitic structure, resulting in the conical shape observed in the microbialites of the genus. However, in this study, the textures on the analysed thin sections point to the existence of different types of biofilms preserved in each dark grey laminae of the stromatolites at the Cabeludo Paleontological Site, revealing at least three communities or populations of microorganisms (distinct or not) growing at the same time. It may imply more than one metabolic group forming the structures, rather than only photosynthesizers competing for sunlight. These three different types of biofilm show a clear tendency to organize into a specific repetitive laminae pattern revealing sequence and cyclicity observed in thin sections across the longitudinal axis of several samples of *Conophyton*. Figure 9 schematizes the evolution of spatial distribution and organization of the three types of biofilms (here called biofilm I, II and III) over the time; the evolution takes place in four stages (denoted in the yellow squares in Figure 9):

Stage 1: in the initial phase of the stromatolite formation, the biofilm I and II were formed. The biofilm I is located in the deeper zone of the mat, while the biofilm II is located in the surface; this arrangement may be due to affinity (synergy) and similar needs of the two constituents for resources such as nutrients and light.

Stage 2: a new type of biofilm (biofilm III) colonizes the preceding two biofilms. It is positioned above the biofilm II, demonstrating a certain competition among the different species for light. This can be observed by the higher concentration of biomass (II and III) starting to accumulate at the apex of the laminae. At this stage, biofilms I and II appear to be distributed in the same pattern observed in stage I, while the biofilm III occupies the upper zone near the apex of the laminations.

Stage 3: the three biofilms appear to have reached a certain equilibrium regarding their spatial distribution and organization according to each metabolic needs: an even pattern of distribution of the biofilms is established, following the sequence of development (from the bottom to the top of the community): biofilm I → biofilm II → biofilm III.

Stage 4: the pattern of spatial distribution and organization of the biofilms reached in the stage 3 starts to repeat until the top of the stromatolites, as observed in thin sections of the top part of the structures.

5.3 Depositional versus post-depositional processes: Origin of internal organization of *Conophyton*

Along the *Conophyton*, laminae with a pointed apex (especially those formed by greater mass of biofilms) may show high competition between constituents. Where the stromatolite apex is more rounded, the biofilms have been assembled and reached an equilibrium stage, which is stage 4. A possible interpretation for the difference in biofilms distribution is that, at certain times of high environmental stress (such as decrease of nutrient availability), probably due to a periodic lack of illumination, the biofilms' community disperses and moves towards the best light and nutrient exposure regions. The competition for the resources is documented by biofilm in stage 2. The stage 1 is the original state of distribution of biofilms (types I and II) in the beginning of the microorganism proliferation; due to a possible increase in light and nutrient provision, the biofilm type III started to associate with the original biofilms I and II. Possibly motivated by environmental stress, biofilm III struggled towards the top after spreading out, establishing an equilibrium situation, which was maintained until the top of the structures. Our most plausible hypothesis to explain this interaction and distribution between biofilms I, II and III is that at least the biofilm II and III were constituted by photoautotrophs. In contrast, the biofilm I, which preferentially remains at the base of the stratification

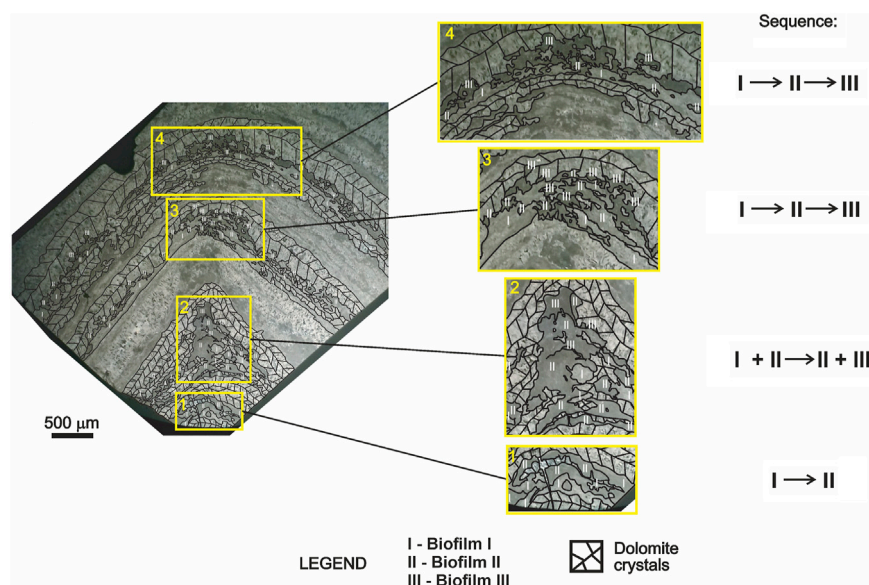


FIGURE 9

Distribution of the three different biofilms in *Conophyton* from the bottom to the top of a thin section (CP6/203b). Sequence of distribution of the different biofilms from the bottom of the structure (stage 1; 1 in yellow square) to the upper laminations towards the top (stage 4; 4 in yellow square) and organization of the biofilms according to resources. In stage 1, the biofilm II is organized above the biofilm I. In stage 2 (2 in yellow square), a new type of biofilm (biofilm III) develops above the biofilm I and II, in the apex of the dark grey laminae. In this stage, the biofilm I and II remain diffusely organized (represented by I + II), while the biofilm III is arranged at the apex, but still seems to mix with the biofilm II (represented by II + III). In the next stage (stage 3 and 4), the sequence of distribution follows the pattern (from the bottom to the top of the laminae: biofilm I → biofilm II → biofilm III.) The pattern is repeated in the subsequent laminations to the top of the stromatolite.

formed, possibly belongs to a non-photosynthetic metabolic type. However, in situations of environmental stress due to the lack of nutrients and sunlight, biofilm III would be more effective than biofilm II, reaching the top to ensure its survival.

Other hypotheses include the influence of textural aspects (crystal size, porosity and permeability) that likely might have controlled the distribution of the organic matter within the rock framework. The repetitive organization of biofilms and their vertical distribution indicates that textural aspects did not exert a major influence in organic matter content. If this was the case, a random distribution of kerogen would be expected. Similarly, heterogeneous modifications by weathering are not the case, since oxidation and chemical reactions would cause degradation of the organic matter from the top toward the bottom, which is not the case in the Cabeludo site. In addition, weathering would damage the internal organization of the *Conophyton* structure. Lastly, although metamorphism and hydrothermalism occur in the vicinity of the study area, some criteria (e.g., preservation of original structures, lack of high temperature/high pressure minerals) indicate that these processes did not cause significant modifications in the composition of the *Conophyton*. Geochemical data exhibit predominance of Ca, Fe and Mn, whereas elements commonly associated with high temperatures (Cu, Pd, Zn) were not detected in the analyzed samples. The only signal of hydrothermalism affecting the Cabeludo site is fracture-filling veins, but this process likely took place after lithification, as

indicated by the predominantly tabular-shaped veinlets that crosscut the *Conophyton*. Metamorphic evidence is not present in the study area, since the recrystallization of dolomite is interpreted to have occurred during diagenesis.

5.4 Geochemical evidence and possible biosignatures for the biofilm differentiation

Exclusively in areas with biofilm I (and sometimes in the biofilm II), phosphate occurs as cryptocrystalline apatite. As shown in Figure 5D very small crystals of apatite appear in the biofilm II area (within the dark grey laminae) while in the other areas, such as the biofilm III and the light grey laminae, the phosphate mineral was not found. As observed, the biofilm I preferentially remains at the base of the stratification in each dark grey laminae, meaning a lower need for sunlight than biofilms II and III. Therefore, there is a possibility that biofilm I may consist of non-photosynthetic species.

Caird et al. (2017), studying Ediacaran stromatolites from Salitre Formation, Brazil, reported the occurrence of phosphorites (francolite) in microbial laminae, whereas strontian fluorapatite occurs between stromatolitic layers. They interpret the accumulation of phosphorites as a consequence of the activity of chemosynthetic bacteria, which, benefiting from the redox gradient caused by the production of photosynthetic oxygen,

promote the *in situ* precipitation of phosphorites. The XRF data in this study showed the presence of Sr in both biofilms I, II and III, but the highest intensity was observed in the biofilm III mapped area. However, we could not identify the link between Sr with the phosphorites in at least the biofilm I and II (in which the phosphorites were found). The Sr is co-located with Ca in some regions in biofilm II and III (Supplementary Figure S2), but it is common the incorporation of metals, such as the strontium (Sr^{2+} , VI-fold coordination, Ionic radius: 1.18 Å), into the CaCO_3 mineral phases, when the metals replace the calcium (Ca^{2+} , VI-fold coordination, Ionic radius: 1.00 Å) in the crystal lattice. As a consequence, there is a co-precipitation of the solid formed, such as the SrCO_3 , or even a calcite doped with Sr^{2+} . Ferris et al. (1995) showed that the incorporation of Sr-rich groundwater during the microbial calcite nucleation promoted the solid solution of SrCO_3 in calcite. In Conophyton, it is possible that Sr may have been associated with the microbially-induced calcite nucleation during the growth of the stromatolite, explaining the co-location of Ca and Sr in the fossilized biofilm zones. However, it is not possible to exclude the hypothesis of substitution of Ca^{2+} by Sr^{2+} in the crystal lattice of carbonates by abiotic way.

Although the formation of phosphatic minerals in marine environments is still poorly understood, the involvement of bacteria in this process is presumed. Dissolved phosphorus in the ocean water is easily incorporated by photosynthetic organisms (Compton et al., 2000). However, organic matter can capture the phosphorus and remobilize it by microbiological processes. Crosby and Bailey (2012) discussed the role of microorganisms in the genesis of phosphatic minerals using several works to exemplify the relationship of microorganisms with different mediation mechanisms in apatite formation. One of them was proposed by Schulz and Schulz (2005), in which the vacuolated sulfide-oxidizing bacteria (SOB) can concentrate polyphosphates in pore water, where apatite is constantly precipitating. According to Crosby and Bailey (2012), several factors may have an effect on the rate of precipitation of apatite, such as the pH, redox potential, the existence of suitable nucleation sites, activation energy for the precipitation, and the microbial activity may influence all of them. Williams and Reimers (1993) and Williams (1984) documented a relation between bacteria and phosphorite formation in fossil record. In their study, they suggest that SOB were involved in phosphogenesis in fossil microbial mats with phosphate-rich laminations under aphotic conditions. In Conophyton, the fact that biofilm I is located in the deepest layer of dark-grey laminae exposes it to constant sunlight deprivation, since photosynthetic biofilms are always above them.

Shukla et al. (2020) described the influence of SOB in the formation of phosphorites in association with biofilms preserved in Neoproterozoic shales. They argue that bacteria, in an extracellular way, create redox conditions favorable to the precipitation of phosphorites. In that case, the bacterial EPS or the chemical ligands in the cell wall provide nucleation sites and decrease the activation energy for the mineral precipitation.

A similar situation may have occurred in the biofilm zones I (and even II) of the Conophyton. The phosphate precipitation is favored due to the acidification of the medium when the oxygen serves as an electron acceptor in the SOB cell walls (Crosby and Bailey, 2012). The inorganic phosphate precipitation could be considered in Conophyton, however, the mineral occur only in areas of biofilm I and sometimes, II, never occurring in the biofilm III laminae. Another evidence for the exclusion of this possibility is the size of the crystals, never reaching more than 10 μm .

The XRF maps show that the region of preserved biofilms in Conophyton is rich in Ca, Fe and Mn (Figure 6). In these areas, Ca is co-located with Fe and Mn (the latter one with low intensity), while in the diagenetic hydrothermal vein, the Ca is co-located with Fe and Mn (with higher intensity than in fossilized biofilm areas). The Raman spectra (Figure 4) and XRD analysis (Supplementary Figure S1) showed the presence of dolomite in both areas. Mn^{2+} is known to induce high luminescence intensity in dolomite even in ppm concentration (i.e., as a trace element), and its emission is represented by a broadband at the orange-red region with maximum wavelength ca. 650 nm (Figure 8C), while the Fe^{3+} works as a luminescence quencher (Pierson, 1981; Marfunin, 1995; Habermann et al., 1998). In the XEOL emission spectra (Figure 8C), it is observed as a broadband that is ascribed as the $3d^5 \rightarrow 3d^5 4T_1(4G) \rightarrow 6A_1(6S) \text{Mn}^{2+}$ (Marfunin, 1995; Shionoya et al., 2007; MacRae and Wilson, 2008; Gaft et al., 2015). In the XEOL emission spectra (Figure 8C) it is observed as a broadband in the orange to red region in the electromagnetic spectrum, which is ascribed as the typical $3d^5 \rightarrow 3d^5 4T_1(4G) \rightarrow 6A_1(6S) \text{Mn}^{2+}$. This is a characteristic electronic transition from this ion that describes the decay from an excited energy level $4T_1(4G)$ to the ground level $6A_1(6S)$. This result indicates that the hydrothermal vein, the region of the most intense luminescence (Figure 8B) is rich in dolomite doped with Mn^{2+} , diagenetically included after the lithification of the stromatolitic structure. Additionally, the X-ray absorption analysis detected the presence of chemical species such as Fe^{2+} , Fe^{3+} in areas of preserved biofilms. The Fe^{3+} are present in hydrothermal veins and cracks, possibly the result of diagenetic incorporation by incursion of hydrothermal fluids and/or groundwater before the stromatolite's lithification.

The decomposition of OM during the early diagenesis by the action of microorganisms from the biofilm itself can produce humic substances, a complex mixture of organic components synthesized during the decomposition of matter original OM (Lovley et al., 1996). This can also be caused by the burial of biofilms due to the mineral precipitation process during the growth of the stromatolitic structure. Once stable, the humic substance can serve as electron donors for other microorganisms, which use them in their energy generation processes (for example, *Geobacter metallireducens* to reduce ferric iron— Fe^{3+}). The reduction of Fe^{3+} is then conducted abiotically, reoxidizing the humic substances previously produced (Lovley et al., 1996). In Conophyton, the iron is

widespread over the biofilm-preserved laminae and in fractures filled diagenetically by fluids. The Fe^{2+} is diffusely distributed in regions of biofilm preservation, possibly being interpreted as a product of abiotic reduction of Fe^{3+} and/or product of the reduction of Fe^{3+} through the action of iron bacteria as electron acceptors from the biotic decomposition of organic matter. The role of iron in microbial ecosystem is diverse: (I) it allows the electron transfer in the system (the Fe^{3+} accept electrons from microbes or Fe^{2+} donate electrons for oxidants); (II) it serves as a sorbent in which the OM absorb Fe^{3+} in minerals, and (III) the Fe^{3+} can serve as connective cement binding OM and minerals (Chen et al., 2020). This last role is what probably happened during the fossilization process of the biofilms in Conophyton of Cabeludo Paleontological Site.

6 Conclusion

The stromatolites of the subgroup *Conophyton cylindricus* Maslov present in the Paleontological Site of Cabeludo, Vazante Group in Brazil, are a typical occurrence of the conical bioconstructions from the Mesoproterozoic. These structures present, at the microscale, morphological characteristics pointing towards the past presence of a stratification of at least three different types of biofilms forming the preserved organic laminae (the dark grey laminae) of the stromatolite. The three different biofilms form a pattern of distribution denoting an equilibrium situation between them towards the top of the structures. The presence of carbonate laminations rich in phosphates in the deepest biofilms in each dark grey laminae (biofilms I and II) are indicative of the possibility of past existence of sulfide-oxidizing bacteria. Thus, the diversity in the microbiota which formed these stromatolites was greater than previously thought, explaining the microscopically observed stratification.

Data availability statement

The datasets presented in this study can be found in online repositories. The names of the repository/repositories and accession number(s) can be found in the article/Supplementary Material.

Author contributions

All the authors contributed in the writhing, interpretations and discussion of the results. FC, F-RB and AM made the field trip for collecting samples; VC, IN, DG, LM, EB, NN, DB and DF participated of the sample's analysis, processing data and interpretation; MA, AR, NN, VC and F-RB participated in the discussion of results; F-RB coordinated the first phase of the study and provided the financial support for the field trip.

Funding

Brazilian Federal Agency for Support and Evaluation of Graduate Education—CAPES and the PDSE Program for the financial support, and scholarship in the beginning of the study; National Council for Scientific and Technological Development—CNPq Research Productivity Grants (310817/2020-0, 310,890/2021-7 and 303527/2017-0) and the São Paulo Research Foundation—FAPESP grants 2016/20927-0 and 2016/06114-6 (for funding the field trips to collect the samples), 2020/02537-5 and 2021/05083-8 for funding analysis and fellowship for this project, and 2015/21810-6 scholarship; the French National Research Agency in the framework of the Investissements d'Avenir program (ANR-15IDEX-02).

Acknowledgments

The authors thank the University of Brasília, Nexa Resources and the geologist Bruno Baptistella for the support in the field trip; the Brazilian Synchrotron Light Laboratory (LNLS) for the facilities (μ -XRF, μ -XEOL, and XANES, proposals 20150076, 20160140 and 20180687) and Carnauba beamline (XANES, proposal 20210014); the microXAS beamline at Swiss Light Source (SLS, proposal 20190823); the Earth and Planets Laboratory at the Carnegie Institution of Science (Washington, DC) for the availability of the Raman spectrometer and EPMA microprobe. We also thank Dr. Silvio Y. Onary Alves (USP) for some clarification on terms and concepts about biological evolution.

Conflict of interest

The authors declare that the research was conducted in the absence of any commercial or financial relationships that could be construed as a potential conflict of interest.

Publisher's note

All claims expressed in this article are solely those of the authors and do not necessarily represent those of their affiliated organizations, or those of the publisher, the editors and the reviewers. Any product that may be evaluated in this article, or claim that may be made by its manufacturer, is not guaranteed or endorsed by the publisher.

Supplementary material

The Supplementary Material for this article can be found online at: <https://www.frontiersin.org/articles/10.3389/feart.2022.804194/full#supplementary-material>

References

- Almeida, F. F. M. (1977). O cráton do São Francisco. *Rev. Bras. Geociências* 7 (4), 349–364. doi:10.25249/0375-7536.1977349364
- Awramik, S. M., and Margulis, L. (1974). “Definition of stromatolite,” in *Stromatolite newsletter*. Editor E. Walter, 2, 5.
- Awramik, S. M. (1992). “The history and significance of stromatolites,” in *Early organic evolution* (Berlin, Heidelberg: Springer), 435–449.
- Bartley, J. K., Knoll, A. H., Grotzinger, J. P., and Sergeev, V. N. (2000). “Lithification and fabric Genesis in precipitated stromatolites and associated peritidal carbonates, Mesoproterozoic Billi Akh Group, Siberia,”. Editors J. P. Grotzinger and M. P. James (SEPM Spec. Publ.), 67, 59–73. *Carbonate Sediment. Diagenesis Evol. Precambrian World*.
- Bertoni, M. E., Rooney, A. D., Selby, D., Alkmim, F. F., and Le Heron, D. P. (2014). Neoproterozoic Re–Os systematics of organic-rich rocks in the São Francisco Basin, Brazil and implications for hydrocarbon exploration. *Precamb. Res.* 255, 355–366. doi:10.1016/j.precamres.2014.10.010
- Bertrand-Sarfati, J., and Moussine-Pouchkine, A. (1985). Evolution and environmental conditions of Conophyton–Jacutophyton associations in the atar dolomite (upper proterozoic, Mauritania). *Precamb. Res.* 29, 207–234. doi:10.1016/0301-9268(85)90069-5
- Bertrand-Sarfati, J. (1972). Paléocologie de certains stromatolites en récifs des formations du Précambrien supérieur du groupe d'Atar (mauritanie, sahara Occidental): création d'espèces nouvelles de ces récifs. *Palaeogeogr. Palaeoclimatol. Palaeoecol.* 11, 33–63.
- Burne, R. V., and Moore, L. S. (1987). Microbialites: Organosedimentary deposits of benthic microbial communities. *Palaio* 2, 241. doi:10.2307/3514674
- Burne, R. V. (2022). A radical reinterpretation of the growth and form of the stromatolite Conophyton lituus (Maslov) from evidence of syngenetic biofilm mineralisation. *J. Paleogeogr.*, 11, 69–84. doi:10.1016/j.jop.2021.09.003
- Caird, R. A., Pufahl, P. K., Hiatt, E. E., Abram, M. B., Dourado, A. R., Kyser, T. K., et al. (2017). Ediacaran stromatolites and intertidal phosphorite of the Salitre Formation, Brazil: Phosphogenesis during the neoproterozoic oxygenation event. *Sediment. Geol.* 350, 55–71. doi:10.1016/j.sedgeo.2017.01.005
- Chen, C., Hall, S. J., Coward, E., and Thompson, A. (2020). Iron-mediated organic matter decomposition in humid soils can counteract protection. *Nat. Commun.* 11, 2255. doi:10.1038/s41467-020-16071-5
- Cloud, P., and Dardenne, M. (1973). Proterozoic age of the bambui group in Brazil. *Geol. Soc. Am. Bull.* 84, 1673–1676. doi:10.1130/0016-7606(1973)84<1673:PAOTBG>2.0.CO;2
- Cloud, P., and Moeri, E. (1973). Conophyton in the bambui group: What form and age? *Geology* 1 (3), 127. doi:10.1130/0091-7613(1973)1<127:CITBGW>2.0.CO;2
- Compton, J., Mallinson, D., Glenn, C. R., Filippelli, G., Föllmi, K., Shields, G., et al. (2000). “Variations in the global phosphorus cycle,” in *Marine authigenesis: From global to microbial* (Tulsa, OK: Society of Economic Paleontologists and Mineralogists Special Publication), 66, 21–33. doi:10.2110/pec.00.66.0021
- Crosby, C. H., and Bailey, J. V. (2012). The role of microbes in the formation of modern and ancient phosphatic mineral deposits. *Front. Microbiol.* 3, 241. doi:10.3389/fmicb.2012.00241
- Dardenne, M. A., Mello, S. M. G., and Moeri, E. (1972). Conophyton: Um fóssil index do precambriano no grupo Bambuí. *Ciênc. Cult.* 24 (2), 199–203.
- Dardenne, M. A. (2000). “The Brasília Fold belt,” in *Tectonic evolution of South America*, 31 international geological congress, Rio de Janeiro, Brazil. Editors U. G. Cordani, E. J. Milani, A. Thomaz Filho, and D. A. Campos, 231–264.
- Dardenne, M. A. (2005). “Conophytos de Cabeludo, Grupo Vazante (MG) – registro de construções dolomíticas por cianobactérias no Proterozóico do Brasil,” in *Sítios Geológicos e Paleontológicos do Brasil*. Editors M. Winge, A. C. S. Fernandes, C. Schobbenhaus, C. R. G. Souza, D. A. Campos, E. T. Queiroz, et al.
- Davey, M. E., and O’Toole, G. A. (2000). Microbial biofilms: From ecology to molecular genetics. *Microbiol. Mol. Biol. Rev.* 64, 847–867. doi:10.1128/MMBR.64.4.847-867.2000
- De Nolf, W., Vanmeert, F., and Janssens, K. (2014). XRDUA: crystalline phase distribution maps by two-dimensional scanning and tomographic (micro) X-ray powder diffraction. *J. Appl. Crystallogr.* 47, 1107–1117. doi:10.1107/S1600576714008218
- Decho, A. W. (1999). “Chemical communication within microbial biofilms: chemotaxis and quorum sensing in bacteria cells,” in *Microbial extracellular polymeric substances*. Editors J. Wingender, T. Neu, and H.-C. Flemming (Berlin: Springer), 155–169. doi:10.1007/978-3-642-60147-7_9
- Des Marais, D. J. (1990). Microbial mats and the early evolution of life. *Trends Ecol. Evol.* 5, 140–144. doi:10.1016/0169-5347(90)90219-4
- Dupraz, C., and Visscher, P. T. (2005). Microbial lithification in marine stromatolites and hypersaline mats. *Trends Microbiol.* 13, 429–438. doi:10.1016/j.tim.2005.07.008
- Dupraz, C., Reid, R. P., Braissant, O., Decho, A. W., Norman, R. S., Visscher, P. T., et al. (2009). Processes of carbonate precipitation in modern microbial mats. *Earth-Science Rev.* 96, 141–162. doi:10.1016/j.earscirev.2008.10.005
- Fairchild, T. R., Rohn, R., Dardenne, M. A., Alvarenga, C. J. S., and Guimarães, E. M. (2015). “Microbialitos dos Grupos Paranoá (Mesoproterozoico) e Vazante (Neoproterozoico), Distrito federal, Goiás e Minas Gerais,” in *Microbialitos do Brasil do pré-cambriano ao recente: um atlas. Rio claro*. Editors T. R. Fairchild, R. Rohn, and D. Dias-Brito (Obra: UNESP-IGCE-UnesPetro), 2, 90–151.
- Falci, A., Caxito, F. A., Seer, H. J., Valeriano, C. M., Dias, P. H., Pedrosa-Soares, A. C., et al. (2018). Provenance shift from a continental margin to a syn-orogenic basin in the Neoproterozoic Araxá nappe system, southern Brasília belt, Brazil. *Precambrian Res.* 306, 209–219. doi:10.1016/j.precamres.2018.01.004
- Ferris, F. G., Frattin, C. M., Gerits, J. P., Schultze-Lam, S., and Sherwood Lollar, B. (1995). Microbial precipitation of a strontium calcite phase at a groundwater discharge zone near rock Creek, British Columbia, Canada. *Geomicrobiol. J.* 13 (1), 57–67. doi:10.1080/01490459509378004
- Foster, J. S., and Green, S. J. (2011). “Microbial diversity in modern stromatolites,” in *Stromatolites: Interaction of microbes with sediments. Cellular origin, life in extreme habitats and astrobiology*. Editors V. Tewari and J. Seckbach (Dordrecht: Springer), 18. doi:10.1007/978-94-007-0397-1_17
- Foster, J. S., and Mobberley, J. M. (2010). “Past, present, and future: microbial mats as models for astrobiological research,” in *Cellular origin, life in extreme habitats and astrobiology: Microbial mats: Modern and ancient microorganisms in stratified systems*. Editors J. Seckbach and A. Oren (Springer), 563–582. doi:10.1007/978-90-481-3799-2_29
- Gaft, M., Reisfeld, R., and Panczer, G. (2015). *Modern luminescence spectroscopy of minerals and materials*. Switzerland: Springer International Publishing, 606.
- Gaucher, C., Cernuschi, F., and Chigolino, L. (2004). “Ocurrencia de Conophyton en Cantera Burguño (Nueva Carrara, Uruguay): nuevos afloramientos del Grupo Mina Verdún y su importancia. IV Congreso Uruguayo de Geología,” in *Cuarto congreso uruguayo de Geología, CD*.
- Graf, D. L. (1961). Crystallographic tables for the rhombohedral carbonates. *Am. Mineral.* 46, 1283–1316.
- Grotzinger, J. P. (1989). “Facies and evolution of precambrian depositional systems: emergence of the modern platform archetype,” in *Controls on carbonate platform and basin development*. Editors P. D. Crevello, J. J. Wilson, J. F. Sarg, and J. F. Read (SEPM Spec. Pub.), 44, 79–106.
- Habermann, D., Neuser, R. D., and Richter, D. K. (1998). Low limit of Mn²⁺-activated cathodoluminescence of calcite: state of the art. *Sediment. Geol.* 116, 13–24. doi:10.1016/S0037-0738(97)00118-8
- Havemann, S. A., and Foster, J. S. (2008). Comparative characterization of the microbial diversities of an artificial microbialite model and a natural stromatolite. *Appl. Environ. Microbiol.* 74, 7410–7421. doi:10.1128/AEM.01710-08
- Hickman-Lewis, K., Cavalazzi, B., Sorieul, S., Gautret, P., Foucher, F., Whitehouse, J. M., et al. (2020). Metallomics in deep time and the influence of ocean chemistry on the metabolic landscapes of Earth’s earliest ecosystems. *Sci. Rep.* 10, 4965. doi:10.1038/s41598-020-61774-w
- Hoffman, P. F. (1976). “Environmental diversity of middle precambrian stromatolites,” in *Stromatolites*. Editor M. R. Walter (Amsterdam: Elsevier), 599–611.
- Hofmann, H. J. (1969). Attributes of stromatolites. *Geol. Surv. Can. Pap.* 58, 69–39.
- Hofmann, H. J. (2000). “Archean stromatolites as microbial archives,” in *Microbial sediments*. Editors R. Riding and S. Awramik (Berlin, Heidelberg: Springer), 315–327.
- Horodyski, R. J. (1985). “Stromatolites of the middle proterozoic belt Supergroup, glacier national park, Montana: a summary and a comment on the relationship between their morphology and paleoenvironment,” in *Paleoalgeology*. Editors D. F. Toomey and M. H. Nitecki (Berlin, Heidelberg: Springer). doi:10.1007/978-3-642-70355-3_4
- Kah, L. C., Bartley, J. K., and Stagner, A. F. (2009). “Reinterpreting a proterozoic enigma: Conophyton–Jacutophyton stromatolites of the mesoproterozoic atar

- group, Mauritania" in *Perspectives in Carbonate Geology, A Tribute to the Career of Robert Nathan Ginsburg*, 41. Chichester, Wiley: International Association of Sedimentologists Spec. Publ., 277–295.
- Kögel-Knabner, I., Guggenberger, G., Kleber, M., Kandeler, E., Kalbitz, K., Scheu, S., et al. (2008). Organo-mineral associations in temperate soils: Integrating biology, mineralogy, and organic matter chemistry. *Z. Pflanzenernähr. Bodenk.*, 171, 61–82. doi:10.1002/jpln.200700048
- Lalonde, K., Mucci, A., Ouellet, A., and Gélinais, Y. (2012). Preservation of organic matter in sediments promoted by iron. *Nature* 483, 198–200. doi:10.1038/nature10855
- Lovley, D. R., Coates, J. D., Blunt-Harris, E. L., Phillips, E. J. P., and Woodward, J. C. (1996). Humic substances as electron acceptors for microbial respiration. *Nature* 382, 445–448. doi:10.1038/382445a0
- MacRae, C., and Wilson, N. (2008). Luminescence database I—minerals and materials. *Microsc. Microanal.*, 14 (2), 184–204. doi:10.1017/S143192760808029X
- Marfunin, A. S. (1995). *Methods and instrumentations: Results and recent developments*. Berlin Heidelberg: Springer-Verlag, 441p.
- Melim, L. A., Northup, D. E., Boston, P. J., and Spilde, M. N. (2016). Preservation of fossil microbes and biofilm in cave pool carbonates and comparison to other microbial carbonate environments. *Palaio* 31 (4), 177–189. doi:10.2110/palo.2015.033
- Moeri, E. (1972). On a columnar stromatolite in the precambrian bambui group of central Brazil. *Eclogae Geol. Helv.* 65 (1), 185–195. doi:10.5169/seals-164084
- Murphy, A. E., Wieman, S. T., Gross, J., Stern, J. C., Steele, A., Glamoclija, M., et al. (2020). Preservation of organic carbon in dolomitized Cambrian stromatolites and implications for microbial biosignatures in diagenetically replaced carbonate rock. *Sediment. Geol.* 410, 105777. doi:10.1016/j.sedgeo.2020.105777
- Neu, T. R. (1994). "Biofilms and microbial mats," in *Biostabilization of sediments*. Editors W. E. Krumbein, D. M. Paterson, and L. Stal (Oldenburg: BIS-Verlag), 6–16.
- Neu, T. R. (1996). Significance of bacterial surface-active compounds in interaction of bacteria with interfaces. *Microbiol. Rev.* 60, 151–166. doi:10.1128/mr.60.1.151-166.1996
- Nielsen, L. P., Risgaard-Petersen, N., Fossing, H., Christensen, P. B., and Sayama, M. (2010). Electric currents couple spatially separated biogeochemical processes in marine sediment. *Nature* 463, 1071–1074. doi:10.1038/nature08790
- Nisbet, E. G., and Fowler, C. M. R. (1999). Archaeal metabolic evolution of microbial mats. *Proc. R. Soc. Lond. B* 266, 2375–2382. doi:10.1098/rspb.1999.0934
- Noffke, N., and Awramik, S. M. (2013). Stromatolites and MISS – differences between relatives. *GSA Today* 23, 4–9. doi:10.1130/GSATG187A.1
- Noffke, N., Christian, D., Wacey, D., and Hazen, R. M. (2013). Microbially induced sedimentary structures recording an ancient ecosystem in the ca. 3.48 billion-year-old Dresser Formation, Pilbara, Western Australia. *Astrobiology* 13 (12), 1103–1124. doi:10.1089/ast.2013.1030
- Pernthaler, A., Dekas, A. E., Brown, T., Goffredi, S. K., Embaye, T., Orphan, V. J., et al. (2008). Diverse Syntrophic partnerships from deep-sea methane vents revealed by direct cell capture and metagenomics. *Proc. Natl. Acad. Sci. U. S. A.*, 105 7052–7057. doi:10.1073/pnas.0711303105
- Pierson, B. J. (1981). The control of cathodoluminescence in dolomite by iron and manganese. *Sedimentology* 28, 601–610. doi:10.1111/j.1365-3091.1981.tb01924.x
- Preiss, W. V. (1976). "Intercontinental correlations," in *Stromatolites*. Editor M. R. Walter (Amsterdam: Elsevier Sci. Publ. Co.), 359–370.
- Reid, R. P., and MacIntyre, I. G. (2000). Microboring versus recrystallization: further insight into the micritization process. *J. Sediment. Res.* 70, 24–28. doi:10.1306/2DC408FA-0E47-11D7-8643000102C1865D
- Riding, R. (2011). "The nature of stromatolites: 3,500 million years of history and a century of research," in *Advances in stromatolite geobiology* (Berlin, Heidelberg: Springer), 131. Lecture notes in Earth sciences. doi:10.1007/978-3-642-10415-2_3
- Rodrigues, J. B., Pimentel, M. M., Bühn, B., Matteini, M., Dardenne, M. A., Alvarenga, C. J. S., et al. (2012). Provenance of the Vazante group: New U–Pb, Sm–Nd, Lu–Hf isotopic data and implications for the tectonic evolution of the neoproterozoic Brasília belt. *Gondwana Res.* 21 (2–3), 439–450. doi:10.1016/j.gr.2011.07.017
- Saghai, A., Gutiérrez-Preciado, A., Deschamps, P., Moreira, D., Bertolino, P., Ragon, et al. (2017). Unveiling microbial interactions in stratified mat communities from a warm saline shallow pond. *Environ. Microbiol.* 19 (6), 2405–2421. doi:10.1111/1462-2920.13754
- Sallun Filho, W., and Fairchild, T. R. (2005). *Estudo comparativo entre estromatólitos do tipo Conophyton das Faixas Ribeira e Brasília*. São Paulo: Revista do Instituto Geológico, 1–18. doi:10.5935/0100-929X.20050001
- Schopf, J. W. (1975). Precambrian paleobiology: problems and perspectives. *Annu. Rev. Earth Planet. Sci.* 3, 213–249. doi:10.1146/annurev.ca.03.050175.001241
- Schopf, J. W., and Yuk, S. (1976). Microfossils in conophyton from the vendian deposits of South Kazakhstan. *Doklady AN SSSR* 230, 1448–1450. (In Russian)
- Schulz, H. N., and Schulz, H. D. (2005). Large sulfur bacteria and the formation of phosphorite. *Science* 307, 416–418. doi:10.1126/science.1103096
- Shionoya, S., Yen, W. M., and Yamamoto, H. (2007). *Phosphor handbook*. 2nd ed.. Boca Raton, FL: CRC Press/Taylor and Francis, 1080. doi:10.1201/9781315222066
- Shukla, Y., Sharma, M., Noffke, N., and Callefo, F. (2020). Biofilm microfacies in phosphoritic units of the neoproterozoic halkal shale, bhima basin, South India. *Precamb. Res.* 349, 105501. doi:10.1016/j.precamres.2019.105501
- Solé, V. A., Papillon, E., Cotte, M., Walter, P., and Susini, J. (2007). A multiplatform code for the analysis of energy-dispersive X-ray fluorescence spectra. *Spectrochim. Acta Part B At. Spectrosc.* 62, 63–68. doi:10.1016/j.sab.2006.12.002
- Stolyar, S., Dien, S. V., Hillesland, K. L., Pinel, N., Lie, T. J., Leigh, J. A., et al. (2007). Metabolic modeling of a mutualistic microbial community. *Mol. Syst. Biol.* 3, 92. doi:10.1038/msb4100131
- Stoodley, P., Sauer, K., Davies, D. G., and Costerton, J. W. (2002). Biofilms as complex differentiated communities. *Annu. Rev. Microbiol.* 56, 187–209. doi:10.1146/annurev.micro.56.012302.160705
- Tolentino, H. C. N., Geraldies, R. R., Moreno, G. B. Z. L., Pinto, A. C., Bueno, C. S. N. C., Kofukuda, L. M., et al. (2021). "X-ray microscopy developments at sirius-LNLS: first commissioning experiments at the Carnauba beamline," in *Proceedings SPIE 11839, X-Ray Nanoimaging: Instruments and Methods V*, 8 September 2021. doi:10.1117/12.25964961183904
- Tolker-Nielsen, T., and Molin, S. (2000). Spatial organization of microbial biofilm communities. *Microb. Ecol.* 40, 75–84. doi:10.1007/s002480000057
- Vasconcelos, A. G., Bittencourt, J. S., Eliziário, N. F., Kraemer, B. M., and Auler, A. S. (2020). Stromatolites in caves in southeastern Brazil and their importance to geoconservation. *Geoh Heritage* 12, 48. doi:10.1007/s12371-020-00469-0
- Walter, M. R. (1976). *Stromatolites*. Amsterdam: Elsevier Sci. Publ. Co., 790.
- Walter, M. R. (1977). Interpreting Stromatolites: These fossils can tell us much about past organisms and environments if we can learn to decode their message. *Am. Sci.* 65 (5), 563–571. Available at: <http://www.jstor.org/stable/27848083>.
- Williams, L. A., and Reimers, C. (1983). Role of bacterial mats in oxygen-deficient marine basins and coastal upwelling regimes: preliminary report. *Geology* 11, 267–269. doi:10.1130/0091-7613(1983)11<267:ROBMIO>2.0.CO;2
- Williams, L. A. (1984). Subtidal stromatolites in monterey formation and other organic-rich rocks as suggested source contributors to petroleum formation. *Am. Assoc. Pet. Geol. Bull.* 68, 1879–1893. doi:10.1306/AD4619F8-16F7-11D7-8645000102C1865D
- Zhang, Y., Li, J., Chen, L., Wei, Y., Shi, Q., Wang, D. G., et al. (2021). Manganese carbonate stromatolites of the ediacaran doushantuo formation in chengkou, northern yangtze Craton, China. *J. Palaeogeogr.* 10, 22. doi:10.1186/s42501-021-00099-9

Advantages of publishing in Frontiers



OPEN ACCESS

Articles are free to read
for greatest visibility
and readership



FAST PUBLICATION

Around 90 days
from submission
to decision



HIGH QUALITY PEER-REVIEW

Rigorous, collaborative,
and constructive
peer-review



TRANSPARENT PEER-REVIEW

Editors and reviewers
acknowledged by name
on published articles

Frontiers

Avenue du Tribunal-Fédéral 34
1005 Lausanne | Switzerland

Visit us: www.frontiersin.org

Contact us: frontiersin.org/about/contact



REPRODUCIBILITY OF RESEARCH

Support open data
and methods to enhance
research reproducibility



DIGITAL PUBLISHING

Articles designed
for optimal readership
across devices



FOLLOW US

@frontiersin



IMPACT METRICS

Advanced article metrics
track visibility across
digital media



EXTENSIVE PROMOTION

Marketing
and promotion
of impactful research



LOOP RESEARCH NETWORK

Our network
increases your
article's readership